University of Southampton

Faculty of Engineering And Physical Sciences

SCHOOL

The Osteology, Palaeoneurology And Systematics Of Theropod (Dinosauria) Material From The Early Cretaceous Of Southern England (UK), With Emphasis On Spinosauridae

by

Chris Tijani Barker

ORCID ID 0000-0001-8792-3307

Thesis for the degree of Doctor of Philosophy

Sept 2023

University of Southampton

Abstract

Faculty of Engineering And Physical Sciences

SCHOOL OF ENGINEERING

Doctor Of Philosophy

The Osteology, Palaeoneurology And Systematics Of Theropod (Dinosauria) Material From The Early Cretaceous Of Southern England (UK), With Emphasis On Spinosauridae

by

Chris Tijani Barker

The Early Cretaceous deposits of the Wealden Supergroup (upper Berriasian–lower Aptian) of southern England and the Isle of Wight are an internationally important source of dinosaur material, however theropod remains are generally rare. The aim of this thesis is to describe and interpret theropod specimens – some recently discovered – from southern England and the Isle of Wight, with a particular focus on fossils belonging to Spinosauridae (Theropoda: Tetanurae). This clade of enigmatic, fish-eating theropods was mainly represented in the British fossil record by the partial skeleton of *Baryonyx walkeri* from the Upper Weald Clay Formation (Barremian) of Surrey, with other isolated fragments—mainly teeth—also known from Wealden Supergroup strata (Chapter 1). Osteological and phylogenetic analyses of new material from the Wessex Formation (Barremian) of the Isle of Wight suggest the presence of multiple spinosaurid lineages and an underappreciated diversity of spinosaurid taxa, including two specimens that are sufficiently diagnostic to warrant naming: *Ceratosuchops inferodios* and *Riparovenator milnerae* (Chapter 2). The latter are phylogenetically closer to the African *Suchomimus tenerensis* than *B. walkeri*, and a novel palaeobiogeographical reconstruction suggests a European (Laurasian) origin for Spinosauridae and multiple dispersal events into Gondwana. Support for a higher diversity of British spinosaurids is provided via additional lines of evidence. Cladistic and morphometric analyses of an isolated spinosaurid tooth, likely from a Valanginian unit of the older Hastings Group of East Sussex, failed to associate with *Baryonyx* in any data run using a large tooth-based dataset (Chapter 3). Meanwhile, the discovery of a notably large-bodied spinosaurid from the overlying Vectis Formation (upper Barremian) of the Isle of Wight also extends the temporal range of British spinosaurids, marking the youngest definitive occurrence of the clade in the British

fossil record (Chapter 4). Phylogenetic analyses of this specimen were inconclusive given its fragmentary nature but the initial results argue for the presence of yet another spinosaurid lineage in the British Mesozoic. This thesis also employs microCT-based reconstruction of the endocranial cavity and associated endocast of *B. walkeri* and *C. inferodios* to shine light on the neuroanatomy and sensory capabilities of earlier branching spinosaurids (Chapter 5). Comparable to various other basal tetanurans in gross morphology, these forms possessed unexceptional hearing and olfaction, suggesting the transition from terrestrial hypercarnivorous ancestors to fish-eating "generalists" did not require substantial modification of the endocranium, or that Barremian spinosaurids already possessed the neuroanatomical adaptations required for this ecological shift. Finally, this thesis also examines rare and highly pneumatic theropod material from the Lower Greensand Group of the Isle of Wight – herein named *Vectaerovenator inopinatus* – whose relationships within Tetanurae could not be presently ascertained (Chapter 6). This fragmentary specimen is one of Britain's youngest non-avian theropods and the first named taxon from the Aptian of Europe, providing valuable data from a poorly sampled period of European Mesozoic. In totality, this work substantially contributes to the diversity and relationships of the theropod fossil record from Britain, provides the first endocranial studies of baryonychine grade spinosaurids, and helps refine the understanding of spinosaurid palaeoecology (Chapter 7).

Table of Contents

Table of Tables

Table of Figures

Research Thesis: Declaration of Authorship

Print name: Chris Tijani Barker

Title of thesis: The Osteology, Palaeoneurology And Systematics Of Theropod (Dinosauria) Material From The Early Cretaceous Of South England (UK), With Emphasis On Spinosauridae

I declare that this thesis and the work presented in it are my own and has been generated by me as the result of my own original research.

I confirm that:

1. This work was done wholly or mainly while in candidature for a research degree at this University;
2. Where any part of this thesis has previously been submitted for a degree or any other qualification at this University or any other institution, this has been clearly stated;
3. Where I have consulted the published work of others, this is always clearly attributed;
4. Where I have quoted from the work of others, the source is always given. With the exception of such quotations, this thesis is entirely my own work;
5. I have acknowledged all main sources of help;
6. Where the thesis is based on work done by myself jointly with others, I have made clear exactly what was done by others and what I have contributed myself;
7. Parts of this work have been published as:

Barker, C.T., Naish, D., Clarkin, C.E., Farrell, P., Hullmann, G., Lockyer, J., Schneider, P., Ward, R.K. and Gostling, N.J., 2020. A highly pneumatic middle Cretaceous theropod from the British Lower Greensand. *Papers in Palaeontology*, 6(4), pp.661-679.

Barker, C.T., Hone, D.W., Naish, D., Cau, A., Lockwood, J.A., Foster, B., Clarkin, C.E., Schneider, P. and Gostling, N.J., 2021. New spinosaurids from the Wessex Formation (Early Cretaceous, UK) and the European origins of Spinosauridae. *Scientific reports*, 11(1), pp.1-15.

Barker, C.T., Lockwood, J.A., Naish, D., Brown, S., Hart, A., Tulloch, E. and Gostling, N.J., 2022. A European giant: a large spinosaurid (Dinosauria: Theropoda) from the Vectis Formation (Wealden Group, Early Cretaceous), UK. *PeerJ*, 10, p.e13543.

Barker, C.T., Naish, D., Trend, J. et al. 2023. Modified skulls but conservative brains? The palaeoneurology and endocranial anatomy of baryonychine dinosaurs (Theropoda: Spinosauridae). *Journal of Anatomy*, 242(6), 1124– 1145.

Barker, C.T., Naish, D. and Gostling, N. J. 2023. Isolated tooth reveals hidden spinosaurid dinosaur diversity in the British Wealden Supergroup (Lower Cretaceous). *PeerJ*, 10, p.e13543.

Signature: .....Date:.....

Acknowledgements

It has been a great privilege to follow a childhood fascination and be able to study theropod dinosaurs in such detail, and I owe a lot to a great many people for helping me fulfil this opportunity. I would firstly like to express my eternal gratitude to my principal supervisor Neil Gostling, for believing in the project and providing infectious enthusiasm long before I stepped into the Life Sciences building. I would also like to thank Claire Clarkin and Philip Schiender for providing support and guidance throughout my doctoral studies, and to John Marshall and Markus Heller for their time and practical criticism of my work during my progress reviews.

To Darren Naish – thank you for the continual support, generosity of time and knowledge, and detailed critique of my work. I have learnt a great deal from you and have appreciated collaborating with you on these theropod projects. Long may this continue.

To Jeremy Lockwood –I admire your drive and dedication to responsible collecting and safeguarding of the Isle of Wight's palaeontological heritage. Thank you for your hospitality, generosity, and help getting this project off the ground.

To Dave Hone – I valued your patience and insight regarding the interpretation of the Wessex Formation spinosaurids, and I appreciate the time you took for our regular catch-ups, which helped focus my efforts.

To the curators: Martin Munt, Susie Maidment, Julian Porter and Phil Hadland – I am extremely grateful for the warm welcomes, helpful advice, and detailed knowledge of the specimens under your care.

To the preparators: Gary Blackwell, Mick Green and Phil James – thank you for the care, skill and expert preparation you all demonstrated, which substantially facilitated the description and interpretation of the specimens studied herein.

To my co-authors –I am proud to have been able to contribute to the field, and it was a great pleasure to work with you on these projects. I am thankful for the attention to detail, hard work and insightful critique you all extended to my drafts.

To the MuVIS team: Katy Rankin, Mark Mavrogordato, Orestis Katsamenis and Roland Smith – I hope that the generally complicated nature of the specimens we repeatedly brought through to your scanners did not prove too taxing for your machines or your sanity.

To Steve Vidovitch and Andrea Cau – I appreciate the time you both took to teach me how to use the software TNT, which formed a substantial part of my methods.

To Alex Peaker, Gary Blackwell, Eleanor Foxwell, Martyn Hornett, Simon Penn, Mick Green, Mark Penn, and Dave Brockhurst – I am grateful for our engaging discussions regarding the palaeontology and geology of the British Lower Cretaceous. And to the team at Dinosaur Isle Museum in particular – your support and enthusiasm was very well received.

To the collectors – this project would not have existed without the hours you put in scouring the British coastlines, or your generosity in donating these specimens and making them accessible to everyone. On both counts, I am extremely grateful.

To the artists: Trudie Wilson, Dan Folkes and Anthony Hutchings – thank you for bringing these extraordinary fossils back to life.

I would like to additionally thank Andrea Cau, Christophe Hendrickx, Tom Land, Tom Smith, Serjoscha Evers, Logan King, Marco Schade, Jon Radley, Jeff Thompson, Denver Fowler and Larry Witmer for their helpfulness in answering queries I had throughout the course of my studies. I am also grateful for the editors at *Scientific Reports*, *PeerJ*, *Papers in Palaeontology*, and *Journal of Anatomy* for handling the manuscripts sent to them. Special thanks are also extended to the reviewers who took the time to check the validity of the findings presented herein, whose comments substantially improved the quality of the work.

To my family and friends – I hope this work is reflective of the unwavering support you have shown me.

And finally, to C and C. –I have been so very, very lucky .

Chapter 1 Introduction

1.1 Theropods and the British fossil record

Theropoda is a clade of saurischian dinosaur whose representatives are more closely related to birds than to sauropods (Sereno, 1998; Padian et al., 1999). British theropod taxa have an important place in the history of theropod research (and dinosaur palaeontology more generally) (Naish et al., 2007): *Megalosaurus bucklandii* from the Jurassic of Oxfordshire was the first scientifically described dinosaur taxon (Buckland, 1824), and was one of three fossil reptiles used to erect the Dinosauria (Owen, 1842). Excluding birds, British theropods are temporally extensive, ranging from the Norian or Rhaetian (Late Triassic) (Spiekman et al., 2021) to possibly the Albian–Cenomanian ("mid" Cretaceous) (Galton et al., 2002; but see Barrett et al., 2021). The British theropod fossil record is rich, and includes representatives from several major clades including Coelophysoidea, basal Tetanurae (e.g. Megalosauridae, Spinosauridae, Allosauroidea) and Coelurosauria (e.g. Tyrannosauroidea, Maniraptora) (Naish et al., 2007; Lomax et al., 2014). British theropods are however less well represented compared with global samples (Naish et al., 2007), and may be rare components in some otherwise dinosaur-rich British successions (e.g. the Wealden Supergroup; see below) (Naish, 2011).

1.2 Spinosaurid palaeobiology: a general background

Spinosaurids are a clade of large-bodied basal tetanuran theropods that have undergone a surge of interest in recent years (Bertin, 2010; Hone et al., 2017). Definitively known from the Cretaceous, their origins likely lie in the Jurassic (Milner, 2003; Holtz et al., 2004; Carrano et al., 2012) (see also Chapter 2). Their unusual and highly specialised morphology is atypical of non-avian theropods (Figure 1.1), and is characterised by elongate, laterally compressed snouts and conidont (cone-shaped) dentition. Multiple lines of evidence point to an ability to exploit semi-aquatic niches that included a partially piscivorous diet (Taquet, 1984; Charig et al., 1997; Holtz, 1998; Holtz et al., 2004; Amiot et al., 2010a; Bertin, 2010; Hassler et al., 2018; McCurry et al., 2019; Ibrahim et al., 2020a; Hone et al., 2021; Fabbri et al., 2022b; Sereno et al., 2022). It has also been suggested spinosaurids became increasingly aquatic during their evolution (Arden et al., 2019; Sereno et al., 2022), with various taxa potentially engaging in specialised underwater foraging or pursuit predation (Ibrahim et al., 2014; Ibrahim et al., 2020a; Fabbri et al., 2022b). Yet, these predators represent a poorly understood clade despite their distinctive morphology; spinosaurid material tends to be fragmentary and body fossils are limited (Hone et al., 2010a; Hone et al., 2017). Further, the loss of the *Spinosaurus* type specimen (Stromer, 1915) during the Second World War (Smith et al., 2006) – the first taxon referred to Spinosauridae (but not the first

spinosaurid discovery; see section 1.3.1) – was a substantial setback to the study of the clade, the repercussions of which are still felt today. As such, various aspects of their palaeobiology remains poorly understood and substantially debated, most notably the degree of specialisation to aquatic life, and the sequence by which such adaptations were acquired during the evolution of the group (Barker et al., 2017; Henderson, 2018; Hone et al., 2019; Hone et al., 2021; Sereno et al., 2022).

1.2.1 Spinosaurid taxonomy and systematics

1.2.1.1 Systematics

Typically recovered as megalosauroid tetanurans that are sister to Megalosauridae (Holtz et al., 2004; Benson, 2010; Carrano et al., 2012; Barker et al., 2021) (Figure 1.2A), some recent phylogenetic work has recovered spinosaurids in an earlier branching position outside of a clade that includes other megalosauroid subclades and allosauroids (Rauhut et al., 2019b) (Figure 1.2B). Regardless, the spinosaurid in-group is traditionally and frequently dichotomised into Baryonychinae and Spinosaurinae (Sereno et al., 1998; Holtz et al., 2004; Benson, 2010; Allain et al., 2012; Carrano et al., 2012; Arden et al., 2019; Rauhut et al., 2019b; Sereno et al., 2022). The differences between the clades are often craniodental, and typical baryonychine characters include the possession of a large number of minutely serrated teeth, a sub-quadrangular quadrate head, and a V-shaped premaxilla-nasal suture; spinosaurines have fewer, more widely space teeth that lack serrations or substantial recurvature.

However the generally fragmentary nature of spinosaurid material has lead to debatable ingroup relationships in recent times. The distinction between the two subclades may be subject to future revision (Evers et al., 2015), and it is possible that baryonychine taxa may represent successive outgroups to a potentially monophyletic Spinosaurinae (i.e. Baryonychinae is paraphyletic) (Sales et al., 2017b) (see also Chapter 2). Additionally, one recent analysis not only recovered the above dichotomous split, but also demonstrated that derived spinosaurines could be grouped into a new clade named “Spinosaurini” (Arden et al., 2019), although no formal diagnosis of the latter was provided. For ease of comparisons, this thesis generally refers to Baryonychinae and Spinosaurinae throughout (unless discussing the validity of the dichotomy specifically).

1.2.1.2 Taxonomy

The number of valid spinosaurid taxa remains a matter of debate, with substantial revisions leading to the synonymisation of various named taxa despite the relatively recent discovery of many of the proposed holotype specimens (Hone et al., 2017). The taxonomic histories of spinosaurid taxa named between 1841–2022 are briefly detailed in Table 1.1.

The sparse and fragmentary spinosaurid fossil record has certainly not aided the taxonomic interpretation of several specimens (one of the key limitations affecting our understanding of the clade in general) (Hone et al., 2017). In some cases, spinosaurid taxa were erected based on isolated dental material, such as *Ostafrikasaurus* (Buffetaut, 2012; the taxon is now referred to a probable ceratosaur; Rauhut, 2011; Hendrickx et al., 2019; Soto et al., 2020). This practice is no longer considered advisable amongst theropod systematicists given the rampant homoplasy displayed by theropod teeth (Hendrickx et al., 2014a; Hendrickx et al., 2019). The taxonomic debates surrounding other taxa have been impacted form the loss of holotype material. For instance, the loss of the *Spinosaurus aegyptiacus* type specimen during the Second World War (Smith et al., 2006), now only known from the original descriptions and several images (Stromer, 1915; Smith et al., 2006), has (in part) lead to conflicting interpretations of the North African spinosaurid fossil record (Ibrahim et al., 2014; Evers et al., 2015; Hendrickx et al., 2016; Arden et al., 2019; Smyth et al., 2020). Assessing the validity of all known spinosaurid taxa is beyond the scope of this thesis – an endeavour that would certainly benefit from the monographic description of several key specimens (Hone et al., 2017).

Table 1.1 Taxonomy of Spinosauridae, focusing on holotype specimens. Modified from (Holtz et al., 2004), and includes results from Chapter 2. Note that the type specimen of *Ostafrikasaurus crassiserratus* MB R 1084, a putative spinosaurid named from the Jurassic of Tanzania (Buffetaut, 2012), is considered a *nomen dubium* with ceratosaurs affinities (Rauhut, 2011; Hendrickx et al., 2019; Smyth et al., 2020; Soto et al., 2020) (*contra* Hone et al. (2017), who considered it Spinosauridae *incertae sedis*), and is not included here.

	Type specimen	**Type occurrence and age**	**Comments**
Spinosauridae Stromer, 1915 (=Baryonychidae Charig and Milner, 1986; =Irritoridae Martill et al., 1996; =Sigilmassasauridae Russell, 1996)			
Sinopliosaurus Young, 1944 ***S. fusuiensis*** Hou et al., 1975	IVPP V 4793	Xinlong Fm. (China, Aptian)	Originally referred to Pliosauridae (Hou et al., 1975). Considered closely related to *Siamosaurus* according to Buffetaut et al. (2008), and referred to Spinosauridae indet. by Samathi et al. (2019).

			Considered a *nomen dubium* by (Sales et al., 2017b).
Siamosaurus Buffetaut and Ingavat, 1986 ***S. suteethorni*** Buffetaut and Ingavat, 1986	SM-TF 2043a	Sao Khua Fm. (Thailand, Barremian)	The taxonomic history of *S. suteethorni* was recently summarised by (Samathi et al., 2019). A re-description dealing with the generic validity of this taxon is apparently in preparation (Bertin, 2010). Bertin (2010) considered it Spinosauridae indet. pending this revision. The spinosaurid affinities suggested by Buffetaut et al. (1986) were questioned by Sues et al. (2002) and Holtz et al. (2004); the latter also considered it a *nomen dubium*, as did Sales et al. (2017b) and Smyth et al. (2020). Referred to ?Spinosauridae indet. by Carrano et al. (2012).
Camarillasaurus Sánchez-Hernández and Benton, 2012 ***C. cirugedae*** Sánchez-Hernández and Benton, 2012	MPG-KPC1– 46	Camarillas Fm. (Spain, Barremian)	Originally referred to Ceratosauria (Sánchez-Hernández et al., 2012). First referred to Spinosauridae by Rauhut et al. (2019a). This revision has since received additional support, with some data runs arguing it is an early branching spinosaurid or spinosaurine (Malafaia et al., 2020a; Barker et al., 2021; Samathi et al., 2021; Sereno et al., 2022). Given the very fragmentary nature of the holotype, it is considered an indeterminate spinosaurid here.
Vallibonavenatrix Malafaia et al., 2019 ***V. cani*** Malafaia et al., 2019	MSMCa-1, 3– 5, 9–15, 18– 20, 22–24, 27–28, 32–33, 53, 55	Arcillas de Morella Fm. (Spain, Barremian)	Initially referred to Spinosaurinae (Malafaia et al., 2020b), a topology supported by Sereno et al. (2022), its phylogenetic position has been unstable in other analyses (Barker et al., 2021; Barker et al., 2022; Mateus et al., 2022).

Iberospinus Mateus and Estraviz-López, 2022 ***I. natarioi*** Mateus and Estraviz-López, 2022	ML1190	Papo Seco Fm. (Portugal, Barremian)	Previously referred to *B. walkeri* (Mateus et al., 2011).
Baryonychinae Charig and Milner, 1986; *sensu* Sereno et al., 1998			
"*Suchosaurus*" Owen 1841 **"*S. cultridens*"** Owen 1840–1845	NHMUK PV R36536	Grinstead Clay Fm. (UK, Valanginian)	Originally considered to be a crocodilian (Owen, 1840–1845; Buffetaut, 2010), *S. cultridens* is a *nomen dubium* and referable to Baryonychinae according to Mateus et al. (2011) and Carrano et al. (2012). Holotype tooth possibly a (senior) synonym of *Baryonyx walkeri* by former authors, however subsuming *Baryonyx* into *Suchosaurus* would be impractical given the nature of holotype material (a single tooth) (Buffetaut, 2007).
"*S. girardi*" Sauvage 1897–1898	MG324	Papo Seco Fm. (Portugal, Barremian)	*Nomen dubium* according to Mateus et al. (2011) and Carrano et al. (2012). Baryonychine affinities presented in Buffetaut (2007) and Mateus et al. (2011). Referred to *Baryonyx* sp. by Buffetaut (2007) and potentially a (senior) synonym of *B. walkeri* according to Mateus et al. (2011) and Carrano et al. (2012). See above regarding the issues of subsuming *Baryonyx* into *Suchosaurus* (Buffetaut, 2007).
Baryonyx Charig and Milner, 1986 ***B. walkeri*** Charig and Milner, 1986	NHMUK PV R9951	Upper Weald Clay Fm. (UK, Barremian)	Arguably a junior synonym of *Suchosaurus*, but see above regarding the issues of subsuming *Baryonyx* into *Suchosaurus* (Buffetaut, 2007).
Cristatusaurus Taquet and Russell, 1998 ***C. lapparenti*** Taquet and Russell, 1998	MNN GDF 366	Elrhaz Fm. (Niger, Aptian)	Type premaxillae initially identified as the dentary symphyses of an indeterminate spinosaurid (Taquet, 1984). Referred to *Baryonyx* sp. by Charig et al. (1997). *Cristatusaurus* a subjective junior synonym of *Baryonyx* in Sues et al. (2002).

			Considered a *nomen dubium* by Sereno et al. (1998), Rauhut (2003), Carrano et al. (2012) and Hendrickx et al. (2016).
			Considered valid by Lacerda et al. (2021).
Protathlitis Santos-Cubedo et al., 2023 ***P. cinctorrensis*** Santos-Cubedo et al., 2023	8ANA-109, 3ANA83, 4ANA43, 4ANA69, 4ANA76, 5ANA78	Arcillas de Morella Fm. (Spain, Barremian)	
Ceratosuchopsini Barker et al., 2021			
Suchomimus Sereno et al., 1998 ***S. tenerensis*** Sereno et al., 1998	MNN GDF 500	Elrhaz Fm. (Niger, Aptian)	*Suchomimus* a subjective junior synonym of *Baryonyx* according to Sues et al. (2002), Milner (2003), Hutt et al. (2004) and Naish et al. (2007), and was considered very similar to the latter by Rauhut (2003) and Holtz et al. (2004). Considered a valid genus by Carrano et al. (2012), Hone et al. (2017) and Lacerda et al. (2021).
Ceratosuchops Barker et al., 2021 ***C. inferodios*** Barker et al., 2021	IWCMS 2014.95.1–3, 5 and 2021.30	Wessex Fm. (UK, Barremian)	
Riparovenator Barker et al., 2021 ***R. milnerae*** Barker et al., 2021	IWCMS 2014.95.6, 2014.96.1–3, 2020.448.1 and 2	Wessex Fm. (UK, Barremian)	Sereno et al. (2022) score *R. milnerae* as a single taxon, *C. inferodios*, in their phylogenetic analysis. Considered distinct by Terras et al. (2022). Analyses by Schade et al. (2023) recovers *Riparovenator* outside of the *Suchomimus*+*Ceratosuchops* clade.
Spinosaurinae Stromer 1915; *sensu* Sereno et al., 1998			
Spinosaurus Stromer, 1915 ***S. aegyptiacus*** Stromer, 1915	BSP 1912 VIII 19	Bahariaya Fm. (Egypt, Cenomanian)	The type specimen named by Stromer (1915) was lost in the night of the 24th/25th April 1944 (Smith et al., 2006). A neotype

			specimen was raised by Ibrahim et al. (2014) following the discovery of FSAC KK11888 from the Kem Kem beds of Morocco, but this has been deemed inadequately justified by some authors (Evers et al., 2015; Chiarenza et al., 2016).
S. maroccanus Russell, 1996	CMN 50791	"Continental Red Beds" (Morocco, Cenomanian)	*S. maroccanus* is a *nomen dubium* according to Sereno et al. (1998), Buffetaut et al. (2002), Rauhut (2003) and Dal Sasso et al. (2005). Also deemed a subjective junior synonym of *Sp. aegyptiacus* in Sereno et al. (1998), Ibrahim et al. (2014), Ibrahim et al. (2020b) and Smyth et al. (2020).
			Considered to be a subjective junior synonym of *S. brevicolis* in Evers et al. (2015).
Sigilmassasaurus Russell, 1996 ***Si. brevicollis*** Russell, 1996	CMN 41857	Ifezoune or Auofous Formation (Morocco; Cenomanian, precise locality of holotype unknown,)	The taxonomic and systematic history of *Si. brevicolis* was summarised by Evers et al. (2015) and McFeeters (2020). *Si. brevicollis* initially described as a theropod of uncertain affinities (Russell, 1996), followed by Holtz et al. (2004) and McFeeters et al. (2013). *Si. brevicollis* considered a subjective junior synonym of *Carcharodontosaurus saharicus* Sereno et al. (1998) and Brusatte et al. (2007). Ornithischian affinities for *Si. brevicollis* also suggested by Canale et al. (2008). Spinosaurid affinities of taxon supported by (Evers et al., 2012a), Evers et al. (2012b), Allain (2014), Evers et al. (2015), Arden et al. (2019) and Barker et al. (2021).

			Si. brevicollis referred to *Sp. marocannus* by Mahler (2005) (but see above).
			Si. brevicollis a subjective junior synonym of *S. aegyptiacus* according to Allain (2014), Ibrahim et al. (2014), Ibrahim et al. (2020b) and Smyth et al. (2020). *Si. brevicollis* considered distinct from *S. aegyptiacus* according to Evers et al. (2015), and presence of at least two distinct spinosaurids from the Kem Kem compound assemblage of Morocco supported by multiple additional lines of evidence (Hendrickx et al., 2016; Arden et al., 2019; Lakin et al., 2019; McFeeters, 2020), although see Ibrahim et al. (2020b) and Smyth et al. (2020). Distinction considered equivocal in Barker et al. (2021).
			Considered a valid taxon by Holtz et al. (2004), McFeeters et al. (2013) and Evers et al. (2015). Considered a *nomen dubium* by Allain (2014).
Irritator Martill et al., 1996 ***I. challengeri*** Martill et al., 1996	SMNS 58022	Romualdo Fm*. (Brazil, Aptian)	Initially considered a maniraptoran (Martill et al., 1996a), *Irritator* was first referred to Spinosauridae by Kellner (1996).
			*The type specimen was originally described from the Romualdo member of the Santana Formation in Martill et al. (1996a), based on the stratigraphy of (Beurlen, 1971). However the formational status of these members was subsequently elevated and included within the Santana Group, with the

			Romualdo Fm. being Aptian in age (Neumann et al., 1999; Assine et al., 2014; Neumann et al., 2015; Arai et al., 2020).
Angaturama Kellner and Campos 1996 ***A. limai*** Kellner and Campos 1996	USP GP/2T-5	Romualdo Fm. (Brazil, Aptian)	Possibility that *Angaturama* represents the same taxon as *Irritator* mentioned in Kellner (1996). It was considered a subjective junior synonym of *I. challengeri* by Charig et al. (1997), Sues et al. (2002) and Bertin (2010). The holotype may even represent the same individual as *I. challengeri* holotype (Sereno et al., 1998; Sues et al., 2002; Dal Sasso et al., 2005), although comparisons are difficult due to non-overlapping nature of both specimens (Sues et al., 2002; Carrano et al., 2012). Sales et al. (2017b) argued these do overlap, and cannot be attributed to the same individual.
Oxalaia Kellner et al., 2011 ***O. quilombensis*** Kellner et al., 2011	MN 6117-V	Alcântara Fm. (Brazil, Cenomanian)	Considered a subjective junior synonym of *Sp. aegyptiacus* in Smyth et al. (2020). Lacerda et al. (2021) and Isasmendi et al. (2022) disagreed with this interpretation, suggesting it differs from material referred to *Sp. aegyptiacus*.
Ichthyovenator Allain et al., 2012 ***I. laosensis*** Allain et al., 2012	MDS BK10-01–15	"Grès supérieurs" Fm. (Laos, Aptian)	Initially considered a baryonychine (Allain et al., 2012), additional material suggests it is related to spinosaurines (Allain, 2014). Spinosaurine affinities have been recovered in subsequent analyses (Arden et al., 2019; Barker et al., 2021; Sereno et al., 2022).

1.2.2 Temporal and spatial patterns

As alluded to previously, definitive spinosaurid material possesses Laurasian (e.g. Europe, Asia) and Gondwanan (e.g. Africa, South America) signals, coupled with a relatively broad temporal spread spanning the Early–"mid" Cretaceous (Holtz et al., 2004; Bertin, 2010; Hone et al., 2017). Key specimens are known from the Cretaceous fossil records of Europe, Asia, Africa and South America (Stromer, 1915; Charig et al., 1986; Martill et al., 1996a; Sereno et al., 1998; Dal Sasso et al., 2005; Kellner et al., 2011; Allain et al., 2012; Ibrahim et al., 2014; Ibrahim et al., 2020a;

Malafaia et al., 2020b; Barker et al., 2021; Mateus et al., 2022). However, the clade's origins remain vexingly obscure. If their position within Megalosauroidea is correct (i.e. Figure 1.2A), then their sister group relationship with megalosaurids generates a c. 30-40 million year ghost lineage that penetrates into the Jurassic (Hone et al., 2017). Unambiguous spinosaurid remains from this time remain elusive, and identifying the fossils needed to break this long branch may be complicated: more basal spinosaurids would only have a few of the derived traits the currently diagnose the clade (Holtz et al., 2004). Teeth reported from the Jurassic of France (Vullo et al., 2014), Tanzania (Buffetaut, 2012) and Niger (Serrano-Martínez et al., 2015) may represent the earliest records of the clade, although doubts have been cast over their referral (Hendrickx et al., 2019). Spinosaurid persistence into the Late Cretaceous is also based on isolated dental remains referred to the clade (Candeiro et al., 2004; Salgado et al., 2009; Hone et al., 2010a), however, like their Jurassic counterparts, it is likely these pertain to other archosaur clades (Hendrickx et al., 2019; Soto et al., 2020). The lack of definitive post-Cenomanian spinosaurids would suggest the clade went extinct around the Cenomanian-Turonian boundary (Candeiro et al., 2017)

Spinosaurid palaeogeographical patterns have only received cursory attention thus far. Sereno et al. (1998) argued for a cosmopolitan Pangaean distribution for the basal spinosaurid stock, which was subsequently divided by the encroaching Tethys Sea as the supercontinent began to fragment into the northern and southern landmasses of Laurasia and Gondwana. This vicariance-based scenario resulted in the evolution of baryonychines in the north and spinosaurines in the south, with dispersal across land bridges during the Early Cretaceous accounting for the presence of baryonychines (i.e. *Suchomimus*) in Gondwanan deposits.

Buffetaut et al. (2002) suggested an alternative scenario, based on the perceived lack of ante-Albian spinosaurine material at the time: spinosaurines did evolve in Gondwana, perhaps from a baryonychine-like ancestral form, but not until the Albian. The proposed baryonychine-like ancestor may have dispersed to southern continents from Laurasia during the Early Cretaceous, or perhaps had a Pangaean distribution that would negate the need for Sereno et al.'s (1998) trans-Tethyan dispersal episode to account for the presence of the Nigerien *Suchomimus*. Buffetaut et al. (2002) also suggested a potential faunal replacement event between African baryonychines and spinosaurines around the Aptian–Albian boundary. Nevertheless, the eventual discovery of European spinosaurines that predate the Albian has since complicated these hypotheses (Malafaia et al., 2020a; Malafaia et al., 2020b). Elsewhere, Milner (2003) considered a Laurasian origin for spinosaurids as a whole based on the European origin of the oldest finds. Taken together, spinosaurid spatiotemporal patterns lack a consensus and remain unclear.

1.2.3 Spinosaurid palaeoecology

Convincing evidence supports the increased aquatic affinities relative to "typical" non-avian theropods and a (partially) piscivorous diet in spinosaurids, which may have exploited resources differently to coeval terrestrial and aquatic carnivores (Charig et al., 1997; Holtz et al., 2004; Hone et al., 2017; Hone et al., 2021). Taquet (1984) were the first to suggest piscivorous habits in spinosaurids, and their highly apomorphic cranial characters were the focus of discussions relating to specialisations to a semi-aquatic way of life (Paul, 1988; Charig et al., 1997; Holtz, 1998;2002; Holtz et al., 2004); known spinosaurid postcrania of the time (e.g. *Baryonyx*, *Suchomimus*) possessed grossly similar anatomies to those of other large-bodied theropods (e.g. bipediality, forelimbs substantially shorter than hindlimbs etc.), which suggested aquatic specialisations did not extend beyond the skull (Holtz, 1998). Potential postcranial adaptations primarily deal with the unusual skeletal remains of certain derived spinosaurines – most notably the proposed *Spinosaurus* neotype specimen FSAC KK11888. Of note, this latter specimen possesses dense long bones, unusually short hindlimbs and a dorsoventrally deep caudal series that was argued to aid underwater locomotion and associated predatory behaviour (Ibrahim et al., 2014; Ibrahim et al., 2020a; Fabbri et al., 2022b). Several aspects of this interpretation and reconstruction have been met with criticism, however, and it does not seem well adapted for this form of lifestyle (Hone et al., 2017; Henderson, 2018; Hone et al., 2019; Hone et al., 2021; Sereno et al., 2022).

Nevertheless, direct evidence for piscivory includes acid etched fish scales (of the genus *Scheenstia* (formerly *Lepidotes*) (Lopez-Arbarello, 2012) in the rib cage of the *Baryonyx* type specimen (Charig et al., 1997). Geochemical analyses support the dietary intake of fish and extended stays in water relative to other theropods (Amiot et al., 2009; Amiot et al., 2010a; Amiot et al., 2010b; Hassler et al., 2018). Conidont (cone-shaped) dentition and fluted crowns (i.e. enamel bearing apicobasal ridges and grooves) may help pierce and grip slippery prey, thus facilitating piscivory (Hendrickx et al., 2019). Indeed, fluted enamel in particular appears to have convergently evolved in multiple aquatically feeding amniote lineages (McCurry et al., 2019). Morphological cranial convergences with fish-eating crocodilians (Holtz, 1998; Rayfield et al., 2007) and pike conger eels (Muraenesocidae) (Vullo et al., 2016) have also been noted. Functional convergence with *Gavialis*, a highly piscivorous crocodilian, has also been previously posited via Finite Element analyses (FEA) (Rayfield et al., 2007). Beam theory argued for the capture of small prey at the tip of the snout (Therrien et al., 2005), whilst representatives of the clade have been considered to be weak or fast biters – an adaptation useful for piscivory (Sakamoto, 2010;2022). However, evidence of small dinosaurs and pterosaurs as spinosaurid food items is known (Charig et al., 1997; Buffetaut et al., 2004), and the previously suggested convergence between

spinosaurid and crocodylian rostra may have been overstated, with spinosaurid diets perhaps determined by individual size and included a wider range of prey (Cuff et al., 2013).

Spinosaurid remains are also typically found in deposits with a degree of aquatic input (e.g. fluvial, lagoonal or palustrine depositional environments) (Bertin, 2010). Several palaeoenvironmental studies have also found correlations between spinosaurid fossils and certain habitats. In southern Tunisia, spinosaurid dental specimens are well represented in coastal or estuarine deposits relative to other theropods (Fanti et al., 2014). More globally, spinosaurids were found to be positively associated with coastal environments relative to other large theropods, but also showed some inland habitat use in a manner similar to the latter (Sales et al., 2016). Indeed, material referred to the purportedly highly-aquatic *Spinosaurus* are known from inland localities, suggesting this predator, like other spinosaurids, is best interpreted as a semi-aquatic bipedal ambush piscivore (Hone et al., 2021; Sereno et al., 2022). Some spinosaurid specimens are also known from deposits lacking permanent water bodies (Ruiz-Omeñaca et al., 2005; Alonso et al., 2016) or in possessing more terrestrial geochemical signals (Amiot et al., 2010a; Amiot et al., 2010b; Hone et al., 2021), suggesting an ability to exploit non-aquatic environments and food sources. Spinosaurids were thus able to access food source beyond the reach of other contemporaneous theropods, whilst retaining increased terrestrial mobility to move between food patches relative to contemporaneous crocodyliforms (Holtz et al., 2004; Hone et al., 2017).

1.3 British spinosaurids

1.3.1 Historical perspectives

Spinosaurids have had an underappreciated place in the history of dinosaur discovery (Buffetaut, 2010). Amongst the first dinosaur remains to be found, described and illustrated were spinosaurid teeth from the Hastings Group of Sussex (UK), collected sometime during the 1820s (Buffetaut, 2010). Of course, the concept of “dinosaurs”, let alone “spinosaurids”, was unknown to Victorian scientists; Richard Owen didn’t erect the Dinosauria until 1842 (Owen, 1842), whilst Spinosauridae was first coined by Ernst Stromer in 1915 (Stromer, 1915). These teeth were originally considered to be crocodilian in nature and given the binomial name “*Crocodilus cultridens*” by Richard Owen’s part ii of his *Odontography*, published in 1841, where he also referred to them by the subgenus “*Suchosaurus”* (Owen, 1840–1845), a misattribution that would remain pervasive for nearly two centuries – one of the longest-lasting cases of palaeontological and taxonomic misinterpretation Buffetaut (2010). “*Suchosaurus cultridens*” is now a *nomen dubium* (see Table 1.1), and specimens referred to this taxon are typically considered Baryonychinae *incertae sedis* (Mateus et al., 2011; Carrano et al., 2012).

It wasn't until the late 20th Century that British spinosaurids benefited from the discovery of more complete specimens following the description and analysis of the *Baryonyx walkeri* type specimen (NHMUK VP R9951) (Charig et al., 1986). This individual represents one of the best-known spinosaurids worldwide, and its discovery in 1983 proved to be integral to the renewed understanding of the Spinosauridae more generally (Naish et al., 2007). However, it must be noted the original diagnosis for this taxon is now largely obsolescent, *sensu* Wilson et al. (2003), following the subsequent discovery of other spinosaurid material worldwide. Attempts to re-diagnose the taxon have appeared in various works (Sereno et al., 1998; Carrano et al., 2012; Hone et al., 2017), but its potentially immature ontogenetic status and lack of thorough descriptive works for key spinosaurid taxa (e.g. *Suchomimus*) are hindering comparisons and diagnostic refinement.

1.3.2 Geological context of British spinosaurids

Notwithstanding the exceptional *B. walkeri* type specimen, the fossil record of spinosaurids in the UK is sparse and fragmentary, although isolated teeth are somewhat more common relative to other theropod clades (Fowler, 2007). Previously documented finds restricted to the Lower Cretaceous sediments of southern England (specifically, the Wealden Supergroup; see 1.5). The 65% complete skeleton of the *B. walkeri* type specimen hails from the Upper Weald Clay Formation (Barremian) of Surrey (Charig et al., 1986; Charig et al., 1997; Milner, 2003). Its discovery precipitated the referral of various isolated Wealden Supergroup elements to this taxon (Charig et al., 1997; Turmine-Juhel et al., 2019). Teeth referred to the *nomen dubium* "*Suchosaurus cultridens*", from the Valanginian Grinstead Clay Formation of West Sussex (Salisbury et al., 2011), a unit considered to be a member of the Tunbridge Wells Sands Formation in some works (Hopson et al., 2008), have also been attributed to *Baryonyx* (Milner, 2003; Buffetaut, 2010). However, as mentioned above, most recent works favour an indeterminate baryonychine position for the latter material (Mateus et al., 2011; Naish, 2011; Salisbury et al., 2011).

Wealden Supergroup spinosaurid remains have also been reported from the Isle of Wight, specifically from the Barremian Wessex Formation. Published material had, until recently (see Chapter 2), consisted only of isolated teeth (Martill et al., 1996b; Naish et al., 2001) and the single dorsal vertebra IWCMS 2012.563 (Hutt et al., 2004). Due to the temporal overlap of the Upper Weald Clay and Wessex Formations, with both recovered as Barremian in aged (Batten, 2011), these finds were previously assumed to belong to *Baryonyx* or a close relative; indeed, the teeth and vertebra have been referred to cf. *Baryonyx*/*Baryonyx* sp. and *Baryonyx* cf. *walkeri* respectively (Naish et al., 2001; Naish et al., 2007; Naish, 2011). Attention has been drawn to

differences in enamel ornamentation that exist between these isolated teeth and the teeth of the *B. walkeri* holotype, leading to suggestions that they might represent an additional baryonychine taxon (Naish et al., 2001; Naish et al., 2007; Naish, 2011). However, variation in spinosaurid crown ornamentation has uncertain taxonomic value within Spinosauridae (Ruiz-Omeñaca, 2003) and may be influenced by both tooth position and ontogeny (Fowler, 2007; Hendrickx et al., 2016).

1.4 Thesis reasoning, importance and research goals

In Britain, enthusiastic fossil collecting efforts remain pervasive, and have contributed to the recent discovery of several new theropod specimens from the Early Cretaceous of the Isle of Wight. Whilst some are from historically dinosaur-rich localities, others are from deposits in which dinosaurs (and particularly theropod) remains are notably rare, and thus contribute greatly to the understanding of the fauna from these poorly known time intervals. This thesis broadly aims to examine the systematics and phylogenetics of this new material – to which taxa do these individuals belong to, and how do they relate to others?

Amongst these finds is new spinosaurid material, which greatly supplements the generally sparse fossil record of the clade. These new spinosaurid specimens include a well-preserved braincase, which also allows for the reconstruction and description of the brain and sensory systems of some of the earliest spinosaurid representatives known from neurocranial material. This is of palaeoecological and palaeoethological importance, as the neuroanatomy of baryonychine spinosaurids has yet to be studied – what does the preserved morphology reveal about baryonychine senses and potential behaviour, and do these systems exhibit adaptations towards a semi-aquatic or piscivorous ecology?

The relatively recent rediscovery of spinosaurid teeth amongst historical collections also allows the examination of previous assumptions regarding British spinosaurid diversity. Quantitative and qualitative methods will be used in order to assess whether the common referral of isolated spinosaurid material to the British taxon *Baryonyx* is warranted.

1.5 General geology of the Lower Cretaceous of southern Britain

This thesis examines new theropod material recovered from Lower Cretaceous strata of southern England and the Isle of Wight. The broad geological context of these finds is briefly described below, with further details provided in the respective chapters. Deposition during this time in the region can be summarised as follows (Figure 1.3): sediments laid down in brief, restricted shallow marine, lagoonal and variably saline freshwater environments (the “Purbeck” facies) were followed by a temporally extensive period of non-marine deposition (The “Wealden” facies) that

culminated in a marine transgression (the Lower Greensand and Selbourne Groups; the latter group, however, is not the focus of this thesis and shan't be discussed further) (Hopson et al., 2008).

1.5.1 The Purbeck Group

Purbeck Group is principally composed of lagoonal and lacustrine carbonates and muds that overlie the marine carbonates of the Portland Group (Jurassic: Tithonian) (Cope, 2006;2007), demonstrating a gradual palaeoenvironmental change towards terrestrial deposition of the Wealden Supergroup (see section 1.5.2) following the marine regression during the latest Jurassic and earliest Cretaceous (Hopson et al., 2015). Formerly split into three "Upper", "Middle" and "Lower" divisions, more recent lithographic schemes follow Casey (1963) and Townson (1975) in describing the older Lulworth Formation and younger Durlston Formation (Hopson et al., 2008), each of which contain several members. It outcrops extensively in Dorset (Westhead et al., 1996; Coram et al., 2021), and as inliers in Wiltshire (Andrews et al., 1894) and in East Sussex (Howitt, 1964). The majority of the Purbeck Group is Berriasian in age, with only a few basal strata deposited during the Jurassic (Tithonian) (Rawson, 2006); the location of the Jurassic-Cretaceous boundary has been debated (Rawson, 2006), but various lines of evidence point to its presence in the lower part of the Lulworth Formation (Cope, 2007; Coram et al., 2021). Some works have also suggested that the highest Purbeck Group strata are possibly Valanginian in age (Ogg et al., 1994).

1.5.2 The Wealden Supergroup

Late Berriasian upfaulting of the surrounding massifs caused the replacement of the lacustrine and lagoonal Purbeck environments by fluvial systems that heralded the Wealden regime (Radley et al., 2012c). This succession of mostly non-marine strata was accumulated during the late Berriasian–early Aptian and deposited in two principal sub-basins (Fig. 1A): the larger Weald sub-basin of south-eastern England, and the smaller Wessex (=Vectian) sub-basin of the Isle of Wight and central-southern England (Batten, 2011; Radley et al., 2012a). These depocentres were separated until the Albian times by an elevated region known as the Portsdown (=Portsdown-Fordingbridge) High (Hopson et al., 2008; Batten, 2011). Both sub-basins contain the following major facies: arenaceous formations that include mudstones, siltstones and sandstones deposited in riparian settings and largely indicative of meander- and braidplains; as well as argillaceous formations principally composed of mudstones that were deposited in lakes, channels, coastal lagoons and mudflats (Radley et al., 2012a). The overall lack of marine influence on the succession has made it difficult to date its constituting formations (Batten, 2011); the chronostratigraphy of

the Weald and Wessex sub-basins has largely been informed by ostracod faunicycles, palynomorphs and charophytes (Radley et al., 2012c;d).

1.5.2.1 The Weald sub-basin

The Wealden Supergroup in this depocentre is typically comprised of two major non-marine units called the Hastings and Weald Clay Groups (Batten et al., 2011; Radley et al., 2012c), however some works consider this subdivision informal (Hopson et al., 2008); this thesis follows Batten (2011) in retaining the subdivision. These are argillaceous or arenaceous in nature, with the main source of these sediments the result of downfaulting/erosion or uplift of the more northerly London Massif (Londinia) respectively (Batten, 2011; Radley et al., 2012a;c).

Within the older Hastings Group, the succession is composed (in ascending order) of the Ashdown Formation, Wadhurst Clay Formation and the Tunbridge Wells Sand Formation (Batten, 2011; Batten et al., 2011; Radley et al., 2012c). The latter formation is informally subdivided into "upper" and "lower" units by the Grinstead Clay Member in the central and western parts of the Weald Sub-basin (Hopson et al., 2008; Batten et al., 2011). The oldest strata within the Ashdown Formation are Berriasian in age, with the Berriasian–Valanginian boundary lying within the middle or higher sections of the formation (Radley et al., 2012c). The succession in the Hastings Group denotes a mixture of alluvial, lacustrine and lagoonal deposits (Radley et al., 2012c).

In the Weald Clay Group, the succession is made up by the Weald Clay Formation, which is subdivided into upper and lower parts in some works that approximates the Hauterivian-Barremian boundary (Batten, 2011; Batten et al., 2011; Radley et al., 2012c). The top of the Weald Clay Formation is latest Barremian or early Aptian (Radley et al., 2012c). The strata in this Group are largely composed of sediments from lacustrine and lagoonal settings (Radley et al., 2012c).

1.5.2.2 The Wessex sub-basin

The succession of the Wealden Supergroup in the Wessex Sub-basin, which is dominated by the Wessex Formation (itself one of two units forming the Wealden Group), is mainly exposed on the Isle of Wight, with smaller outcrops in Dorset (Batten, 2011; Sweetman, 2011; Radley et al., 2012d). These overlay the Purbeck Group (Batten, 2011; Radley et al., 2011), which is not exposed on the Isle of Wight (Hopson et al., 2015). The Wealden Group predominantly crops out along the island's southwest coast, with a smaller exposure occurring along the southeast coast. Both of these coastal areas reveal the entirely Barremian and predominately alluvial upper facies of the Wessex Formation (the majority of this formation is in fact concealed), which are overlain by the late Barremian–early Aptian Vectis Formation (Sweetman, 2011; Radley et al., 2012d). Small exposures of the Wessex and Vectis formations are also observed in Dorset (Radley et al., 2012d;

Penn et al., 2020). The Cornubian Massif to the west was a major source of sediments, with some input from the Portsdown High along the sub-basin's northern border (Batten, 2011). The Vectis Formation shows evidence of coastal lagoonal deposition (Stewart et al., 1991; Sweetman, 2011), however its upper portion provides an early glimpse of the return to fully marine conditions seen in the overlying Lower Greensand Group (see 1.5.3 below) (Hopson et al., 2015).

1.5.3 The Lower Greensand Group

The Lower Greensand Group provides the most complete record of Aptian and Lower Albian stages in Britain, and signals the beginning of an extensive period of marine sedimentation that lasted throughout of the rest of Cretaceous (Casey, 1961). More specifically, it represents a return to mainly shallow-marine environments, and includes shallow-marine and estuarine sediments deposited following the major Aptian marine transgression (Insole et al., 1998; Rawson, 2006; Hopson et al., 2015). Laid down in northern and southern basins, the Group crops out in Bedfordshire, Buckinghamshire, Cambridgeshire, Dorset, Hampshire, the Isle of Wight, Kent, Lincolnshire, Norfolk, Oxfordshire, Wiltshire and Yorkshire (Casey, 1961; Hopson et al., 2008; Barrett, 2021). Pertinent to this thesis, the Group in the Wessex sub-basin and on the Isle of Wight is composed of four units (in ascending order): the Atherfield Clay Formation, the Ferruginous Sands Formation, the Sandrock Formation and the Monk's Bay Sandstone Formation (Hopson et al., 2008); each is further subdivided by various members (Hopson et al., 2015). The Lower Greensand Group rests on a disconformity over the Wealden Supergroup deposits (Casey, 1961; Hopson et al., 2008).

1.6 Methods: an overview

Outlined below are brief introductory descriptions of the main methods used in the systematic and morphological interpretation of the studied theropod specimens, with the aim of defining important or common terms and (where applicable) highlight major strengths, weaknesses and other considerations. Supplementary analyses used in this thesis to support the results of these main methods, and methods used to examine specific neurological attributes (e.g. hearing, olfaction) are presented in their respective chapters.

1.6.1 Phylogenetic analyses

The cladistic analyses will be based on two differing optimality criteria: maximum parsimony and Bayesian inference. These tree-searching strategies differ in their approaches towards tree reconstruction: statistical methods such as Bayesian inference require an explicit model of evolution, unlike their non-statistical counterparts (e.g. parsimony) (Goloboff et al., 2005). The

appropriateness of each method is a running source of disagreement (Wright et al., 2014; Sansom et al., 2018; Smith, 2019), however the philosophical and methodological debates surrounding tree-building procedures are far beyond the scope of this thesis. Both will employ morphological data distributed amongst a set of operational taxonomic units (OTUs) focusing on basal tetanuran theropods. Regarding the spinosaurid OTUs specifically, most will be scored from single specimens (i.e. individuals), however the use of hypodigms (a sample of several individuals referred to the same taxon) is unfortunately unavoidable for some OTUs.

1.6.1.1 Maximum parsimony

This character-based approach aims to untangle evolutionary relationships using the minimalist principle of parsimony: the simplest explanations that require the fewest assumptions are to be preferred over more complex ones (cf. "Ockham's razor") (Steel et al., 2000). With maximum parsimony as the optimality criterion, the most parsimonious trees (MPTs) are those explaining the data with the fewest evolutionary changes or "steps" (i.e. the shortest tress recovered) (St. John, 2017).

1.6.1.1.1 Tree searching algorithms

Phylogenetic reconstruction can be computationally intensive, as each additional OTU increases the number of possible solutions (the number of possible topologies grows super-exponentially with the number of taxa) (Lewis, 1998; St. John, 2017). Finding optimal trees is unlikely to have solution in polynomial time (Giribet, 2007). As such, whilst the following cannot guarantee the recovery of an optimal solution (Giribet, 2007), heuristic searches are conducted in order to decreases time spent evaluating nonoptimal trees (notably for the case of large datasets in excess of 20–30 OTUs (Hovenkamp, 2004), were exact or exhaustive methods are effectively impossible) (Lewis, 1998).

TNT's "new technology" (NT) search function combines multiple algorithms, including a modified ratchet (RAT) procedure (Nixon, 1999) as well as tree drifting (DFT), tree fusing (TF) and sectorial searches (SS) (Goloboff, 1999), to efficiently search for shortest trees (Goloboff, 2002; Hovenkamp, 2004; Goloboff et al., 2007; Goloboff et al., 2008). RAT, DFT and SS are algorithms that improve existing trees, whilst TF mixes sets of trees to produce combined trees (Goloboff et al., 2007). Details of the mechanisms behind the algorithms can be found in Goloboff (2002) and Goloboff et al. (2007).

Applying a branch-swapping algorithm, such as tree bisection and reconnection (TBR), on the MPTs recovered in the initial NT search allows the researcher to recover additional topologies with the same or shorter lengths, providing a more complete overview of the number of MPTs.

TBR functions by “cutting” an internal branch of a tree to produce two subtrees, selecting a branch in each in order reconnect and form a new tree (Goloboff, 2002; Yang, 2014). This is repeated for various branch combinations.

Some have nevertheless noted issues with the repeatability of the NT searches due to inherent random effects in the search algorithms (Hovenkamp, 2004). Despite this, TNT remains one of the most commonly used cladistics software for morphological data.

1.6.1.1.2 Clade support

Clade support is calculated in this thesis using Bremer support (decay indices), which evaluates the number of additional steps required to collapse a node relative to the MPT(s) (Bremer, 1988;1994); larger numbers indicate stronger support for a particular clade. Assessing what constitutes “good” support is nevertheless unclear and will differ amongst and within datasets, potentially affecting comparisons (Lee, 2000).

JACKNIFE?? A resampling programe

1.6.1.1.3 Consistency and Retention Indices

The “quality” of the trees, or rather how well the data fits the trees produced by a phylogenetic analysis, can be assessed via goodness of fit metrics such as ensemble consistency and retention indices (CI and RI respectively) (Kitching et al., 1998; Egan, 2006). Ensemble values are a summation of the individual consistency and retention indices (ci and ri respectively) for every character within a dataset, and gives a measure how well the entire dataset performs (Kitching et al., 1998). CI (Kluge et al., 1969) is a direct measure of homoplasy whilst RI (Farris, 1989) is based on levels of synapomorphy within a dataset. These are intended to express the relative amount of homoplasy within a dataset, where values closer to 0 than 1 indicate increased homoplasy; datasets with high values are thus considered superior (Kitching et al., 1998).

The ci for an individual character is calculated with the equation:

$$m/s$$

where m is the minimum amount of change exhibited by a character and s is the sum of the observed number of changes in the character on the tree (Kitching et al., 1998). The CI is the summation of m (=M) and s (=S) within the character suite, resulting in CI = M/S. It should be noted that CI has been found to correlate with number of OTUs and characters, and can be inflated in the presence of autapomorphies and symplesiomorphies in the dataset (Siebert, 1992).

The RI examines the observed degree of homoplasy relative to the maximum possible amount of homoplasy in a dataset (Siebert, 1992). The ri for an individual character is calculated with the equation:

$$(g–s)/(g–m)$$

where *s* and *m* are the same as for the ci, and *g* represents the most number of steps a character can have on any cladograms (Kitching et al., 1998). The RI is calculated using the summed values of *s*, *m* and *g*, such the RI = (*G*–*S*)/(*G*–*M*). Unlike CI, RI is insensitive to autapomorphies and symplesiomorphies as these admit no potential for synapomorphy, which therefore do not inflate RI values (Siebert, 1992).

1.6.1.1.4 Consensus trees

When multiple MPTs are recovered, a consensus tree can be generated that is representative of this collection of results (Bryant, 2003). The strict consensus only shows topologies that are shared by all trees in the set, collapsing those that are not into polytomies. As mentioned above, so-called "rogue/wildcard" OTUs can drastically reduce the resolution of the strict consensus tree and the support of clades with in it (Deepak et al., 2012; Goloboff et al., 2015). A reduced consensus approach can help identify and "prune" these problematic OTUs from the trees in order to improve consensus tree resolution (Deepak et al., 2012; Goloboff et al., 2015). This differs from eliminating OTUs from the matrix completely, as rogue OTUs possess character information that must be considered and their outright removal may affect the relationships between other OTUs (Goloboff et al., 2015).

1.6.1.1.5 Constrained searches

Constrained searches are useful ways of exploring phylogenetic hypotheses by decreasing the number of nodes to be swapped without decreasing the number of taxa/OTUs (as larger samples increase tree accuracy) (Giribet, 2007). They can also help deal with issues of rampant homoplasy in certain datasets by forcing the analysis to find the correct assumed topology (Hendrickx et al., 2020b).

The Templeton test (Templeton, 1983) can be used to calculate the significance of these constrained (cf. "alternative") topologies relative to the MPT(s). Such assessments of clade significance are useful tools for evaluating tree robustness (Lee, 2000); insignificant results indicate that the constrained topologies are not significantly worse explanations of the data.

1.6.1.1.6 Software employed

The freely available cladistics software TNT (Tree searching using New Technologies) (Goloboff et al., 2008) is employed for the parsimony analyses. Outperforming other cladistics software, it is comfortable with large datasets, recovering results rapidly and efficiently (Hovenkamp, 2004; Giribet, 2005) with a number of available options with which to analyse morphological data (Goloboff et al., 2016).

1.6.1.2 Bayesian Inference

Bayesian inference in phylogenetics is a model-based method that allows users to incorporate prior information into parameter values used within the model, and is a powerful tool in addressing questions in evolutionary biology (Huelsenbeck et al., 2001; Wright, 2019; Warnock et al., 2021). Unlike parsimony, which looks for the shortest evolutionary path, Bayesian inference accounts for all possible paths of character evolution (Huelsenbeck et al., 2001; Wright, 2019).

1.6.1.2.1 Fundamentals of phylogenetic Bayesian inference

Bayesian inference can be thought of as having three core components: a likelihood model (which describes the processes creating the data), "priors" (statistical distributions denoting prior beliefs/knowledge about the data-generating processes), and the posterior probability (the outcome of the analysis – a set of plausible solutions which denotes the combined understanding based on the two previous components) (Wright, 2019; Warnock et al., 2021). Taken together, the posterior probability (also denoted Pr $[Tree|Data]$) is derived from Bayes' theorem, where ϑ denotes the parameters of a model (Alfaro et al., 2006):

$$\Pr\left[Tree|Data\right] = \frac{\int \Pr[Data|Tree,\theta] \times \Pr\left[Tree,\theta\right] d\theta}{\Pr\left[Data\right]}$$

The posterior probability denotes whether the probability of a tree is correct given the data (including the model and assumptions imposed) (Goloboff et al., 2005; Nascimento et al., 2017). It cannot be calculated analytically (Alfaro et al., 2006), however, and is instead approximated using an algorithm known as Markov Chain Monte Carlo sampling (MCMC) (Alfaro et al., 2006; Warnock et al., 2021). The MCMC produces a "posterior sample", consisting of a log of trees, branch lengths and parameters examined during the phylogenetic analysis, upon which a summary tree can then be built (see 1.6.1.2.3) (Wright, 2019).

1.6.1.2.2 Time-calibrated Bayesian phylogenies

Time calibration allows dating of the inferred phylogenies, determination of the evolutionary rates of the sampled OTUs, and patterns of historical biogeography (Heath et al., 2014; Warnock

et al., 2021). Time-calibrated Bayesian phylogenies typically assume a tripartite model of evolution, which can be separated into component models (briefly described below): the substitution model (=site model, describing the accumulation of character change over time), the clock model (describing the rate of character change distributed throughout a tree) and the tree model (=tree prior, describing the distribution of speciation events throughout a tree) (Warnock et al., 2021). The component models employed in this thesis are described below. The results of the Bayesian analysis are summarised via a maximum clade credibility tree (MCCT).

The substitution model describes the process of character evolution via the probability of character state changes (Warnock et al., 2021). Bayesian phylogenetics based on morphological data have previously employed fewer sets of models relative to molecular counterparts due to difficulties in describing character state transitions over evolutionary time (Warnock et al., 2021). The Markov-k (Mk) model (Lewis, 2001) is employed in this thesis, as is common for morphological datasets (Warnock et al., 2021). Based on Jukes-Cantor model for molecular sequence evolution (Jukes et al., 1969), the Mk model for morphological evolution assumes exchangeabilities (i.e. expected rate of a given change between two character states) are equal amongst all character states, and that the latter all have equal equilibrium frequencies (i.e. the observed frequency of each state in a dataset is equal, assuming an infinite evolutionary process) (Wright, 2019; Warnock et al., 2021). Summarily, the basic MK model assumes all character state changes are equally likely and occur at the same rate (Keating et al., 2020).

The clock model describes the variation in substitution rate (if any) across a tree (Warnock et al., 2021). A relaxed clock model is employed herein. Unlike strict clock models, which assumes constant substitution rates across both time and the tree, the relaxed clock model allows for variation (Dos Reis et al., 2016), as is seen in most clades (Warnock et al., 2021). Further, relaxed-clock models appear to fit real data better compared to strict molecular clocks (Drummond et al., 2006; Drummond et al., 2010).

The tree model denotes the speciation, extinction and sampling processes that generated the tree, and is the only component in the tripartite model to employ age information, helping infer plausible age ranges for recovered nodes (Warnock et al., 2021). Birth-death process models are commonly used in macroevolutionary studies, allowing researchers to quantify speciation (birth) and extinction (death) rates of lineages (Warnock et al., 2021). A subset of models, collectively known as Fossilised Birth-Death (FBD) processes (Stadler, 2010; Heath et al., 2014), allow for more rigorous integration of fossil taxa into phylogenetic dating analyses (Wright et al., 2022). Composed of four main parameters, the FBD model incorporates data regarding the speciation and extinction rates mentioned above as well as two metrics that describe the sampling rates of

fossils and extant lineages. The FBD's sampling model provides further inferences regarding tree topology, using fossil ages to assign increased likelihoods to certain trees and thus increasing the probability that the recovered trees agree with the historical record of the fossil sample (Wright et al., 2022).

More specifically, a variant of the FBD model, the Sampled Ancestor Fossilised Birth-Death Skyline Model (SAFBS) (Gavryushkina et al., 2014) is used as the tree model in this work, which allows the possibility of direct ancestors within the sample. Initially developed for molecular datasets, the model was soon extended to include morphological characters as well (Gavryushkina et al., 2017). Ignoring sampled ancestors increases diversification rates, and may lead to biases in nodal age inference and estimates of fossil diversity (Gavryushkina et al., 2014; Cau, 2017; Gavryushkina et al., 2017).

1.6.1.2.3 Maximum Clade Credibility Trees

Several consensus tree construction methods can be used to summarise the trees obtained by MCMC sampling of the posterior distribution (Heled et al., 2013; O'Reilly et al., 2018; Warnock et al., 2021). The maximum clade credibility tree (MCCT) is one such method, and one that has become popular in tip calibrated analyses of morphological data (O'Reilly et al., 2018). This method picks out the single tree in the posterior sample with the largest sum of posterior clade probabilities (O'Reilly et al., 2018). The posterior probability value at a node of a consensus tree is the proportion of trees in the posterior sample that have the node in question (Alfaro et al., 2006).

1.6.1.2.4 Software employed

The Bayesian analysis conducted in this thesis uses the software BEAST (Bayesian Evolutionary Analysis Sampling Trees) (Suchard et al., 2018). BEAUti (Bayesian Evolutionary Analysis Utility) was used to generate BEAST XML files, whilst Tracer (Rambaut et al., 2018) was employed to visualise the output generated by the Markov Chain Monte Carlo (MCMC), an algorithm that approximates the posterior probability (Alfaro et al., 2006; Warnock et al., 2021).

1.6.2 CT Scanning

X-ray Computed tomography (CT) scanning is widely considered to have revolutionised the study of fossil material, being part of a computational era where fossils and their internal structures can be non-destructively visualised as digital or virtual representations in three dimensions (Carlson et al., 2003; Witmer et al., 2008; Abel et al., 2012; Cunningham et al., 2014; Sutton et al., 2016). CT-based methods were first applied to vertebrate palaeontology in the early 1980's (Tate et al.,

1982; Conroy et al., 1984), with *Archaeopteryx* (Haubitz et al., 1988) and an unnamed dinosaur egg (Hirsch et al., 1989) among the first dinosaur specimens examined.

Palaeoneurology – the study of brains and nervous systems in extinct taxa (notably vertebrates) – is one of the major beneficiaries of this "CT revolution". The discipline, founded almost single-handedly by vertebrate palaeontologist Tilly Edinger (1897–1967) in the 1920s, was built on earlier works that sought to describe and interpret endocranial morphology and examine trends in brain evolution through time (Buchholtz et al., 1999; Walsh et al., 2011). Naturally, the study of brains and sensory systems of fossil taxa at the time required the use of destructive methods such as sectioning, serial grinding and latex casting, with rare, natural stony casts of the endocranial cavity (termed "steinkerns") or fortuitous breaks providing additional glimpses into the endocrania of fossil forms (Witmer et al., 2008). Given the unpalatable or simply unfeasible nature of most of these methods, the introduction of CT-based approaches not only preserved the integrity of fossil specimens of interest, but also increased the number of extinct specimens available for palaeoneurological study (Witmer et al., 2008; Walsh et al., 2011). Further, they produce a digital record that can be distributed and accessed widely (Racicot, 2017).

In terms of dinosaur palaeoneurology, Hulke (1871) was the first to interpret the internal surfaces and cranial nerves of a partial "*Iguanodon*" braincase from the Isle of Wight (Bucholtz, 2012), a find that tangentially cements the importance of the Isle's fossil record and role in the history of dinosaur research. Over a century later, the palaeoneurology of *Allosaurus* would be studied using CT methods (Rogers, 1998), and virtual endocasts (digital representations of enclosed cranial cavities, such as the brain cavity or inner ear; henceforth referred to as "endocasts") are now known for many species belonging to the five major dinosaur clades (King, 2021). Whilst research on endocasts remains largely descriptive, especially for works dealing with sauropsids (Walsh et al., 2011), their reconstruction has nevertheless provided information on comparative morphology, encephalisation and correlative changes between neurological structures and their associated functions (Balanoff et al., 2020).

1.6.2.1 Scanning

The methods and protocols involved in CT scanning in palaeontological contexts have been recently overviewed by Racicot (2017). At its core, CT produces a 3D-representation of an object (volume) computed from a series of X-ray projections taken at different angles (Racicot, 2017). Scanners thus consist of an X-ray source, a detector, and (in the case of machines built for inanimate objects) a rotating stage (Sutton, 2008). The advent of high-resolution micro-CT (µCT) has been successfully used on numerous palaeontological specimens. These often possess smaller focal spot sizes (which determine the spatial resolution of the CT system), and higher voltages (kV,

which help penetrate denser materials) and currents (mA, which affect the clarity of the scan images) to generate better resolution scans of dense objects such as fossils relative to many medical CT scanners (Cunningham et al., 2014; Racicot, 2017; Pérez-Ramos et al., 2020).

1.6.2.2 Reconstruction and segmentation

The output of a scan generates a series of stacked projections (or "sinogram"), made up on lines containing detector readings for each individual projection, which can be converted into a volume of 2D slices in a process known as reconstruction (Racicot, 2017). Segmentation involves the automatic or manual delimitation of regions of interest based on greyscale thresholds from the CT volume (Lautenschlager, 2016; Racicot, 2017). Pertinent to this thesis, a guide to the segmentation of endocasts was published by (Balanoff et al., 2016a).

1.6.2.3 Limitations of micro-CT

Whilst micro-CT setups are becoming staple laboratory equipment in modern research institutions (Cunningham et al., 2014), several limitations can affect scan outcomes or interpretation, some of which are briefly detailed here. Sample size may limit resolution (Racicot, 2017), with larger samples limited to lower resolutions. X-ray penetration may be insufficient for particularly dense specimens/regions of interest, and modification of the scan parameters to counter this problem may lead to downstream visualisation issues (Walsh et al., 2011). Further, scanned materials need to contain different X-ray attenuation properties to visualise fine details (Racicot, 2017), and techniques such as micro-CT may have difficulties imaging chemically homogenous samples that lack substantial X-ray attenuation contrast (Cunningham et al., 2014). Manual segmentation, especially in poor contrast scans, is qualitative and down to operator interpretation, introducing issues of replicability (Walsh et al., 2011), and computational issues may also arise when working on large datasets in the absence of powerful hardware (Racicot, 2017). Artefacts within the scanned specimen, which in fossil specimens may be due to the inclusion of dense minerals for example, may also cloud or confuse the interpretation of CT slices (Racicot, 2017; Orhan et al., 2020). Additional limitations concern the longevity of the data collected (i.e. file type, data corruption), amount of cloud data storage, and the ability to disseminate datasets (Racicot, 2017).

1.7 Figures

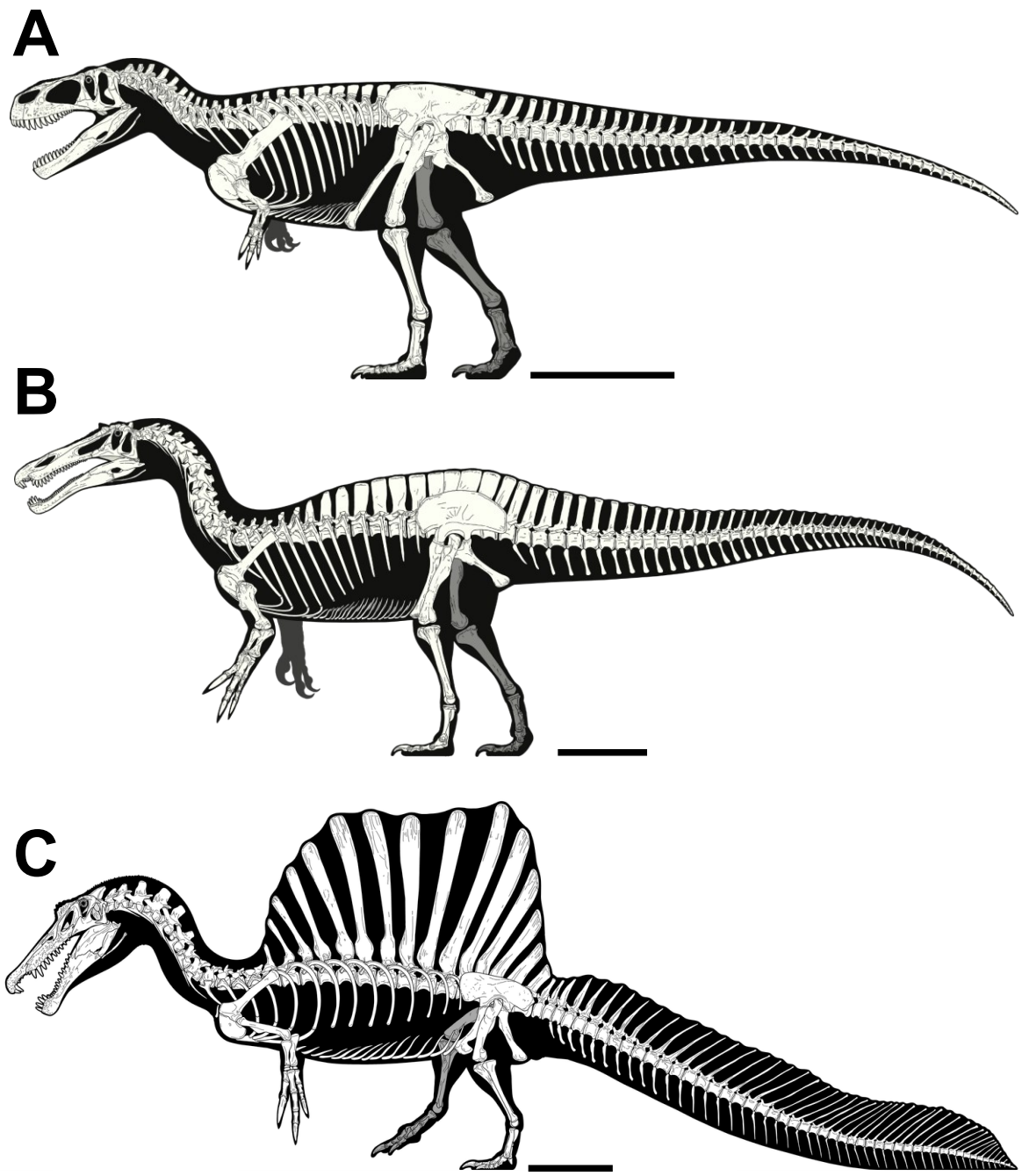

Figure 1.1 The spinosaurid bauplan. A "typical" theropod *Megalosaurus* (A) compared to the baryonychine spinosaurid *Suchomimus* (B) and the spinosaurine spinosaurid *Spinosaurus* (C). Note these reconstructions include holotype and referred specimens; in the case of *Spinosaurus*, this also includes the proposed neotype specimen FSAC KK11888 (see section 1.2.1.2 for further information regarding the taxonomic history of this genus). Scale bar: 1m. Credit: Dan Folkes (used with kind permission).

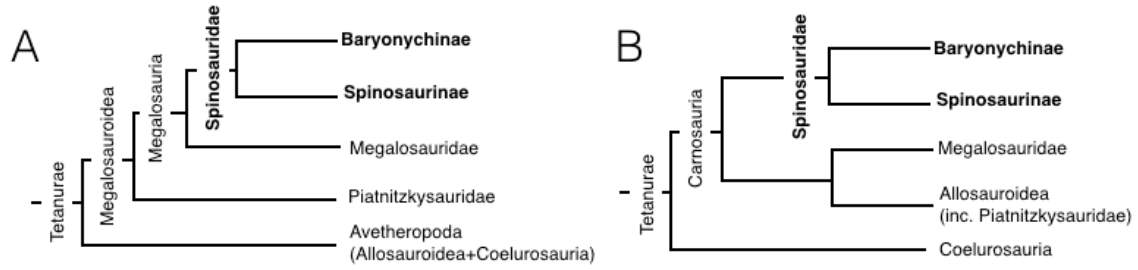

Figure 1.2 Recent competing hypotheses for the relationships of Spinosauridae within Tetanurae. Schematic cladograms based on the analyses of A) Carrano et al. (2012) and B) Rauhut et al. (2019b). Note the dissolution of the clade Avetheropoda in the latter topology.

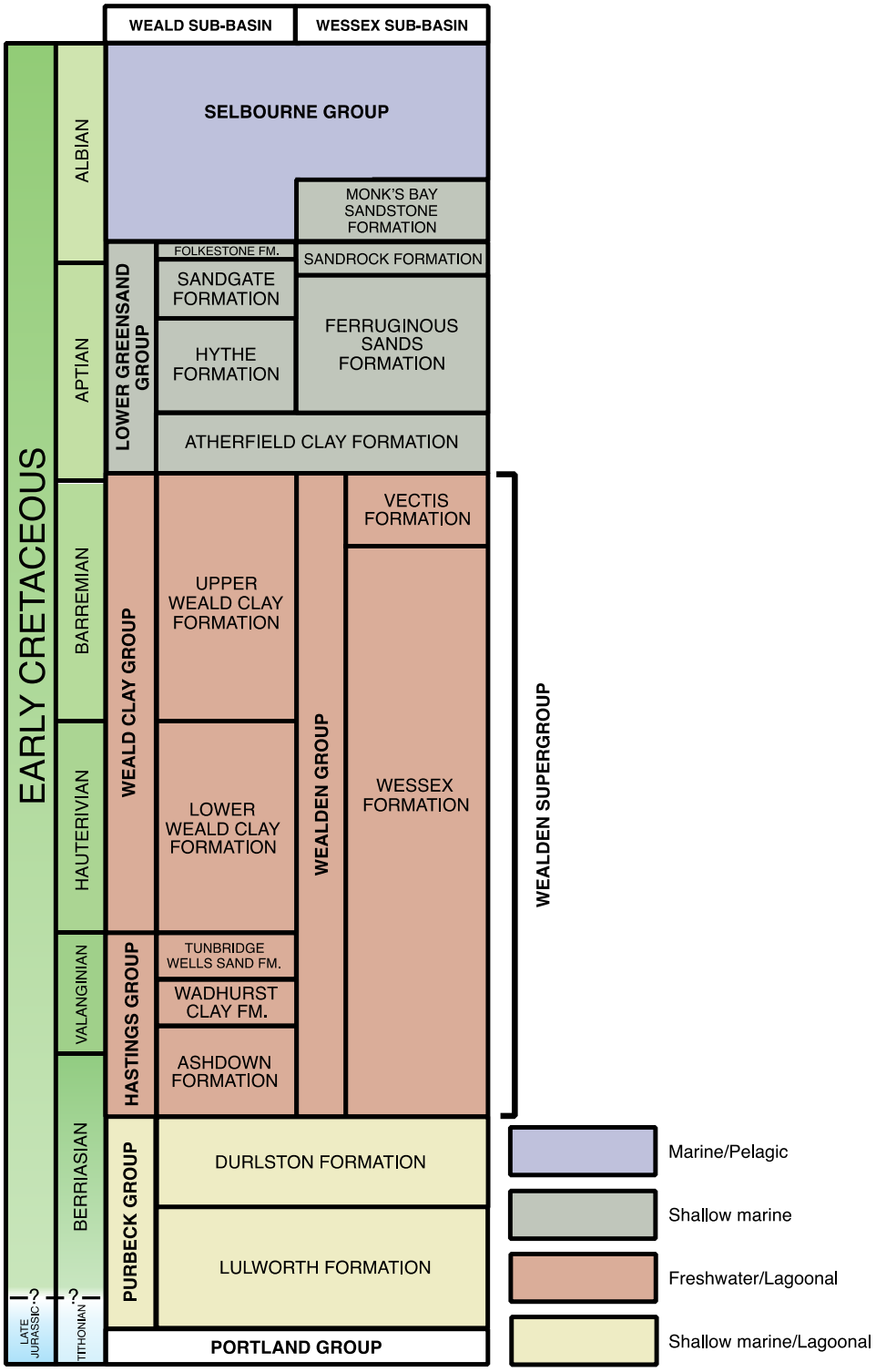

Figure 1.3 Schematic overview of the Lower Cretaceous succession of southern England and its major depositional environments. Based on Hopson et al. (2008) and Batten (2011). Note that the nomenclature within the succession, as well as that of the basins in which they were deposited, can be confusing (Batten, 2011), and interested readers may which to consult Hopson et al. (2008) for further comments or alternative nomenclature.

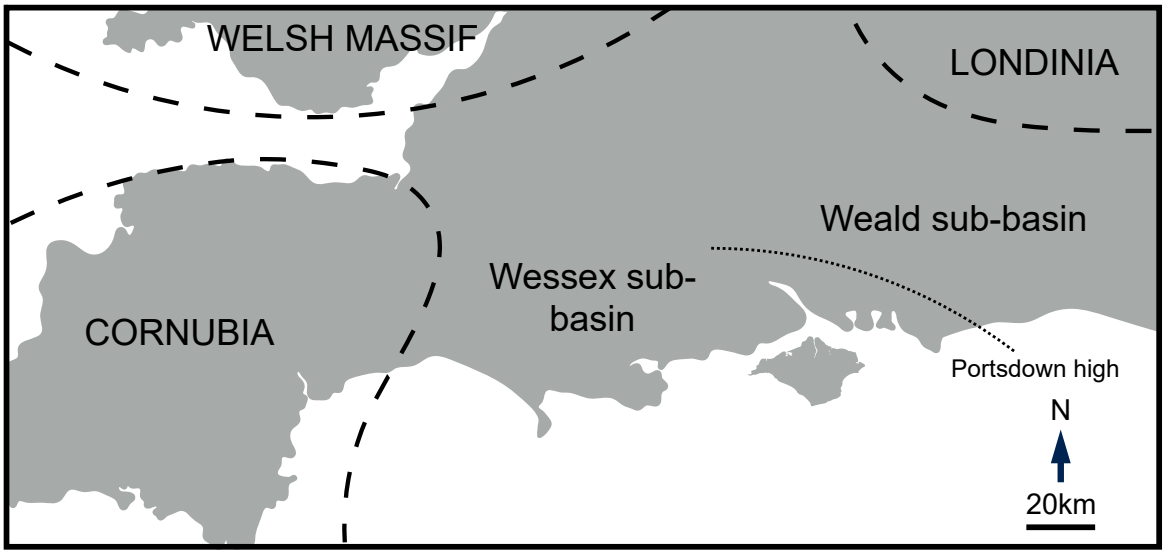

Figure 1.4 Schematic overview of the Weald and Wessex sub-basins of southern England. The upland areas surrounding these depocentres are also approximately delimited (dashed lines). Based on Hopson et al. (2008), Batten (2011) and Penn et al. (2020)

Chapter 2 New spinosaurids from the Wessex Formation (Early Cretaceous, UK) and the European Origins of Spinosauridae

2.1 Authorship statement

This chapter is the product of: **Barker, C.T.**, Hone, D.W., Naish, D., Cau, A., Lockwood, J.A., Foster, B., Clarkin, C.E., Schneider, P. and Gostling, N.J., 2021. New spinosaurids from the Wessex Formation (Early Cretaceous, UK) and the European origins of Spinosauridae. *Scientific reports*, *11*(1), pp.1-15.

CTB, DN and NJG conceived the study. BF and JFAL found and donated material from Chilton Chine; BF prepared cranial elements. CTB wrote the first drafts (main text and supplementary information), compiled the supplementary materials and created Figs. 2–5 and 7; AC compiled the character list and scored the OTUs used in the phylogenetic analyses; CTB, AC and DEH edited the scores for the spinosaurid OTUs. AC conducted the phylogenetic analyses, drafted the methods and results sections, and created Figs. 6 and S1 and S2. All authors contributed to the interpretation of the specimens and editing of the manuscript and its supplementary information.

The supplementary information for this chapter can be found in Appendix A and online.

2.2 Abstract

Spinosaurids are among the most distinctive and yet poorly-known of large-bodied theropod dinosaurs, a situation exacerbated by their mostly fragmentary fossil record and competing views regarding their palaeobiology. Here, we report two new Early Cretaceous spinosaurid specimens from the Wessex Formation (Barremian) of the Isle of Wight. Large-scale phylogenetic analyses using parsimony and Bayesian techniques recover the pair in a new clade within Baryonychinae that also includes a hypodigm of the African spinosaurid *Suchomimus*. Both specimens represent distinct and novel taxa, herein named *Ceratosuchops inferodios* gen. et sp. nov. and *Riparovenator milnerae* gen. et sp. nov. A palaeogeographic reconstruction suggests a European origin for Spinosauridae, with at least two dispersal events into Africa. These new finds provide welcome information on poorly sampled areas of spinosaurid anatomy, suggest that sympatry was present and potentially common in baryonychines and spinosaurids as a whole, and contribute to updated palaeobiogeographic reconstructions for the clade.

2.2.1 Keywords

Spinosaurid, Theropod, Wessex Formation, Early Cretaceous, paleobiogeography

2.3 Introduction

Spinosaurids are among the most distinctive, unusual and controversial of theropods; they are characterised by an elongate, laterally compressed rostrum, sub-conical dentition and, in a subset of taxa, a dorsal sail formed by elongate neural spines. Their unusual cranial (and in derived forms, postcranial) morphology is atypical of non-avian theropods, and multiple lines of evidence point to an ability to exploit semi-aquatic niches (Charig et al., 1997; Amiot et al., 2009; Amiot et al., 2010a; Ibrahim et al., 2014; Aureliano et al., 2018; Hassler et al., 2018; McCurry et al., 2019; Ibrahim et al., 2020a). A "generalist" or varied diet may have included a range of terrestrial and aquatic prey (Ruiz-Omeñaca et al., 2005; Bertin, 2010; Hone et al., 2017; Schade et al., 2020) and was potentially influenced by individual size (Cuff et al., 2013) or habitat (Alonso et al., 2016). It has been suggested that spinosaurids became increasingly aquatic during their evolution (Arden et al., 2019) and that highly modified taxa like *Spinosaurus* engaged in specialised underwater pursuit predation (Ibrahim et al., 2014; Ibrahim et al., 2020a). However, the sequence by which semiaquatic adaptations were acquired, and the degree of specialisation to aquatic life in *Spinosaurus* and other spinosaurids, remain debatable and the topic of ongoing research (Barker et al., 2017; Henderson, 2018; Hone et al., 2019; Hone et al., 2021).

The majority of spinosaurid material comes from Early and "mid" Cretaceous strata, although isolated dental remains suggest persistence of the group into the Late Cretaceous (Santonian) (Hone et al., 2010a). Views on how spinosaurids relate to other theropods, and on the relationships within Spinosauridae itself, are controversial. The majority of recent studies find spinosaurids to be nested within Megalosauroidea (Carrano et al., 2012; Evers et al., 2015; Malafaia et al., 2020b), a position requiring an origin during the Early Jurassic at least. An alternative is that they are outside a Megalosauridae + Allosauroidea clade (Rauhut et al., 2019b). Spinosauridae itself is agreed by most to consist of the two clades, Baryonychinae and Spinosaurinae (Sereno et al., 1998; Benson, 2010; Carrano et al., 2012; Arden et al., 2019; Rauhut et al., 2019b), although the number of valid taxa within these clades remains uncertain. Several – typically based on dental or fragmentary material – have been considered *nomina dubia* or subsumed into synonymy by some workers (e.g. Sereno et al., 1998; Smyth et al., 2020). Support for the spinosaurine/baryonychine dichotomy may not, however, be as strong as conventionally supposed (Evers et al., 2015) and baryonychines may be paraphyletic to a monophyletic Spinosaurinae (Sales et al., 2017b).

Discussions of spinosaurid phylogeny have frequently been coupled to evaluations of the clade's biogeographical history, in part because spinosaurines exhibit a strong Gondwanan signal and baryonychines a mostly Laurasian one (though neither clade is restricted to these two regions). However, rigorous attempts to reconstruct the clade's palaeogeographic patterns have yet to be undertaken, largely due to the phylogenetic instability of the spinosaurid in-group. Sereno et al. (1998) proposed an ancestral pan-Pangaean distribution followed by a Laurasian baryonychine and Gondwanan spinosaurine divergence driven by the opening of the Tethys. More recent discoveries (including of the Iberian *Vallibonaventarix*, initially identified as a spinosaurine) provide complications for this model, rendering the biogeographical history of the clade unresolved (Malafaia et al., 2020b).

In the UK, spinosaurid fossils are restricted to the Lower Cretaceous Wealden Supergroup (see "Geological Context" below), a fossiliferous succession of mudstones, sandstones and siltstones well known for its dinosaurs and other vertebrates that is mostly exposed in the English south-east and Isle of Wight (Martill et al., 2001a; Naish, 2011). The partial holotype skeleton (NHMUK PV R9951) of *Baryonyx walkeri* – one of the world's best spinosaurid specimens and the first to reveal the true appearance of members of this group – is from the Upper Weald Clay Formation (Barremian) of Surrey (Charig et al., 1986; Charig et al., 1997). Its discovery precipitated the referral of various isolated Wealden Supergroup elements to this taxon; these include specimens from other Upper Weald Clay locations in Surrey, as well as the upper Berriasian–lower Valanginian Ashdown and Valanginian Wadhurst Clay formations of East Sussex (Charig et al., 1997; Turmine-Juhel et al., 2019). Teeth referred to the *nomen dubium* "*Suchosaurus cultridens*" from the Valanginian Grinstead Clay Formation have also been attributed to *Baryonyx* (Milner, 2003; Buffetaut, 2010), although other work has favoured an indeterminate baryonychine position (Mateus et al., 2011; Naish, 2011; Salisbury et al., 2011).

Wealden Group spinosaurid remains have also been reported from the Isle of Wight, specifically from the Barremian Wessex Formation. Published material has, until now, consisted only of isolated teeth (Martill et al., 1996b; Naish et al., 2001) and the single dorsal vertebra IWCMS 2012.563 (Hutt et al., 2004). Due to the temporal overlap of the Upper Weald Clay and Wessex Formations (both are Barremian; Batten, 2011), these were previously assumed to belong to *Baryonyx* or a close relative; indeed, the teeth and vertebra have been referred to cf. *Baryonyx*/*Baryonyx* sp. and *Baryonyx* cf. *walkeri* respectively (Naish et al., 2001; Naish et al., 2007; Naish, 2011). Attention has been drawn to differences in enamel ornamentation that exist between these isolated teeth and the teeth of the *B. walkeri* holotype, leading to suggestions that they might represent an additional baryonychine taxon (Naish et al., 2001; Naish et al., 2007; Naish, 2011). The presence of multiple spinosaurids based on the presence of several tooth

morphotypes has also been put forward for other palaeoecosystems (e.g. Richter et al., 2013). However, variation in spinosaurid crown ornamentation has uncertain taxonomic value within Spinosauridae (Ruiz-Omeñaca, 2003) and may be influenced by both tooth position and ontogeny (Fowler, 2007; Hendrickx et al., 2016).

The fragmentary and incomplete remains of two new baryonychine spinosaurid specimens were recovered at Chilton Chine on the Isle of Wight's southwest coast and are herein named *Ceratosuchops inferodios* gen. et sp. nov. and *Riparovenator milnerae* gen. et sp. nov. (Figure 2.1 and Figure 2.2). Both include partial skulls, the latter being associated with a series of caudal vertebrae (see Appendix A for allocation of the material recovered and brief osteological descriptions). Surprisingly, both specimens differ from the broadly contemporaneous *B. walkeri* and from each other, and our interpretation demonstrates the presence of multiple spinosaurid taxa within the Wealden Supergroup. In this article, we explore their position within Spinosauridae via a new phylogenetic analysis and use this to re-evaluate spinosaurid palaeobiogeography. Finally, we discuss the possible implications of these new taxa for baryonychine diversity and ecology. A more detailed work on the osteology of the Wealden Group spinosaurids (including the additional spinosaurid elements recovered from Chilton Chine that could not be attributed to either taxon) is in preparation.

2.3.1 Institutional abbreviations

IWCMS: Dinosaur Isle Museum (Isle of Wight County Museum Service), Sandown, UK; ML: Museu de Lourinhã, Lourinhã, Portugal; MNN: Musée National du Niger, Niamey, Republic of Niger; MSNM: Museo di Storia Naturale di Milano; NHMUK: Natural History Museum, London, UK.

2.4 Geological context

The Lower Cretaceous Wealden Supergroup of southern England includes a succession of principally non-marine strata, accumulated between the late Berriasian and early Aptian. These are mainly deposited in two sub-basins: the larger Weald sub-basin of south-eastern England (where the strata are subdivided into the younger Weald Clay Group and older Hastings Group), and the smaller Wessex sub-basin of the Isle of Wight and central-southern England (composed of the younger Wealden Group and older Purbeck Limestone Group) (Batten, 2011) (Figure 2.2a). The Wealden Group on the Isle of Wight crops out along the southwest coast and less extensively so along the southeast coast (Figure 2.2b), with both areas revealing exposures of the entirely Barremian Wessex Formation and overlying late Barremian–early Aptian Vectis Formation (Sweetman, 2011; Radley et al., 2012d). The Wessex Formation is formed of sandstones and

varicoloured mudstones with interspersed plant debris beds. These sediments are mostly of alluvial origin and were deposited by a perennial, moderately sized, highly sinuous, west-to-east flowing river; some represent lacustrine environments as well (Batten, 2011; Sweetman, 2011; Radley et al., 2012d).

The new spinosaurid material reported here was collected at beach level, between 2013-2017, some of which originated from an exposure of the Wessex Formation located just east of Chilton Chine. The latter is a coastal geological feature situated approximately 1km from Brighstone on the island's southwest coast (Figure 2.2b, c). The strata at Chilton Chine have experienced a substantial rotational slump, and additional, smaller slumps have further complicated the area's stratigraphy. The braincase and caudal series referred to *Riparovenator* were recovered *in situ* and in close association (c. 10m), likely from an unnamed layer between the Brighstone and Chilton Chine Sandstones (Figure 2.2d); additional elements were recovered as isolated surface finds (see also Appendix A). The sandstone matrix surrounding this specimen is largely fine-grained but does include small clasts; comparatively little plant debris (usually typical of the plant debris beds) was present during preparation. The premaxillae, braincase and postorbital referred to *Ceratosuchops* were recovered from isolated sandstone blocks found on the foreshore, and as such their precise original stratigraphic location remains uncertain.

2.5 Methods

2.5.1 Phylogenetic analysis

Each of the new Wessex Formation specimens was entered into a phylogenetic dataset based on a modified version of the Cau (2018) analysis implemented by Dal Sasso et al. (2018), focusing on non-coelurosaurian tetanurans (see Appendix A for further details). The Triassic saurischian *Eoraptor* was used as a root for the assessment of character polarity. The dataset was analysed using maximum parsimony as the tree search strategy using TNT version 1.5 (Goloboff et al., 2016). The search strategy involved 100 "New Technology" search analyses using the default setting, followed by a series of "Traditional Search" analyses exploring the tree islands found during the first round. Nodal support was calculated saving all trees up to 10 steps longer than the shortest topologies found and using the "Bremer Supports" function of TNT. In an attempt to improve tree resolution, rogue spinosaurid OTUs (*Irritator*, ML 1190, MSNM V4047 and "*Spinosaurus* B") were identified using the command pcrprune (Goloboff et al., 2015). Alternative relationships not recovered in the shortest found topologies were then enforced in TNT, and the statistical significance of their step difference from the most parsimonious trees found was calculated using the Templeton test (Schmidt-Lebuhn, 2016) implemented in TNT (see 0).

2.5.2 Bayesian Inference analysis

The phylogenetic dataset was analysed integrating the morphological data matrices with absolute ages of the least inclusive stratigraphic range including each terminal unit. The Sampled Ancestor Fossilized Birth Death Skyline Model (SAFBD; Gavryushkina et al., 2014) implemented in BEAST 2.4.4. (Drummond et al., 2012; Bouckaert et al., 2014) was used as the tree model. In our analysis, rate variation across traits was modelled using the multi-gamma parameter (implemented for the analysis of morphological data in BEAST 2). The rate variation across branches was modelled using the relaxed log-normal clock model, with the number of discrete rate categories that approximate the rate distribution set as n-1 (with n the number of branches), the mean clock rate using default setting, and not setting to normalize the average rate. Since the character matrix includes autapomorphies of the sampled taxa, the Lewis (2001) model was not conditioned to variable characters only. Stratigraphic information for the taxa was converted to geochronological ages. Stratigraphic data and age constraints for each terminal were obtained from the Paleobiology Database (http://paleobiodb.org/), checked against the International Chronostratigraphic Chart (http://stratigraphy.org/), and included as uniform priors for tip-dating. The extant taxon included (the avian *Meleagris*) calibrates the height for the tip-date setting (the uniform prior setting used for incorporating uncertainty in the age of the fossil taxa requires at least one terminal taxon to have the tip age fixed to a value; see Gavryushkina et al., 2014). The analysis used four replicate runs of 10 million generations, with sampling every 1,000 generations, that were subsequently combined using LogCombiner 1.7.3 (included in the BEAST package) (Drummond et al., 2012; Bouckaert et al., 2014). In the analyses, burnin was set at 20%. Convergence and effective sample sizes of every numerical parameter among the different analyses were identified using Tracer (included in the BEAST package). The root age of the tree model was conservatively set as a uniform prior spanning between the age of the oldest in-group taxa and 252 Mya (near the Permian-Triassic boundary), which consistently pre-dates the diversification of all theropod branches.

We used the MCCT resulting from the Bayesian analysis as a temporally calibrated phylogenetic framework for palaeobiogeographic reconstruction, inferring ancestral geographic placement of nodes using RASP (Reconstruct Ancestral State in Phylogenies) (Yu et al., 2015). The distribution range of the taxa was *a priori* divided into five areas: Asia (A), North America (B), Europe (C), Africa (D), and South America (E). Each terminal taxon was scored for the geographic area character state according to the continent(s) it was recovered in. Biogeographic inferences on the phylogenetic frameworks were obtained by applying the Dispersal-Extinction-Cladogenesis model (DEC) (Ree et al., 2008), with no *a priori* constraints on range and dispersal parameters.

2.6 Results

2.6.1 Systematic palaeontology

DINOSAURIA Owen, 1842

THEROPODA Marsh, 1881

TETANURAE Gauthier, 1986

SPINOSAURIDAE Stromer, 1915

BARYONYCHINAE Charig and Milner, 1986, *sensu* Sereno et al., 1998

CERATOSUCHOPSINI clade nov.

LSID urn:lsid:zoobank.org:act:D2370EE2-B5B3-4921-B2F6-FA5207CE85BF

Definition. The most inclusive branch-based clade containing *Ceratosuchops inferodios* but not *Baryonyx walkeri* and *Spinosaurus aegyptiacus*.

Included taxa: *Ceratosuchops inferodios*; *Riparovenator milnerae*; *Suchomimus tenerensis* Sereno et al., 1998.

Diagnosis: postorbital facet of frontal dorsoventrally thick (height more than 40% of length) and excavated by a deep, longitudinal slot; well-defined and strongly curved anterior margins of supratemporal fossa; occipital surface of the basisphenoid collateral oval scars excavated.

Genus *Ceratosuchops* nov.

LSID urn:lsid:zoobank.org:act:5EB49885-7AF9-45DF-854A-C75A1AED16A1

Etymology: kératos (Greek, κέρας) – “horn”, prominent postorbital boss and rugose orbital brow; soûkhos (Greek, Σοῦχος) – “crocodile”; óps (Greek, ὄψ) – “face”.

Type species: Ceratosuchops inferodios

Diagnosis: as for type and only species.

Ceratosuchops inferodios sp. nov.

LSID. urn:lsid:zoobank.org:act:1957EEF7-F3DD-49FF-BB90-82F53EF8E34A

Etymology: īnfernus (Latin) – underworld, hell; erodiós (Greek, ερωδιός) – heron, in reference to its presumed heron-like ecology.

Holotype. Associated premaxillary bodies (IWCMS 2014.95.5) and posterior premaxillary fragment (IWCMS 2021.30); a near complete but disarticulated braincase (IWCMS 2014.95.1–3) (Figure 2.3).

Referred material. Right postorbital (IWCMS 2014.95.4) (Figure 2.3).

Diagnosis. Baryonychine distinguished by the presence of the following unique traits: premaxillae displaying a pair of bilaterally located tuberosities on the anterior margin of the external nares; narrow (reversal of the ancestral megalosauroid condition) and ventrally restricted subcondylar recess of the basioccipital; oval scars of the basisphenoid excavated by deep, elongate sulci; anteroposteriorly thick interbasipterygoidal web; supraoccipital dorsal process possessing a gently curving posteroventral surface in coronal section.

This taxon can be further separated from other baryonychines by the following combination of traits: presence of narial fossae on the premaxilla (as in cf. *Suchomimus* but not *Baryonyx*); short subnarial (maxillary) process of the premaxilla (as in *Baryonyx* but not cf. *Suchomimus*); lack of premaxillary sagittal crest (as in *Baryonyx* but not cf. *Suchomimus*); curved anterior margin of the dorsal facet of the paroccipital process (angular in *Baryonyx* and probably *Riparovenator*); posterolaterally directed paroccipital processes of the otoccipitals (more laterally directed in *Baryonyx*); exoccipital components of the occipital condyle closely spaced (as in *Riparovenator* and cf. *Suchomimus* but not *Baryonyx*); subcondylar recess lacking mediolaterally thick lateral crests (as in cf. *Suchomimus* but not *Baryonyx* or *Riparovenator*); relatively stout supraoccipital dorsal process (as in *Baryonyx* but not cf. *Suchomimus*); lack of a dorsal extension of the basisphenoid recess under the basioccipital apron (recess extends dorsally in *Baryonyx* and *Riparovenator*).

Type locality and type horizon: Wessex Fm. (Barremian), Chilton Chine, near Brighstone (Isle of Wight, UK).

Genus *Riparovenator* gen. nov.

LSID urn:lsid:zoobank.org:act:9F4B6370-138E-443E-9650-DE6134FD9CC0

Etymology: Rīpārius (Latin)–relating to the riverbank; vēnātor (Latin) –hunter

Type species: Riparovenator milnerae

Diagnosis: as for type and only species

Riparovenator milnerae sp. nov.

LSID urn:lsid:zoobank.org:act:791F5DA4-1BDB-47DC-8ABF-BC24F14722B1

Etymology: In honour of Angela Milner and her contributions to spinosaurid palaeobiology (and palaeontology as whole).

Holotype. Associated premaxillary bodies (IWCMS 2014.95.6); a disarticulated braincase (IWCMS 2014.96.1, 2; 2020.448.1, 2); a left "preorbital" fragment (partial lacrimal and near complete prefrontal) (IWCMS 2014.96.3) (Figure 2.4).

Referred material. A posterior nasal fragment (IWCMS 2014.95.7) (Figure 2.4); an extensive caudal axial series (IWCMS 2020.447.1–39) (Figure 2.5).

Diagnosis. Baryonychine distinguished by the presence of the following unique traits: notched dorsal orbital margin between prefrontal and postorbital process of the frontal; deeply inset facial nerve (CN VII) foramen that is largely obscured from lateral view; deep subcondylar recess (depth over 1/3 of its mediolateral width; depth less than 1/5 in other baryonychines); reduced exposure of ventral surface of the basipterygoid processes in lateral view.

This taxon can be further separated from other baryonychines by the following combination of traits: curved dorsal margin of the frontal process of the nasal in lateral view (margin effectively straight in *Baryonyx*); straight dorsal margin of the dorsum sellae (V-shaped in *Baryonyx* and *Ceratosuchops*); exoccipital components of the occipital condyle closely spaced (as in *Ceratosuchops* and cf. *Suchomimus* but not *Baryonyx*); mediolaterally thick crests bordering the subcondylar recess (as in *Baryonyx* but not *Ceratosuchops* or cf. *Suchomimus*); lateral margins of the basipterygoid processes concave in ventral view.

Type locality and type horizon: Between the Chilton Chine and Brighstone Sandstones, Wessex Fm. (Barremian), Chilton Chine, near Brighstone (Isle of Wight, UK).

2.6.2 Parsimony analysis

The parsimony analysis of 1810 characters and 40 Operational Taxonomic Units (OTUs) found 2660 shortest trees of 2448 steps each (CI=0.4939; RI=0.4551). The strict consensus is partially

resolved, and we find support for the monophyly of Coelurosauria, Allosauroidea and Megalosauria. Among spinosaurids, the strict consensus topology weakly supports a dichotomous Baryonychinae-Spinosaurinae split, although their in-group relationships are completely unresolved. Pruning rogue spinosaurid OTUs (recovered by the TNT command *pcrprune*), improved in-group resolution but did little to alter the poor nodal (Bremer) support (Figure 2.6). Jackknife resampling (see Appendix A) also weakly supports the above-mentioned dichotomy, although it is unable to resolve the relationships between most of the spinosaurine in-group.

These results are in accordance with the majority of previous works regarding the well supported monophyly of Spinosauridae (Carrano et al., 2012; Hone et al., 2017) and the sister-group relationship between Baryonychinae and Spinosaurinae (Sereno et al., 1998; Benson, 2010; Carrano et al., 2012; Arden et al., 2019; Rauhut et al., 2019b) (the synapomorphies of these clades are listed in Appendix A). However, the results of the Templeton test (discussed below; see also Appendix A) and poor nodal support reveal that the relationships of the spinosaurid in-group remain elusive and are hindered by the incompleteness of the sampled OTUs (see below). With respect to the broader affinities of Spinosauridae, our results generally conform to those of Cau (2018) and Rauhut et al. (2019b) in that they support the dissolution of the "traditional" avetheropodan node within Tetanurae, recovering instead an early-branching position for Coelurosauria, and (in this case) a polytomous Carnosauria that includes Allosauroidea and Megalosauroidea. In contrast, we find Megalosauridae to retain a traditional sister-group relationship with Spinosauridae.

2.6.3 Bayesian analysis

The Maximum Clade Credibility Tree (MCCT) obtained by the Bayesian inference analysis is in overall agreement with the strict consensus of the shortest trees recovered by the parsimony analysis, though resolution is substantially improved (

Figure 2.7, Appendix A). The MCCT indicates that the [megalosaurid-spinosaurid] divergence occur at over 180 Mya and thus requires a c. 36 MY ghost lineage pre-dating an Early Cretaceous radiation of Spinosauridae. The monophyly of Spinosauridae is strongly supported (*pp* = 0.94), and relatively strong support is recovered for Baryonychinae (*pp* = 0.71) and Spinosaurinae (*pp* of the subclade excluding *Camarillasaurus* = 0.81). Within Baryonychinae, the two Wessex Fm. specimens are recovered as sister taxa and form a moderately supported clade with *Suchomimus* (*pp* = 0.64). Within Spinosaurinae, the hypothesis that all North African spinosaurines form a clade (to the exclusion of non-African taxa) is weak, with almost all in-group nodes possessing *pp* values <50. The MCCT topology is thus equivocal on the distinction between *Sigilmassasaurus* and

Spinosaurus. Of additional note is the early-branching position of *Vallibonavenatrix* outside the baryonychine-spinosaurine clade.

2.7 Discussion

2.7.1 Taxonomic interpretation

Ceratosuchops inferodios and *Riparovenator milnerae* represent new Wealden Group theropod taxa, differing from the other broadly contemporaneous spinosaurid *Baryonyx walkeri* in numerous anatomical features (see Diagnoses in section 2.6.1; further comparisons are also described in Appendix A).

Our taxonomic interpretation nevertheless overlaps with several vexing and interrelated issues: the relative maturity of the Wessex Formation taxa and the broadly coeval *Baryonyx* is unknown, as is the scope of variation amongst spinosaurid cranial characters. Regarding the former, no unambiguous methodology is currently available to distinguish the ontogenetic status of non-coelurosaurian theropods (Griffin et al., 2020): while similar fusion patterns (e.g. premaxillae, nasals) and relatively comparable body sizes suggest overarching similitudes between these Wealden Supergroup specimens, we accept that there are caveats to these indicators of maturity (Griffin et al., 2020). Multi-element histological sectioning of the more complete *Baryonyx* type specimen could nonetheless prove an informative starting point. We are cognisant that some of the differences we report for our two new baryonychine taxa are associated with individual and/or ontogenetic variation in better-sampled theropods (see also Appendix A); indeed, intraspecific variation is seen to increase throughout the extreme ontogenetic series of the tyrannosaurid *Tyrannosaurus* (Carr, 2020), for instance. Meanwhile, the presence of a mosaic of states in the Wessex Fm. pair, regarded as “mature” and “immature” in other theropods, could be interpreted as revealing high variation in the order of ontogenetic character maturation (sequence polymorphism) within a single taxon (as seen in non-tetanuran theropods; Griffin et al., 2016); conversely, it is unknown whether spinosaurids were affected by such variability and there are currently no good reasons to assume that all are applicable to the clade. Simply put, the interpretation of spinosaurid cranial characters requires larger samples before we can properly assess the tempo and sequence of ontogenetic character state maturation and scope of intraspecific variation. In the absence of these data, we opt to name the two Wessex Fm. taxa given the presence of unique characters and character combinations.

Osteologically, the Wessex Fm. spinosaurid pair provides welcome new cranial and caudal information, all of which will be expanded upon in future work. Of note is the rugose brow region

of the skull in both specimens: in *Ceratosuchops*, this terminates posteriorly in an enlarged postorbital boss (Figure 2.3b). Given the similarity in frontal postorbital facet shape in *Riparovenator* and cf. *Suchomimus* (MNN GDF 214), a similarly built postorbital (and thus brow region) is inferred. Such cranial ornamentation suggests a role in socio-sexual signalling (Hone et al., 2017), although "overbuilt" brow regions may have also had a role in intraspecific antagonism (Sereno et al., 2008a); biomechanical analyses, such as Finite Element analysis (FEA) could shed light on this interpretation. Several previously diagnostic cranial features in *Baryonyx*, such as the deep occiput (*sensu* Hone et al., 2017), are here interpreted as obsolescent given our recovered topologies and taxonomic interpretation of the new finds; others, for instance the cruciform process of the nasal (*sensu* Hone et al., 2017), require refinement to take into account differing morphologies. In the caudal series, the relatively elongate neural spines of *Riparovenator* in particular push back the appearance of a dorsoventrally deep tail in spinosaurids, this feature being previously known from the Aptian in *Ichthyovenator* and *Suchomimus*.

2.7.2 Spinosaurid diversity in the Wealden Supergroup

Theropods appear rare in the Wealden Supergroup generally (Naish, 2011), despite the strata being the subject of enthusiastic collecting efforts and producing numerous specimens of herbivorous dinosaurs (Brusatte et al., 2008). As new Wealden Group taxa, *Ceratosuchops* and *Riparovenator* are thus substantial additions for the British theropod record, sharing the Wessex Fm. with at least three other mid-to-large theropods: the 7–8 m allosauroid Neovenator (Hutt et al., 1996; Brusatte et al., 2008), an indeterminate tetanuran (Benson et al., 2009a), and the 4–5 m tyrannosauroid *Eotyrannus* (Hutt et al., 2001). These new spinosaurid finds corroborate previous suggestions that the Early Cretaceous Wealden Supergroup faunas were inhabited by more than one baryonychine taxon (Naish et al., 2001; Naish et al., 2007; Naish, 2011), a discovery with potential implications for ecological separation within the clade, and for the Spinosauridae as a whole.

The presence of more than one baryonychine taxon in the British Wealden was previously suggested from the discovery of at least two spinosaurid dental morphotypes (Naish et al., 2001; Buffetaut, 2007; Naish, 2011). However, it has been argued (Smyth et al., 2020) that the presence of multiple spinosaurid dental morphotypes within deposits containing a single known taxon was indicative of a "significant degree of subtle heterodonty" within the given putative taxon, rather than the presence of multiple taxa. Spinosaurids did exhibit heterodonty, but the discovery of these new Wessex Fm. baryonychines, coupled with the occurrence of at least two taxa and multiple dental morphotypes (representing baryonychines and spinosaurines) from the Early Cretaceous deposits, of the Iberian Peninsula (Sánchez-Hernández et al., 2007; Canudo et al.,

2008; Gasca et al., 2018; Isasmendi et al., 2020; Malafaia et al., 2020a), paints a more complex picture. Diagnostic Iberian taxa from the Barremian specifically include *Baryonyx*, *Vallibonavenatrix* and possibly *Camarillasaurus* (see below), though their remains currently occur in non-overlapping formations and the true taxonomic diversity of the Iberian sample remains elusive (Isasmendi et al., 2020; Malafaia et al., 2020a). The validity of Iberian spinosaurine dental morphotypes has also been questioned (Smyth et al., 2020), despite there being some quantitative support for this referral (e.g., Alonso et al., 2018) and the presence of unambiguous spinosaurine synapomorphies (carinae lacking serrations *sensu* Hendrickx et al., 2019). The presence of more than one spinosaurid taxon is also indicated by dental variation present in a Lower Cretaceous assemblage from Tunisia (Fanti et al., 2014). We are aware of, and reject, claims that the profound variation present in this sample – in this case, the presence of denticulated and non-denticulated morphotypes – can be explained by intraspecific variation (Smyth et al., 2020) in the absence of a clear morphological gradient or variably denticulated in situ dental series. Isolated Iberian spinosaurid teeth are known to possess variably denticulated carinae (Isasmendi et al., 2020), however their taxonomic implications are presently unclear.

Returning to the British Wealden Supergroup, labial and lingual enamel ornamentation (e.g. Figure 2.3c) can be observed in both Wessex Formation taxa, as it can in isolated baryonychine teeth from this formation. This is a trait shared with "*Suchosaurus*" crowns from the neighbouring Weald sub-basin (and the Nigerien *Suchomimus*) (Hendrickx et al., 2019) and it is distinct from the largely lingually fluted condition of *Baryonyx walkeri* (Hendrickx et al., 2019) (the caveat being the aforementioned variability and incomplete understanding of spinosaurid enamel ornamentation more generally). Regardless, assuming our taxonomic interpretation is correct, the discovery of the new Wessex Formation specimens renders the presence of *Baryonyx* in the Wessex Formation ambiguous. Indeed, the dorsal vertebra IWCMS 2012.563 previously referred to *Baryonyx* (Naish, 2011) differs in its prominent spinodiapophyseal lamina and taller neural spine (potential damage to the *Baryonyx* type dorsal vertebrae notwithstanding) (Naish, 2011). We argue that the specimen is best identified as an indeterminate baryonychine or spinosaurid; this can be extended to other isolated Wealden Supergroup spinosaurid material previously referred to "*Baryonyx*".

Ecological demands require that large predators occur at low taxonomic diversity (Molnar, 1990). Despite this, numerous Jurassic and Cretaceous dinosaur assemblages include two or more comparably sized, morphologically similar, sympatric theropods (Van Valkenburgh et al., 2002); examples are present in various geological formations worldwide (e.g., Russell, 1970; Farlow et al., 2002b; Currie, 2003; Rauhut, 2005; Novas et al., 2010; Hone et al., 2011; Carrano et al., 2012; Cau et al., 2013; Gianechini et al., 2021). The presence of two or more spinosaurid taxa in the same geological unit is therefore not without precedent and may in fact be typical (Samathi et al.,

2021) – the above mentioned Early Cretaceous of Iberia appears to testify this diversity. Indeed, when present, spinosaurids may have been locally abundant, perhaps when environmental circumstances benefited their specialised niche (Hone et al., 2010a; Hone et al., 2017), a feature potentially driving high diversity within the clade. As such, the possible presence of broadly coeval spinosaurid taxa in the British Wealden Supergroup may represent the norm based on our knowledge of other assemblages. A view, popular in the Mesozoic dinosaur literature is that large theropod taxa can only coexist when anatomical traits indicative of resource partitioning are identifiable (Henderson, 2000; Farlow et al., 2002a; Barrett et al., 2006; Brusatte et al., 2012). This view obviously has merit, but is not incompatible with the possibility that similar, closely related taxa can co-exist and even overlap in ecological requirements; niche separation may be temporal (seasonal or daily), spatial (between habitats within ecosystems), or conditional. It should also be noted that those baryonychines inhabiting the regions represented by the Wessex and Weald sub-basins may have been separated in habitat choice (possible sub-basin habitat differences or climates have been previously suggested; Batten, 2011; Radley et al., 2012b; Raven et al., 2020). Nonetheless, these hypotheses assume *Baryonyx*, *Ceratosuchops* and *Riparovenator* were contemporaries and subject to interspecific interactions. Alternatively, given the variable and intermittent sedimentation of fluvial systems (Robinson et al., 2004), the expanse of time deposited within the Upper Weald Clay and exposed Wessex Fms., and the difficulties correlating their respective stratigraphies, it remains possible one or more of these spinosaurids were separated by geological time.

2.7.3 Phylogenetic analyses

We have determined through a large-scale phylogenetic analysis that the Wessex Formation specimens are more closely related to (a hypodigm OTU coding of) the Nigerien *Suchomimus tenerensis* than to *Baryonyx*, forming with it the newly recognised clade Ceratosuchopsini. This clade, and its internal relationships, is recovered under Bayesian and reduced consensus search strategies as well as through jackknife resampling (see Appendix A), suggesting a potentially stable topology with albeit limited support. Moreover, the extent to which the recovered topology is influenced by ontogenetically controlled character states is uncertain (see above). Additional characters, not currently included in the clade's diagnosis, may further unite the Ceratosuchopsini, (e.g. shallow rise of the parietal nuchal crest, boss-like process on the anterior prefrontal; see Table A 2), however comparisons with sufficient, adequately preserved spinosaurid material is required.

Comparing the consensus trees produced by the two phylogenetic methodologies reveals grossly congruent topologies. However, some of the finer aspects of the ingroup relationships remain

debatable: while Baryonychinae is recovered regardless of the phylogenetic methodology employed, we cannot reject alternative suboptimal scenarios where baryonychines form a paraphyletic grade to spinosaurines; constrained topologies forcing the Wessex Fm. pair outside of a *Baryonyx*+*Suchomimus* node, Ceratosuchopsini outside of a *Baryonyx*+Spinosaurinae node, and *Baryonyx* outside of a Ceratosuchopsini+Spinosaurinae node, required 2, 4 and 6 extra steps respectively, with all results insignificant under the Templeton test (see Appendix A). This echoes previous works (Evers et al., 2015; Sales et al., 2017b) questioning the robusticity of the traditional spinosaurid in-group dichotomy. Similarly, differing topologies recovered within Spinosaurinae indicate a continued lack of in-group resolution. This impacts the perceived number of coeval North African spinosaurines, a topic that has attracted considerable debate in recent years (Ibrahim et al., 2014; Evers et al., 2015; McFeeters, 2020; Smyth et al., 2020). The polytomous, parsimony-based strict consensus, coupled with the insignificance of the constrained analysis performed to group North African specimens (see Appendix A), are unable to support or reject the existence of a spinosaurine subclade incorporating all North African material – a topology required to corroborate the proposed synonymy of these specimens (i.e. *Spinosaurus sensu* Ibrahim et al., 2014). This is somewhat echoed in our Bayesian analysis: a North African subclade is recovered, but its support is weak. Thus, the proposed synonymy of *Spinosaurus* and *Sigilmassasaurus* (Smyth et al., 2020) is regarded as equivocal here. It should be noted these results might be affected by our decision to employ a composite OTU for *Sigilmassasaurus*, otherwise known from highly fragmentary type material; future analyses may consider removal of this OTU. Moreover, a better understanding of North African spinosaurine relationships requires the discovery of more complete individuals regardless.

Other minor topological differences include the Bayesian recovery of the Portuguese spinosaurid ML 1190 with the *Baryonyx walkeri* type specimen, a result differing from Arden et al.'s (2019) parsimony-driven placement of this specimen as an indeterminate spinosaurid. Our Bayesian findings are instead consistent with the specimen's original referral to *Baryonyx* (2011). The low posterior probabilities for this grouping hinder support for this association, as does the instability of ML 1190 in our parsimony analysis, but these likely originate from the fragmentary nature of the latter OTU in particular. Meanwhile, *Vallibonaventarix* – initially described as a spinosaurine (Malafaia et al., 2020b) – is recovered as a baryonychine (Figure 2.6) or a basal spinosaurid outside the baryonychine-spinosaurine spilt (Figure 2.7), indicating an unstable position within Spinosauridae. Elsewhere, the recovery of *Camarillasaurus* as a spinosaurine (originally described as a ceratosaur; Sánchez-Hernández et al., 2012), lends further support to recently published reinterpretations of this taxon's systematic position (Rauhut et al., 2019a; Malafaia et al., 2020a; Samathi et al., 2021). This interpretation may help explain the presence of spinosaurine-like teeth

recovered from the same deposits (Sánchez-Hernández et al., 2007). The "wildcard" status of *Irritator* within Spinosaurinae in our parsimony-driven analysis is perhaps unexpected given its well-preserved cranial material. Whilst derived apomorphies in the dentition and narial region (that are absent in baryonychines) support its association to other spinosaurine OTUs with overlapping osteologies (e.g. MSNM V4047, *Spinosaurus* holotype), its unstable nature is likely explained by the inability to compare it to other known predominantly from postcranial material.

Our phylogenetic analyses involved a substantial character list and large sample of spinosaurid OTUs, improving upon most previous studies that used comparatively smaller datasets. It also represents a first attempt to reconstruct spinosaurid palaeogeographic patterns using Bayesian methods. However, some spinosaurid OTUs could only be scored based on initial reports rather than first-hand observation or detailed monographs. This was the case for the *Suchomimus* OTU, for instance, and we favour using a hypodigm until the holotype specimen is thoroughly inventoried and described. We are nevertheless cognisant of the problematic inclusion of composite OTUs (Palci et al., 2013; Madzia et al., 2017). The lack of thorough descriptive works for many spinosaurid specimens remains a running hindrance in the study of the clade's systematics and taxonomy, and is exacerbated by the incomplete nature of most specimens. This incompleteness likely contributes to the labile positions of various spinosaurid OTUs as well as the moderate to poor in-group node support throughout the consensus topologies.

2.7.4 Spinosaurid palaeobiogeography

From a palaeogeographical perspective, our analysis supports a European origin of Spinosauridae generally consistent with the Laurasian origin model suggested by Milner (2003), with regionalisation and vicariance explaining the subsequent distribution of genus-level taxa. The Dispersal-Extinction-Cladogenesis (DEC) model supports the expansion of spinosaurid distribution during the first half of the Early Cretaceous to Asia and Western Gondwana, followed by progressive contraction of their distribution into the "mid" Cretaceous. In contrast, our findings are not consistent with Sereno et al.'s (1998) suggestion of an ancestral cosmopolitan distribution for spinosaurids followed by a vicariance-led divergence of Laurasian baryonychines and Gondwanan spinosaurines, and a *single* dispersal event invoked to explain the presence of *Suchomimus* in Africa. Our results instead indicate a European origin followed by at least two Early Cretaceous migrations to Africa, these leading, respectively, to *Suchomimus* and a clade within Spinosaurinae. An opposite direction of dispersal (Gheerbrant et al., 2006; Canudo et al., 2009) is not consistent with our results. This European origin and recovery of *Camarillasaurus* as an early-branching spinosaurine would appear to simplify the "complex" palaeogeographic pattern suggested by the presence of putative Iberian spinosaurines (Malafaia et al., 2020b). The

Aptian extinction of the Eurasian Spinosauridae is potentially contradicted by evidence indicating their persistence well into the Late Cretaceous of Asia (Hone et al., 2010a). The highly fragmentary specimen (a single tooth) was not, however, included among our OTUs, and its omission has likely influenced the tempo of the clade's perceived Eurasian extinction. Importantly, its potential baryonychine affinities may complicate the clade's palaeogeographic patterns.

2.8 Acknowledgements

We thank Martin Munt and Alex Peaker (Dinosaur Isle Museum, Sandown) for access to specimens and help with the stratigraphic relationship of the fossils; Gary Blackwell, Martin New, Eleanor Foxwell (Dinosaur Isle Museum) and Shaun Smith for preparation of the material; Martin Munt, Gary Blackwell and Alex Peaker, as well as volunteers Eleanor Foxwell, Callum Atkinson, Steve Hutt and Trudie Wilson, who helped excavate the site in 2017; Tim Medland, Andrew Cocks, Jon and Lou Moody, and Shaun Smith for donating their finds to the museum; Kai Bailey for finding and preparing remains attributable to *Ceratosuchops*; Replicate 3D for providing printed models; Susie Maidment (Natural History Museum, London) for providing access to the *Baryonyx* type specimen; Serjoscha Evers (University of Fribourg), Simone Maganuco (Natural History Museum of Milan) and Marco Schade (University of Greifswald) for providing additional imagery and discussion of *Suchomimus*, spinosaurid material from the Kem Kem beds, and *Irritator* respectively; Christophe Hendrickx for comments regarding spinosaurid dental variation, and John Radley for discussions regarding Wealden geology. We also thank Dan Folkes (University of Bristol), Scott Hartman (University of Wisconsin-Maddison) and Alex Vieira for the skeletals and silhouettes used in the figures. The program TNT was made available thanks to the Willi Hennig Society. We would like to extend out gratitude to the editorial team at Scientific Reports, and also to the reviewers for the thorough comments that helped improve this manuscript. This study was funded by the Engineering and Physical Science Research Council (EPSRC) and Institute for Life Sciences (University of Southampton). The acquisition of material was supported by the Friends of Dinosaur Isle (Charity No. 1170688).

2.9 Figures

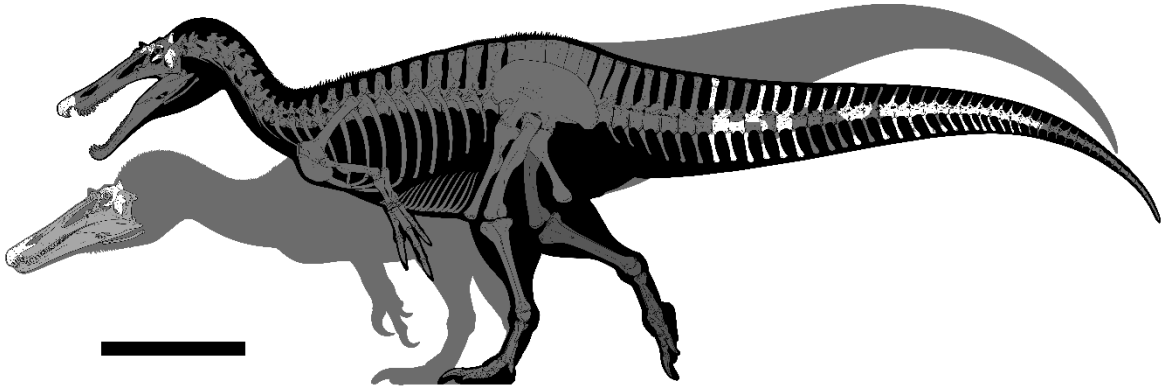

Figure 2.1 Known material referred to the baryonychines *Ceratosuchops inferodios* (grey silhouette) and *Riparovenator milnerae* (black silhouette) recovered at Chilton Chine (Isle of Wight, UK). White bones represent recovered elements. The arrangement of the elements in the caudal series is estimated; their relative position in the true series, and relationship with respect to each other (bar for those of the largely articulated mid-caudal series), are estimated. Image credit: Dan Folkes (CC-BY 4.0). Scale bar: 100cm.

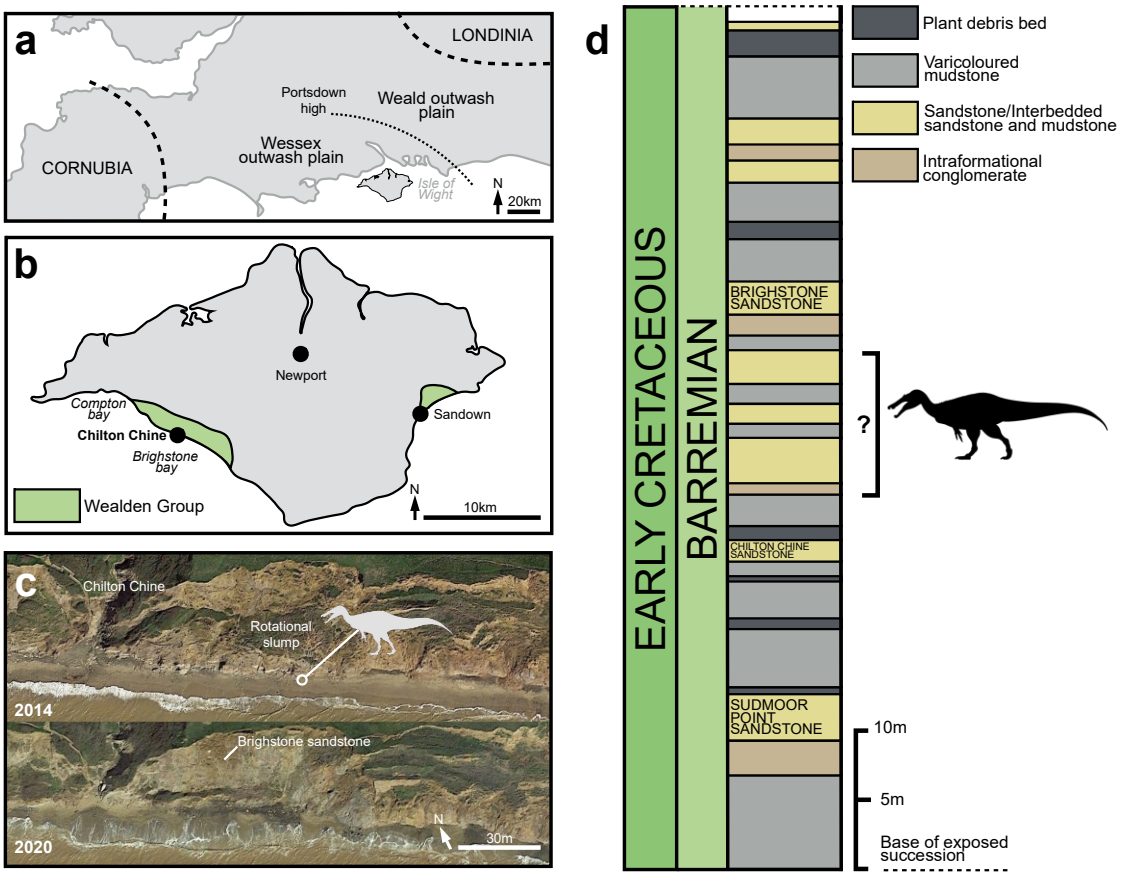

Figure 2.2 Locality information and stratigraphy of Chilton Chine. a) Schematic palaeogeographic map of the Wessex and Weald sub-basins of southern England (modified from Penn et al., 2020); b) map of the Isle Wight, highlighting the location of Chilton Chine and Wealden Group outcrops; c) aerial photographs of Chilton Chine, highlighting the approximate position of the in situ material referred to *Riparovenator milnerae* (see 0) and the extensive coastal processes affecting the locality since the initial discoveries (map data: Google, Landsat/Copernicus, TerraMetrics, Maxmar Technologies); d) schematic lithological log of the base of the exposed Wessex Fm. at Brighstone Bay (modified from Sweetman et al., 2014), highlighting approximate position of the *R. milnerae* in situ material. Silhouette credit: Dan Folkes (CC-BY 4.0).

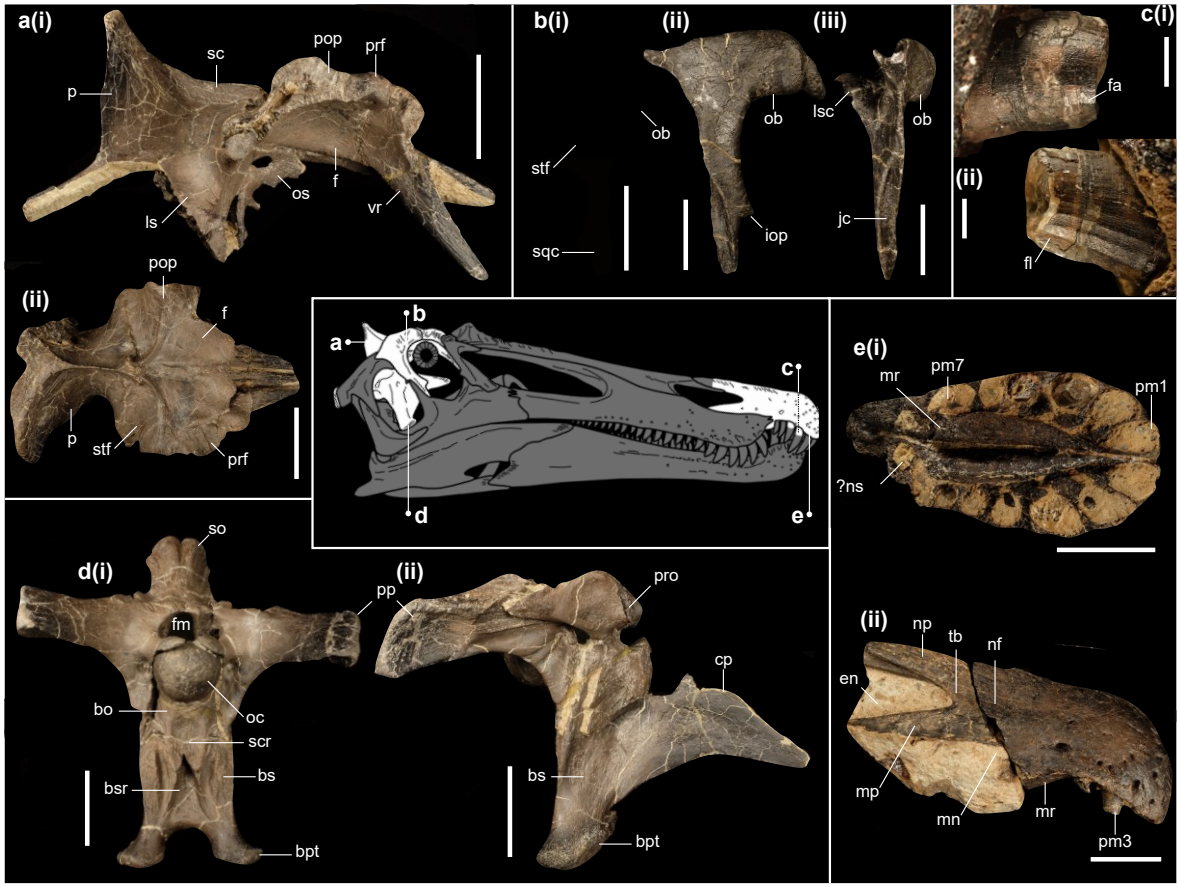

Figure 2.3 Cranial material of *Ceratosuchops inferodios*. a) Holotype skull roof fragment (IWCMS 2014.95.1), in (i) right lateral and (ii) dorsal views; b) referred right postorbital (IWCMS 2014.95.4), in (i) dorsal, (ii) lateral and (iii) posterior views; c) close up of holotype in situ Rpm3 (IWCMS 2014.95.5) in (i) labial and (ii) lingual views; d) holotype basicranium (IWCMS 2014.95.3), in (i) posterior (rearticulated with the supraoccipital+left otoccipital fragment IWCMS 2014.95.2) and (ii) right lateral views; e) holotype premaxillae (IWCMS 2014.95.5, 2021.30), in (i) ventral and (ii) right lateral views. Abbreviations: bo, basioccipital; bs, basisphenoid; bpt, basipterygoid process; bsr, basisphenoid recess; cp, cultriform process; en, external naris; f, frontal; fa: faceting; fl, fluting; fm, foramen magnum; iop, infraorbital process; jc, jugal contact; ls, laterosphenoid; lsc, laterosphenoid contact; mn, maxillary notch; mp, maxillary process; mr, median ridge; nf, narial fossa; np, nasal process; ns, nasal sinus; ob, orbital boss; oc, occipital condyle; os, orbitosphenoid; p, parietal; pop, postorbital process; pm(n), premaxillary tooth/alveolus (tooth position); prf, prefrontal; pro, prootic; sc, sagittal crest; scr, subcondylar recess; so, supraoccipital; sqf, squamosal contact; stf, supratemporal fossa; tb: tuberosity; vp: ventral process

of the prefrontal. Skull reconstruction credit: Dan Folkes (CC-BY 4.0). Scale bars a–b, d–e: 50mm; c: 5mm.

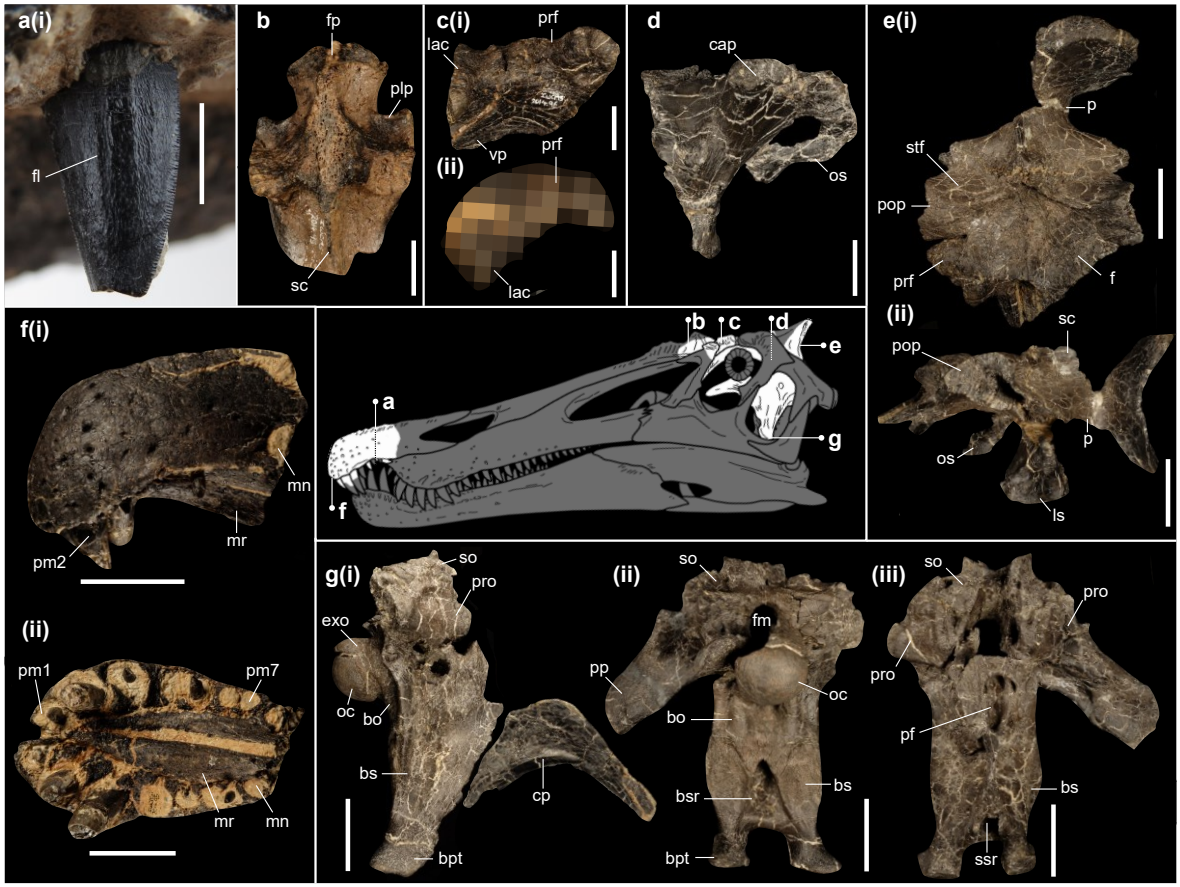

Figure 2.4 Cranial material of *Riparovenator milnerae*. a) Close up of holotype in situ RpmVII (IWCMS 2014.95.6), in labial view; b) referred posterior nasal fragment (IWCMS 2014.95.7) in dorsal view; c) holotype left preorbital fragment (IWCMS 2014.96.3) in (i) lateral and (ii) anterodorsal view; d) holotype right laterosphenoid (IWCMS 2014.96.2) in lateral view; e) holotype skull roof and associated left laterosphenoid (IWCMS 2014.96.1) in (i) dorsal and (ii) left lateral views; f) holotype premaxillary bodies (IWCMS 2014.95.6) in (i) left lateral and (ii) ventral views; g) holotype basicranium (IWCMS 2020.448.1) in (i) right lateral (with fractured cultriform process IWCMS 2020.448.2), (ii) posterior and (ii) anterior views. Abbreviations: bo, basioccipital; bs, basisphenoid; bpt, basipterygoid process; bsr, basisphenoid recess; cap, capitate process of the laterosphenoid; cp, cultriform process; exo, exoccipital; f, frontal; fl, fluting; fm, foramen magnum; fp, frontal process; lac: lacrimal; ls, laterosphenoid; mn, maxillary notch; mr, median ridge; oc, occipital condyle; os, orbitosphenoid; p, parietal; plp, posterolateral process; pop, postorbital process; pm(n), premaxillary tooth/alveolus (tooth position); prf, prefrontal; pro, prootic; sc, sagittal crest; scr, subcondylar recess; so, supraoccipital; ssr, subsellar recess; stf,

supratemporal fossa; vp: ventral process of the prefrontal. Skull reconstruction credit: Dan Folkes (CC-BY 4.0). Scale bars a: 5mm; b–d: 20mm; e–g: 50mm.

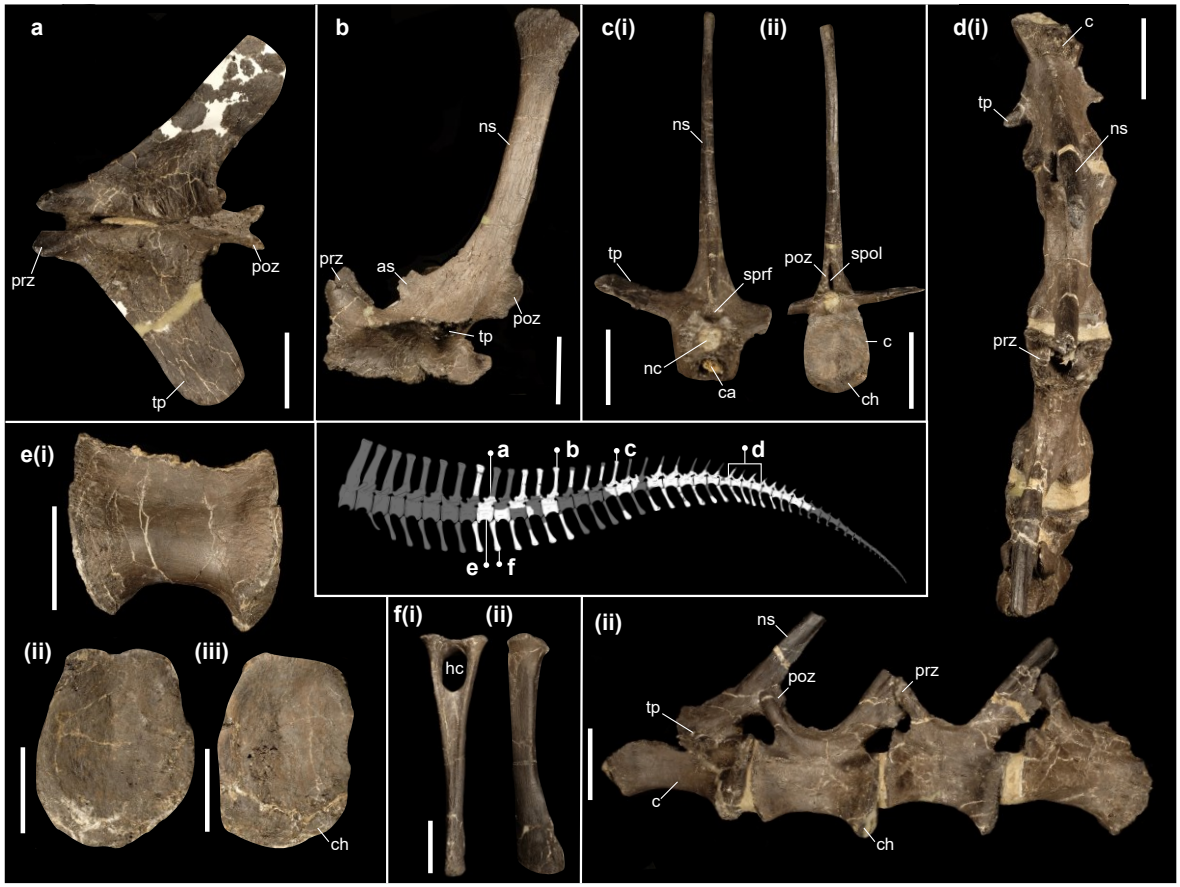

Figure 2.5 Caudal material referred to *Riparovenator milnerae*. a) Anterior neural arch (IWCMS 2020.447.3) in dorsal view; b) anterior neural arch (IWCMS 2020.447.2) in left lateral view; c) partial middle vertebra (IWCMS 2020.447.8) in (i) anterior and (ii) posterior views; d) articulated mid-caudal series (IWCMS 2020.447.12) in (i) dorsal and (ii) left lateral views; e) anterior centrum (IWCMS 2020.447.5) in (i) left lateral, (ii) anterior and (iii) posterior views; f) anterior chevron (IWCMS 2020.447.20) in (i) anterior and (ii) left lateral views. Abbreviations: as, anterior spur; c, centrum; ca, cavity; ch, chevron contact; h, haemal canal; nc, neural canal; ns, neural spine; poz, postzygapophysis; prz, prezygapophysis; spof, spinopostygapophyseal fossa; sprf, spinoprezygapophyseal fossa; tp, transverse process. Tail reconstruction credit: Dan Folkes (CC-BY 4.0). Scale bars: 50mm.

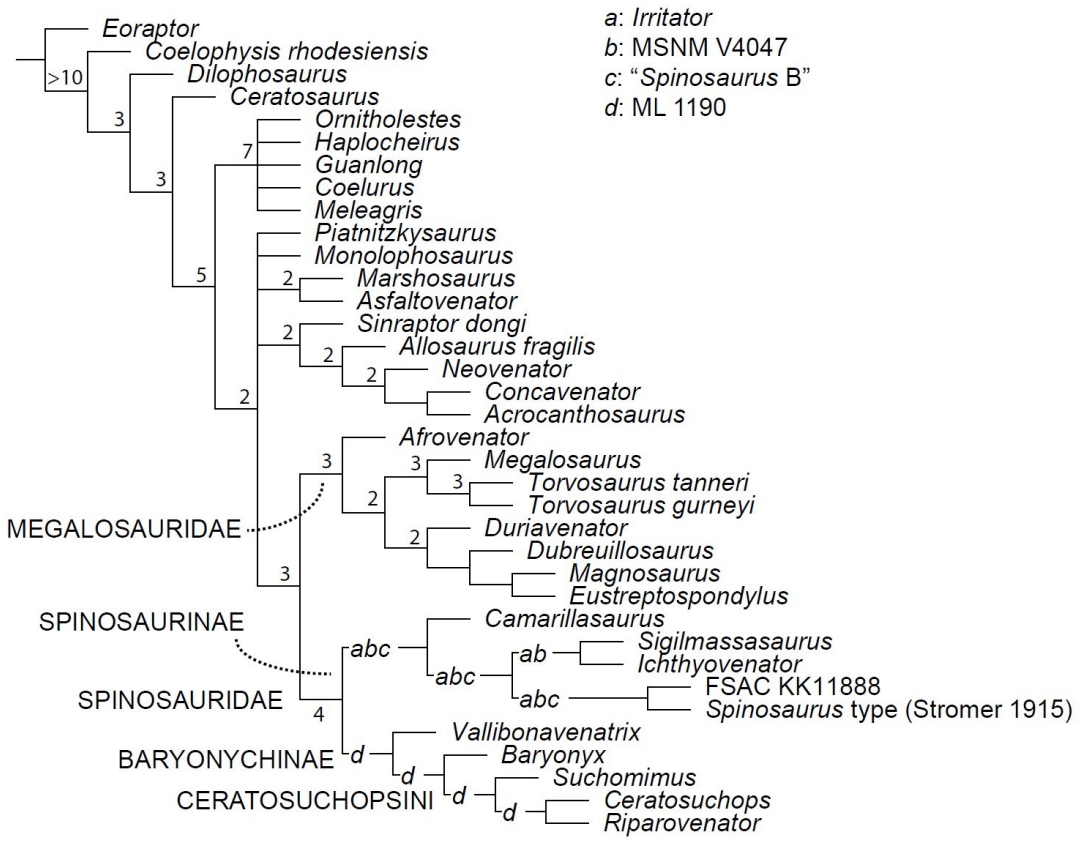

Figure 2.6 Phylogenetic relationships of Spinosauridae, based on parsimony analyses. Reduced consensus tree following a posteriori pruning of rogue spinosaurid OTUs. Values at nodes indicate the Bremer support values following pruning of rogue spinosaurid OTUs as well as select fragmentary taxa (see main text). Letters represent potential placement of rogue spinosaurid OTUs: a, *Irritator*; b, MSNM V4047; c, "*Spinosaurus* B"; d, ML 1190.

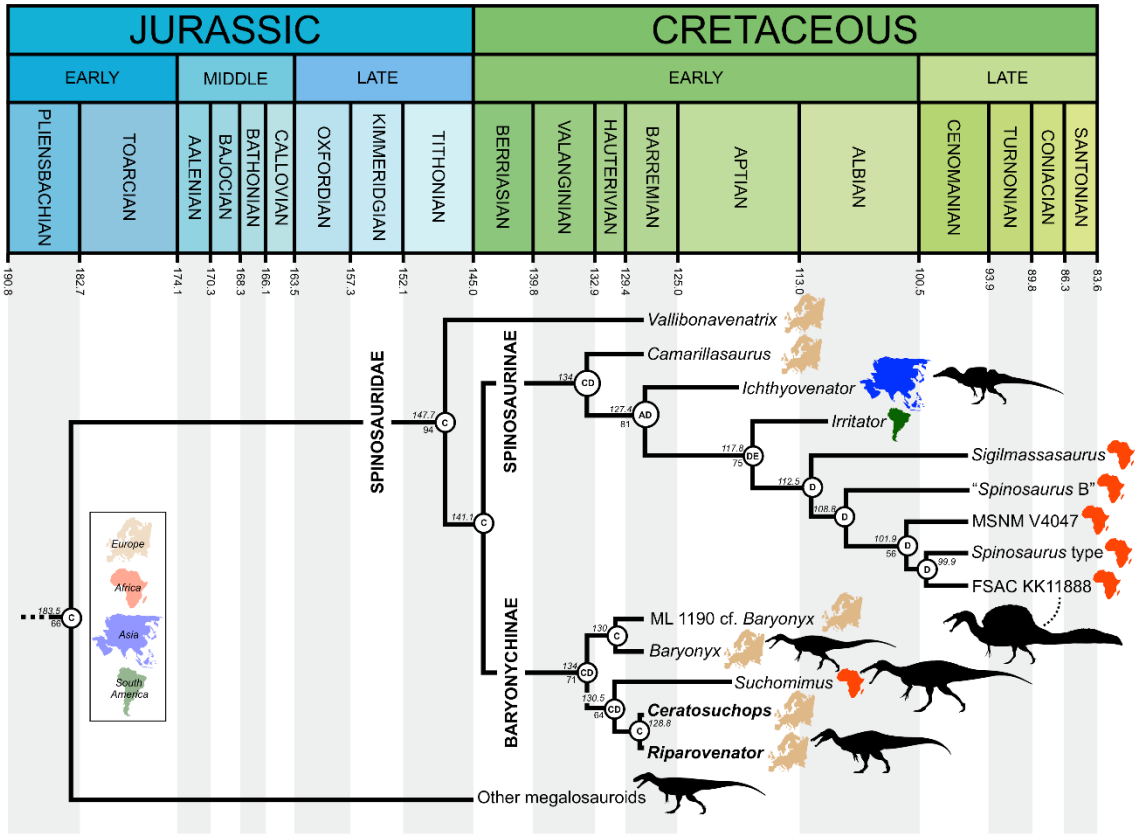

Figure 2.7 Time-calibrated phylogenetic relationships of Spinosauridae, based on the Maximum Clade Credibility Tree inferred by the Bayesian analysis (see Appendix A for extended figure). Numbers at nodes represent node age (top, in million years) and posterior probability values >50% (bottom). Letters at nodes refer to the most likely ancestral area reconstructed. Geologic timescale from Walker et al., (2018). See Appendix A for the extended figure. Abbreviations: A, Asia; B, North America; C, Europe; D, Africa; E, South America. Silhouette credits: *Riparovenator* – Dan Folkes (CC-BY 4.0); *Baryonyx*, *Megalosaurus*, *Suchomimus* – Scott Hartman/Phylopic (CC-BY-NC-SA 3.0); FSAC KK 11888 – Scott Hartman; *Ichthyovenator* – Alex Vieira (CC-BY-NC-SA 4.0)

Chapter 3 Isolated tooth reveals hidden spinosaurid dinosaur diversity in the British Wealden Supergroup (Lower Cretaceous)

3.1 Authorship statement

This chapter is the product of: **Barker, C.T.**, Naish, D. and Gostling, N. J. 2023. Isolated tooth reveals hidden spinosaurid dinosaur diversity in the British Wealden Supergroup (Lower Cretaceous). *PeerJ*, 10, p.e13543.

CTB, DN and NJG conceived the study. CTB wrote the first drafts (main text and supplementary information), conducted the analyses, compiled the supplementary materials and created the figures. All authors contributed to the interpretation of the specimen and editing of the manuscript and its supplementary information. The supplementary information for this chapter can be found in Appendix B and online.

3.2 Abstract

Isolated spinosaurid teeth are relatively well represented in the Lower Cretaceous Wealden Supergroup of southern England, UK. Until recently it was assumed that these teeth were referable to *Baryonyx*, the type species (*B. walkeri*) and specimen of which is from the Barremian Upper Weald Clay Formation of Surrey. British spinosaurid teeth are known from formations that span much of the c. 25 Ma depositional history of the Wealden Supergroup, and recent works suggest that British spinosaurids were more taxonomically diverse than previously thought. On the basis of both arguments, it is appropriate to doubt the hypothesis that isolated teeth from outside the Upper Weald Clay Formation are referable to *Baryonyx*. Here, we use phylogenetic, discriminant and cluster analyses to test whether an isolated spinosaurid tooth (HASMG G369a, consisting of a crown and part of the root) from a non-Weald Clay Formation unit can be referred to *Baryonyx*. HASMG G369a was recovered from an uncertain Lower Cretaceous locality in East Sussex but is probably from a Valanginian exposure of the Hastings Group and among the oldest spinosaurid material known from the UK. Spinosaurid affinities are both quantitatively and qualitatively supported, and HASMG G369a does not associate with *Baryonyx* in any analysis. This supports recent reinterpretations of the diversity of spinosaurid in the Early Cretaceous of Britain, which appears to have been populated by multiple spinosaurid lineages in a manner comparable to coeval Iberian deposits. This work also reviews the British and global records of early

spinosaurids (known mainly from dental specimens), and revisits evidence for post-Cenomanian spinosaurid persistence.

3.3 Introduction

Spinosaurids are an unusual clade of large-bodied tetanuran theropods best known for the multiple lines of evidence indicating specialisation for a semi-aquatic ecology and the associated controversy over their lifestyle (Taquet, 1984; Charig et al., 1997; Holtz, 1998; Amiot et al., 2010a; Bertin, 2010; Hassler et al., 2018; Ibrahim et al., 2020a; Hone et al., 2021; Fabbri et al., 2022b; Sereno et al., 2022). Spinosaurids are currently known from Cretaceous deposits and possess a wide spatial distribution, with important specimens coming from England, Brazil, northern Africa, the Iberian Peninsula and Southeast Asia. The clade is generally considered to consist of the sister-clades Baryonychinae (anchored on *Baryonyx walkeri* from southern England) and Spinosaurinae (anchored on *Spinosaurus aegyptiacus*, first described from Egypt though since reported from other north African countries) (Stromer, 1915; Charig et al., 1997; Sereno et al., 1998; Sues et al., 2002; Holtz et al., 2004; Benson, 2010; Bertin, 2010; Allain et al., 2012; Carrano et al., 2012; Ibrahim et al., 2014; Arden et al., 2019; Rauhut et al., 2019b; Ibrahim et al., 2020a; Mateus et al., 2022; Sereno et al., 2022). However, several recent analyses suggest that support for this dichotomy may not be as robust as usually supposed (Evers et al., 2015; Sales et al., 2017b; Barker et al., 2021).

The fossiliferous Lower Cretaceous (late Berriasian–early Aptian) Wealden Supergroup of southern England is a significant location for the clade, notably following the 1983 discovery of the *Baryonyx walkeri* holotype (Charig et al., 1986; Charig et al., 1997). The discovery of *B. walkeri*, represented by a partial skeleton, was integral to the reinterpretation of Spinosauridae (Naish et al., 2007), and resulted in the realisation that isolated teeth known from throughout the succession – traditionally regarded as crocodilian – also pertain to spinosaurids (Buffetaut, 2007; Fowler, 2007; Buffetaut, 2010). Indeed, among the first dinosaur remains to be scientifically illustrated and described are spinosaurid teeth from the English Wealden Supergroup, discovered in or around 1820 and given the binomial name "*Suchosaurus cultridens*" (Owen, 1840–1845; Buffetaut, 2010). These were misinterpreted as crocodilian for nearly two centuries (one of the longest cases of taxonomic misidentification), and were not correctly identified as spinosaurid until more recently (Buffetaut, 2007; Buffetaut, 2010). "*Suchosaurus cultridens*" is currently considered a *nomen dubium*, being best interpreted as an indeterminate spinosaurid (Mateus et al., 2011; Salisbury et al., 2011). More recent finds from the Wealden Supergroup succession on the Isle of Wight include the incomplete skeletons of the baryonychine taxa *Ceratosuchops inferodios* and *Riparovenator milnerae* from the Wessex Formation (Barker et al., 2021), and the

as-yet-unnamed “White Rock” spinosaurid (a possible spinosaurine) from the overlying Vectis Formation (Barker et al., 2022).

Spinosaurid skeletal material is rare (Hone et al., 2010a), but tooth crowns attributed to the group are regularly discovered; numerous isolated specimens have been reported from England (Martill et al., 1996b; Charig et al., 1997; Fowler, 2007; Turmine-Juhel et al., 2019), Spain (Ruiz-Omeñaca et al., 2005; Alonso et al., 2016; Isasmendi et al., 2020), China (Buffetaut et al., 2008; Shu'an et al., 2022), Malaysia (Sone et al., 2015), Japan (Hasegawa et al., 2003; Katsuhiro et al., 2017), Thailand (Buffetaut et al., 1986; Buffetaut et al., 2019; Wongko et al., 2019), Algeria (Benyoucef et al., 2015; Benyoucef et al., 2022), Cameroon (Congleton, 1990), Morocco (Richter et al., 2013), Libya (Le Loeuff et al., 2010), Niger (Sereno et al., 1998), Tunisia (Bouaziz et al., 1988; Benton et al., 2000) and Brazil (Medeiros, 2006; Sales et al., 2017a; Lacerda et al., 2023) (see also Bertin (2010) for further references and notes). Putative spinosaurid dental material may also extend the temporal span of the clade, though reported teeth from the Jurassic of France (Vullo et al., 2014), Tanzania (Buffetaut, 2012) and Niger (Serrano-Martínez et al., 2015; Serrano-Martínez et al., 2016), as well as the Late Cretaceous of China (Hone et al., 2010a) and Patagonia (Salgado et al., 2009), likely belong to other archosaur clades (Hendrickx et al., 2019; Soto et al., 2020).

Spinosaurid teeth are specialised and distinctive relative to those of other theropods, and possess a list of autapomorphies (Hendrickx et al., 2014a; Hendrickx et al., 2019). These allow them to be differentiated from the teeth of crocodylomorphs and plesiosaurs, two groups with which they have occasionally been confused (Sánchez-Hernández et al., 2007; Bertin, 2010; Buffetaut, 2010; Hone et al., 2010a; Sanguino, 2020; Soto et al., 2020). Key spinosaurid tooth characters, which are likely adaptions towards piscivory, include conidont (cone-shaped) morphology, fluted enamel surfaces, and veined enamel surface texture (Charig et al., 1997; Hendrickx et al., 2019; McCurry et al., 2019). Spinosaurid teeth are not homogenous: those conventionally attributed to baryonychines possess minutely denticulated carinae, while those conventionally attributed to spinosaurines are unserrated and weakly recurved (Carrano et al., 2012; Hendrickx et al., 2019; Barker et al., 2021). Spinosaurid teeth have been important with respect to discussions on the palaeobiology of the clade: they not only provide data on diet, ecology and lifestyle (Buffetaut et al., 2004; Amiot et al., 2009; Amiot et al., 2010a; Amiot et al., 2010b; Hassler et al., 2018; Hone et al., 2021) but also physiology (Heckeberg et al., 2020) and – most importantly for the present study – species-level diversity and palaeoenvironmental and stratigraphic distribution (Ruiz-Omeñaca et al., 2005; Fanti et al., 2014; Alonso et al., 2016; Sales et al., 2016; Beevor et al., 2021).

Those spinosaurid teeth discovered throughout Wealden Supergroup strata were initially assumed to be referable to *Baryonyx* (albeit not necessarily to *B. walkeri*) on the basis of general

similarity. Charig et al. (1997) referred isolated crowns from the Wessex, Upper Weald Clay and "Ashdown Sands" formations to cf. *Baryonyx*. Isolated teeth of the NHMUK collections, some previously referred to "*Megalosaurus*" and "*Suchosaurus*", were also referred to *Baryonyx* by Milner (2003). Buffetaut (2010) agreed that many of the "*Suchosaurus*" crowns from the Wealden Supergroup could be attributed to *Baryonyx*. More recently, Turmine-Juhel et al. (2019) referred incomplete crowns from the Wadhurst Clay Formation to *Baryonyx* sp. Attributing these various Wealden teeth to *Baryonyx* (or cf. *Baryonyx*) was a reasonable proposal in view of knowledge of Wealden spinosaurid diversity at the time but recent finds demonstrate higher diversity across the supergroup (Barker et al., 2021; Barker et al., 2022). In addition, it should be noted that these fossils come from strata spanning a time frame (~25 million years) not considered typical for the duration of a genus-level dinosaur taxon (Naish, 2011). However, these teeth differ in several ways from the dentition of the *Baryonyx walkeri* holotype and we consider it plausible that they represent additional taxa (Naish et al., 2007; Buffetaut, 2010; Naish, 2011).

A collection of archosaur teeth (HASMG G369) accessioned at Hastings Museum and Art Gallery (East Sussex, UK) includes one specimen (HASMG G369a) bearing the conidont appearance and minute denticles typical of baryonychine spinosaurids. An associated note indicates that these teeth were discovered close to the village of Netherfield in West Sussex (Figure 3.1), and from the Purbeck Group, a succession that underlies the Wealden Supergroup and spans the Jurassic-Cretaceous boundary (Tithonian–Berriasian; see below). A Purbeck origin for HASMG G369a would be important, as theropods are the rarest terrestrial vertebrate fossils from the Purbeck Group (Milner, 2002; Benson et al., 2009b; Barrett et al., 2010) and Purbeck spinosaurid remains have not previously been reported.

Isolated theropod teeth are common in the Mesozoic fossil record (Smith et al., 2005; Hendrickx et al., 2019) but their identification to lower taxonomic levels has been fraught with issues, among which are rampant homoplasy and a scarcity of sufficiently detailed anatomical accounts (Hendrickx et al., 2015a; Hendrickx et al., 2020b). Obviously, theropods possess a wide variety of dental morphologies (Hendrickx et al., 2014a; Hendrickx et al., 2015b; Hendrickx et al., 2019), and various characters have the potential to allow the identification of isolated specimens to their respective clades (Hendrickx et al., 2020b). Recent works advocate for the combined use of cladistic, discriminant and cluster methods in order to provide robust support and minimise the misleading impact of homoplasy (Hendrickx et al., 2014a; Hendrickx et al., 2020b). Here, we aim to identify HASMG G369a via the application of these methods, and to test the aforementioned assumption that British spinosaurid material should be considered referable to *Baryonyx* by default. The specimen's provenance is also discussed, and the fossil record of early and post-Cenomanian spinosaurids is reviewed.

3.3.1 Instutitional abbreviations

BEXHM, Bexhill Museum, Bexhill, UK; DCM, Dorset County Museum, Dorchester, UK; HASMG, Hastings Museum and Art Gallery, Hastings, UK; IWCMS, Dinosaur Isle Museum (Isle of Wight County Museum Services) Sandown, Isle of Wight, UK; IVPP, Institute of Vertebrate Paleontology and Paleoanthropology, Beijing, China; LUPFS, Laboratorio de Paleontologia of the Universidade Federal de Sergipe, São Cristóvao, Brazil; ML, Museu de Lourinhã, Lourinhã, Portugal; MNEMG, Maidstone Museum, Kent, UK; MNN, Musée National du Niger, Niamey, Republic of Niger; NHMUK, Natural History Museum, London, UK; SMNS, Staatliches Museum für Naturkunde Stuttgart, Germany; XMDFEC, Xixia Museum of Dinosaur Fossil Eggs of China, Xixia, China.

3.4 Geological context and provenance of HASMG G369a

The collection of teeth labelled as HASMG G369 consists of 10 specimens, and is associated with a note, which states:

"*If no specific locality is mentioned, these specimens are from Netherfield (Purbeck)*"

No specific locality is mentioned for any of the specimens, and it is unclear when or by whom this note was written. Importantly, the note is inconsistent with the accession record for HASMG G369, which details a "*collection of local Wealden fossils*" gifted by the Reverend Pierre Tielhard de Chardin (1881–1955); the provenance and contents of this "collection" are unknown. Tielhard is known to have collected from the Ashdown and Wadhurst Clay formations around Hastings, and donated many specimens (including some vertebrate remains) to Hastings Museum (Brooks, 2008). Thus, within the Weald sub-basin, HASMG G369a was either found from the Purbeck Group near Netherfield or the overlying Wealden Supergroup strata surrounding Hastings (Figure 3.1A).

Three fault-bounded inliers result in surface exposures of the Purbeck Group within the Weald sub-basin, located north and northwest of Battle in East Sussex, and are surrounded by the overlying Hastings Group (most of which comprise deposits of the Ashdown Formation) (Milner, 1922; Howitt, 1964; Radley et al., 2012c). These are the oldest exposed rocks in the region, with the inliers located north of Brightling, between Hollingrove and Netherfield, and near Archer Wood (Lake et al., 1987); the foremost pair have been respectively referred to as the Rounden Wood/Brightling-Heathfield and Limekiln Wood/Mountfield inliers (White, 1928; Howitt, 1964). The Purbeck Group in the area was previously quarried and mined, with data also provided from boreholes; however, surface exposures are poor and are mainly visible following valley denudation; those exposed in stream valleys have often been disturbed by valley-bulging,

landslips and slope cambers (Topley, 1875; Lake et al., 1987). Nevertheless, exposures of the Purbeck Group in the region are represented by both of its constituent Lulworth and Durlston Formations (Figure 3.1B), which are principally Berriasian in age (Howitt, 1964; Lake et al., 1987; Cope, 2007; Hopson et al., 2008). As mentioned above, Purbeck theropods are very rare, and documented specimens from Sussex outcrops include material referred to "*Megalosaurus* sp." (Topley, 1875; White, 1928; Benton et al., 1995b).

The Hastings Group, itself the basal unit of the Wealden Supergroup within the Weald sub-basin (Batten, 2011), dominates the area surrounding Hasting and is comprised of the older (late Berriasian–early Valanginian) Ashdown Formation, followed by the Wadhurst Clay Formation (Valanginian) and Tunbridge Wells Formation (late Valanginian; Figure 3.1B), several of which are well exposed along coastal sections (Lake et al., 1987; Hopson et al., 2008; Radley et al., 2012c). Only a small outcrop of the overlying Weald Clay Group is known near Cooden (Lake et al., 1987). Vertebrate fossils from the coastal exposures around Hastings in particular have been collected for over a century (Benton et al., 1995b). Documented theropod finds from the Hastings area include an allosauroid tibia (HASMG G378) (Naish, 2003) and material referred to "*Megalosaurus dunkeri*" (e.g. NHMUK PV R19154) and "*M. oweni*" (White, 1928; Benton et al., 1995b). Allosauroid and spinosaurid teeth are also known from the Wadhurst Clay around Bexhill (Charig et al., 1997; Turmine-Juhel et al., 2019), as are the remains of a tiny maniraptoran (Naish et al., 2011). The enigmatic theropod *Altispinax* (NHMUK PV R1828) is also known from the Hastings Group of Battle (von Huene, 1923; Naish, 2011; Maisch, 2016), located between Netherfield and Hastings.

We were unable to clarify the conflicting accession information surrounding HASMG G369a or ascertain its provenance. Given the rarity of Purbeck Group theropods, limited exposure of the succession around Netherfield, and accession history, we consider it highly unlikely this tooth originates from the Purbeck Group. Further, in the overlying Hastings Group, vertebrate fossils (bar fish detritus) are also extremely rare in the Ashdown Formation around Hastings and the exposures of the Weald Clay Formation are highly limited (Lake et al., 1987). Taken together, the upper units of the Hastings Group succession are thus the more likely candidates regarding HASMG G369a's provenance, and we thus provisionally consider the specimen to be Valanginian in age.

3.5 Materials & methods

3.5.1 Orientation and terminology

Dental nomenclature and protocols for crown and denticle morphometry follow the recommendations of Hendrickx et al. (2015b) and references therein.

3.5.2 Measurements

The specimen was examined via a DinoLite (AM4113TL) digital microscope. Measurements were taken using a 150mm digital calliper (accuracy 0.01mm), as well as the measurement tools in DinoXcope (v2.0.4) software. A full list of measurements is provided in the supplementary information.

Table 3.1 Measurements of the reconstructed HASMG G369a used in the morphometric analyses. Measurements in millimetres (mm) and crown angle in degrees (º). Asterisk (*) marks measurements derived from reconstructed, rather than observed, crown height (see main text).

Crown base length (CBL)	8.16
Crown base width (CBW)	7.03
Crown height (CH)*	17.2
Apical length (AL)	?
Midcrown length (MCL)*	5.67
Midcrown width (MCW)*	4.54
Mesial serrated carina length (MSL)	?
Number of labial flutes (+1) (LAF)	7 (8)
Number of lingual flutes (+1) (LIF)	5 (6)
Crown angle (CA)	74
Mesial denticle length (MDL)	?
Distal denticle length (DDL)	0.171

As HASMG G369a is missing its apex, several ordinary least-squares regression analyses were conducted where the specimen's crown height (CH) was compared against crown base length (CBL) and crown base width (CBW) for other spinosaurid teeth. Measurements were collected from the dataset of Hendrickx et al. (2020b). Variables were log-transformed to fit a normal

distribution and the analyses were conducted using the *Bivariate regression* function (*Model*>*Linear*) in Past4 (v.4.11) (Hammer et al., 2001). Of the different spinosaurid samples analysed (see supplementary information), logCBW from *Baryonyx walkeri* lateral teeth provided the most favourable regression coefficient (r^2=0.86), the slope and intercept of which was then used to estimate crown height in HASMG G369a. Other measurements or descriptions derived from CH (e.g. mid-crown length and width, number of denticles at mid-crown etc.) were based on the estimation detailed above.

Crown angle (CA) was estimated using the *Angle* tool in FIJI (Schindelin et al., 2012) via the creation of a vertex delimited by the CBL and a line trending through the midpoint of the preserved apex as the specimen was observed in lateral view. The landmarks used to delineate CBL follows Hendrickx et al. (2015b). Hendrickx et al. (2015b) described a method to calculate CA using the law of cosines and several morphometric landmarks, but photographs and FIJI has also been employed for isolated theropod crowns (Hendrickx et al., 2020b).

3.5.3 Cladistic analysis

We examined the phylogenetic affinities of HASMG G369a by including it in an updated version of the Hendrickx et al. (2014a) data matrix designed to test the affinities of non-avian theropod teeth (Hendrickx et al., 2020b). This updated matrix was used to assess the affinities of an isolated theropod tooth associated with the *Aerosteon riocoloradensis* holotype: the latter operational taxonomic unit (OTU) was replaced by HASMG G369a, and the final matrix was composed of 146 characters (Ch.) scored across 106 theropod OTUs (the “whole dentition” dataset). The mesial and lateral dentitions of spinosaurids are difficult to distinguish (Hendrickx et al., 2015b). However, as early spinosaurids possessed supernumerary lateral teeth (e.g. *Baryonyx* NHMUK PV R9951), it is more likely that HASMG G369a originated from the more distal maxillary or dentary dentition. HASMG G369a was thus scored as a lateral tooth.

We performed the cladistic analysis in TNT 1.5 (Goloboff et al., 2016) following the methods outlined in Young et al. (2019) and Hendrickx et al. (2020b), based on a backbone tree topology and the positive constraint command (*force +*), setting HASMG G369a as a floating terminal. The references used to create the backbone tree can be found in Hendrickx et al. (2020b). A pair of additional cladistic analyses was also performed using the whole dentition dataset without constraints, and a reduced matrix consisting only of crown-based characters (see Young et al. 2019; Hendrickx et al. 2020b: 11). The latter included 91 characters (Ch. 38–122 and 141–146) scored for 101 OTUs, with all edentulous taxa removed.

The tree searching strategy involved a combination of algorithms: Wagner trees, TBR branch swapping, sectorial searches, Ratchet (perturbation phase stopped after 20 substitutions) and Tree Fusing (5 rounds) were used until 100 hits of the same minimum tree length were reached. The recovered trees were subsequently subjected to an additional round of TBR branch swapping. In the unconstrained analyses, wildcard OTUs were identified using the iterPCR function (Pol et al., 2009; Goloboff et al., 2015), and Bremer support values were calculated as a measure of nodal support in the resulting reduced consensus.

Hendrickx et al. (2014a) use hypodigms for their spinosaurid OTUs, given the type specimens for several do not preserve dental elements (e.g. *Suchomimus*) or have been lost entirely (e.g. *Spinosaurus*). We note that their *Baryonyx* OTU includes the *B. walkeri* holotype NHMUK PV R9951 and the Iberian specimen ML 1190, and that the latter was recently considered the type specimen of a distinct taxon, *Iberospinus natarioi* (Mateus et al., 2022). Mateus et al. (2022) combined the dental character matrix of Hendrickx et al. (2020a) – itself a version of the matrix used in the present work – with the modified pan-skeletal matrix of Arden et al. (2019) in their phylogenetic analysis of ML 1190. The latter specimen was coded for 36 observable dental characters, however it would appear that Mateus et al. (2022) did not realise that the *Baryonyx* OTU employed in their analysis is a hypodigm and already contained ML 1190 (Hendrickx et al., 2014a). Nevertheless, the spinosaurid OTUs used in our analysis of the Hendrickx et al. (2020b) matrix were not modified given the fact that the dental material of *I. natarioi* is limited, positionally overlaps with that of *B. walkeri*, and possesses the same (observable) character scores as the *Baryonyx* OTU.

Elsewhere, the OTU of *Irritator* also includes the type specimen of *Angaturama*, following previous authors who consider the latter congeneric with the former (Charig et al., 1997; Sereno et al., 1998; Buffetaut et al., 2002; Sues et al., 2002; Dal Sasso et al., 2005). Specimens used for the cf. *Suchomimus* and cf. *Spinosaurus* hypodigm OTUs can be found in Hendrickx et al. (2014a: Table 1).

Regarding character scores, those of Ch. 82 (concerning the basalmost position of the mesial serration in lateral teeth) were scored by a process of elimination: although the basalmost mesial serration is not preserved in HASMG G369a, it likely possessed state 1 given the preserved extent of the mesial denticles and the probable inapplicability of states 0 and 2. Meanwhile, Ch. 90 (denticle number in lateral teeth respectively) were extrapolated from the observable data due to the incomplete nature of the carinae and preservation of denticles.

3.5.4 Discriminant function analyses

3.5.4.1 Pan-theropodan datasets

To classify and predict its optimal classifications inside "family-level" groupings based on quantitative data, HASMG G369a was included in a large published dataset of theropod teeth (Hendrickx et al., 2020b) and subjected to a discriminant function analysis (DFA) in Past4, where it was treated as an unknown taxon and classified at genus or clade levels. Pertinent to this work, the British spinosaurids previously included in this dataset were the type specimens of *Baryonyx walkeri* (NHMUK PV R9951) and "*Suchosaurus cultridens*" (NHMUK PV R36536). As above, HASMG G369a replaced the tooth associated with the *Aerosteon* holotype examined in Hendrickx et al. (2020b). The discriminant function analysis was performed following the protocol detailed by Young et al. (2019) and implemented in Hendrickx et al. (2020b), where all variables were log-transformed to normalize the quantitative variables, and a log (x+1) correction was applied to LAF and LIF to account for the absence of flutes on the crown, and an arbitrary value of 100 denticles per five mm was used for unserrated carinae (see Young et al. (2019) regarding justification of the latter modification).

The final dataset included 1335 teeth belonging to 89 taxa (84 species and five indeterminate family-based taxa) separated into 20 monophyletic or paraphyletic group measured for 12 variables (CBL, CBW, CH, AL, MCL, MCW, MSL, LAF, LIF, CA, MDL, DDL; see Table 3.1). As noted in Hendrickx et al. (2020a), Young et al. (2019) and Hendrickx et al. (2020b) incorrectly use the abbreviation DCL and DDC for DDL. Due to inconsistencies between authors when measuring dinosaur tooth crowns (Hendrickx et al., 2020b), a second analysis was conducted on a reduced dataset restricted to measurements previously taken by a single author using a consistent measuring protocol. This reduced dataset includes 594 teeth belonging to 72 theropod taxa separated into 20 monophyletic or paraphyletic groups.

In sum, clade- and genus-level discriminant function analyses were conducted on both the whole and reduced pan-theropodan datasets. These datasets were subject to an additional round of clade- and genus-level analyses where the absence of denticles was considered inapplicable (no denticles = "?").

3.5.4.2 Spinosaurid-only datasets

In order to assess the morphospace occupied by each spinosaurid specimen, additional discriminant function analyses were conducted on the raw morphometric data from Hendrickx et al. (2020b) focussing only on Spinosauridae. HASMG G369a was thus added to a dataset that included teeth from *Baryonyx*, cf. *Suchomimus*, *Irritator*, "*Sinopliosaurus fusuiensis"* and

"*Suchosaurus cultridens"*, as well as teeth referred to cf. Baryonychinae (XMDFEC V10010) and various indeterminate Spinosaurinae (the specimens and their associated data are compiled from Hendrickx et al. (2020b); see supplementary information). Only teeth from *Baryonyx*, *Irritator*, "*Suchosaurus*" and "*Sinopliosaurus*" are from holotype specimens.

We follow Hendrickx et al. (2015a) in performing two analyses in Past4 where all morphometric variables of interest (n=35) were included in the first instance, followed by an analysis were ratio variables (MAVG, DAVG, CBR, CHR, MCR, MEC, DSDI, CA, CDA, CMA and CAA) were excluded; CDA is derived from two ratio variables (Richter et al., 2013) and thus also excluded from this second analysis. The variables "transverse undulations" and "interdenticular sulci" were excluded from both analyses as the former contained qualitatively described data whilst the presence of the latter is not a character associated with spinosaurid dentition (Hendrickx et al., 2019). Alternative versions of variables (i.e. CA2, DAVG2), were also excluded so as not to inflate the dataset.

As in Hendrickx et al. (2015a), measurements were not log-transformed. Missing or uncertain data were coded as "?", whilst characters with an uncertain data range were averaged (e.g. the value 11.5 was used for the "11 or 12" lingual flutes scored for "*Suchosaurus*" NHMUK PV R36536). Data prefaced with a greater or less than sign were arbitrarily adjusted by plus or minus one point respectively (i.e. ">5" was changed to "6"). Data scored as "absent" or "not applicable" (represented by a dash) were replaced with the value zero. The "absent?" data point for the lingual flutes of cf. *Suchomimus* specimen UC G73-3 was changed to "?" given the uncertainty of the interpretation. These changes are compiled with the supplementary information.

A second round of analyses was undertaken, based on a reduced spinosaurid sample excluding the *nomina dubia* "*Suchosaurus*" (NHMUK PVR 36536) and "*Sinopliosaurus fusuiensis"* (IVPP V4793.1), as well as cf. Baryonychinae (XMDFEC V10010) given suggestions this specimen does not represent a spinosaurid taxon (see also below) (Katsuhiro et al., 2017; Buffetaut et al., 2019; Soto et al., 2020). The remaining spinosaurids were subjected to the same analyses described above (i.e. one DFA using all variables and another excluding ratio variables).

3.5.5 Cluster analysis

Cluster analyses were also performed in Past4 on the different pan-theropodan datasets mentioned above. Hierarchical clustering with a Paired group algorithm and Neighbour joining clustering were used, rooting the tree with the final branch, whilst selecting Euclidean distances as the similarity index.

3.6 Results

3.6.1 Systematic palaeontology

DINOSAURIA Owen 1842

THEROPODA Marsh 1881

TETANURAE Gauthier 1986

SPINOSAURIDAE Stromer 1915

Spinosauridae gen. and sp. indet.

3.6.2 Description

3.6.2.1 Orientation

The slight distal recurvature of the crown means that HASMG G369a can be oriented along its mesiodistal axis but the labiolingual axis is less clear. A basal depression, ordinarily lingually situated in theropods (Hendrickx et al., 2015b), is absent on either side of HASMG G369a. This crown subunit may appear planar in some theropods (Hendrickx et al., 2015b), but this is also not the case in HASMG G396a. The crown does, however, display slight labiolingual curvature when viewed distally, and we use this feature to differentiate the lingual and labial surfaces.

3.6.2.2 Condition

HASMG G369a comprises a near-complete crown (lacking its apex) associated with the basal portion of the root. The enamel is largely well preserved on the labial surface excepting a small chip apically. Large parts of the enamel on the lingual surface however have been worn.

The preserved mesial carina has been abraded in several places, such that only two short sections remain: one just above the cervix and the other located mesiocentrally; the denticles – where preserved – appear slightly worn. The distal carina is more complete, with wear mainly affecting the apical-most portion.

3.6.2.3 Crown

HASMG G369a is a conidont crown with a lenticular cross section at the cervix and at mid-crown (Figure 3.2A–B); as such, the crown is weakly labiolingually compressed (CBR: 0.86). The crown is

not particularly large (preserved CH: 13.2mm; reconstructed CH: 17.2mm) and only moderately elongated (preserved CHR: 1.68; reconstructed CHR: 2.1).

The mesial and distal carinae are both denticulated (Figure 3.2C–D, Figure 3.3), lacking adjacent concave surfaces. The former is straight, undivided, and not notably developed, and is positioned largely centrally on the mesial profile. Whilst the basalmost portion has been chipped off (see above), what remains suggests the mesial carina almost certainly reached the cervix. The distal carina is slightly diagonally oriented, and as mentioned above, trending towards the labial side basally. It too is not markedly developed and lacks any twisting of splitting. It extends basally past the cervix a short distance. The apical extent of either carina cannot be determined for this specimen.

The crown displays weak distal recurvature in labiolingual views (Figure 3.2A). Its mesial profile is weakly convex, whilst the distal profile is almost straight for the majority of its preserved length. The preserved apex is almost centrally positioned. When viewed distally (Figure 3.2D), the crown also possesses minor lingual curvature, with the apex closer to the lingual side. Both the labial and lingual crown surfaces are convex.

The cervix assumes a parabolic morphology on the better-preserved labial side of the crown, such that the basalmost extent of the enamel occurs roughly centrally (Figure 3.2E). The equivalent features, or relative extent of the enamel on the lingual side, cannot be reliably ascertained due to preservation. However, the extent of the enamel on the mesial and distal surfaces appears largely similar.

3.6.2.4 Denticles

The denticles (Figure 3.3) of the mesial carina are best preserved at mid-crown, although some incipiently visible ones are also observed at the basalmost preserved portion of the carina. Those of the distal carina are present across a large extent but are worn distoapically and between the distocentral and distobasal portion of the crown.

There are approximately 7 denticles per millimetre on both the mesial and distal carinae at midcrown. These are typically mesiodistally longer than apicobasally tall and are oriented perpendicularly relative to their respective carina. Their external margins are flattened, giving them a mesiodistally subrectangular appearance in lateral view. The interdenticular spaces are relatively broad and well developed, though the interdenticular diaphyses are not easily recognised, perhaps due to preservation. The mesial and distal denticles at midcrown are approximately the same size (denticle size density index (DSDI): 1), and interdenticular sulci are

not observed on either carina. The more complete distal carina also reveals a regular variation in denticle size; this attribute can also be extended to those sections preserved on the mesial carina.

The basalmost segments of the carinae are also denticulated. However, those present mesially are difficult to measure and describe, being visible only under certain light conditions and orientations. Those situated distobasally appear to extend to the cervix (if not just beyond the latter) and are generally similar to those of the midcrown, being smaller and slightly more numerous per millimetre.

3.6.2.5 Ornamentations

The crown is ornamented, possessing weakly developed flutes, of which seven (possibly eight) are present on the lingual side and five on the labial one (Figure 3.2A, E). Those adorning the latter surface are less prominent. Transverse and marginal undulations appear absent. The crown possesses veined enamel texture basally, which is particularly fine near the cervix and whose grooves/ridges are generally apicobasally oriented barring those that curve towards the carina. More apically however, the texture becomes irregular (Figure 3.2F–H).

3.6.3 Cladistic analyses

The results of the various cladistic analyses, detailed below, are summarised in Table 3.2. Full versions of the recovered trees are available in the supplementary information.

3.6.3.1 Whole dentition dataset

Two MPTs of 1318 steps were recovered following the constrained search on the whole dentition dataset (CI=0.204097, RI=0.451360). HASMG G369a either assumed a position outside the baryonychine + spinosaurine clade or at the base of Spinosaurinae; the latter position was supported by a single synapomorphy: a slightly convex mesial margin (Ch. 73:1). Accordingly, the strict consensus recovered HASMG G369a in a polytomous Spinosauridae alongside Baryonychinae and Spinosaurinae (Figure 3.4A), with the clade supported by numerous synapomorphies. Of these, HASMG G69a shared: 1) weak labiolingual compression of the crown with a CBR exceeding 0.75 (Ch. 70:2), 2) subcircular basal cross-section of the crown (Ch. 76:0), 3) over 30 distocentral denticles per 5mm (Ch. 89:0), 4) fluted enamel surfaces present on both labiolingual surfaces (Ch. 111:2) and 5) veined enamel texture (Ch. 121:3).

The unconstrained search on the whole dentition dataset initially returned 248 MPTs of 1074 steps (CI=0.250466, RI=0.578975). This increased to 87576 MPTs following the round of TBR. The strict consensus is largely unresolved and predominantly formed by two large polytomies

containing well over 25 OTUs each. Few traditional clades can be recognised but those present include Spinosauridae and Abelisauridae. The strict consensus nevertheless recovered HASMG G369a within a polytomous Spinosauridae alongside Baryonychinae and Spinosaurinae.

A reduced consensus was achieved following the pruning of 23 wildcard OTUs (*Limusaurus* (juvenile), *Masiakasaurus*, *Indosuchus, Chilesaurus*, *Piatnitzkysaurus*, *Sciuruminus*, *Eustreptospondylus*, *Afrovenator*, *Dubreuillosaurus*, *Duriavenator*, *Sinraptor*, *Allosaurus*, *Orkoraptor, Acrocanthosaurus*, *Aorun, Guanlong*, *Eotyrannus*, *Raptorex*, *Gorgosaurus*, *Alioramus, Daspletosaurus, Tyrannosaurus* and *Ornitholestes*) identified via the iterPCR function (Figure 3.4B). As above, HASMG G369a is again recovered in a polytomous Spinosauridae alongside Spinosaurinae and Baryonychinae, which is supported by several synapomorphies; those present in HASMG G369a are: 1) the basalmost denticle on the mesial carina of lateral teeth extending to the base of the crown or slightly above the cervix (Ch. 82; see comment in the "Cladistic analysis3.5.3" section above), 2) basalmost serration on the distal carina situated below the cervix (Ch. 85), and 3) flutes present on both labial and lingual surfaces (Ch. 111).

3.6.3.2 Crown-based dataset

The unconstrained search on the crown-based dataset initially recovered 244 MPTs of 648 steps (CI=0.251543, RI=0.62139). The additional round of TBR returned over 99999 trees found (overflow). The strict consensus produced a huge polytomy incorporating the vast majority of OTUs including HASMG G369a (see supplementary information for the full result). HASMG G369a was one of 74 OTUs acting as wildcard taxa (the others include: *Daemonosaurus*, *Eodromaeus*, *Eoraptor*, *Dracovenator*, *Coelophysis*, *Liliensternus*, *Dilophosaurus*, *Ceratosaurus*, *Genyodectes*, *Berberosaurus*, *Masiakasaurus, Kryptops*, *Rugops*, *Abelisaurus*, *Aucasaurus*, *Arcovenator*, *Chenanisaurus*, *Indosuchus*, *Majungasaurus*, *Skorpiovenator*, *Piatnitzkysaurus*, *Marshosaurus*, *Monolophosaurus*, *Sciuriminus*, *Eustreptospondylus*, *Afrovenator*, *Dubreuillosaurus*, *Duriavenator*, *Megalosaurus*, *Torvosaurus*, *Baryonyx*, *Suchomimus*, *Irritator*, *Spinosaurus*, *Erectopus*, *Sinraptor*, *Allosaurus*, *Neovenator*, *Fukuiraptor*, *Australovenator*, *Megaraptor*, *Orkoraptor*, *Acrocanthosaurus*, *Eocarcharia*, *Carcharodontosaurus*, *Giganotosaurus*, *Mapusaurus*, *Bicentenaria*, *Aorun*, *Zuolong*, *Proceratosaurus*, *Guanlong*, *Dilong*, *Compsognathus*, *Ornitholestes, Haplocheirus*, *Eshanosaurus*, *Falcarius*, *Jianchangosaurus*, *Segnosaurus*, *Erlikosaurus*, *Incisivosaurus*, *Halszkaraptor*, *Sinornithosaurus*, *Graciliraptor*, *Dromaeosaurus*, *Bambiraptor*, *Tsaagan*, *Velociraptor*, *Sinusonasus*, *Zanabazar*, *Troodon* and *Archaeopteryx*).

Table 3.2 Summary of the cladistic analyses, describing the position of HASMG G369a in Newick format.

Dataset	Position	Constrained	Unconstrained	
			Strict Consensus	Reduced Consensus
Whole dentition	Lateral	(HASMG G369a, Spinosaurinae, Baryonychinae)	(HASMG G369a, Spinosaurinae, Baryonychinae)	(HASMG G369a, Spinosaurinae, Baryonychinae)
Crown only	Lateral	–	Polytomy with majority of theropod OTUs	n/a

3.6.4 Discriminant function analysis

3.6.4.1 Pan-theropodan datasets

The analyses conducted on the whole dataset (Figure 3.5), regardless of whether the absence of denticles was considered inapplicable or not, consistently classified HASMG G369a as a spinosaurid (clade-level analyses) or referred the tooth to the baryonychine spinosaurid *Suchomimus* (genus-level analyses) (Table 3.3). Reclassification rates (RR) are, however, generally low, ranging between 59.37–62.07%. Similarly, the reduced datasets based on single-author measurements classified HASMG G369a as a spinosaurid and as *Suchomimus* in the respective analyses (again, with low RR between 59.19–63.74%).

Table 3.3 Results of the discriminant function analyses on the various iterations of the pan-theropodan dataset, with HASMG G369a treated as an unknown taxon.

Dataset	Discriminant Function Analysis		Reclassification Rate (RR)	
	Clade level	Genus level	Clade level (%)	Taxon level (%)
Whole dataset	Spinosauridae	*Suchomimus*	61.02	61.17
Whole dataset (no denticles = ?)	Spinosauridae	*Suchomimus*	62.07	59.37
Reduced dataset	Spinosauridae	*Suchomimus*	59.36	63.74
Reduced dataset (no denticles = ?)	Spinosauridae	*Suchomimus*	59.19	60.37

Dataset	Clade level		Genus level		Clade level (Eigenvalue)		Taxon level (Eigenvalue)	
	PC1 (%)	PC2 (%)	PC1 (%)	PC2 (%)	Axis 1	Axis 2	Axis 1	Axis 2
Whole dataset	51.01	19.8	41.04	21.56	5.71	2.22	18.38	9.65
Whole dataset (no denticles = ?)	50.2	19.04	42.87	17.08	5.79	2.20	18.01	7.18
Reduced dataset	57.1	21.9	41.07	24.72	12.19	4.67	24.99	15.04
Reduced dataset (no denticles = ?)	54.27	22.94	41.4	25.66	10.98	4.64	23.75	14.72

3.6.4.2 Spinosaurid-only datasets

The DFA results for the spinosaurid-only morphometric datasets (Table 3.4) consistently classified HASMG G369a as a non-*Baryonyx* spinosaurid. Reclassification rates are very high (98.18–100%), especially in comparison to the pan-theropodan datasets used above, with HASMG G369a classified as cf. *Suchomimus* in the majority of analyses (PC1 63.73–84.32%, PC2 14.84–26.12%). Interestingly, the results from the dataset including all spinosaurids and all variables classified HASMG G369a as "*Suchosaurus*" (PC1 72.53%, PC2 20.03%), which is also known from the Hastings Group.

Visualisation of the DFA plots also shows that spinosaurid teeth are readily differentiable based on the data from Hendrickx et al. (2020b) (Figure 3.6 and Figure 3.7): spinosaurine and baryonychine taxa occupy different morphospace areas, whilst *Baryonyx* and cf. *Suchomimus* do not overlap in any iteration of the analyses. This suggests that *Baryonyx* and cf. *Suchomimus* teeth are morphologically distinct. Whether this impacts discussions regarding the congeneric status of the two taxa remains to be seen, especially given the non-cranial nature of the *Suchomimus* holotype skeleton (Sereno et al., 1998; Carrano et al., 2012). Also of note is the tendency for "*Suchosaurus*" to cluster closely with the cf. *Suchomimus* morphospace in the analyses containing all spinosaurid specimens, whilst "*Sinopliosaurus*" plotted close to the morphospace occupied by spinosaurine teeth.

As an aside, the isolated specimen XMDFEC V10010 from the Santonian (Late Cretaceous) Majiacun Formation of China, referred to Baryonychinae by Hone et al. (2010a), does not cluster closely or share morphospace with any spinosaurid taxon in the DFA analyses of the spinosaurid sample. To explore this further, we tested the specimen using discriminant function and cluster analyses on the "whole", "personal" and "large crown" pan-theropodan datasets from Hendrickx

et al. (2020b), treating XMDFEC V10010 as an unknown taxon. These results are presented in full in the supplementary information and are briefly discussed below.

Table 3.4 Results of the discriminant function analyses on the various iterations of the spinosaurid-only dataset, with HASMG G369a treated as an unknown taxon.

Dataset	**Discriminant Function Analysis**	**Reclassification Rate (RR) (%)**
All spinosaurid dataset	*"Suchosaurus"*	98.28
All spinosaurid dataset no ratios	*Suchomimus*	98.28
Reduced spinosaurid dataset	*Suchomimus*	100
Reduced spinosaurid dataset no ratios	*Suchomimus*	98.18

Dataset	**Taxon level**		**Taxon level (Eigenvalue)**	
	PC1 (%)	**PC2 (%)**	**Axis 1**	**Axis 2**
All spinosaurid dataset	72.53	20.03	89.905	24.824
All spinosaurid dataset no ratios	63.73	26.12	40.277	16.506
Reduced spinosaurid dataset	84.32	14.84	73.009	12.846
Reduced spinosaurid dataset no ratios	82.02	17.34	36.934	7.807

3.6.5 Cluster analysis

The cluster analyses based on the pan-theropodan dataset (Table 3.5, supplementary information), regardless of the method employed (i.e. hierarchical vs. neighbour joining), unanimously support spinosaurid affinities of HASMG G369a. Almost all results recover the crown as a sister taxon to *Suchomimus*, except for the Neighbour joining analysis performed on the whole dataset (no denticles = "?"), where it is recovered as sister to a clade containing *Irritator* + *Suchomimus*.

Table 3.5 Results of the cluster analyses on the various iterations of the pan-theropodan datasets, with HASMG G369a treated as an unknown taxon.

Dataset	**Cluster Analysis**	
	Hierarchical clustering	**Neighbour joining**
Whole dataset	*Suchomimus*	*Suchomimus*
Whole dataset (no denticles = ?)	*Suchomimus*	*Suchomimus+Irritator*
Reduced dataset	*Suchomimus*	*Suchomimus*
Reduced dataset (no denticles = ?)	*Suchomimus*	*Suchomimus*

3.7 Discussion

3.7.1 Affinities of HASMG G369a and the diversity of British spinosaurids

The results from the cladistic, discriminant and cluster analyses clearly support the spinosaurid affinities of HASMG G369a. HASMG G369a shares multiple dental characters in common with spinosaurids, including a sub-circular outline, fluted enamel ornamentation and veined enamel texture, extension of the mesial carina to the cervix and a centrally positioned distal carina (Hendrickx et al., 2019).

Of particular note is the finding that HASMG G369a (its wildcard status within the crown-only phylogenetic analyses excepting) failed to associate with *Baryonyx* in any data run. This further supports previous arguments that the Wealden Supergroup contains multiple spinosaurid lineages (Naish et al., 2007; Buffetaut, 2010; Naish, 2011; Barker et al., 2021). These results also suggest that the spinosaurid diversity within the Wealden Supergroup reflects the situation of coeval Iberian localities, which appear to have contained a more diverse spinosaurid fauna than previously assumed (Isasmendi et al., 2020; Malafaia et al., 2020a; Mateus et al., 2022).

The dentition of *Ceratosuchops* and *Riparovenator* were not scored for this analysis due to poor preservation; however, future work should aim to use cladistic and discriminant methods on spinosaurid crowns found in known strata within the Wealden Supergroup in order to further assess the diversity of its spinosaurids. It would be of particular interest to examine isolated spinosaurid teeth from the Upper Weald Clay Formation, in order to test whether these can be confidently referred to *Baryonyx*. Revisiting coeval Lower Cretaceous localities from Iberia may also be useful given the widespread presence of spinosaurids in these deposits (Malafaia et al.,

2020a); several morphometric-based (PCA and DFA) analyses have already been undertaken on Iberian spinosaurid crowns (the results of which also hint at high spinosaurid diversity) (Alonso et al., 2016; Alonso et al., 2018; Isasmendi et al., 2020). However, cladistic analyses are recommended (if not preferred) for the identification of isolated theropod teeth (Hendrickx et al., 2020b), although some alternative machine learning techniques (e.g. decision trees) may be attractive tools with which to assess morphometric data from isolated theropod teeth (Wills et al., 2021). It should be noted that performing cladistic analyses on single teeth can be time consuming: each individual tooth in a batch of "unknown" specimens has to be tested separately, or appropriately grouped into morphotypes (Hendrickx et al., 2020b). This is further exacerbated by the difficulty distinguishing the position of isolated spinosaurid teeth (Hendrickx et al., 2015b); whilst we believe a lateral position for HASMG G369a is a more likely origin (see above), spinosaurid samples could alternatively be tested in both positions. Another potential technique for investigating spinosaurid diversity in the Wealden Supergroup might be to conduct specimen-level phylogenetic analyses using Bayesian methods and incorporating stratigraphical information, a method inspired by Cau (2017).

3.7.2 Comparative anatomy

The large number of minute denticles recalls the condition present in baryonychine spinosaurids (Hendrickx et al., 2019). The presence of minute denticles on both carinae most recalls the situation of other British spinosaurid crowns, including those of *Baryonyx* (Charig et al., 1997), *Riparovenator* (Barker et al., 2021), and BEXHM 1995.485 (Barker, pers. obs., 2022; Charig et al. (1997) misreported the accession number of this specimen as "BEXHM 1993.485"); the carinae of *Ceratosuchops* are poorly preserved and its dentition will be revisited elsewhere, but denticles are present on some distal carinae at least. The denticles of the "*Suchosaurus cultridens*" type specimen (NHMUK PV R36536) are difficult to discern but this is probably due to wear (Buffetaut, 2010). Nevertheless, HASMG G369a differs from some Iberian spinosaurid teeth where a baryonychine dental morphotype lacking mesial denticles has been reported (Isasmendi et al., 2020).

Sporadic variation in denticle size is noted in baryonychines and is particularly developed in *Baryonyx* and *Iberospinus* (Hendrickx et al., 2019; Mateus et al., 2022). In contrast, those of cf. *Suchomimus* change more gradually and sporadic variation in denticle size is mainly observed on the basal portions of the teeth (Hendrickx et al., 2019). Those of the preserved mesial dentition of *Riparovenator* are similarly regular (Barker, pers. obs., 2022), as are baryonychine teeth from the Barremian–lower Aptian Cameros Basin of Spain (Isasmendi et al., 2020). HASMG G369a mirrors

the latter specimens in this regard, with the more complete distal carina possessing a largely gradual change of denticle size.

Although damaged in its basal portion, the mesial carina likely reaches or terminates very near the cervix in HASMG G369a, as is common for spinosaurids generally (Hendrickx et al., 2019). However, a few spinosaurid crowns, notably from Lower Cretaceous Iberian deposits, do display shorter carinae that extend over only half or two-thirds of the crown height (Canudo et al., 2008; Hendrickx et al., 2019; Isasmendi et al., 2020). A similar feature is also seen in *Iberospinus* (Mateus et al., 2022). Charig et al. (1997) described the carinae of BEXHM 1995.485 as failing to reach the cervix, however it would appear that the carinae have been chipped in places, and what remains basally seems to extend past the cervix.

Fluted enamel is typical of spinosaurid crowns (Hendrickx et al., 2019), and some have noted that these tend to be more numerous and better developed on the lingual surface (Buffetaut, 2012), further corroborating the orientation of the specimen described above. Those present on HASMG G369a, whilst generally weakly developed, are nevertheless in the range of several other spinosaurids: *Baryonyx* and cf. *Suchomimus* average around 6–7 flutes (range 4–8 and 2–10 respectively), whilst an average of 7–8 flutes are observed in *Irritator* (range 5–10) (Hendrickx et al., 2019). A similar range (3–9 flutes) has been observed in spinosaurid crowns from Lower Cretaceous Iberian localities (Ruiz-Omeñaca et al., 2005). However, the number of flutes in HASMG G369a differs from "*Suchosaurus*" (10–12 flutes) and several spinosaurines (17–20 flutes) (Hendrickx et al., 2019). The presence of flutes on both sides of the tooth also makes HASMG G369a different from *Baryonyx walkeri* (where the flutes are almost entirely lingually located), and is instead similar to the condition present in *Ceratosuchops*, *Riparovenator*, "*Suchosaurus*" and cf. *Suchomimus*.

Other forms of enamel ornamentation, such as the transverse undulations observed in some *Baryonyx* (NHMUK PV R9951), *Iberospinus* (ML1190) and cf. *Suchomimus* crowns (e.g. MNN G67-1), or the marginal undulations present in *Baryonyx*, *Irritator* (SMNS 58022), cf. *Suchomimus* (e.g. MNN G35-9) and indeterminate Brazilian spinosaurines (Medeiros, 2006; Hendrickx et al., 2019; Hendrickx et al., 2020b), are absent in HASMG G369a. Elsewhere, HASMG G369a shares with spinosaurids a lack of interdenticular sulci (Hendrickx et al., 2019).

The enamel texture of HASMG G369a is unusual in that two morphotypes are present: a veined textured basally and a more irregular texture apically. The former is common in spinosaurids and synapomorphic for the clade: it is present in *Baryonyx* (NHMUK PV R9951), *Iberospinus* (ML 1190) and various cf. *Suchomimus* crowns (e.g. MNN G35-9) (Hendrickx et al., 2019). Veined enamel texture is also present in *Ceratosuchops inferodios* (IWCMS 2014.95.5) and *Riparovenator*

milnerae (IWCMS 2014.95.6) (Barker, pers. obs., 2022). Indeed, HASMG 639a also possesses the strong basal curvature of the veined texture towards the adjacent carinae, which is characteristic of the clade (Mateus et al., 2011; Hendrickx et al., 2019). However, an irregular enamel texture has so far only been reported for some *Irritator* crowns among spinosaurids (Hendrickx et al., 2019).

Differences in dental characters have been used to discuss the taxonomy of isolated spinosaurid teeth (Richter et al., 2013; Fanti et al., 2014), though the utility of several traits has been questioned (Hendrickx et al., 2016). Tooth-bearing spinosaurid bones often lack erupted in-situ teeth, rendering variation between teeth within a complete tooth row poorly understood. Where teeth can be assigned to a single individual, as in the *Baryonyx walkeri* holotype NHMUK PV R9951, variation in ornamentation is documented (Hendrickx et al., 2016). Theropod dentition is also known to vary ontogenetically (Hendrickx et al., 2019) and it remains possible that differences in spinosaurid crown ornamentation may reflect ontogeny or tooth position more than phylogenetic position (Hendrickx et al., 2016).

Spinosaurid teeth are sometimes confused for those of crocodyliforms (Sánchez-Hernández et al., 2007; Bertin, 2010; Buffetaut, 2010; Hone et al., 2010a), and the latter are well represented and taxonomically diverse in the Purbeck Group and Wealden Supergroup of southern England (Benton et al., 1995b; Salisbury, 2002; Salisbury et al., 2011). The crocodyliform fauna recovered from the Hastings Group is dominated by goniopholidids but also includes atoposaurids, bernissartiids and indeterminate mesoeucrocodylians and eusuchians (Salisbury et al., 2011). However, we can confidently dismiss a crocodyliform origin for HASMG G396a based on several lines of evidence.

Numerous “ridges” (i.e. flutes) ornament the enamel of goniopholidid and pholidosaurid crowns; in *Goniopholis* and *Pholidosaurus* for instance, these are well defined and closely packed (Owen, 1840–1845; Owen, 1878;1879; de Andrade et al., 2011; Martin et al., 2016; Allain et al., 2022), whereas those of HASMG G369a are fewer and poorly defined. Interestingly, Owen (1840–1845) drew attention to the differences present between enamel ornamentation of “*Suchosaurus cultridens*” relative to that of *Goniopholis*. Smooth carinae are observed in goniopholidids generally, although false-ziphodont serrations are present in some taxa (e.g. *G. kiplingi*) (Salisbury et al., 1999; de Andrade et al., 2011; Puértolas-Pascual et al., 2015). The latter are clearly distinguishable from the true denticles of HASMG G369a. Similarly, the mesial and distal carinae of pholidosaurids such as *Pholidosaurus* lack denticles, and can barely be differentiated from the flutes on the enamel surface (Martin et al., 2016). HASMG G396a is evidently not referable to atoposaurids, due both to the small size (<1m) of representative taxa (e.g. *Theriosuchus*) (Schwarz

et al., 2005) and their distinctive distal dentition (Salisbury et al., 2011; Young et al., 2016). Fluted, conical teeth are present in the mesial dentition of bernissartiids, but these are also represented by small (<1m) taxa (Sweetman et al., 2015; Martin et al., 2020). In addition, their mesial teeth lack serrations and possess incipient cervical constriction (Norell et al., 1990; Martin et al., 2020). The short, rounded posterior crowns of bernissartiids are also obviously incompatible with the conidont morphology of HASMG G369a (Norell et al., 1990; Sweetman et al., 2015; Martin et al., 2020). In conclusion, we can reject with confidence the possibility that HASMG G369a might be considered referable to Crocodyliformes.

3.7.3 The British spinosaurid record and biogeography of early spinosaurids

Most British spinosaurid skeletal (i.e. non-dental) material has been recovered from the Barremian strata of Surrey (Upper Weald Clay Formation) and the Isle of Wight (Wessex Formation and base of the Vectis Formation) (Charig et al., 1986; Martill et al., 1996b; Charig et al., 1997; Milner, 2003; Barker et al., 2021; Barker et al., 2022). However, spinosaurid teeth are relatively common throughout the Wealden Supergroup (Fowler, 2007; Turmine-Juhel et al., 2019). While this is well known, the extent of the British spinosaurid record, and how it compares to that of other localities globally, has yet to be rigorously analysed.

The spinosaurid crown BEXHM 1995.485 is briefly described by Charig et al. (1997) as originating from the “Ashdown Sand (Hauterivian)” near Bexhill in East Sussex, which Milner (2003) considered to be the earliest record of Spinosauridae. The term “Ashdown Sands” is now defunct (Hopson et al., 2008), having been introduced by Drew (1861) before being formalised to Ashdown Formation by Rawson (1992). The latter is now considered late Berriasian to early Valanginian in age (Hopson et al., 2008). More recently, Turmine-Juhel et al. (2019) described and figured two poorly preserved crowns (BEXHM 2019.49.251 and BEXHM 2019.49.253) which they referred to *Baryonyx* sp. All three teeth were found at the same site – the Pevensey Pit at Ashdown Brickworks (Turkey Road, Bexhill-on-Sea; J. Porter and D. Brockhurst, pers. comms., 2022) – where the only exposures are of the Valanginian Wadhurst Clay Formation (Turmine-Juhel et al., 2019). BEXHM 1995.485 therefore cannot be Hauterivian or from the Ashdown Formation, contra Charig et al. (1997) and Milner (2003).

Modern interest in spinosaurids has resulted in the discovery of several Wealden Supergroup teeth in collections of crocodylomorph material housed in various institutions (Milner, 2003; Buffetaut, 2007; Fowler, 2007; Buffetaut, 2010). However, the historic nature of many of these specimens impacts our ability to identify their precise stratigraphic position. Fowler (2007) described a pair of spinosaurid crowns within a collection of goniopholidid teeth (NHMUK PV

R1901) from the "Wealden" of Hastings, a provenance which would make them Valanginian or possibly Berriasian. Elsewhere, Bertin (2010), following Lydekker (1888), listed a "*Suchosaurus cultridens*" crown (NHMUK PV R635) as originating from the Berriasian-Valanginian "Hastings Sands" of Sandown. Older works suggested that the "Hastings Sands" were represented on the Isle of Wight (White, 1921). However, the oldest exposed Wealden Supergroup strata on the Isle of Wight are from the entirely Barremian upper portion of the Wessex Formation (Sweetman, 2011; Radley et al., 2012d) and this specimen is probably Barremian in age.

It would thus appear that the oldest British spinosaurid material is definitively Valanginian in age, with Berriasian occurrences remaining a possibility for some specimens of undetermined provenance. In comparison, the oldest specimens from Iberia – the other European hotspot for spinosaurid remains – are late Hauterivian in age (Malafaia et al., 2020a). Fowler (2007) described and figured a "saurian" tooth (DCM-G95a) potentially recovered from the Purbeck Group of Swanage (Dorset, UK), which possesses several spinosaurid characters such as fluted enamel ornamentation. However, it is not dissimilar to plesiosaur tooth crowns (Fowler, 2007) and is indeed most likely from a marine reptile (D. Fowler pers. comms., 2022).

Alleged Jurassic spinosaurid teeth have been reported from Tanzania (Buffetaut, 2012) and Niger (Serrano-Martínez et al., 2015; Serrano-Martínez et al., 2016). However, similarities with other theropod clades (notably ceratosaurs and megalosaurids) have been noted and doubts have been cast on the identification of these specimens (Hendrickx et al., 2019; Soto et al., 2020). An additional putative spinosaurid tooth – initially compared with the above mentioned Tanzanian material – has been described from the Jurassic of France (Vullo et al., 2014). Insufficient data exists to regard this identity as secured and, like the above Tanzanian "spinosaurid" specimens, it is probable that this tooth is also non-spinosaurid. Thus, whilst Spinosauridae likely evolved during the Jurassic (Carrano et al., 2012; Barker et al., 2021), definitive Jurassic material pertaining to the group remains elusive. Moreover, associated discussion regarding the early evolution of spinosaurid teeth, with a proposed gradual acquisition of adaptations towards piscivory (Buffetaut, 2012; Serrano-Martínez et al., 2015; Serrano-Martínez et al., 2016), are best considered speculative pending further data (Hendrickx et al., 2019; Soto et al., 2020).

A small, conidont crown (LPUFS 5737) from the Berriasian–Valanginian of Brazil (Sales et al., 2017a) may represent one of the oldest spinosaurid occurrences globally. Additional spinosaurine teeth, as well as specimens referred to Baryonychinae (e.g. LPUFS 5870) or regarded as indeterminate spinosaurids (e.g. LPUFS 5871), have also been recently recovered from the locality (Aragão, 2021; Lacerda et al., 2023). We note that the identification of these specimens is based on (sometimes limited) qualitative data and would benefit from additional support generated

using cladistic, discriminant and cluster analyses, as advocated for isolated theropod teeth in general (Hendrickx et al., 2020b). Nevertheless, evidence for spinosaurids in deposits of Berriasian–Valanginian age could complicate the biogeographic scenario proposed for the clade by Barker et al. (2021), as independently suggested by Lacerda et al. (2023). Barker et al. (2021) regarded Europe as the ancestral region but did not include specimens known from isolated teeth in their analyses. As a result, alternative biogeographical scenarios include earlier instances of dispersal from the proposed European ancestral area, or a different ancestral area altogether.

3.7.4 Spinosaurid persistence in the Late Cretaceous and status of specimen XMDFEC V10010

The results of the discriminant function analyses (supplementary information) show that XMDFEC V10010 does not associate with Spinosauridae when classified at either the clade or genus level. At the clade-level, the specimen was consistently classified as an allosauroid (Metriacanthosauridae or Allosauridae; reclassification rates = 54.46–62.12%; PC1 37.97–57.88%, PC2 19.11–31.01%), regardless of the dataset or whether serrations were considered inapplicable. At the genus-level, the allosauroid signal was retained, with the tooth most commonly referred to Early Cretaceous *Erectopus*, a tetanuran previously referred to Allosauroidea (and possibly Metriacanthosauridae) (Carrano et al., 2012). XMDFEC V10010 was also referred to the megalosauroid *Condorraptor* and the abelisaurid *Skorpiovenator* in some genus-level DFAs. Reclassification rates in the genus level analyses were generally similar to those at the clade level analyses, and ranged between 57.4–63.68%.

The cluster analyses using the hierarchical clustering option consistently recovered XMDFEC V10010 as the sister taxon to an indeterminate abelisaurid. Similarly, the neighbour-joining option also commonly recovered the tooth as sister to an indeterminate abelisaurid, with several analyses of the whole dataset also recovering XMDFEC V10010 as a sister taxon to Abelisauridae indet.+*Fukuiraptor*.

The conflicting signals produced by the above quantitative analyses on XMDFEC V10010 are perhaps expected given that the dentition of Metriacanthosauridae and Allosauridae are considered the closest to that of Abelisauridae (Hendrickx et al., 2020b), although these allosauroid clades are not known from the Late Cretaceous (Carrano et al., 2012). In comparison, abelisaurids were successful and diverse during the Late Cretaceous but are poorly represented in Asian deposits (outside of India) (Carrano et al., 2008; Delcourt, 2018). Their teeth are nevertheless relatively diagnostic; however, the dental characters that unite Abelisauridae involve the shape of the premaxillary and maxillary alveoli (which are unknown for XMDFEC V10010) or

relate to the morphology of the denticles (which are somewhat worn in XMDFEC V10010; Hone et al., 2010) (Hendrickx et al., 2019; Hendrickx et al., 2020b). Cladistic analyses of XMDFEC V10010 based on first hand examination of the specimen would be beneficial, and we refrain from referring the tooth to a theropod clade without this additional line of evidence. However the quantitative evidence presented herein corroborates previous suggestions that XMDFEC V10010 cannot be referred to Spinosauridae (Katsuhiro et al., 2017; Buffetaut et al., 2019; Soto et al., 2020). With the Patagonian late Cenomanian-early Turonian tooth referred to Spinosauridae in Salgado et al. (2009) also likely from a different theropod lineage (Soto et al., 2020), the youngest definitive spinosaurid remains appear to come from Cenomanian deposits of Africa (Ibrahim et al., 2020b; Benyoucef et al., 2022; Sereno et al., 2022).

Assuming the reinterpretation of the above-mentioned Chinese and Patagonian specimens is correct, the potential extinction of Spinosauridae around the Cenomanian–Turonian boundary (CTB) remains poorly understood (Candeiro et al., 2017). This time interval coincides with the peak Cretaceous greenhouse climate and a major marine transgression, and a marine extinction event has been documented (Sepkoski, 1986; Kerr, 2014). However, studies of the faunal changes in terrestrial, freshwater and brackish water environments during this transition are rare, and available data from North America suggests these faunas were not (a few taxa excepting) overly affected (Eaton et al., 1997; Benson et al., 2013). Spinosaurids are not definitively known from the Mesozoic of North America, however, and it may be that results inferred from these deposits may not be applicable elsewhere. Moreover, as theropods that have been positively associated with costal palaeoenvironments (Sales et al., 2016), it is interesting to speculate upon the impact of the CTB marine transgression on available spinosaurid habitat, and certainly warrants further consideration as a potential driver of their apparent extinction.

3.8 Conclusions

An isolated spinosaurid tooth crown HASMG G369a cannot be referred to *Baryonyx* based on the results of multiple quantitative and qualitative analyses, and further supports suggestions that multiple spinosaurid taxa are present within the Wealden Supergroup. Although the precise provenance of HASMG G369a could not be ascertained with certainty, it is among the oldest spinosaurid remains found in Britain and is probably Valanginian in age. Indeed, while the oldest definitive British spinosaurid material comes from this stage, Berriasian occurrences cannot be completely ruled out for some specimens. Future work should look to apply cladistic and discriminant methods on spinosaurid crowns from known strata within the Wealden Supergroup, which may help further assess the British diversity of the clade and provide information on the dental evolution of these atypical theropods.

Following the general consensus that Jurassic spinosaurid material is currently unknown, and that previously referred material represent other theropod clades (see above), a literal interpretation of the fossil record highlights Western Europe as a key region for early spinosaurid evolution, given the wealth of (albeit largely fragmentary) Early Cretaceous material. However, the presence of isolated spinosaurid teeth from the Berriasian-Valanginian of Brazil suggests that early spinosaurids were more spatially widespread, and underlines the palaeobiogeographical importance of fragmentary specimens. As such, alternative biogeographic scenarios regarding the place of origin and early movements of the clade should be examined. Meanwhile, evidence for post-Cenomanian spinosaurid persistence is not supported based on quantitative reinterpretation of dental material previously referred to the clade, and the lack of spinosaurid remains in the latter stages of the Cretaceous hints at an extinction event around the Cenomanian-Turonian boundary.

3.9 Acknowledgements

We would like to thank: Phil Hadland for access to the specimen and discussions regarding provenance; Julian Porter and David Brockhurst for information pertaining to BEXHM 1995.485; Christophe Hendrickx for discussion regarding methods; Denver Fowler for discussion regarding spinosaurid dentition; Luis Coy and Charlotte Collier for help with imagery; and Andrea Cau for help with the programme TNT. Martin Simpson is additionally thanked for assisting DN's research on the historic specimens accessioned at HASMG and BEXMH. The programme TNT is made available thanks to the Willi Hennig Society. Thanks are also extended to editor Fabien Knoll and reviewers Kirstin Brink and Marco Sales for their attention to this work.

3.10 Figures

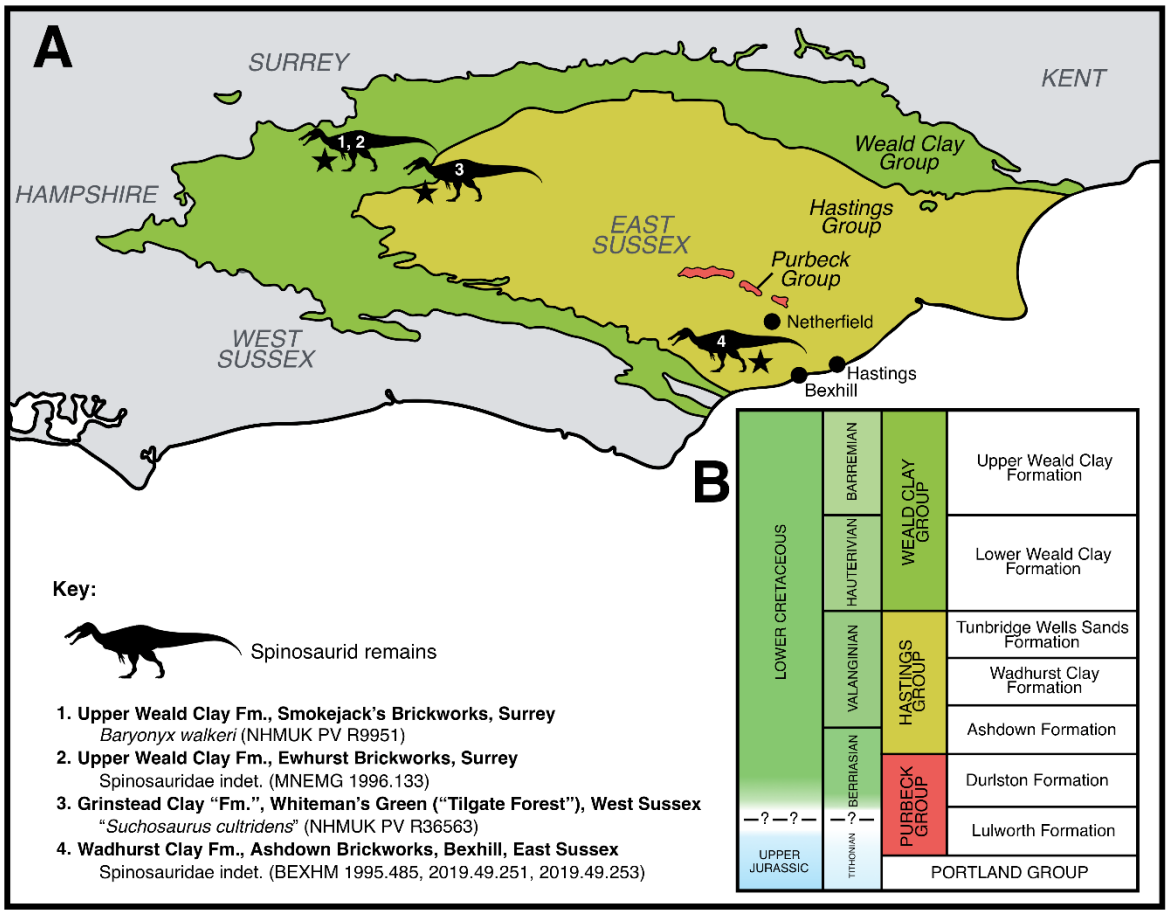

Figure 3.1 Geological context of the Lower Cretaceous deposits of southeast England, focussing on the Purbeck Group and Wealden Supergroup. A) Schematic geology of the Lower Cretaceous deposits of the Weald Sub-basin (southeast England), highlighting published spinosaurid finds (Charig et al., 1997; Salisbury et al., 2011; Turmine-Juhel et al., 2019). Based on Fig. 2 in Austen et al. (2018). Note that various additional spinosaurid teeth are known from the region but remain undescribed in detail (Fowler, 2007). B) Simplified stratigraphic column of the Weald Group in southeast England, based on Fig. 3.2 in Batten et al. (2011). Note that the Grinstead Clay Formation, which subdivides the Tunbridge Wells Sands Formation in Batten et al. (2011) and from which the "*Suchosaurus cultridens*" type specimen was discovered (Salisbury et al., 2011), is downgraded to a member of the latter formation in other works (Hopson et al., 2008) and has not been included in this column. Spinosaurid silhouette courtesy of Dan Folkes.

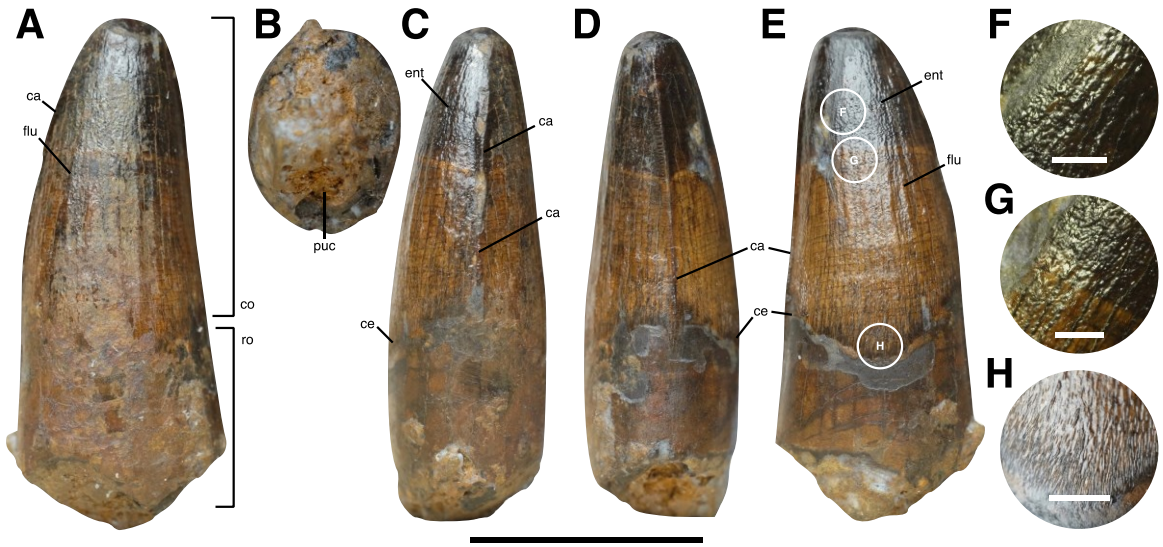

Figure 3.2 HASMG G369a, in A) lingual, B) basal, C) mesial, D) distal and E) labial view. F–G) Close up of the enamel texture on the labial tooth surface. Abbreviations: ca, carina; ce, cervix; co, crown; ent, enamel texture; flu, flute; puc, pulp cavity (infilled); ro, root. Scale bars A–E:10mm, F–G: 1mm.

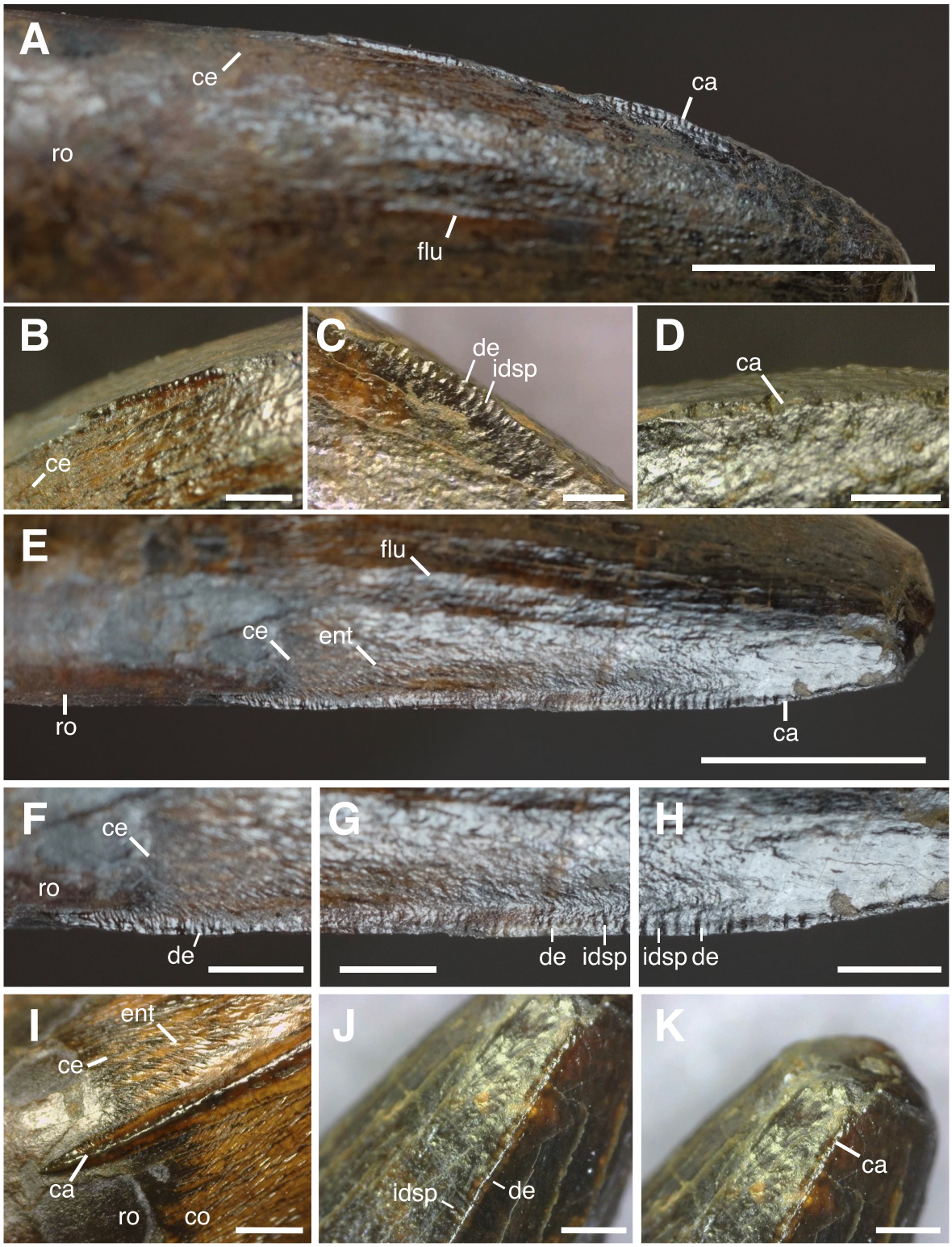

Figure 3.3 Close up of carinae and denticles of HASMG G369a under various lighting conditions. Mesial carina in A) lateral view. Close up of mesial carina in B) mesiobasal, C) mesiocentral and D) mesioapical views. Distal carina in E–H) lateral and I–J) distal views. Close up of F) distobasal carina, G) distocentral carina, H) distoapical carina. Abbreviations: flu, ca, carina; ce, cervix; co, crown; de, denticle; ent, enamel texture; flute; idsp, interdenticular space; ro, root. Scale bars: A, E) 5mm, B–D, F–K) 1mm.

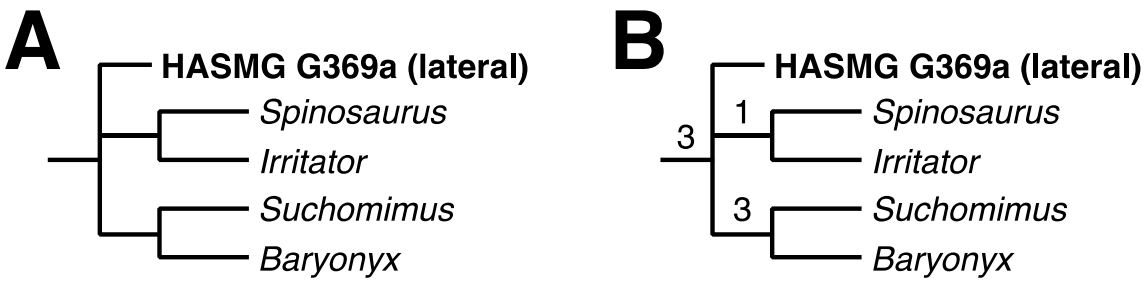

Figure 3.4 Results of the cladistic analyses. A) Strict consensus of the analysis using the whole dataset under constrained conditions. B) Reduced consensus of the unconstrained analysis using the whole dataset. Numbers at nodes indicate Bremer supports values. Full results can be found in the supplementary information.

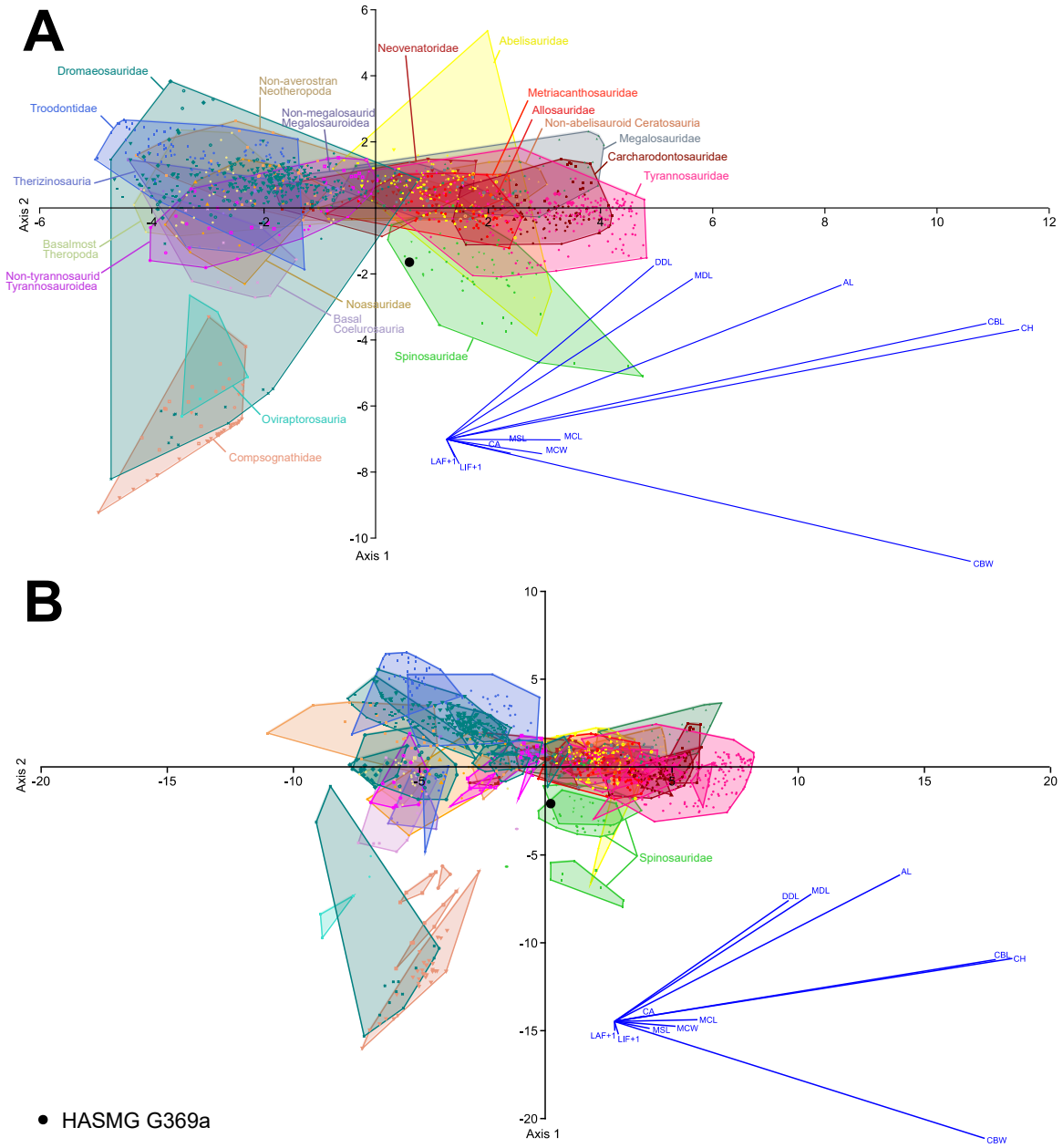

Figure 3.5 Results of the discriminant function analysis of the pan-theropodan dataset plotted along the first two canonical axes of maximum discrimination in the dataset at the A) clade level (Eigenvalue of Axis 1=5.7073, which accounts for 51.01% of the total variation; Eigenvalue of Axis 2=2.2155, which accounts for 19.8% of the total variation) and B) taxon level (Eigenvalue of Axis 1=18.377, which accounts for 41.04% of the total variation; Eigenvalue of Axis 2=9.6544, which accounts for 21.56% of the total variation), on the whole dataset consisting of 1335 crowns belonging to 89 taxa (i.e., 84 species and five indeterminate family-based taxa) separated into 20 monophyletic or paraphyletic groups. 61.02% and 61.17% of the theropod specimens were correctly classified to their respective groups and taxa, with HASMG G369a (black dot) respectively classified as a spinosaurid and *Suchomimus* at the clade and taxon-level. Abbreviations: AL, apical length; CA, crown angle; CBW, crown base

width; CH, crown height; DDC, distal denticle length; LAF+1, number of labial flutes plus one; LIF+1, number of lingual flutes plus one; MCL, mid-crown length; MCW, mid-crown width; MDL, mesial denticle length.

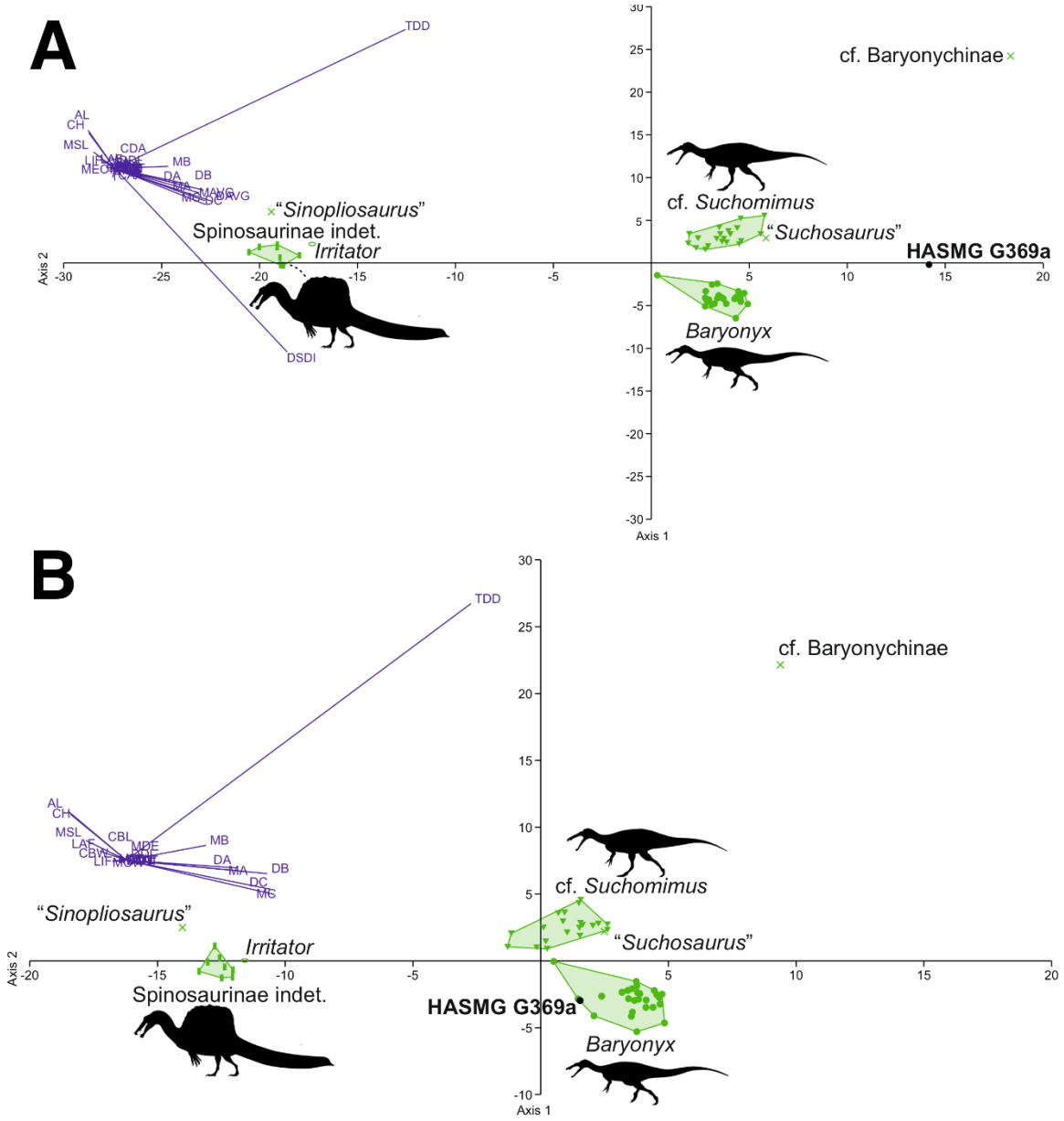

Figure 3.6 Graphical results of the discriminant analyses using a spinosaurid-only dataset comprised of 59 teeth from 7 taxa (*Baryonyx*, cf. *Suchomimus*, *Irritator*, Spinosaurinae indet., cf. Baryonychinae, "*Suchosaurus*", "*Sinopliosaurus*"), including HASMG G369a as an unknown taxon. A) Results of the analysis including all variables (PC1 72.53, PC2 20.03; Eigenvalue of axis 1: 89.905, axis 2: 24.824; reclassification rate = 98.28%), where HASMG G369a was referred to "*Suchosaurus*". B) Results of the analysis excluding ratio variables (PC1 63.73, PC2 26.12; Eigenvalue of axis 40.277, axis 2: 16.506; RR = 98.28%), where HASMG G369a was referred to cf. *Suchomimus*. Abbreviations: see Hendrickx et al. (2015a) and Richter et al. (2013). Phylopic silhouette credits: Spinosaurinae indet.: Ivan Iofrida (CC-BY-4.0, https://creativecommons.org/licenses/by/4.0/); *Baryonyx* and *Suchomimus:* Scot t Hartman (CC-BY-NC-SA-3.0, https://creativecommons.org/licenses/by-nc-sa/3.0/).

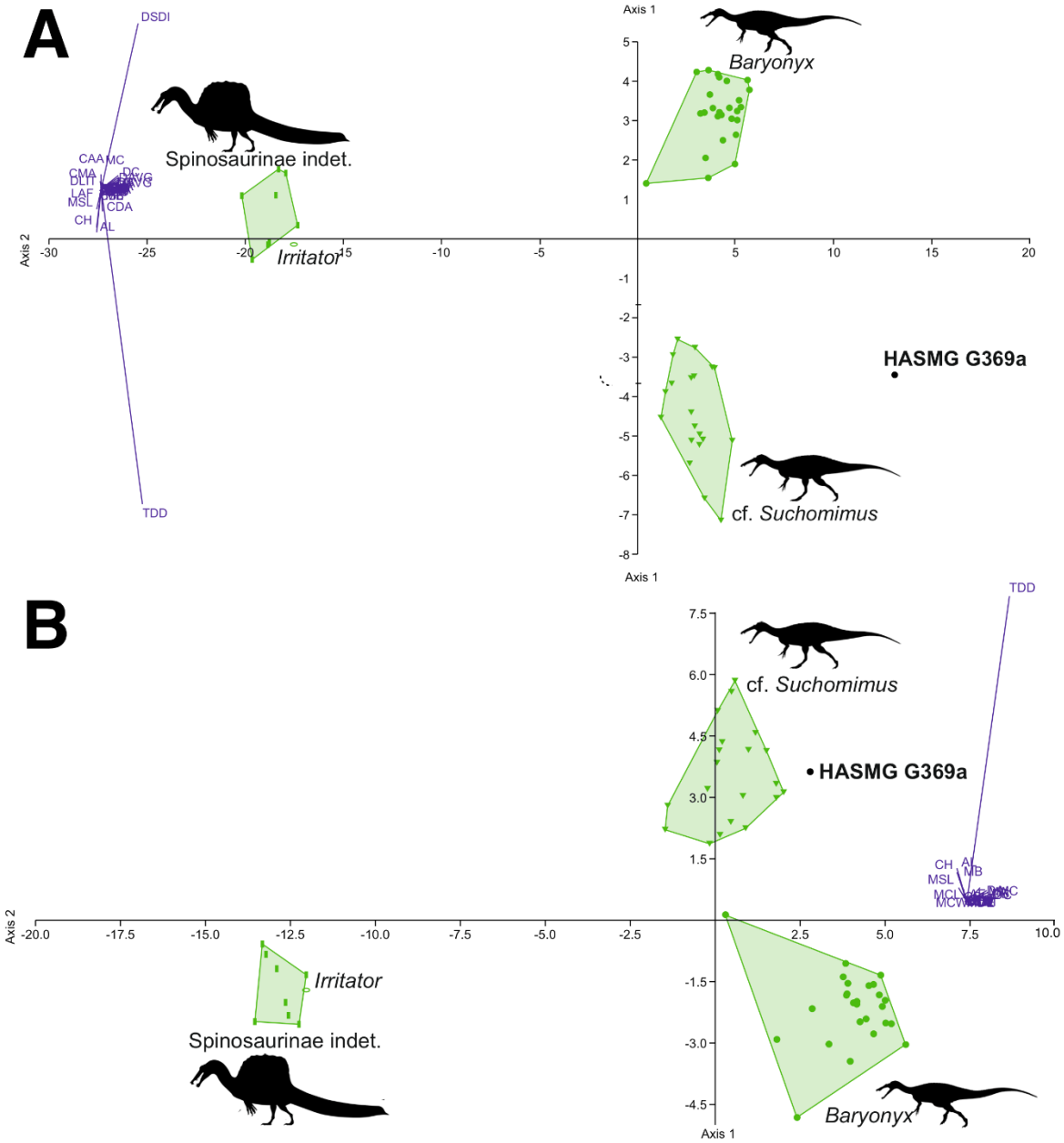

Figure 3.7 Graphical results of the discriminant analyses using a reduced spinosaurid-only dataset comprised of 56 teeth from 4 taxa (*Baryonyx*, cf. *Suchomimus*, Spinosaurinae indet., *Irritator*), including HASMG G369a as an unknown taxon. A) Results of the analysis including all variables (PC1 84.32, PC2 14.84; Eigenvalue of axis 1: 73.009, axis 2: 12.846; reclassification rate = 100%), where HASMG G369a was referred to cf. *Suchomimus*. B) Results of the analysis excluding ratio variables (PC1 82.02, PC2 17.34; Eigenvalue of axis 36.934, axis 2: 7.807; RR = 98.18%), where HASMG G369a was referred to cf. *Suchomimus*. Abbreviations and silhouette credits: as in Figure 3.6.

Chapter 4 A European giant: a large spinosaurid (Dinosauria: Theropoda) from the Vectis Formation (Wealden Group, Early Cretaceous), UK.

4.1 Authorship statement

This chapter is the product of: **Barker, C.T.**, Lockwood, J.A., Naish, D., Brown, S., Hart, A., Tulloch, E. and Gostling, N.J., 2022. A European giant: a large spinosaurid (Dinosauria: Theropoda) from the Vectis Formation (Wealden Group, Early Cretaceous), UK. *PeerJ*, 10, p.e13543.

CTB, DN, JL and NJG devised the study. CTB wrote the first draft, conducted the analysis, and created the figures. JL drafted section of the geological context as well as the biostratinomy. SB, AH and ET contributed to the interpretation of the material. All authors edited the manuscript.

The supplementary information for this chapter can be found in Appendix C and online.

4.2 Abstract

Postcranial elements (cervical, sacral and caudal vertebrae, as well as ilium, rib and limb bone fragments) belonging to a gigantic tetanuran theropod were recovered from the basal unit (the White Rock Sandstone equivalent) of the Vectis Formation near Compton Chine, on the southwest coast of the Isle of Wight. These remains appear to pertain to the same individual, with enormous dimensions similar to those of the *Spinosaurus* holotype and exceeding those of the largest European theropods previously reported. A combination of features – including the presence of spinodiapophyseal webbing on an anterior caudal vertebra – suggest that this is a member of Spinosauridae, though a lack of convincing autapomorphies precludes the identification of a new taxon. Phylogenetic analysis supports spinosaurid affinities but we were unable to determine a more precise position within the clade: weak support for a position within Spinosaurinae or an early-diverging position within Spinosauridae were found in some data runs. Bioerosion in the form of curved tubes is evident on several pieces, potentially related to harvesting behaviour by coleopteran bioeroders. This is the first spinosaurid reported from the Vectis Formation and the youngest British material referred to the clade. This Vectis Formation spinosaurid is unusual in that the majority of dinosaurs from the Lower Cretaceous units of the Wealden Supergroup are

from the fluviolacustrine deposits of the underlying Barremian Wessex Formation. In contrast, the lagoonal facies of the upper Barremian–lower Aptian Vectis Formation only rarely yield dinosaur material. Our conclusions are in keeping with previous studies that emphasise western Europe as a pivotal region within spinosaurid origination and diversification.

4.3 Introduction

The deposits of the internationally important Wessex Formation of the Isle of Wight – part of the Wealden Group (itself part of the Wealden Supergroup) – have been and remain exceptionally productive regarding dinosaur material and research (Insole et al., 1994; Sweetman, 2011; Radley et al., 2012d). Indeed, the Wessex Formation has yielded almost all dinosaur fossils known from the Isle of Wight (Martill et al., 2001b). Its fluviolacustrine sediments preserve the remains of various tetanuran theropods, rebbachisaurid and titanosauriform sauropods, and a variety of ornithischians, including ankylosaurs and ornithopods (Benton et al., 1995b; Martill et al., 2001a; Naish et al., 2007;2008; Lomax et al., 2014). In contrast, dinosaur remains are rare in the overlying Vectis Formation (Radley et al., 1998b), documented finds being limited to a handful of ornithopod, ankylosaur and indeterminate theropod specimens (White, 1921; Hooley, 1925; Blows, 1987; Benton et al., 1995b; Martill et al., 2001a; Weishampel et al., 2004; Naish et al., 2008). Ichnological remains referred to theropod, thyreophoran and ornithopod track-makers have also been reported from the Vectis Formation (Radley et al., 1998b; Pond et al., 2014).

A number of large, fragmentary dinosaur bones, encased in a matrix matching the basal unit (the White Rock Sandstone) of the Vectis Formation, were found east of Compton Chine on the southwest coast of the Isle of Wight by Mr Nick Chase, Mr Mark Penn and Dr Jeremy Lockwood. The material was found loose in an intermittently exposed gutter located around 10 m from the cliff face, and its discovery here occurred over a period of several months. Taphonomic and anatomical evidence (discussed below) show that they belong to a single individual. Some of these bones were figured and alluded to in Austen et al. (2018) but they have not previously been described. A list of character traits show that the specimen likely belongs to Spinosauridae and is thus the first member of this clade reported from the Vectis Formation. The specimen's large size is noteworthy and it appears to represent the largest theropod yet reported from the Wealden Supergroup and potentially from the European fossil record in general.

Our identification of this specimen as a spinosaurid is interesting in view of recent discoveries pertaining to spinosaurid diversity within the Wealden Supergroup. Spinosauridae is characterised by atypical cranial (and sometimes postcranial) morphologies indicative of divergent, semi-aquatic ecologies relative to related lineages (Charig et al., 1997; Amiot et al., 2009; Amiot et al., 2010a;

Ibrahim et al., 2014; Aureliano et al., 2018; Hassler et al., 2018; McCurry et al., 2019; Ibrahim et al., 2020a). Most studies support the division of Spinosauridae into Baryonychinae and Spinosaurinae (Sereno et al., 1998; Benson, 2010; Carrano et al., 2012; Arden et al., 2019; Rauhut et al., 2019b), although there are indications that support for this dichotomy may be weaker than customarily supposed (Evers et al., 2015; Barker et al., 2021). Most spinosaurids are from Early and "mid" Cretaceous strata but phylogenetic analyses support a Jurassic origin for the clade (Carrano et al., 2012; Hone et al., 2017; Barker et al., 2021) and isolated teeth suggest spinosaurid persistence into the Late Cretaceous (Santonian) (Hone et al., 2010a).

To date, all formally published British spinosaurid remains come from the Berriasian–lower Aptian Wealden Supergroup, and include *Baryonyx walkeri* from the Upper Weald Clay Formation of the Weald sub-basin (Charig et al., 1986; Charig et al., 1997), and *Ceratosuchops inferodios* and *Riparovenator milnerae* from the Wessex Formation of the Wessex sub-basin (Barker et al., 2021). Additional fragmentary material has been recovered throughout the Wealden succession (Martill et al., 1996b; Charig et al., 1997; Naish et al., 2001; Milner, 2003; Hutt et al., 2004; Buffetaut, 2010; Naish, 2011; Salisbury et al., 2011; Turmine-Juhel et al., 2019). This Wealden Supergroup material pertains exclusively to Baryonychinae and spinosaurines are currently unknown from the British fossil record. This contrasts with equivalent strata in Iberia, where evidence of both clades is known (see Malafaia et al. (2020a) for a review of the Iberian spinosaurid record).

In the present contribution, we provide osteological descriptions and comparisons of the better-preserved remains (several additional fragments, including some large pieces, could not be readily identified but are briefly reported in Appendix C), and include the "White Rock spinosaurid" in a phylogenetic analysis in order to further test its affinities. We also remark upon the biostratinomic context of these finds, and briefly describe the bioerosion apparent on several elements.

4.3.1 Institutional abbreviations

FSAC Faculté des Sciences, Casablanca University, Casablanca, Morocco; IWCMS Isle of Wight County Museum Services, Dinosaur Isle Museum, Isle of Wight, UK; MDS, Dinosaur Museum, Savannahket, Laos; MN Museu Nacional, Rio de Janeiro, Brazil; MNBN Musée National Boubou Hama, Niamey, Niger; MNEMG Maidstone Museum, Kent, UK; MNN Musée National du Niger, Niamey, Niger; MSM Museo Paleontológico Juan Cano Forner, Sant Mateu, Castellón, Spain; MUJA Museo del Jurásico de Asturias, Colunga, Spain; NHMUK Natural History Museum, London, UK; SM Sirindhorn Museum, Department of Mineral Resources, Kalasin, Thailand.

4.4 Geological context

The Wealden Supergroup of southern England is a succession of largely non-marine strata accumulated during the Early Cretaceous (late Berriasian–early Aptian) and mainly deposited in two sub-basins (Figure 4.1A): the larger Weald sub-basin of south-eastern England, and the smaller Wessex sub-basin of the Isle of Wight and central-southern England (Batten, 2011; Radley et al., 2012a).

Within the latter, the succession consists of the younger Wealden Group and older Purbeck Limestone Group. The Wealden Group on the Isle of Wight (Figure 4.1B) predominantly crops out along the island's southwest coast, with a smaller exposure occurring along the southeast coast. Both areas reveal the entirely Barremian and predominately alluvial facies of the Wessex Formation (deposited in a fluviolacustrine setting) as well as the overlying late Barremian–early Aptian Vectis Formation (Sweetman, 2011; Radley et al., 2012d) (Figure 4.1C).

The three constituent members of the 67 m thick Vectis Formation represent the return to coastal lagoonal environments that occurred prior to the Aptian marine transgression and are characterised by low diversity ostracod and mollusc assemblages (Ruffell, 1988; Radley et al., 1998b; Sweetman, 2011). The largely argillaceous Cowleaze Chine and Shepherd's Chine members form the base and top of the formation respectively, denoting low-energy subaqueous or mudflat environments. The Barremian–Aptian boundary occurs within the Shepherd's Chine Member (Kerth et al., 1988; Robinson et al., 2004). The interposing Barnes High Sandstone Member represents deltaic inundation into the lagoon (Radley et al., 1998b).

At the Atherfield type locality and extending west of Cowleaze Chine, a pale, metre-thick sandstone unit in-fills the "dinoturbated" uppermost stratum (the *Hypsilophodon* bed) of the underlying Wessex Formation and forms the base of the Cowleaze Chine Member (Radley et al., 1998b; Sweetman, 2011). Known as the White Rock Sandstone, it is interpreted as narrow fluvial channels intersecting a marginal lagoonal sand-flat deposit laid down by climatically-controlled terrestrial runoff and intermittent lagoonal influxes (Radley et al., 1998b; Sweetman, 2011). The lower part of the White Rock Sandstone is formed of laminated, cross-laminated or burrow-mottled sandstone (Radley et al., 1998b). Lenses of fusain-rich carbonaceous sandstone, organic-rich mudstones, and poorly sorted conglomerate are interspersed throughout this lower part; the conglomerates occasionally yield worn reptilian bone fragments (Radley et al., 1998b).

Due to a fault, the Vectis Formation crops out at two sites in Compton Bay, the larger exposure being located to the east near Shippards Chine and the other towards the west, nearer Compton Chine (Figure 4.2A). The specimens were all found in front of the ~34 m thick (Radley et al.,

2012d) more westerly exposure, along an approximately 50 m stretch of foreshore. Here, the basal ~60 cm unit of the Vectis Formation is lithologically variable and includes a fine sandstone and a pale jarositic siltstone, resembling the higher part of the White Rock Sandstone at the previously described type locality, and is marked at the outcrop by a line of water seepage (Radley et al., 1998a). This White Rock Sandstone equivalent forms an obvious layer that is distinct from the dark grey mud and siltstones of the lagoonal sediments of the Cowleaze Chine member and the varicoloured palaeosols or grey plant debris beds of the Wessex Formation (Figure 4.2B). Although all the spinosaurid specimens reported here were found on the foreshore, adhering matrix closely matches that of the White Rock Sandstone equivalent in all specimens, and the remains were likely present on the foreshore due to a cliff fall (though the possibility remains that their presence is due to erosion through a wave cut platform) (Figure 4.2C). Generally, the White Rock equivalent at this location contains few macroscopic fossils except for sporadic fragments of fusain and bone. Ichnites are represented by the occasional gastrolith and infrequent burrows usually ~1 cm in diameter.

4.5 Methods

4.5.1 Measurements

Measurements were taken in millimetres using digital callipers and rounded to one decimal point.

4.5.2 Terminology

Nomenclature of the vertebral neural arch fossae and laminae follows Wilson et al. (2011). Relative position within the axial series is based on the suggestions of Evers et al. (2015) and we also follow the latter authors in their repositioning of the *Baryonyx walkeri* type presacral series. Nomenclature of the various ichnological features found on these specimens follows the ichnotaxobases provided by Pirrone et al. (2014).

4.5.3 Phylogenetic analysis

The White Rock spinosaurid was included in a comprehensive phylogenetic matrix derived from Cau (2018) and implemented in Barker et al. (2021), focusing on non-coelurosaurian tetanurans. Following our positional identifications (see 4.7), IWCMS 2018.30.1 was scored as an anterior dorsal vertebra, whilst IWCMS 2018.30.3 was scored as an anterior caudal vertebra.

Scores for five character statements concerning the caudal vertebrae of the two operational taxonomic units (OTUs) *Baryonyx* (NHMUK PV R 9951) and *Riparovenator* (IWCMS 2020.447.1, 2)

were changed relative to the analysis in Barker et al. (2021). For *Baryonyx*, these changes related to the caudal neural arch characters (Ch.) 358, 359, 868 and 1576. An isolated neural arch belonging to NHMUK PV R 9951 was identified as that of an anterior caudal vertebra by Charig et al. (1997). However, the presence of a hyposphene and well-developed centrodiapophyseal laminae alternatively suggest that the element instead belongs to a posterior dorsal vertebra, an identification also proposed by Charig et al. (1997). Given this uncertainty, we opt to re-code the above character as "?". Regarding *Riparovenator*, Ch. 1035 (originally Ch. 99 of Carrano et al. (2008) and concerning caudal neural spine morphology) was mis-scored and has been changed to state 1 to reflect their abbreviated state. All other scores and OTUs remained the same as in the Barker et al. (2021) analysis, although we acknowledge the recent designation of the specimen ML 1190 as the holotype of the new spinosaurid taxon *Iberospinus natarioi* (Mateus et al., 2022), which also includes some fragmentary new material.

The final matrix contains 41 operational taxonomic units coded for 1810 binary character statements. The analysis was performed in TNT v1.5 (Goloboff et al., 2016). A driven search using 100 initial addition sequences was performed via the "New Technology Search" function, with default settings employed for sectorial, ratchet, drift and fusion. Tree islands were further explored via a round of tree bisection and reconnection (TBR) using the "Traditional search" function, and results were initially explored via a strict consensus. Improved resolution was achieved via the identification of wildcard OTUs using the iterPCR method (Pol et al., 2009) implemented in TNT (*Trees>Comparisons>Iter PCR*). A reduced consensus tree was calculated following the pruning of these OTUs.

Nodal support was assessed via Bremer (decay indices; *Trees>Bremer*) and jackknife (*Analyze>Resampling*) values. The former were obtained for the strict consensus by retaining trees suboptimal by 10 steps, whilst those of the reduced consensus were calculated using existing suboptimal trees with the exclusion of the wildcard OTUs identified previously. Jackknife values were calculated using 1000 pseudoreplicates under a "traditional search" function, also excluding *a priori* the wildcard OTUs. We report both absolute and GC frequency values.

4.6 Results

4.6.1 Systematic palaeontology

DINOSAURIA (Owen, 1842)

THEROPODA (Marsh, 1881)

TETANURAE (Gauthier, 1986)

SPINOSAURIDAE (Stromer, 1915)

Spinosauridae indet.

Referred specimens: IWCMS 2018.30, which includes a probable yet fragmentary anterior dorsal vertebra (2018.30.1), a pair of fused sacral centra (2018.30.2), a partial anterior caudal vertebra (2018.30.3), a sacrocaudal centrum fragment (2018.30.4), rib fragments (2018.30.5, 6), pieces of ilium (2018.30.7, 8) and portions of long bone (2018.30.9, 10). Several other indeterminate fragments have also been recovered (see also Appendix C).

Locality and Horizon: White Rock Sandstone equivalent, Compton Chine, Vectis Formation (late Barremian).

4.7 Descriptive osteology

4.7.1 Axial elements

4.7.1.1 IWCMS 2018.30.1 (Anterior dorsal vertebra)

This element is represented by the majority of the centrum and a portion of the right neural arch (Figure 4.3), metric data of which are presented in Table 4.1. The left side of the anterior and posterior articular facets are substantially abraded, as is the ventral rim of the anterior facet, exposing cancellous bone and its trabeculae; this ventral abrasion has also affected the anterior part of the ventral keel. A sub-circular portion of the bone has been lost from the right ventral surface, including a part of the ventral keel. The extensive damage to the neural arch and loss of most of its structures has also exposed cancellous bone across the dorsal surface, as well as on the floor of the wide neural canal. The specimen has likely experienced some plastic deformation; given the posterolaterally facing rather than laterally facing parapophysis, this deformation may be related to compressive forces.

The anteroposteriorly abbreviated centrum is opisthocoelous, with a pronounced anterior convexity and posterior concavity. The nature of the neurocentral suture is ambiguous; a suture-like feature is visible in anterior and right lateral view and located above the parapophysis, suggesting the latter is thus entirely centrum-bound if genuine. However, this structure may be a taphonomic artefact and not a suture at all.

Both articular facets are mediolaterally wide and in line with one another (i.e. the anterior facet is not dorsally offset relative to the posterior facet); the posterior facet protrudes lateral to the

extremities of the anterior equivalent when the specimen is viewed dorsally. The anterior facet lacks any notable inclination but is not uniformly convex since a subtle, median tuberosity is present. This tuberosity is visible in lateral view and protrudes a short distance anteriorly (Figure 4.3A). The dorsal margin of the anterior facet is subtly concave dorsal to the tuberosity, such that the dorsal margin is indented in anterior view. A distinct flattened rim is present on the undamaged dorsal portion of the right side of the facet, demarcated posteriorly by a low ridge.

The concave right lateral surface possesses a sediment-filled pneumatic foramen, located posteroventral to the ipsilateral parapophysis. The original shape of the foramen cannot be ascertained, and damage precludes identification of the foramen on the left side. The foramen appears to communicate with a shallow yet broad sulcus that cuts into the centrum ventral to the parapophysis (Figure 4.3A). The parapophysis is sub-circular and largely flattened.

Ventrally, the centrum possesses a stout keel, which is better developed anteriorly. A ventral fossa on the left side of the centrum contributes somewhat to the keel's pronounced nature, although this is not mirrored on the right. The posterior portion of the keel expands mediolaterally as it becomes confluent with the posterior articular margin.

Regarding its position within the axial series, the anterodorsal location of the parapophysis, sub-parallel (rather than offset) relationship between the articular facets, and possession of a prominent ventral keel (Evers et al., 2015) suggest an anterior dorsal position for IWCMS 2018.30.1. Tetanuran parapophyses typically migrate onto the neural arch between the 2nd and 7th dorsal (Holtz et al., 2004). It is unclear whether the parapophysis remains restricted to the centrum in the specimen discussed here but its position is most similar to that present in the second dorsal vertebrae of *Baryonyx* (NHMUK PV R9951; fourth dorsal of Charig et al., 1997) and second and third dorsals of cf. *Suchomimus* (MNBH GAD70, Ibrahim et al. (2020b): Figure 130). Accordingly, we identify IWCMS 2018.30.1 as a second or third dorsal vertebra.

Table 4.1 Metric data for IWCMS 2018.30.1. Asterisk denotes taphonomic damage. Measurements are in millimetres (mm).

Anteroposterior length of the centrum (between ventral rims)*	69.4
Dorsoventral midline height of the anterior articular facet*	75.3
Mediolateral width of the anterior articular facet*	99.2
Dorsoventral midline height of the posterior facet*	92.5
Mediolateral width of the posterior facet*	118.5
Dorsoventral height of the right parapophysis	27.8

Anteroposterior length of the right parapophysis	25.7
Mediolateral width of the neural canal	39.7

4.7.1.2 IWCMS 2018.30.2 (Sacral vertebrae)

Two sacral centra, fused at their intercentral junction, are known (Figure 4.4): the centra are relatively well preserved, but the neural arches and sacral ribs are missing. The only breakage consists of shallow cracks on the smooth external surfaces of the centra, and a large oblique transverse crack near the posterior articular facet of the more posterior centrum. Abrasion has damaged several surfaces to some extent, but most notably affects the sacral rib attachments as well as both articular facet rims and the conjoined intercentral junction, where the underlying trabeculae are exposed. With regard to abrasion of the exposed anterior and posterior facets, the external bone in the more anterior centrum is largely intact in anterior view, whereas abrasion of the facet rims is more extensive in the posterior element when it is viewed posteriorly (the central portion of this facet is nonetheless preserved). An indeterminate mass of bone and matrix is cemented onto the floor of the neural canal of the more posterior centrum. Metric data are presented in Table 4.2.

The robust centra are longer than tall, and are approximately in line with one another. The exposed hemielliptical anterior facet of the anterior element is flat and notably larger than the sub-circular posterior facet of the more posterior element. The latter appears convex, although this is likely due to abrasion of the facet's rim.

The sacral rib attachments are large, subtriangular and located anterodorsally on the lateral surfaces of the centra. They are asymmetrical in the anterior element, and the right attachment facet appears larger and more prominent. On the posterior centrum, the sacral rib attachments appear less developed, although it seems likely they have been substantially weathered. The floors of the intervertebral foramina are visible bilaterally as wide and posteroventrally trending channels present on the dorsal surface of the more posterior centrum.

The dorsolateral surfaces, ventral to the neurocentral junction, are variably indented. The right lateral depression on the anterior centrum is best developed, in contrast to its far shallower counterpart, whilst those on the posterior centrum are more similar in development. These depressions do not house pneumatic foramina, and their poor development indicates these are unlikely to pertain to a pneumatic system.

The ventral margins are only shallowly concave in lateral view. The ventral surface of the anterior centrum is rounded in transverse section along its length. Similar rounding is present on the

posterior centrum; however, this element goes on to develop a shallow midline sulcus posteriorly. This sulcus is associated with a degree of mediolateral expansion of the bone, with the latter centrum thus appearing posteriorly wider relative to the equivalent end of the anterior element when viewed ventrally.

The relative position of the sacral vertebrae is difficult to determine given their incompleteness, and it is perhaps unusual that elements of this size are not more extensively fused to other sacral elements. The plesiomorphic dinosaurian (and archosaurian) sacrum consisted of two “primordial vertebrae” (Langer et al., 2006; Moro et al., 2021). This count increased to five in tetanurans via the addition of dorso- and caudosacrals (Holtz et al., 2004). The primordial sacral vertebrae are thought to fuse prior to the evolutionarily ‘younger’ elements (O'Connor, 2007), suggesting that IWCMS 2018.30.2 may represent this pair in the absence of a completely fused series. However, recognition of sacral fusion patterns in theropods remain complicated (Moro et al., 2021) and the identification of primordial sacrals is largely based on their sacral ribs and associated attachment points on the ilium (Nesbitt, 2011), neither of which can be assessed here.

Table 4.2 Metric data for IWCMS 2018.30.2. Asterisk denotes taphonomic damage. Measurements are in millimetres (mm).

Maximum anteroposterior length of the conjoined centra	298
Anteroposterior length of anterior centrum	~156
Anteroposterior length of posterior centrum	~142
Dorsoventral midline height of the exposed anterior articular facet*	118.1
Mediolateral midline width of the exposed anterior articular facet*	126.2
Dorsoventral midline height of the exposed posterior facet*	107.9
Mediolateral width of the exposed posterior facet*	102.7
Mediolateral width of the neural canal	40.7

4.7.1.3 IWCMS 2018.30.3 (Anterior caudal vertebra)

A large partial caudal vertebra preserves only its posterior portion, having suffered a transverse shear posterior to the prezygapophyses (Figure 4.5). It is among the most complete and informative of the elements known for this dinosaur. Fine cracks are apparent across the external bone surfaces, most notably affecting the centra. Both transverse processes and the neural spine have been lost, whilst abrasion to the postzygapophyses and margins of various neural arch laminae is apparent. Minor crushing appears to affect the left side of the element, as evidenced

by the flattening of the ipsilateral rim of the posterior articular facet in posterior view. The left portion of said facet also appears abraded such that the underlying trabecular bone is exposed; abrasion also affects the rim of the right half of the facet. Metric data are presented in Table 4.3.

In life, the centrum was tall relative to its width (Figure 4.5A), with the dorsoventral midline height of the posterior facet appearing unaffected by the crushing experienced along its left lateral side. The lateral margins are concave in coronal section, as is the ventral margin in lateral view. It is difficult to determine whether the neurocentral suture is closed: in places, the suture looks highlighted by specks of a black mineral (which also dots many of the abraded surfaces and cracks throughout the element), but it is unclear if this represents retention of the open state or is a taphonomic artefact. The broken anterior surface does not preserve obvious evidence of internal pneumatic features such as camerae or camellae (Britt, 1993;1997) (Figure 4.5B). The distinction between the cortical and cancellous bone is obvious in places, with the former measuring 4.8mm on the left ventrolateral side; it appears to thin dorsally towards the neurocentral suture. The cross-section of the infilled neural canal is visible in anterior view. It is largely circular, but its mid-ventral margin bulges ventrally.

The ventral surface of the centrum is heavily distorted. Although no keel is present, crushing on the left side has distorted the surface and its original shape can only be supposed; based on the better-preserved right side, it was likely largely convex in transverse section (Figure 4.5C).

The lateral surfaces of the centrum present an elongate pleurocentral depression dorsally. On the better-preserved right side, a trifecta of small and presumably vascular foramina penetrate the right lateral surface. The dorsal two are smaller and located along the anterior and posterior ventral margins of the pleurocentral depression, with the larger, more ventral foramen positioned in line with the latter. Posteriorly, the mid-dorsal rim of the tall and moderately concave posterior articular facet is shallowly indented, above which sits the inversely ovate neural canal.

The neural arch is robust, with thick walls made visible in the anterior cross-section. It preserves various fossae, some of which are delimited by stout laminae and may bilaterally vary in shape (Figure 4.5D–F). Along the anterodorsal midline, the spinoprezygapophyseal fossa is deepest posteriorly and narrows mediolaterally towards the neural spine, being bordered by variably developed laminae; the right lamina is sharper than the contralateral structure. The dorsal rim of the former lamina is more complete, preserving a dorsally curving anterior portion where it rose to meet the ipsilateral prezygapophyseal pedicle in lateral view.

Prezygocentrodiapophyseal and centrodiapophyseal fossae excavate the lateral neural arch surfaces. The former are deep and possess a largely triangular outline via two constraining

laminae: the largely horizontal prezygodiapophyseal lamina forms its dorsal border, while the notably thick and obliquely oriented anterior centrodiapophyseal lamina delimits the fossa ventrally. The latter also forms the anterior margin of the bilaterally asymmetrical centrodiapophyseal fossae. The left is more developed, excavating the neural arch ventral to the transverse process to a deeper extent; the right, fossa, in contrast, is hardly perceptible. Posteriorly, the posterior centrodiapophyseal lamina forms a thick buttress to the transverse process. What remains of the transverse processes indicate these were massively constructed and possibly posterolaterally projecting. Postzygocentrodiapophyseal fossae are absent in this element.

The neural spine is posteriorly positioned on the neural arch. The base of the spine is mediolaterally thin and anteroposteriorly short. It is bilaterally webbed via variably developed spinodiapophyseal sulci and ridges (Figure 4.5F, G). The postzygapophyses are insufficiently preserved at their posterior ends to warrant useful description, although the dorsoventrally tall spinopostyzygapophyseal fossa they enclosed is narrow and slit-like. No obvious hyposphene is present ventral to the remnants of the postzygapophyses (indeed, there appears to be no space between the spinopostzygapophyseal fossa and dorsal margin of the neural canal in which one could be present), although a small mass of cemented bone and sandstone overhangs the neural canal posteriorly.

The positioning of IWCMS 2018.30.3 within the caudal series derives from multiple lines of evidence. Indeed, several more anterior axial positions can be readily excluded. The dorsal positions of the transverse processes and their buttressing laminae eliminate most of the cervical series from consideration. In addition, the absence of a ventral keel is inconsistent with the condition present in posterior cervicals and anterior dorsals. The absence of internal pneumaticity within the centrum also indicates a more posterior position given that pneumatisation of the cervical and anterior dorsal centra is the “common pattern” amongst theropods (Benson et al., 2012). The lack of sacral ribs or their facets excludes a sacral position. Finally, the ovate shape of the posterior articular facet resembles the condition present in theropod posterior dorsal and anterior caudal vertebrae (Rauhut, 2003), as does the presence of spinodiapophyseal webbing (observed in such elements in spinosaurid taxa especially).

We consider it most likely that IWCMS 2018.30.3 represents an anterior caudal vertebra, rather than the mid- or posterior dorsal vertebra for several reasons: a hyposphene, postzygocentrodiapophyseal fossae and accessory centrodiapophyseal laminae are all absent, and the neural spine is anteroposteriorly short. Hyposphenes are typical of dorsal vertebrae in large saurischians (although they can occur in the posterior cervical and anterior caudal vertebrae too)

(Rauhut, 2003; Langer, 2004; Stefanic et al., 2019), and are present in the mid- and posterior dorsal vertebrae of *Baryonyx* (NHMUK PV R9951) (Charig et al., 1997), IWCMS 2012.563 (Hutt et al., 2004), *Suchomimus* (MNN GDF 500) and *Ichthyovenator* (MDS BK 10-01) (Allain et al., 2012) where they are ventral to a broad spinopostzygapophyseal fossa and separate the latter from the neural canal. Hyposphene-free anterior caudal vertebrae are common amongst spinosaurids (Barker et al., 2021): a hyposphene is present in the putative anterior caudal neural arch of *Baryonyx* (Charig et al., 1997) but – as discussed above – the identification of this element as an anterior caudal vertebra may be an error. The absence of a hyposphene means that the spinopostzygapophyseal fossa is located dorsal to the neural canal (as seen in IWCMS 2018.30.3). The fossae concerned may also be narrower than their equivalents in the dorsal vertebrae, as noted in the anterior caudal vertebrae of *Riparovenator* (Barker et al., 2021) and *Vallibonavenatrix* (Malafaia et al., 2020b), although we concede that the narrow condition present in IWCMS 2018.30.3 may be exaggerated by loss of its postzygapophyses.

The pair of centrodiapophyseal fossae in IWCMS 2018.30.3 also differs from the three present in the mid and posterior dorsal vertebrae of such spinosaurids as *Baryonyx* (Charig et al., 1997), *Ichthyovenator* (Allain et al., 2012), *Vallibonavenatrix* (Malafaia et al., 2020b), *Spinosaurus* (Stromer, 1915) and *Suchomimus* (MNN GDF 500). Some of these taxa present an accessory centrodiapophyseal lamina in this vicinity, a trait typically recovered as synapomorphic of Baryonychinae but also present in the phylogenetically labile taxon *Ichthyovenator* (Holtz et al., 2004; Benson, 2010; Allain et al., 2012; Carrano et al., 2012; Rauhut et al., 2019b; Barker et al., 2021). Given the absence to date of spinosaurine spinosaurids (see also below) in the Wealden Supergroup, an accessory lamina might be expected if this element were a mid- or posterior dorsal vertebra.

The lack of a chevron facet – a characteristic feature of caudal vertebrae – would appear to count against a caudal identification for IWCMS 2018.30.3. However, chevron facets are absent on the anteriormost caudal centra of some tetanurans (Holtz et al., 2004). Further support for a caudal identification is provided by the anteroposteriorly short and posteriorly positioned neural spine, the position and anatomy of which recalls the condition in the anterior caudal vertebrae of *Riparovenator* (Barker et al., 2021) (see also Table 4.4). Caudal vertebrae of basal tetanurans may be amphicoelous or amphiplatyan (Holtz et al., 2004), and the concave posterior facet of IWCMS 2018.30.3 recalls the amphicoelous anatomy of *Spinosaurus* (Stromer, 1915), *Ichthyovenator* (Allain et al., 2012), the spinosaurine FSAC-KK 11888 (Ibrahim et al., 2020a) and *Vallibonavenatrix* (Malafaia et al., 2020b).

Table 4.3 Metric data for IWCMS 2018.30.3. Asterisk denotes taphonomic damage. Measurements are in millimetres (mm).

Dorsoventral height of posterior articular facet	159.8
Mediolateral width of the posterior articular facet*	112.8
Anteroposterior depth of the concavity of the posterior articular facet*	25.3
Anteroposterior length of the preserved centrum (right side)	106.5
Dorsoventral height of the anterior neural canal	38.6
Mediolateral width of the anterior neural canal	29.5
Anteroposterior length of the base of the neural spine	49.6
Mediolateral width of the base of the neural spine	16.8

4.7.1.4 IWCMS 2018.30.4 (Sacrocaudal fragment)

The damaged and fragmentary vertebra (Figure 4.6A–D) was also recovered; it lacks many of its original margins and its dorsal surface is obscured by matrix. Useful morphometric data is difficult to obtain in light of its preservation. Its asymmetry presumably represents a degree of plastic deformation. The anterior and posterior surfaces have been damaged, although one surface (perhaps the posterior one, see below) appears to preserve a degree of bevelling in its ventral part, though this may be taphonomic in origin. The fragment possesses a width of 68.1 mm (measured across the ventral midpoint), a maximum height of 70.6 mm, and a maximum length of 74.6 mm. The most noteworthy osteological feature pertains to a prominent and wide anteroposteriorly oriented sulcus on its ventral surface.

The longitudinal ventral sulcus of IWCMS 2018.30.4 suggests that this fragment might be an incomplete caudal centrum. Ventral sulci are common on theropod caudal vertebrae including those of spinosaurids (Samathi et al., 2021), although we note that Rauhut (2003) did not observe any in the cf. *Suchomimus* caudal element MNN GDF 510. Whilst ventral sulci can be narrow in theropod caudal centra (Rauhut (2003), they are broad in some taxa, including some large megalosaurids (Rauhut et al., 2018). Additionally, the fragment is similar in ventral view to the anterior caudal vertebrae of *Vallibonavenatrix* (Malafaia et al. (2020b): Fig 6E), which also possess a broad ventral sulcus bordered by parallel crests. The somewhat bevelled ventral portion of the posterior surface may be a chevron facet. However, we cannot exclude the possibility that IWCMS 2018.30.4 is a sacral vertebra: it is similar to the other sacral elements in width, and the presence

of a ventral sulcus is a feature seen in spinosaurid sacral vertebrae, including those of *Vallibonavenatrix* (Malafaia et al., 2020b) and possibly *Camarillasaurus* (Samathi et al., 2021).

4.7.1.5 IWCMS 2018.30.5 and 6 (Rib fragments)

A pair of rib shaft fragments are preserved (Figure 4.6E–J), although it cannot be determined whether they pertain to the same element. The larger one, which is associated with a confused mess of bone fragments cemented to its surfaces, has a length of 194.0 mm. The other measures 144.3 mm and is largely well preserved despite the loss of its dorsal and ventral segments. A triangular cross-section with rounded corners is apparent in the latter, the widest of the three surfaces measuring 80.8 mm. Whilst this morphology was likely present ventrally in the larger piece (despite the damage sustained to one of the margins), this fragment appears to flare and flatten dorsally. The internal cross-section of the smaller fragment is infilled with cancellous bone. Such internal organisation could not be reliably ascertained via macroscopic examination of the larger fragment's extremities.

4.7.2 Appendicular elements

4.7.2.1 IWCMS 2018.30.7 and 8 (Ilium fragments)

A pair of fragments representing a single, postacetabular process of a right-sided ilium were recovered. The fragments are poorly preserved and do not fit back together, though it would appear that only a slither of material is missing (Figure 4.7). The fragments are large and robustly built, and lack any evidence of pneumaticity.

The remains of the brevis fossa can be distinguished, preserved as at least two separate pieces; the anterior piece measures ~135 mm (anteroposterior length), and the more posterior fragment ~145 mm. The medial side has been mostly stripped of its overlying cortical bone. The dorsally projecting postacetabular blade is missing, and what remains are medial and lateral blades that together enclose the brevis fossa. The former is incomplete and its extent difficult to assess, although it likely faced mainly ventrally. Enough of the ventrolaterally projecting lateral blade is well preserved to describe its generally thick and rounded morphology, posteriorly increasing ventrolateral projection, and flattened lateral surface. While stout anteriorly (with a dorsoventral thickness of 41.9 mm), it appears to thin posteriorly (dorsoventral height: 21.9 mm) before thickening again (dorsoventral height: 34.1 mm). When viewed ventrally, both pieces describe a posteriorly expanding fossa. A small neurovascular foramen is present on the anterior margin of the more anterior piece.

Additional fragments probably pertain to the ilium given their triradiate and triangular cross-section, but are very poorly preserved. These are briefly reported in Appendix C.

4.7.2.2 IWCMS 2018.30.9 and 10 (Long bone fragments)

Two transverse slices of a long bone are preserved (Figure 4.8), one with a largely sub-circular cross-section while the other likely possessed a more ovate cross-section in life. Both are damaged and offer little of note bar their diameter (107.8 mm and 123.7 mm respectively) and asymmetrical cortical bone thickness. The space enclosed by the cortical bone is occupied by cancellous bone with no evidence of a medullary cavity, perhaps suggesting the pieces derived from the metaphyseal region of the limb bone. It is uncertain as to whether both belong to the same element, and to which element that may be, although we presume it originates from the pelvic limb given the rest of the material recovered for this individual.

4.8 Theropod affinity of the material

Multiple lines of evidence suggest the material pertains to a large theropod dinosaur. Whilst the neural arch fossae and delimiting laminae support the saurischian affinities of IWCMS 2018.30.3 more generally (Wilson et al., 2011), the presence of a pneumatic foramen posterior to the parapophysis supports theropodan or neotheropodan affinities of the anterior presacral vertebra IWCMS 2018.30.1 (Carrano et al., 2012; Cau, 2018). The opisthocoelous condition of the latter's centrum (Holtz et al., 2004) is common within the cervical and anterior dorsal vertebrae of non-coelurosaurian tetanurans; indeed, opisthocoely is synapomorphic of carnosaur cervicals in certain analyses (Rauhut, 2003; Rauhut et al., 2019b) and is notably pronounced in allosauroids and megalosauroids (Evers et al., 2015). Elsewhere, the pronounced, well-developed brevis fossa of the ilium has been considered diagnostic of Theropoda in some previous works (Gauthier, 1986), although a large and expanded brevis fossa on the ilium is observed for dinosaurs more generally (Hutchinson, 2001). Also of note is the relatively thin-walled nature of the long bones fragments, a trait also deemed synapomorphic for Theropoda (Gauthier, 1986).

Sauropods share opisthocoelous and pneumatic cervical and anterior dorsal vertebrae with some theropods (Upchurch et al., 2004; Upchurch et al., 2011) but several lines of evidence are inconsistent with a sauropod identity for the Compton Chine material. If a cervical position is assumed for IWCMS 2018.30.1 (see 4.7 for further comments regarding element position), subdivision of the pneumatic foramen would be expected (Upchurch, 1995; Whitlock, 2011). Moreover, cervical ventral keels are rare in sauropods and their parapophyses – which are typically indented – consistently maintain a ventral position throughout the series (Upchurch et al., 2004). Similarly, if an anterior dorsal position is assumed, the element's generally abbreviated

dimensions are inconsistent with a sauropod identity, since these vertebrae are the longest of the dorsal series in Sauropoda (Upchurch et al., 2004). In addition, while opisthocoelous and ventrally keeled cervical and anterior dorsal vertebrae are present in large ornithopod vertebrae from the Wealden Supergroup (Norman, 2011), skeletal pneumaticity is absent within Ornithischia (Rauhut, 2003). Further, the proposed caudal element IWCMS 2018.30.3 lacks the ossified tendons present on the neural spines of ornithopod vertebrae near the pelvis (Norman, 2011), and lacks the rectangular outline of the anterior caudal vertebrae of basal iguanodontians (Norman, 2004). Referral to either Sauropoda or Ornithopoda can thus be rejected.

More specifically, the flattened peripheral rim around the anterior articular surface observed in IWCMS 2018.30.1 is characteristic of megalosaurian cervical vertebrae (Carrano et al., 2012), although it can be observed in anterior dorsal vertebrae as well (e.g. *Baryonyx*; Charig et al. (1997)). Additionally, the presence of spinodiapophyseal webbing in IWCMS 2018.30.3 is characteristic of spinosaurid dorsal vertebrae (or various spinosaurid in-groups, depending on the analysis) (Rauhut, 2003; Holtz et al., 2004; Benson, 2010; Carrano et al., 2012; Evers et al., 2015; Rauhut et al., 2019b; Barker et al., 2021) and have been documented in spinosaurid anterior caudal vertebrae as well (Barker et al., 2021; Samathi et al., 2021). Coria et al. (2016) described the presence of webbing in the dorsals of some megaraptorans, although the clade currently lacks any presence in the European record (White et al., 2020). Thus, combined with our phylogenetic results (see 4.9), we consider the presently discussed material to pertain to a large spinosaurid.

4.9 Phylogenetic analysis

The New Technology Search returned 30 trees of 2451 steps and consistency (excluding the 1068 parsimony uninformative characters deactivated using the command *xinact*), rescaled consistency, and retention indices (CI, RCI and RI) of 0.374, 0.171 and 0.456 respectively. The round of TBR recovered 22535 trees. The strict consensus tree finds Spinosauridae to be completely unresolved (Figure 4.9A). Seven other spinosaurid OTUs (*Irritator*, MSNM V4047, *Sigilmassasaurus*, '*Spinosaurus* B', ML 1190, *Vallibonavenatrix* and *Camarillasaurus*) were identified as wildcard taxa following the iterPCR method.

Interestingly, the reduced consensus recovered a baryonychine-spinosaurine split, with the White Rock spinosaurid placed as an early-branching member of Spinosaurinae (Figure 4.9B), albeit with limited support. Three characters were shared between the White Rock spinosaurid and other spinosaurines, all from the anterior caudal series: the presence of centrodiapophyseal laminae (Ch. 358:1), the presence of prezygodiapophyseal laminae (Ch. 626:1), and the presence of a deep

prezygocentrodiapophyseal fossa (Ch. 1605:1). Jackknife resampling (Figure 4.9C, D) also recovered low nodal support (both absolute and GC frequency values), with the White Rock spinosaurid instead assuming a position amongst Spinosaurinae or recovered in a polytomy outside Baryonychinae and Spinosaurinae.

4.10 Remarks

4.10.1 The White Rock spinosaurid: a British spinosaurine?

The recovery of the White Rock spinosaurid as an early branching member of Spinosaurinae in some data runs is intriguing, especially considering the current absence of the clade from Lower Cretaceous deposits of the British Isles. Spinosaurines may have originated in Europe (Barker et al., 2021), and phylogenetic and quantitative analyses of fragmentary materials support their presence in the quasi-contemporaneous deposits of Iberia (Sánchez-Hernández et al., 2007; Alonso et al., 2016; Alonso et al., 2018; Isasmendi et al., 2020; Malafaia et al., 2020a). The three above-listed spinosaurine synapomorphies were also recovered in the previous iteration of the analysis used here (Barker et al., 2021).

However, the distribution of these three caudal character states could potentially be a function of the relative position of these elements along the axial column. Indeed, specimens such as FSAC-KK 11888 (Ibrahim et al., 2020a) and MN 4743-V (Bittencourt et al., 2004) appear to show that fossae and laminae become less prominent in the more posterior parts of the axial skeleton. We consider IWCMS 2018.30.3 to be more anteriorly placed than any of the known caudal elements of *Riparovenator* or *Vallibonavenatrix* (specimens that are also known from anterior caudal material); scores regarding fossae or laminae for the latter pair's anterior caudal series might thus be affected by a lack of positional overlap. Comparisons are exacerbated by our incomplete knowledge of the anteriormost caudal series of other relevant taxa, such as *Baryonyx* and *Suchomimus* (Charig et al., 1997; Sereno et al., 1998). In addition, the presence of centrodiapophyseal (Ch. 358:1) and prezygodiapophyseal laminae (Ch. 626:1) is not unique to Spinosaurinae: rather, these character states are homoplastic amongst tetanurans. Our understanding of character distribution within spinosaurid tails would very obviously benefit from the discovery of more complete (i.e. overlapping) anterior caudal vertebrae from non-spinosaurine taxa.

In sum, we do not consider the recovered synapomorphies to be sufficiently diagnostic or the nodal support sufficiently robust to warrant referral of the White Rock spinosaurid to Spinosaurinae at this time.

4.10.2 Further comparisons

The presence of a sub-parapophyseal sulcus in the probable dorsal vertebra IWCMS 2018.30.1 is similar to the (albeit better developed) sulci described in the anterior dorsal centrum of the indeterminate tetanuran *Vectaerovenator* (Barker et al., 2020). Similarly positioned sulci are present in the possible megalosauroid *Yunyangosaurus* (Dai et al., 2020). While *Vectaerovenator*'s incomplete nature requires that its phylogenetic position remains ambiguous, it is interesting that constrained phylogenetic analyses found that few extra steps were required to recover it within Megalosauroidea (Barker et al., 2020) and it possesses at least some features (including enlarged pneumatic foramina) akin to the synapomorphic condition of megalosaurian anterior dorsal centra (Carrano et al., 2012). However, caution is advised when discussing this character in IWCMS 2018.30.1, given the state of preservation on the contralateral side that precludes assessment of any mirroring.

The possible presence of a median tuberosity in IWCMS 2018.30.1 is similar to that observed in the posterior cervical and anterior dorsals of *Sigilmassasaurus* (Evers et al., 2015), and would suggest the feature is more broadly distributed amongst spinosaurids. What remains of the ventral keel in this specimen is prominent and straight, as seen in Spinosauridae (Evers et al., 2015; Barker et al., 2021). The robust ventral keel differs from theropods more generally, however, with anterior dorsal centra in particular typically producing deep, sharp keels (Rauhut, 2003). However, robust keels may occur around the cervicodorsal region and are perhaps a function of overall size, given the tendency for increased keel robusticity in larger elements of some spinosaurid material (Evers et al., 2015).

The shallowly concave, nearly horizontal lateral profile of the ventral margins of the sacral vertebrae (IWCMS 2018.30.2) is typical of many theropods. They lack the strongly arched condition of various ceratosaurs (Carrano et al., 2008; Carrano et al., 2012; Rauhut et al., 2019b). The anteroposteriorly elongate centra are similar to those of other spinosaurids including *Suchomimus*, *Vallibonavenatrix* and *Camarillasaurus*, although such dimensions also occur in some ceratosaurs and *Megalosaurus* (Samathi et al., 2021). The presence of a ventral sulcus on the posterior sacral centrum recalls a similar structure on the third sacral of *Vallibonaventrix* (Malafaia et al., 2020b) but it does not extend as far anteriorly in the White Rock spinosaurid. The sacral centra also recalls *Vallibonaventrix* and the lost *Spinosaurus aegyptiacus* type specimen (Stromer, 1915) in possessing depressed lateral surfaces. So called sacral “pleurocentral depressions” have been deemed synapomorphic for Allosauria and Megalosauridae in some analyses (Carrano et al., 2012; Rauhut et al., 2019b), but are also present in various coelurosaurs (Holtz et al., 2004), with those of IWCMS 2018.30.2 poorly developed compared to such taxa as

Megalosaurus (Benson, 2010) and *Allosaurus* (Gilmore, 1920). As above, we consider the features in IWCMS 2018.30.2 to represent non-pneumatic lateral indentations; the centra thus remain apneumatic, as is typical of non-avian theropods but contrasts with the condition in *Vallibonavenatrix* (Malafaia et al., 2020b).

The anteroposteriorly narrow neural spine (relative to neural arch length) of IWCMS 2018.30.3 differs from longer condition observed in the "pelvic" axial series (i.e. the vertebral series encompassing the posterior dorsals to the anterior caudals) of such spinosaurids as *Baryonyx* (Charig et al., 1997), *Ichthyovenator* (Allain et al., 2012) and *Suchomimus* (the latter only preserves large, sheet-like neural spine tips in its anterior caudal series; Sereno et al. (1998): Fig. 3). When caudal elements are compared (Table 4.4), IWCMS 2018.30.3 is closest to *Riparovenator*, although (as mentioned previously) we consider the anteriormost preserved caudal element of the latter to occupy a comparatively more posterior position. Indeed, IWCMS 2018.30.3 differs from *Riparovenator* in the absence of an anterior spur (=accessory neural spine of some) at the base of the neural spine. Anterior spurs are more common towards the mid-caudal series in taxa possessing this feature (Rauhut, 2003), and are similarly absent from the anteriormost elements of *Ichthyovenator* (Allain et al., 2012) and the entirety of the caudal series of FSAC-KK 11888 (Ibrahim et al., 2020a).

Table 4.4 Size of the anterior caudal neural spine base (collected from the most anterior preserved caudal element) relative to their respective neural arch in select spinosaurids. Note that data for key taxa (e.g. *Baryonyx* and *Suchomimus*) is missing due to preservation. Asterisk denotes minimum metric due to preservation. Where neural arch base lengths are unknown, centrum length is used (denoted by †). Data collected from Allain et al. (2012), Ibrahim et al. (2020a) and Samathi et al. (2021). *Riparovenator* and FSAC-KK 11888 calculated via images using the scale function in FIJI (Schindelin et al., 2012).

Specimen	**Spinosauridae indet. (IWCMS 2018.30.3)**	**" Phuwiang spinosaurid B" (SM-PW9B-15)**	***Riparovenator* (IWCMS 2020.447.3)**	***Ichthyovenator* (MDS BK10-02)**	**Spinosaurinae indet. (FSAC-KK 11888)**
Basal neural arch length (mm)	112.9*	69	~138	101†	~55
Basal neural spine length (mm)	49.6	53	~45	68	~101
Neural spine length:neural arch length	0.43*	0.77	0.33	0.67	0.54

Additionally, the lack of postzygocentrodiapophyseal fossae in IWCMS 2018.30.3 suggests a difference in centrodiapophyseal fossae morphology in this individual relative to some other spinosaurids. Three centrodiapophyseal fossae are present in the neural arches of the anterior caudal vertebrae of such specimens as the spinosaurine FSAC-KK 11888 (Ibrahim et al., 2020a), MN 4743-V (Bittencourt et al., 2004), and the 'Phuwiang spinosaurid B' material (SMPW9B-14, 15) (Samathi et al., 2021). However, as noted above, more convincing comparison can only take place when better corroboration pertaining to the proposed axial position of IWCMS 2018.30.3 occurs. Elsewhere on IWCMS 2018.30.3, the presence of pleurocentral depressions is also shared with the anterior caudal vertebrae of *Vallibonavenatrix* (Malafaia et al., 2020b) and *Iberospinus* (Mateus et al., 2022), as well as the megalosaurids *Torvosaurus*, *Megalosaurus* and *Wiehenvenator* (Rauhut et al., 2016; Rauhut et al., 2019b).

The posteriorly diverging margins of the brevis fossa (IWCMS 2018.30.7, 8) recall the condition in *Baryonyx* (Charig et al., 1997) and *Vallibonaventarix* (Malafaia et al., 2020b); indeed, this character state has previously been suggested as a synapomorphy of Baryonychinae *sensu* Barker et al. (2021). It is, however, also wide in the spinosaurine FSAC KK11888 (O. Rauhut, pers. comms. 2022). In *Ichthyovenator*, a taxon recovered in Barker et al. (2021) as a spinosaurine but whose affinities are not entirely clear (Evers et al., 2015), the fossa is narrow and with subparallel margins (Allain et al., 2012). Posterior expansion of the brevis fossa is nevertheless common in Neotheropoda (Carrano et al., 2012) and is present in a variety of tetanurans (Benson, 2010), indicating a wider distribution of the character state.

4.10.3 Brief biostratinomic comments

All elements that make up the specimens described here are highly fragmented. The transverse slices of long bone show variation in cortical thickness, perhaps exacerbated by varying degrees of delamination. Other elements display cracked, crazed and irregular surface markings. The best-preserved bones – the fused sacral vertebral centra (Figure 4.4) – show longitudinal cracking, while some other bored elements (see below; Figure 4.10) possess reasonably preserved cortex on one surface but roughened, irregular looking cortical surfaces elsewhere. These changes equate to stages 1-3 in Behrensmeyer's (1978) scale of weathering and abrasion, suggesting a possible pre-burial interval of 3-4 years. Given the highly fragmentary state, we note that trampling may also have occurred (Britt et al., 2009), and perhaps accounts for the crushed in left lateral surface of IWCMS 2018.30.3 in particular.

Bioerosion, represented by curved tubes of uniform width, is present on several elements and is interpreted as representing invertebrate feeding traces (Figure 4.10A–G). These extend into the

cancellous bone for ~80 mm and have circular cross-sections with a diameter of ~10 mm. Terrestrial bone borings with equivalent diameters have been recorded in the Upper Jurassic and throughout the Cretaceous (Rogers, 1992; Paik, 2000; Csiki, 2006; Britt et al., 2008). In all cases, beetles (Coleoptera) were considered the most likely bioeroders. No bioglyphs are visible on our specimen, although the boring infills have been left in situ. When reassembled, the more medially placed circular cross-section in Figure 4.10G abuts the marginally placed end of the longitudinal section of its counterpart in Figure 4.10F, indicating the possibility of a right-angled branch or direction change. The borings were infilled by matrix and macroscopic bone chippings or frass are absent. This suggests that burial occurred after the bioerosion occurred.

Britt et al. (2008) considered borings more than 5 mm in depth to be ethologically indicative of internal mining or harvesting of bone. Necrophagous coleopterans and their larvae (in particular desmestids) are among the most common invertebrate bone modifiers (Xing et al., 2013) and feed on desiccated carcasses that are subaerially exposed (Bader et al., 2009; Cruzado-Caballero et al., 2021); osteophagy occurs when other food sources are exhausted (Bader et al., 2009), bone borings being more typically related to pupation (Höpner et al., 2017). Regardless, bioerosion created by dermestid-type beetles can involve the creation of tunnel (=tube)-like structures (Britt et al., 2008; Höpner et al., 2017; Cruzado-Caballero et al., 2021).

Circumstantial support for the possible importance of dermestids as bone modifiers in Wealden environments is provided by the existence of this group in the Middle Jurassic (Deng et al., 2017) and the fact that beetles are the most abundant Wealden Supergroup insect, the caveat here being that they are mostly represented by elytra (which are largely non-diagnostic to family level) (Jarzembowski, 2011).

Several other necrophagous insect groups can be excluded from consideration (Bader et al., 2009; Xing et al., 2013; Cruzado-Caballero et al., 2021): hymenopterans and isopterans typically produce star-shaped features and isopterans tend to cause more widespread, irregular damage, rather than tunnels (Huchet, 2014); tineid moths (Lepidoptera) specialise in keratinous tissues and traces made by them have yet to be identified in the fossil record; and the burrows of mayfly (Ephemeroptera) larvae are typically narrow, U-shaped, thin walled, and limited to aquatic environments anyway. Damage by other aquatic organisms such as burrowing bivalves are also improbable given the taphonomic circumstances and the curved form of the structures (such molluscs usually produce clavate-shaped borings; McHugh *et al.,* 2020), whilst the parallel-sided morphology with lack of splitting makes plant root damage unlikely (Rogers, 1992).

An additional trace can be observed on the abraded medial surface of a fragment of ilium. It takes the form of a straight, wide, parallel-sided ‘furrow’ that extends across the exposed cancellous

bone (Figure 4.7A) (at mid-length, some of the furrow's margins have seemingly been eroded). As furrows typically describe open excavations affecting cortical bone (Britt et al., 2008; Pirrone et al., 2014), this structure might represent one side of a tube akin to those described above. Additional divot-like impressions are present on other pieces of the ilium, but these are difficult to separate from non-biological damage and are not considered further here. Elsewhere, several tooth mark-like traces are observed on the smaller rib fragment. However, they likely do not represent vertebrate feeding traces (D. Hone, pers. comms. 2021). In sum, we tentatively attribute the traces to coleopteran bioerosion related to harvesting behaviour, but note that additional study is required.

4.11 Discussion

The presence of multiple theropod – and specifically spinosaurid – characters across various elements, combined with the consistency in specimen size, preservation and adhering matrix, supports their referral to a single spinosaurid individual. Given the material's state of preservation, more precise identification is not currently possible, and the specimen is best classified as Spinosauridae indet. The White Rock spinosaurid likely does represent a new taxon, but we are unable to diagnose it based on the material to hand.

The discovery of this specimen in the basal unit of the Vectis Formation renders it the youngest documented spinosaurid material from the Wealden Supergroup. Previous finds from the Wealden Group had been restricted to the underlying Wessex Formation (Martill et al., 1996b; Hutt et al., 2004; Barker et al., 2021) and no spinosaurid material is known from equivalent outcrops in Dorset (Penn et al., 2020). A possible contemporary is perhaps represented be a worn tooth crown (NHMUK PV R 5165, initially referred to *Goniopholis crassidens*) recovered from Atherfield on the Isle of Wight (Fowler, 2007), a locality that contains outcrops of the Vectis Formation. Unfortunately, precise stratigraphic information is missing for this specimen.

Comparisons with the spinosaurid record from the younger members of the neighbouring Weald Clay Group are more difficult. The Upper Weald Clay Formation yielded the type specimen of *Baryonyx walkeri* (Charig et al., 1986) and is largely synchronous with the exposed Wealden Group strata on the Isle of Wight. The base of this formation is Barremian in age, but its upper age has proven difficult to constrain and may be late Barremian or early Aptian (Radley et al., 2012c); indeed, the palynomorph, ostracod and mollusc faunas of the upper units of the Upper Weald Clay Formation are similar to those of the Vectis Formation (Radley et al., 2012c). However, the *Baryonyx walkeri* type specimen was recovered from Smokejacks Pit in Ockley, Surrey, whose exposures in the Upper Weald Clay Formation are consistent with an early Barremian age (Ross et

al., 1995; Radley et al., 2012c). A baryonychine tooth crown (MNEMG 1996.133) was recovered from Ewhurst's Brickworks (Surrey) from a layer equivalent to the top of the Smokejacks beds (Charig et al., 1997). We are unaware of any younger spinosaurid occurrences from the Weald Clay Group, although the historical nature of many accessioned Wealden specimens renders it difficult to collate precise stratigraphic information. Nevertheless, spinosaurids are known from the late Barremian and early Aptian of Iberia (Malafaia et al., 2020a), suggesting the potential existence of younger British specimens.

Despite the general rarity of Vectis Formation dinosaur remains, ichnological evidence from the White Rock Sandstone suggests the sandflat facies supported large dinosaur populations that visited the fluctuating, plant colonised shoreline (Radley et al., 1998b; Radley et al., 2012d). More generally, the recovery of spinosaurid remains from this formation is perhaps expected. Not only are its units within the temporal span of the clade, spinosaurid remains from lagoonal deposits have been documented elsewhere (see Bertin (2010) for a review of depositional environments containing spinosaurid remains), and their occurrences have been shown to correlate with 'coastal' palaeoenvironments (relative to other sampled taxa) (Sales et al., 2016), a broad category that includes paralic environments (Butler et al., 2008).

A remarkable feature of the White Rock spinosaurid is its large size (Table 4.5). Large theropods from the underlying Wessex Formation include the allosauroid *Neovenator salerii* (Hutt et al., 1996; Brusatte et al., 2008) and the spinosaurids *Ceratosuchops* and *Riparovenator* (Barker et al., 2021). While ichnological evidence reinforces the presence of particularly large forms in the Wessex Formation (Lockwood, 2016), the size of the Vectis Formation spinosaurid appears to eclipse the above taxa, as well as other European theropods.

The fragmentary megalosaurine caudal vertebra MUJA-1913 is currently regarded as the largest European theropod skeletal material (based on the dorsoventral height of its posterior articular facet). Its size suggests an individual more than 10m in length (Rauhut et al., 2018). A set of large caudal vertebrae from the Oxfordian (Jurassic) of France with potential megalosaurid affinities are said to be of comparable size, but have yet to be published in detail (Pharisat, 1993; Rauhut et al., 2018). IWCMS 2018.30.3 exceeds the dorsoventral proportions of MUJA-1913 (Table 4.5). Similarly, the anterior sacral vertebra of the White Rock spinosaurid is larger anteroposteriorly (~156 mm) than that of spinosaurids for which data is known, including *Vallibonavenatrix* (five recovered vertebrae, length range: 90–96 mm) (Malafaia et al., 2020b) and FSAC KK-11888 (three vertebrae, length range: 135–145 mm) (Ibrahim et al., 2014), being sub-equal to the largest sacral element of the *Spinosaurus* type specimen (of the three recovered vertebrae, lengths for the two most complete ones are >130 mm and 155 mm) (Stromer, 1915). The brevis fossa in IWCMS

2018.30.7 also supports these extrapolations: the maximum measurable width is 84.6 mm but the fossa probably flared to a greater width when complete. In comparison, the fossa has a maximum width of ~50 mm in *Ichthyovenator* (based on Allain *et al*. 2012: Fig. S7), 60 mm in *Vallibonavenatrix* (Malafaia et al., 2020b), and ~70 mm in *Allosaurus* (based on Madsen (1976): pl. 46B).

Table 4.5 Comparative dorsoventral heights (in millimetres) of the posterior articular facets of the caudal vertebrae of various tetanurans. Where several caudal vertebrae are known, the largest is presented here. Note that only data for the anterior articular facet is available for the lost *Spinosaurus* holotype and FSAC KK-11888 (marked by an asterisk). Data collected from Stromer (1915); Dong et al. (1983); Charig et al. (1997); Brochu (2003): Fig. 59A; Allain et al. (2012); Hendrickx et al. (2014b); Rauhut et al. (2018); Ibrahim et al. (2020a); Samathi et al. (2021) and Mateus et al. (2022). Measurements for *Riparovenator* taken by CTB.

Spinosauridae								**Other tetanurans**			
Spinosauridae indet. (IWCMS 2018.30.3)	*Baryonyx* (NHMUK PV R9951)	*Riparovenator* (IWCMS 2020.447.7)	*Ichthyovenator* (MDS BK10-03)	*Spinosaurus* (BSP 1912 VII 19)	Spinosaurinae indet. (FSAC KK-11888)	Phuwiang spinosaurid B" (SM-PW-9B-17)	*Iberospinus* (ML 1190-15)	*Tyrannosaurus rex* (FMNH PR2081)	*Yangchuanosaurus magnus* (CV00216)	*Torvosaurus gurneyi* (ML 1100)	Megalosaurinae indet. (MUJA-1913)
159.8	110	125.6	128	135*	129*	88	100.7	~257	140	145	150

Aureliano et al. (2018) suggested that the evolution of large body sizes (i.e. 10–15 m) in Spinosaurinae may be linked to their semi-aquatic specialisations; indeed, selection for increased size has been noted amongst aquatic vertebrates in general (Heim et al., 2015; Gearty et al., 2018). However, the definition of 'semi-aquatic' remains problematic within the context of spinosaurid ecology; not only is the degree of aquatic adaptation within spinosaurines a disputed issue (Hone et al., 2019), there is also the fact that the apparently less aquatic baryonychines (Arden et al., 2019; Hone et al., 2021), such as *Suchomimus*, also exceeded 10 m (Sereno et al., 1998; Therrien et al., 2007). At the time of writing the degree and nature of aquatic adaptations within spinosaurids remains the topic of research (Ibrahim et al., 2014; Barker et al., 2017; Henderson, 2018; Hone et al., 2019; Ibrahim et al., 2020a; Hone et al., 2021; Fabbri et al., 2022b); nevertheless, it is not clear that giant size in Spinosaurinae is linked to aquatic habits. Indeed, the

especially large baryonychine *Suchomimus* was recently inferred to be less aquatically adapted than the "subaqueous" foragers *Baryonyx* or material referred to *Spinosaurus* (Fabbri et al., 2022b) on the basis of histological data. If valid, this indicates a lack of correlation between size and aquatic ecology. Moreover, these histological results are not incompatible with the wading hypothesis suggested for Spinosauridae (Hone et al., 2021), rather than the more specialised "subaqueous foraging" ecology suggested for *Baryonyx* and cf. *Spinosaurus* in particular (Fabbri et al., 2022b). The discovery of the large-bodied White Rock spinosaurid, lacking unambiguous spinosaurine affinities or obvious traits suggestive of enhanced aquatic specialisation (e.g. the long bone cross-sections do not appear to be particularly dense), also lends support to this contention. Histological sectioning of this material, and comparison to results collected for other spinosaurids (Fabbri et al., 2022b), would nevertheless be beneficial, especially given the limited histological data known for spinosaurids (Cullen et al., 2020). Such analysis is beyond the scope of the present report.

In sum, whilst the precariousness of extrapolating overall body size from singular bones and dimensions cannot be understated, the impressive proportions of the White Rock spinosaurid material (IWCMS 2018.30.3 in particular) demonstrate the presence of a notably large tetanuran in the Wealden Supergroup of Britain: one that rivalled or even exceeded the largest theropods recovered elsewhere from the European Mesozoic.

4.12 Conclusions

The White Rock spinosaurid represents the first documented spinosaurid from the Vectis Formation of the Isle of Wight, extending the temporal span of the clade in the British fossil record to the late Barremian. This stratigraphic positioning also renders it the youngest spinosaurid known from the UK. The White Rock spinosaurid is likely a novel taxon: however, the specimen lacks convincing autapomorphies and we presently opt to identify the specimen as Spinosauridae indet. Our phylogenetic analysis was unable to resolve its position within Spinosauridae but weakly supported spinosaurine or early-branching spinosaurid affinities were recovered in some data runs. Though fragmentary, it is the largest theropod currently known from the Wealden Supergroup, with some metrics exceeding those of the largest theropods known from Europe more generally.

4.13 Acknowledgements

We thank Serjoscha Evers and Steve Hutt for useful comments regarding spinosaurid vertebral anatomy; Dave Hone for thoughts on vertebrate feeding traces; Steve Vidovich for advice on the

phylogenetic analysis; Phil James (ilium and long bone fragments) and Mick Green (axial elements) for their expert preparation of the material; and Mark Penn for kindly donating a vertebral fragment. We also thank editor Andrew Farke and the two reviewers, whose comments and expertise improved the manuscript. The program TNT is made available thanks to the Willi Hennig Society.

4.14 Figures

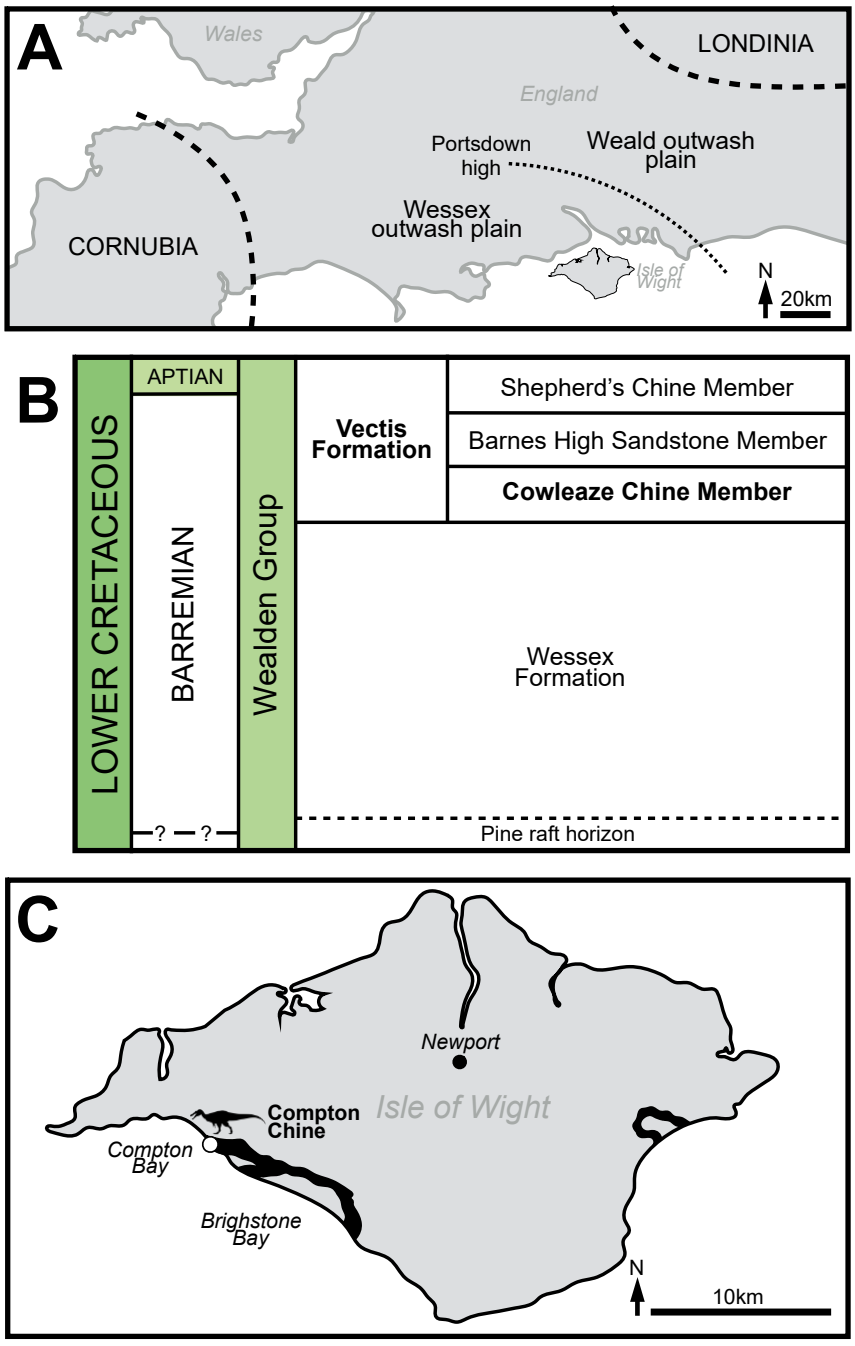

Figure 4.1. General geological context of the White Rock spinosaurid material. A) Schematic palaeogeographic map of the Wealden Supergroup, highlighting the Wessex and

Weald sub-basins (from Barker et al. (2021), modified from Penn et al. (2020): Fig. 2); B) Schematic stratigraphy of the Wealden Group on the Isle of Wight (modified from Radley and Allen (2012c): Fig. 6), with relevant strata highlighted; C) Map of the Isle of Wight, highlighting the outcrops of the Vectis Fm. and location of the spinosaurid remains (modified from Ruffell (1988): Fig. 1). Spinosaurid silhouette courtesy of Dan Folkes.

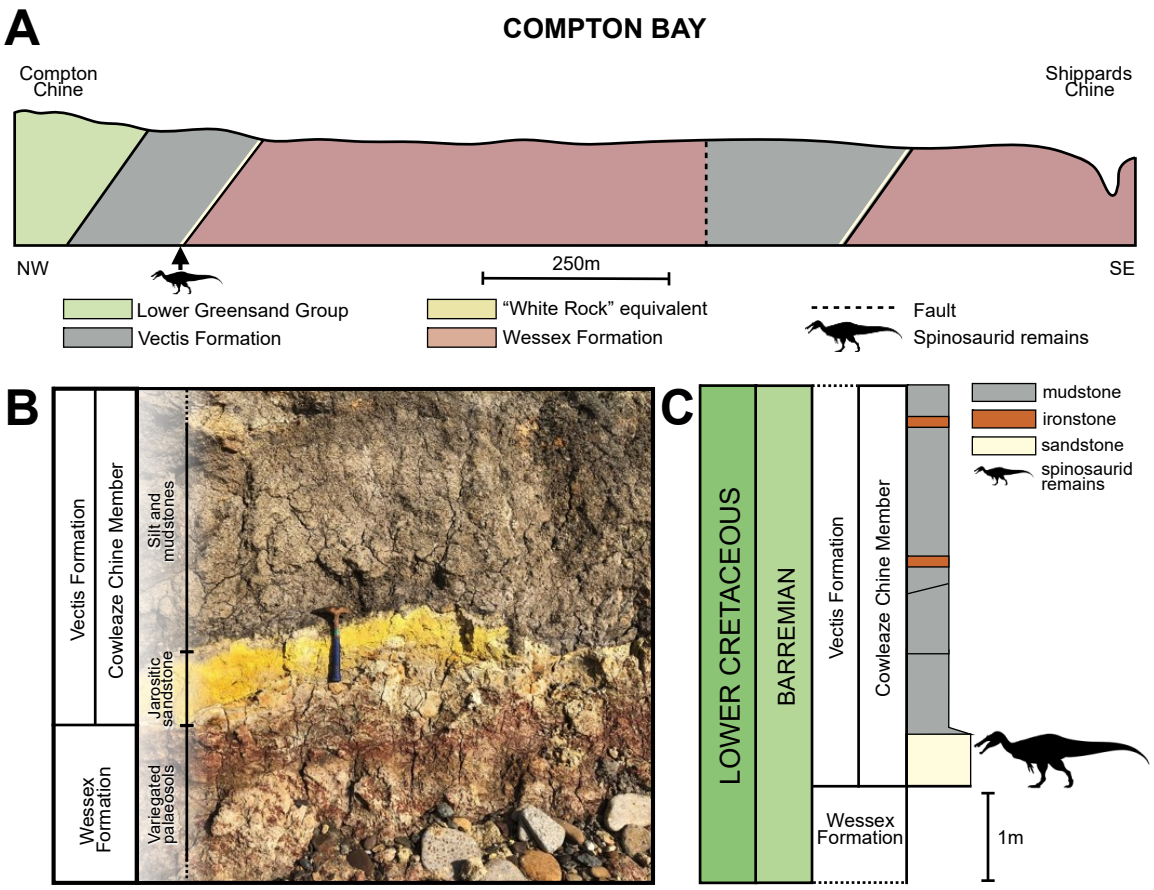

Figure 4.2 Stratigraphic context of the White Rock spinosaurid material. A) View of the cliff between Compton Chine and Shippards Chine (Compton Bay), highlighting the members of the Weald Group and overlying Lower Greensand Group (from Radley et al. (1998a): Fig. 2); B) Junction between the Wessex and Vectis formations located towards Compton Chine; C) Vertical section through the lower unit of the Vectis Formation, Compton Bay, Isle of Wight (modified from Radley et al. (2012d): Fig. 26). Spinosaurid silhouette courtesy of Dan Folkes (CC-BY 4.0).

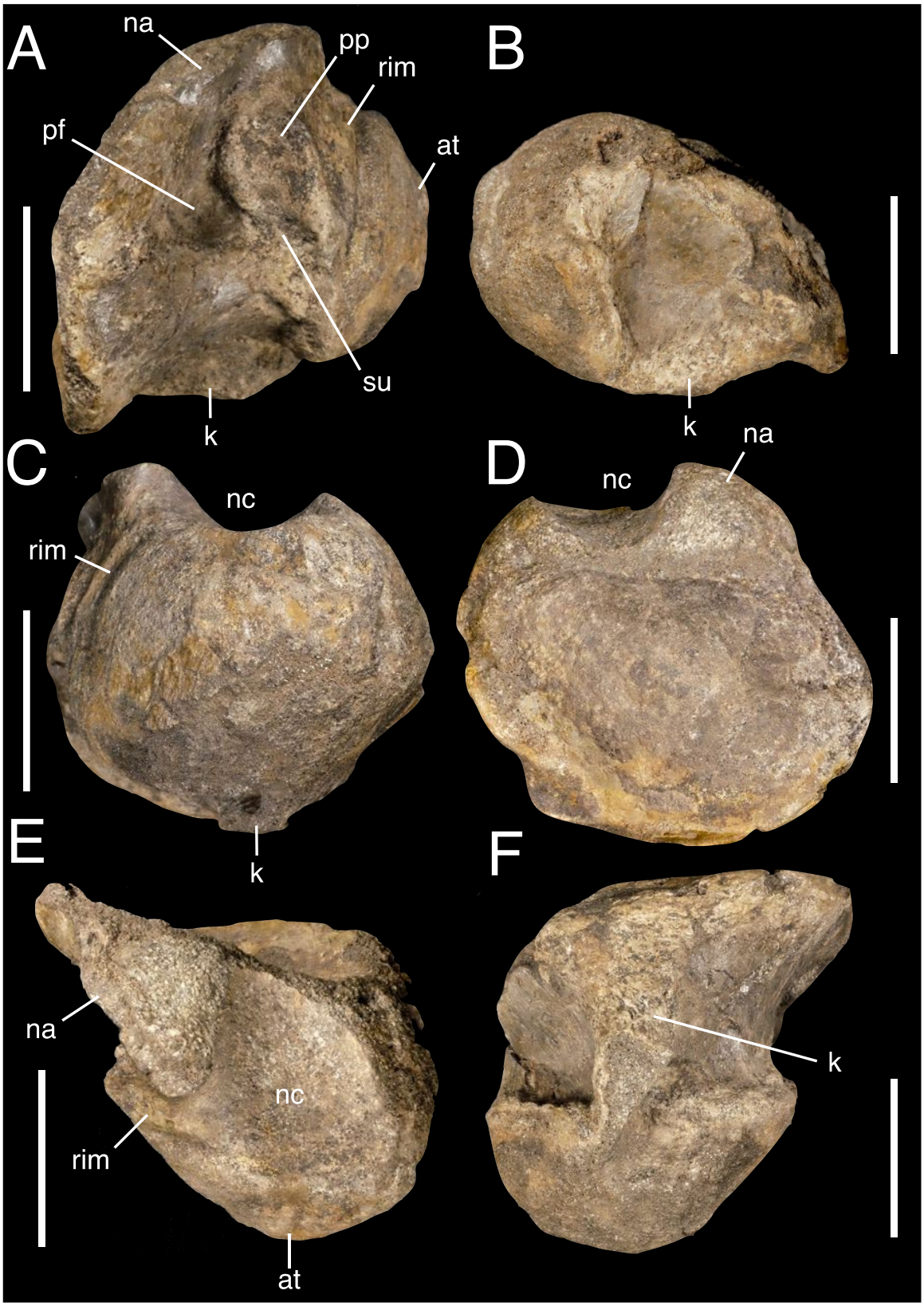

Figure 4.3 Anterior dorsal vertebral fragment IWCMS 2018.30.1, in A) right lateral, B) left lateral, C) anterior, D) posterior, E) dorsal and F) ventral views. *Abbreviations:* at, anterior tuberosity; k, keel; na, neural arch; nc, neural canal; pf, pneumatic foramen; pp, parapophysis; rim, flattened rim around the anterior articular facet; su, sulcus. Scale bar: 50 mm.

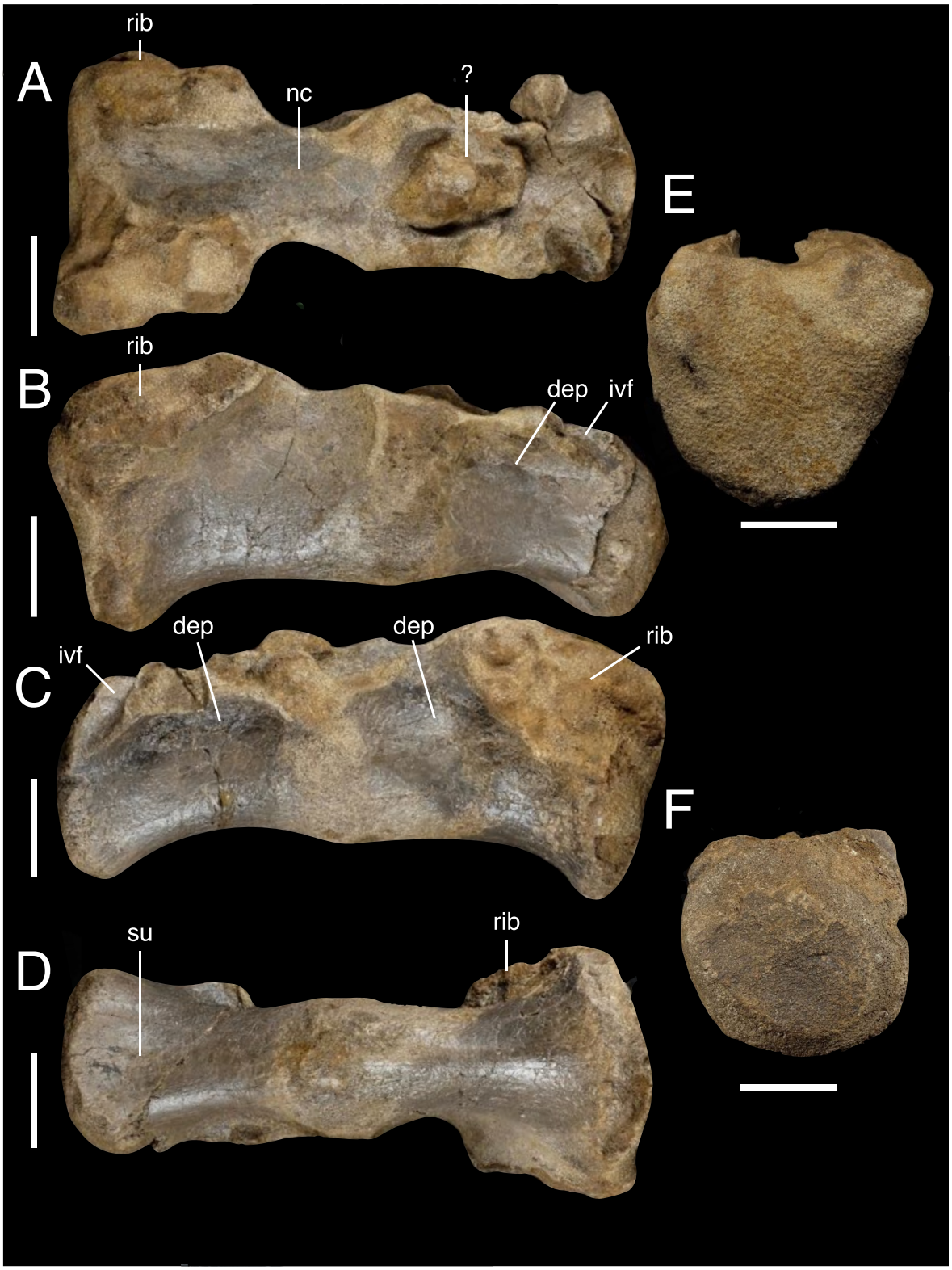

Figure 4.4 Conjoined sacral centra IWCMS 2018.30.2 in A) dorsal, B) right lateral, C) left lateral, D) ventral, E) anterior and F) posterior views. *Abbreviations*: dep, depression; ivf, floor of the intervertebral foramen; nc, neural canal; rib, sacral rib attachment; su, sulcus. Scale bars: 50 mm.

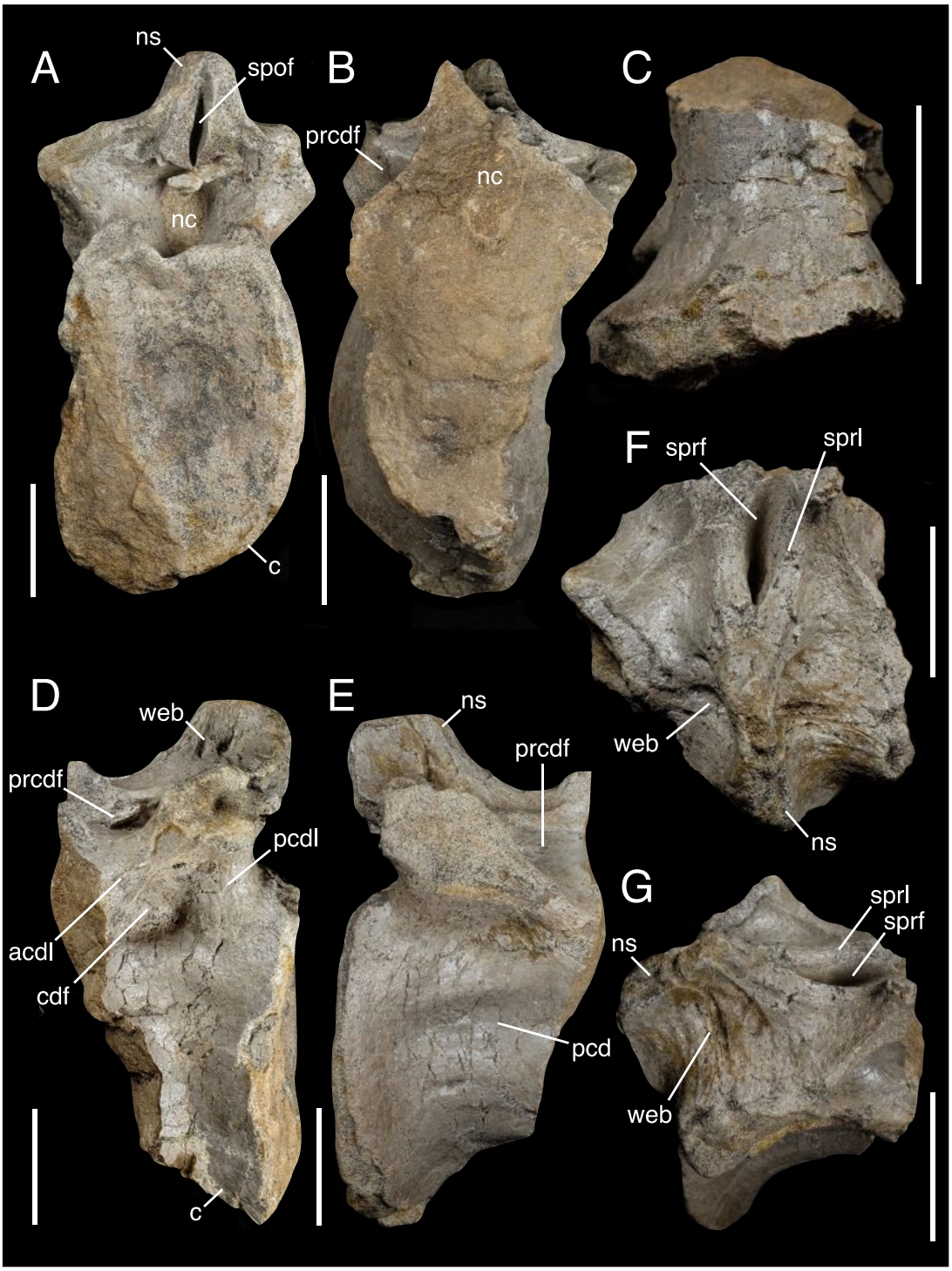

Figure 4.5 Partial anterior caudal vertebra IWCMS 2018.30.3 in A) posterior, B) anterior, C) ventral, D) left lateral, E) right lateral, F) dorsal and G) right dorsolateral oblique views. *Abbreviations*: acdl, anterior centrodiapophyseal lamina; c, centrum; cdf, centrodiapophyseal fossa; nc, neural canal; ns, neural spine; pcd, pleurocentral depression; pcdl, posterior centrodiapophyseal lamina; prcdf, prezygocentrodiapophyseal fossa; sprf, spinoprezygapophyseal fossa; sprl, spinoprezygapophyseal lamina; spof, spinopostzygapophyseal fossa; web, spinodiapophyseal webbing. Scale bars: 50 mm.

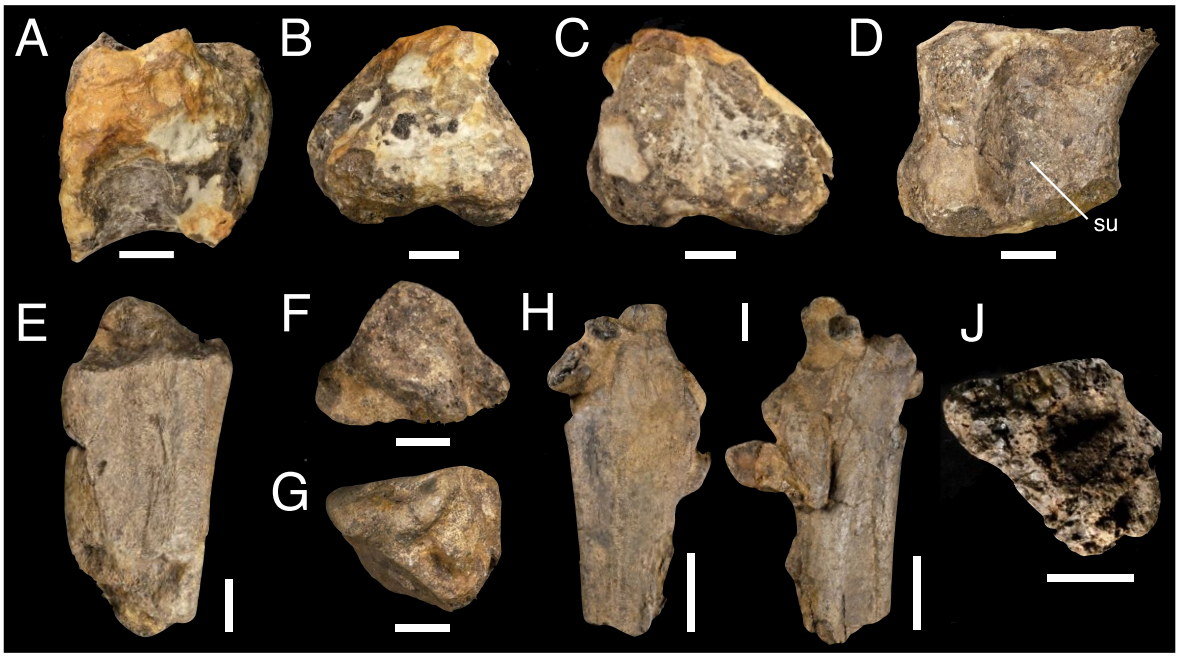

Figure 4.6 Sacrocaudal fragment IWCMS 2018.30.4 in A) dorsal, B) posterior, C) anterior, D) ventral views. Rib fragments IWCMS 2018.30.5 (E–G) and 2018.30.6 (H–J), views uncertain. *Abbreviations:* su: sulcus. Scale bars: 20 mm (A–G, J); 50 mm (H–I).

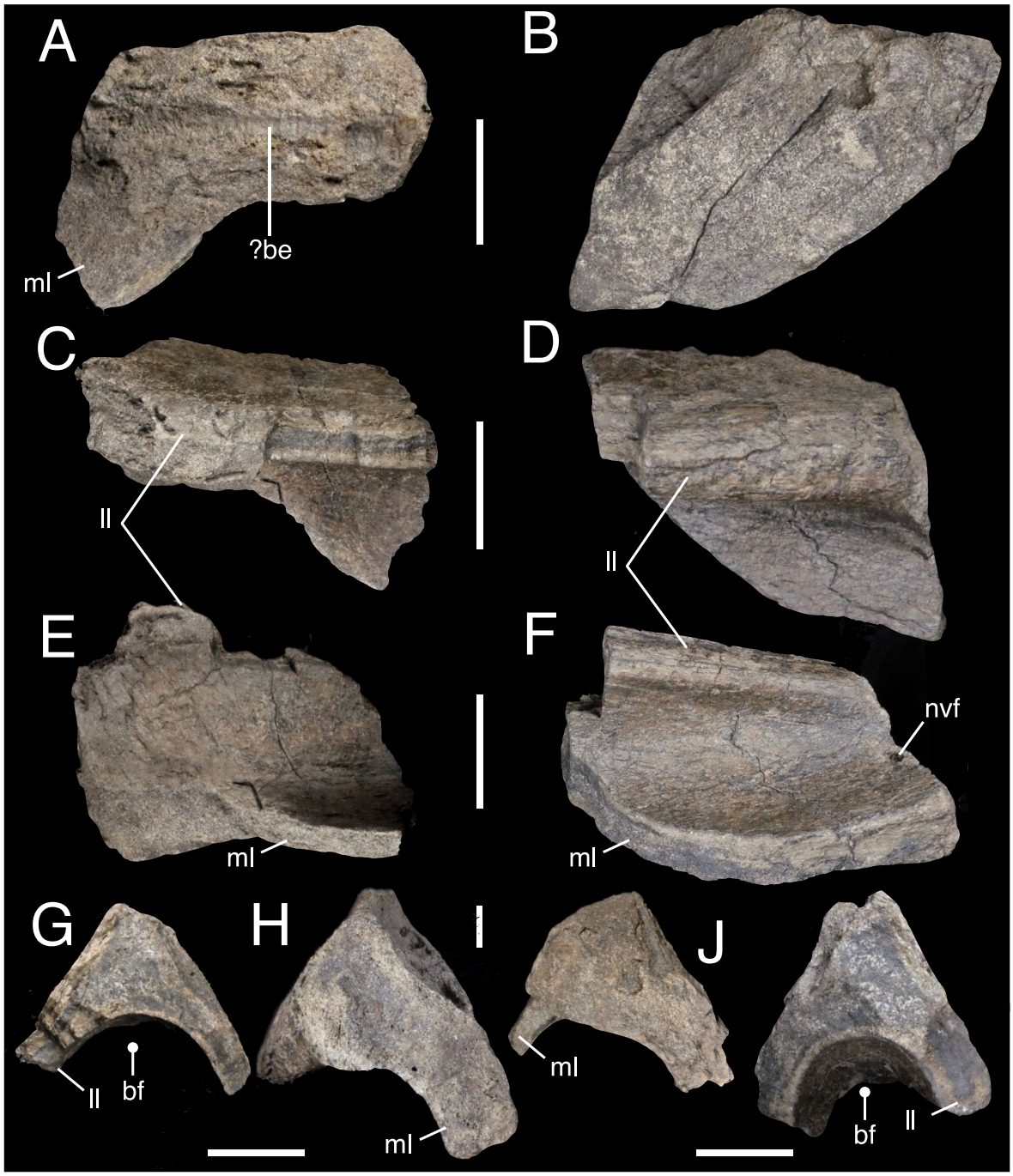

Figure 4.7 Fragmentary postacetabular process of the right ilium IWCMS 2018.30.7 (A, C, E, G, I) and 2018.30.8 (B, D, F, H, J) in A–B) medial; C–D) ventrolateral oblique, E–F) ventral, G–H) anterior and I-J) posterior views. *Abbreviations:* be, bioerosion; bf, brevis fossa; ll, lateral lamina; ml, medial lamina; nvf, neurovascular foramen. Scale bars: 50 mm.

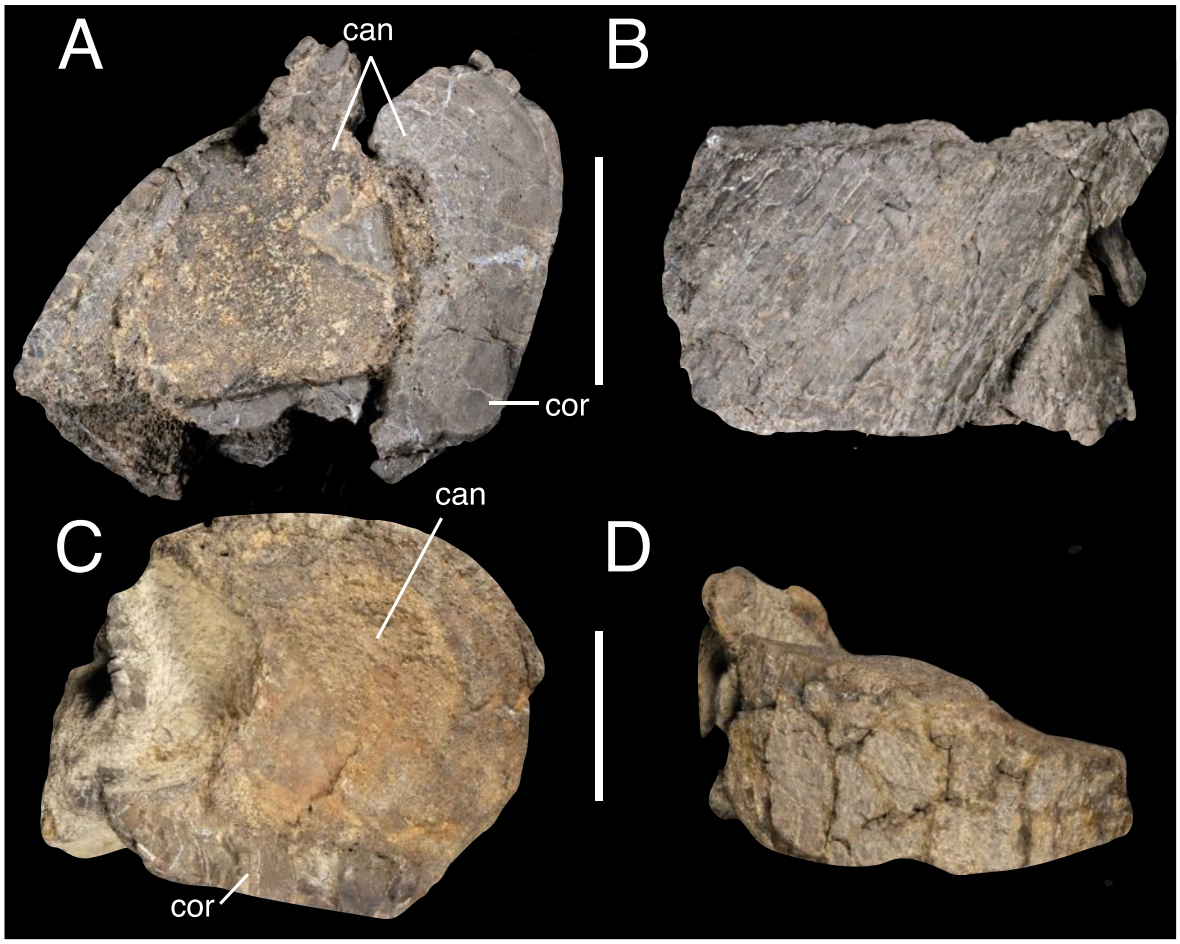

Figure 4.8 Long bone fragments IWCMS 2018.30.9 (A, B) and 2018.30.10 (C, D). Views uncertain.

Abbreviations: can, cancellous bone; cor, cortical bone. Scale bars: 50 mm.

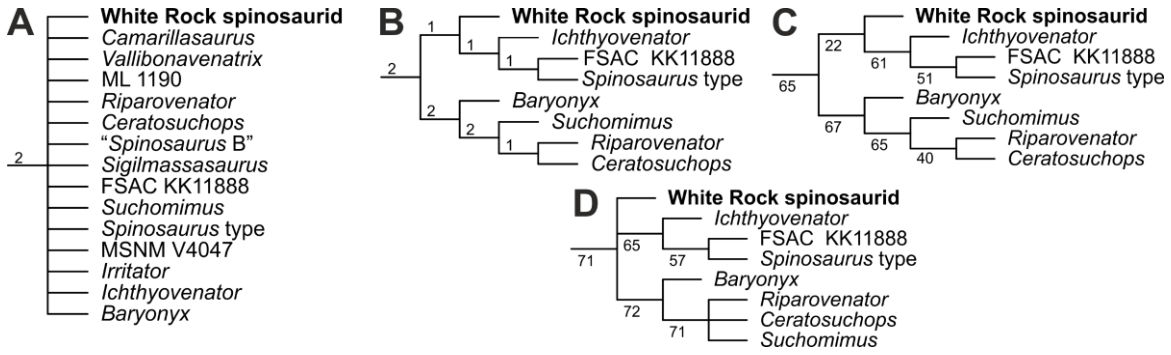

Figure 4.9 Phylogenetic results following the addition of the White Rock spinosaurid to the modified dataset of Barker et al. (2021), focusing on Spinosauridae. A) Strict consensus tree; B) reduced consensus tree showing stable spinosaurid OTUs; Jackknife values based on absolute (C) and GC frequencies (D) after wildcard OTUs were pruned. Numbers above and below nodes indicate Bremer and jackknife values respectively. Full versions available in Appendix C.

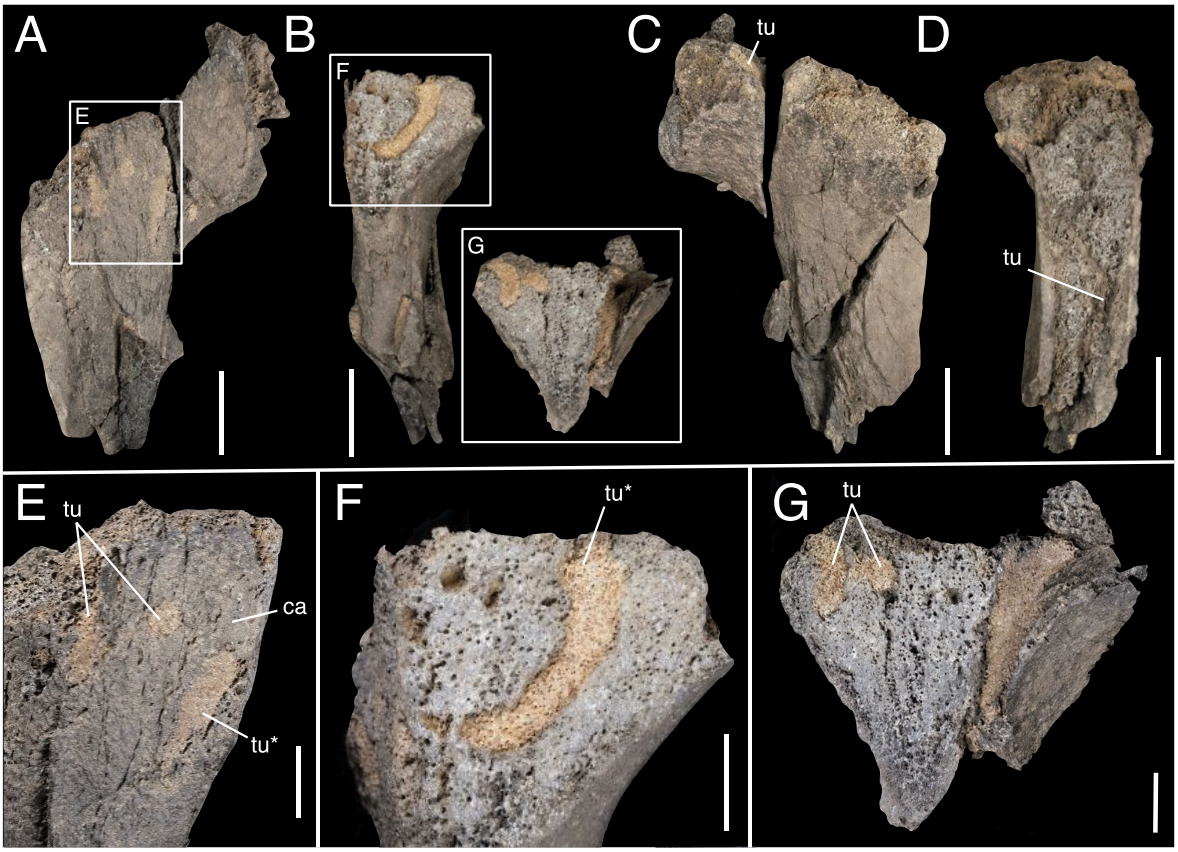

Figure 4.10 Bioeroded indeterminate bone fragment IWCMS 2018.30, displaying cross-sections of internal tubes. Figures F and G are counterparts. Asterisks denote continuation of a single tube visible in different views. *Abbreviations:* ca: cancellous bone; tu: tubes (preserved in cross-section). Scale bars: 50 mm (A–D); 20 mm (E–G).

Chapter 5 Modified skulls but conservative brains? The palaeoneurology and endocranial anatomy of baryonychine dinosaurs (Theropoda: Spinosauridae)

5.1 Authorship statement

This chapter is the product: **Barker, C.T.**, Naish, D., Trend, J. et al. (2023) Modified skulls but conservative brains? The palaeoneurology and endocranial anatomy of baryonychine dinosaurs (Theropoda: Spinosauridae). *Journal of Anatomy*, 243(6), 1124– 1145.

CTB, NJG, DN, CEC and PS devised the project. CTB wrote the first draft of the manuscript, conducted the analyses and created the figures. KR optimised the scanning of the *Ceratosuchops* braincase. CTB, JT and LVM segmented the *Ceratosuchops* micro-CT dataset; CTB reconstructed the full endocast and associated neurovasculature. RR and LW reconstructed the *Baryonyx* endocast and wrote the associated segmentation methodology and scanning protocol. All authors edited the manuscript.

The supplementary information for this chapter can be found in Appendix D and online.

5.2 Abstract

The digital reconstruction of neurocranial endocasts has elucidated the gross brain structure and potential ecological attributes of many fossil taxa, including *Irritator*, a spinosaurine spinosaurid from the “mid” Cretaceous (Aptian) of Brazil. With unexceptional hearing capabilities, this taxon was inferred to integrate rapid and controlled pitch-down movements of the head that perhaps aided in the predation of small and agile prey such as fish. However, the neuroanatomy of baryonychine spinosaurids remains to be described, and potentially informs on the condition of early spinosaurids. Using micro-computed tomographic scanning (µCT), we reconstruct the braincase endocasts of *Baryonyx walkeri* and *Ceratosuchops inferodios* from the Wealden Supergroup (Lower Cretaceous) of England. We show that the gross endocranial morphology is similar to other non-maniraptoriform theropods, and corroborates previous observations of overall endocranial conservatism amongst more basal theropods. Several differences of unknown taxonomic utility are noted between the pair. Baryonychine neurosensory capabilities include low

frequency hearing and unexceptional olfaction, whilst the differing morphology of the floccular lobe tentatively suggests less developed gaze stabilisation mechanisms relative to spinosaurines. Given the morphological similarities observed with other basal tetanurans, baryonychines likely possessed comparable behavioural sophistication, suggesting that the transition from terrestrial hypercarnivorous ancestors to semi-aquatic "generalists" during the evolution of Spinosauridae did not require substantial modification of the brain and sensory systems.

5.3 Keywords

Spinosauridae, Baryonychinae, endocast, sensory anatomy, Theropoda, palaeoneurology

5.4 Introduction

Spinosauridae is an aberrant clade of long-snouted, large-bodied theropod dinosaurs, with representative taxa and key specimens known from the fossil records of Europe, Asia, Africa and South America (Stromer, 1915; Charig et al., 1986; Sereno et al., 1998; Sues et al., 2002; Dal Sasso et al., 2005; Kellner et al., 2011; Allain et al., 2012; Ibrahim et al., 2014; Ibrahim et al., 2020a; Malafaia et al., 2020b; Barker et al., 2021; Mateus et al., 2022). Generally limited to Lower to "mid" Cretaceous deposits (Holtz et al., 2004; Bertin, 2010), phylogenetic analyses nevertheless support a Jurassic origin for the clade (Carrano et al., 2012; Barker et al., 2021), although definitive material from this period remains unknown (Hendrickx et al., 2019; Soto et al., 2020). Spinosauridae is typically subdivided into Baryonychinae and Spinosaurinae (Sereno et al., 1998; Benson, 2010; Carrano et al., 2012; Arden et al., 2019; Rauhut et al., 2019b), although support for this dichotomy may be weaker than previously thought (Evers et al., 2015; Sales et al., 2017b; Barker et al., 2021). Nevertheless, for ease of comparison, we follow the baryonychine-spinosaurine dichotomy throughout this work.

All spinosaurids reported thus far possess atypical craniodental (and sometimes postcranial) features (Stromer, 1915; Charig et al., 1997; Allain et al., 2012; Ibrahim et al., 2014; Ibrahim et al., 2020a; Fabbri et al., 2022b), the most noteworthy of which is a long, narrow, superficially crocodile-like rostrum. Multiple lines of evidence indicate that spinosaurids exploited divergent, semi-aquatic ecologies relative to related lineages, which included a degree of piscivory (Taquet, 1984; Charig et al., 1997; Holtz, 1998; Amiot et al., 2009; Amiot et al., 2010a; Hone et al., 2014; Ibrahim et al., 2014; Hassler et al., 2018; McCurry et al., 2019; Ibrahim et al., 2020a; Hone et al., 2021; Sakamoto, 2022). A range of terrestrial and aquatic prey were likely taken under a "generalist" or "opportunistic" foraging strategy (Ruiz-Omeñaca et al., 2005; Bertin, 2010; Hone et al., 2017), with individual size (Cuff et al., 2013) or habitat (Alonso et al., 2016) perhaps impacting

prey availability and/or selection. Indeed, despite their apparent ties to water, spinosaurid specimens are known from several semi-arid or arid palaeoenvironments (Ruiz-Omeñaca et al., 2005; Amiot et al., 2010b), and direct evidence indicates that small dinosaurs and pterosaurs, in addition to fish, were consumed (Charig et al., 1997; Buffetaut et al., 2004). Spinosaurines may well have exhibited increased aquatic specialisation (in some respects) relative to baryonychines, but the degree to which they were adapted to water, and how this adaptation was reflected in behaviour and ecology, remains the subject of ongoing research and controversy (Ibrahim et al., 2014; Barker et al., 2017; Henderson, 2018; Arden et al., 2019; Hone et al., 2019; Ibrahim et al., 2020a; Hone et al., 2021; Fabbri et al., 2022a; Fabbri et al., 2022b; Myhrvold et al., 2022; Sereno et al., 2022).

Given the strong evidence for aquatic behaviour in the skeletal (and particularly cranial) anatomy of these dinosaurs, it follows that the brain and nervous system may be expected to exhibit specialisations for aquatic foraging or swimming. Schade et al. (2020) described the endocranial anatomy of the South American spinosaurine *Irritator challengeri* (SMNS 58022) from the Romualdo Formation (Lower Cretaceous: Aptian) of Brazil (Martill et al., 1996a; Sues et al., 2002; Arai et al., 2020). *Irritator* shares similarities with the endocasts of other non-maniraptoran theropods and possesses unexceptional hearing capabilities; more interesting is the tentative evidence from the inner ear that suggest an ability to rapidly move and tightly control ventral movements of the head that may have aided in the capture of small, agile prey such as fish (Schade et al., 2020).

Endocasts are now known for a range of theropod taxa, including early neotheropods (Xing et al., 2014; Paulina-Carabajal et al., 2019a) and ceratosaurs (Sanders et al., 2005; Sampson et al., 2007; Paulina-Carabajal et al., 2014; Paulina-Carabajal et al., 2018; Cerroni et al., 2019; Gianechini et al., 2021), as well as basal (i.e. non-coelurosaur) (Rogers, 1998; Eddy et al., 2011; Paulina-Carabajal et al., 2019b) and coelurosaurian tetanurans (Brochu, 2000; Kundrát, 2007; Witmer et al., 2009; Bever et al., 2011; Lautenschlager et al., 2012; Balanoff et al., 2014; King et al., 2020; Knoll et al., 2020). Work on theropod endocast has also elucidated adaptational trends (Larsson et al., 2000; Zelenitsky et al., 2011; Kundrát et al., 2018; Choiniere et al., 2021) and changes in brain modularity across the theropod-bird transition (Balanoff et al., 2016b).

However, to date, no study has examined the endocranial morphology or neurosensory capabilities of baryonychine spinosaurids. Here, we fill this knowledge gap via the description and interpretation of X-ray computed tomography (CT) scan data pertaining to *Baryonyx walkeri* and *Ceratosuchops inferodios*. Both are from Barremian strata of the Wealden Supergroup (Lower Cretaceous) of southern England, and both possess well-preserved (albeit partially disarticulated)

braincases (Charig et al., 1986; Charig et al., 1997; Barker et al., 2021). Given the temporal and phylogenetic relationship of these specimens relative to *Irritator*, the baryonychines *Baryonyx* and *Ceratosuchops* may provide some context regarding the evolution of the spinosaurid endocranium and associated neurosensory capabilities.

5.4.1 Institutional abbreviations

IGM: Geological Institute of the Mongolian Academy of Sciences, Ulaan Baatar, Mongolia; IWCMS, Isle of Wight County Museum Services, Dinosaur Isle Museum, Sandown, UK; IVPP: Institute of Vertebrate Paleontology and Paleoanthropology, Beijing, China; NHMUK, Natural History Museum, London, UK; MAU: Museo Municipal Argentino Urquiza, Rinco n de los Sauces, Neuquén, Argentina; MCF: Museo "Carmen Funes," Plaza Huincul, Neuquén, Argentina; SMNS, Staatliches Museum für Naturkunde, Stuttgart, Germany; YPM, Yale Peabody Museum, New Haven, CT, USA.

5.5 Materials and methods

5.5.1 Spinosaurid material

The spinosaurid material examined first hand for this study includes the following specimens: *Baryonyx walkeri* (NHMUK PV R9951) and *Ceratosuchops inferodios* (IWCMS 2014.95.1–3) (Figure 5.1).

5.5.2 Terminology

Unlike that of birds or mammals, the brains of non-avian reptiles such as *Alligator* (Hurlburt et al., 2013), turtles (Evers et al., 2019) and squamates (Allemand et al., 2022) do not typically fill the endocranial cavity. As such, a reptilian endocast represents the total soft tissues within the braincase and only provides superficial information regarding brain topography (the extent of which depending on the species and neuroanatomical regions) (Hopson, 1979; Hu et al., 2021; Allemand et al., 2022). As such, we follow previous works by referring to the digital casts of the space within the braincase as "endocasts". Similarly, the segmented labyrinths do not truly represent the membranous or osseous features of the inner ear, and we also follow previous authors in adopting "endosseous" throughout when referring to the reconstructed structure (Witmer et al., 2008). Other segmented structures (e.g. neurovascular canals, pituitary fossae) are referred to as if they were the structures themselves.

5.5.3 CT Scanning and endocast generation

5.5.3.1 Data archiving

The data used in this study were archived on Morphosource (https://www.morphosource.org/projects/000491312). Data pertaining to *Baryonyx walkeri* and *Ceratosuchops inferodios* can be respectively found under project IDs 000491194 (https://www.morphosource.org/projects/000491194) and 000491949 (https://www.morphosource.org/projects/000491949).

5.5.3.2 *Baryonyx walkeri* (NHMUK PV R9951)

5.5.3.2.1 CT Scanning

The preserved braincase consists of three fragments (i.e., a large posterior basicranial fragment, a smaller skull roof fragment with portions of the frontals, parietals and left laterosphenoid, and the left otoccipital with its paroccipital process) that were scanned at OhioHealth O'Bleness Hospital in Athens, Ohio, USA, on a General Electric LightSpeed Ultra at 140kV and 200–300mA, with voxel sizes of 432x432x625µm and using Extended Hounsfield and bow-tie filtration.

5.5.3.2.2 Volume reconstruction and image processing

Scan data were reconstructed using a bone algorithm and were exported as a DICOM image stack, which were then imported into Windows-based workstations running Amira-Avizo (Thermo Fisher Scientific, Waltham, MA) for analysis and segmentation. To generate 3D PDFs, 3D models were exported as OBJ files and imported into SimLab 3D Composer (Amman, Jordan).

5.5.3.2.3 Braincase rearticulation

The three preserved braincase fragments show some amount of plastic deformation and, although close, do not fit together perfectly. Different models were generated based on different optimization criteria: (1) best overall fit considering both bony structure and enclosed soft tissues (e.g., semicircular canals); (2) best fit optimizing bony structure, especially the otoccipital fragment; and (3) best fit optimizing the structure of the labyrinth, which is the most consistently symmetrical aspect of endocranial anatomy (Cerio et al., 2019). The differences between the resulting models are slight, and Figure 5.1 and Figure 5.2 presents the result of the second optimization criterion above. It is also worth noting that portions of the bony braincase overlying the left cerebral region were not preserved (or were lost during collection or preparation) but the underlying cerebral endocast is preserved in matrix as a natural endocast.

5.5.3.3 *Ceratosuchops inferodios* (IWCMS 2014.95.1–3)

5.5.3.3.1 CT Scanning

The three braincase fragments were scanned at the μ-VIS X-Ray Imaging Centre at the University of Southampton (UK), using a custom 225/450 kVp Hutch dual source walk-in micro-focus CT system (Nikon Metrology, UK). Peak voltage and current were set at 300 kVp and 250 μA respectively. A total of 3142 projections were collected over a 360º rotation, averaging 16 frames per projection with 250ms exposure time per frame.

5.5.3.3.2 Volume reconstruction and image processing

Projection data were reconstructed as 32-bit float raw volumes with an isotropic voxel size using filtered back-projection algorithms implemented in CT Pro 3D and CT Agent software (v. XT 2.2 SP10, Nikon Metrology, UK). Voxel dimensions were 103.3μm^3 for IWCMS 2014.95.1, 89.3μm^3 for IWCMS 2014.95.2, and 109.7μm^3 for IWCMS 2014.95.3. These were converted to 8-bit (raw) volume files to reduce computational load.

To improve contrast, the raw image files of the basicranium fragment (IWCMS 2014.95.3) were manipulated in FIJI (Schindelin et al., 2012) using the “sharpen” filter and background subtract function. Additional sharpening of the *Ceratosuchops* braincase material was conducted within Object Research Systems (ORS) Dragonfly (v. 2022.1, build 1249) via the *Unsharp* filter (*Workflow*>*Image Filtering*>*Operations*>*Sharpening*) using a factor of 4–9 (standard deviation=1), depending on the specimen/region of interest (ROI).

5.5.3.3.3 Braincase rearticulation and segmentation

A landmark-based rearticulation process in 3D Slicer (v. 4.11.20210226) (Fedorov et al., 2012) was used to reconstruct the braincase, whilst segmentation of the endocranial features was achieved using ORS Dragonfly (Object Research Systems (ORS) Inc, Montreal, Canada; v. 2021.3 and 2022.1). Final endocast generation employed Autodesk Meshmixer. The methodological details are expanded upon in the Appendix D.

5.5.4 Measurements

Morphological measurements were taken digitally using the measuring tools in Autodesk Meshmixer, ORS Dragonfly and FIJI (Schindelin et al., 2012).

5.5.5 Reptile encephalisation quotient

The reptile encephalisation quotient (REQ) (Hurlburt, 1996) is a measure of relative brain size and gross cognitive capacities. We generated an estimated REQ based on the brain and body mass of the more skeletally complete *Baryonyx* type specimen. Body mass estimates are unknown for *Ceratosuchops*, but both taxa are of similar proportions where their known anatomy overlaps (Barker et al. (2021); see also Table 5.1), and the REQ estimated for *Baryonyx* likely approximates that of *Ceratosuchops*. The equation is as follows:

$$REQ = \frac{M_{Br}}{0.0155 \times M_{Bd}{}^{0.553}}$$

where M_{Br} is brain mass (in grams, excluding the olfactory tract and bulbs) and M_{Bd} is body mass (in grams). Following Hurlburt et al. (2013), we assumed the brain occupied 37% or 50% of the endocast volume. As the relative density of brain tissues nears unity, brain volume and mass are interchangeable (Hurlburt et al., 2013). Endocast volume was calculated in Meshmixer (*Analysis*>*Stability*).

A mass estimate for *Baryonyx* was generated based on the equation of Campione et al. (2014) implemented in Benson et al. (2018):

$$mass_{biped} = \frac{10^{\left(2.749 \times log_{10}\left(FC \times 2^{0.5}\right) - 1.104\right)}}{1000}$$

where FC is minimum femoral circumference (in millimetres). Inputting the available femoral data for *Baryonyx* (minimum preserved circumference of the incomplete right shaft: 350mm; S. Maidment, pers. comms., 2022) produced a mass estimate of 2011kg. However, the measured *Baryonyx* femur is not only incomplete but also damaged (Charig et al., 1997), which affected the ability to collect reliable data (S. Maidment, pers. comms., 2022). Nevertheless, this estimate is comparable to the 1981kg calculated by Therrien et al. (2007) using least-squares regressions involving skull length, and is used herein pending the discovery of better preserved material.

5.5.6 Hearing frequency and range

The length of the endosseous cochlear duct (lagena of some authors) is often used as a proxy for hearing range and sensitivity (Walsh et al., 2009; Hanson et al., 2021). We employ the methods used by Walsh et al. (2009) in estimating hearing parameters. Two metrics are required: endosseous cochlear duct (ECD; pars cochlearis) length and basicranial length (BCL). The dorsal limit of the former is usually defined by a marked constriction where the ECD meets the saccule ((Walsh et al., 2009): preservation does not allow us to determinate this with absolute confidence

in *Ceratosuchops* but we were still able to provide an estimate. The measurement tools in Meshmixer were employed for both spinosaurids.

The constraints of the BCL were not outlined in Walsh et al. (2009) but this measure is defined as the anteroposterior distance between the anterior limit of the basisphenoid (excluding the cultriform process of the parasphenoid) and the posterior margin of the occipital condyle (Dudgeon et al., 2020). In *Ceratosuchops*, the basisphenoid and parasphenoid are indiscernibly fused together; the anterior limit of the basisphenoid was herein defined by following an obliquely trending line from the anterior margin of the basipterygoid process pedicel towards the region of the pituitary fossa in lateral view.

The ECD was scaled to the BCL and log transformed. For hearing range, we followed the equation:

$$y = 6104.3x + 6975$$

with x being the scaled and log-transformed ECD, and y being the best hearing range in Hz. For mean hearing frequency we followed the equation:

$$y = 3311.3x + 4000.8$$

with x being the scaled and log-transformed ECD length, and y being the mean best hearing frequency in Hz.

We also calculated the hearing capabilities of several other theropods for further comparisons, using the STL models of theropod inner ears from Choiniere et al. (2021). These included: *Viavenator exonii* (MAU Pv LI 530), *Sinraptor dongi* (IVPP 10600), *Murusraptor barrosaensis* (MCF PVPH 411), and *Erlikosaurus andrewsi* (IGM 100.111). These are based on models from Lautenschlager et al. (2012), Paulina-Carabajal et al. (2012), Paulina-Carabajal et al. (2017), and Paulina-Carabajal et al. (2018). Approximate ECD dimensions were measured using the tools in Meshmixer, and BCL was estimated from published images (Lautenschlager et al. (2012): Fig. 2A; Paulina-Carabajal et al. (2012): Fig. 5A; Paulina-Carabajal et al. (2017): Fig. 7.3; Paulina-Carabajal et al. (2018): Fig. 1D) using FIJI.

5.5.7 Olfactory acuity

The form and external limits of the olfactory bulbs are difficult to determine in the *Ceratosuchops* endocast, being located at the anterior end of the expanding olfactory tract and separated by a midline sulcus in dorsal view (see below). An olfactory ratio was calculated by measuring the longest diameters of the bulbs and cerebral hemisphere (regardless of orientation); this is expressed as a percentage following previous studies (Zelenitsky et al., 2009; Zelenitsky et al.,

2011). Raw olfactory ratios should not be directly compared across taxa due to the influence of body size (Zelenitsky et al., 2009). As the mass of *Ceratosuchops* cannot be presently estimated but likely approximates that of *Baryonyx* (see above), we used the *Baryonyx* mass estimate employed in our REQ calculations and log-transformed both metrics. These were subsequently plotted onto the graph produced by Zelenitsky et al. (2009: Fig. 2). Given the use of both specimens in this analysis, we provisionally consider the latter result representative of the generalised baryonychine condition.

5.6 Results

5.6.1 Baryonychine endocranial morphology

5.6.1.1 Preservation

5.6.1.1.1 *Baryonyx* (NHMUK PV R9951)

The cerebral endocast is preserved in three disjunct pieces (Figure 5.2). A transverse break posterior to the dural peak and anterior to the trigeminal nerve (CN V) trunk separates the two main anterior and posterior portions, with a third located on the disarticulated left otoccipital. The left side of the anterior cerebral endocast is preserved as a natural cast and is visible macroscopically following the loss of the left frontoparietal and laterosphenoid. Unfortunately, the anterior four cranial nerve trunks, the left vestibulocochlear (CN VIII) and glossopharyngeal (CN IX) nerve trunks, and olfactory bulbs or tracts are not preserved.

Nevertheless, what remains of the endocast is well preserved, though a degree of plastic deformation affects the anterior braincase piece and the internal left otoccipital (as evidenced by the dorsoventrally compressed semicircular canals). The endosseous labyrinth of the right inner ear is well preserved and can be reconstructed in full (Figure 5.2, Figure 5.4A and Figure 5.5A–D), unlike its damaged and disjoined left counterpart, and this right-side structure forms the basis of the structure's description and comparison.

5.6.1.1.2 *Ceratosuchops inferodios* (IWCMS 2014.95.1–3)

The endocast, once reassembled, is largely complete and includes all major cranial nerves and major vascular features (Figure 5.3). However, our effort to rearticulate the braincase has introduced three morphological artefacts to the endocast. These are as follows: (1) a divot on the posterior dorsal expansion, which was presumably smoother in life given the morphology of other theropods (Sampson et al., 2007; Witmer et al., 2009); (2) the bilateral, transverse sinus-like ridges posterior to the cerebral hemispheres do not represent cerebral topography but the

supraoccipital-parietal contacts; and (3) an artificial 'step' between the ventral laterosphenoid-prootic contacts which, when combined with the loss of a portion of the right dorsum sellae (exposing some of the right abducens (CN VI) nerve trunk in cross-section), produces an anteriorly projecting ventral "lobe" on earlier iterations of the endocast near the right trigeminal (CN V) trunk. To avoid confusion or interpretation of this artefact as a genuine endocranial feature, this region of the endocast was bevelled in 3D view using the *Polygon* tool in ORS Dragonfly. This loss of bone and suboptimal laterosphenoid-prootic contact also rendered it difficult to visualise the ventral border of the trigeminal nerve trunk, which was inferred based on the preserved margins of the trigeminal foramen.

Elsewhere, the floccular lobes could not be reconstructed in full: the left lobe exists as two disjointed pieces and the lateral extent of both cannot be determined. Image contrast issues mean that the posterior dorsal head veins were difficult to trace, while the secondary, more ventral passages for the hypoglossal (CN XII) nerve trunks could only be traced over a short distance. The left vestibulocochlear nerve trunks (CN VIII) could not be visualised.

The endosseous labyrinths are partially preserved (Figure 5.3, Figure 5.4B and Figure 5.5E–H). The left side is missing its vestibule, cochlear duct and portions of the anterior and lateral semicircular canals, which could not be visualised due to the lack of contrast and presence of a substantial quantity of radiopaque matrix in the region. The right labyrinth is more complete and forms the basis of the structure's description and comparison, although the midsection of the anterior semicircular canal (within the prootic) could not be segmented (this was also due to the presence of radiopaque matrix obscuring its path). The posterior margin of the cochlear duct could not be reconstructed due to disarticulation of the prootic and otoccipital.

5.6.2 Endocranial morphology

Baryonychine endocasts (Figure 5.2 and Figure 5.3) conform to the general morphology of other non-coelurosaurian theropods, the details of which are discussed below, and corroborate previous suggestions of endocranial conservatism amongst the taxa concerned (Hopson, 1979; Sampson et al., 2007). As is typical for most non-maniraptoriform sauropsids, the brain did not fill the endocranial cavity, with much obscured by a dural envelope and its extensive venous sinuses (Hopson, 1979; Sedlmayr, 2002; Sampson et al., 2007; Witmer et al., 2008; Witmer et al., 2009). To facilitate interspecific comparisons, the endocasts will be oriented with the lateral semicircular canal assuming a horizontal path.

Table 5.1 Metric data for the baryonychine endocasts. Linear measurements in millimetres (mm). Volume data in cubic centimetres (cm^3). Asterisk (*) denotes incomplete data due to preservation.

	Baryonyx	***Ceratosuchops***
Preserved anteroposterior length (measured from the anterodorsal-most tip to the dorsal margin of the foramen magnum)	128.4*	173.5
Anteroposterior length (excluding olfactory tract)	128.4	122.2
Endocranial volume (excluding neurovascular features)	150.487*	185.603
Mediolateral width across cerebral hemispheres	47.5	47.9
Cephalic flexure	63º	78º
Pontine flexure	55º	66º

The olfactory tract is well preserved in *Ceratosuchops*. It is an elongate, narrow structure that expands anteriorly towards the olfactory bulbs. The anterior portion is indented along its dorsal midline by a shallow sulcus, as in *Irritator* (Schade et al., 2020), likely marking the position of the olfactory bulbs. The tracts are in line with the forebrain in both these specimens, and their elongate proportions conform to the plesiomorphic archosaurian condition present in many non-avian theropods (Franzosa, 2004; Bever et al., 2013); though incomplete, the base of the olfactory tract is also present in *Baryonyx*, and a similar morphology is thus inferred. The spinosaurids lack evidence of medial separation of their respective bony olfactory tracts, as in *Majungasaurus* (Sampson et al., 2007) and various allosauroids excluding *Acrocanthosaurus* (Franzosa et al., 2005; Eddy et al., 2011; Paulina-Carabajal et al., 2012).

Although the brain does not completely occupy the endocranial cavity, the portion of the endocast corresponding to the telencephalon is considered to approximate the underlying brain contours, especially laterally (Sedlmayr, 2002; Sampson et al., 2007; Witmer et al., 2008); the cerebral hemispheres can be clearly observed. The studied baryonychines possess the relatively small and unexpanded ancestral morphology typical of non-maniraptoriform theropods (Larsson et al., 2000; Rauhut, 2003; Franzosa, 2004). Despite the limited expansion, the widest part of the endocast appears located at the level of the cerebral hemispheres, as is typical for fossil reptiles (Hopson, 1979) and observed in such theropods as *Irritator* (Schade et al., 2020), abelisaurids (Sampson et al., 2007; Paulina-Carabajal et al., 2018), *Murusraptor* (Paulina-Carabajal et al., 2017) and allosauroids such as *Allosaurus* (Rogers, 1998) and *Sinraptor* (Paulina-Carabajal et al., 2012).

The forebrain and hindbrain are generally horizontally oriented in both baryonychines, as is typical for non-coelurosaurian theropods and also early-branching coelurosaurs such as tyrannosaurids (Witmer et al., 2009). A nuance is that the forebrain is directly slightly anteroventrally along its length in *Ceratosuchops*. Differences are noted in the degree of flexure between the baryonychine endocasts. The estimated cephalic and pontine flexures *sensu* Hopson (1979) are presented in Table 5.1 and suggest that the midbrain region is more strongly angled in *Ceratosuchops*, although precise measurement of these angles is problematic due to the obscuring nature of the surrounding dural envelope (Witmer et al., 2009). Midbrain angulation of around 45–60º is observed in non-coelurosaurian theropods generally (Hopson, 1979; Witmer et al., 2009).

In contrast to *Baryonyx*, the dorsal surface of the *Ceratosuchops* endocast preserves a narrow midline sulcus (Figure 5.3E). This likely does not represent the interhemispheric fissure, a feature typically obscured by the dorsal longitudinal sinus in non-avian theropods (Hopson, 1979; Witmer et al., 2008; Cerroni et al., 2019) but reported in various maniraptorans (Balanoff et al., 2009; Lautenschlager et al., 2012; Balanoff et al., 2014; Hattori et al., 2021). Instead, these potentially represent anteriorly diverging venous channels emanating from the dorsal expansion.

The dorsal expansion of the endocast – an eminence just posterior to the cerebrum – has been thought to house (at least in part) the pineal apparatus in non-coelurosaurian theropods, although the expansion is absent in more basal theropods (Sampson et al., 2007; Witmer et al., 2009). However, recent work on extinct and extant turtles suggests that a cartilaginous origin, rather than one relating to the pineal gland also merits consideration (Werneburg et al., 2021), as does a venous interpretation as the dorsal expansion is associated with a variety of clearly venous structures in a variety of extinct and extant diapsids (Witmer et al., 2008; Witmer et al., 2009; Porter et al., 2015;2020). The dorsal expansion is pronounced and ascends above the dorsal margin of the forebrain in *Baryonyx*, in contrast to *Ceratosuchops*. As such, the dorsal margin of the latter's forebrain assumes a largely linear trend in lateral view, contrasting against the more concave margin in *Baryonyx*. As in *Majungasaurus* and *Allosaurus* (Sampson et al., 2007), the dorsal expansion in *Baryonyx* is located within the parietals, whereas *Ceratosuchops* recalls the condition in tyrannosaurids, where the apex is situated at the parietal-supraoccipital suture (Bever et al., 2013). Variation in the development of the dorsal expansion has been noted in *Tyrannosaurus*; however, it is likely that this structure is non-homologous with that of non-coelurosaurian taxa (Witmer et al., 2009). Damage to this region in *Irritator* (Schade et al., 2020) precludes accurate comparisons with the baryonychines.

The dorsal expansion's peak is approximately level with the trigeminal nerve trunk in both baryonychines, recalling the condition in *Majungasaurus* (Sampson et al., 2007), *Murusraptor* and *Tyrannosaurus* (Paulina-Carabajal et al., 2017), whereas it is more anteriorly positioned in various allosauroids and ceratosaurs (Rogers, 1998; Paulina-Carabajal et al., 2012; Paulina-Carabajal et al., 2017). Conversely, the peak is more posteriorly positioned in *Alioramus* and *Viavenator*, being respectively level with the facial (CN VII) nerve trunk and floccular lobe (Bever et al., 2013; Paulina-Carabajal et al., 2018). The dorsal expansion has also been used to approximate the size of the midbrain region in theropods, with many non-coelurosaurian tetanurans and ceratosaurs possessing elongated midbrain regions (Paulina-Carabajal et al., 2017). The sampled baryonychines follow this trend (Table 5.2), although the elongation is less marked compared to such forms as *Majungasaurus* or *Allosaurus*.

Table 5.2 Approximate elongation of the midbrain region in select theropods. Midbrain and medulla lengths follow Paulina-Carabajal et al. (2017): midbrain length measured from the anterior border of the floccular lobe to the peak of the dorsal expansion; medulla length measured from the foramen magnum to the trigeminal nerve (CN V) trunk. We note that the medulla was likely obscured by the dural envelope (see main text), and the medulla measurement of Paulina-Carabajal et al. (2017) instead approximates the length of the rhombencephalon. Measurements for non-spinosaurids taken from images using FIJI.

	Midbrain length (mm)	**"Medulla" length (mm)**	**Midbrain:"medulla" ratio**	**References**
Sinosaurus	50.2	52.5	0.96	Xing et al. (2014: Fig. 6A)
Majungasaurus	52.8	36.2	1.46	Sampson et al. (2007: Fig. 18A)
Viavenator	49.8	41.7	1.19	Paulina-Carabajal et al. (2018: Fig. 4A)
Baryonyx	61.6	46.9	1.31	This paper
Ceratosuchops	61.1	49.9	1.22	This paper
Allosaurus	58.9	38.6	1.53	Witmer et al. (2009: Fig. 4B)
Acrocanthosaurus	55.6	44	1.26	Franzosa et al. (2005: 2B)

	Midbrain length (mm)	"Medulla" length (mm)	Midbrain:"medulla" ratio	References
Murusraptor	33.5	32	1.05	(Paulina-Carabajal et al., 2017: Fig. 7.4)
Tyrannosaurus	40.7	50.9	0.8	Witmer et al. (2009: Fig. 4C)
Erlikosaurus	20.4	27.7	0.74	Lautenschlanger et al., (2012: Fig. 3A)
Deinonychus	16.3	20.7	0.79	Witmer et al. (2009: Fig. 4E)

The optic lobes (optic tecta) in the baryonychines are imperceptible, recalling the plesiomorphic sauropsid condition (Franzosa, 2004; Schade et al., 2020); this is also the case in *Irritator* (Schade et al., 2020). These lobes are equivocally visible in some *Tyrannosaurus* specimens, and a trend whereby these structures become increasingly obvious is observed within coelurosaurs on the line to birds (Witmer et al., 2009). The course of the transverse sinus and middle cerebral vein can be used to identify the gross position of the optic lobes and cerebellum, given that these structures pass between these brain regions in extant sauropsids (Sampson et al., 2007; Witmer et al., 2009). The transverse sinus is difficult to differentiate in the *Baryonyx* endocast, while an artificial ridge in *Ceratosuchops* corresponds to the rearticulated laterosphenoid-prootic and supraoccipital-parietal contacts. There is also no clear evidence of a canal or foramen corresponding to the passage of the middle cerebral vein in either baryonychines (the implications of which are discussed below). In sum, the positions of the optic lobes remain obscured.

The cast of the baryonychine pituitary (hypophyseal) fossa, which mostly housed the pituitary gland (Sampson et al., 2007) but likely contained various other soft tissue structures (Hopson, 1979), is a largely vertically oriented structure located just anterior to the level of the dural peak when viewed laterally. It produces a pair of dorsal and ventral posterior projections in the baryonychines, imparting a "wavy" posterior margin in lateral view. In *Irritator*, the posterior margin is more uniformly convex (Schade et al., 2020), although variation in the shape of the pituitary fossa is known amongst well sampled theropods such as *Tyrannosaurus* (Bever et al., 2013). A minor degree of posterior angulation is also noted in the *Irritator* pituitary, which would follow the conservative theropod pattern (Bever et al., 2013); baryonychines, however, do not appear to deviate substantially from the vertical.

Within the region of the pituitary fossa, *Ceratosuchops* possesses the plesiomorphic cavernous sinus present in archosaurs and many non-coelurosaurian theropods through which pass the

trochlear (CN IV) and abducens (CN VI) nerves, their associated vasculature, and likely the encephalic branches of the cerebral carotid artery (Sampson et al., 2007; Witmer et al., 2009; Bever et al., 2011). This feature could not be discerned in *Baryonyx* due to preservation.

Discrimination of the posterior regions of the brain, including the cerebellum, medulla and pons, is difficult in the baryonychine endocasts, and it most probably resembled other basal theropods and archosaurian outgroups in possessing extensive dural venous sinuses that obscured morphological details (Sedlmayr, 2002; Sampson et al., 2007). We note, however, that the ventral morphology of the rhombencephalon (i.e. the region posterior to the trigeminal (CN V) nerve trunk in lateral view) is markedly more convex in *Baryonyx* (Figure 5.2A) than in *Ceratosuchops* (Figure 5.3A) when viewed laterally, and recalls the condition observed in *Irritator*.

The floccular lobes (part of the cerebellum) are distinguishable, however, as is typical for theropods (Franzosa, 2004) and dinosaurs more generally (compared to extant non-avian reptiles) (Witmer et al., 2003). The lobes themselves, best visualised on the well-preserved right side of the *Baryonyx* endocast, display the mediolaterally thin and somewhat triangular/tabular lateral morphology of many non-maniraptoriform theropods, lacking the bulbous derived condition (Franzosa, 2004; Witmer et al., 2009; Paulina-Carabajal et al., 2017). Like *Irritator*, these project posterolaterally from the endocast, passing the plane of the anterior semicircular canal to occupy the space delineated by these vestibular structures, as in many theropods other than adult tyrannosaurids (Witmer et al., 2009), whose floccular lobes barely project into this space (but may not truly represent the size of the neural structure in life.

The lateral extent of the lobes could not be reliably reconstructed in *Ceratosuchops*; however, the floccular lobes of *Baryonyx* terminate medially to the lateral semicircular canal when viewed dorsally (Figure 5.2E). In contrast, said lobes were described as notably large in *Irritator*, additionally exhibiting lateral extent to reach the level of the lateral semicircular canal (Schade et al., 2020). Floccular lobes that reach the level of the lateral semicircular canal are observed in such theropods as *Velociraptor* (which also displays the more bulbous morphology typical of coelurosaurs) (King et al., 2020).

Two small, conical, lateral protrusions are present bilaterally on the posterior endocasts of both baryonychines, posterior to the endosseous labyrinth and dorsal to the hypoglossal (CN XII) canals. Equivalently positioned “blind dural sinus of the hindbrain” have been documented in an indeterminate theropod (Knoll et al., 1999), *Tyrannosaurus* (Witmer et al., 2009) and the sauropod *Spinophorosaurus* (Knoll et al., 2012), and a similar feature was tentatively identified as an “endolymphatic duct” in *Murusraptor* (Paulina-Carabajal et al., 2017). Rounded protuberances

in this region are nevertheless noted in many archosaurs, where they have been interpreted as diverticula of the longitudinal sinus (Hopson, 1979).

5.6.3 Cranial nerve trunks

Cranial nerve trunk organisation is highly conserved within Dinosauria (Hopson, 1979; Witmer et al., 2009), and the baryonychine endocasts do not deviate from this general pattern (Figure 5.1–Figure 5.3). As above, however, cranial nerves I–IV are unfortunately not preserved in *Baryonyx*, although the more posterior nerve trunks can all be readily distinguished. We reiterate previous works in noting that veins, as well as nerves, likely passed through the cranial nerve foramina, as is the case in extant archosaurs (Sedlmayr, 2002; Sampson et al., 2007), such that segmented canals likely contained both soft tissue structures.

In *Ceratosuchops*, both the olfactory bulbs and tract and optic nerve (CN II) trunk are situated medially and project anteriorly from the endocast. The latter is large and undivided in contrast to the condition present in some abelisaurids, whose optic nerve trunk may be subdivided by the calcified interorbital septum (Sampson et al., 2007). The small, ovate trochlear nerve (CN IV) trunks are located ventral to the cerebral hemispheres. These are usually situated dorsally to the oculomotor nerve (CN III) trunks in archosaurs (Hopson, 1979), however independent foramina for the latter could not be distinguished. The trochlear nerve trunks identified in *Irritator* (Sues et al., 2002; Schade et al., 2020) are too dorsally located to correspond to this cranial nerve, which always passes behind and then ventral to the optic lobe in extant taxa (Witmer et al., 2009). Instead, these most likely correspond to passages for orbitocerebral veins, as observed in *Majungasaurus* (Sampson et al., 2007).

The trigeminal nerve (CN V) trunks possess a large diameter and project laterally from the ventrolateral endocast surface in both baryonychines. This structure is undivided and exits the lateral braincase via a single foramen in both specimens. This mirrors the condition in *Irritator* (Sues et al., 2002) and most carcharodontosaurids (Brusatte et al., 2010), indicating an extracranial position of the trigeminal (Gasserian) ganglion (Witmer et al., 2008). In contrast, most tetanurans possess the derived condition whereby separate foramina are present for the transmission of the trigeminal's ophthalmic (CN V_1) and maxillomandibular (CN $V_{2,3}$) rami (this demonstrating an intracranial position of the ganglion) (Franzosa, 2004; Witmer et al., 2008; Witmer et al., 2009). The partial canal for the ophthalmic ramus could be segmented in *Ceratosuchops*: it splits from the lateral (extracranial) part of the trigeminal nerve trunk and extends anteriorly within a shallow sulcus on the ventrolateral surface of the laterosphenoid.

The horizontal abducens nerve (CN VI) canals are located ventrally and medially to the trigeminal nerve (CN V) trunks and are present anterior to the latter to open into the dorsal pituitary fossa. This positioning within the pituitary fossa in the baryonychines is plesiomorphic for theropods; it has been reported in *Irritator* and various allosauroids (Franzosa, 2004) and differs from the derived and more laterally projecting coelurosaur condition (Witmer et al., 2009; Bever et al., 2011). This more lateral course results from the loss of the above-mentioned cavernous sinus in members of the latter clade, although it is present in some tyrannosauroids (Witmer et al., 2009; Bever et al., 2011).

The facial nerve (CN VII) trunk becomes dorsoventrally expanded as it approaches its lateral exit through the prootic. Dorsoventral elongation of the associated external foramen has been recovered as a spinosaurid synapomorphy in some studies (Barker et al., 2021). The associated palatine and hyomandibular rami most probably diverged upon exiting the external facial nerve foramen, and thus indicate an extracranial position of the associated geniculate ganglion that is typical of theropods bar *Alioramus* (Bever et al., 2011). Indeed, sulci on the lateral surface of the prootic, whilst difficult to discern in *Baryonyx*, are visible in the better-preserved *Ceratosuchops* braincase and bear testament to this extracranial condition.

Dorsal to the facial nerve trunk is the vestibular ramus of the vestibulocochlear nerve (CN $VIII_{vest}$), which shares a common internal foramen with the former in *Ceratosuchops* (and probably *Baryonyx* as well). This ramus courses dorsolaterally towards the vestibule of the ipsilateral endosseous labyrinth in both baryonychines (Figure 5.4). The diminutive cochlear ramus of the vestibulocochlear nerve (CN $VIII_{co}$) trunk is located posterior to the facial nerve trunk, projecting laterally towards the endosseous labyrinth. This ramus appears to split laterally as it approaches the labyrinth in *Ceratosuchops* (Figure 5.5G).

The dorsoventrally elongate glossopharyngeal nerve (CN IX) trunk and more tubular vagal canal for the vagus (CN X) and accessory nerve (CN XI) trunks diverge from a common protruding feature on the hindbrain of the endocast: the metotic foramen. The foremost nerve trunk transmits laterally posterior to the fenestra ovalis and is level with the cochlear duct of the endosseous labyrinth. The vagus and accessory nerve trunks, as well as a probable small jugular vein (Sampson et al., 2007; Bever et al., 2013), take a more posterior course and open on the occiput. This organisation, and notably the posterior diversion of the vagal canal, is indicative of the subdivision of the metotic foramen by the anteromedial aspect of the otoccipital (or, more specifically, its crista tuberalis) (Gower et al., 1998; Sampson et al., 2007; Bever et al., 2013). *Baryonyx* and *Ceratosuchops* thus possess the derived theropod condition (Rauhut, 2003; Sampson et al., 2007), which is also observed in *Irritator*. The subdivision of the cavum metoticum

is incomplete in the baryonychines and the crista tuberalis does not meet the lateral endocast wall; the medial aperture of the cavum is thus undivided, as in most archosaurs (Bever et al., 2013).

Only a single hypoglossal nerve (CN XII) trunk is bilaterally present in *Baryonyx* (Figure 5.2D): this opens within a common fossa on the occiput alongside the vagal canal. Ceratosuchopsin spinosaurids, in contrast, possess a smaller third external foramen located ventrally to the vagal and hypoglossal foramina (and thus display three external foramina penetrating the occiput) (Barker et al., 2021). The path of the corresponding third canal can only be traced a short distance in *Ceratosuchops*, and its identity is unclear (Figure 5.3D); it may represent an accessory hypoglossal nerve trunk or a venous canal (Witmer et al., 2009). Three canals can also be seen in *Irritator* (M. Schade pers. comms, 2022), *contra* Sues et al. (2002) and Schade et al. (2020). Elsewhere among Theropoda, single hypoglossal canals/foramina have been noted in abelisaurids (Sampson et al., 2007; Paulina-Carabajal et al., 2018; Cerroni et al., 2019) and *Alioramus* (Bever et al., 2013), whilst two are observed in *Dilophosaurus* (Marsh et al., 2020) and *Allosaurus* (Hopson, 1979), though we note that Franzosa (2004) scores the latter taxon as possessing only a single foramen in specimen UMNH VP 18055 (previously UUVP 5961). Two hypoglossal canals are also present in various maniraptoriforms (Franzosa, 2004; Lautenschlager et al., 2012).

The presence of three external foramina on the occiput was deemed synapomorphic for megalosauroids in a previous phylogenetic analysis, the spinosaurid condition whereby two are present being regarded as a reversal (Carrano et al., 2012). The new information from *Irritator* and ceratosuchopin baryonychines (*sensu* Barker et al., 2021) would instead suggest that three passages is the more probable ancestral state amongst the spinosaurids, with the two canals in *Baryonyx* potentially representing an autapomorphic condition. However, we note here that polymorphism in hypoglossal foramen and internal canal number has been reported in *Tyrannosaurus* (Witmer et al., 2009; Bever et al., 2013), a well-sampled theropod taxon, and the character may not be as phylogenetically relevant as previously assumed.

5.6.4 Vascular structures

As mentioned above, a pair of the large, ovoid channels located on the anteroventral surface of the cerebral hemispheres corresponds to passages for the orbitocerebral veins. Posterodorsally, the paired canals of the posterior middle cerebral veins (=transversooccipital veins) adjoin the endocast posterior to the dural peak in both baryonychines, as is common for theropods. The canals are short and posterodorsally trending, opening on the occipital surface of the supraoccipital bone near its contact with the parietal.

Laterally, the lack of an obvious independent foramen in the laterosphenoid for the anterior middle cerebral vein (=transversotrigeminal vein) in either baryonychine suggests this vessel passed through the trigeminal foramen (or, potentially the prootic-laterosphenoid suture), in contrast to the condition present in many other saurischians (Rauhut, 2003).

Ventrally, the canals of the internal carotid arteries unite anteriorly prior to entering the posteroventral pituitary fossa, imparting a V-shaped morphology in the baryonychines when viewed ventrally. Such organisation is unusual among non-coelurosaurian theropods: certain ceratosaurs, allosauroids and early neotheropods possess carotid canals that enter the pituitary fossa separately (Franzosa, 2004; Sampson et al., 2007; Marsh et al., 2020). The condition in *Irritator* cannot be ascertained (Schade et al., 2020), but that in *Baryonyx* and *Ceratosuchops* recalls the condition observed in *Tyrannosaurus* and several other coelurosaurs (Franzosa, 2004), as well as *Giganotosaurus* (Paulina-Carabajal et al., 2010).

5.6.5 Endosseous labyrinth

The inner ear can be grossly subdivided into two mechanosensory organs that are respectively responsible for the detection of head movements and sound – the vestibular labyrinth (composed of the three semicircular canals, the utriculus and sacculus) and cochlea (which includes the cochlear and perilymphatic ducts) (Wever, 1978; Witmer et al., 2003; Pfaff et al., 2019; Bronzati et al., 2021; Hanson et al., 2021). Despite representing a (slightly) smaller individual, the *Baryonyx* inner ear is a slightly larger structure compared to the reassembled organ of *Ceratosuchops*, but the disarticulation experienced by the latter's braincase may have impacted some of its dimensions (Figure 5.5). Nevertheless, the semicircular canals are also slightly larger in diameter in *Baryonyx*.

The baryonychine semicircular canals are generally thin structures organised roughly orthogonally relative to one another, as seen in other theropods (Sampson et al., 2007; Witmer et al., 2009). The vertical semicircular canals are asymmetrical – a common feature among theropods including *Irritator* (Bever et al., 2013; Schade et al., 2020). The anterior semicircular canal is tall – a typical morphotype amongst avemetatarsalians (Hanson et al., 2021) – and like other dinosaurs (Sampson et al., 2007), it is the longest of the three canals in both baryonychines. These possess the elliptical morphology observed in other noncoelurosaurian theropods, lacking the anterior and posterodorsal expansion noted in tyrannosaurids and other coelurosaurs (Witmer et al., 2009). It rises above the dorsal level of the posterior canal prior to deflecting ventrally to meet the common crus between the pair. The anterior canal remains in line with the common crus, such that latter does not show the twisting seen in various coelurosaurs (Sampson et al., 2007;

Witmer et al., 2009). It maintains a near-uniform diameter throughout most of its length, however a slight ventral dilation – the anterior ampulla – can be observed in both of the Wealden Supergroup spinosaurids where the canal contacts the vestibule.

The shorter posterior semicircular canal in both baryonychines forms a simple, near-vertically oriented arc, generally comparable to the non-coelurosaurian condition (Bever et al., 2013). Its parasagittal orientation, which helps create a sub-triangular space between the three semicircular canals in lateral view, is representative of the plesiomorphic theropodan condition observed amongst various non-maniraptoriform theropods (Franzosa, 2004), including *Irritator* (Schade et al., 2020). Baryonychines also lack the anterior bowing of the posterior canal observed in tyrannosaurids and most other coelurosaurs (Witmer et al., 2009).

The lateral semicircular canal in *Baryonyx*, like that of *Irritator*, is not particularly bowed laterally in dorsal view: its anterior portion assumes a largely linear initial trajectory. This is again typical of non-coelurosaurian theropods (Bever et al., 2013), and the canal in both spinosaurids only "hooks" towards the secondary common crus in their posterior halves. *Allosaurus* produces a similar (if not slightly more exaggerated) posterior "hook" (Rogers, 1998; Witmer et al., 2009). In comparison, the lateral semicircular canal of *Ceratosuchops* is more uniformly bowed along its length, although the arc through which it sweeps is not as broad as that of various coelurosaurs (Witmer et al., 2009). Nevertheless, distinction between the posterior and lateral semicircular canals is impossible to determine in posterior view in any of the above-mentioned spinosaurids, a characteristic of non-maniraptoran theropods (Witmer et al., 2009).

The vestibule is typically archosaurian (some exceptions not withstanding) in failing to extend dorsally above the level of the lateral semicircular canal (Sampson et al., 2007; Witmer et al., 2009; Bever et al., 2013). The ventrally projecting cochlea is relatively long, as in archosaurs generally (Hanson et al., 2021), and accounts for approximately two-thirds of the dorsoventral height of the vestibular labyrinth in both baryonychines. Intriguingly, this is different from the subequal proportions described for *Irritator* (Schade et al., 2020) and the relatively short cochlea of abelisaurids (Cerroni et al., 2019). A subtle degree of medial inclination is also observed in *Baryonyx* and *Ceratosuchops* when viewed anteriorly, as in *Irritator* (Schade et al., 2020) and tyrannosaurids (Witmer et al., 2009). In comparison, the medial inclination of the cochlea is more exaggerated in *Sinraptor* and *Murusraptor* (Choiniere et al. (2021): supplementary data S2). A small, dorsally situated lateral projection on the cochlear duct in both baryonychines marks the passage from the fenestra ovalis, through which the columella passes.

5.6.6 Basicranial pneumaticity

Details of the braincase pneumaticity will be presented elsewhere; here, we include brief comments given their effects on hearing capabilities, which are discussed below. Relative to that of some other theropods such as tyrannosaurids (Witmer et al., 2009), pneumaticity is only subtly developed in the *Baryonyx* and *Ceratosuchops* braincase: pneumatic structures include indentations on the lateral basisphenoid for the lateral tympanic recess, and deeper subsellar and basisphenoidal recesses within the cultriform process and basisphenoid, respectively.

An indentation on the posterior basioccipital and ventral to the occipital condyle is present in both taxa, which varies substantially in form and development. This was incorrectly referred to as a "subcondylar recess" in *Ceratosuchops* in Barker et al. (2021); however, such a recess usually refers to paired structures and is only present in a few theropod clades such as tyrannosaurids and ornithomimosaurs (Witmer, 1997a). It remains unclear whether these indentations pertain to an excavation by a pneumatic system or are simply epiphenomena related to the elevation of the muscular ridges that delimit them laterally.

5.7 Discussion

The cranial endocasts of the Wealden Supergroup baryonychines provide insight into the early evolution and anatomy of the spinosaurid endocranium. Like *Irritator* (Schade et al., 2020), both *Baryonyx* and *Ceratosuchops* possess neuroanatomical features typical of their phylogenetic position as non-coelurosaurian tetanurans. These include the possession of weakly demarcated brain regions, prominent cranial flexures, mediolaterally thin, "tabular" floccular lobes, and asymmetrical vertical semicircular canals.

With the above-described caveats regarding the body mass estimation used in our assessment of relative encephalisation, the calculated REQ for *Baryonyx* is approximately between 1.2 ($REQ_{37\%}$) and 1.6 ($REQ_{50\%}$). Some question exists on the utility of encephalisation quotients (Balanoff et al., 2020); nevertheless, we note that the degree of encephalisation calculated for large predatory theropods is generally comparable, the exception being select tyrannosaurids (Table 5.3). This, combined with the conservative nature of non-coelurosaurian theropod endocranial morphology, implies comparable cognitive capacity and behavioural sophistication among the taxa concerned.

Table 5.3 Reptile Encephalisation Quotients (REQ) calculated for a range of theropods. Modified from (Cerroni et al., 2019). Note that the endocranial volumes (EV) at 37% and 50% of *Giganotosaurus* were misreported in Cerroni et al. (2019). Mbd, body mass.

Taxon	**EV (cm^3)**	**EV (cm^3) 37%**	**EV (cm^3) 50%**	**Mbd (g)**	**REQ 37%**	**REQ 50%**
Baryonyx	150.5	55.7	75.3	2011000	1.2	1.6
Carnotaurus	169.8	62.8	84.9	1419000–1743000	1.4–1.6	1.9–2.2
Majungasaurus	106.4	39.4	53.2	1130000	1.14	1.54
Ceratosaurus	–	–	–	–	1.2	1.7
Allosaurus	169–188	62.5–69.5	84.5–93.9	1400000–2300000	1.3–1.8	1.8-2.4
Sinraptor	95	35.1	47.5	1700000	0.8	1.1
Giganotosaurus	275	101.7	137.5	7000000	1.1	1.4
Murusraptor	148.2	54.8	74.1	1551000	1.33	1.8
Tyrannosaurus	414.2	153.2	207.1	5654000–7000000	1.8–1.6	2.5–2.2
Gorgosaurus	128.9	47.7	64.5	1100000	1.4	1.9

Some differences in endocranial and neurovascular morphology are present between *Ceratosuchops* and *Baryonyx*. These include the number of hypoglossal nerve (CN XII) canals (and their associated external foramina), the cranial flexure angles, the relative position of the dorsal expansion, the shape of the dorsal margin in the regions of the telencephalon and ventral margin of the rhombencephalon, the shape of the lateral semicircular canal, and the dimensions of the inner ear. It is not clear whether any of these lend support to the osteological characters used to differentiate the Wealden Supergroup baryonychines by Barker et al. (2021): endocasts of better-sampled theropods such as *Allosaurus* (Hopson, 1979) and *Tyrannosaurus* (Witmer et al., 2009) have been described as “very similar” or “[showing] little variation”. Variation, when present, is possibly taphonomic or ontogenetic in nature, but studies examining this variation is rare (Lautenschlager et al., 2013) or speculative (McKeown et al., 2020), and our understanding of its influence between and within taxa remains preliminary (Hu et al., 2021).

5.7.1 Inferred sensory capabilities of the Wealden Supergroup spinosaurids

5.7.1.1 Vision and gaze stabilisation

As with many other studied theropods (Witmer et al., 2009), the imperceptible optic lobes in both baryonychine endocasts provide little information regarding visual acuity or sensitivity. The floccular lobes, however, may provide some information on the visual system. Integrating information from the latter as well as the vestibular systems of the inner ear (Voogd et al., 2004), the floccular lobes regulate gaze stabilisation via compensatory movements of the eyes in response to rotation of the head (vestibulo-ocular reflex, VOR), help track moving objects within the field of view (smooth pursuit), and (in some taxa) stabilise the head via recruitment of the cervical musculature (vestibulo-collic reflex, VCR) (Ito, 1982; Witmer et al., 2003; Ferreira-Cardoso et al., 2017).

Relative floccular lobe size has been used (in part) to reconstruct theropod ethology, where enlargement has been qualitatively correlated with increased capacity for gaze stabilisation (Lautenschlager et al., 2012; Cerroni et al., 2019; King et al., 2020). The relatively large floccular lobe in *Irritator* (compared to other non-coelurosaurian theropods but not many coelurosaurs) was regarded as evidence of improved performance of the VOR and VCR systems (Schade et al., 2020). However, the size of this structure appears to correlate negatively with body size in theropods (Paulina-Carabajal et al., 2021). Size may also reflect differing ontogenetic status, as has been noted during tyrannosaurid ontogeny, for example, and the small condition in mature individuals may not necessarily reflect of the size of the neural structure in life (Witmer et al., 2009). Indeed, rather than being indicative of differing ecologies, the influence of allometry or ontogeny could explain the difference in floccular lobe size in *Baryonyx* and *Irritator*, whose estimated skull lengths (*Irritator,* 600mm; *Baryonyx*, 910mm; Sues et al., 2002; Therrien et al., 2007) tentatively suggest differing ontogenetic status. We note, however, the assessment of ontogenetic status in non-coelurosaurian theropods is complicated (Griffin et al., 2020), and as a result, the relative age of the above spinosaurids has not been rigorously determined. Further clouding the interpretation of floccular lobe size is the fact that the reconstructed structures may not be indicative of the neural tissues themselves, since additional tissues were likely also present alongside the floccular lobes (Walsh et al., 2013; Ferreira-Cardoso et al., 2017).

The more complete right floccular lobe of *Baryonyx* is grossly comparable to other non-coelurosaurian tetanurans in shape and extent. With the above caveats in mind and assuming the preserved lobe contained comparable amounts of neural tissue per unit volume, this similarity crudely implies *Baryonyx* possessed similarly developed gaze stabilisation mechanisms, and that these were potentially less developed than in *Irritator*.

Although beyond the scope of this study, some preliminary inferences regarding the visual capabilities of *Ceratosuchops* can be additionally made via the skeletal elements. Rearticulation of the holotype braincase (IWCMS 2014.95.1–3) and the referred and mirrored postorbital (IWCMS 2014.95.4) shows that the orbits appear more anteriorly facing compared to some other theropods (e.g. *Ceratosaurus*), which display the plesiomorphic, laterally facing condition (Zelenitsky et al., 2009). If correct, this could indicate a higher degree of stereoscopic vision, which perhaps aided in to the calculation of prey position during hunting. However, we note that stereopsis can evolve in animals with laterally facing orbits, and that it may not necessarily be present in animals with binocular overlap (Nityananda et al., 2017).

5.7.1.2 Hearing

The endosseous cochlear duct (housing the cochlea or basilar papilla), is closely associated with hearing performance (sensitivity and frequency range) (Walsh et al., 2009; Choiniere et al., 2021). Indeed, longer cochlear ducts provide improved sensitivity to low frequency sounds (Gleich et al., 2005; Walsh et al., 2009). The auditory capabilities of the Wealden Supergroup baryonychines, as well as various other saurischians, are presented in Table 5.4.

Table 5.4 Auditory capabilities of various saurischians based on the equations of Walsh et al. (2009). See methods for data collected for *Baryonyx*, *Ceratosuchops*, *Viavenator*, *Sinraptor*, *Murusraptor* and *Erlikosaurus*. Data for *Irritator* from Schade et al. (2020); *Phuwiangosaurus* from (Kaikaew et al., 2023); *Thecodontosaurus* from Ballell et al. (2020); and *Velociraptor* (IGM 100/976) from King et al. (2020). All other data from Hanson et al. (2021).

Taxon	Specimen Number	Cochlear duct length (ECD; mm)	Basicranial length (BCL; mm)	Best hearing frequency (Hz)	Mean hearing frequency (Hz)
Baryonyx	NHMUK PV R9951	19.6	104.5	2538	1594
Ceratosuchops	IWCMS 2014.95.3	17.7	106.8	2210	1416
Irritator	SMNS 58022	18.1	75.3	3196	1950
Viavenator	MAU Pv LI 530	15.5	99.1	2057	1333

Taxon	Specimen Number	Cochlear duct length (ECD; mm)	Basicranial length (BCL; mm)	Best hearing frequency (Hz)	Mean hearing frequency (Hz)
Sinraptor	IVPP 10600	17.8	102.7	2329	1480
Murusraptor	MCF PVPH 411	19.2	75.3	3352	2036
Erlikosaurus	IGM 100.111	11.1	55.2	2723	1694
Velociraptor	IGM 100/976	11.15	34.71	3965	2368
	IGM 100/0977	7.44	24.66	3798	2278
Alioramus	IGM 100/1844	17.88	104.63	2292	1460
Citipati	IGM 100/3006	8.75	21.42	4602	2713
Byronosaurus	IGM 100/0983	7.97	19.24	4639	2733
Troodontidae indet.	IGM 100/3500	6.68	15.54	4737	2787
Thecodontosaurus	YPM 2192	9.3	40.28	3089	1893
Phuwiangosaurus	SM K11-006	9.48	n/a	1687	1132

Archosaurs display elongate cochlear ducts relative to most other reptiles (Hanson et al., 2021). An increased degree of cochlear ducts elongation is observed in several theropods and is potentially related to adaptations for auditory foraging (Choiniere et al., 2021). Moderate elongation is present in coelurosaurs including hypercarnivorous tyrannosaurids, dromaeosaurids, alvarezsaurids and troodontids as well as secondarily herbivorous therizinosaurs. However, some hypercarnivorous non-coelurosaurian theropods (e.g. *Viavenator* and *Sinraptor*) and some herbivorous/omnivorous coelurosaurs (e.g. oviraptorids and ornithomimosaurs) have relatively short ducts, suggesting they relied on other senses (Choiniere et al., 2021).

Although some works have critiqued the use of Walsh et al.'s (2009) equations (Knoll et al., 2021), they have been commonly used as an approximation of hearing capabilities in extinct taxa and provide a basis for comparisons (Table 5.4). Previous works estimated that most saurischians have an optimal hearing frequency between 3500–5500 Hz (akin to modern birds) and best mean

hearing frequencies between 2250–3250 Hz (Hanson et al., 2021), although the extinct sample was biased towards smaller maniraptoran taxa. However, Gleich et al. (2005), using a different method, suggested large dinosaurs were capable of low frequency perception up to 3000 Hz. The baryonychines share gross hearing capabilities in common with other large theropods such as abelisaurids, allosauroids and tyrannosauroids in having lower-pitched optimal frequency ranges (Table 5.4). *Baryonyx* and *Ceratosuchops* also both possessed lower estimated auditory capabilities relative to those reported for *Irritator* (Schade et al., 2020), suggesting differing hearing ecologies between the clades.

The lack of extensive tympanic pneumaticity in either baryonychine also suggests that, like *Irritator* (Schade et al., 2020), the middle ear system was not as specialised for the reception of low-frequency sounds as those of tyrannosaurids (Witmer et al., 2009). Extensive pneumaticity (and thus volume of these sinuses) in this region affects the impedance-matching capabilities of the middle ear and permits the emphasis of low-frequency sounds (Witmer et al. (2009), and references therein), which spinosaurids were seemingly less reliant upon.

5.7.1.3 Equilibrium and head posture

Semicircular canal shape has been previously used to infer aspects of spinosaurid ecology: Schade et al. (2020) discussed the possible behavioural ecology of *Irritator* based on the elongate anterior semicircular canal, which they considered to impart enhanced sensitivity to pitch-down movements of the head. The morphology of the vestibular labyrinth observed in both *Irritator* and the Wealden Supergroup baryonychines (i.e. vertically tall anterior semicircular canals) meanwhile resembles the bipedal locomotor morphotype described in Hanson et al. (2021). While the bipedal nature of baryonychines is now uncontroversial, it is of historic interest that *Baryonyx* was initially considered to be quadrupedal (Charig et al., 1986), a stance that was revised in subsequent works (Charig et al., 1997). However, it is becoming increasingly difficult to support correlations between semicircular canal geometry and specific ecological or locomotor functions, which may instead be linked to spatial and developmental constraints (Benson et al., 2017; Bronzati et al., 2021; David et al., 2022; Evers et al., 2022). We note that some quadrupedal dinosaurs, such as *Spinophorosaurus* (Knoll et al., 2012), also possess vertically tall anterior semicircular canals, as do some pterosaurs such as *Anhanguera* (Witmer et al., 2003), and increases in relative height of the anterior semicircular canal may not only be affected by bipedal locomotion but also erect limb postures (Bronzati et al., 2021). Taken together, the above inferences regarding spinosaurid locomotion/ecology and semicircular canal geometry are incompatible with the current consensus.

Similarly, previous trends that used lateral semicircular canal orientation to infer "alert" or "habitual" head posture have since been questioned (Marugán-Lobón et al., 2013; Benoit et al., 2020). Nevertheless, independent support for a down-turned position of the skull in *Irritator* was provided by the slight ventral rotation of the occipital condyle (Sues et al., 2002; Schade et al., 2020). Such rotation is absent in *Baryonyx* and *Ceratosuchops*, with the condyle projecting largely posteriorly in the baryonychines. Thus, regardless of lateral semicircular canal orientation, the craniocervical articulation suggests differing "standard" head postures within Spinosauridae.

5.7.1.4 Olfaction

Ceratosuchops possess raw olfactory ratios (olfactory bulb length: 26.4mm; cerebral hemisphere diameter: 52.2mm) similar to those of most other non-maniraptoran theropods (Table 5.5). When the log-transformed olfactory ratio and estimated body mass are considered and subsequently plotted onto the graph in Zelenitsky et al. (2009: Fig. 2), the generalised baryonychine olfactory ratio is near that predicted for a theropod of this size. Baryonychines thus possess the "typical" (c.f. plesiomorphic) condition amongst Mesozoic theropods (Zelenitsky et al., 2009). Such olfactory capabilities are shared with ceratosaurs, allosauroids and basal tyrannosauroids, with the taxa concerned perhaps being less reliant on olfaction than tyrannosaurids and dromaeosaurids (Zelenitsky et al., 2009).

Table 5.5 Olfactory ratios of select theropods. Data from Zelenitsky et al., (2009; 2011), and supplemented by [a]Cerroni et al. (2019), [b]Paulina-Carabajal et al. (2018) and [c]Paulina-Carabajal et al. (2017).

Taxon	**Olfactory Ratio (%)**
Spinosauridae	
Ceratosuchops	50.6
Ceratosauria	
Ceratosaurus	48.1
Majungasaurus	48.3
Carnotaurus[a]	50
Viavenator[b]	57
Allosauroidea	
Allosaurus	50–51.6

Taxon	Olfactory Ratio (%)
Acrocanthosaurus	58.1
Carcharodontosaurus	56
Giganotosaurus	57.7
Sinraptor[a]	55
Tyrannosauroidea	
Dilong	27
Tarbosaurus	65.1–67.4
Tyrannosaurus	68.3–71
Murusraptor[c]	45–50
Ornithomimosauria	28.2–32.5
Oviraptoridae	31.5
Dromaeosauridae	28.5–36
Troodontidae	32.6–33.5

Regarding spinosaurine olfactory bulbs, Arden et al. (2019) suggested that the reduced condition of the bulbs based on frontal specimens from the Ifezouan Formation of Morocco was consistent with an "aquatic" lifestyle. The correlation (or lack thereof) between spinosaurid olfactory bulb size and aquatic ecology was commented on by Hone et al. (2019). We supplement this discussion with the discovery that baryonychines did not (based on the mass estimates mentioned above) possess reduced olfactory bulbs relative to their body size; our results indicate retention of the ancestral theropod condition in spinosaurids. Comments regarding the spinosaurine condition thus await better-preserved specimens that allow for more accurate measurements of endocranial features and estimations of mass.

5.7.2 Implications of baryonychine sensory systems

Consensus exists that spinosaurids exhibit specialisation for some (almost certainly varying) degree of aquatic or semiaquatic adaptation. This view has to be evaluated within the broader debate on which endocranial features are indicative of semi-aquatic or aquatic behaviour amongst archosaurs. Some studies suggest that shape changes in the inner ear of various amniotes correlate with transitions from terrestrial to semi- and fully-aquatic ecologies (Spoor et

al., 2002; Neenan et al., 2017; Schwab et al., 2020), for example. Others, as mentioned above, find no evidence for change in labyrinth shape being associated with such transitions and, furthermore, question previous form-function inferences based on vestibular geometry (Bronzati et al., 2021; Evers et al., 2022). Furthermore, derived ecologies can arise in the absence of significant shifts in endocranial anatomy, as observed in the extant diving bird *Cinclus* (Passeriformes: Cinclidae), whose endocasts and inner ears are very similar to non-diving passeriform relatives (Smith et al., 2022).

The grossly comparable endocranial morphologies and REQ scores, relative to other non-coelurosaurian tetanurans and ceratosaurs, suggests that baryonychines shared similar cognitive capacities with terrestrial, hypercarnivorous forms. This might indicate that spinosaurids were pre-adapted in terms of neural and sensory adaptations for the exploitation of aquatic prey, or that modification of the rostrum and dentition were sufficient for successful prey capture in aquatic settings and that substantial reorganisation of the endocranium was apparently not required. Further, the unremarkable hearing and olfactory capabilities inferred here also indicates that baryonychines did not deviate substantially from the auditory and olfactory capabilities of "typical" non-coelurosaurian theropods.

The tactile capabilities of the spinosaurid rostrum have also been deemed important in the context of prey detection and capture in some previous works, with neurovascular networks and patterning of the associated external foramina perhaps imparting crocodile-like sensitivity to prey movement in water (Ibrahim et al., 2014). Tactile sensation of the face and jaws of vertebrates is detected by the trigeminal nerve (CN V) (Schneider et al., 2016; Vermeiren et al., 2020); however, the available endocranial data for spinosaurids suggests, qualitatively at least, that there is little evidence of an emphasised trigeminal nerve system in these theropods, as is consistent with previous observations of other dinosaur endocasts (Porter et al., 2020). Difficulties persist in collecting the relevant quantitative data in theropod dinosaurs, such as trigeminal ganglion volume, a proxy for facial sensation in crocodyliforms and possibly other archosaurs (George et al., 2013; Lessner et al., 2022). Meanwhile, measurements based on neurovascular foramen size alone would be unreliable due to the likely passage of concomitant vasculature (see above). Whilst some tetanurans with clear adaptations for terrestrial predation possessed rostral neurovascular features akin to spinosaurids and suggestive of tactile jaw edges (Barker et al., 2017; Kawabe et al., 2022), there is no a priori reason to assume theropods had enhanced sensitivity around the oral margin (Porter et al., 2020). Nevertheless, spinosaurids may prove to be an exception (Porter et al., 2020), with the degree of neurovascular branching perhaps more developed relative to other tetanurans (Bouabdellah et al., 2022). Further work, perhaps focusing on the branching pattern of canals within the dentary (which may provide the clearest signal for

facial tactile sensation) (Lessner, 2021), for instance, is clearly needed before rostral neurovascular specialisations can be inferred for the clade.

Intriguingly, low frequency hearing in the tyrannosaurid *Alioramus* has been tentatively associated with the detection of abnormally low juvenile vocalisations, a possible lack of parental care, or an adaptation for the detection of sounds made by large prey (Hanson et al., 2021). We show that using a larger sample of basal tetanurans and ceratosaurs that low frequency hearing is not autapomorphic to *Alioramus* and is seen in a range of large predatory theropod taxa (Table 5.4). It would be extremely speculative to link this with inferred parental behaviour (or the lack of it), and dietary characteristics related to cochlear duct dimensions failed to produce significant signals (Hanson et al., 2021). Nevertheless, low frequency hearing in baryonychines as an adaptation for detecting large prey would not corroborate with evidence of spinosaurids as predators of generally small vertebrates (Therrien et al., 2005; Hone et al., 2017), as shown by their relatively weak bite force for instance (Sakamoto, 2022). Indeed, small prey items were likely commonly selected and depredated by carnivorous theropods in general (Hone et al., 2010b).

5.8 Conclusions

Baryonyx and *Ceratosuchops* possess well-preserved endocranial features, and provide insight into the evolution of the brain and sensory systems in earlier branching spinosaurids. The overall morphology of the reconstructed endocasts is reflective of their phylogenetic position and follows previous observations of endocranial conservatism in non-maniraptoriform theropods. Similarly, the morphology of the endosseous labyrinth, and in particular the shape of the semicircular canals, is comparable to other non-coelurosaurian tetanurans. REQ values imply that baryonychines did not deviate substantially in terms of cognitive capacity and behavioural sophistication relative to other basal theropods, and these predators possessed unexceptional hearing and olfactory capabilities on par with several other large-bodied terrestrial theropods. There is no tangible evidence for adaptations to semi-aquatic ecologies in the baryonychine endocrania, suggesting that neural and sensory systems of spinosaurids were pre-adapted for the successful detection and capture of aquatic prey, or that the initial transition to semi-aquatic ecologies simply required modifications of the craniodental apparatus.

5.9 Acknowledgments

We would like to thank: Martin Munt and Alex Peaker (Dinosaur Isle Museum) and Angela Milner and Sandra Chapman (Natural History Museum) for access to the specimens; Gary Blackwell (Dinosaur Isle Museum) for expert preparation of the *Ceratosuchops* braincase; Orestis

Katsamenis, Ronan Smith, Rich Broadman and Mark Mavrogordato (µ-VIS X-Ray Imaging Centre, University of Southampton, UK) for their help and advice with the *Ceratosuchops* scans; Susannah Maidment (Natural History Museum) for providing the *Baryonyx* femoral shaft data; Michael Hanson for providing the dataset for the hearing inferences; Logan King for discussion; and Arjan Westerdiep for help with the *Voxeliser* application. We would also like to thank Marco Schade for commenting on an earlier draft of the manuscript. We are grateful for the detailed comments of Ariana Paulina-Carabajal and Serjoscha Evers, which improved the manuscript. Phil Cox and Edward Fenton are additionally thanked for handling the paper. Chris Tijani Barker is funded by the Institute for Life Sciences (University of Southampton) and the Engineering and Physical Sciences Research Council (EPSRC; Project Ref: 2283360). Grant to Lawrence Witmer & Ryan Ridgley from the United States National Science Foundation (NSF IOB-0517257, IOS-1050154, IOS-1456503) and the Swedish Research Council (SRC 2021-02973).

5.10 Data availability statement

The data that support the findings of this study are available on Morphosource (https://www.morphosource.org/projects/000491312)

5.11 Figures

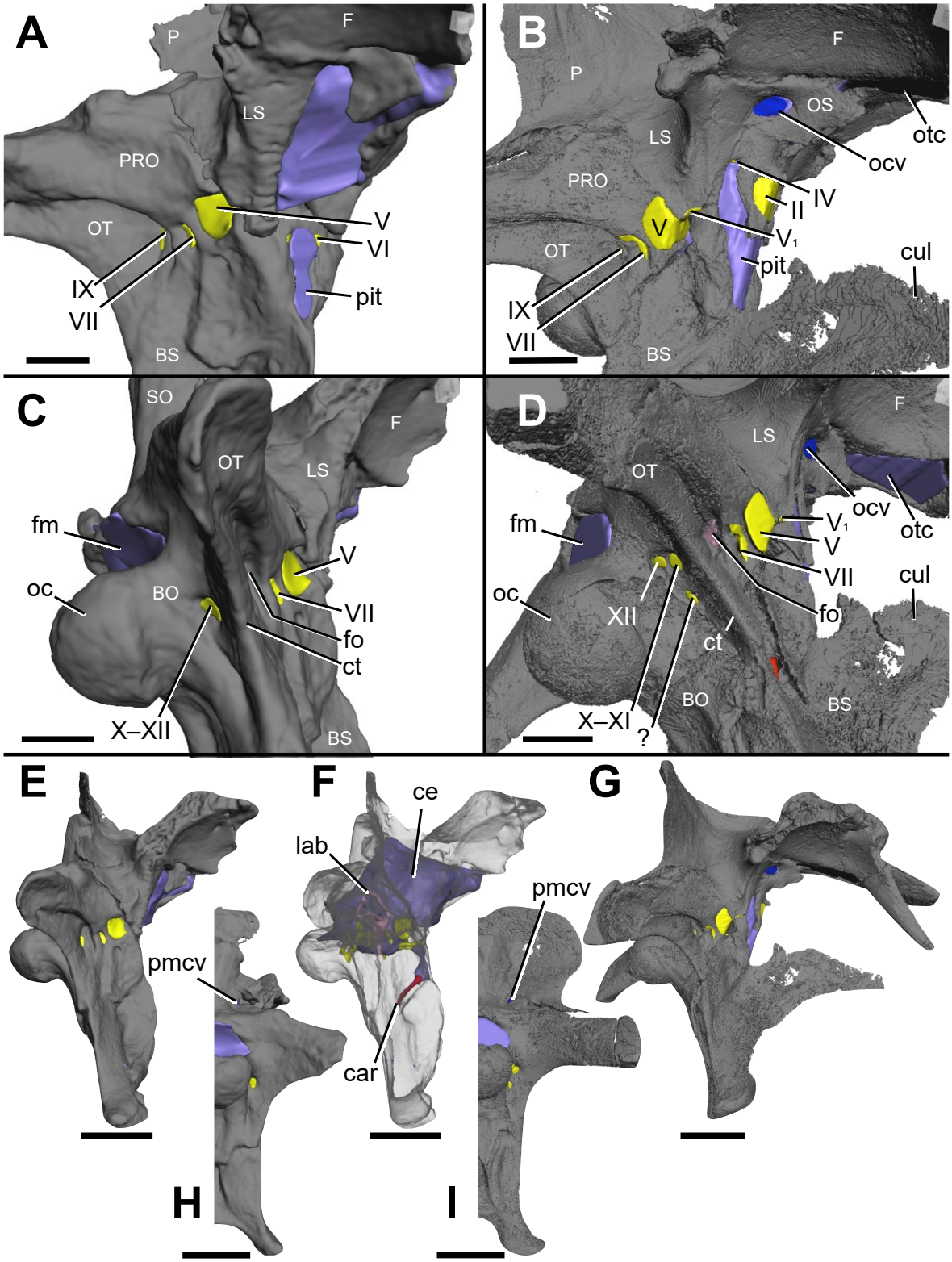

Figure 5.1 Braincases of A, C, E, F, H) *Baryonyx walkeri* (NHMUK PV R9951) and B, D, G, I) *Ceratosuchops inferodios* (IWCMS 2014.95.1–3), in A–B) right anterolateral and C–D) right posterolateral, E–G) right lateral and H–I) posterior (right side) views, showing the major neurovascular features (and associated foramina) and braincase anatomy.

Note that in *Baryonyx*, the separate cranial nerve trunks X—XI and XII open into a common fossa lateral to the occipital condyle, which is depicted here. Abbreviations: ce, cranial endocast; cul, cultriform process; ct, crista tuberalis; BO, basioccipital; BS, basisphenoid; car, cerebral internal carotid artery canal; F, frontal; fm, foramen magnum; fo, fenestra ovalis; lab, endosseous labyrinth; LS, laterosphenoid; ocv, orbitocerebral vein; oc, occipital condyle; OS, orbitosphenoid; OT, otoccipital; otc, olfactory tract; P, parietal; pit, pituitary; pmcv, posterior middle cerebral vein canal; PRO, prootic; II, optic nerve canal; IV, trochlear nerve canal; V, trigeminal nerve canal; V_1, ophthalmic nerve canal; VI, abducens nerve canal; VII, facial nerve canal; IX, glossopharyngeal nerve canal; X–XI, shared canal for the vagus and accessory nerves, and accompanying vessels; XII, hypoglossal nerve canal; ?, potential accessory hypoglossal nerve or venous canal. Scale bars: A–D) 20mm and E–I) 50mm.

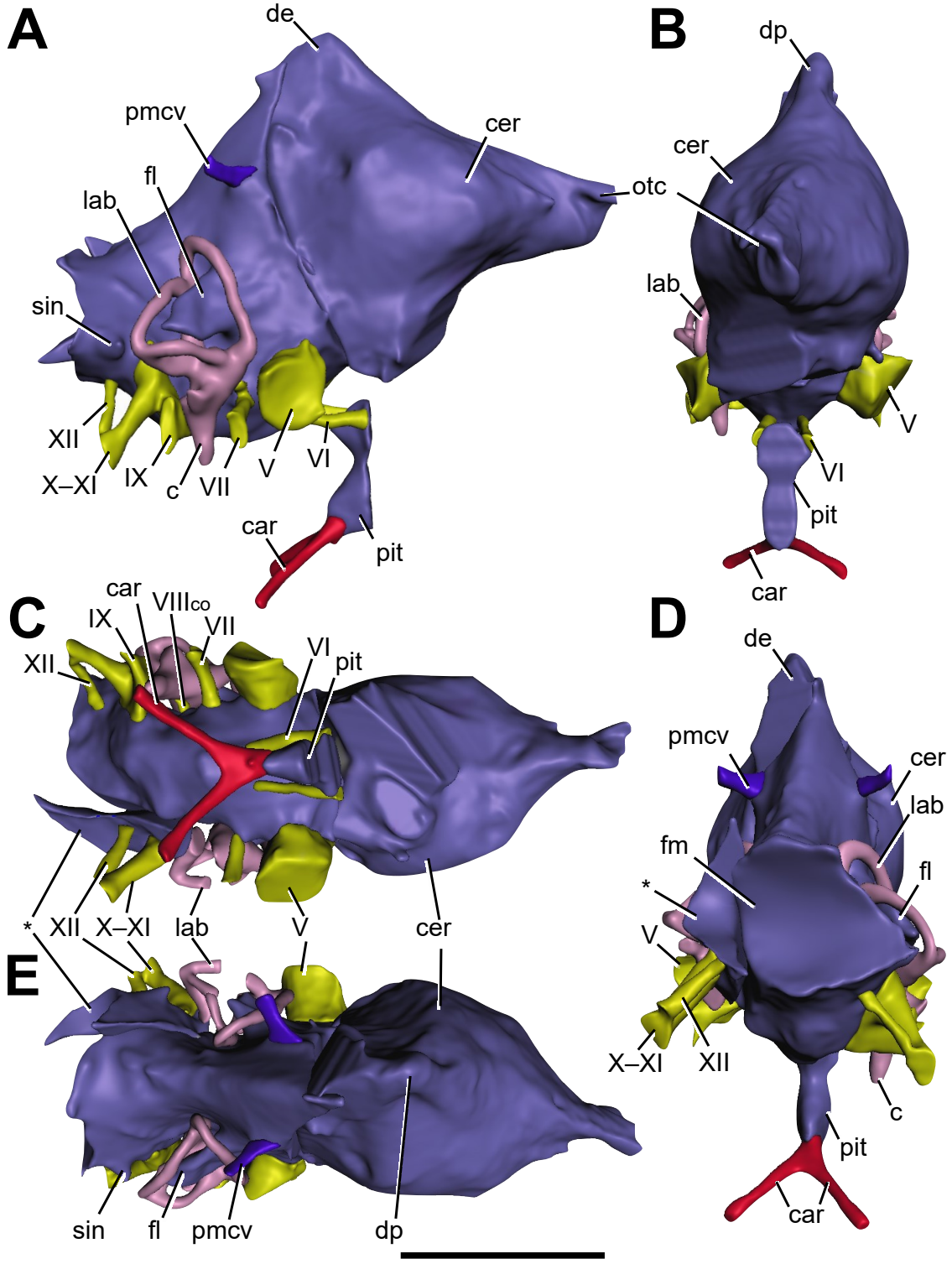

Figure 5.2 Cranial endocast of *Baryonyx walkeri* (NHMUK PV R9951), reconstructed from CT scans, in A) right lateral, B) anterior, C) ventral, D) posterior and E) dorsal views. Vascular structures and endosseous labyrinth also depicted. Abbreviations: c, cochlea; car, cerebral internal carotid artery canal; cer, cerebral hemisphere; de, dorsal expansion; fl, floccular lobe; lab, endosseous labyrinth; otc, olfactory tract; pit, pituitary; pmcv,

posterior middle cerebral vein canal; sin, blind dural venous sinus of the hindbrain; V, trigeminal nerve canal; VI, abducens nerve canal; VII, facial nerve canal, $VIII_{co}$, cochlear ramus of the vestibulocochlear nerve; IX, glossopharyngeal nerve canal; X–XI, shared canal for the vagus, and accessory nerves, and accompanying vessels; XII, hypoglossal nerve canal. Asterisk (*) marks the disarticulated left otoccipital portion of the endocast. Scale bar: 50mm.

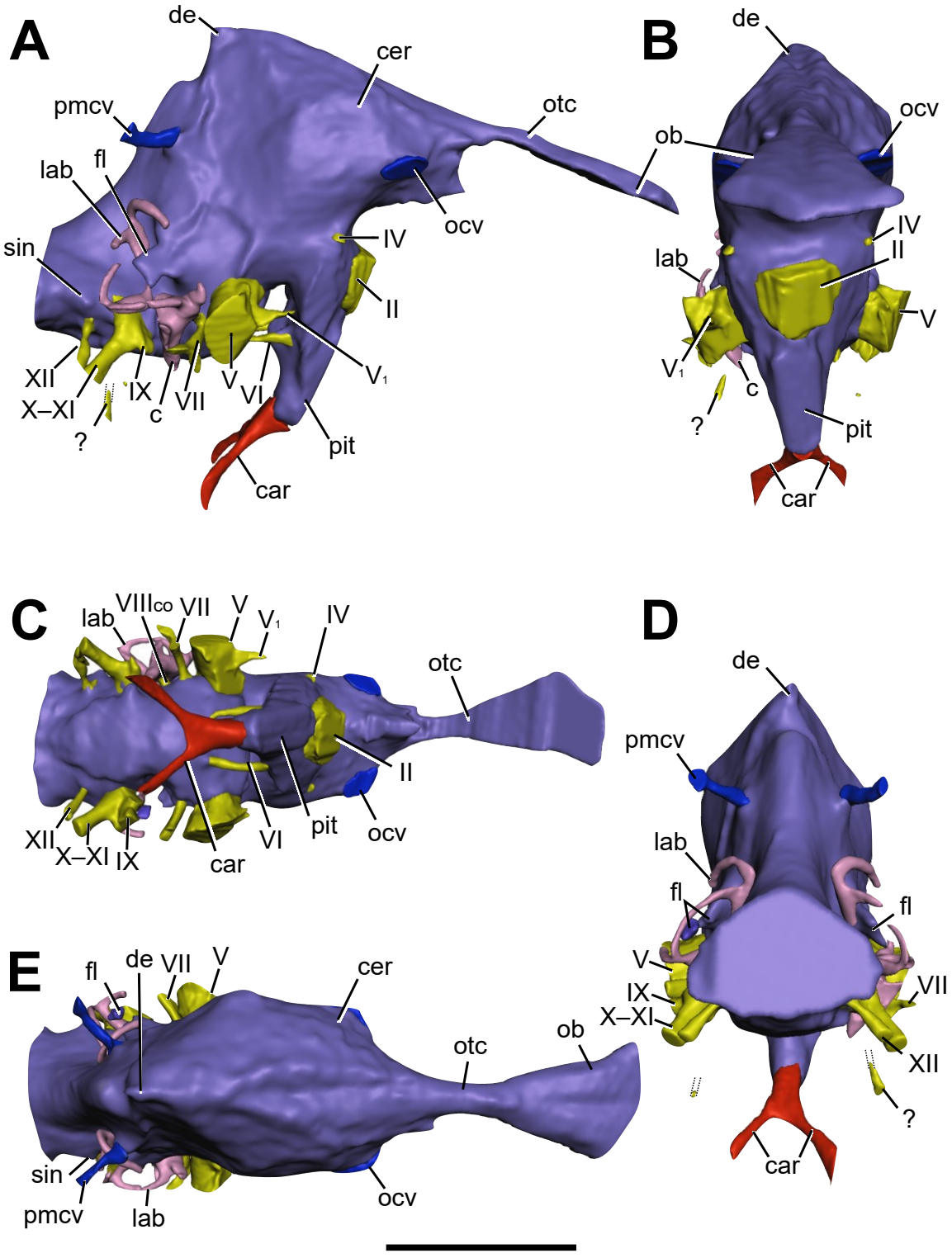

Figure 5.3 Cranial endocast of *Ceratosuchops inferodios* (IWCMS 2014.95.1–3), reconstructed from CT scans, in A) right lateral, B) anterior, C) ventral, D) posterior and E) dorsal views. Vascular structures and endosseous labyrinth also depicted. Abbreviations: c, cochlea; car, cerebral internal carotid artery canal; cer, cerebral hemisphere; de, dorsal expansion; fl, floccular lobe; lab, endosseous labyrinth; ocv, orbitocerebral vein; pit, pituitary; pmcv, posterior middle cerebral vein canal; sin, blind dural venous

sinus of the hindbrain; II, optic nerve canal; IV, trochlear nerve canal; V, trigeminal nerve canal; V_1, ophthalmic nerve canal; VI, abducens nerve canal; VII, facial nerve canal, $VIII_{co}$, cochlear ramus of the vestibulocochlear nerve; IX, glossopharyngeal nerve canal; X–XI, shared canal for the vagus, and accessory nerves, and accompanying vessels; XII, hypoglossal nerve canal; ?, potential accessory hypoglossal nerve or venous canal. Scale bar: 50mm.

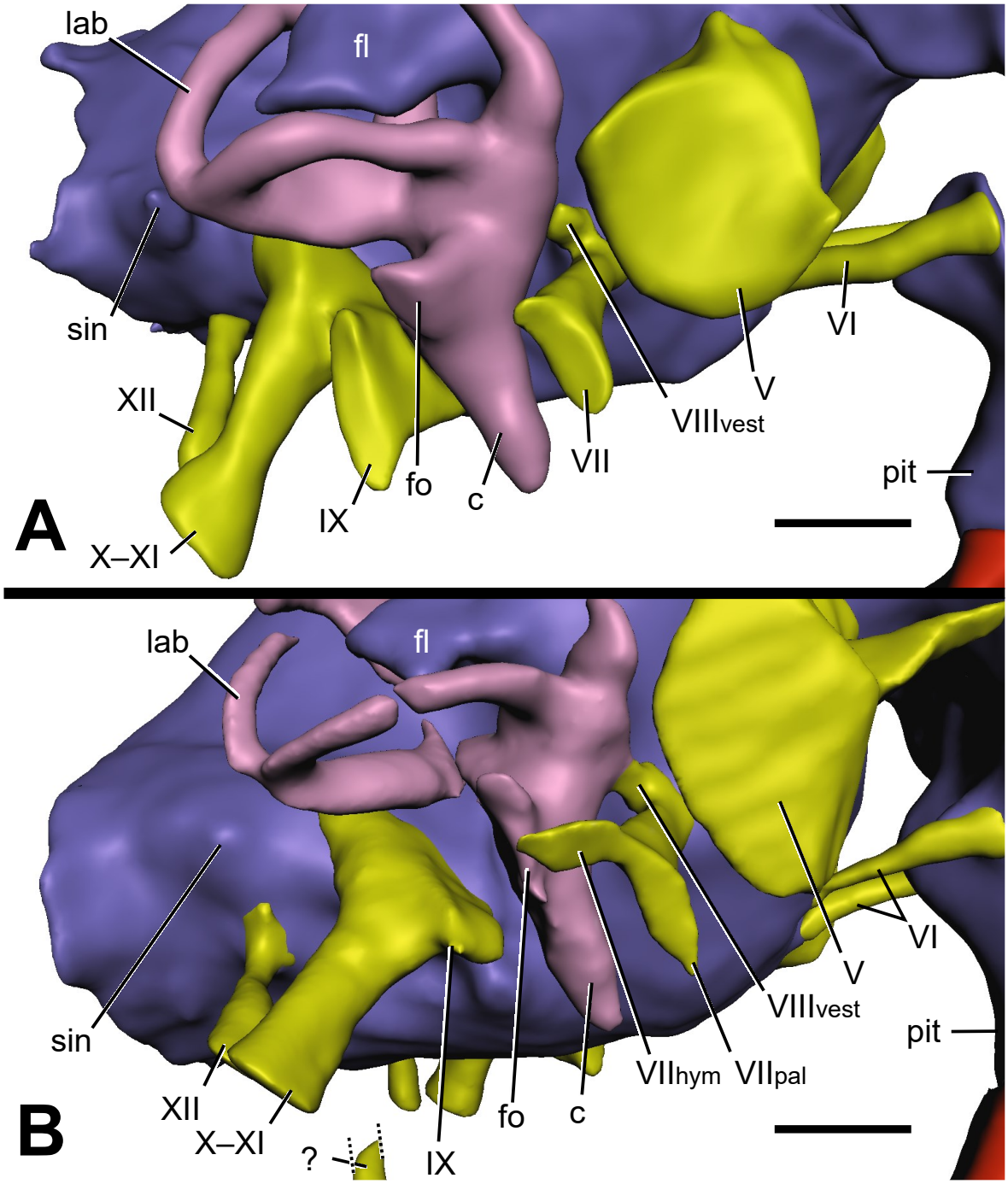

Figure 5.4 The baryonychine rhombencephalon, in right lateral views. A) *Baryonyx walkeri*, B) *Ceratosuchops inferodios*. Abbreviations: c, cochlea; fl, floccular lobe; fo, fenestra ovalis; lab, endosseous labyrinth; pit, pituitary; sin, blind dural venous sinus of the hindbrain; V, trigeminal nerve canal; VI, abducens nerve canal; VII_{hym}, hyomandibular ramus of the facial nerve; VII_{pal}, palatine ramus of the facial nerve; $VIII_{vest}$, vestibular ramus of the vestibulocochlear nerve; IX, glossopharyngeal nerve canal; X–XI, shared canal for the vagus and accessory nerves, and accompanying vessels; XII, hypoglossal

nerve canal; ?, potential accessory hypoglossal nerve or venous canal.. Scale bar: 10mm.

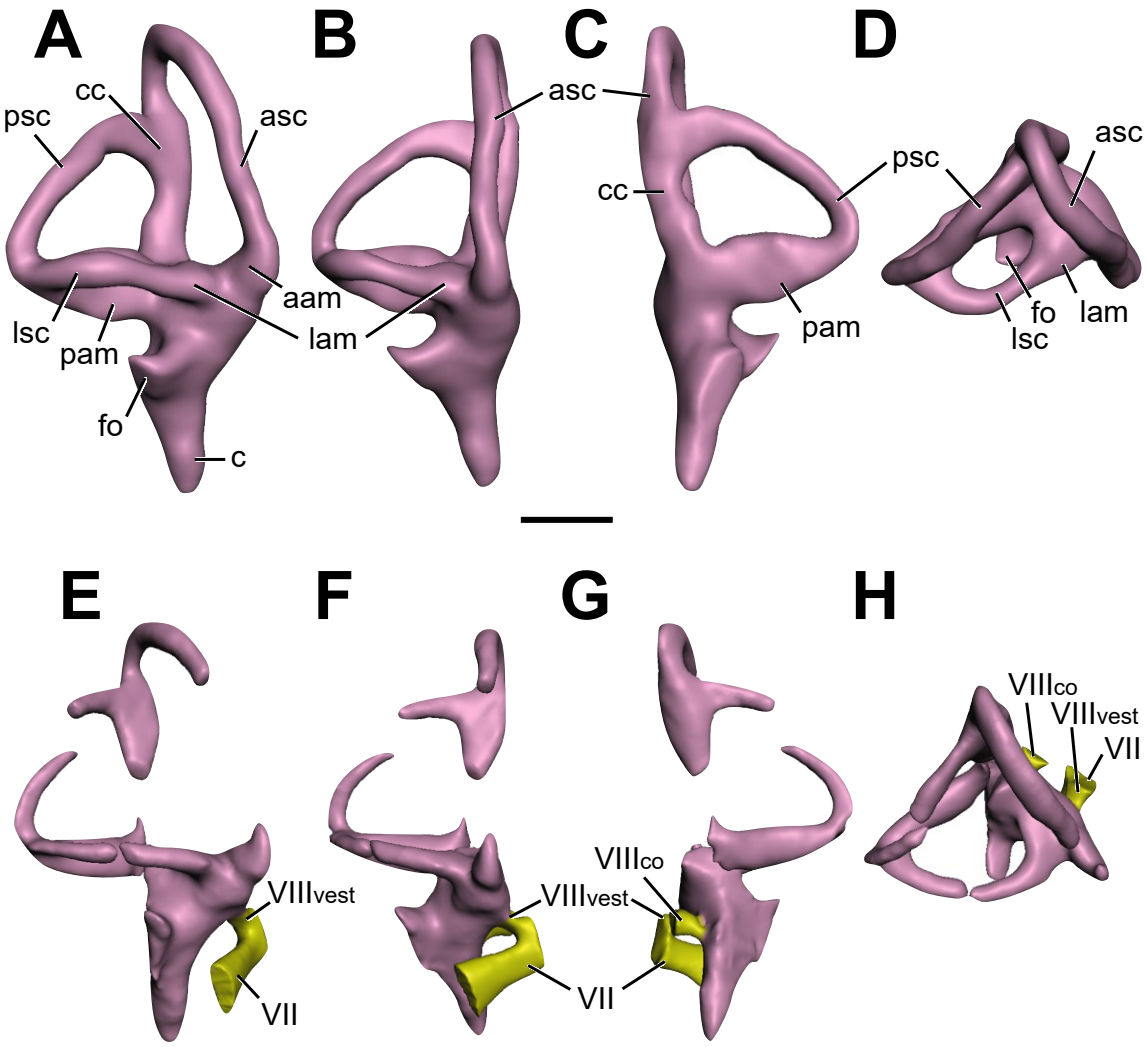

Figure 5.5 Baryonychine endosseous labyrinths. *Baryonyx walkeri* (A-D) and *Ceratosuchops inferodios* (E–H), in A, E) lateral, B, F) anterior, C, G) posterior, D, H) dorsal views. Note that the facial nerve (CN VII) trunk has been abbreviated in the *Ceratosuchops* model. Abbreviations: aam, anterior ampulla; asc, anterior semicircular canal; c, cochlea; cc, common crus; fo, fenestra ovalis; lam, lateral ampulla; lsc, lateral semicircular canal; pam, posterior ampula; psc, posterior semicircular canal; VII, facial nerve canal; $VIII_{co}$, cochlear ramus of the vestibulocochlear nerve; $VIII_{vest}$, vestibular ramus of the vestibulocochlear nerve. Scale bar 10mm.

Chapter 6 A highly pneumatic 'mid Cretaceous' theropod from the British Lower Greensand

6.1 Authorship statement

This chapter is the product of: **Barker, C.T.**, Naish, D., Clarkin, C.E., Farrell, P., Hullmann, G., Lockyer, J., Schneider, P., Ward, R.K. and Gostling, N.J., 2020. A highly pneumatic middle Cretaceous theropod from the British Lower Greensand. *Papers in Palaeontology*, 6(4), 661-679.

CTB, DN, GH and NJG conceived the study. CTB wrote the first draft, conducted the analyses, and created the figures. PF, JL and RKW discovered the elements. All authors edited the manuscript.

The supplementary information for this chapter can be found in Appendix E and online.

6.2 Abstract

A series of axial elements from the Aptian Ferruginous Sands Formation of the Lower Greensand Group, discovered on the foreshore near Knock Cliff on the Isle of Wight, United Kingdom (UK) are (bar some isolated teeth and fragmentary postcranial material from the Cenomanian Cambridge Greensand) the youngest non-avian theropod remains reported from the British Mesozoic. These specimens have the potential to shed light on a poorly known section of the European dinosaur record. A consistency in size, appearance and adhering matrix indicate that the vertebrae belong to the same individual. This was a mid-sized tetanuran, the presence of several diagnostic characters indicating that it should be recognised as a new taxon, herein named *Vectaerovenator inopinatus*. The cervical and dorsal vertebrae are camerate and highly pneumatic. Tetanuran features include opisthocoelous cervicals and pneumatic foramina located within fossae, however assigning this specimen to a specific clade is problematic. Within Tetanurae, *Vectaerovenator* possesses axial structures and homoplastic features seen in megalosauroids, carcharodontosaurians and certain coelurosaurs. Not only is *Vectaerovenator* one of the UK's youngest non-bird dinosaurs, and one of few valid British Greensand taxa, it is also the first diagnosable theropod taxon to be named from Aptian deposits of Europe.

6.2.1 Keywords

Aptian, Cretaceous, pneumaticity, theropod, vertebrae.

6.3 Introduction

Western Europe has a rich Early Cretaceous dinosaur record. The majority of British Lower Cretaceous dinosaurs are from the Wealden Supergroup (Berriasian to lower Aptian) (Martill et al., 2001a; Naish et al., 2007;2008; Sweetman et al., 2010), exposures of which crop out on the southern coasts of the Isle of Wight and East Sussex. Wealden dinosaur fossils mostly come from floodplain and flood channel deposits, and only those in the Vectis Formation (Barremian to lower Aptian) come from strata with an obvious marine contribution. The Early Cretaceous dinosaurs represented by these fossils include tetanuran theropods of several lineages, rebbachisaurid and titanosauriform sauropods, ankylosaurs and ornithopods (Martill et al., 2001a; Naish et al., 2007; Lomax et al., 2014). Among theropods, baryonychines are known from isolated teeth and the holotype of *Baryonyx walkeri* (Charig et al., 1997), *Neovenator salerii* represents carcharodontosaurian allosauroids (Brusatte et al., 2008), and there are fragments that may belong to noasaurids (Naish, 2011) and early-diverging tetanurans (Benson et al., 2009a); coelurosaurs include the probable compsognathid *Aristosuchus pusillus*, the tyrannosauroid *Eotyrannus lengi* and fragmentary remains belonging to dromaeosaurids and perhaps other maniraptoran groups (Hutt et al., 2001; Naish et al., 2001; Sweetman, 2004; Naish et al., 2007; Naish, 2011; Naish et al., 2011).

Of those British Cretaceous units overlying the Wealden, the lower Aptian-lower Albian Lower Greensand and mid-upper Albian/lower Cenomanian Upper Greensand formations have yielded dinosaurs, while the chalk – a wholly marine deposit – preserves fragmentary and dubious ornithischian remains (Naish et al., 2008; Lomax et al., 2014). In contrast to the Wealden, the Greensand has yielded few dinosaur specimens and low taxonomic diversity. Fragmentary remains and isolated teeth referred to *Iguanodon*, *Polacanthus* and a putative brachiosaurid sauropod have been recovered from the Lower Greensand of the Isle of Wight (Blows, 1998), as has the famous 'Mantel–piece' iguanodontian, today referred to *Mantellisaurus*, from Kent (Naish et al., 2008). Teeth assigned to indeterminate theropods are also known from the Lower Greensand of Dorset (Barrett et al., 2010). Meanwhile, the Upper Greensand has yielded indeterminate sauropod remains from the Isle of Wight (Wilson et al., 2003), nodosaurid remains from Folkestone (Naish et al., 2007), and indeterminate theropod teeth from Charmouth (Barrett et al., 2010).

These units represent generally shallow marine depositional environments, and the paucity of dinosaur material known from them likely reflects the overall lack of terrestrial strata deposited around this time (Buffetaut et al., 2012; Krumenacker et al., 2017). Diagnostic Aptian dinosaur material is rare in the European fossil record as a whole, most likely due to a return to marine

conditions following the early Aptian transgression (Hopson, 2011). Non-bird dinosaur remains are considered uncommon in marine sediments (Pasch et al., 1997), and are often fragmentary (Farke et al., 2017), though their rarity may reflect a collection bias in some localities (Horner, 1979). Several mechanisms have been suggested for the allochthonous or parautochthonous presence of dinosaurs in marine sediments (Benton et al., 1995a), including the passive drifting of carcasses out to sea from river systems, the exploitation of marine environments as a source of food, or that their remains represent the product of predation by marine vertebrates using hunting strategies akin to modern crocodilians or orcas.

Despite rarity overall, members of all major dinosaurian groups are known from marine rocks (Horner, 1979; Bartholomai et al., 1981; Pasch et al., 1997; Martill et al., 2000; Pereda-Suberbiola et al., 2015; Brown et al., 2017; Longrich et al., 2017) – though marginocephalians are notably scarce (Farke et al., 2017) – and some marine sediments, such as those of the Middle and Upper Jurassic of England (Benton et al., 1995a; Martill et al., 2006), are well known sources of dinosaur material. Members of some non-bird dinosaur groups – in particular nodosaurids and hadrosaurids – show a significant association with marine palaeoenvironments and their representation in these deposits is perhaps linked to a preference for fluvial and/or coastal habitats (Butler et al., 2008).

Nevertheless, no theropod type specimens are known from the Aptian of Europe, though fragmentary body fossils of spinosaurids, allosauroids, maniraptoriforms and other indeterminate theropods have been reported (Pereda-Suberbiola et al., 2012). Here, we report the fragmentary remains of a new Aptian tetanuran from the Lower Greensand of Knock Cliff on the Isle of Wight, which we diagnose and name. This species possesses a mix of features seen elsewhere within Tetanurae, notably with members of Allosauroidea, Megalosauroidea and Megaraptora (a controversial group regarded by some workers as part of Allosauroidea, and by others as part of Coelurosauria and perhaps Tyrannosauroidea). However the presence of probable homoplastic character states renders its position within Tetanurae uncertain, pending the discovery of further material.

The Knock Cliff theropod is therefore significant in being the first diagnosable non-avian theropod from the Greensand, whilst also being the youngest named non-avian theropod yet reported from the British fossil record and first diagnosable Aptian theropod taxon from Europe. As described below, it possesses a complex degree of pneumatisation, some detailed aspects of which are unlike those reported elsewhere within Theropoda. Our aim in this work is to describe and diagnose the remains of this new taxon, to identify its vertebrae to specific anatomical location, and to evaluate the new taxon's phylogenetic position.

6.3.1 Institutional abbreviations

IWCMS: Dinosaur Isle Museum (Isle of Wight County Museum Service).

6.4 Geological setting

The specimens described here were recovered on the foreshore at Knock Cliff (Figure 6.1A), between Shanklin and Luccombe, Isle of Wight, as three independent sets of remains over a period of several months: the more anterior dorsal and caudal vertebrae were collected in tandem, and whilst the cervical and more posterior dorsal was recovered as singular elements (Figure 6.2). All were surface finds, discovered with adhering glauconitic sandstone matrix.

The succession at Knock Cliff is formed of the three strata of the Lower Greensand Group: the uppermost members of the Ferruginous Sands Formation (late Aptian in age) (Ruffell et al., 2002), the Sandrock Formation (age undetermined) and the Monk's Bay Sandstone Formation (Albian) (Ruffell et al., 2002; Gale, 2019). The last of these can be discounted as a source for the fossils since sediment from this formation is gritty and dark brown; furthermore, vertebrate fossils remain unreported (Young et al., 2014). The Sandrock formation can also be discounted based on the fine-grained, yellow and white sands that form its strata (Gale, 2019). This renders the relatively fossiliferous Ferruginous Sands Formation the most plausible provenance. This is supported by the sedimentology of the matrix surrounding the specimens, as discussed further below.

Eleven informal (="local", Rawson 2006) "members" (units) have been identified within the Ferruginous Sands Formation (Insole et al., 1998; Hopson et al., 2008). Those exposed at Shanklin form its uppermost members, and include the Old Walpen Chine (XII) Member, the New Walpen Chine (XIII) Member and the unnamed Member XIV (Ruffell et al., 2002; Young et al., 2014). All are late Aptian in age. The glauconitic, fine to medium grained sandstone matrix adhering to the vertebrae matches that of the New Walpen (XIII) Member (Insole et al., 1998) (Figure 6.1B). Specifically, the material may originate from the "Urchin bed", located on top of Horse ledge (Ruffell et al., 2002), of the *T. subarticum* subzone within this member (M. I. Simpson, pers. comm.). Moreover, it is unlike the dark, pebbly clays that mark the base of Member XIII, or the more argillaceous and pyritic greensands of Member XIV above (White, 1921; Ruffell et al., 2002; Gale, 2019). In addition, longshore drift trends from southwest to northeast at Sandown Bay, making transport of the fossils from the nearest Wealden beds at Yaverland unlikely, and there are no indication that they might represent reworked or transported material from the underlying Wessex or Vectis Formations.

The Lower Greensand Group was deposited in shallow-marine and possibly estuarine environments following the major Aptian marine transgression (Insole et al., 1998; Rawson, 2006). Specifically, the majority of the Ferruginous Sands Formation, and thus the New Walpen (XIII) Member, are regarded as shallow marine shelf deposits (Insole et al., 1998). Dinosaur remains are very rare in these deposits, the material reported here all shares the same matrix, and the substantial pneumaticity and thus fragile nature of the material make it unlikely that the remains of several individuals have been rolling around on the beach for any length of time prior to recovery. We therefore consider it likely that the remains described here belong to the same individual.

6.5 Methods and terminology

Measurements were recorded in millimetres using digital callipers and the results rounded to one decimal place (Table 6.1 and Table 6.2). Nomenclature of vertebral fossae and laminae follows Wilson et al. (2011). Positioning within the axial series follows the suggestions of Evers et al. (2015), who identified potentially useful anatomical traits to help position isolated material.

6.6 Systematic palaeontology

DINOSAURIA Owen, 1842

THEROPODA Marsh, 1881

TETANURAE Gauthier, 1986

incertae sedis.

Vectaerovenator gen. nov.

LSID. urn:lsid:zoobank.org:act:316560EA-1314-4413-8C55-2D4E0BD6A204

Derivation of name. Vectis (Latin): referring to the discovery of this new taxon on the Isle of Wight; aero (Greek): “air”, referring to its high degree of skeletal pneumaticity; -venator (Latin): meaning hunter. We imagine the name to be pronounced ‘vect-air-oh-ven-ah-tor’.

Vectaerovenator inopinatus sp. nov.

LSID. urn:lsid:zoobank.org:act:E88CFD45-34CF-4C47-BC31-FADC7AE483E9

Derivation of name. inopinatus (Latin): “unexpected”, referring to its surprise discovery in the notably dinosaur-poor Lower Greensand strata of the Isle of Wight. The name thus translates as ‘unexpected Isle of Wight air-filled hunter’.

Holotype: IWCMS 2020.407, 2019.84, 2020.400.

Diagnosis: Tetanuran theropod diagnosed by: conspicuous lateral furrow between the lateral margin of the postzygapophysis and prezygoepipophyseal lamina in cervical vertebrae; convex spinoprezygopophyseal laminae in anterior cervical vertebra; curved lamina bisecting the postzygocentrodiapophyseal fossa; external extension of the air sac ventral to the parapophysis of anterior dorsal vertebra; complex partitioning of the anteriormost dorsal pneumatic foramen into several internal pneumatic features; anterior articular facet of anterior dorsal vertebrae wider than centrum such that vertebra is T-shaped in dorsal or ventral view; shallow fossae lateral to the base of the postzygapophyses in mid caudal vertebrae.

Type locality and horizon: Knock Cliff, Isle of White, United Kingdom. Upper Aptian, Lower Greensand, Ferruginous Sands Formation, Member XIII, *Parahoplites nutfieldensis* Zone (possibly *Tropaeum subarcticum* subzone) (Figure 6.1).

6.7 Description

6.7.1 Cervical vertebrae and rib

Three components of the cervical series are known for *Vectaerovenator*: a well preserved cervical vertebra lacking some or most of the neural spine, left prezygapophysis, diapophysis and epipophysis (the right epipophysis and lateral margin of the posterior articular surface are also damaged), an associated cervical rib, and a portion of a second cervical vertebra represented only by a prezygapophysis (IWCMS 2020.407, Figure 6.3A–B). We here describe each of these elements in turn bar the second prezygapophyseal fragment, which offers little additional insight.

The more complete cervical vertebra is ‘mid-sized’ for a non-avian theropod, with a total centrum length of 54.7 mm. The neurocentral sutures are still visible externally. The centrum is opisthocoelous: its posterior articular facet being markedly concave yet the anterior articular facet is only incipiently convex. The anterior facet is anteroposteriorly thickest dorsally, such that the anterior facet margin trends posteroventrally in lateral view. The anterior facet is dorsoventrally shorter than the posterior articular facet, but their dorsal margins are at the same horizontal level. Both surfaces are wider than tall and punctate, unlike the smooth cortical bone covering most of the specimen. The anterior articular surface is generally ellipsoidal, however the

neural canal marginally excavates its dorsal margin (Figure 6.3C). The posterior articular surface has a straight dorsal margin and is wider than the anterior articular surface (Figure 6.3D). The ventral surface of the centrum is convex and lacks a keel, and minor mediolateral constriction of the centrum can be clearly noted (Figure 6.3E). Anteriorly, this surface possesses irregular radial grooves between the parapophyses, the median of which extend posteriorly to the ventral midpoint of the centrum.

The parapophyses are small and located just ventral to the centrum's midline; they project laterally only slightly. They possess a flat, punctate lateral surface. An elongate, anterodorsally-posteroventrally trending pneumatic fossa excavates the centrum posterodorsal to each parapophysis, the left posterodorsal margin of which is marked by a poorly developed lamina. A rounded pneumatic foramen is present anteriorly within each fossa, and penetrates the anterior and medial regions of the centrum. The entrance of the left foramen, the largest of the two, measures 15.7mm dorsoventrally and 15.1mm mediolaterally. Together, the fossa and foramen form a pneumatic feature that spans much of the centrum's length. Internally, the foramen is incompletely divided by a low, anteriorly tapering septum, such that a shallow ventral portion lateral to the septum excavates the medial surface of the parapophysis while a larger, mediodorsal portion opens into a substantial chamber within the centrum (Figure 6.3A and Figure 6.4A).

The incomplete neural arch is tall and highly pneumatic. The broken left prezygapophysis reveals a matrix-infilled hollow. The complete right prezygapophysis projects anteriorly from the base of the neural arch, and only just extends past the anterior articular surface of the centrum. Its inclined facet is flat and ovate, and faces dorsomedially. Its long axis is almost perpendicular to the long axis of the neural arch. A small medial projection of the prezygapophyseal facet is visible in dorsal view (Figure 6.3F). In lateral view, the pedicle of the right prezygapophysis has a crenulated cortical bone texture. The anterior surface of this pedicle is perforate by a small, presumably vascular foramen just above the diapophysis.

Anteriorly, the neural canal is vaguely heart-shaped, with a subtly concave dorsal margin (Figure 6.3C). A poorly developed centroprezygapophyseal fossa is present laterodorsal to the neural canal, and is best preserved ventral to the complete right prezygapophysis. The intraprezygapophyseal laminae are short due to the close proximity of the prezygapophysis, and have incurred slight damage at their midpoint. The margins of the spinoprezygapophyseal laminae are rounded (i.e. not sharp ridges) and do not contact the prezygapophyseal facets anteriorly. They are prominently convex in lateral view. These laminae delineate an anteriorly diamond-shaped spinoprezygapophyseal fossa. A narrow, rugose prespinal ligamentous attachment site

medially bisects this fossa. The right ventral margin of the ligamentous attachment site contacts a small pneumatic foramen that is not mirrored on the left-hand side. The right prezygapophysis is connected to the right epipophysis by a pronounced prezygoepipophyseal lamina. This is slightly concave in lateral and dorsal view and possesses a sharp margin. The elongate right epipophysis is abraded, projecting posterodorsally and tapering dorsally.

The complete right diapophysis projects posteroventrally and is located ventral to the neurocentral suture. It is mediolaterally compressed and slightly abraded at its ventral end (Figure 6.3B). In lateral view, the prezygodiapophyseal lamina projects anterodorsally from the diapophysis while the postzygodiapophyseal lamina is sub-vertical. Consequently, the generally ventrally projecting diapophysis has a triangular outline. In anterior view, the prezygodiapophyseal lamina is slightly concave laterally. The anterior and posterior centrodiapophyseal laminae are very weakly developed. The exposed left postzygocentrodiapophyseal fossa is deep and contains three internal pneumatic features: two visible camerae and a pneumatic foramen (Figure 6.4A). The medial camera is the largest and excavates the neural arch medially. It is separated from the smaller lateral camera by a thin, anteriorly curved lamina. The lateral camera likely excavates the left pedicle of the prezygapophysis, and may connect to the aforementioned hollow made visible by the loss of the left prezygapophyseal facet. The posterior foramen excavates the thin left ventral wall of the spinopostzygapophyseal fossa, such that the latter communicates with the postzygocentrodiapophyseal fossa. This latter condition is not mirrored on the right side.

Posteriorly, the complete right postzygapophyseal facet is flat and somewhat inclined (Figure 6.3D). It possesses a sub-triangular outline that tapers medially. A strongly projecting, convex lateral margin, running almost parallel to the prezygoepipophyseal lamina, demarcates the ventral border of a lateral furrow leading to the long, thin epipophysis (Figure 6.3B). We are not aware of such a prominently demarcated furrow elsewhere within Theropoda and hence regard this as an autapomorphy. The postzygapophyses border a deep, roughly rhomboidal spinopostzygapophyseal fossa. This fossa is bisected medially by a rugose triangle of bone, the postspinal ligamentous attachment site. The spinopostzygapophyseal laminae are thick, with rounded margins. The thinner intrapostzygapophyseal laminae curve ventrally and meet medially as a broad, U-shaped hyposphene-like structure. This latter structure overhangs the neural canal, which is horizontally oval in shape. The exposed cross-section of the anteroposteriorly short, posteriorly placed and posterodorsally projecting neural spine is triangular. Two small pneumatic chambers suggest the spine was also pneumatic, perhaps communicating with one of the aforementioned pneumatic foramina excavating the postzygocentrodiapophyseal fossa.

The cervical vertebrae are associated with a well-preserved right cervical rib (Figure 6.4B). Its medial surface is obscured by matrix, and whether it belonged to the more complete vertebra is uncertain. However, the distances between the articular surfaces of the rib are roughly equivalent to the distance between the right diapophysis and parapophysis. The anterolateral process of the cervical rib is poorly developed. The posterior process is anteriorly convex, flattens posteriorly, and barely tapers along its preserved length. A sharp ridge extends posteriorly to form the ventral margin of the rib, separating the lateral and ventral surfaces. A large pneumatic fossa is present on the rib's anterior surface, which measures 9.9mm dorsoventrally and 11.6mm mediolaterally (Figure 6.4H). The pneumatic fossa houses two pneumatic foramina, the larger and more ventrally placed of which is separated by a thin lamina from its substantially smaller dorsal neighbour. The larger foramen is further bisected internally, with a deeply inset lamina separating it into medial and lateral portions. In medial view the tuberculum facet is subtriangular in shape, whereas the capitulum is ovate. Both lie in the same plane relative to one another and are separated by 6.7mm of bone.

Table 6.1 Measurements (in mm) of IWCMS 2020.407, 2019.84 and 2020.400. Abbreviations: AP: anteroposterior; DV: dorsoventral; ML: mediolateral.

	Cervical (IWCMS 2020.407)	**Dorsal (IWCMS 2019.84)**	**Dorsal (IWCMS 2020.400)**	**Caudal (IWCMS 2019.84)**
AP length of centrum (from laterodorsal extremities of anterior and posterior articular surfaces)	54.7	52	52.3	77.7
DV height of anterior articular surface	36.4	60.1	59.5	47.4
ML width of anterior articular surface	51.4	64.1	66.2	41.5
ML width across parapophyses	59.8	69.3	77.9	-
DV height of posterior articular surface	44.9	41.4 (incomplete)	61.6	48 (inc. chevron facet)
ML width of posterior articular surface	54.7	59.2	57.4 (incomplete)	40.8
DV height of anterior neural canal	15.7	23	21.9	13.9
ML width of anterior neural	17.7	22.7	19.8	13.1

canal				
DV height of posterior neural canal	12.5	20.8	20.5	13.3
ML width of posterior neural canal	19.2	18.4	18.3	13.5
ML width across prezygapophyses	72.2 (incomplete)	n/a	n/a	n/a
ML width across postzygapophyses	74.1	n/a	n/a	n/a
Length of neural arch from anterior end of prezygapophyses to posterior end of postzygapophyses	80.7	n/a	n/a	n/a

Table 6.2 Measurements of IWCMS 2020.407 rib. Abbreviations: AP: anteroposterior; DV: dorsoventral; ML: mediolateral.

	Rib (IWCMS 2020.407)
DV height of anterior rib surface	33.3
ML width of anterior rib surface	23.5
AP length of cervical rib	87.4 (incomplete)
ML width of capitulum	12.9
AP length of capitulum	18.7
ML width of tuberculum	12
AP length of tuberculum	16.9

6.7.2 Dorsal vertebrae

Dorsal vertebra IWCMS 2019.84 lacks the posteroventral portion of the centrum and most components of the neural arch (Figure 6.5A–C and E). The centrum is anteroposteriorly short; its anterior articular facet is complete, and taller than the centrum's length (Figure 6.5A–B). The margins of the articular facets are eroded and have a punctate bone texture. At the dorsal midline, the margin of the anterior articular facet is concave, but rounded elsewhere (Figure 6.5B). The mediodorsal section of the anterior articular facet possesses a cambered portion that flattens out ventrally and laterally. A portion of bone on the left side is missing, revealing a matrix-infilled hole that penetrates the centrum and communicates with a pneumatic chamber

posteriorly. The incomplete posterior articular facet is concave and reniform in outline (Figure 6.5C). It is narrower than its anterior counterpart, rendering both pneumatic foramina visible in posterior view. Both facets are parallel and their dorsal margins are in line with one another. The neural canal excavates the dorsal surface of the centrum, forming a recessed area delimited laterally by the base of the neural arch. The anterior recess is mediolaterally narrow relative to the posterior excavation.

Laterally, the centrum contacts the neural arch via a medially constricted, inverted "V"-shaped neurocentral suture. The most prominent features of the centrum's lateral surfaces are the extensive, elongate pneumatic fossae, which occupy much of the centrum's length and are demarcated dorsally and ventrally by thick, sub-parallel laminae, the latter of which extends posteriorly from the parapophysis. Both of these laminae are gently concave in coronal view. Single, bilateral pneumatic foramina excavate the centrum dorsal to the flat parapophyses: the latter are situated anteroventrolaterally, roughly midway between the anterior-most end of the neurocentral suture and the ventral margin of the anterior articular facet. The pneumatic foramina are large and somewhat ovate, the left hand of which measures 19mm dorsoventrally and 24.3mm mediolaterally, and both are divided into three, sequentially organised internal pneumatic features (Figure 6.5F), namely two medially positioned camerae that are bordered laterally by a shallow internal fossa. The medial-most camera is anteroposteriorly elongate and penetrates the medial centrum body. It is separated from its more dorsoventrally oriented lateral neighbour by a thin lamina. The shallow fossa that borders both camerae is variably indented depending on the side examined; the left internal fossa possesses several indentations relative to the smoother right-hand equivalent, which likely represent small outpocketings of the air sac system. Both excavate the mediodorsal surface of the parapophysis and the anterodorsal and anterior portion of the centrum (behind the rim of the anterior articular surface).

As noted above, the posteroventral portion of the centrum is absent, leaving behind a large, matrix-infilled hollow. The ventral surface of the centrum is pinched but fails to produce a substantial keel or ridge.

The extensively pneumatic neural arch is very eroded and is missing its zygapophyses, both transverse processes and the neural spine (Figure 6.5E). Camerae and internal septa are visible throughout. In anterior view, the neural canal is slightly wider than it is tall, and the mediodorsal margin of the canal becomes concave. Immediately dorsal to this, a shallow, medially placed recess is present and is interpreted here as the remains of a spinoprezygapophyseal fossa. Posteriorly, the neural canal is taller than wide, and has a straight dorsal margin.

Laterally, and ventral to the incomplete left diapophysis, a triangular centrodiapophyseal fossa is demarcated anteriorly by the vertically oriented anterior centrodiapophyseal lamina and an anterodorsally inclined posterior centrodiapophyseal lamina. In its ventral part, the left fossa contains two pneumatic foramina, a configuration that is not mirrored on the element's right side. Instead, the right posterior centrodiapophyseal lamina possesses an accessory lamina that projects anteroventrally to delimit a small fossa (Figure 6.5E). This fossa is perforated by a pinhole-like foramen that communicates with a large internal hollow, made visible by the loss of the right diapophysis. Internally, a lamina bisects the hollow into anteroventral and posterior camerae.

A second dorsal vertebra (IWCMS 2020.400) has a complete and well-preserved centrum missing only the right margin of the posterior articular surface (Figure 6.6A–G). Only the base of the neural arch is present; all of the more dorsal structures are absent.

The centrum is anteroposteriorly short, possessing articular surfaces that are taller relative to centrum length (Figure 6.6A–C). In coronal view, the mediolaterally broad anterior surface, combined with the weakly constricted midsection and mediolaterally narrower posterior articular surface, gives the element a roughly T-shaped appearance (Figure 6.6D–E). Thanks to this configuration, the pneumatic fossae and lateral margins of the anterior articular surface are visible in posterior view (Figure 6.6B).

The anterior articular facet is sub-circular but for a straight section present along the dorsal midline (Figure 6.6A). The articular face is flat bar for a subtle mediodorsal convexity. The shallowly concave posterior articular facet is taller than wide, again with a straight edge along its dorsal margin (Figure 6.6B). The preserved left lateral margin is convex before descending steeply to the ventral midpoint. The neural canal excavates the dorsal surface of the centrum. However, in contrast to the other dorsal vertebra, the canal only barely excavates the dorsal margin of the posterior articular facet..

The parapophyses project weakly laterally from the margins of the anterior articular surface, and are bisected by the neurocentral sutures. The better-preserved left parapophysis shows that these structures were dorsoventrally tall (Figure 6.6C). The centrum-bound portion of the left parapophysis extends posteriorly to form the anterolateral wall of the pneumatic foramen. It has a concave lateral margin in anterior view, compared to the flatter on right element. The left parapophysis narrows dorsally, and the section that extends onto the neural arch has a shallowly concave lateral surface. The ventral margin of the centrum is concave in lateral view and "pinched" in transverse section, forming a small, ventrally rounded median ridge (Figure 6.6E-F).

Anteroposteriorly short radial grooves ornament the median anteroventral surface of the centrum.

The bilateral, elongate pneumatic fossae excavate much of the posterodorsal lateral surface and their single anterior foramina deeply penetrate the anterior centrum body. These fossae are demarcated dorsally by a small lamina just ventral to the neurocentral suture. The left foramen opens medially and ventrally into the centrum where it splits into four further pneumatic features: three camerae and an internal pneumatic fossa (Figure 6.6G). The three camerae are separated from one another by two thin laminae; two camerae excavate the medial centrum body, whilst a third excavates the centrum ventrally. The shallow, laterally placed internal fossa borders the camerae and excavates the medial wall of the parapophysis and anterodorsal corner of the centrum. Ventral to the parapophyses, shallow, anteroventrally-posterodorsally trending sulci communicate with the large pneumatic fossae that excavate the laterodorsal centrum surface. These sulci suggest an external lateroventral expansion of the pneumatic features. The neural arch is incomplete and eroded, revealing a camerate internal structure. The camerae are broadly symmetrical in dorsal view; an anterior pair excavates the prezygopophyseal pedicles and dorsal part of the parapophysis, the left side of which is bisected by an internal lamina; whilst two dorsoventrally deep camerae excavate the neural arch medially to the centrodiapophyseal fossae (Figure 6.6D). The mid-section of the neural arch is constricted, such that the neurocentral suture is V-shaped in coronal view. A shallow, subtriangular centrodiapophyseal fossa is present, dorsal to the neurocentral suture. The neural canal is tall and relatively broad, and as previously stated excavates the dorsal margin of the centrum.

6.7.3 Caudal vertebra

A single caudal vertebra (IWCMS 2019.84) is a heavier, more robust element than the others described above (Figure 6.7A–D). Its centrum is complete and well preserved; the neural arch is missing its zygapophyses, neural spine, and lateral ends of the transverse processes. Erosion of the rims of the articular surfaces, and loss of the aforementioned neural arch structures has exposed the interior trabeculae. The neurocentral suture is visible and has a somewhat irregular, sinusoidal shape.

The centrum is anteroposteriorly elongate and almost 1.7 times its height (Figure 6.7A); its articular surfaces are shallowly concave and taller than wide (Figure 6.7B–C). The dorsal margins of the articular surfaces are straight. The anterior articular surface shows slight transverse expansion across its midpoint. The posterior articular surface is more rounded and a chevron facet is present. Some damage, however, has occurred to the left side of the articular surface just

dorsal to the facet. Minor mediolateral constriction is present along the middle portion of the centrum, such that the articular facets are wider. In lateral view, the dorsal portion of the centrum bears a shallow pleurocentral depression that occupies nearly the entire dorsal width of the centrum. Ventrally, the centrum has a somewhat pinched, featureless underside.

The neural arch roofs a generally subcircular neural canal whose ventral margins also excavate the dorsal surface of the centrum. The left spinoprezygadiapophyseal lamina is present, delimiting a small yet deep spinoprezygapophyseal fossa that extends posteriorly beneath the anterior portion of the neural arch (Figure 6.7B and D). A low, thin prespinal lamina roofs the fossa and extends posteriorly to the abraded base of the neural spine. The diapophyses are dorsoventrally flat and hemispherical in dorsal view due to the erosion of their lateral tips.

Ventral to the diapophyses, the remnants of the anterior and posterior centrodiapophyseal laminae are perceptible as subtle ridges, whose ventral ends do not reach the centrum (Figure 6.7A). These delineate a poorly developed centrodiapophyseal fossa. The postzygapophyses are missing except for their bases, the lateral surfaces of which are concave. These depressions are bounded dorsally by the postzygodiapophyseal laminae and anteroventrally by accessory laminae (Figure 6.7C). These resemble centropostzygopophyseal fossae however they are not bound laterally by centropostzygopophyseal lamina, and are thus unnamed for the sake of brevity. The postygapophyseal bases, along with the abraded spinopostzygapophyseal laminae, delimit a narrow, oval spinopostzygapophyseal fossa

6.8 Remarks

The anteroventral position of the parapophysis and presence of epipophyses indicates that the more complete vertebra of IWCMS 2020.407 belongs to the cervical series. The ventrolaterally projecting diapophyses and anteroventral inclination of the anterior articular facet are present in the anterior cervicals of several other theropods. The absence of a ventral keel – typically present in more posterior cervical vertebrae – supports its position in the anterior to middle part of the cervical series. Typically, cervical vertebrae VI to IX are longest in Neotheropoda (Holtz Jr, 2000), though comparisons are difficult owing to the lack of additional cervical elements. The capitulum and tuberculum are closely spaced, their articular facets lying in a same plane. In contrast, the articular facets of posterior cervical ribs are widely separated, although they do also lie in the same plane (Dai et al., 2020). The proximity of the rib with the more complete cervical vertebra indicates that it pertains to this bone or an adjacent vertebra, and indeed its detailed anatomy appears inconsistent with a more posterior position. Based on comparisons with *Allosaurus* (Madsen, 1976), this vertebra is most similar to cervical III in the relative distance between the

diapophysis and parapophysis (which increases posteriorly) and the anterior projection of the prezygapophysis (which project further anteriorly in the mid-series and sit atop taller pedicles in the posterior elements) (Chokchaloemwong et al., 2019). All neurocentral sutures in this specimen are "open", consistent with putative measures of relative morphological immaturity (Brochu, 1996) (a trait that can be extended to the other recovered axial elements).

Presacral vertebra IWCMS 2019.84 could either be a posterior cervical or anterior dorsal. The parapophyses are restricted to the ventral portion of the anterior centrum; in most non-bird theropods, these are located anteroventrally up to the tenth cervical vertebra (Evers et al., 2015). They are usually more dorsally situated in the anterior dorsal series and migrate to the neural arch in the posterior rib-bearing vertebrae (Currie et al., 2001). However, this transition is less marked in the anterior dorsals of certain taxa (Evers et al., 2015). The first dorsal vertebra figured for *Aerosteon* possesses an anteroventrally situated parapophysis, for example (Sereno et al., 2008b). Similarly, Madsen (1976) figured the first to third dorsal vertebrae of *Allosaurus* as having anteroventrally-situated parapophyses. Regardless, the cervical-dorsal transition is difficult to ascertain in the absence of associated ribs (Harris, 1998). Horizontal or dorsolaterally projecting diapophyses may also help identify a position in the dorsal series (Evers et al., 2015), but again these are lacking in this specimen. The orientations of the anterior and posterior centrodiapophyseal laminae suggest, however, that the diapophyses of IWCMS 2019.84 were laterally projecting. In summary, we provisionally identify the specimen as the first or second dorsal vertebra.

In IWCMS 2020.400, the presence of parapophyses that span the neurocentral suture and the orientation of the posterior centrodiapophyseal laminae clearly support an anterior position among the dorsal vertebrae. Such vertebrae have been termed "cervicodorsals" (e.g. Coria et al. 2006) or "pectorals" (Currie et al., 1993), and typically represent the 11th to 13th/14th presacral vertebrae, although this nomenclature has not been widely adopted. The position of the parapophysis in IWCMS 2020.400 resembles the condition in the fourth and fifth dorsal vertebrae of *Allosaurus* (Madsen, 1976). The specimen also resembles the fourth dorsal vertebra of *Aerosteon* (Sereno et al., 2008b), further suggesting a position at or near this point in the dorsal series.

The identification of IWCMS 2019.84 as a caudal vertebra is supported by its lack of parapophyses, sacral rib attachments and pneumatic fossae (Charig et al., 1997; Brougham et al., 2019). The presence of transverse processes indicate that it is a proximal caudal, belonging to the part of the tail anterior to the "transition point" that separates the proximal and distal parts of the tail skeleton (Russell, 1972). Its exact position in the proximal caudal series cannot be

determined, but an approximate position can be deduced based on several traits. The lack of a hyposphene (which is variably present in theropod caudals), elongate centrum body, poorly developed centrodiapophyseal laminae (Rauhut et al., 2018), rounded ventral margin and presence of a chevron facet suggests it was part of the posterior proximal series, located closer to the "transition point" than the sacrum. This corresponds to the "mid" caudals of some authors.

6.9 Discussion

6.9.1 Theropod affinity of the material

The overall appearance of the cervical (IWCMS 2020.407) and combination of epipophyses, anteroventrally situated parapophyses, a neural arch with lateral depressions, distinct pre- and postzygapophyses as well as pneumatisation of the vertebra (a trait that can be extended to dorsal elements IWCMS 2019.84 and 2020.400) and associated rib clearly identifies IWCMS 2020.407 as belonging to a saurischian dinosaur (Gauthier, 1986; Rauhut, 2003). Moreover, it shares several synapomorphies with Theropoda: closely placed diapophyses and parapophyses in anterior (and mid-) cervicals, as well as "pleurocoels" in anterior presacral vertebrae (Gauthier, 1986; Cau, 2018). Further, the camerate internal chambers within the cervicals have been tentatively suggested as an additional theropodan apomorphy in some analyses (Rauhut, 2003).

A sauropod identification can also be discredited, despite the presence within this group of opisthocoelous cervical vertebrae and pneumatisation in the vertebral column, as well as the discovery of a putative brachiosaurid from the nearby Lower Greensand locality of Luccombe Chine (Blows, 1995). In contrast to sauropods (Rauhut, 2003; Nicholl et al., 2018), the cervical postzygapophyses of *Vectaerovenator* are in line relative to the prezygapophyses, a keel is absent on the anterior cervical vertebra, and the anterior articular facet of the anterior cervical vertebra is horizontally ovate rather than rounded or high-oval in shape. In addition, the cervical is not strongly opisthocoelous as in most sauropods (Upchurch, 1995), the cervical pneumatic foramina are undivided, unlike most neosauropods (Upchurch, 1995; Whitlock, 2011), and the cervical rib is elongate and most probably overlapped the posterior centrum in life, unlike the short non-overlapping ribs of diplodocoid neosauropods (Whitlock, 2011).

Theropod traits are also evident in the caudal vertebra of *Vectaerovenator*: it has dorsoventrally compressed transverse processes elevated above the dorsal margin of the centrum and weakly developed laminae (Brougham et al., 2019). Furthermore, whilst synapomorphic ornithopodan characters are typically restricted to cranial and appendicular elements, the caudal vertebra retains its transverse processes and lacks the hexagonal or octagonal cross-section present in

iguanodontians (Norman, 2004; Verdú et al., 2019), further supporting the element's theropodan affinities.

6.9.2 Comparative anatomy

Within Theropoda, *Vectaerovenator* possesses traits indicative of averostran and tetanuran affinities: the opisthocoely (albeit subtle) of its cervical centrum is consistent with this, as are its bilateral cervical pneumatic foramina located within fossae (Rauhut, 2003; Benson et al., 2012; Cau, 2018). Dorsoventral compression of the anterior cervicals has also been recovered as a tetanuran synapomorphy (Cau, 2018), and the non-fusion of the cervical rib to its vertebra and lack of an elongate anterolateral process also supports this placement (Poropat et al., 2019). However, *Vectaerovenator* is unusual with respect to two proposed tetanuran synapomorphies: the width between the prezygapophyses is subequal to that of the neural canal (i.e. the median margins of the prezygapophyses are not strongly laterally displaced relative to the neural canal), and the ventral narrowing of the anterior dorsals is not quite as pronounced and fails to produce a sharp keel (Rauhut, 2003; Carrano et al., 2012).

Nevertheless, in certain analyses, cervical opisthocoely is characteristic of Neotetanurae in particular (Cau, 2018), and is notably pronounced in megalosauroids and allosauroids (Evers et al., 2015); while the one sufficiently complete cervical of *Vectaerovenator* is opisthocoelous, the condition is weak and about comparable to that present in such tetanurans as *Monolophosaurus* (Xi-Jin et al., 2009), *Sinraptor* (Currie et al., 1993), *Piatnitzkysaurus*, such tyrannosauroids as *Dilong* (Rauhut, 2003) and basal carcharodontosaurians such as *Siamraptor* (Chokchaloemwong et al., 2019) and *Concavenator* (the latter reflecting the basal condition within allosauroids) (Cuesta et al., 2019). *Vectaerovenator* lacks a conspicuous rim around the anterior articular facet – a probable synapomorphy of Megalosauroidea (Evers et al., 2015; Dai et al., 2020) – but does possess "enlarged" pneumatic foramina in the anteriormost dorsals, a character considered synapomorphic of the megalosauroid clade Megalosauria (Carrano et al., 2012).

The cervical prezygapophyses of *Vectaerovenator* are not flexed, as in most coelurosaurs (Gauthier, 1986). However, the cervical does possess a synapomorphy of coelurosaurian clade Tyrannoraptora: the centrum does not extend beyond the neural arch (Cau, 2018). The presence of a prezygoepipophyseal lamina in the cervical vertebra – effectively separating the lateral and dorsal surfaces of the neural arch – has been recovered as an allosauroid synapomorphy in some analyses (Chokchaloemwong et al., 2019), although it is also present (and developed more prominently) in abelisauroids and megaraptorans (Calvo et al., 2004; Carrano et al., 2008) as well as some megalosauroids (Rauhut et al., 2012). In addition, the offset between the articular

surfaces in *Vectaerovenator* is minimal and similar to that present in the mid cervicals of carcharodontosaurids (Calvo et al., 2004; Chokchaloemwong et al., 2019). However, the cervical parapophyses are not located at the midlength of the centrum, as they are in carcharodontosaurids and *Megaraptor* (Calvo et al., 2004).

The postzygodiapophyseal lamina of *Vectaerovenator* is sub-vertically oriented as it is in carcharodontosaurians (Chokchaloemwong et al., 2019) and megaraptorans (Calvo et al., 2004). Posteriorly, the cervical possesses a hyposphene-like structure: the presence of this structure anterior to the dorsal vertebrae is rare in saurischians but is present, however, in carcharodontosaurians (Chokchaloemwong et al., 2019), megaraptorans (Smith et al., 2008) and tyrannosaurids (Novas et al., 2013). In addition, the cervical epipophyses of *Vectaerovenator* appear to point posterodorsally, as they do in carcharodontosaurids (Novas, 2009). Long epipophyses have been proposed as a carcharodontosaurid synapomorphy, though in some analyses they are also present in ceratosaurians and metriacanthosaurids (Cuesta et al., 2019).

Postaxial cervical (and anterior dorsal, see below) pneumaticity is typical for non-avian theropods (Benson et al., 2012), and most tetanurans present with single bilateral pneumatic foramina in the centrum; carcharodontosaurids (Sereno, 1991; Chokchaloemwong et al., 2019; Cuesta et al., 2019) and megaraptorids (Novas et al., 2013; Porfiri et al., 2018; Aranciaga Rolando et al., 2019) are unusual in that these pneumatic foramina are bisected by lamina. Cervical rib pneumaticity is present in a range of non-avian theropods, including *Majungasaurus* (O'Connor, 2006) (where it is extensive), *Tyrannosaurus* (Brochu, 2003) and *Aerosteon* (Sereno et al., 2008b). It is thus not indicative of affinity with any particular clade. Nevertheless, the development and organisation of pneumaticity in theropod vertebrae may vary within an individual or element, potentially reducing their use as indicators of phylogenetic position (O'Connor, 2006; Brougham et al., 2019). The known cervical and dorsal vertebrae of *Vectaerovenator* are camerate, as they are in *Piatnitzkysaurus*, *Allosaurus*, *Torvosaurus*, sinraptorids, dromaeosaurids (Rauhut, 2003) and the carcharodontosaurian *Siamraptor* (Chokchaloemwong et al., 2019). This is unlike the camellate condition of most carcharodontosaurians (Benson et al., 2010) and megaraptorans (Benson et al., 2012), although the camerate/camellate internal structure can vary within a single vertebra of members of the latter clade, as it does in *Megaraptor* (Porfiri et al., 2014).

The dorsal vertebrae of *Vectaerovenator* recall those of *Lajasvenator* in that the incipiently convex dorsal part of the anterior articular surface is just visible in lateral view (Coria et al., 2019). As mentioned above, the large foramina are similar to the condition present in various megalosaurians such as *Eustreptospondylus* (Sadlier et al., 2008; Carrano et al., 2012), though they are more centrally placed in the latter than they are in *Vectaerovenator*. However, the

parapophyses on the more posterior dorsal of *Vectaerovenator* are large, as is the case in allosauroids and *Aerosteon* Carrano et al. (2012). Further, the parapophyses project only slightly laterally, as they do in allosauroids (Carrano et al., 2008). The conspicuous fossa ventral to the parapophyses is of note, and a similarly placed fossa is present in the megalosauroid *Yunyangosaurus* (Dai et al., 2020).

The pair of conspicuous, laterally placed fossae on the pedicels of the postzygapophyses are also noteworthy in the caudal element, and similar structures have been in noted in the anterior caudals of some megalosauroids (Rauhut et al., 2018). Similarly placed small depressions are also noted in the holotype mid caudal vertebra of the carcharodontosaurid *Veterupristisaurus* (Rauhut, 2011), however, their relatively larger size and associated laminae in *Vectaerovenator* may be diagnostic.

6.10 Phylogenetic analysis

Vectaerovenator was added to a comprehensive dataset of pan-avian taxa (Cau, 2018). The final matrix included 1781 characters and 133 operational taxonomic units (OTUs) (see Appendix E). All characters were treated as unordered. The analysis was performed in TNT 1.5 (Goloboff et al., 2016). A “New Technology Search” was undertaken, using a driven search that stabilised consensus twice with a factor of 25, and default settings for ratchet, sectorial and tree fusion. This retained 98 trees, with a tree length of 6797 steps, a CI=0.244, and an RI=0.563. These trees were then subjected to tree bisection and reconnection (TBR) branch swapping using the “Traditional Search” function in order to explore the tree islands recovered in the former search, recovering 10920 trees. Strict consensus recovered *Vectaerovenator* as the sister taxon to Megaraptora+*Gualicho*, nested within Tyrannosauroidea. As a measure of absolute tree support, Bremer (decay indices) were calculated using the “Bremer Supports” function, using “TBR from existing trees” option and retaining trees suboptimal by ten steps. While *Vectaerovenator*’s phylogenetic position appears relatively well resolved, the Bremer support values of 1 across most nodes indicates low support for this result (Figure 6.8). Several constrained analyses were undertaken to assess the number of steps required to place *Vectaerovenator* in alternative positions within basal tetanurans. Using the command “force = (taxon a taxon b … taxon n)”, only two extra steps were required to place *Vectaerovenator* as a megalosauroid, and three additional steps were required to recover it as an allosauroid.

6.10.1 Comments on the phylogenetic position of *Vectaerovenator*

The recovery of *Vectaerovenator* as a tyrannoraptoran (*sensu* Cau, 2018) – and, more specifically, a tyrannosauroid – is perhaps unexpected, as the axial elements resemble those of allosauroids and megalosauroids in some respects. Nevertheless, as previously stated, *Vectaerovenator* does possess a tyrannoraptoran axial synapomorphy (*sensu* Cau 2018) (the centrum does not extend beyond the neural arch), and its similarities with more basal tetanurans could be the result of homoplasy. Placement of *Vectaerovenator* on a tyrannosauroid branch leading to Megaraptora is potentially significant as the latter clade has yet to be recovered in Europe despite their wide temporal and geographical distribution (Aranciaga Rolando et al., 2019; White et al., 2020). Porfiri et al. (2014) found *Eotyrannus* from the Isle of Wight to be a megaraptoran but examination of the character codings that support this phylogenetic position shows them to be erroneous (Naish and Cau, unpub. data.). Megaraptorans are known to exhibit homoplasy with allosauroids, and their position within Coelurosauria has been supported and refined in recent phylogenetic analyses. Originally described as unusual allosauroids (Benson et al., 2010), Megaraptora has since been recovered as an early-diverging lineage within Coelurosauria, lacking close ties to any other recognised coelurosaurian lineage (Novas et al., 2013; Porfiri et al., 2014), or nested within Tyrannosauroidea (Aranciaga Rolando et al., 2019), occasionally positioned as the sister group to tyrannosaurids (Novas et al., 2013; Porfiri et al., 2014). Our tree topography closely follows that recovered by Cau's (2018) original analysis, in that Megaraptora is nested within Tyrannosauroidea.

However, the three synapomorphies supporting *Vectaerovenator*'s association with the clade Megaraptora+*Gualicho* possess a broad distribution throughout Theropoda. These include the presence of a prezygoepipophyseal lamina (character (CH) 209), which as previously stated is present in several tetanuran and ceratosaur clades; the possession of a "peduncular fossa" lateral to the neural canal in presacral vertebrae (CH 668), which are also found in abelisaurids such as *Majungasaurus* (O'Connor, 2007) and tetanurans such as *Monolophosaurus* (Xi-Jin et al., 2009); and a subvertical cervical postzygodiapophyseal lamina (CH 1591) which, as discussed above, is also noted in carcharodontosaurians. Further, *Vectaerovenator* cannot be allocated to Megaraptora. This is due to the incomplete nature of the *Vectaerovenator* holotype, the few axial synapomorphies recovered for megaraptorans (Aranciaga Rolando et al. (2019) reported no axial synapomorphies for this clade, for instance), and the fact that the relevant characters are present not just in megaraptorans but also in carcharodontosaurids and non-megaraptoran tyrannosauroids (Novas et al., 2013). Furthermore, our phylogenetic analysis finds *Vectaerovenator* in an earlier branching position than *Gualicho* (the latter occupying the same

position as in Cau's (2018) original phylogeny), a taxon often considered a basal coelurosaur (Apesteguía et al., 2016; Aranciaga Rolando et al., 2019).

In sum, the low Bremer supports, combined with the low CI value (and thus high number of homoplastic characters within the dataset) and few additional steps required to recover *Vectaerovenator* amongst other basal tetanuran clades suggests this taxon's position within Tetanurae remains highly uncertain, and as such we find is more parsimonious to currently identify it as Tetanurae incertae sedis. Our understanding of this dinosaur would thus benefit greatly from the recovery of further material.

6.11 Conclusions

The new taxon described here – *Vectaerovenator inopinatus* – is a highly pneumatic, 'mid-sized' theropod, its autapomorphies mostly concerning the distribution of pneumatic features on the centra and neural arches of the cervical and dorsal vertebrae. *Vectaerovenator* recalls several basal tetanuran clades in overall anatomy, but our inclusion of this new taxon in a phylogenetic analysis supports a position within Tyrannosauroidea. Nevertheless, as detailed above, we find it more parsimonious to diagnose this theropod as an indeterminate tetanuran given the fragmentary nature of the holotype, the low support for the phylogenetic result, the numerous homoplastic traits and the few extra steps required to recover *Vectaerovenator* amongst megalosauroids or allosauroids respectively.

The recognition of a new tetanuran theropod from the English 'mid' Cretaceous – specifically, a late Aptian upper "member" of the Ferruginous Sands Formation of the Lower Greensand Group of the Isle of Wight – is significant in enhancing our knowledge of the diversity of European dinosaurs of this age. As a Lower Greensand dinosaur, *Vectaerovenator* is locally important in being the youngest diagnosable non-avian theropod yet reported from the British fossil record (some indeterminate theropod teeth are of similar age, whilst fragmentary postcranial material from the Cenomanian Cambridge Greensand – reported by Galton et al. (2002) as perhaps belonging to a small non-avian theropod – is younger). Furthermore, Vectaerovenator is the first European theropod from the Aptian to be considered diagnostic and worthy of a taxonomic name.

6.12 Acknowledgments

We thank Martin Munt and Alex Peaker (both Dinosaur Isle Museum, Sandown, Isle of Wight) for access to the material and for help and guidance regarding the geology of the Lower Greensand;

Gary Blackwell (Dinosaur Isle Museum) for his excellent preparatory work on these delicate specimens; Martin Simpson for his help identifying the geological provenance of the material; Mark Chapman, Steve Vidovic (both University of Southampton) and Tom Smith (University of Bristol) for their advice with the phylogenetic analyses; Dom Barker and Luis Coy (both University of Southampton) for their help with specimen photography. We would also like to thank Phillip Mannion and Sally Thomas, and reviewers Andrea Cau and Fernando Novas for their input and detailed insights during the review process that substantially improved the manuscript. The program TNT is being made available thanks to the Willi Hennig Society. This study was supported by the Engineering and Physical Sciences Research Council (EPSRC), UK and the Institute for Life Sciences, University of Southampton, UK.

6.13 Data Archiving Statement

This published work and the nomenclatural acts it contains, have been registered in ZooBank: http://zoobank.org/References/7C7C4F6C-BC1D-42B5-8EBA-5D59C726EC1D.

Data for this study are available in the Dryad Digital Repository: https://doi.org/10.5061/dryad.8cz8w9gmj.

6.14 Figures

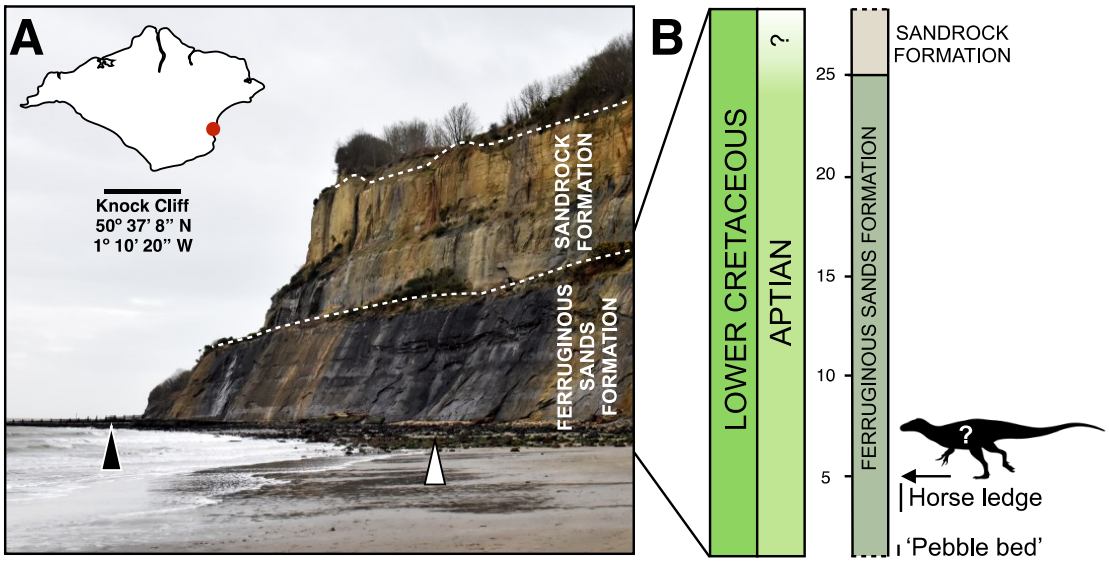

Figure 6.1 Locality map of the new theropod taxon and stratigraphy of the Ferruginous Sands Formation at Knock Cliff, Isle of Wight (UK). A) Map of the Isle of Wight (inset) and photograph of Knock Cliff at Shanklin (credit: Trudie Wilson), where the specimens

were collected. B) Stratigraphy of Knock Cliff, focusing on the Ferruginous Sands Formation. Black triangle indicates Horse Ledge. The white triangle indicates the location the 'pebble bed'. Based on Ruffell et al. (2002), Young et al. (2014) and Gale (2019). Scale bar: 10km.

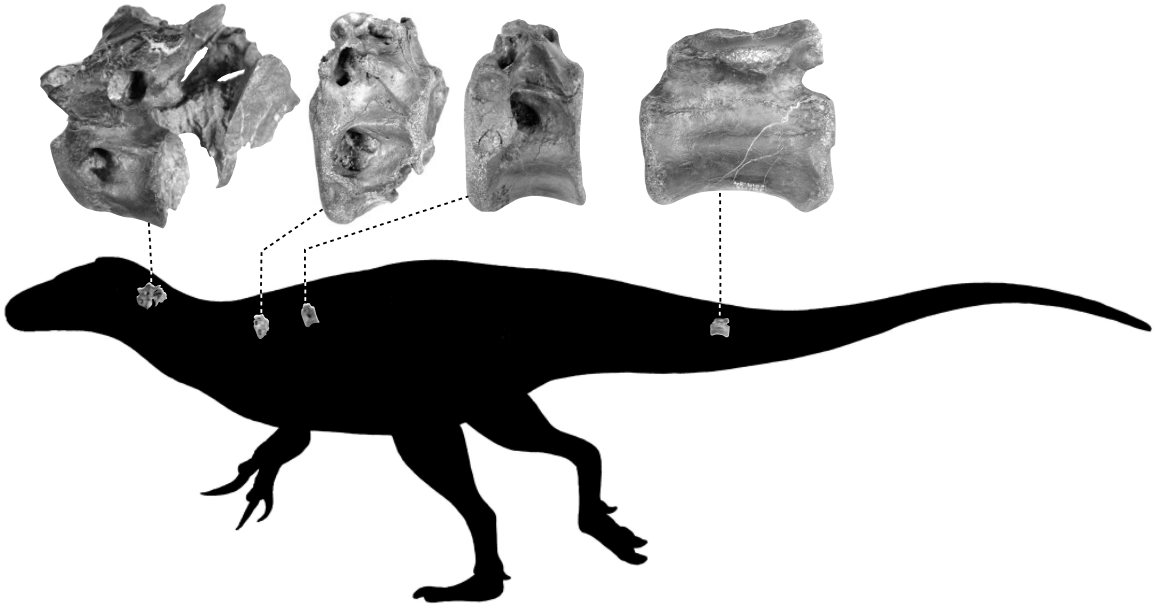

Figure 6.2 Silhouette of *Vectaerovenator* showing the approximate position of the vertebral elements (see description for further discussion). Elements not to scale.

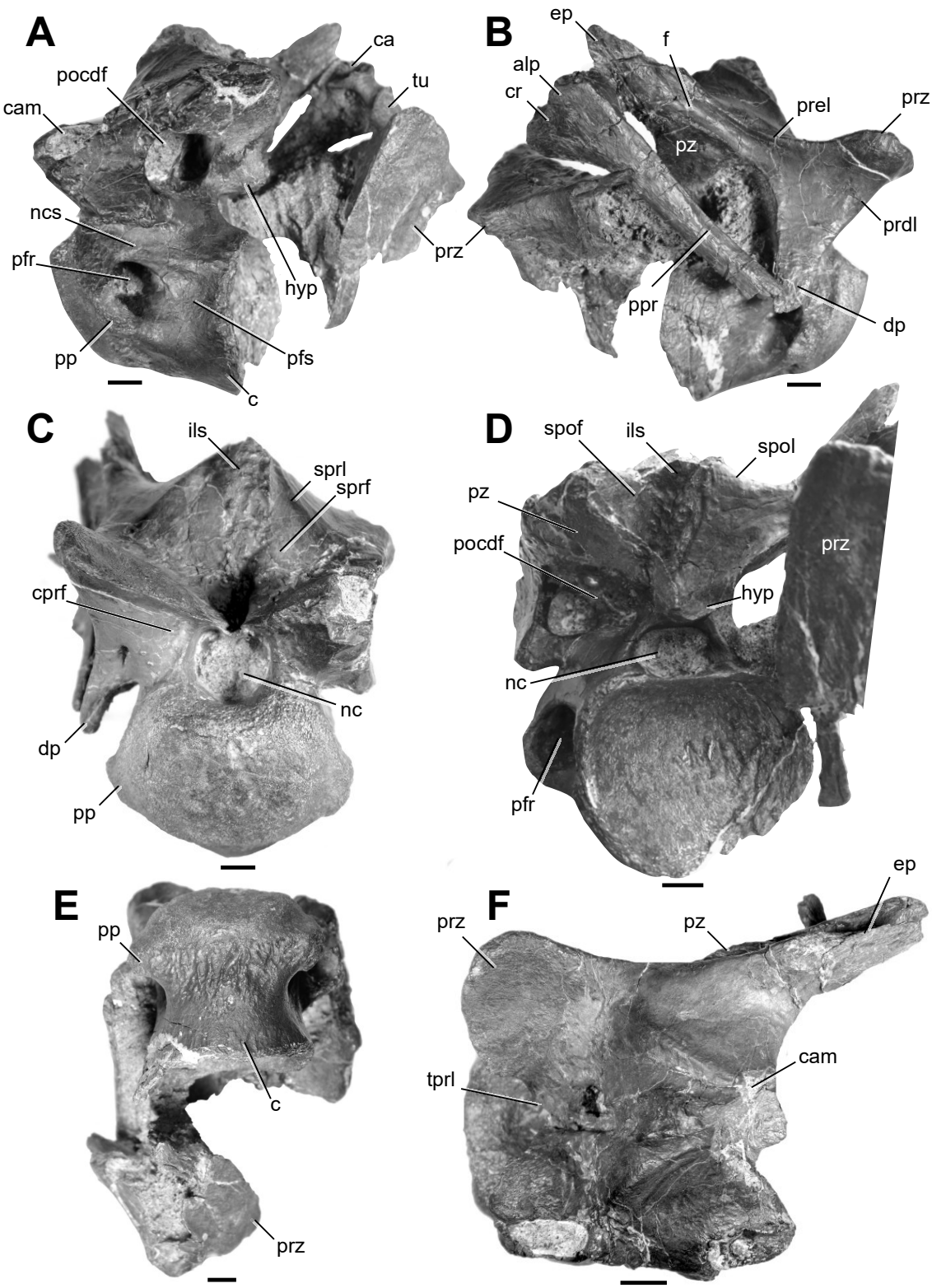

Figure 6.3 Cervical vertebrae (IWCMS 2020.407), in: A) left lateral, B) right lateral, C) anterior, D) posterolateral, E) ventral and F) dorsal views. Abbreviations: alp, anterolateral process of cervical rib; c, centrum; ca, capitulum; cam, camera; cprf, centroprezygapophyseal fossa; cr, cervical rib; dp, diapophysis; ep, epipophysis; f, furrow; hyp: hyposphene-like lamina; ils, interspinous ligament scar; nc, neural canal; ncs, neurocentral suture; pfr, pneumatic foramen; pfs, pneumatic fossa; pocdf,

postzygocentrodiapophyseal fossa; pp, parapophysis; ppr, posterior process of cervical rib; prdl, prezygodiapophyseal lamina; prel, prezygoepipophyseal lamina; prz, prezygapophysis; pz, postzygapophysis; spof, spinopostzygopophyseal fossa; spol, spinopostzygopophyseal lamina; sprf,; spinoprezygopophyseal fossa; sprl, spinopostzygopophyseal lamina; tb, tuberculum; tprl, intraprezygopophyseal lamina. Scale bars represent 1cm.

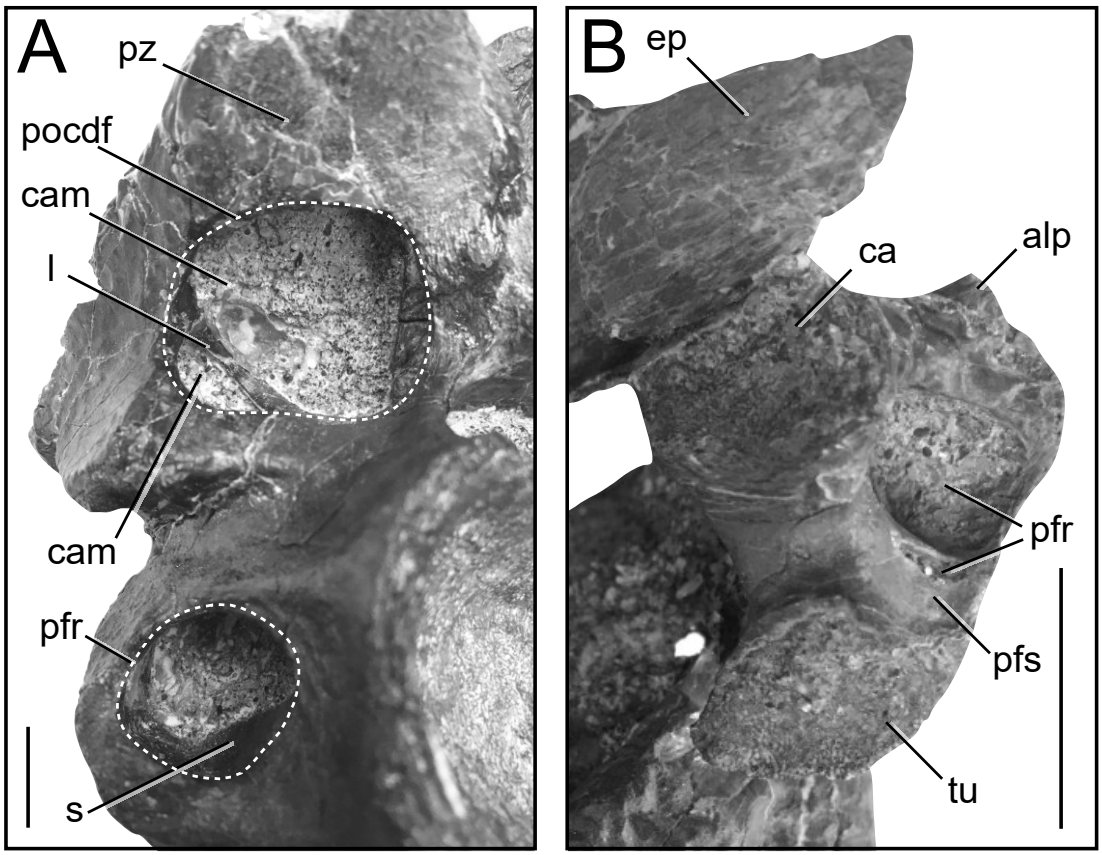

Figure 6.4 A) Details of the pneumatic features of IWCMS 2020.407, in posterolateral view. B) Details of the articular facets and pneumaticity of the associated cervical rib, in anterior view. Dotted lines delineate entrances to pneumatic features. Abbreviations: alp, anterolateral process of cervical rib; ca, capitulum; cam: camera; ep, epipophysis; l, lamina; pfr, pneumatic foramen; pfs, pneumatic fossa; pocdf, postzygocentrodiapophyseal fossa; pz, postzygapophysis; s, septum; tb, tuberculum. Scale bars represent 1cm.

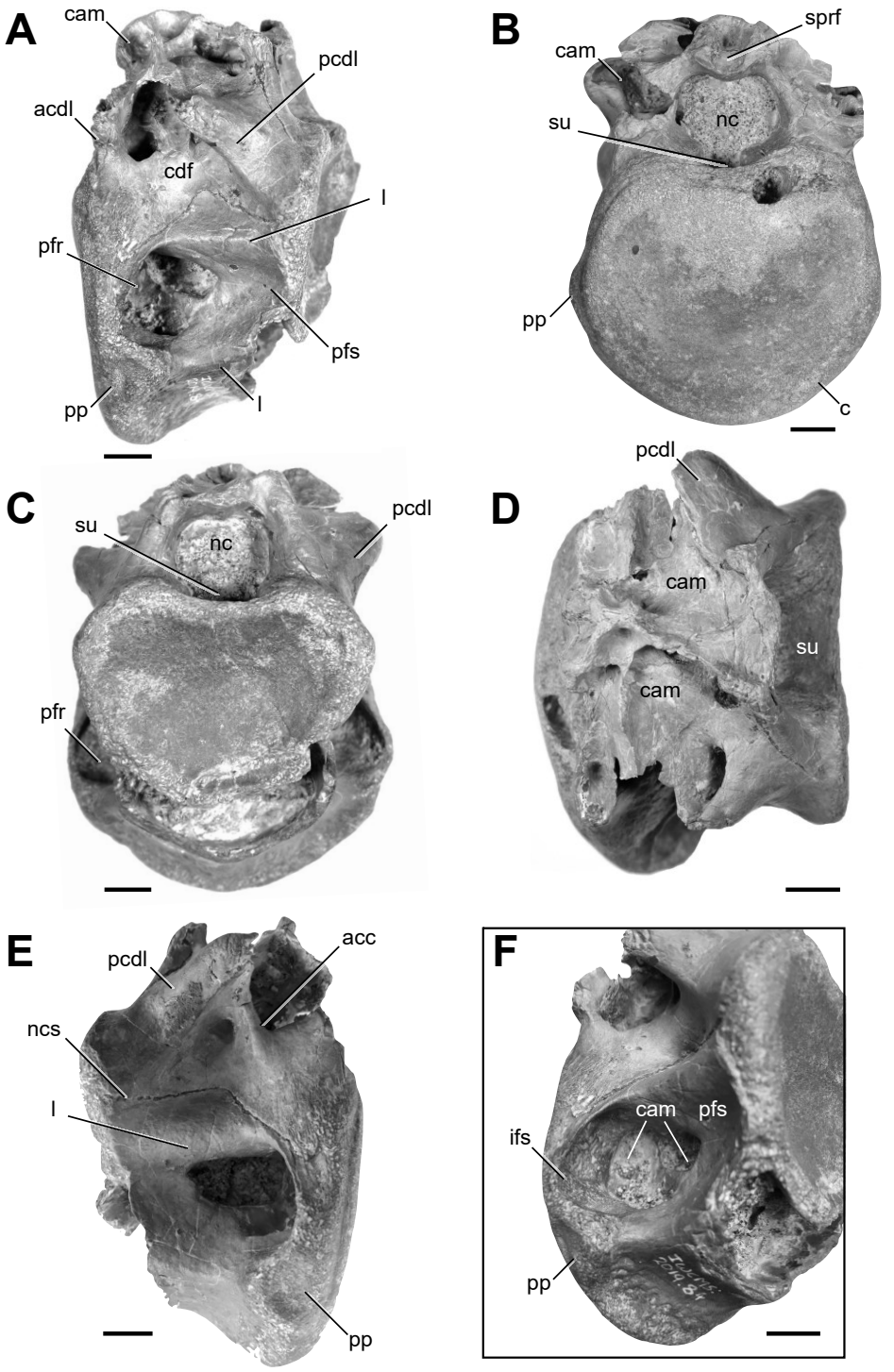

Figure 6.5 Anterior dorsal vertebra (IWCMS 2019.84), in: A) Left lateral, B) anterior, C) posterior, D) dorsal and E) right lateral view. F) Detail of the pneumatic features of the centrum in left posterolateroventral view. Abbreviations: acdl, anterior centrodiapophyseal lamina; acc, accessory centrodiapophyseal lamina; c, centrum; cam, camera; cdf, centrodiapophyseal fossa; ifs: internal pneumatic fossa; l, lamina; nc, neural canal; ncs, neurocentral suture; pcdl, posterior centrodiapophyseal lamina; pfr, pneumatic foramen; pfs, pneumatic fossa; pp, parapophysis; sprf,; spinoprezygopophyseal fossa; su, sulcus. Scale bars represent 1cm.

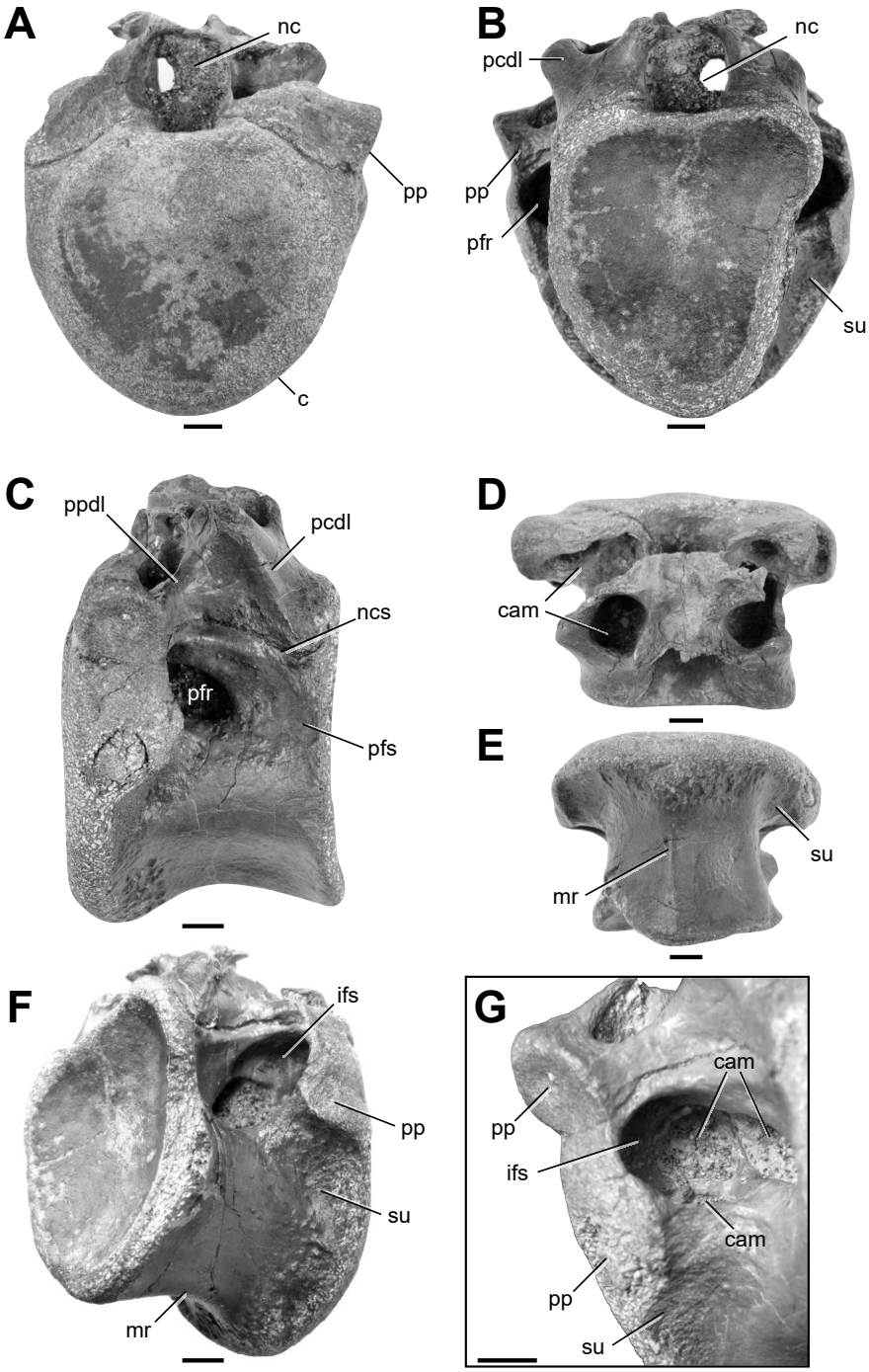

Figure 6.6 Anterior dorsal vertebra (IWCMS 2020.400), in: A) anterior, B) posterior, C) left lateral, D) dorsal, and E) ventral views. F) Details of the pneumatic fossa in right posterolateroventral view. G) Detail of the pneumatic features of the centrum in left posterolateral view (credit: Alex Peaker). Abbreviations: c, centrum; cam, camera; ifs: internal pneumatic fossa; nc, neural canal; ncs, neurocentral suture; pcdl, posterior centrodiapophyseal lamina; mr, median ridge; pfr, pneumatic foramen; pfs, pneumatic fossa; pp, parapophysis; ppdl, paradiapophyseal lamina; su, sulcus. Scale bars represent 1cm.

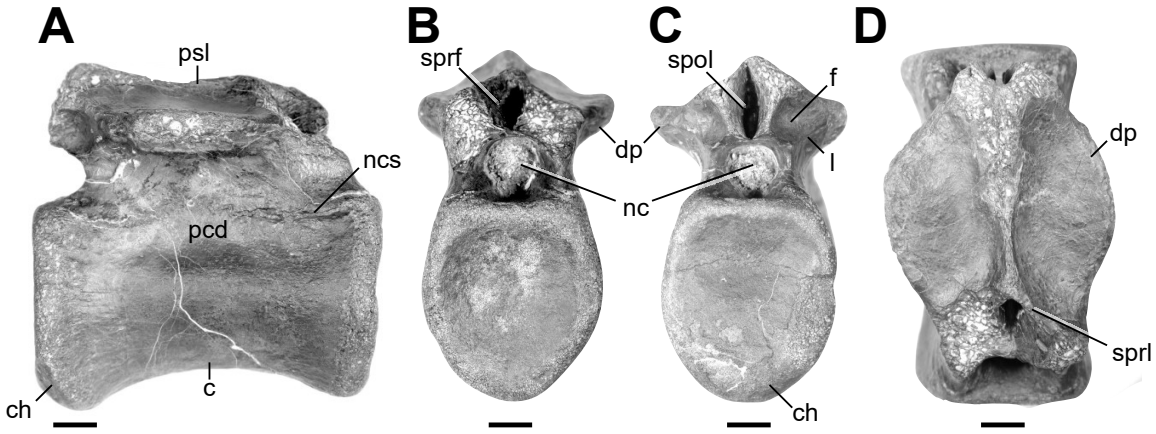

Figure 6.7 Mid caudal vertebra (IWCMS 2019.84), in: A) right lateral, B) anterior, C) posterior and D) dorsal views. Abbreviations: c, centrum; ch, chevron facet; dp, diapophysis; f: fossa; l, lamina; nc, neural canal; ncs, neurocentral suture; pcd, pleurocentral depression; psl, prespinal lamina; spof, spinopostzygopophyseal fossa; spol, spinopostzygopophyseal lamina; sprf,; spinoprezygopophyseal fossa; sprl, spinopostzygopophyseal lamina. Scale bar represents 1cm.

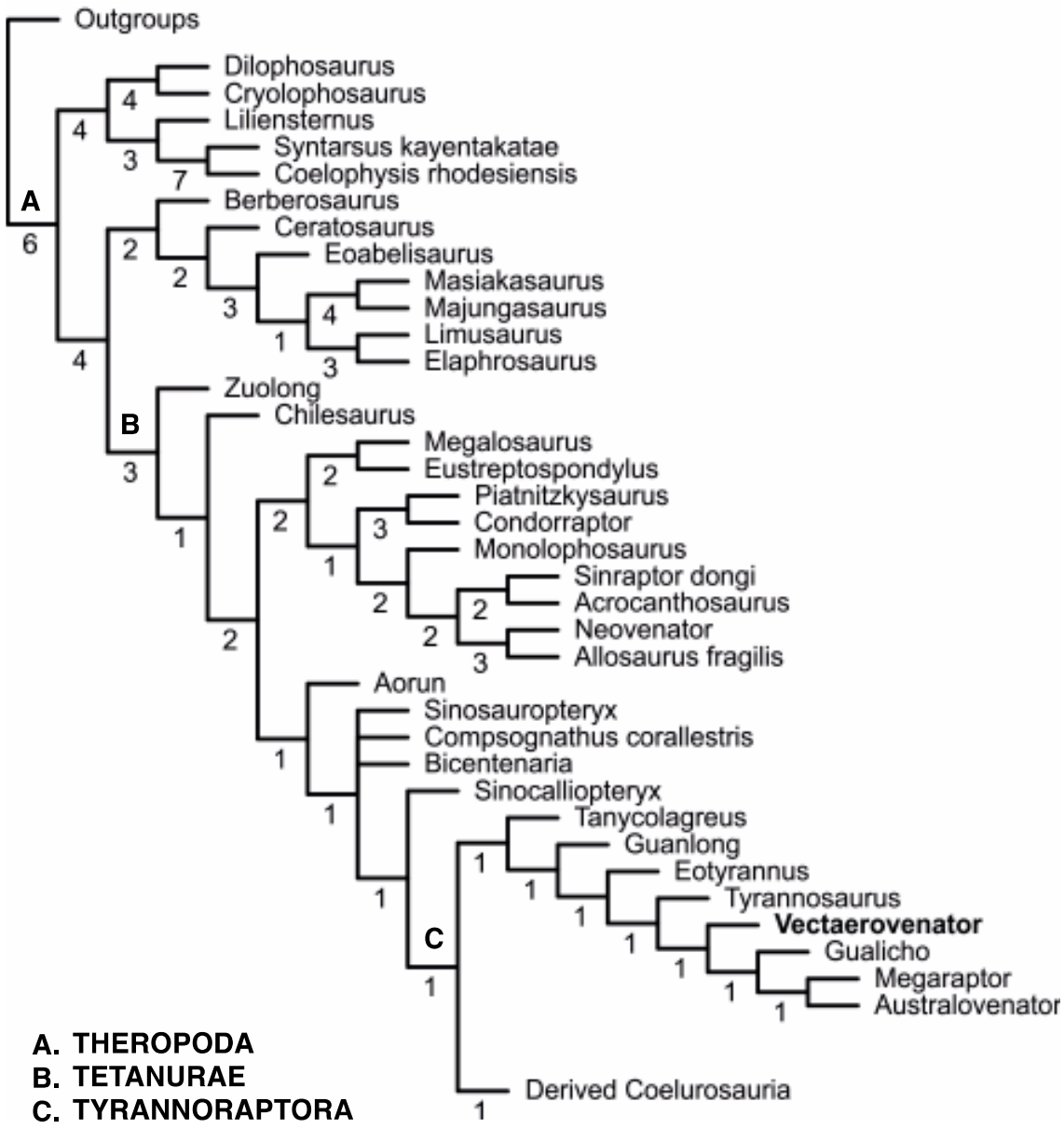

Figure 6.8 Strict consensus tree based on the data matrix of Cau (2018). Numbers below the nodes indicate Bremer support values; letters above nodes indicate clade names. See text regarding the context of this result, which reflects the fragmentary nature of the material, low Bremer support values and low CI value.

Chapter 7 General discussion

7.1 Summary of results

Despite intensive fossil collecting for over two hundred years, theropod dinosaurs are generally rare and fragmentary in the British fossil record (Chapter 1). This thesis sought to explore the taxonomy and phylogenetic relationships of new and historical British theropod specimens, the majority of which pertain to the remains of Spinosauridae. Notably, this work questioned previous assumptions regarding spinosaurid diversity in the British fossil record, and tested whether spinosaurid specimens could be referred to the previously known British taxon *Baryonyx*. In addition, this thesis examined the palaeoneurology of the earliest spinosaurids known from braincase material, and assessed the sensory capabilities of these partially piscivorous predators relative to other theropods, with the aim of refining palaeoecological inferences based on neuroanatomical traits.

The remarkable discovery of two large-bodied spinosaurid specimens from the Wessex Formation (Early Cretaceous: Barremian) at Chilton Chine (Chapter 2), on the Isle of Wight, show unique characters and can be distinguished from *Baryonyx* (known from the broadly coeval Upper Weald Clay Formation of Surrey) in areas of overlapping anatomy. Using a large-scale phylogenetic analyses focusing on Spinosauridae, these specimens were shown to cluster with the Nigerien spinosaurid *Suchomimus*, a topology recovered under both maximum parsimony (reduced consensus) and Bayesian inference. These results, combined with the presence of unique characters, have been deemed sufficiently diagnostic to erect new taxa – *Ceratosuchops inferodios* and *Riparovenator milnerae*. This taxonomic and phylogenetic interpretation suggests the presence of multiple lineages of spinosaurid in the British Barremian. Furthermore, this would indicate that *Baryonyx* has yet to be recovered from the Wessex Formation of the Isle of Wight, and that other fragmentary spinosaurid material previously referred to the taxon is best identified as belonging to indeterminate Spinosauridae. The results of the Bayesian phylogenetic analysis also provided a new palaeobiogeographic hypothesis, highlighting Europe as the potential area of origin for spinosaurids.

Further evidence for multiple spinosaurid lineages in the British Cretaceous were recovered in Chapter 3 and Chapter 4. In the former, an isolated spinosaurid tooth (HASMG G369a), likely from the Hastings Group of East Sussex, failed to associate with *Baryonyx* in any cladistic, discriminant function or cluster analysis. The identity of this tooth unfortunately remains uncertain – several characters (e.g. the lack of sporadic variation in denticle size, presence of enamel fluting on both

labiolingual surfaces) are similar to those observed in teeth referred to cf. *Suchomimus*, with the majority of iterations of the cluster and discriminant analyses repeatedly classifying it to the Nigerien taxon. However, the constrained cladistic analyses, argued by Hendrickx et al. (2020b) to be the preferred method for identifying isolated theropod crowns, failed to recover an association with cf. *Suchomimus*, instead recovering HASMG G369a outside both Baryonychinae and Spinosaurinae within Spinosauridae. The tooth is best identified as belonging to an indeterminate spinosaurid. Nevertheless, this result suggests the referral of spinosaurid teeth from the Wealden Supergroup to *Baryonyx*, as had been done in the past, may not be reflective of the clade's actual diversity within the succession. Given that isolated spinosaurid teeth are the most common spinosaurid elements recovered from the Wealden Supergroup, additional tooth-based analyses may be attractive means with which to assess spinosaurid diversity within the succession.

In Chapter 4, fragmentary new spinosaurid material from the Vectis Formation, herein dubbed the "White Rock spinosaurid", not only marks the first documented occurrence of the clade from this geological unit (and probably accounts for the youngest British spinosaurid material yet known), but several cladistic data runs hint at the possibility this individual belonged to a non-*Baryonyx* or non-baryonychine taxon. More broadly, this notably large individual (likely the largest terrestrial predator known from Europe) also supplements the known fauna from this generally dinosaur-poor deposit, being the first Vectis Formation theropod identifiable to lower taxonomic rank.

The palaeoneurology of the British spinosaurids *Ceratosuchops* and *Baryonyx* (Chapter 5), uncovered via micro-CT scanning and digital reconstruction, revealed brain morphologies and sensory capabilities similar to various other large-bodied non-maniraptoriform theropods, further supporting previous observations of morphological conservatism in the endocrania of more basal taxa. Several morphological differences were noted between the two taxa, however it is unclear whether any of these support the osteological differentiation put forward in Chapter 2. Both taxa possessed unexceptional hearing and olfactory capabilities, and likely exhibited similar behavioural sophistication and cognitive abilities to other basal tetanuran theropods. The overarching similarity in form and development of various endocranial regions suggests that the brains of these early spinosaurids were either preadapted for exploiting aquatic resources, or that the modifications to the snout and teeth (e.g. elongation of the rostrum, transition from ziphodont to conidont dentition) was sufficient to do so; these hypotheses are not mutually exclusive.

Finally, the series of axial elements recovered from the Lower Greensand deposits of the Isle of Wight are diagnostic of a new taxon, *Vectaerovenator inopinatus* (Chapter 6). Within Tetanurae,

the cladistic analysis recovered *Vectaerovenator* amongst Tyrannosauroidea, but the specimen possesses axial structures and homoplastic features seen in megalosauroids, carcharodontosaurians and certain coelurosaurs. Exploration of the data via a constrained cladistic analyses demonstrated that few extra steps were required for the taxon to nest amongst megalosauroids or allosauroids, and the taxon is best interpreted as Tetanurae *incertae sedis* pending the recovery of additional material. *Vectaerovenator* is one of the UK's youngest non-avian dinosaurs, one of few valid British Greensand taxa, and appears to be the first diagnosable theropod taxon to be named from Aptian deposits of Europe.

7.2 Relevancy of findings

Theropods are generally rare in the Wealden Supergroup (Naish, 2011), and were only known from isolated teeth in the Lower Greensand Group (Barrett et al., 2010). The discovery of the new spinosaurid specimens from the Wealden Group and *Vectaerovenator* from the Lower Greensand Group of the Isle of Wight help to fill in these gaps in the Early Cretaceous British theropod fossil record. These finds also cements the importance of the Isle of Wight's Early Cretaceous succession (and notably, the strata comprising the Wealden Group) in the field of dinosaur palaeontology (Martill et al., 2001c). Meanwhile, *Vectaerovenator* is a temporally important data point that may be of palaeoecological or palaeobiogeographical importance, as has been suggested for "post-Wealden" dinosaur remains in general (Barrett, 2021).

Regarding the spinosaurid sample in particular, not only do these specimens present welcome skeletal data for a clade known mainly from fragmentary material (Hone et al., 2017), the results collected in this thesis have challenged previous assumptions that spinosaurid material from the temporally extensive Early Cretaceous Wealden Supergroup of southern Britain could be referred to *Baryonyx* by default. The increased diversity of British spinosaurids proposed in this thesis is in line with updated views regarding spinosaurid systematics from the Early Cretaceous of Iberia, where dental morphotypes have hinted at a diverse fauna and specimens traditionally referred to *Baryonyx* have been reappraised as new taxa (Malafaia et al., 2020a; Mateus et al., 2022).

Regarding palaeoethological/ecological reconstructions, spinosaurids are somewhat exemplar fossil taxa as multiple lines of convincing evidence exists for their ability to exploit aquatic resources to varying degrees (Charig et al., 1997; Taquet et al., 1998; Holtz et al., 2004; Hone et al., 2014; Hone et al., 2017). The use of microCT to explore the endocranial anatomy and sensory capabilities in baryonychine spinosaurids for the first time supplements discussions regarding the potential behaviours exhibited by spinosaurids. Indeed, constructing hypotheses using multiple lines of evidence and a cross-disciplinary approach form parts of the palaeobehavioural inference

framework proposed by Hone et al. (2014). In the case of the better-known *Baryonyx*, this is of particular interest given the colourful history of its hypothesised way of life. Initially considered to be a facultative terrestrial quadruped with a predominantly piscivorous diet (Charig et al., 1986), *Baryonyx* (in common with other spinosaurids) was latter considered to have adopted a more traditional bipedal stance and broader dietary envelope, perhaps wading into shallows to strike aquatic prey in a heron-like manner (Paul, 1988; Charig et al., 1997; Holtz, 2002; Holtz et al., 2004; Hone et al., 2017; Hone et al., 2021). More recent and unsual reinterpretations have posited that *Baryonyx* was a "subaqueous forager" (i.e. capable of fully submerged foraging) based on bone histology (Fabbri et al., 2022b). The limitations of palaeoneurological studies notwithstanding (see below), endocranial and sensorial evidence relating to olfaction and hearing suggests limited divergence from the ancestral or "typical" basal tetanuran condition, and the lack of clear neurological adaptations to aquatic life (subtle changes to the underlying neural wiring notwithstanding, which would not be detected in the segmented endocast) might favour more conservative palaeoethological reconstructions.

As an aside, these specimens and their associated findings highlight the impact of appropriate media campaigns, which helped garner public interest in the UK's palaeontological heritage and, in the case of *Vectaerovenator*, prompted the donation of additional fragmentary caudal material. Charismatic fossil taxa are important tools in effective science communication, and can act as ambassadors to help preserve scientifically important aspects of the UK's palaeontological heritage, all whilst solidifying the relationship between collectors, museums and researchers by underlining the value and role of natural history collections.

In summary, this work has provided evidence that the previously held assumption regarding British spinosaurid taxonomy (i.e. that material spanning a substantial period of time is referable to *Baryonyx* by default) is likely flawed, and that the Early Cretaceous of Britain likely contained several distinct spinosaurid lineages. This thesis has also reviewed and expanded the temporal range of the British spinosaurid record, and has described important new theropod samples from dinosaur poor strata (i.e. from the Vectis Formation and the Lower Greensand Group). Palaeoneurological examination of *Ceratosuchops* and *Baryonyx* has also revealed the endocranial anatomy and potential sensory capabilities of these predators, a first for baryonychine-grade spinosaurids. This has helped refine previous ethological reconstructions and suggests that these spinosaurids did not deviate substantially in terms of inferred behavioural sophistication, cognitive abilities, olfaction and hearing relative to many other basal tetanurans despite their atypical craniodental morphology.

7.3 Limitations

7.3.1 Origin and preservation of the studied material

The British theropod material that forms the focus of this thesis is fragmentary and displays varying degrees of preservation, which has impacted the amount of information available and thus subsequent interpretation.

The majority of the studied specimens come from coastal localities (e.g. Chapter 2, Chapter 4 and Chapter 6) that proved difficult to work with. Not only were some surface finds (e.g. *Ceratosuchops*, the "White Rock" spinosaurid, *Vectaerovenator*), tides and bad weather affecting the ability to safely remove specimens, locate potential additional material, and conduct appropriate field studies. As a result, various details are absent (depending on the material considered), including important anatomical, stratigraphic and taphonomic data. The missing anatomical data, combined with the state of preservation for several recovered elements, hindered the systematic interpretation of the studied material (see below). The absence of clear stratigraphic data was a particular issue regarding the association (or lack thereof) between *Ceratosuchops* and *Riparovenator*, and only a vague stratigraphic position could be obtained for the latter (see Chapter 2). This impacted the taxonomic and palaeoecological interpretation of the two individuals.

Elsewhere, the historical nature and confused accession information of HASMG G369a meant its relative stratigraphic position proved difficult to pin down (Chapter 3). Whilst a likely stratigraphic position was discussed, it remains unclear where and from which strata this specimen was collected from in particular.

MicroCT scanning of the Wessex Formation *Ceratosuchops* braincase (Chapter 5) was also affected by the preservation of the material. Originally scanned within a large sandstone block prior to the start of my PhD studies, very poor contrast led to the re-preparation of the block: the disjoined braincase was extracted, and matrix infilling the brain cavity was removed to further reduce the amount of material through which the x-rays needed to pass. This improved contrast, however the lack of supporting matrix has rendered the specimen fragile. Despite the improvements to the scan data, several regions of interest, such as some cranial nerves and portions of the semicircular canals, could not be segmented largely due to the presence of radiopaque artefacts; fortunately, this did not negatively impact the description or examination of these features to a great degree. Spaces within the bones from the Wealden Group of the Isle of Wight are often infilled by minerals, several of which include metallic components (e.g. pyrite, siderite, ferroan calcite) (Martill, 2001) that can have a detrimental effect on scan quality

(Garwood et al., 2014). The effects of these artefacts were worse in the more poorly preserved *Riparovenator* brain case elements, and it was deemed too time consuming to extract what available information remained; as such, the neuroanatomy of *Riparovenator* remains poorly understood.

7.3.2 Comparability of the studied material to other taxa/specimens

Spinosaurid skeletal material is generally rare and fragmentary (Bertin, 2010; Hone et al., 2017), as attested by the specimens examined within this thesis. Fortunately, in the case of *Ceratosuchops* and *Riparovenator*, the recovered cranial material overlaps with that of *Baryonyx* (the other Barremian spinosaurid from Britain), allowing some detailed comparisons (Chapter 2, Chapter 5, Appendix A). Similarly, spinosaurid dental material is well documented, allowing HASMG G369a to be rigorously examined relative to others (Chapter 3). Comparisons proved more difficult with the known material of the "White Rock" spinosaurid and *Vectaerovenator*, whose very fragmentary (and, in the case of the former, rather degraded) skeletal elements could only be sparingly compared (Chapter 4 and Chapter 6). Where decent anatomical data was available for the "White Rock" spinosaurid in particular, comparisons were further hampered by the lack of overlapping data with other specimens.

7.3.2.1 Taxonomic interpretation of *Ceratosuchops* and *Riparovenator*

The named spinosaurids from the Wealden Supergroup of southern England differ from one another across multiple cranial characters (Chapter 2 and Appendix A), but do the differences represent genuine speciation or are these simply "normal" variation within a single population? This thesis argues that the multiple spinosaurid lineages are present in the Lower Cretaceous of Southern England, and presence of unique morphological traits, character combinations and phylogenetic topologies warrants the distinction of *Ceratosuchops* and *Riparovenator* from one another as well as from *Baryonyx*. However, as acknowledged in Chapter 2, the lack of a large, well-preserved spinosaurid sample rendered it difficult to adequately assess the studied specimens against other (named) individuals.

7.3.2.1.1 Comparisons with *Baryonyx*

Two major issues hampered comparisons with the *Baryonyx walkeri* type specimen NHMUK PV R9951: its diagnosis and uncertain degree of maturity. The original diagnoses by Charig et al. (1986) and Charig et al. (1997) are now largely obsolescent, *sensu* Wilson et al. (2003), following the subsequent discovery of new spinosaurid material worldwide. For instance, the terminal rosette and sinusoidal jaw margin highlighted in these works have a much wider distribution

within Spinosauridae. Attempts to re-diagnose the taxon have appeared in various works (Sereno et al., 1998; Carrano et al., 2012; Hone et al., 2017). However, clouding such endeavours is the ontogenetic status of this animal: Charig et al. (1997) considered it immature despite its large size, whilst histology of comparably sized material from *Iberopsinus* (specimen ML 1190, then referred to *B. walkeri*) implies it could well have been near skeletal maturity (Waskow et al., 2017). With the ambiguity of what constitutes an "adult" dinosaur (Hone et al., 2016) and the difficulty of assessing ontogeny in non-ceolurosaur theropods (Griffin et al., 2020) in mind, the assessment of the ontogenetic status of *Baryonyx* through multi-element histology would have been a useful starting point. Histology probably represents the most accurate current method for assessing vertebrate maturity (Bailleul et al., 2019), and could provide a foundation with which to interpret the *Baryonyx* holotype and guide subsequent interpretation of the new material described herein.

Quite what constitutes "normal" intraspecific variation in spinosaurids is also unknown. Sexual dimorphism is very difficult to recognise in the fossil record (Mallon, 2017; Hone et al., 2020), so to dismiss differences in morphology between specimens using such reasoning is reductive. Assuming spinosaurids followed the same ontogenetic trends or scope of variation as better-known theropods is also flawed unless such variation can been demonstrated to affect disparate groups across Theropoda. Several differences between the Wealden Supergroup spinosaurids could be considered ontogenetic based on patterns seen in tyrannosaurids (*Tyrannosaurus* in particular), for instance (see Appendix A), however the latter are known to have undergone extreme skeletal changes during growth (Carr, 2020) and it remains unclear how many are applicable to spinosaurids.

Intriguingly, low intraspecific variation in growth is inferred for Avetheropoda (i.e. allosauroids + coelurosaurs) (Griffin et al., 2016; D'Emic et al., 2023), although quite when this appeared relative to the increased variation seen in more basal theropods (e.g. coelophysoids, ceratosaurs) is uncertain (Griffin et al., 2016). Avetheropoda was not recovered in the phylogenetic analyses conducted in Chapter 2. Instead, Coelurosauria and Allosauroidea bracketed Spinosauridae, suggesting low intraspecific variation in growth could be inferred for the latter. This would temper the issues of *Baryonyx*'s uncertain ontogenetic status, and facilitate comparisons between the Wealden Supergroup spinosaurids due to the largely similar size (and thus similar ontogenetic status). In summary, and unaided by limited histological studies (Cullen et al., 2020), the growth patterns of spinosaurids remain unclear and comparisons between the British specimens studied herein were made on the plausible yet untested assumption that they represented individuals at similar developmental stages.

Whilst *Ceratosuchops*, *Riparovenator* and *Baryonyx* occur in broadly contemporaneous formations (all are Barremian), the finescale correlation of the strata within the Wessex and Weald sub-basins has proven difficult. It thus remains unclear whether these animals were genuinely coeval, not only impacting the interpretation of the taxa at hand, but also their possible palaeoecological attributes.

7.3.2.1.2 Comparisons with *Suchomimus*

This thesis assumes *Suchomimus tenerensis* from the GAD 5 horizon (Elrahz Formation) of Gadoufoua (Niger) represents a distinct genus, following previous authors (Sereno et al., 1998; Carrano et al., 2012; Hendrickx et al., 2016; Hone et al., 2017; Lacerda et al., 2021). Importantly, the *Suchomimus* type specimen (MNN GDF 500) is only known from postcranial material (Sereno et al., 1998; Carrano et al., 2012), however the taxon's diagnosis is based on a hypodigm of several specimens including a referred partial rostrum (MNN GDF 501) (Sereno et al., 1998). *Suchomimus* is considered to be very similar to *Baryonyx* in some works (Milner, 2003; Rauhut, 2003) and possibly represents an adult of the latter (Naish et al., 2001). Although generic synonymisation has been proposed (Buffetaut et al., 2002; Sues et al., 2002; Hutt et al., 2004; Naish et al., 2007), this has largely been argued in a cursory manner, a situation exacerbated by the lack of detailed accounts describing the *Suchomimus* type and referred material or assessment of their ontogenetic status (the above-described issues regarding non-coelurosaur ontogeny notwithstanding).

Further muddying the water is the possible presence of a second spinosaurid from the GAD 5 horizon at Gadoufoua, *Cristatusaurus lapparenti*, the holotype of which is known from fragmentary rostral and mandibular elements (Taquet et al., 1998). Due to an uninformative diagnosis and a lack of apomorphies, *Cristatusaurus* is widely considered a *nomen dubium* (Sereno et al., 1998; Sues et al., 2002; Bertin, 2010; Carrano et al., 2012; Hendrickx et al., 2016). Should *Cristatusaurus* and *Suchomimus* be shown to be the same animal, the former name would have priority (Holtz et al., 2004), although this is complicated by the non-overlapping nature of both type specimens. *Cristatusaurus* has also been considered an indeterminate species of *Baryonyx* (Charig et al., 1997; Buffetaut et al., 2002). However some recent works argue that the *Cristatusaurus* can be differentiated from cf. *Suchomimus* and other spinosaurids (Sales et al., 2017b; Lacerda et al., 2021).

Comparisons of Wessex Formation cranial material was made against specimens referred to *Suchomimus* (e.g. MNN GDF 501 and GDF 214, the latter a near-complete braincase), whereas this should ideally be conducted against holotype material in the first instance. It is clear that a rigorous description of the *Suchomimus* type specimen is needed: should *Suchomimus* be shown

to be congeneric with *Baryonyx*, the taxonomic nomenclature of the Wessex Formation spinosaurids will likely change as a result.

7.3.3 Phylogenetic results

The perceived irrelevancy of the fossil record in phylogenetic reconstruction by certain late 20th Century cladists is now a footnote in phylogenetic systematics, and fossil specimens are now accepted to contribute to such efforts (Grantham, 2004). The specimens studied herein are not without flaws, however. Temporally recent and superlatively preserved fossil specimens excepting, the phylogenetic placement of fossil taxa is effectively scored on morphological data only (Wiens, 2009). The number of available characters is thus limited relative to a molecular dataset, whilst issues of non-independence within the character list may bias results (Wiens, 2009). Conversley, some recent works have also promoted the usefulness of fragmentary fossil organisms in phylogenetic reconstruction (Woolley et al., 2022).

Non-random biological and sampling factors result in morphological datasets with missing or uncertain values that, under the additional influence of taphonomic processes, combine to reduce the amount of information available (Cobbett et al., 2007; Brown et al., 2012). The fragmentary nature of the fossil record mean these are certainly not immune to such issues, and the theropod specimens examined herein are indeed largely incomplete. The impact of missing data in phylogenetic contexts is varied: on the one hand, it may lead to the *a priori* exclusion of potentially informative specimens; on the other, their addition may decrease the accuracy of the phylogenetic results (Wiens, 2006; Wiens et al., 2011). As phylogenetic analyses depend on homology (shared ancestry) statements between OTUs, missing data may reduce the number of homologies assessed for incomplete OTUs, and the resolution of their relationships may suffer as a result (Kearney et al., 2003). As seen in Chapter 2 and Chapter 4, “rogue” or “wildcard” (i.e. unstable) OTUs may thus occupy differing positions throughout the MPTs, and various palaeontological cladistic studies have suggested that highly incomplete OTUs may generate many equally parsimonious trees, decrease the resolution of the consensus tree, and reduce branch support (e.g. Bremer support) values (Gauthier et al., 1988; Wilkinson, 1995;2003; Wiens, 2006; Cobbett et al., 2007).

Conversely, whilst adding incomplete OTUs increases the relative amount of missing data, it increases the absolute amount of potentially informative data, which can improve the final results (Wiens, 2006; Cobbett et al., 2007; Tschopp et al., 2018). In general, highly incomplete OTUs may be problematic in small datasets with few characters, but generally not the case in large ones (such as the ones used in this thesis) regardless of the optimality criterion employed (Wiens et al.,

2011). Indeed, OTU completeness is not necessarily synonymous with its stability; rather, missing data in key characters and homoplasy (or a combination of both) may be at the root of this issue (Kearney, 2002; Kearney et al., 2003; Pol et al., 2009).

The incompleteness of the sampled spinosaurid OTUs, and the effect of missing data on tree resolution and branch support values (Wilkinson, 2003; Cobbett et al., 2007), likely explains the fact that Spinosauridae was completely unresolved in unconstrained parsimony-based analyses and recovered generally low in-group support values under both parsimony and Bayesian searches (Chapter 2, Chapter 4). Whilst this was partially mitigated by the use of reduced consensus trees and removal of unstable taxa in the analyses focussing on Spinosauridae, the removal of these wildcard OTUs failed to produce spinosaurid ingroup topologies with robustly supported nodes. As alluded to elsewhere, refinement of the in-group relationships within Spinosauridae requires the discovery of further, well-preserved specimens. In a similar vein, the issues described above can be extended to the type material of *Vectaerovenator*, whose fragmentary nature impacted the ability to accurately classify it within Tetanurae (Chapter 6). Nevertheless, several works interestingly note that the impact of missing data on phylogenies generally appears to be small (Wiens et al., 2008; Wiens, 2009; Dávalos et al., 2014).

The use of morphological datasets in Bayesian phylogenetics (Chapter 2) also presents challenges, with outputted tree topologies, divergence time estimates and evolutionary rates more variably impacted by model specifications relative to molecular counterparts (Simões et al., 2020). Nevertheless, the greater influence of natural selection on organismal phenotype has affected the ability to develop realistic morphological models, whilst difficulties comparing the equivalence of character states between character statements has hindered the generation of more complex morphological substitution models (Keating et al., 2020; Simões et al., 2020). Indeed, whilst the MK model is commonly used in Bayesian phylogenetics of fossil taxa and posesses several positive aspects (Wright et al., 2014; Wright, 2019), complications may arise when the model is applied to morphological data (Lewis, 2001). The model itself may be somewhat restrictive (Warnock et al., 2021), and doubts exist over its ability to reflect the complex nature of morphological evolution with its intrinsically simple framework (Caldas et al. (2019), and references therein). For instance, whilst the MK model assumes the likelihood and rate of state changes are the same, morphological characters may in fact be gained or lost at varying rates (Keating et al., 2020). Further, the assumption that morphological characters evolve under a common mechanism (i.e. linearly correlated rates of evolution among characters at each branch) may not be a normal feature of morphological evolution (Lee, 2016; Caldas et al., 2019). Developing methods to model the evolution of such characters is one obvious direction that could improve Bayesian analyses of

morphological datasets (Gavryushkina et al., 2017). Nevertheless, resolving issues relating to model complexity is far beyond the scope of this work.

7.3.4 Palaeobiogeographic patterns

Although Chapter 2 presents a novel palaeobiogeographical hypothesis for the evolution and dispersal patterns of spinosaurids, the matrix only contained specimens (of varying completeness) that span the Barremian through to the Cenomanian and scored for pan-skeletal characters. However, the spinosaurid fossil record contains a far larger number of fragmentary specimens, including numerous isolated teeth (Bertin, 2010; Hone et al., 2017). Dubious Jurassic elements aside (Hendrickx et al., 2019), isolated dental records in particular extend the spinosaurid spatiotemporal record to the Berriasian-Valanginian of Brazil (Sales et al., 2017a; Aragão, 2021; Lacerda et al., 2023) and possibly the Santonian of China (Hone et al., 2010a). However, as mentioned previously (see Chapter 3 in particular), some works have questioned the spinosaurid nature of these Late Cretaceous dental records in particular (Katsuhiro et al., 2017; Soto et al., 2020). Regardless, in a similar manner to the research conducted by Gavryushkina et al. (2017) on fossil penguins, the analysis herein struck a balance between incorporating spinosaurid specimens with a reasonable degree of skeletal completion from a wide spatiotemporal spread (which informs the sampling rate and time), and the potential impact of including a larger sample of spinosaurid specimens containing a limited number of informative characters. These fragmentary specimens may nevertheless have important palaeobiogeographic implications regarding the origins and dispersal patterns of the clade, as independently suggested by Lacerda et al. (2023), and subsequent research should look to incorporate them in order to refine spinosaurid spatiotemporal evolution.

7.3.5 Other methodological limitations – discriminant function analyses

Discriminant function analyses (DFAs) are a multivariate analysis that can be employed to predict group membership of unknown samples (Hammer et al., 2008; Kovarovic et al., 2011), and have been a standard technique for the identification of theropod teeth (Hendrickx et al., 2020b; Wills et al., 2021). However, the DFA reclassification results were low in some data runs, and it appears that this method possesses some limitations when classifying isolated theropod teeth (Hendrickx et al., 2015a; Wills et al., 2021).

Hendrickx et al. (2015a) suggested that the results of DFAs conducted on theropod teeth could be improved by increasing the sample size of each taxon or inclusion of additional morphometric variables. However the choice and number of predictor variables need to be properly assessed:

too many and one may amplify over-fitting effects (where the correct classification rate that exceeds that expected by chance) or peaking effects (where the addition of variables beyond a threshold worsens classification) (Kovarovic et al., 2011). Conversely, excluding valuable predictor variables could remove interesting information (Kovarovic et al., 2011). Indeed, Hendrickx et al. (2020b) later demonstrated that the addition of theropod teeth from a broader phylogenetic range, as well as from a wider distribution along the toothrow, resulted in less successful discrimination to lower taxonomic or genus levels. Furthermore, DFAs may also be less able to discriminate between closely related taxa with similar crown morphologies (Hendrickx et al., 2020b), although this did not appear to be the case in the spinosaurid-only iterations of the discrimant analyses.

The incomplete preservation of fossil material can affect morphometric analyses, where missing, distorted or obscured data can limit the amount of information available for the analysis (Wills et al., 2021) and affect the performance of the classifier (i.e. DFA) constructed based on the training sample (Acuna et al., 2004). To compensate for the minor damage sustained at the crown apex of HASMG G369a and calculate an estimated complete crown height, a series of linear regressions examining the relationship between crown height and crown width/length were undertaken based on various samples of spinosaurid teeth (Appendix B). Whilst inferred values, such as those imputed from multiple regressions for instance, may distort a dataset and impact the resulting classification (Feldesman, 2002; Wills et al., 2021), only a single specimen (i.e. HASMG G369a) was subjected to the above described size estimation and any negative effects on the entire dataset are expected to be minimal.

Following the recommendation of Hendrickx et al. (2020b), the identification of the isolated spinosaurid tooth in Chapter 3 to lower taxonomic levels was mostly based on the qualitative (phylogenetic) techniques, with quantitative methods such as DFA used as auxiliary support. New methods for distinguishing isolated theropod teeth using decisions trees and machine learning were recently shown to possess several advantages over DFA, resulting in improved classification rates (Wills et al., 2021). These may prove to be an attractive substitute for DFA, and could compliment the apomorphy-based methods favoured by Hendrickx et al. (2020b).

7.3.6 Palaeoneurological limitations

The palaeoneurological study of *Ceratosuchops* and *Baryonyx* – the earliest spinosaurids known from neurocranial material – was conducted with the aim of assessing whether their endocranial anatomy reflected, in part, their ability to exploit aquatic resources for prey (Chapter 5). Schade et al. (2020) suggested various traits in the endocranium of the spinosaurine *Irritator*, notably the

vestibular region of the endosseous labyrinth, the reconstructed “alert” head posture, and the floccular lobes, were potentially adaptations towards the capture of small elusive prey such as fish. These features have, however, been shown to be poor predictors of ecology or foraging style (Ferreira-Cardoso et al., 2017; Benoit et al., 2020; Bronzati et al., 2021). Aspects of other sensory capabilities, such as vision or degree of rostral sensitivity, cannot be reliably demonstrated with the presented endocasts, although the latter is an interesting avenue of future research (see below). This begs the question: what is a spinosaurid endocranial trait that accurately reflects their semi-aquatic ecology and associated behaviours? Spinosaurids are deeply nested within Theropoda and semiaq uatic adaptations may not be prominent within the endocranium due to potential overriding effect of the ancestral theropod bauplan, as suggested for the morphology of the *Irritator* endosseous labyrinth (Schade et al., 2020). Paraphrasing Balanoff et al. (2020), if we accept that spinosaurids like *Baryonyx* or *Ceratosuchops* examined herein could catch fish with some sort of regularity, then we accept that their brains had the processing power to do so. These traits, in turn, may be beyond what is gleanable from the reconstruction of their endocasts.

This thesis also presented an estimated reptilian encephalisation quotient (REQ) for *Baryonyx* as a general proxy for gross cognitive capacities and behavioural sophistication. The utility of encephalisation quotients aside, one prominent issue with such calculations is that it relies on brain and body mass estimates, with the latter are notoriously difficult to ascertain for fossil taxa and may impact results (Balanoff et al., 2020). Indeed, the mass estimate for *Baryonyx* used herein is based on minimum femur circumference (Campione et al., 2014), however this element in *Baryonyx* is incomplete (Charig et al., 1997) and what remains has sustained some damage (S. Maidment, pers. comms. 2022). Meanwhile, the study of fossil cranial endocasts is based on reconstructions of the space immediately deep to the skeleton-soft tissue interface and lacks internal structure (Balanoff et al., 2016a). Moreover, the soft tissue at this interface is not the brain itself, but the dural envelope and associated vasculature, which can vary in extent across taxa and throughout ontogeny (Hopson, 1979; Witmer et al., 2008; Hurlburt et al., 2013; Balanoff et al., 2016a; Watanabe et al., 2019). Thus, brain masses of extinct taxa remain difficult to constrain. Moreover, the utility of the EQ may be on the wane, as several other proxies may prove to be better predictors of cognitive capabilities (Balanoff et al., 2020).

As above, the small sample of known spinosaurid braincases also means few endocasts are known, rendering it difficult to interpret differences in morphology when present. Several differences are observed in between *Baryonyx* and *Ceratosuchops*, however it is unclear whether these support the osteological traits that differentiate the taxa.

The spinosaurid endocast described herein were manually segmented, a process that is both time consuming and difficult to replicate. The advent of deep learning methods to segment palaeontological CT datasets may help resolve these issues, being notably more efficient (but perhaps less meticulous) than manual attempts (Yu et al., 2022). However, the ability to implement these novel techniques will depend on the quality of the scan and preservation of the specimen of interest; in the case of *Ceratosuchops*, internal features such as the endosseous labyrinths possessed similar greyscale values as the surrounding bone, suggesting a limited ability for deep learning algorithms to differentiate regions of interest from undesired content.

7.4 Future research

Spinosaurid palaeobiology remains a propitious field for further enquiry. Importantly, with certain "mid" Cretaceous spinosaurines arguably displaying more specialised traits (Hone et al., 2021; Sereno et al., 2022), the older British spinosaurid fossil record provides valuable data points with which to compare and test the evolution of various characteristics. Below is a selection of research avenues that could shed further light on the palaeobiology of these atypical predators, whilst several other areas should also be revisited in order refine our current understanding.

7.4.1 Taxonomy and systematics

The fragmentary nature of spinosaurid specimens means their taxonomy and systematics will require further work before a consensus is achieved regarding phylogenetic topologies and taxon splitting or synonymisation. Revisiting the *Baryonyx walkeri* (NHMUK PV R9951) and *Suchomimus tenerensis* (MNN GDF 500) type specimens will inform on their potential con-generic status and provide updated diagnoses where applicable. Whilst some works have argued the distinction is more semantic than scientific (Candeiro et al., 2017), providing a well-supported consensus has knock-on effects on the taxonomy proposed in this thesis.

Although spinosaurid phylogenetics was herein explored with large-scale analyses, the low node support values and Templeton test results suggest that the relationships between taxa are still labile. Whilst the discovery of more complete specimens would provide a welcome and obvious improvement, so would the rigorous description and illustration of important finds (e.g. *Suchomimus* holotype, the proposed "*Spinosaurus* neotype" FSAC KK11888) with which to appropriately score OTUs. Further, the implementation of new models for probalistic phylogenetic methods, such as novel Markov models for dealing with dependent (inapplicable) morphological characters (Tarasov, 2023), may help refine future phylogenetic analyses.

7.4.2 Ontogeny and growth patterns

Whilst the assessment of ontogenetic maturity in non-coelurosaur theropods remains somewhat ambiguous in terms of preferred methodology (Griffin et al., 2020), multi-element histological sampling of the *Baryonyx* type specimen is of taxonomic interest given its uncertain ontogenetic status. Characters used to diagnose *Ceratosuchops*, *Riprovenator*, or Ceratosuchopini could be reappraised in light of this information. Further, histological analysis of the "White Rock" spinosaurid, preservation allowing, could provide important preliminary data regarding the growth patterns of a large-bodied individual and supplement recent discussions regarding spinosaurid growth rates (D'Emic et al., 2023).

Given the relatively common nature of spinosaurid teeth in the British Wealden Supergroup, histological sampling to assess tooth replacement rate could contextualise the findings of Heckeberg et al. (2020), who sampled spinosaurine material from the younger Kem Kem compound assemblage of Morocco. The temporally extensive British sample could help describe the evolution of rapid tooth replacement in spinosaurids.

7.4.3 Diversity and spatiotemporal patterns

Given that isolated dental remains are the most common spinosaurid elements known from the Wealden Supergroup, further cladistic and morphometric analyses should be employed to assess diversity at a larger stratigraphical scale. Whilst the historical nature of some of these finds may frustrate efforts, several specimens referred to other clades should be revisited to assess their spinosaurid affinities (D. Fowler, pers. comms. 2022). Moreover, the use of decision trees could help extract more reliable patterns from the available morphometric data, a could replace the DFAs traditionally used to classify isolated theropod teeth (Wills et al., 2021).

The palaeobiogeographic scenario presented in Chapter 2 provided an updated hypothesis for the spatiotemporal evolution of Spinosauridae. However, as mentioned above, the lack of important samples based on isolated dental elements may alter the proposed patterns (Chapter 3), and it would be of interest to assess how their inclusion might affect the temporal distribution of the clade. This would require certain dental specimens to be revisited to validate their spinosaurid affinities. Given that some important spinosaurid taxa (e.g. *Vallibonaventarix* type specimen) are not known from dental material, it might be tempting to combine whole skeleton and dental phylogenetic matrices to not only improve the sample size of spinosaurid taxa, but to also constrain the topology of the resulting trees and allow select dental specimens to act as floating OTUs. Combining dental and pan-skeletal matrices has been used for some theropod tooth

studies (Hendrickx et al., 2014a), however it may be problematic, inflating the number of dental characters and resulting in unusual topologies for some clades (Hendrickx et al., 2020b).

Assuming that post-Cenomanian spinosaurid teeth (Hone et al., 2010a) do not pertain to spinosaurids, as questioned by (Soto et al., 2020), the potential extinction of the clade around Cenomanian–Turonian boundary (CTB), a time interval known to involve palaeoenvironmental changes and an extinction event within marine ecosystems (Sepkoski, 1986; Kerr, 2014), remains obscured (Candeiro et al., 2017).The recent adoption of ecological niche and occupancy modelling in palaeobiological studies (Chiarenza et al., 2019; Jones et al., 2021) may help address whether the climactic events (and especially sea level rises) around the CTB had a role in the perceived disappearance of spinosaurids.

7.4.4 Palaeoneurology

Whilst spinosaurids have been thought to possess sensitive snouts for the detection of prey in water by virtue of an internal neurovascular system (Ibrahim et al., 2014), rigorous assessment of such capabilities has yet to be undertaken. Known spinosaurid rostral neurovasculature is possibly more complex compared to other theropod (Bouabdellah et al., 2022), and examination of the size and branching patterns of the neurovascular canals within the spinosaurid rostrum could be the first step into understanding the role of the snout in prey detection. Such patterns could be quantified using the methodology of Lessner (2021), for example, although a survey of a large number of diapsids is likely necessary (Porter et al., 2020).

7.4.5 Palaeoecology

Whilst the semi-aquatic ecology of spinosaurids is well supported (Chapter 1), little is known about their hunting ecology or the extent of their relationship with water bodies. Hydrodynamic modelling may be an attractive avenue in an attempt to understand how spinosaurids caught underwater prey, a technique that has been successfully applied to a range of fossil organisms (Gutarra et al., 2022). Indeed, water is a constraining medium, and interest into how the spinosaurid bauplan interacts with environment and overcomes possible constraints has only recently been recently been ignited (Henderson, 2018; Ibrahim et al., 2020a; Sereno et al., 2022). Physical models or computational fluid dynamics could be used to test these constraints. As an example, swimming capabilities of the proposed *Spinosaurus* neotype FSAC KK11888 were recently assessed using physical models of the tail (Ibrahim et al., 2020a), with follow up work using a more holistic, 3D modelling approach (Sereno et al., 2022). Expanding upon these results could include data from the caudal series of *Riparovenator*, for example.

Additionally, enamel calcium isotope studies on spinosaurid crowns from the Wealden Supergroup could provide further lines of dietary evidence. Direct evidence for piscivory is known for *Baryonyx* (Charig et al., 1997), and calcium isotope studies have been used on younger spinosaurid-bearing deposits from Africa (Hassler et al., 2018). Combining calcium isotopic studies with more traditional isotopes such as carbon or oxygen, both of which have been previously used to infer semi-aquatic ecologies for spinosaurids (Amiot et al., 2010a; Amiot et al., 2010b), would be beneficial. Importantly, the extensive temporal range of the known British spinosaurid record would provide an excellent sample with which to examine the evolution of the spinosaurid diet through time.

7.4.6 Overlooked localities of interest

Regarding the discovery of new British spinosaurid material, the Wealden Group of Dorset is a succession of interest, preserving some of the oldest Wessex Formation faunas that date to the late Berriasian-early Valanginian (Penn et al., 2020; Penn et al., 2022). Dinosaur material from the Wealden Group of Dorset (especially remains pertaining to theropods) is generally rare (Benson et al., 2009b), and whilst no spinosaurid material has yet been found (Penn et al., 2020), several (albeit uncommon to rare) reptile teeth have been recently described from micro-vertebrate rich gutter casts (Penn et al., 2022).

These gutter casts generally preserve hydraulically sorted aquatic faunas, with limited terrestrial vertebrate material (Penn et al., 2022), and the small size of the tetrapod dental material recovered may hinder the discovery of spinosaurid specimens. However, spinosaurids exhibited rapid tooth replacement rates, high tooth counts (in baryonychine taxa at least) and an ability to exploit aquatic environments, traits that have been used to explain the abundance of spinosaurid teeth in several other deposits worldwide (Heckeberg et al., 2020; Hone et al., 2021; Isasmendi et al., 2022)and that might favour the preservation of their crowns in these gutter casts relative to other dinosaur taxa. As such, these gutter casts may be a resource for the discovery and study of spinosaurids from the basal Wessex Formation and allow comparison with younger Barremian fauna from the Isle of Wight.

Appendix A Supplementary information for Chapter 2

New spinosaurids from the Wessex Formation (Early Cretaceous, UK) and the European origins of Spinosauridae

Note that the full supplementary files, including scripts for the phylogenetic analyses, can be found with the published article online.

A.1 Methods and Materials

A.1.1 Allocation of material recovered at Chilton Chine

Here we provide brief comments regarding the allocation of the spinosaurid material recovered at Chilton Chine (Isle of Wight, UK) to the pair of individuals. In general, the material referred to *Riparovenator* is less well preserved than *Ceratosuchops*, possessing extensive cracking across the external surfaces.

A.1.1.1 *Ceratosuchops inferodios*

The material allocated to *Ceratosuchops inferodios* involves conjoined premaxillae, a braincase and a right postorbital, all found on the beach surface within separate blocks.

The premaxillae were found separately in two blocks on the beach surface; one contained the conjoined premaxillary bodies (IWCMS 2014.95.5) and the other its posterior processes (IWCMS 2021.30). These rearticulate well along the taphonomic crack that caused their separation, and are smaller than the rostral material recovered for *Riparovenator* (see below), supporting their association with the relatively smaller *Ceratosuchops* braincase. Further, their mode of preservation (which is superior to that of *Riparovenator milnerae*), suggests similar taphonomic histories. This confidence in the association permits the designation of the premaxillae to the holotype individual.

The disarticulated braincase material was recovered in very close association within a large but cracked sandstone block. This included a detached “skull roof complex” (paired frontoparietals, orbitosphenoids and laterosphenoids, with articulated right prefrontal) (IWCMS 2014.95.1), and a disarticulated supraoccipital+left otoccipital complex (IWCMS 2014.95.2) that had detached from the rest of the basicranium (articulated basioccipital-basisphenoid complex that includes both

prootics and a disarticulated but closely associated right otoccipital) (IWCMS 2014.95.3). This unambiguously represents the remains of a single individual.

We refer an isolated right postorbital (IWCMS 2014.95.4) to the *Ceratosuchops* type individual as the dimensions of the articular facets of the postorbital, while damaged, match those of the respective frontal and laterosphenoid articulations. An adequate degree of articulation can be achieved and, in concert with the above comment regarding the mode of preservation, the element possesses a well-preserved external surface. Whilst uniformly darker relative to some of the material listed above, we note that several elements of the *Ceratosuchops* type specimen are variably coloured and possess darker regions (e.g. cultriform process, paroccipital processes, basipterygoid processes; see main text Fig. 3), suggesting the overall difference in colour may be the result of the local taphonomic processes affecting particular bone properties within a disarticulated skull.

A.1.1.2 *Riparovenator milnerae*

As mentioned in the main text, the *Riparovenator milnerae* material comprises of a mix of surface and in-situ finds. The former include associated premaxillary bodies (IWCMS 2014.95.6), a left preorbital fragment (IWCMS 2014.96.3) and a posterior nasal fragment (IWCMS.95.7). As above, the premaxillary bodies are consistent in size with the in-situ braincase elements attributed to *Riparovenator* (see below), and also share comparable modes of preservation; we thus designate it as part of the holotype. Similarly, the preorbital fragment articulates with the exposed facet on the holotype frontal and is clearly part of the same individual. We refer the nasal fragment to *Riparovenator* due to its size (the ventral frontal facet appears too large for the nasal process of the *Ceratosuchops* frontal) and similar state of preservation.

Additional cranial in-situ finds include the holotype braincase. This includes a skull roof (paired frontoparietals with articulated but incomplete right prefrontal and disarticulated left laterosphenoid and orbitosphenoid fragment) (IWCMS 2014.96.1) and an isolated right laterosphenoid (and partial orbitosphenoid) (IWCMS 2014.96.2), which were found on a separate occasion from the in situ basicranial complex (which included variably complete basioccipital, basisphenoid, supraoccipital, and paired prootics and otoccipitals) (IWCMS 2020.448.1, 2).

We also refer a series of in-situ axial elements (denoting at least 22 caudal vertebrae and include including four anterior centra, three anterior neural arches, and nine middle vertebrae and nine post-transition point vertebrae in largely good condition, as well as 21 chevrons and various neural spine fragments) (IWCMS 2020.447.1–39) to *Riparovenator* due to their close proximity (c. 10m) to the holotype basicranial complex.

A.1.2 Spinosaurid specimens used in the phylogenetic analyses

Spinosaurid OTU	Specimen(s)	Examined	Photo Credits	Literature
Baryonyx walkeri	NHMUK PV R9951	Yes (premaxillae, nasal, lacrimal, skull roof fragment, occiput)		(Charig et al., 1986; Charig et al., 1997); axial series (Evers et al., 2015); quadrate (Hendrickx et al., 2016); dentition (Hendrickx et al., 2019).
cf. *Baryonyx walkeri*	ML1190	No		(Mateus et al., 2011)
Camarillasaurus cirugedae	MPG-KPC1–46	No		(Sánchez-Hernández et al., 2012; Rauhut et al., 2019a; Samathi et al., 2021)
Ichthyovenator laosensis	MDS BK10-01–25	No		(Allain et al., 2012; Evers et al., 2015)
Irritator challengeri (inc. *Angaturama limai*)	SMNS 58022, USP GP/2T-5	Photos of SMNS 58022	Marco Schade	Quadrate (Hendrickx et al., 2016); dentition (Hendrickx et al., 2019); (Sues et al., 2002; Sales et al., 2017b).
Sigilmassasaurus brevicollis	BSPG 2006 I 53, 54, 55, 56; BSPG 2011 I 115, 116, 117, 118; BSPG 2013 I 95 CMN 41774, 41790, 41850, 41856, 41857, 41858;	No		(Russell, 1996; Evers et al., 2015)

	CMN 41857; MNN IGU11; NHMUK PV R 16427, 16434, 16435; P.P.No 481; CMN 50791; SGM–DIN 3, 5.			
Spinosaurinae indet.	MSNM V4047	Yes		Dentition (Hendrickx et al., 2019); (Dal Sasso et al., 2005).
Spinosaurus aegyptiacus	BSP 1912 VIII 19	No		(Evers et al., 2015); (Stromer, 1915) (translation by Zanon, 1989); (Smith et al., 2006).
Spinosaurinae indet.	FSAC-KK 11888	No		(Ibrahim et al., 2014; Evers et al., 2015; Ibrahim et al., 2020a)
"*Spinosaurus* B"	Nr. 1922 X 45	No		(Stromer, 1934; Evers et al., 2015)
cf. *Suchomimus tenerensis*	MNN GDF 500–511, 214, MNN GAD 513, MNBH GAD 70. Additional dental interpretation based on comments in Hendrickx et al. (2019)	Photos MNN GDF 500-511, cast of MNN GDF 501, 3D model of MNN GDF 214	Serjoscha Evers, Marco Schade	Quadrate (Hendrickx et al., 2016); dentition (Hendrickx et al., 2019); holotype and referred specimens (Sereno et al., 1998); furcula (Lipkin et al., 2007); ulna (Smith et al., 2008); anterior axial series (Ibrahim et al. (2020b): Fig, 130).
Ceratosuchops inferodios (WightA)	IWCMS 2014.95.1–5, 2021.30	Yes		

Riparovenator milnerae (WightB)	IWCMS 2014.95.6–7, 2014.96.1–3, 2020.447.1–39, 2020.448.1–2	Yes		
Vallibonavenatrix cani	MSMCa-1, 3–5, 9–15, 18–20, 22–24, 27–28, 32–33, 53, 55	No		(Malafaia et al., 2020b)

A.1.3 Brief comments on spinosaurid OTU selection and interpretation

The number of spinosaurine taxa represented by “mid-Cretaceous” remains from North Africa is controversial (Ibrahim et al., 2014; Evers et al., 2015; Chiarenza et al., 2016; Ibrahim et al., 2020b; McFeeters, 2020). We use the name “*Spinosaurus aegyptiacus*” to refer specifically to the holotype material from Egypt (Stromer, 1915): other specimens which could eventually be referred to this taxon, such as the Moroccan specimens described by Dal Sasso et al. (2005), Ibrahim et al. (2014) and Ibrahim et al. (2020a), are referred to as “Spinosaurinae gen. et sp. indet.”. Stromer (1915) described two cervical vertebrae for the *Spinosaurus* type specimen (“Wirbel a” and “b”); Smith et al. (2006) tentatively identified "a" as an axis and "b" as a middle element, while Evers et al. (2015) interpreted "a" as the third cervical 3 (i.e. anterior) and "b" as cervical 4 or 5 (i.e. middle); we follow the latter interpretation when scoring cervical characters. We use the name “*Sigilmassasaurus brevicollis*” for the type material described by (Russell, 1996) but follow Evers et al. (2015) in including additional material referred to this taxon. A theropod from the Bahariya Formation of Egypt described by Stromer (1934) and informally referred as “*Spinosaurus* B” is here assumed to represent a single individual (see also Ibrahim et al. (2014) and Evers et al. (2015) for further comments) and included in the analysis to test its affinities. As the precise inventory of material included in the *Suchomimus tenerensis* type specimen remains unclear (Sereno et al. (1998) only mention a “partial disarticulated skeleton”), we treat this OTU as a hypodigm and also score referred material pending publication of thorough osteological descriptions of the spinosaurid material from Niger.

Cristatusaurus lapparenti, *Spinosaurus maroccanus* and *Oxalaia quilombensis* are based on fragmentary material (Bertin, 2010; Kellner et al., 2011; Carrano et al., 2012); since their character score strings are redundant with subsets of those of other included OTUs (e.g., *Oxalaia* is redundant with a subset of the scores of the unnamed Moroccan specimen MSNM V4704), we

excluded them *a priori* from our analysis. We follow previous authors (Charig et al., 1997; Sereno et al., 1998; Buffetaut et al., 2002; Sues et al., 2002; Bertin, 2010; Benyoucef et al., 2015) in considering "*Angaturama*" a junior synonym of *Irritator*: both are scored into a single OTU (i.e., *Irritator*).

A.1.4 Character amendments and additions

The following character statements were emended:

- 974) Rephrased as: "Basioccipital contribution to foramen magnum margin: large, exoccipitals widely separated (0); reduced, exoccipitals closely placed (1)".
- 1120) Rephrased as: "Long bone, medullary cavity diameter: more (0); less (1) than 1/3 of bone diameter".

Four new characters replace previously included characters that are uninformative with the present taxon sample:

- 509): Basioccipital apron, basisphenoid overlap, dorsoventral extent: less (0); more (1) than 1/3 of the basisphenoid.
- 510): Basisphenoid, excavation of the collateral scars placed lateral to middle depression: absent (0); present and distinct on both sides (1).
- 511): Premaxilla, narial margin, overlap with oral margin: present (0); absent (1).
- 512): Premaxilla, interalveolar space between 3rd and 4th alveoli, mesiodistal diameter: less (0); subequal or more (1) than ½ of 4th alveolus mesiodistal diameter.

Additionally, Cau's (2018) character list includes the following new character statements:

- 1782): Frontal, parietal suture, position relative to postorbital process: at same level (0); posteriorly placed, resulting in a concave posterolateral margin of frontal in dorsal view (1).
- 1783): Femur, shaft, distal half, elongate crest on posterior surface (accessory distal trochanter of Sereno et al. 1996): absent (0); present (1).
- 1784): Prootic, lateral surface, anterior end, large fossa housing foramina of cranial nerves V and VII: absent (0); present (1). (Brusatte et al., 2014).
- 1785): Anterior tympanic recess, development: narrow groove facing anterolaterally (0); wide foramen facing laterally (1). (Pei et al., 2017).
- 1786): Astragalus/tibiotarsus, distal condyles, ventral surface, shape in extensor/flexor view: flattened (0); rounded (1).
- 1787): Scapula, dorsal margin distal to acromion, flange distinct from acromion by cleft/concavity: absent (0); present (1).
- 1788): Manual digit IV: phalanx p2-IV: present (0); absent (1). Inapplicable in taxa lacking mc IV.
- 1789): Manual digit IV: phalanx p3-IV: present (0); absent (1). Inapplicable in taxa lacking mc IV.
- 1790): Manual digit V: phalanx p2-V: present (0); absent (1). Inapplicable in taxa lacking mc V.
- 1791): Dentary, first tooth crown, shape: similar to other rostral teeth (0); elongate, fang-like (1).
- 1792): †Dentary, lateral surface, neurovascular foramina, vertical sulci linking foramina to alveolar margin: absent (0); present (1).
- 1793): †Axis, centrum, shape in ventral view: mediolaterally constricted posterior to the intercentral suture (0); lateral margins subparallel (1). (Wang et al., 2017).

- 1794): †Presacral vertebrae, cervical and anterior dorsal centra, posterior surface, shape: flat to slightly concave (0); deeply concave (1). (Modified from Rauhut 2003; Holtz 2000; Carrano and Sampson 2008).
- 1795): Metatarsal IV, shaft, ventral view, proximodistally extended medial flange overlapping metatarsal III in articulated specimens: absent (0); present, metatarsal III shaft not exposed for most of its length ventrally (1).
- 1796): Premaxilla, lateral and dorsal surface, extensive pitting of neurovascular foramina: absent (0); present (1).
- 1797): Maxilla and dentary, paradental laminae (interdental plates), contact between adjacent elements: absent, widely spaced elements and crown base exposed lingually (0); contacting, crown base not exposed lingually (1).
- 1798): Pennaceous feathers (if present), vanes: open (no hocklets) (0); closed (hooklets present) (1).
- 1799): Elongate, semi-rigid tubular tegumentary structures (rachis or unbranched rachis-like elements, including those inserted on ulnar papillae): absent (0); present (1).
- 1800): Femur, intertrochanteric fossa between greater and anterior trochanter, nutrient foramen: absent (0); present (1). (Zanno et al. 2019).
- 1801): Postorbital, ventral (jugal) process, lateral surface, proximodistally (dorsoventrally) elongate ridge: absent (0); present (1). (Modified from Aranciaga et al. 2019).
- 1802): Prearticular, participation to milohioid foramen: absent (0); present as a distinct cleft or concavity (1). (Modified from Aranciaga et al. 2019).
- 1803): Ilium, preacetabular process, ventral margin, orientation of lateral surface relative to rest of blade: aligned dorsoventrally and facing laterally (0); flared laterally and facing ventrolaterally (1).
- 1804): Humerus, deltopectoral crest, anteromedial surface, pectoral scar along distal margin: absent or indistinct (0); present as a marked oval scar (1). (Rauhut et al., 2019).
- 1805): Basipterygoid processes, lateral view, angle formed with culfriform process and basal tubera (measured at basal tuber): less (0); more (1) than 30∞.
- 1806): Braincase, endocast, dorsal sinus (dural peak), distinction from the dorsal roof of the cast: poorly distinct (0); markedly distinct peak (1). (Paulina-Carabajal et al., 2019).
- 1807): Tibia, proximal end, posterior margin, accessory cleft lateral to main posterior sulcus between condyles: absent (0); present (1). (Modified from Ezcurra & Brusatte, 2011).
- 1808): Caudal vertebrae, accessory longitudinal ridge running along dorsolateral surface of neural arch, lateral to zygapophyses and medial to ribs: absent (0); present (1). (Rauhut, 2011).
- 1809): Caudal vertebrae, anterior and middle neural arches, posterior view, fossa on peduncle, ventrolateral to poszygapophyseal bases: absent (0); present (1). (Rauhut, 2011).
- 1810): Anterior caudal vertebrae, prespinal lamina, development: poorly- to moderately-developed, not markedly protruding anteriorly in lateral view (0); prominent, forming a distinct convex anterior margin of the neural spine at mid-height (1).

A.1.5 TNT Scripts

xread

1810 40

Eoraptor
100000?0000010000?0000011010??000001000000000000?0000000110101110?100???????0?0?0??11000000010?0????0000000?????????10????00???????????1??000?0???000000???0000?0?00000?00???00000???01?00000??000?0??0?1???1000000?0000?0000000000?00?0??0000??1

?000?0011000100?1?0????0???000?1??0??10??0?0?0000?001?0000011??000010000100?001
00000010001????????10?0?100?0000000?1??0?100?0?00?0?000?0101?01?0000001?0?0010?1
100010?001?000010000?1010?000010010????0??00?1?0000001??0000??1000???0000000?000
00000?110?00?1000000?0110??00????00?????00?10?10?0??00?1?0??101?100?0????0?010?10
?????000???????0000?00?????00???0?0??00???000?000?????00000?0??0???????000??00????0
??0?0??10?000?0?00???????00????1????010000?0???0?01????000??01???????000??????0?0??
000?011?00000111?000?0??0000100100??0?00??1???0?01???01?00?00????000?0??0?00??1??
00?100?001???0??0?0000?0??00000?????0000???0?0?0100000??1??0?0001?000???0??0??0??
?000??0000???0?0?0?0???100???0000??1?????????????0?00?001??????????00???0????00???
??0?0??????00????0100000?0???000??0????????0?????00???11???0?0??0?????0010110??0???
?11????00?000??0????0?000??0?00??0??????????00?0????????1?00?0?0??0????1??0????????0??
?0??0??00???????????00?0??1?0?????????????0???????????1?????0?0010???00??0?0???0??0
??000?1?000??0?0????0?????0??0?????????00???????00?000000???0??0?????????????????0???
0?0?00??????1?????00???0?001??100???????000?0?000?????0?0?0???00?????????????000??
??1?00????01??0??01??????0???0??0??0??0?1??00?00?10000001?100???0??0????????00?000
???0?01001?00?0?0??0?????0????000000?0?00??0??0?0?0?????????????????00???1??????1?
?0???????0?????0?????????0?????0?0?????1???0????????00??10?000??0??????????0????????
?0?0?????0??????00??0001?????????0??0???000?????????????????????0?000000000?00?0000
00??00000??0??0?0???001??0???000?0?1??010????0???00??0?00?????10???00?0??0???0?0??
?0???

Meleagris
1111?1??01100???00?????0?11010111?00101101000000100 1?????0????????0????0100011011
00???00?000?10?1?1?0110??1?10011???01??1101100?????????01100?11????00?1??11???????
????100???1?0?0??1100?00??100?0111010001??1000100000110101110110111101?0?????110
101?1?0101110111001010101011100011100010110?0101?011?11110100?01?1110010?1???1
?0??????1???111101111?01?011?11????001??010?0?011????1111000?10101??00????0011110
0?1010?010?1?111000100001011101000111?110000001010??1?110?0??11????1??0111000011
??11011?0?101?11110?00110001?1001???1?0?11??0??0????1101??0000?110?10??10?01???11
??101?????10??01?0?0101001 0??11110??0??0?010????0??001?1100?0?1?????????0????0????
?0?1???011001??????11?1????0?0????1??11??01?01????0??11101?????1??110??0???????0?10
?0?0?1?11??1?0?1110?0????0?001?01?010?01??10??0?0??11??10?00?0??000?0001?10?110??
???0??000?????110?110?00???0????????????011000??0?????????????0111???1?????1??11??
??1111110?0111?01??0??010?????011??001?110011011??11??0????????0?000??0?0?1??0????
????01?0???001?11?101?11?1?11000010?0??????0?111???0??11???0?11???111??010011??0??
1110???000??10000????0?0?1?????10??00?110?1?00111111???11?0?0?01?0?0????1??01?0?0
0??????0???????0??00??1100?00?0???00???01?????????????????01?????1??10?0???1???01?0??
0??0??1?01????0???100???1??11101111111?????????10?????????01110???11010000?01111??
00?????1?1???00?1?????00001?000??1??????11?0??????0111??????????1?01111110 1?????11
0101?1??1?000???????0??11???1?1??0??????1000?01?????????????01?1?110??1??0?????01??
??????01?0????0?00?????0???????????011?11?1?0???00?010??????1??0?????1100????110???
????????0???????????0????01??1????11????10??0???01??????0???00??000??0???????????10?
?????0??001111001?1?1?1?1?????10??????0???0??0????100????10?01111???0??1111111111??
?1000101??00??01??00000?????????????????0???0??1??????????11???0101?0??10???????????11?
??0????????

Acrocanthosaurus
1000000100011001010011001010000010000010001001110000101111100010011?10001000?0
0100110001011000010 00???000001000000001?01100??10?10???00?????1?1010?10100000000
000?0110?00001???1010??00?0000111?1110?101101111110?1100??011100?001011000000010
0100100???01111001010 1?0010?11000010100000101000 1?0011?0100101101100 01?00?0?0??
0?101?00?0???1001????????1?0?10?00?0100?0100100001010 00?000111?11?0?101?0000???00
010?11??011011?0010010010111100111110011110000110 1????011010?0??1??1?01???1??010
00010000001?000?0?101?0000?01?0?00????0000100001100?001010000????100001?00?0???0

001110??000000110000?000?01000?000?000000000????010101?0010?00000??11?01?111?110
100?1?00001101??1??01100??01110???00?0?11????0?0000?000?010011??0000011?0??0??000
0??0?01000?000001??1?1?0011??01?00?01?0??111???0001?01000?000?0??0?11000???010100
0000000????10??010001?1100001010000 0?000?00000?10??0?0????0???0?10?0000?00000000
0100000?0????000001000??00????????101001?1?1000??01?0?????????001??00?011?11?10?1
000?0?0???0?????0?0??00??01??0?010?11100?1?000100?11?0?0?01?0??100?1110?00????0?0
01?00100110???00010?1???0??10101??0?000?0??1?00??1???0?000??0?00000?001?0??0???01
01010?011??00000??????00010??0011?1?00?001????1?10?0?0?1?????0?10?00010???0000010
0??010??0000?00????00??1?10?0010??0?0??0?0?????0??????????????????1000???0??000??0??
00?000????0????00????01110?0?00??0101101010?010?11000??01?00111110?000????0?000?0
1000??0???00??????000???01?00????0011011011100000000 0???000??00?01010011010?00110
000???00??0?01?000001101??1?00??00100??10000?010?00000??000000000???1000?00??0?0?
?0?010?0?110????????100?01?1?0010011???011?1???00?1??11??101000?001011????0?0000?
?000000?00??0??????????????0?0?0?0??????????????00000100?????????1000?011000??0??0??
???000????0?110000000?00000?100??000?0?000?0?0???000000000101?0?1000??1?0?000??0?
?0000?000??0???0?01001???01???10000

Afrovenator
10??????????1???????1101???10000?01100100??0??????????01110101111100?00???????????
?0000010010???0?0??0000?0?0??0????0000???1
?????????????????????????????1???100011?11111?110???001000???101??????000??0001?0?0?
??????????????????????000?1??0001010?????????0110?01101100010001 0?0??0???1???1?????
001???????????????????0000?0???????0?01?001?0011101110?1?1001?000000010 0101?01??0?
?00100110000??10?110010011???0???10??????110?00?11??1?0?011?1??010000?0000??11100
1001??1?????11?????????00???000??1?00001??00????0?10?0?10?0??0??0?0?11?0?0??00???0
0?0?00???1?0???00?00?0???0?0??00??101??0????00?0????11????0?0?0??0???0???01?0??10??
??00?0?1?0??0?0???????????0?0????0??????1?????0??0???1?0??????1????0?????00?001??????
?1?0??0??????1??1?1?????0?11???0????11?000??0????0?????1?0?????0??1??0???0???????1?
0?0??1?0????00???????01?00???????1?????10????1?1??0??100???????????????????00???00??
1000?0??00???1????????????????????0??1???0?00??????0???0??0?????????????????011000?10
??1??11????0????0??0?????????1?0?000????1????????????????0???11??1????1?0???????101?1?
?0?????0??1??0??0????????????????????????0?0???0???1?0??0???0??????????0?000??0?????1
00?0?0??1?0?0?00?0?0???????00?1??1?0?100?10000???10??0????0??????0??1?10???001????
??0?0????0???????????????????1001??????1????0????????????????????????100??0????00????
???????????10???????0?0100?????0??????0?0?????????????00??????000????0?00??????1??0??
??????????00???0?0????0?1010?0??1????1??????1????????????0?00010??0?0????0?????01?0?
??????0????0?0?00????0???1????00???????0?????0?????????????1?????????????????????1?10?
??0??1???????00??00?0?0??0????0?01???????0??????????????0???????????????????????????0?
00010??????????0?????01????????0?????????????????????????????????0??0???00???????????0
00101000?1???????????????????0????0???????????????1??0???0?????????

Allosaurus_fragilis
10000001000011010100110010010000100100101010001000000101111100100 01?01001100000
00001100001000000101000100100100000000111111000010110000101010100101001000 01000
00000000100010010101000100110000101111101101111010010011000100100010000101010 0
00000100100000000111001010100010011000000010000010100000000 1?0100101101100011001
000110?101?00101??1001??????0111000000100000000000110000101000100011101110110 0011
1010000010011110110100001001001001110011011001110000011 01?0110110100011 1011001
111100010000100000001?100100101100000110000 0????000010000110010010000 01001?10110
1000000000000111010000000110000?000000000000011000000000000000001010000000000000 1
1111001001001000100000011010?100010001001100000000 0?0101?0001000000000000011??001
0011100000000001000001000?001101111110001100010001010010111000100100000000000?00
0001110000000101000000000001011000010011011000010100000?000100000?10100011010001
1000000000?000000000100000110000000001000??00?000000100000?01100000001?0????????

0001000001010001101100000000000010000000000110000000010011100010000000000?0010?0
000001000011000000??000000001001100100001001000000100010000100000010000000?000
00?0010000000001000000?0000001?00001?00000000?10?00010000100001000000000000000000
010000000110000101010?000001000001000000000000000000?0101000010?00?000000001?000000
0000???00?00111010?00100000000?000?00??0?0????0000?0010000100000000001100000011
1000?001?000101000000000000000000?00000??0???0000000?0001?00000000000000000000110000
000000000000??000010100010100001100000100100?00??000001101101000??011000010000?
0100000000000000000000??0000000?0000000000000000000000100100100?0?10??000???011?
10??00??10110?1000000000010?000000000?1000000?000001000010?0000000?1?00??00000
0?0010000001000111011010000?0110000?000011?0?000000000110000000?0000001000?0000
0?00000?000000010100011??0?100010000000000000?00000?000010???0001001???0100110000

Asfaltovenator
?000?0010001?00?0?0011011000??00100100100110001?00?0??01110000101100001????????1
0?1000?011010001????????110101?00??001??1?????????????????????0????0001000000000?
00??00???101010?01??1100001001?0??????00????01??010????????0??0001???000?00?00??1?
?????01110?????0???1??11???0101????0?010??1?0011?001?101101???01100?0101?0??01?00
??0??1001??1?
0??????????????????????????11???????000??10??0???0???????????????????????????????????????
???????????????0??????0???0?00?????001?000?0???????0?100?????0?0?????????000????????
??????0?0?00?0??000???0????0?0?0???????00??????????????0??0??????0??????0???0??11?0?
0?1?????????????1?1??0?0?0???0????11????00??0?1??1?????00??????1?0??0010?01?1???????
??0??0???1?01???????0??0???1?????0?000??1??0?0???111???????00?????1??0???11??0????1
01???????0???????010??0???1??0??00?00????1010?0?????1???0??1???1??1???000???0??????
00?0?????1?0??????1?????????????????00?1?0?????????0??0??0?00???????????00?01????01??
?1??0??????0????0?????00?????????1??????????????????00??????????????????????????0?1?1
00?????0??0????0???????0???????1????0????0???????0???????????????0???0??????????????00?
?????????1???1?0?0?????0?1????????????0?0????????????????0??0??1?????????????0????0???
???????????????0?0????001??????100??0??????????????????????0100?00??00?0??????10?????
0??1??0?????00?000????????0???00??????0???????00??????00???????00??0?????0???1???????
?0????????????????01??????0?001???0????0???0?0????0?????????00??????0???1?????????0??
????0?00???00???0??????????????????????10??????????????0??1??0???0???0????1???0???????
???1?????????????????????1????0?????????0????????????0?????1?????????????????0????1??????
????1?????0?????????????11??000????0?????????0?00?0??10???00??00?0??0?????????????????
????1???1????????????????????????????????1????????????????

Ceratosaurus
1000000100011001010011000001000000001001010001011000010011010010101010?0000100000
0000110000000000000?0?00?000000100000001?11?0?010000?0000???0????00??10000100001
000?0010000001??0100100??100000?1110110001101000110?110010001000111011110000100
10000100?0?0111100100010000000000000001?000010100000010???0???01011?????00?0?0??
0010010????001????????????1??0000000000000100100100000?00110111111010?1?000110??00
?01101010011?1010?00010?00011??01000110110?00000111?00101101000?11001000111??00
?000000000??10001??????????????00?0?????0?0000?00000?00?1000000?00?1010?0?00?0000
010011?0?000000?110?0?100101000?00100000000000??1?00?00?10???0???0????01??000010
0101??00?000?01??100?00?00?1?10????0??01?101??000?0??0000000010??000001110000??00
0110??00000?000101111?10011100?0?1?1010011111111100010000??00?00?0??001000????0?01
0000?000??1??0001010101??0?00000?0??01??001010??01000000001000??0000?0000?010?1?
1100?000001??01000001000??10?01?00001010?0?0000001000?0????????00001000110?0????
0000?010000001?0100000011111000000?01???1110000000000?00?0?0?0?00??00001110?011??
?000010?0100110?0?01010??10?????0001100?010001110001010?0000???0?0??00000100?01
?0?0010?00?001??100?0??????00000?000????10??000????1?0?00?000?????0?00?0?0001?001
00011?01000??0000?00??0?00?0101000000000?00??????0??0??0????0???01000100000?01000
000100?00?00?????0????00????0000?00?00?0??1??100000000??1000??11?001101?00001????

0000000?000??????????0?????01??00?00?00000??00?00001000?00?0?0??00??00?0100?00001
0000110?0001?1?00?????0010000011000??0000000101100?00???00000?000000000?????00?
0?0??0???0?000?0???000????0?01??000??10??0?01??0?1?10??????000?0?100010?000?00?0??
???000?100?000??0?0000000000??110000?0?1?????00???00????000100011001100100??01101
0??0000?11??????0000?111?0000??00000?1000?000000?0??0?0???001000001?01?0?0??0000?
0?100?00??0?0??100?10???00?1001??00?0??10000

Coelophysis_rhodesiensis
1010?0?10000101001001101101 00?000101001000000000000001?0100000001??0?10001001000
1?01?1010000?0??000?0?1???00001?00?1?00010?01010?00?110?0??1???1?1?0?0?0000000?00
0?0???000?00?0000???????000?0????0?1?00010100?11000000?00?1?0110001 0?0?000100100?
?10000000110001 00?10??0??1?0??0?00000?010100?0?00?000110100101100010001 0?0110000
0000?000010?1??????011?000001??001??010?100?0010?000??111111010010010010 00?00101
?110110?00101?0?10100?1110010001101010?00??000???10??0?00??1??0?100???00111?0?0
?0100001100?10??0?1100?01????0??????01?00001?00??000???101??0?111?0?00?????001??1
?0??0?000??010???1?1111010?001000001??0?0??00010100??????0?00???0????1?0?1?0??00?
?0?1?11?00?10??00?000011???0?0???001???10?0?00000?0000100??00??0010000??0000????0
?0?00?110?011?1?1000?11001?000011011?1111100?1?011????00?0001?00?00000010100??10
000?????0?10??001??0?0?000000001?10???00?0010?01???0?000000?00??0?1?100????00??0?
?0???1???10??0000??10??1000?00001??000000????1???????????1?001001001???1?00?00000?
0?00000???00?0????011?????1?????0??00?0?00?000?0???000000?0???11??00????010?0??011
111?00????1?????0???000?0??0?000000?10?0??00??00???00??0???????1????0???00???00000
0??00??0???1??0?0?0??010?001???00????0??0000?????????0?000?00?100?0???0?000100???0
?00??0????00??1010?0000?0??0???00??0?????????????0?0??00010??1?1?1000?0??0???0????
??????00???000??010?00?00????10000??00?0000???0?010?000000?01??????00?00??0???0???
000?101000?00?01??01?1?00??0??00??1??00000?0????0???00?001?0??10010111?10000?1?00
??????0???00000?00???1??10??000000?00??000??0?0?0000?000??0????0000?0?1?0???0?0000
0?00010??0??10??0?00????0?????1?1??????10???0?0?00?0??11?00?1?????00??0?0??00????0
0?0??????0??00????1?0???0??0??????00?00000?????????10??000???????0110000?0000?0?00
?110000000?00?000100??000?0?????0??????????????????????10??10??0?000??0??0000???0?1?
11?0??0???????????100???

Coelurus
??
??00??0????????????????
??????1????????????????????0?????????1100000001001??0?00101100?00?00?01??1?0?0?0?11?
???????0?????????00000?00001010??0?0001?0?1?????????????10??101????????0??????????
??????????????0?0???0?000100000?0??0???0????????????0?????????????????1111111000100?
?????????0110010111??000?11?1?0?1?11?00??011?1?0111?????0?1????0??????10?1??0?????
??????????????????01???????0?????????1???????1???????0?00?00??????0????1??011?00??0?
??0??0??00???0????????0??0????????????0?????0?????0?0?0?????0?????????????0????0?11?
?????0????????0???0?0?????????????????1?????0????????0????00?????????111???1110?????
????0101?1??0?????0???0?0???0???0????????0?0?00?0?0?11?0?1?????????????????01?00??
?0????????01?0?????0?0?0??????000?????????????????????????00????0?????0?00????????0??
??10?0??0?????????????00???0?????0????0?????????????????000???????????0?????????????0
???100??????0????0???????1?0??0????0??????0?????????????1??????????0?0????????0?????
0???0??0?0???????0????001????0????????10???0?????????????0?0???0??????????001???1?
???????????0?????????????1?1???????00??????????00??01??1??????0??????00?1????00
000?????????????????0???????0???0????????1????
?????0??0?????00?????????????????????????????????0???0?????????????????0??????1??
???????????0?0?????0????????1?????????????????????0?????0?????????????????0????????0
0?????????????????000?????????????????1?????????????????0????????01????????????
???0???1??????????????????

?0????????1??1?00???????????????????0???????????????????0110?????????????0?????????
???0??0??0?0??????????????0?????1???0??????

Concavenator
00??00????????0?????1100101???00100100?0?010011?0?001?0110100110?1??????????????1?
?????1?11?0?0???1??0????00?0?10000000?001?
???????111?????00????0??11?1?0?1????1???11???100??0??000?0?000???10?000?000???00?0
0111100101?100??0?1????0000????01010?00?000???????0?10????0???0??1?110???1?0???0??
1000???????11??????0?0000000?0010000111?001??011101010011000100101000100111001??
10000?001000101?1001?001??1????0???1???0?10????00??0??0?000???0?00?0000?0??00011?
01?0?1???0?0?0000??0??0??00?????00????1001??00?1?00?10???1?00???0000??11??????000?
1?????????00???????100???0?0?0??00???000?????00000?0?110????????0???0??0?????????10
?01000?0111?????0???1??????0???0??1??0?001?1??0????11????0???0?0??????0???0?10?1???
?1????1???0??0??1?01??1101?0?????0??00??0???00?0??0????0??1?00?0??00?1??0???0?0????
???0???0?000????0???????010?0??????000??0?00??1?1?1?0????0?????0?????????1?0?0????0
00?0?10???010????1000????????????????1????010??????01????0????????0??????????1???00
00???1??0????????????????0??1??00???1??????1???0??????0?????10?????1????1???0?00?????
00??0?0?001??0??0?????????????00?0????0?????000????0????0??10??1???????0??????0??0?1
???1?0?00????01???0??????????00??0???1??0??????1??010?0???0?0???????0???10?????010?
0?????00?????0????????????0??????001????0??0??????0????0????????????0???0???00???0?1??
??1?10???000?11000?????0???01??0??0????0???0????0???0???00??????00????0??00???????
01?1???0??01??0????????????1???0?0???1???0110?0????????1?1???0??0?1?????00??000????0
????00?0??0?00000?00000?000?00????0???0????0???0??????0?0??0?????1???1????1??????0?
1?10??1????0?????001?00?0??0?????????0???0??000??0??0????????0???0????0?0???????????
??00??001?????????01??0???????0???????????????0???0?11000000??0000?01?00???0?0?????0
??0?0?????????????????0?0101????0???0??000???????????0?????????0?0???????

Dilophosaurus
101000010000000011001000101000000000000100010000??0?0?00101100?11010?100????0????
???10000101000000100000 1?01000?00?0000110000010000000001???????0???1000010000100
0?0100000001?001000?????00001?10100??00000100111000000000011?01?01011?0000010010
0??100?0?0011000000010000000100000001000001010000?0000??010?001011??000001000010
0000100001000001????????100000000?00000010010?00001?00?00111111010?1??100100000?
010?1100010000001?0010000011100010001?01000000001011001011010001110 0??001111??01
10000000000000000010?1??1100?0110000?????00?000?0011?000?1000001?00?1000?0000??000
0100110??0010000?00?0?00111?000?0010000000000000000000100??0?0?00000?00?001?11011?
0?00010?0001100??10000000?0011100??00?01?1?0?001000000?00110110??000001??00?0000
000???001000?111?01??11100111 0000?0?1?101111111?10?01000?000000?000001?0000?0010
100?0?0?0000??00110??011??00000000?0000?0001100??010001000000001100000000 0?000??
00000?000011????00000?000??0??010000??000?1?000000?000??????????010001000000 0????
0??????00???00????000?0?1???11000?11??1110??0?000000?00?010?0?00001000?010?000???
0?00??0011111??00???10010000000000000000000?00000000000000?0000??00?0???????100000?
0?0010??00000??????0???1??000000000????10?0000????0?000??000?????000000?1000?0000
00000010?0??0000?00000?00?01010000000?0?00???0?????0???????0???00000000000?101010
00000?00?00?????0?????0????000?000?00??0?????10??0??0111000?????100100000000?????0
?000??000??????00??0???00????0??00?????00????00001000000?0?0??00??0000100?00?0100
001?000?00?0??????????0?0001010000001011000?01000??????0?000000000000000??1?00?00
00?????0000??0?00????0?1?000?1???0????00?0???001?1???????0???0?1?0???0?0??00???????
000??100000??0?000??00000?0???0?0?1?0?????00?????1???0??10????????001?0??0?10000?0
000000?00000???0?1?0000000?000000100??00000??0?00?0???00000001100 0???10???00??00
00??0??0?0??????101110?01011?????001?0000

Dubreuillosaurus
?01000010000?0010100110010110001100100101??0????0?????011100?11001??000010000000

0000000000010?????????00?000??00000000??000???01????0001????????1??1000000000000
?010000000?????0101???10???1????11???????????1????????????0?0??01010?000?0?00?0??1?
??????1?0?01??????????????0??
??001????????11???00???00000010?1?000001?0010???????????????????????????????????????
?????????????????1?0010???0??0??01?000???????00??????1?????????????????????????????
1?????????1???00??????1??0?00??????00?0000????????????0??0?0??1??11?0????000???????
??0???0???0???00??000????????01?????0??0?0????0??0?010???0?1?????????0?10???0???000
????????????????10?0?0??????????0??1????0???0?1???????00?1?01????????????01????1?????
????0?0101?0????????0?11??????0??1???????????0??0??1??0??0???????0???0?0011?10???0?
??????????0?000?0??0?0???????1???0000????0?1?000?10???000?01??000?0????????????0????
?0?000?0????000??????????????0?0?10?0?0001????????0??0????00???0??????0???10?1???1?
?1???0???????????????????0????????0??0000????????0??0?00??0???????????????????????0??0
????????0???1????????????????????????0?????0???????0???????????????00?????????????????
??????????0????????????00??101???????0????????0??000??0??????????????????0???0??0??????
????????????????????????????????0???0?????????????????????????1?0?00?00?0?????11000?0
0???1??0??00?0???0??0000?????000???0?00???????00????????????0??0??0???01??????1????
????00?????????????1?0????????001???0???1?0??????????00??011?0?????0??????????0??????
00???0??00?00?0????00??0????????0???0???00?????????0???0??0?1???????????????0????????
????1??????????????????????????0??????0???0?????1????????????0??????????1???0?000?0???
???????00????00?????0?????????????????1?000000??00?0??????????00??000?0???????????????
????0?1??????00??????????????0????????00????1???0?????????

Duriavenator
??1?????000?1????10??1??????0????0110??????0???
??1??????????000000000000?010??0
00????????1??
??
??
??
??????????0?????????0???0???????????????0?0?????????????????0?0??????????0???0??????????
?10?????????1??10??????????????????????????1??
0?????????????????????0???0???1????????0?01???????00???????????????????1??1???0????????
???????0??0??????????????????????????????????????0????????????1???????????????0?1??????????
???????1??????????????????????????000?01???????????????????????????0?0????????????????????
??????????0???10???????????????????????0??????????????????1??????????????????????????1?
?????????????????????????????0??????????????????????????0?????????????????1???????????????
????????????????0??????????????????????????0?????????????????????????????0????????????10???
?1?????????????????0??0????0?????????????????????0????????????????????0?????????????????
????0??????????????????????????????1????0??
??0??0?????????????????1?????????????1????????????
1????????1???00??????????00??0????????
????????????????????1??
???????????????????????????????????????0??????0???0???????????00????01?????????1??????????
1??????????????00????????????00??00??????????????????????0?????????????????????????????????
???0??????0??????????????

Eustreptospondylus
101000?100?0100101001100??11??01???10?1?1??0????????00011?0000?????0??00100?0?000
000000000100??000?0000?????000000001110001?110??01?001?????????????000000000?0??
01000000????????1?????????????????1?0?000101?110100100000001??0100001?000000000000?1
0??0?001110?10?11??????????0000100000010100?0???
????????????????110000??0?0??0010000000?000?00?0?0111010100101001000000010010?10100
110000001001100001 0??01100100111000 0?0101000101101000111?11?111?????0??00000000
0011000100????0000?0?0??00????0?0110????1?01?000100?00?0?10?????00??000?100??00??

?000?1?0010?000??1010?001?00??00?0?0000?00?011?000????000?0?1000?0??000?0?0?010?0
0?10??1?00?0?00?0??0????0?00??1010?01??0?00?000?00?1??0?10011?1?00?000?0?0100?000
?10??01??0?1??11??0????0101?1101110?0001?00?100?0???0???00?????000?0?000?0000?00?
001?10??011?11???0????0??0?0??0?00??11?0??0000?010?????00000???0?0010???000?11?0?
?001????????10?00?00?0?000????0???0?000??????????0???000?000?0??0?0???0?00???0000?
?0000???0000100?0??1???11?0100???0???????00??0???00?????10??0????0?0?0??0??0???????
??1??10????????00????????0?01???0?10?????????????????????10?00???000????000?0?????????
?0??0?000??00????10?0??0????010?00???0?????0?10?110?00?1000000??0?010??0??0?00??00
0???10???0000??0?00?????????0???????0?????????1001???0???0???0?????????????????0???
??100??0?00?0?????110?0000???1?0???01100010000?000?????00?0?0?00?????????0?0?????0
???010?????0?????0??000?0000??00????0?????0?10??0??01??0?1??0?0?110??????1??0000??0
110001???0010??0???????????000????0000????????00??0?00?????000????000????????0000?0
????1?????0?????1?1?0????01?0???1???????0??00???????0?10??00?00?????????????10?0???0?
????0??????????0???0?00?10?????????000??000?000?0?????????????????11000000??00????
????0??0??????00?0???000100000?1??0?1???????????0?????0?0?????????????1????????????
000?

Guanlong

1000?0?10001000100??11011100??001001001001101111000000011110??111?101000100000?
?0000110000000010?0?0????0010100000??001??000??10?10??1??1????????10??0??00000?000
0?0?000???00?11101?????00000?0??0?0????????00?10000?0?0?0?0??10??01?0?0?0???0???10?
1?00???0111??10??10??1??1???00001??00?1??0??0?0001?0111?011010??010101010110?1111
001?01?1001????????110?00????010000?010??0???0??0????11101110011101100?110010111
110111100?0?0010000??0100111111011110?00??10????1?110000011??11?1?1?????0110?1?00
?0??11?0110?1??10?00011???00????00??10?00???0?0001000?1??0?10?1?1000??00?00?1?1??
????00??1??00?0?0?011??0?0?????0011?00??00101??0?01??00000?0?01???0101?00??????0??
?11?0???0?00?00?001?????????0??1??1?0?????100?0??10????00????1???????000????0?1?0??
000??1????1??1??00?1?00?00?01?11?????1?1?1??000???00??00?01?000?0?0101?0??1?011?????
??0?1?001??????0?01???????00????????0??0???0??1?????0?????1?010?00??0?011?0??????0?
0??1000??0??000?0???0???10??000?????????????????1??00??0????0?0???0??00????0???0??
?????00?01?????1?????????????????1????0??0???0????1?????????????0??010???0?1????1??
???????1???0????0?0???????0??1?????????????00??????1?00?0???????0???000??0???0???1??0
0??00000????10??010????????00?001??????0?1?????0??????00??00???0??0??000???00?0??1?
0?????0??0?0??000?????????????????????????????000??0??0?????????????0????0?0?0
01?11????????00???0?0?????????0??0???0??0??0??????000?0?0001??????001?????00001??100
0?00010??0??0??????????0100110?????1?10010?1?10?0011??00?????00?01???00?0?????????
??00??0?0??0?0??????0??0?00000000000???100??00?????1?0??100??00?????????1111?10?1
????00???????0???00?0001???1100?0000?010???1????0???0??????0000000100?0????????0?1
?0?????????????0?000?????????????0?????????????????11?0?000????00110000000?00?00?10?
??000?0?????0?1?00?????????????????10??1?????1?0??0????0??1?????11?0??1?????????0?????
?

Haplocheirus

100?1??100?0101000001101101110001101?0?0111000100010000?1???00011110?10101??0??1?
???1?000?000?00??000???001010??????001?10?0???001??0???1????1110?10?00?0?00000000
?00?01?0000?001?100???100000?10?0?????????????1??000???1???0???11?0?0?00????1??0?1
10010?01100010??100?1??110??00?1??0??1??00?0?0001??01???1101???0101010?0110?11??1
01?0??1001????????110?00????000???????00?00?0??01??01??01??1?1?0001?0??10??11010?0
111?0100000010000011110l1?01?011???00??1?????1???000??????11??1?????00?1??0?0???0
??1?0?1??1?????????1???10????01?????01??00?100?101?1??0?1??1?000?1?????00?1???0??10
?0?0??0??0?0?????0?0?0?00?000??0???000010????0?000000?0?11?????0??0???001?????????
??10??1??0?101????0????????1?1?00?0?0?????????0????00????1??0?????00??0?0?1?0???0???
?????????????1???0????1?0??10????????00??0100??00?????0?10??1?000????1100???0??1?1?
?01??????010?00?????1?????????0?????????0???1????????0??01?00?000?000?????1?11???00

0???0?11???01?10????0?00??????????????????01??10?????????1?0?0??0?????????0??????0??
??1?1??1???1?????1???????1??0????00??????????1????????1?0??????1??????????1??????0??
?0???????0?00??????0??1??1?00??????0?????????0??0????0???11??10?????????????0???0???
1???????10????1000?1????????00?0???????1????????110?01??0??????000??????0??1?01?????
??0?0????0?????????????????????????????????0????0??0???????????????0???0????00??10???
?????0??????0??????????1????0?????0???????00?????00??????00?????????????0??????0????
?????????????????????????????0????1??0??01?1100?????????0??0?????????????????????????0
????????0?00???0000?0000???0100?00?1?????0??????0??????0?0???11?1??001???00?0??01??
00??0?????0???10???100??0??????????0???????????0??00?1??0????????????1?1?????00?0????
????????0????????11????????????????11?1?0?0??????110000000?00000?1000?000?1?????0?0
0???????????????0?1?????0??????0?0????????????????0??0????????????????

Magnosaurus
???0??
???000000000?000?010??000
???????11???0?0?0?????0?????????????????
???
??????????????????0????????????0??????????????????1???????????????0????????????????????
?????0?????1100?0?0?0?????01101???1??
???????????0????????????????????????????????0??????????1????????????1????0?0??????????0????
??0???????????????1???????????????????????????1?
00??1????0?????????????0????????????????0??1???????????0??????????????????????0??????0
???????????0????????????????0?????????????????0???????????????????????????????????????
??????????????????????????????????0??11??????????????????????????0???????????????????
??????????????0???0????0?????0???????????0??0???????????????????1?????????????????????
???1???
??????10??0?????0???????????????????????????0???
??????00??00???????????????00????????????????????0?0????????????????????????????????????
???
???1?
??????1?????????????????????????????????0?????????????????????????????????0????????????0?
??0????????????????
???????????????????????????????????????0???
???0
0???????????????????

Marshosaurus
??00?0?10000?000?1001101?00?0?00?00?0?000??000?????????????????????0????????????????
0?0????010???00??????0????????0??01?10?????????????????????????????010000000000?0???
0000???????1?????????????????1???0?00??11?01??1?????????????0???0010??0?????0????????????0
1??
??????1?????????????????????????????????01111100????0101?01?000?10?1100111?010???001
001001110??
???????????????????00??????0??0???0??1??0?1??????000????????????0????0??????0????0???0??
???0?????00???00????0?1??????????????????1????????????????????????00???????0??????????????
?????1??????????00??00??1????????0?1?0??????0????00????????0?????????????????1???????
0???1?0?????????0???0????????0?????0????????????0?0????1??????????1???0????0?????0?1
???????0?????????????????????1???????0????1?0?????????0????????0??????0?0?0??????????
????????????????????00??000?????1????0?????????????0??????????????????????????????????
????????1?????????????????????????????????1???1????
??????????????????????????0???0?????????0????????0??????????????????0????0?0000??0???
????010?000?10???????????????0?????0?0???????????????????0?????00??????????????????????
????1???0????0??0?????????0????????????????????010
0???0???0????0??0????????????????00?????????????10

1?????????01?????????????????????01010????00?????1???0?????????????????00??????????
???0?????????????????????????1??1???0????1?????????????1???????0?11?????????????????
?????01?????????????????????0?0?????????????????????????0?????0??????????0????????????
??0??????????????1?000000?????????????????0?????????????????????????0?1????011?1?????
??????????????????001??0?????????????

Megalosaurus
??????????????????????1?0??????00?001?0?????0?????????????????????011?????????????????
??000000000?000?001??00
0???????0????????00??0??100???????????1??1?0????????0?001010??00?00?00???1???0??111
10010?010??0??00??00001??0001010??0???
???????1?100?010?0???0110??0?0?100??0?0?01?11?1?00100001101001O?10?101001100??011
??11?010?11?0110010??111000?11?????????????????1??1?????????0???0000???0?11?????????
?????????????????????0?0???????0???0??0???????????0??????0101????????0?01????0?????
?1??0???0100???0????????00?0?0?????????????1???????0???0?????0????1?????0??0??0????
???????????1?00?????0?????????0????0???0???0????????1??10???00?00???????????1?000???
??1???01?11???????????0??0?????????0?0???????0?0???0??00????11?1????????1???????????
???0?????????????????????0?????1??101?????????????????0100????1????????1?0?1??0?0?000?
????1??0?0?1??????????0????00??01?0??0????????0?????????1??????????????0????????????
????0?1?????????1???0???????0?00??????0????0???????1??????????????????0??0????????????
???1?0?????????????????????0?????0???000?????????????1??0??0?????????1?????0????0?0
000?0?0?????0011????1??11001?00??0??1???0??0?00????????1???????0??0?00?0???????0???
????0??????????001???0???????0?????????????????????????1????0?????????????????????1???
??????0??000??????????0????????0???0???0???0
0?????0??0?00???1???01????????0???????????0001???????0??01????0?????????????????000
0?????????0??0????0???0??0????????????01?011?????????????????1?0??0??1?0??????000
?000?????0???0?1?0?????????????????????0???????????0??????????0?????????????????1??
???01????????0?????????????11000000????????????0???0??0?????????????????????0?????
????????????????????????????00???00?????????????

Monolophosaurus
1000000100000100?0100?1001011000010010000011011100000101101100110111?100010?0?10
001010000101?000100000?00100001?00??1111?1???010?10???0?????1???????100000000000
00?0000000001???100110?010000100111?0100111110001 1?1?0?01001??0100101000000000 1
010010??0?00???
??????????????????1?0000????????0110?1??0??????0?1?01111111001001011 00?0000100101
0011?0000010010000 0?0?0??
?????????????????????00??????0??0?00??00??0100000???0?1?0??1?00????0?????1?????0000
?1???????0??100??0?00?????0??000?0??0?0?0000??0????????0????11?0?10??????0???1?00???
0?????0?????1??????????1????0?????000?00000?1??0?????1????0??100?????0?????0011?1??
1???????00?1?10?01?0?0?11???00010?0???0??1?0??0?1000??????01??000?0??????100?01001
1??????0????0?????00?0????010?000?????1???0?00????0?0100?1000??0000?1???000????????
?0??????0?100??00?????????????????????0???00?0?1001??1???0101?0?0??00????00????????
00????110?????0??????0?????????????????0??????1???0????0???0????0011??1?????1?????????
???1??0?00000??1?????1????0?????????????????0???????01??00??0????0??????1??0???000?0
??????????0??0?0?0?00??0??????00??0?00?0??0????????0??00??0?0??0???0????010?????00?
?0?0??0???????0???????????0?000?1001??????00000?????????????????????00?00?0??00??
?????110?1?000??1????????000100?0000??????0?0??0?000?????????????????100?0??00000
??00?0???????????0???0?????????0000??0???0011??00??????0??1?????00010?1???00?0???0?
0?????0?0????0?0?????000??00???1????0????????????0???10??????????0?10?10?0??00?0???
??000?0??0??0?0???11000?????????????????000?000?????00?00000000?0?0???????1??????????
??1???100001??????????1?00?????????????????????????0?11000000??00?0?????????0????0
??0?????000100???101???10?01?110?????????????????????????0?1??????010???????

Neovenator
101000?10000010?0100110010110?00?001101011100101?000????????????????????????????
??1???????0000100?00000?011
??00????????0???????????????1?1???111?1??0???11?0?0001??010000110?0??001001??10???
?00??10010??1??????11???
????????????000??00?0000?0?000001????0010?01?1?10??0???001?0??01??1??11??0110?000
0100100000?01001111001110?001?10100110110100???1??1?????????0??00010?0???10100?
0?1?????0?0?10??00????0???10?????00??0???0?????0?1??????00??00???01???0????0?0????0
0?000???00???01?00??00?0???????0????0??????000???111?????01?????0????????00???????0
??1?0?1????????0??101??00???0???0?0?00????0???0?1?0?????00?0??????????001???????1?0
01?0??1?10????0???????0???????0100????0???????????00?0??0?0?0???????10??0????1??1??
?0????0??0????????????10000??111?1?????00???00?00?????????000??0?????00????????0??00
??0?000????????000?0????????????10??10??010?10???1???0??00????????0????0?0??????0??
????1110???????1????????????0?0?1?00???1??????????????????00?????????1????000?0??0????
????????????????1?????????????????????10?0?????1011110?0?1??1??????????00?0?????1??0??
0???0????0110101??1?????0?110???101?0000011?????10??0??0?00????0??010???001?0?0?0?
?????????0???????0???????????001???????0???0????????????????????????1??????00?????0???
0????????1?????????0?111????0???????0??????????????????????????????0????????011?????0
0??0?0??0??????????????01?00??1????1????????0?????????0?00???????10???0??0??0???????
?????00????000?00???????0??0?00?????0????????????????10??1??0??0??????????????????0????
??1?1???1??01??001?0???????00???????00???????????????0???????????0??????????0???1????
1???????????100????11?0??????0?????????????????????????00??????00????0??00????0?0?????
?????????0?1???????????????0??0?0???0???????00?1?01?????????0001

Ornitholestes
000100?000?0?0110?1111011110?0001001001001 0??00?00?001011?0101111100000?0????010
0?010??0000000000100??001?000???0???01??0?0??10???0?1??????????1?1???000000000000
?000000001?101100????11?001?1010????????????1110001000?101??0?011?0?0?000000001??
110???00?1??????????????????0000000001010??????0??????????01?00010???1????????????
??????000????????1?000???0?0100???0010?10??0?001?1011101010010101 1000?11001001110
01??0100000010000010100???????010???0?0??0?????????????????1??????????01?0?0?000000
10101?0?????1?0??1?0??0?????00?010001?10???00?000?1??0?10???1000??1????0?11?????10
00?10?1????0?010?0?0?0????0000000000?011011000??0??00?0?1110?0???000??000?0???1??
0??10?0?0?0?00??0????0??0??1????0?000?00??0??00????0??????1?01?0??00??????0??0??00??
01??1?1?????000??10?01?0001110?00????0?11??101?000?0???0?0????000000100100???00??
0??001????0?0??????????0????????0?00?0???0??0???1?001?0?0?00000000???0000????0100??
??0????00?????011?0?0???0?000???????????????010?0?0?00?????0?0???1??00????0????0???
??????10?10?010?????0??00000?00?00??0??0?0???????110??0????0???0??0?00????1?1??1???
????????0?0??0?0?0?0?????00?00???0?00??000???00001?0??????00????0??0???0????????1??0
00?00000????1?0???0010000???0???????0?0?????????0?????0????????0??000????0???0???????
??????0??0?0?????0?1??0110100?????0?????????1???0???00??0????????????????????0????0?0??
00?0?1???????00???000?1??????????00?00000??00?????00???0?001??0????????0??????0??00110
0?????0?????0???????????0??00????????0??01?????1??0001??00???????????????0?00?10????00??
?00?0??0????0????????0?0???00000000???0????0????????0?0?0??0??????????????010??00????
0?0???0???10?????00?????1???????????10????????00???0??????00011?1?0000?0?????0?1????
?????????????000??1????????????????????00????0?????????????????0?11000000??00?0??????????
0??????0?????00110?001?01???1??????????????000????0??1?0??????0??00?????????0??????

Piatnitzkysaurus
10????????????????????11?01???0?0??0?1?0100??0????????????????????????????010000?0000?
?????????????????????????????00000011?000?0100110000??????????????01000000000000?001
??01??????????????????????????1???1000?1011010011000001??0100101000000000100??10??
0?00111001010100000011?000001?01001010000?001???????????????????????????????????????
???????????????110?0000???????010???01??????0???01?111110?1?0001?00?00001???010011?

1000010010000011100100010011 10?00??10????10110100?1????1?01??????0?0000000000000
100?0????????????0???????0?1?00??????0??0?01??01??0?10?????00??0?00100???0???00???
?0?00?00?????00??0??00???0?0?00?0?0??01???0??????00???0?1111??000?0?????00???0???1?
?0?0??????10?0??0???????1?00???0?00??0???0????0???0???0????0???1????0??00?0???????1
??????100?????1???0??11?????????0?????????0???0?0??????0?0?000000000????11?????????
11???0??????0??0????00??01?00?????0?1?????00??????????0???0??000??1????00000??????0
??01??0?0?0???0???0????001?????????000??00?0?0??????0???0??????????0??00????0?????
0?0??????11?0?0?0001?0????0?0??1?0?01????11????????0???00?0?????0??????10??????????
??1????????0?01?????1?????????????????????1???0?????0???00?1?1??0???????1??0??1???00?
????0???00????0?0001?0?0???????10??001?0?1001000???1?0??????0?0?????????10??0000???
0?0??0???????0?????????????????1001???0???????0?????????????????????????1????0????????
???1?????????1?????????01000???0???????0?????0?????????????????????0??????????0???
0?1??1???0???????0??????0?10?000??1????1????????0?????????0??1??????1000?000????0??
?0???10??0???0???000????????????0?0?????????????????1?????01011?????0?1?????0?????1?1
????0??000??????0?0??00?0????????00??1?????????????????1????????????1??????????0???
0?000????????????0??????100????000?????????????11000000?????????????0??????????
?????????????????????????1??????????0????0?1??????????1???????1?0???

Sinraptor_dongi
1000000100001001010011001000000010000010001000100000101111100010011?0000100000
00001110100?1000000100010000010110001011111?0?0101100000000010110101001000000000
0000?0000100100??011101000100000011111011001111100110110001011100100101000000011
1001001000000110??010001000000?00?????????????????????????1???????10????00??????0
110110????111001100000??110000?0?????????10?1000??????0?0?0111111100100001?010000
010?10110110?000110010001011100110110011111000011011001011010001110110011111000
1100010000001010010010110000001100?00????0?0000?0011000?0100000???0?101?01?000100
0?00111010??0000110000?0000?000?00000000?100000000??01010000?00?00000?10?1?01??1
00??0?100?001101??100001?0????11?0?00000?11?1?001????000000000110?0?100111000???
0001??000?0???001001111110101100?1000101?010?110?000010?000000?0?0??0?101000?0??
01?000010?0011?110?010011?010??0????0?00?000100000010000000000000110000???10?0000
000001000000100010 0?00??00?000101000001 0??10??0?????0????????????00??00?0000000?1
?0?10000000?000????000?0?0??1?10???110?111000?0???00?0??00?0??1?0?0??000?1????0??
00??000??100110010???11?000000010001?00?00000?01??00?00??00000??00????????10000??
?000000000001??00000???1??0?000000000000100???0??100?0000??010????00100100?00?100
10010?0?000??0?00?00??0??0?010???0110?00?00?0???????0???????0???00000?0001?0?010?0
00000?00?00???0??????00???00000?00?00?0?0??0110000000?11000??01?00?101100000????0
0100?0?0001?0???000???????01?100000?00000?00010?000??00??00?00000??0000101000101
?00011?00001?00000?01??00001100?01000?10?10000??0?0?0100?0?0000?0000??000?0000??
0?0?00???00?1000?000???0010011?101?0?10?00000??01101????1??0?1???11001???0000??0?
??0000001000000?000000100001 0?0???0?0?0?0?????00???10?00000011????????0?000???11?
000????0?????????000001100000??000000???????00??00000?0000000100000101?0?1000?00
?001?0000?00?0??0?0??????00?1000???01??1?0???

Torvosaurus_gurneyi
??????????????????????01?0????0?00101100?0???0??
??1???00000?0?1????
??
??
??????????????????0?0???
??
????????0?????????0???0????????????????????????????0????0????????????????????????
0?????????????1????????????????????????????????????0????????????????????????????
??????????????0????????0????????????1?0????????00??????????????????0??1?????????????

?????0??0?????????0????????????????????????1???????????0???0???????????0????????????
?????0?????00?0??0?1??????????0????????????????????????????0?????????????0?????????
?0??????0???11??????????0??0???
??00??????????????0????????????????
???????????????????????????00???????????????1?????????????????????????????00????1
??????????????????0????0???
?????????????????????????????1?????????????????????????????0?????????????????????????
??????????????????????0???????????????0??????????????10?????????0???01??????????1???
???????0??????????0?????????????????????????????????????000?????????????0????????????
???????????????0???
????????????????????????????????????0?000????????????11??????????????1??????????????
??????????????????????00??000???
?????1?????????0???

Torvosaurus_tanneri
10100001000000000010001?0??110?0??01100101??0?????????1?011?0001?0110?00??????????
??????0?1010?0?0?0?1?00???00??????????????????????????????????????0000100000000?00
1?????????????0???????????????1?000?110100111001100000001??0100101000000000001??10?
?0?001110010101000000000000001?0000?010000?001????00??11011000??00??????0??01?0?
??????0???????????1?1010010?00000110010000000??011000111011000100000110?00100100101
0011010?01000?10000101001100100111010?1100000101101000111011001??1?00????0000
000?01100?????????????????00????0???00100?1?010?1???0?0?00?10???1?00??00001011??0?
?0??0?1?0010?000001000??00?000000?0?0000?0??01??0???????00?0?1?????0?0?010????100
0??00??100?10?00?1?10?0??0?0???101??01??0000?000?00????001?0?1?1??0??0??1??100?00
0?00?001??1110001000?011?1?0?0101100000?1??00?10?00??0??0????????00?0100?000?00?1
?111?10??0?1??00??0?0?00?00?0?01?????01000000?0?010??0010???10????0??10???000?0???
??00100??00??1??00?00?0?000???001?00?000???????1??0001100??11?0??0?0?????00???0?0?
???00??0?0??000010??1???11??100000001?00??10?0?00?0000?011?0?00???0?????00??0?????
0???10?00??????0001?0??0?0?0??1?0?00100?0?00?????0???????10??1??0000??1000001??00?
?????1??0??00????0???10??000????00000??00??????0?01?1??101?1000000??0?000??00?0?00
?????0?01010?00001?0?0???????????0???????0???0?????0001???0?010???00?00?00???0??????
?0????0100??0?00?0??????10?????????1?0??????00?11?????0?????000?0????0????????????0??
???????0???????????1?????00?0?000?????0?000????0??00001?01?0?01???0??1?01??0?????000
0?10??0?010?001?00?0?0?0????????000??0000000?0?????0??0?0??????0000??00???????????
0???0?????????????????00100??0??100?0?1?0000??0?000?0???0?01100?00000?0???0???????0
?0???0?????0???????????0??????0?1????????????01?0?01100???0??1?????????????0?11000000?
?00????1?000??00?????????0???000100010?1????00????100??????0????0???????????????1??1?
????????????

Baryonyx
?00?00??00101100?00???0???111??????????????0010?0???01?011?0101???????????1???0?????
1??????????????0?00010??????10?001001100??0011?10??00?1?????????????00?000000?000?0?
1??000???????1000??1????????1?110?1011?1001011000000000010???101101?1?0000?0000??10?
?000?111?0?0??10??00?1?0?00001??00010100?00001??????????????????????????????????????
???0011??????????????????????110???00??????0??????1?????????10?1??1?0???????1?1?0?0?0?
??????1000?0?1???1??0100?111000??1?0?0????????00????0???????11???????????????????????
??????????????1011?????0?0?0???????????1010?00????1?1????00??10001??01??0??0?001?????
???1?1?0010??1?00??010????0??0010???0????????????1?10?0??0?0100??00?0???1?????????10
110??11?10????????1??000???0???010??0??1??0?????01???0?000??000????00?110?0?111???0
?11101?0????0?1101??00000??0?????0????00?10?0???0000?0?0????0000????01??0?00?1????
?0?????000??0?1??01??000?0100?0??1?00?????0?????10??10?0??0?001???1100??0??????????
???00?00???00??00??1??0???????????010?110??00?0????0??0?100??0??01000100?0?0??0???0
???1??????100?0?01?1?0010?0????????0????11????11??0?0??0?0??0110???????100?????????11
1?????????00110?0???????0??0???0?000?100?????0?????0?0100?1?1???0???0?????1????1??000

001??1??0??1?0?0?0??1?0????????0?111011?11???1?00?1??0??0??0?000???????10???000?0?
???0????1????0???????0???0?0???1000???????0?000??0?0???????0???????????00??????????0
?????00??0????10???????0?0101???00??0??0??0????0????????00?1???????01?0???0???0?01?
????0??0?00?00???????????????????0??01?0?0?1??0???0???0???????11????0?0100????111??0
???00?0??10??0????0?0?????????01??0000?1?00?????0????00?0????1??01??????0????0???0?
101?1????????????1???0000?1??0??0???00?10?10???????????0?0???0????0?0????0??????????
0???????????0????????0?0??0111??????????????????0000????????????11?????????????0??0?1??
?1???10000001011??0?100?0?????????????????????0??0????0?1?10??????0??????

Ichthyovenator
??
???1????1?0???1??????
??????????????????????1?1???11?1011011011????000??1101101?1?0000100??0?10??0?01???
??
???1?0?0??0???????100?0?00?01???0?1?01?11001001?100110100000100111101100011?1001
000000010???
?????????????0???0?????????????????????0?1???????0??1??????????????????????0???????1????
??0??????0???000?????0?1?????????????101?1?????????????????????????????1??1????1?????
??????????0??????0??0????????????????????????????1??????????????????0????0???????????
10?111??????????0??0???????????????????0?????0????0???01?1??????????????????0????0????
????0???0?????????1?????00??????????????????????????0??????????0?????0?????????????0?0
?10?????????????1??????0??????0?????????????????????0??????????????????????????????0????
???1???????0??????1???0?????????????????????10????????????????110?????????????00?????0???
?????????????????????0????????10001????0??????01????????????????1??0?????0?1?0?0???????
???00??????1?1?0????????00?1????0????????0???01????00??????????????????0??????????????
????10??????????????0???1?????????1??0
?0???????????????????1??????????????0?????????01???????????????????0??0????????????????????
??0???10???????????????????????00??????????????????
????01?????????????????????0????1???1??????????????????101?1????00?0????????????????????
1??0????1????????????????????0?0????0???
???????????????????11000000??0??????????????0?
?????????????????????????????0????001

Irritator
?00?00?10010?1?0?00?10001011100110110010?00010?00000100101100 10?11???000100?00??
0?11?000000??0?????1?????????????0010011?00??011010??00?1??????????????????11????100??
?1?????????????????00??0001?1??
??
??
??
??0011??????0??0?00??0????1010??????????1??0??????????????1??0??000???????????1???0???0
??0?????1??????????????????1??0???????????????0????????????0???1??0??????????1?????????????
???????0?????????????????1???????1???1????0?0??0???????????10??1???????????????????00????
??????0??1??0???0??0???????00?????????1??1???0??????0?0?0100?1?1????0???????????01?10
1????0??????????1????100????0?01000???0?????0????????????????????????????????0???000??????
???????????????????0??0?????????????00?1?0?10??011?????????????00??????0?????1??????????
???0?????????????????????????????0?0????1???????0????????????????????0?????????????1????
1???????????????????????????????????????1?0???????????00??0?00??????????????????1??????
?????????111???????????????????0?0??0???0?????????????????0?????????????????????????0??
??????????????0??????????????????????????0?0??01?????????0?0????00?????????00?0?????
?0?????????0?00??1?000??????????1???????01????0????00????????????????????????????????10
0?????????011??0???????0??0????11?0100?11???????11?????????0????1??????100???01????
????0????1?0?????0?????????????????????10?0???0?1???0??????????????????1????????????????
?????0????1??????0??0??????????????????1???????????????????00?0?????????0?????????????

???0????????????0???????????11?0??????????0??????????????????????100???1?????000?????
???????????0?????????????????????0????

MSNM_V4047
??00001?001?1110?00?1?00101110?1??10??10010010???000?????????????????????????????
??11????100??????
??
??
??
??1
1?????????0????????????????0?????????????????????????????0???????????????1???0??0???????
??1?????????0????0?????????????????????????????????????0????????????????????????????
???????????????????0??????????0?1?????00??00????????110???????????????????0?????????????
??????????0???????0???????0????????????????????????01???1??????0???????????1????????1??
???????1????101????1?01??
?????????1????0????????1?????????????????????????????????1?????????????????????????
????????????????????????????1???1?????????????????
????????????????????????????1?0???????0?????????????????????????????1?????????????????
1?????????????????0??
??0??0????????????????????????????????
??????????????????????????0?????????????????0?????????????0???????????001?????????1??
????????????????????0?????????????????1?????????????????????????00????????1????0???????????
??????????????????????????0?????????????????????????????1?????????????????????1?????
??0??000???????????0?????????????????????????0
???????????????10???????????0?????1?????????????????????????1????????????????????????????
??????1?????????????????

Spinosaurus_type
??
??01?011001?100???0?1000
???????000???1?????????1?0??????????01001?0?1?01?????1???1????0001100???10??1001???
??
??????????????????1?0???0??0????0?0??
??
??0?????????????????0?????????????????????????
??10????????0?0?????????????????1???????????0????????0???1????????0?????????????????1??
??0????????0??????????0?????????????????00?????????????????1???????1???????????11???????
??????????0????0?????????????????0?????????????????0?????????????????0???01??????0???1
?????????10?????????????????????????001???10?0?????????????????????0??????????0?1???????
?????0???????????0?????????????????????0?1?????????????????????????????0????????????
?????????????0????0?????????????????????????????111????????1???0?????????????????????
???????????????????0??110??
?1????????????01?????0????0?????????1????000???0??0?????????1???????0??????0????0???
?????????0??0?????????????????1??0?????0????
????????????????????????????????0?????????0??
0????????????????????????????????0?????????????????????????????100???????????1????00?1??
????????????????????????????????????0????1?1?1?????????????????????????????1??1?????1?
????????????????????????????????????00??????????0??????????0?????????????????????????
????????????????????????????????0????????????????????????????0????????????????????????????
????00?1?????????????0?1

Suchomimus
?00000??00101100?00?1000??101001?11100101??010??00001?????????????????110??01110
?1?????????????????0?????????1??0?10011???0?011?10??00?1????????????00?000000?000?0?

1??00?????????????????????????1?0?1??1?10???1??10000?0?10??10110101??000??00????00?0
00111??0101110?00001???00001??0001010??00001?????????????????????????????0???????????
??001?????01110000???????????0????0??0???????01????1?0????0??????0?????????10?0?00
?????0100000011001?00100111?000??11100010?101?0?1????00?????????????????????????????
????????????????1111????00?0?0???????????010?000?0?1?????000??10001?1?1?00???0?01???0
0???1?1?0010?01?000?01????0???0010??0?????????????????00??000?0?????0?0???00???0??1
?1?01?10?10???????1?1?000??0??????0?10?1??0??01?1?1??0?0?0??00????000?11??0?1?1110
0???001?00??0??1?????000?0??????1?0????00?10?0???0000?0?0?0??00000????1??0100?1??0
??00????00?????1??01???00??1?0000?1??????00??00?0?0?0???0??0?0????01?0???0?????????
00??????0???00??00?????0??????????0?0?110??00??????0?????0???0???11??1?000?0?????0?
???1???01?1?0???0??1?10?0???????0?0?00?11???01?????00?000??0111?????????1?????????1
???0?????0??10????10??0??0???00000?1?0?10??0??0??0?01?0?????110?0?0?????1????1??000
00?????00????010001?1?0?????????0??110????10000??0?1??0???000?00?0?0????10??000????
????????0????0???????0?????0??01000???0???0??????0?0???00??0???????????0????1?0????0
????1?0??00?0?100???00??0010?????????????0?????0????0???00?1?010??00??0????0????01?
????0???000??0?0??0?????????100?????1?0?01???0????0?0??????0?11????0??1000????11?00
????0?01?10???0????00?????????????000????000????0????0??0?????10010????10????1?????
101????0??????0?1????000?0??0??????0??10?10???????0????????1?0???000????00????0????
??????000?0??????????0??0?01010????000?????????000????????????11?????????????????1??
?10?00000000??11????10??0???????????0?00?????00??0???00?1?10??????0??????

FSAC_KK11888

??
????????????????1??
??????????????????????1??????????????????????0???????????100????0???????0???1????1???????
??1
???????0000100100000?0000?000000111000?0010000?000??00?10??10?001?0?????0?10000
???101100010?1110010?111????10???100??0???1010???1??00?????????????????????0?0?0?0
1?0????????0?????1?????????????????????0??1???0?????????????0??????????1???????????1?????
???00?????????????????0????????0??01?10??????0??0??0?????????????????1??????1?1????000
?????0????????????1?????????????????????????????????1????????0?????1?0????0???????????
??1?????????????????????0????????0??00???????00?????????????????????????0???????????
??0??????1???0?0??????000?????????????????????????????????????1??0????00????1?010?
10?????????????????????????0?0?????0?????????????0??????????0????????0????????0?????
??1??????0????0??1011?????????????????????10???1??10101?1????1????????????00???00???
????0??????????1??0???1???????????0??0???????1???0???????????1?????0????0????????1???
??00???????????1???1???0??1????0????0????0??010???????0?????????????1??????????????
?????????????????0???????0???1?0??????????00?
?????0?????????????????????????????????????0????????????01??0?0?????????????1???
?????1???????1?????01???????0?????????0?????????????????????????00??0????000????0???
????????????0??0??????????0?????1?????????????????????1?????0????????????0?0???????1
?0???0?????????????????????????????00
??????????????????11000000??????????00?????????????????0100000?1011????????0??????????0
??0?0???0??????????1?????????????001

Sigilmassasaurus

??
??
????????????????????????1?????????????110??00????0????0110101???00??00????0????????????
??
??
??
?????0?????????????????????????????????????1?0?????????????????????????????????????
???????????0?????????????????????????0?????????????????????0???????0?0?????????????0

????????????????????????????0????????????????????????????????00??????????01?????????
??0??0????????????????????
??0??
????????????????????????????????????0????????????????????????????0????????0?????????
?????????????0?????????????????????0??????????1??????????0???0????????????????????????
??????????????1?0?1?????????????????????????????0??0????????????????????????????1??
????????????1????0??????????????????10?????0????????????????????????????????????010????????
??1???????????0????????????????????
????????????????????????0??0?????????
????????????????????????00??1???????????????
????01?????1?????????????????????????00????????????????????????????????1?????????????????
??
????????????????????????????????1????????????????????????????0??????????????????????????1
??????????????????

Spinosaurus_B
??
??
????????????????????????1?0????????????????????????0???????0?????0???100?????1????????????????
??
???????0?0???0????????0?00??
?????????1100?0?1???0?010?101??01????1???0????
??0?0???1???????????1????1?????????????????????
??0????????????????????????0?????????????????????01?
?00??0????1?????????????????1????????
????????????????????????????0??
?0???????????00?????????????????????????0?????????????0????????0????????0?0?????????
????????????????????0?????0?????????????0?????????????????????1????????0????????????0?0
????????001???????????0?????????????????1??0??1??1?????????????????0?????1?????????????????
????10?0?????????1???1?????????????????0?1???
????0???0????????????????????????????1????????????????????????0????????????????????????
??????0??1???????????0?????????????
??00?????????????????????1??????????????????
??0???0????????????????????????????
??0????????0????????0???1???????1???
??
??
??1???????????????????

Wight_A
??0?0?1?0010?1?0??????????1?????????????????0????????1?????????????????????110010111001
????00111?????????????????????10?00100110000001 1?100?00?1????????????????????????????????
??
??
??
??1 1
10?????????0??0????????01??0?????????????????????????1??0??0????????????1???0??0?????
???0?0????????0??????1?????????????????0?0???0?????????????????????1?????????????????
???0???????????0?0???????????1??????0?0?????????????????????1?????????????1??0?????????
???01?????????????????????????0???????0???0????????????00?1?????????????????????01????0
??1??????????1???????????0?0???0?????????????????????????????0?????10?????????????????
???????????1??0?????????????????0?100??11????????????1??????1??????1?????????????0????
?????????1?????????????010???????1?????????????????????????????11?????????????????????
????????????????????????????1????????0???????????1??0?00????????????????????????????????

?01??????????????????????0??0?00???0????????
??????0??????????????????????????????0????0??1?00??11?00?00?????????00??????????????
?????????1?0????????????1???????01?????????????1??1?????????????????????????????????????
???????00???????0??????1????00??1???????11???????0?0111?1??????????????????????????0
??0?????????000?????????????0????10?0??1??????????????????????1?0??????????????????????
?0????????????0?????????????0???????????????????????????????????????0??????????????????
????????0???????????11??1?10?????????0??????????
?0????????????1????0?????????

Wight_B
??0???1?00???100???????????????????????????010?0???01???????0??????????1100101110?1
???????????????????????????0?00?001100?00011?100?00?1??????????????????????????0????
??1???
???
???????????0?00000000??0000001??000???
???1
110??????0??0????????????01?????0????1????????????????01??0??0??????????????1???0??0????
??????0????????0??????1?????????0??0?000???0?1????????????????????????1??1?????????????
?0??0?????????????????????????????????0?????????????????0???1??????????????????0????????
????0?????????????????????0????0???????0???0?????????????0??1??????????????????????01????
?????????????????000????10?0???0???????????????????????????????0?0?00?00???000100??
?????????????1?????????????????0?1???10???11????????????????0????????????1?????????????001?
??????????????0000????????10???????1????????????????????????????????????0??0??0????????
?????????????????????????????????????0??????0???1??0?00???????????????????????????????0??
???11?????????????????????00??0??0??0??0?????????0??????????????????????????????0??????
????????0??????????????????????????????????????0???11?0??00?????????0???????????????
????????????0????????????1???????01???????????0?1???0???00?0????????????????????????0????
????????0????????????????1?????01?????????11???????0?0110?100????????00??????????????
???0???0?????000???????????????????10????1??????????????????????1?????????????????0??????
??0?????????????????????????0???0???????
?????????0???????????11???????0???????????????????????????????????1?1???????????0?????????
??0?????????????1????????????00?

ML_1190_cf_Baryonyx
???0???
???0??000?0?000?0?1??00??
??0?0
???
???????0?0??????0?1000??????0???????????????????????????????????0??????????????????????
?????????????????????????????????????0??????11??
????????0??1
?????????0????????????????????0??????????????????????????????1??????????????????1?????
????????????????????0??0???????????????0?????????????????????????????????????1??????????
???0??
????????????00??????????????????0????????????????????????????000??????0001?????????????
??????????????????????????????????????0??
???????????????????????????????????????0???0??????????????????????????????0?????????????
????0??????0??
?????????????????00?0?0?????????????????????????0???????????????????0????????????????????????
?????0??0????????????????????????????000??????????
??0??????????0?0???????????????0??0????????????????????
??0??????????????1?????????????????????????????????????0????0???????????????????????1?????????
??0????????????????????????????????????
??????????????0?????????????????????0????????????0??

??????????0?????????????????????????????????????0?????????????????????????????????????
???????????????

Vallibonavenatrix
??
??
?????????????????????1?????????????????0?????????????0?10101?000??000????1??0??1??????
??
111010??0?????0000?1?00??????0?0?01?11111??1?0101000?0????001?1?????????????0?00?
?0??
??????0????????????????????????0?1???????0????0????0?????????????????????????????1???
?????????0?????????????????????0?1?????????????????????????????1?????????????????????
???0?????????0?????????????????????????????0?????????????????????10??????????10?1?0?
??????????????????????????????0??????????0????1?0?????????????????????????????????
???????????0????00?????????????????????1??0??????????????????0?????0??????0?0??0?????
??????????????0??0????????0???
???1??????????0?????????????????????0?????????????????1?????????????0??????0??????????
???????????0????????10??1???????????????0?????????????????1????????101?0?1??????????0?????
??????1????????0?????????????????????01????00??
?????????0??1???????????1000????????
??0?????????????????????0????????
??????0?????????????????????????1?????????0?????????????00??????0?????????????0??????
?????????????0????????1?????????????????????0??0??1?????????????????????0??0????????
???????????????0?0?0?????????????001????0??
?????11000000????0??????0?????????????????????????????????????0?????????????????????
???????1?????????????00?

Camarillasaurus
??
??
??1?????0?????1?????????????????????1????
??10??1??1?0??
1?0?0???0?0??????0?1??0?000??0???
??????????????????????0?0?010??0?????????0???
??0?????????????????????????0???????
??1?????????????????????1??0???????????0??
?0??1???????????1?????????
??
0????????????00?????????????????????0?????????????????1???????0???????0?????????????????
??0????????0????????????????????????????????????
????????1???????0??0??????
??10?????1??
??????????????????0?????????0??
??
??0??0????????????????????????????
??0??0????????????????????????????????
??0??
???????????00??1???0??????????????????11??
??
???????????????

;

A.1.6 Bayesian analysis

Scripts for the Bayesian analysis can be found online.

A.2 Synapomorphies of Spinosauridae

Common synapomorphies of the spinosaurid nodes reconstructed in all shortest trees are detailed below.

A.2.1 Spinosauridae

Char. 11.1: premaxillae fused.

Char. 1796.1: external surface of premaxilla extensively pitted.

Char. 1485.1: ventral margin of premaxilla concave in lateral view.

Char. 14.1: fifth premaxillary alveolus present.

Char. 1717.1: sixth premaxillary alveolus present.

Char. 511.1: external naris retracted, does not overlap oral border of premaxilla.

Char. 582.1: mediolateral constriction of rostrum at premaxilla-maxilla transition.

Char. 1468.1: subnarial foramen replaced by a dorsoventrally oriented channel.

Char. 731.1: anteroventral border of dentigerous margin of maxilla curved dorsally.

Char. 18.0: medial palatal alae of maxilla expanded as large shelves.

Char. 1736.1: thick torus maxillaris confluent with anteromedial process.

Char. 707.1: anteromedial process of maxilla long, low and anteriorly projected beyond lateral surface of maxilla.

Char. 1175.1: promaxillary recess not exposed in lateral view.

Char. 1315.1: promaxillary recess penetrates anteroventral corner of antorbital fossa.

Char. 22.0: maxillary recess absent.

Char. 732.1: first maxillary alveolus oriented anteroventrally.

Char. 1500.1: nasal extensively overlaps nasal process of frontal.

Char. 662.1: angle between anterodorsal and ventral rami of lacrimal <60°.

Char. 756.0: straight anterior margin of lateral lamina of lacrimal.

Char. 1001.1: dorsoventrally vaulted frontals.

Char. 844.1: dorsoventrally elongate facial nerve foramen.

Char. 1751.1: medial condyle of quadrate with anterior concavity.

Char. 1747.0: quadrate ridge does not contact lateral condyle.

Char. 115.1: occipital condyle forms acute angle with basituberal processes in lateral view.

Char. 1192.1: basipterygoid processes placed ventral to basituberal region.

Char. 1566.1: deep ventral recess of basisphenoid.

Char. 758.1: anterodorsal margin of dentary raised relative to rest of dentigerous margin.

Char. 892.1: enlarged splenial foramen.

Char. 180.0: posterior margin of splenial straight (not concave).

Char. 1467.1: premaxillary and symphiseal dentary tooth crowns with apicobasal striations.

Char. 599.1: maxilla/dentary tooth crowns labiolingual diameter > 60% of mesiodistal diameter.

Char. 840.1: labial flutes on maxillary and post-symphiseal dentary tooth crowns.

Char. 1528.1: tooth roots narrowing basally.

Char. 200.1: distinct axial diapophyses.

Char. 1195.1: prominent axial parapophyses.

Char. 1550.1: large foramina on ventral surface of diapophyses in posterior cervical and cervicodorsal vertebrae.

Char. 943.1: pre- and postspinal laminae in dorsal vertebrae do not reach apex of neural spine.

Char. 555.1: anterior surface of cervical centra reniform, dorsally concave.

Char. 1194.1: pleurocoels penetrate parapophyses in middle cervical vertebrae.

Char. 1273.0: middle cervical neural spines subvertically oriented.

Char. 225.1: prominent ventral keel in anterior dorsal vertebrae.

Char. 230.1: anterior dorsal centra wider than tall in anterior view.

Char. 1740.1: dorsoventrally expanded anterior dorsal parapophyses.

Char. 1073.1: dorsal neural arches with spinodiapophyseal basal webbing.

Char. 250.1: neural spines in posterior dorsal, sacral and anterior caudal vertebrae at least 250% taller than long.

Char. 359.0: hyposphene absent in anterior caudal vertebrae.

Char. 562.0: anterior chevron lacking anteroproximal process.

Char. 406.1: distinct anterior convexity in the ambiens region of proximal pubis.

Char. 425.0: distal ischial shaft mediolaterally compressed.

Char. 693.1: distinct posterolateral projection on distal femur.

A.2.2 Baryonychinae

Char. 1146.1: interdigitate premaxilla-maxilla suture in lateral view.

Char. 785.1: posterior end of nasal processes of premaxillae appressed.

Char. 72.1: dorsal surface of frontal with abrupt transition between anterior half and postorbital process.

Char. 78.1: parietal longer than ¾ of frontal.

Char. 509.1: basioccipital apron with extensive overlap over basisphenoid.

Char. 1151.1: marked muscle scars on basisphenoid.

Char. 1193.0: tooth serration in basal half of mesial carina.

Char. 212.0: anterior postaxial cervical neural spines not taller than long.

Char. 670.1: dorsal fossae in presacral neural arches.

Char. 660.1: accessory centrodiapophyseal lamina in dorsal vertebrae.

Char. 592.1: lateral margin of brevis fossa posterolaterally diverging in ventral view.

Char. 409.0: pubis lacking posterior extension of distal foot.

A.2.3 Spinosaurinae

Char. 1136.1: maxilla included in narial fossa.

Char. 1050.1: dentigerous margin interrupted at the premaxilla-maxilla transition.

Char. 100.1: paraquadrate foramen reaches level of mandibular condyles.

Char. 1614.1: paired alveoli in premaxilla and anterior dentary.

Char. 153.1: maxilla/dentary paradental laminae indistinct.

Char. 154.1: maxillary/post-symphyseal tooth crowns unrecurved.

Char. 159.1: maxillary/post-symphyseal tooth crowns unserrated.

Char. 1507.1: maxillary/dentary tooth crowns with fluted labial surfaces.

Char. 1347.1: posterior dorsal neural spines taller than 12 times their width.

Char. 1349.0: absence of pneumatic foramina in anterior dorsal neural arches.

Char. 1608.1: reduced middle and posterior dorsal parapophyses.

Char. 1605.1: deep prezygocostal fossae in anterior caudal vertebrae.

Char. 358.1: centrocostal laminae in anterior caudal vertebrae.

Char. 626.1: prezygocostal laminae in anterior end middle caudal vertebrae.

Char. 929.1: elongate anterior and middle caudal ribs.

Char. 1034.1: mediolaterally thick middle caudal neural spines.

Char. 381.0: iliac supracetabular shelf reduced.

Char. 382.0: vertical crest dorsal to acetabulum absent.

Char. 245.1: tibia and femur relatively short compared to dorsal centra.

Char. 1120.1: reduced internal cavitation in long bones.

Char. 1069.1: collateral sulci in pedal unguals confluent with ventral surface of bone.

Char. 1433.1: pedal unguals with lateral ridges.

A.3 Templeton test results

Topology (T) 1: unconstrained MPT; T2: Wessex Fm. OTUs not included in the node (*Baryonyx*, *Suchomimus*); T3: Ceratosuchopsini not included in the node (*Baryonyx*, Spinosaurinae); T4: *Baryonyx* not included in the node (Ceratosuchopsini, Spinosaurinae); T5: *Spinosaurus sensu lato* (all North African Cenomanian OTUs forced as a monophyletic unit).

Topology	Floater OTUs not constrained by enforced topology	Steps	Negative Ranks	Non-zero scores	Significance	Comment
T1	None	2448	n/a	n/a	n/a	n/a
T2	ML 1190, *Vallibonavenatrix*	2450	370	38	p>0.05	Non-significant
T3	ML 1190, *Vallibonavenatrix*	2452	430	42	p>0.05	Non-significant
T4	ML 1190, *Vallibonavenatrix*	2454	561	50	p>0.05	Non-significant
T5	None	2449	2	3	p>0.05	Non-significant

A.4 Preliminary specimen descriptions

Below are brief preliminary descriptions focusing on the major osteological features pending a more complete assessment (in prep.). Comparisons have been explored further in Table A 2.

A.4.1 Select cranial measurements.

Table A 1 Measurements (in millimetres) were taken using digital callipers and rounded to the nearest decimal point. Asterisk denotes measurements influenced by taphonomic damage. AP= anteroposterior, DV=dorsoventral, ML=mediolateral). Values in square brackets indicate normalised ratio to occipital condyle width

Measurement	*Ceratosuchops*	*Riparovenator*	*Baryonyx*
Premaxilla, maximum interpremaxillary (ML) width	86.3 [1.88]	100.6* [2.17]	83.3 [1.86]
Frontal, maximum interfrontal (ML) width	136.2 [2.97]	164 [3.53]	–
Frontal body (exc. nasal process), sagittal AP length	75.9 [1.66]	81.7 [1.76]	–
Parietal, sagittal AP length	81.6 [1.78]	93 [2.00]	–

Basioccipital, occipital condyle ML width	45.8	46.4	44.8
Basisphenoid, maximum ML width across oval scars	67.2 [1.47]	84.3 [1.82]	65.6 [1.46]
Supraoccipital, ML width across main body	111.6 [2.44]	112.6 [2.42]	104 [2.32]
Postorbital, maximum DV height	167.9	–	–
Postorbital maximum AP length	140.7	–	–
Postorbital, orbital boss DV height	48.7	–	–

A.4.2 *Ceratosuchops inferodios*

A.4.2.1 General notes

Taxon represented by a partial cranium (see above, main text). Elements generally well preserved. Cracking present across most surfaces but original bone texture remains largely visible. Premaxillary dentition poorly preserved with few teeth remaining in situ. Conjoined premaxillary nasal processes missing the posterior tip. Postorbital well preserved bar some damage to the ventral surface of the orbital brow and extremity of the ventral process. Braincase disarticulated into three closely associated parts. Abrasion to some articular surfaces and minor plastic deformation amongst certain braincase elements impairs clean manual rearticulation. Minor damage to the extremities of various braincase elements (e.g. left capitate process of laterosphenoid, ventral cristae tuberalis etc.) can also be observed. Comparative osteology is available in Table A 2.

A.4.2.2 Osteology

Premaxillae

Premaxillae dorsally conjoined, interpremaxillary suture remains open anteriorly and ventrally. Body expanded to form a terminal rosette. Nasal and subnarial process project posteriorly and enclose an acute external naris. External surfaces peppered with many prominent neurovascular foramina. Dentigerous margin “hooked” anteriorly. Seven dental alveoli present per element; all located anterior to the external nares. No paradental laminae observed. Posteriorly keeled median ridges situated lingually to the alveoli and visible in lateral view. Two large vacuities extend anteriorly into the premaxillary body (made visible by transverse break), interpreted here as extensions of the nasal sinuses (Dal Sasso et al., 2014; Ibrahim et al., 2014).

Dentition

Premaxillary dentition poorly preserved. Available teeth largely conidont with minor labiolingual compression. Size heterodonty noted along the tooth row, with largest crowns in the mesial three tooth positions. Fluted/facetted enamel observed on both the labial and lingual surfaces. Enamel texture appears veined (*sensu* Hendrickx et al. 2019) where preserved intact.

Prefrontal

Prefrontal possessing a conspicuous, boss-like cornual process anteriorly. Anterior and ventral rami project from main body at an acute angle; lateral surface of latter possessing narrow facet for the lacrimal. Lateral surface posterior to rami excavated by a prominent notch.

Orbitosphenoids

Orbitosphenoids preserved as extremely thin elements whose sutural contacts with the adjacent laterosphenoids are not obviously discernible due to taphonomic cracking. Elements seemingly partaking in the olfactory (CN I), oculomotor (CN III) and the abducens (CN VI) nerve borders, while also enclosing the optic (CN II) nerve in its entirety.

Frontals

Frontal bodies coossified dorsally; however, interfrontal suture remains open ventrally. Nasal processes elongate and anteroventrally projecting; nasal facet does not overlap frontal body. Anterior frontal body concave in transverse section and bisected by a low, incomplete sagittal ridge. Anterior margins of the supratemporal fossae sharply defined and laterally curving. Prefrontal facet deepest anteriorly. Postorbital processes well developed and laterally projecting, forming posterior wall of a dorsally right-angled articular space for the prefrontal; anterior surface of process possesses articular facet to contact prefrontal. Frontals excluded from the orbital margin. Frontals convex in lateral view, exposing the orbital fossae. Frontoparietal suture V-shaped; suture marked medially by small bilaterally projecting frontoparietal processes.

Parietals

Parietals hourglass in shape in dorsal view. Sagittal crest thin and undivided; supratemporal fenestrae narrowly separated on skull roof. Posterior nuchal crest thin and projects laterally and somewhat dorsally; mid-dorsal margin flattened. Posterolateral ala of the parietal present as a narrow, spike-like process.

Laterosphenoids

Antotic crests bilaterally asymmetrical (right crest forms a sharp ridge terminating ventrally in a small protrusion; left poorly developed). Capitate process ovate and generally mediolaterally directed. Laterosphenoids form anterior margins of the trigeminal nerve (CN V) foramina; ophthalmic ramus (CN V_1) excavates ventral element via sulcus. Likely forming posterior borders to the oculomotor (CN III) and the abducens (CN VI) nerve foramina (but see orbitosphenoids above).

Prootics

Trigeminal nerve (CN V) foramen margin largely formed by prootic. Element also delineates anterior border of the fenestra ovalis and entirely encapsulates the facial (CN VII) nerve. Prootic overhangs a shallow columellar recess. Internal facial (CN VII) and vestibulocochlear (CN VIII) nerve foramina visible endocranially due to disarticulation of the braincase, as are the ventral portions of the floccular recesses. Prootics seemingly contribute to dorsal pituitary fossa; if correct, the abducens nerve (CN VI) foramina exit through prootics and open into fossa.

Otoccipital

Otoccipitals formed via the extensive fusion of the opisthotics and the exoccipitals. Both otoccipitals contribute extensively to the lateral margins of the foramen magnum, bar for minor median input by the supraoccipital dorsally and basioccipital ventrally. Paroccipital processes well developed and posterolaterally projecting, with concave anterolateral surfaces. Crista tuberalis forming the posterior borders of the fenestra ovalis, and encapsulating the adjacent fenestra pseudorotunda (glossopharyngeal nerve (CN IX) foramen). Posterior otoccipital pierced by three neurovascular foramina (for CN X–XII), lateral to the occipital condyle.

Supraoccipital

Supraoccipital producing a conspicuous dorsal process projecting from the platform-like main body. Posterior surface of the dorsal process excavated along its dorsal midline by a shallow sulcus; median crest or keel lacking. Posterior middle cerebral vein foramina penetrate the supraoccipital bilaterally at the base of the dorsal process, internal foramina also visible endocranially, as are the dorsal portions of the floccular recesses. Main body of the supraoccipital indented by bilateral crescentic depressions; depressions contour tab-like processes.

Basioccipital

Occipital condyle largely hemispherical and mainly formed by basioccipital. Condylar neck short and subtly inset from condyle margins. Basioccipital apron convex dorsally and indented ventrally by a subtle subcondylar recess; the recess excavates well below the occipital condyle. Basitubera unclear but presumably represented by the pair of flat ventral extensions of the apron that overlap the basisphenoid and form the apex of the basisphenoid recess margin.

Basisphenoid

Basisphenoid and parasphenoid indiscernibly fused together. Cultriform process mediolaterally thin and anteriorly projecting (when in life position), with a gently curved ventral margin. Process excavated dorsally by *sulcus septalis* (for the presumably cartilaginous interorbital septum) and ventrally by the anterior portion of the subsellar recess. Anterior (=lateral) tympanic recesses bilaterally excavate basisphenoid and are overhung by conspicuous preotic pendants. Oval "scars" (*sensu* Bakker et al. 1988) well developed; lateral margins only incipiently curved. Basisphenoid recess opening triangular; recess anteroposteriorly deep but fails to extend dorsally under the basioccipital apron. "Scars" deeply excavated by narrow, dorsoventrally trending sulci. Basipterygoid processes strongly taper anteriorly and generally rounded posteriorly however asymmetry may be observed in ventral view. Both project anteroventrally and slightly laterally (in life position). Interbasipterygoidal space largely semicircular. Interbasipterygoidal web anteroposteriorly thick.

Postorbital

Postorbital brow displaying a large, laterally projecting ovoid boss at the posterodorsal corner of the orbit. Anterior dorsal surface excavated by supratemporal fossa. Ventral process elongate and ventrally tapering, with a U-shaped cross section at its midshaft due to concave posterior jugal facet; jugal facet visible in lateral view. Infraorbital process present as a small, triangular projection.

A.4.3 *Riparovenator milnerae*

A.4.3.1 General notes

Taxon represented by a partial cranium and semi-articulated portion of the caudal vertebral series (see above, main text). Taphonomic damage is more extensive relative to *Ceratosuchops*, with substantial cracking evident across the cranial elements in particular. Various element extremities

lost (e.g. premaxillary processes, right paroccipital process, supraoccipital dorsal process, various caudal transverse processes and neural spines) or damaged (e.g. cultriform process broken from the basisphenoid, crushed caudal centra). Plastic deformation mainly affecting a select few processes of the caudal series and not observed in the braincase. Interpremaxillary suture open and premaxillary bodies disarticulated due to damage sustained along presumably fused dorsal margin; few teeth remaining in situ and erupted teeth damaged. Braincase disarticulation includes the skull roof from the basicranium, bilateral isolation of the laterosphenoids, and detachment of the left preorbital elements and otoccipital. For comparative osteology, see Table A 2.

A.4.3.2 Osteology

Premaxillae

Premaxillae only preserving the anterior terminal rosette. Dentigerous margin “hooked” anteriorly; seven dental alveoli present per element. Interdental plates not observed. Lateral surfaces peppered with many prominent neurovascular foramina. Keeled median ridges visible in lateral view.

Dentition

Size heterodonty noted along the tooth row. First premaxillary alveoli notably smaller relative to the second. Preserved teeth largely conidont with minor labiolingual compression. Teeth posteriorly recurved. Fine serrations (5-8 denticles/mm) noted on intact carinae. Fluted/facetted enamel observed on both the labial and lingual surfaces. Enamel texture appears veined on intact replacement teeth apices.

Nasals

Nasals coossified along their midline into a low sagittal crest that develops posteriorly into an abraded median knob. Nasal ornamentation cruciform in dorsal view. Posterolateral processes triangular and horizontally projecting. Frontal (=posterior) process stout with a curved dorsal margin. Small fragment of a ventral median ridge, visible on posterior ventral surface.

Lacrimals and prefrontals

Prefrontal possessing a boss-like cornual process. Anterior and ventral rami diverge at an acute angle; latter possesses facet for the lacrimal along lateral surface. Lateral surface posterior to the

rami notched. Posterior lacrimal fragment articulated to the left prefrontal via a visible, foramina-lined suture.

Orbitosphenoids

Orbitosphenoid fragments preserved but offer little of osteological note.

Frontals

Frontal bodies coossified dorsally; however, interfrontal suture remains open ventrally. Incomplete nasal processes anteroventrally projecting; nasal facet does not overlap frontal body. Anterior frontal body concave in transverse section and bisected by a low, incomplete sagittal ridge. Anterior margins of the supratemporal fossae sharply defined and laterally curving. Frontals arched in lateral view to expose the orbital fossae. Prefrontal facet deepest anteriorly; posterior portion of facet accepts prefrontal via a transversely V-shaped facet. Postorbital processes well developed and lacking an anterior facet for prefrontal; the processes anterolateral corner is thus exposed, potentially allowing for a minor frontal contribution to the dorsal orbital margin. Frontoparietal suture initially transverse medially, before coursing posteriorly for a short distance and then regaining a generally transverse trend. Frontoparietal processes prominent but asymmetrical.

Parietals

Parietals hourglass-shaped in dorsal view. Sagittal crest present; supratemporal fenestrae narrowly separated on skull roof. Nuchal crest present and flattened along dorsal margin, but badly damaged more generally.

Laterosphenoids

Antotic crest poorly developed with rounded cross section, leading to an ovate and mediolaterally directed capitate process. Lateral (adductor) surface producing a low tuberosity posterior to antotic crest. Sulcus for the ophthalmic ramus of the trigeminal nerve present ventrally.

Prootics

Trigeminal nerve foramen margin principally formed by prootic. Element delineates anterior border of the fenestra ovalis and entirely encapsulates the facial (CN VII) nerve. Facial nerve (CN VII) deeply inset and obscured in lateral view. Posterior process overhangs columellar recess.

Abducens nerve (CN VI) foramina open into pituitary fossa and are separated by a deep, posteriorly directed conical space.

Otoccipitals

Otoccipitals formed via the extensive fusion of the opisthotics and the exoccipitals. Contribution by elements to foramen magnum margin substantial, bar for minor median input by the supraoccipital dorsally and basioccipital ventrally. Paroccipital process well developed with concave lateral anterior surface. Posterior otoccipital pierced by three foramina lateral to the occipital condyle.

Supraoccipital

Dorsal process largely missing, although coronal section clearly demonstrates pinching of ventral posterior surface into a low, rounded midline ridge. Body indented with bilateral crescentic depressions. Posterior middle cerebral vein foramina penetrate the supraoccipital bilaterally at the base of the dorsal process.

Basioccipital

Basioccipital forming majority of hemispherical occipital condyle; condyle neck short and inset from condyle margins. Basioccipital apron extends ventrally and excavated by a deep subcondylar recess; recess extends from ventral neck of the condyle (but possibly exaggerated by taphonomic damage) and delimited laterally by robust crests. As above, basitubera presumably represented by the pair of flat ventral extensions of the basioccipital apron that overlap the basisphenoid and form the apex of the basisphenoid recess.

Basisphenoid

Cultriform process mediolaterally thin; tip ventrally downturned to give ventral margin a more strongly arched outline. Process excavated dorsally by *sulcus septalis* and ventrally by the anterior portion of the subsellar recess; subsellar recess bisected by thin lamina. Anterior (=lateral) tympanic recesses bilaterally excavating lateral basisphenoid and overhung by conspicuous preotic pendants. Oval “scars” well developed with rounded lateral margins. Basisphenoid recess opening triangular; recess anteroposteriorly deep and extends dorsally under the basioccipital apron. “Scars” excavated by short, shallow depressions. Basipterygoid processes strongly tapers anteriorly; posterior margins somewhat pinched in ventral view. Exposure of ventral surface of basipterygoid process reduced in lateral view. Processes project anteroventrally and slightly

laterally when in life position. Interbasipterygoidal space with somewhat flattened dorsal margin in posterior view. Interbasipterygoidal web relatively thin anteroposteriorly.

Caudal vertebrae

Partially articulated caudal series includes at least 22 vertebrae and 18 chevrons. Series preserves "transition point" between vertebrae possessing and lacking caudal ribs (Russell, 1972); all bar nine of the recovered vertebrae are anterior to this point. Closure of neurocentral sutures follows a posterior-anterior trend.

Centra shallowly amphicoelous. Anterior centra are only slightly longer than tall and constricted about their mid point; centra become more elongate posteriorly. Centra internally hollow.

Neural arches typified by tall neural spines; spine height decreases posteriorly but remains taller than centra facet heights well into middle series where preserved. Intact anterior and middle neural spines show minor anteroposterior expansion at the dorsal extremities. Spine inclination increases posteriorly. Spine cross-section thin and anteroposteriorly elongate in anterior series, becoming ovate more posteriorly. Accessory neural spines (=anterior spurs) project from the anterior base of pre-transition point neural spines; reduced to small ridges in elements immediately posterior before disappearing. Webbing present at lateral spine base of anteriormost elements.

Prezygapophyses anterodorsally projecting in lateral view; anterior facet overlap minimal to absent. Prezygapophyseal facets face mainly medially. Spinoprezygapophyseal fossa narrow and deep anteriorly, becoming boarder and shallower in middle elements. Postzygapophyses thin and medially trending in more anterior elements, becoming more parallel posteriorly.

Caudal ribs generally project posterolaterally with minor dorsal inclination in undeformed anterior elements; reduced to small "fin"-like process by transition point. Ventral laminae absent bar for stout buttress (?centrodiapophyseal lamina) in anterior neural arches.

Chevrons lacking anterior processes. Haemal canal generally tall and ovate in anterior elements, becoming stouter and flat-topped posteriorly. Chevron articular facets divided into anterior and posterior portions. Haemal spines elongate with anteroposteriorly spatulate ventral tips in anterior elements; spine rod-like in posterior elements.

A.5 Supplementary Figures

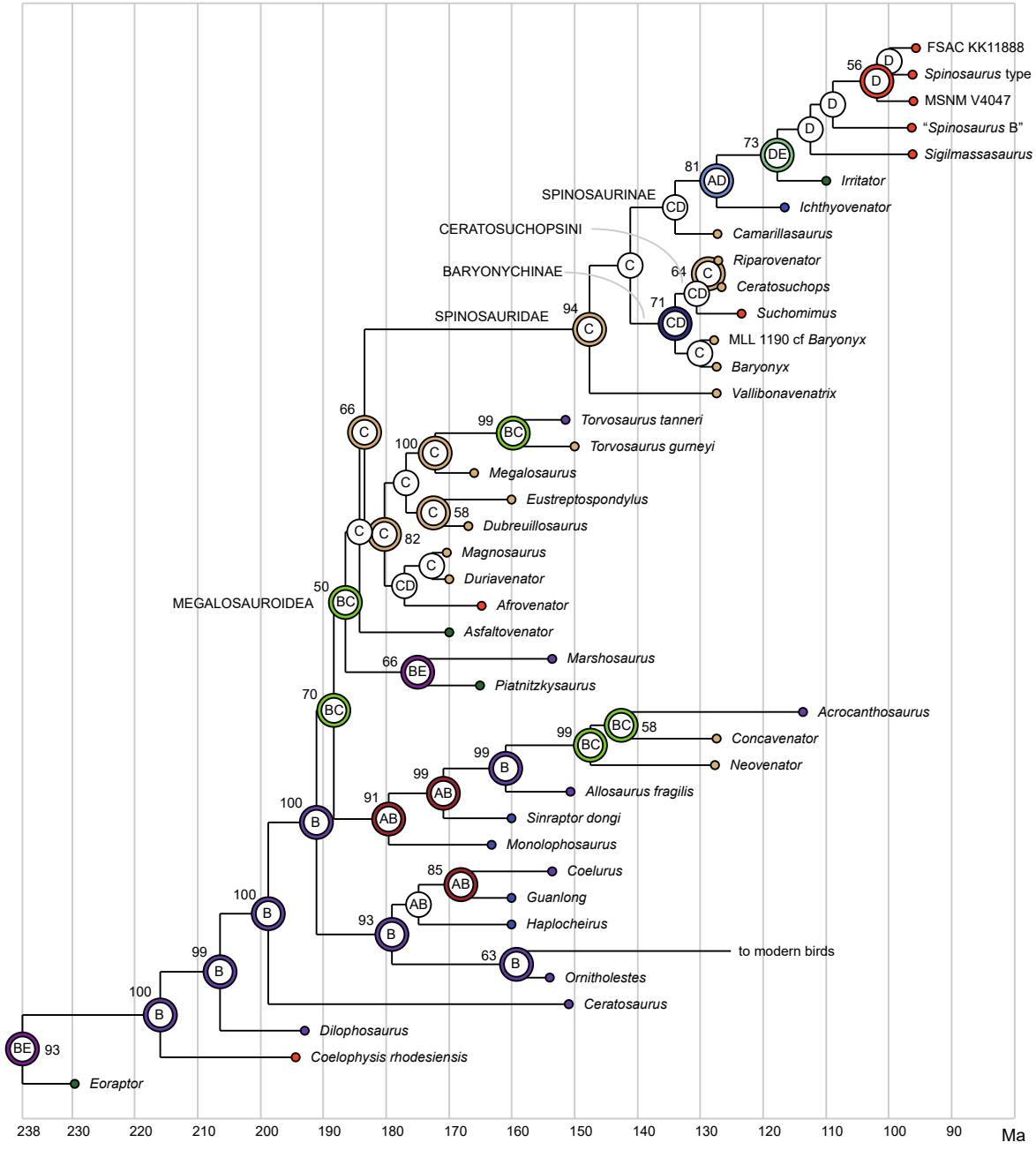

Fig. A 1 Time-calibrated phylogeny of theropod relationships based on the Maximum Clade Credibility Tree inferred by the Bayesian analysis. Numbers at nodes represent posterior probability values >50%. Letters at nodes refer to the most likely ancestral area reconstructed. Colored circles indicate ancestral area inference with frequency >50%. Abbreviations: A, Asia; B, North America; C, Europe; D, Africa; E, South America.

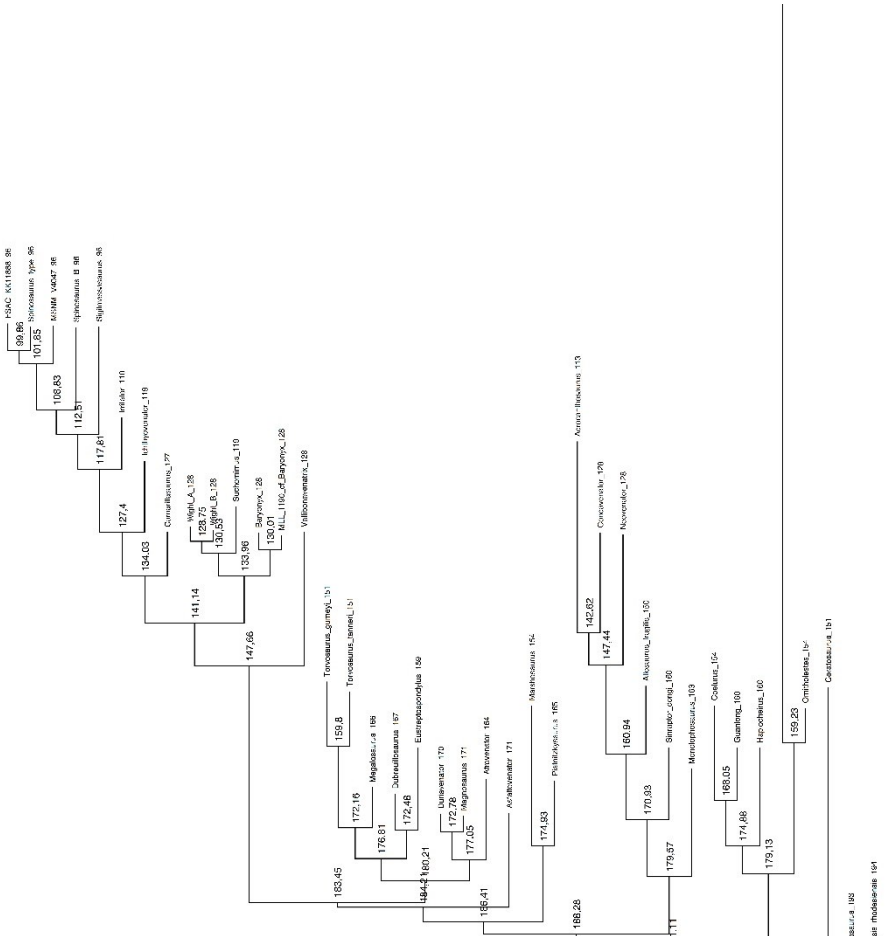

Fig. A 2 Time-calibrated phylogeny of theropod relationships based on the Maximum Clade Credibility Tree inferred by the Bayesian analysis, showing age of node divergences.

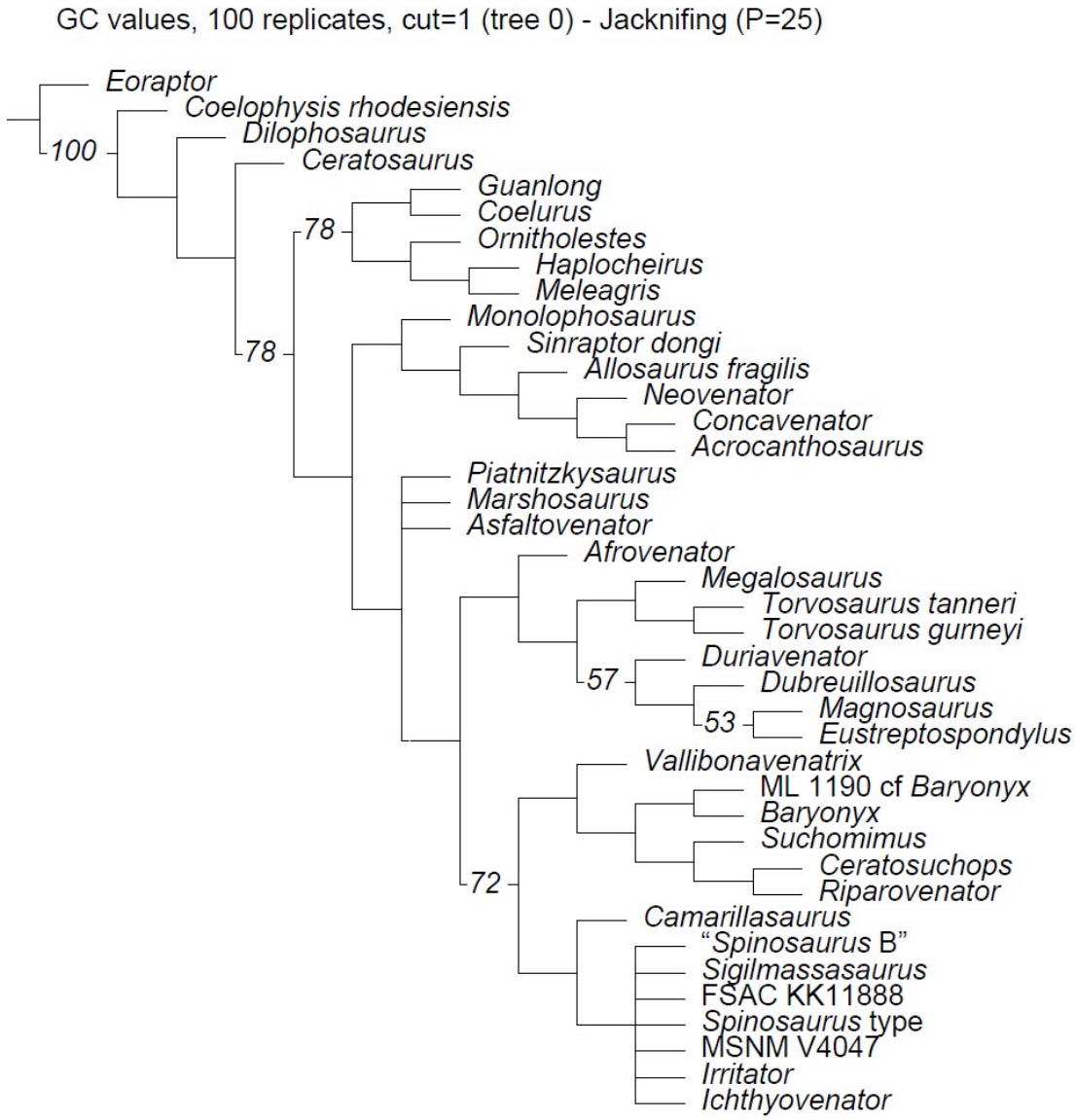

Fig. A 3 Jackknife resampling for nodal support. Numbers at nodes indicate jackknife values in excess of 50%.

A.6 Baryonychine osteological comparisons

Table A 2 Comparison of osteological characters between *Ceratosuchops*, *Riparovenator*, *Baryonyx* (holotype specimen NHMUK PV R9951) and material referred to *Suchomimus* (MNN GDF 500, 501, 214).

	#	Character statements (character polarity arbitrary in this context; parentheses containing "Ch. XX" refer to equivalent characters used in our phylogenetic analyses)	*Ceratosuchops*	*Riparovenator*	*Baryonyx* type	*cf. Suchomimus***	Caveats and points of consideration
Unique characters observed in the Wessex Fm. specimens							
Ceratosuchops	1	Basioccipital, width and position of the subcondylar recess: mediolaterally narrow and ventrally restricted (surface directly below condyle convex) (0); mediolaterally wide (~2/3 condyle width) and dorsoventrally tall (recess reaches the occipital condyle neck) (1) (see also Ch. 1191).	0	1	1	1	Reversal of the wide megalosaur condition. Ambiguous due to individual/ontogenetic variability of pneumatic features (Witmer, 1990; Chure et al., 1996; Witmer, 1997a; Witmer, 1997b; Sampson et al., 2007; Witmer et al., 2010; Carr, 2020). Surface below condyle develops from convex ("large stage 1" specimens) to concave ("stage 3 specimens") during *Gorgosaurus* growth series (Carr, 1999: 519).
	2	Basisphenoid, excavation of the oval scars: shallow depressions (0); elongate, narrow sulci (1).	1	0	n/a	0	Oval scar excavation apomorphic for Ceratosuchopsini (see main text; row 37), *Ceratosuchops* could simply represent individual variation of this trait (albeit arguably extreme in terms of morphological difference).
	3	Basisphenoid, width of the interbasipterygoidal web: thin (0); thick (1).	1	0	0	0	Ambiguous if individual variability affecting pneumatic features bordering it; Web becomes thicker during *Tyrannosaurus* ontogeny (Carr (2020): ch 1050 – blade-like in young adults, long and convex in adults), although Wealden Supergroup spinosaurids do not display blade-like morphology.
	4	Supraoccipital, dorsal process, posterior surface in coronal view (below more dorsally positioned sulcus): gently curved (0); V-shaped or produces a midline ridge (1).	0	1	1	1	Variation in ridge presence and development is present in various coelurosaurs and may characterise early members of the clade (Bever et al., 2013). Midline ridge also present in *Irritator* (Sues et al., 2002).

Riparovenator	5	Premaxilla, shape of pm1tooth/alveolus relative to pm2: pm1 at least half the size of pm2 (0); pm1 less than half the size of pm2 (1).	0	1	0	0	Heterodonty exhibited by spinosaurids generally; possibly too variable to be taxonomically useful (C. Hendrickx, pers. comm. 2021).
	6	Frontal, prefrontal contact in dorsal view: prefrontal articulates along anterior surface of the frontal postorbital process, no notch (0); prefrontal does not contact frontal postorbital process, notch present (1) (see also Ch. 1498)	0	1	0	0	Possibly an immature trait displaying incomplete closure in *Riparovenator*; Orbital notch closure ontogenetically and individually variable in *Tyrannosaurus* (Carr (2020): Ch 90)
	7	Prootic, visibility of the facial nerve (CN VII) foramen in lateral view: foramen visible (0); foramen largely obscured by thick otosphenoidal crest (1).	0	1	0	0	
	8	Basioccipital, depth of the subcondylar recess: shallow, depth less than 1/5 of recess mediolateral width (0); deep, depth over 1/3 recess mediolateral width (1).	0	1	0	0	Potentially ambiguous due to variability of pneumatic features (see above); surface ventral to the condyle convex to concave (in *Daspletosaurus)* (Carr, 1999: 519). However, excavation of "ventral plate" (deep vs shallow) helped distinguish *Daspletosaurus horneri* and *D. torosus* (Carr et al., 2017); whilst "subcondylar recess" depth changes during *Tyrannosaurus* ontogeny (Carr (2020): Ch 111 – deep in large juveniles, shallow by young adult stage), these refer to different set of pneumatic features not situated directly ventral to condyle (see also Witmer and Ridgley, 2009).
Potentially obsolescent/ambiguous "unique" characters in *Ceratosuchops* or *Riparovenator*							
Ceratosuchops	9	Premaxillae, antenarial tuberosities (located on the anterior margin of external narial margin): absent (0); present (1).	1	?	0	0	
	10	Premaxilla, subnarial process, length: subequal to or more than (0); less than (1) the length of the buccal margin of the premaxilla (Ch. 752)	1	?	?	0	Process lengths generally variable (Molnar, 1990), longer process in *Suchomimus* affects slightly larger specimen; Ontogenetic/individual variation observed in *Tyrannosaurus* (Carr (2020): Ch 265 – some adults display immature "short" state, despite mature state already acquired by some young adult morphs).

Ceratosuchops (cont.)	11	Skull roof, path of the frontoparietal suture: V-shaped (0); "step"-like (intitally transverse medially, before trending posteriorly a short distance and regaining a transverse orientation laterally) (1); sigmoidal (2)	0	1	?	2	Frontoparietal suture changes observed in tyrannosaurid ontogeny (Carr 2020): Ch92 – some adult *Tyrannosaurus* display immature"wedge-shaped" state, vice versa for some large juveniles (Carr et al., 2004); however frontoparietal contact differences helped distinguish *Daspletosaurus horneri* and *D. torosus* (Carr et al., 2017).
	12	Otoccipitals, angle of projection of paroccipital proccesses: laterally (sub-horizontally) (0); posterolaterally (1).	1	?	0	?	Variation in projection angle apparently observed in some tyrannosaurid taxa (development from more posterior to more lateral projection) (Bever et al., 2013: 19).
	13	Otoccipitals, anterior margin of the facet on the dorsal paroccipital process: angular, margin projects anteriorly (0); curved, minimal anterior projection (1).	1	0*	0*	?	*Potentially ambiguous as the right otoccipitals in *Baryonyx* and *Riparovenator* are missing lateral part of the process; unable to test for intra-individual variation in facet shape.
	14	Basisphenoid, basisphenoid recess, dorsoventral extent: recess short and does not extend far under basioccipital (0); extends dorsally under basioccipital apron (1)	0	1	1	?	Ambiguous due to individual variability of pneumatic features. See Dufeau (2011) for *Baryonyx*.
	15	Cultriform process, direction of projection of process tip (relative to the horizontally oriented skull roof): anteriorly (0); anteroventrally (1).	0	1	?	?	Strongly arched processes observed in *Tyrannosaurus* ontogeny (Witmer et al. (2009)– on basis CMNH 7541 "*Nanotyannus*" is a immature morph of *Tyrannosaurus*) and *D. torosus* (Carr, 1999: 507).
	16	Occiput, crista tuberalis (=metotic strut), mediolateral width across opposing cristae in posterior view: less than (0); more than (1) 1/2 the dorsoventral depth of the braincase from the dorsal tip of the supraoccipital to the ventral tip of the basal tubera (ch 1014).	0	?	1	?	Possibly influenced by ontogenetic variation in paraoccipital process projection (see also #12)

Riparovenator	17	Nasal, cruciform process, shape of posterodorsal margin (i.e. dorsal margin of the frontal process) in lateral view: straight (0); curved (1).	?	1	0	?	
	18	Skull roof, path of the frontoparietal suture: V-shaped (0); "step"-like (intitally transverse medially, before trending posteriorly a short distance and regaining a transverse orientation laterally) (1); sigmoidal (2)	0	1	?	2	Replicate (see #11)
	19	Dorsum sellae, shape of the dorsal margin in anterior view: V-shaped (0); sub horizontal (1).	0*	1	0	?	*based on mirroring the undamaged right side of the dorsum sellae.
	20	Cultriform process, direction of projection of process tip (relative to the horizontally oriented skull roof): anteriorly (0); anteroventrally (1).	0	1	?	?	Replicate (see #15)
	21	Cultriform process, subdivsion of the subsellar recess by thin lamina: absent (0); present (1)	?	1	?	?	Pneumatic features generally variable, comparative sample unknown for baryonychines.
	22	Basisphenoid, basipterygoid process, shape of lateral margin in ventral view: convex (0); concave (1).	0	1	?	0	
	23	Basiphenoid, basipterygoid process, exposure of the ventral surface in lateral view: thick (0); reduced (1).	0	1*	?	0	*minor damage to left process' ventral margin
	24	Caudal vertebrae, anteroposterior width of anterior neural spines: narrow (0); wide (1).	?	0	1*	1	*Fragmentary evidence suggest some breadth in *Baryonyx* (Charig et al., 1990; Charig et al., 1997); Comparisons potentially affected by non-overlapping elements. Anterior caudal neural spines also anteroposteriorly narrow in *Ichthyovenator* (Allain et al., 2012).
	25	Caudal vertebrae, anterior neural arches, ventral rib laminae: absent (0); present (1) (Ch. 358)	?	0	1	?	Not unique as *Vallibonavenatrix* is also scored the same (taxon recovered as baryonychine in parsimony analysis) (Malafaia et al., 2020b); Comparisons potentially affected by non-overlapping elements e.g. more distal anterior *Ichthyovenator* caudals appear to lack ventral rib lamina relative to laminated anteriormost element (Allain et al., 2012).

Riparovenator (cont.)	26	Caudal vertebrae, anterior neural arches, hyposphene: absent (0); present (1) (Ch. 359).	?	0	1	?	Not unique as *Vallibonavenatrix* is also scored the same (taxon recovered as baryonychine in parsimony analysis) (Malafaia et al., 2020b); Comparisons potentially affected by non-overlapping elements.
	27	Caudal vertebrae, constriction of the centrum midpoint: less than (0) or more than (1) 40% anterior facet width.	?	1	0	?	Possibly allometric, state 1 affects larger specimen; overlap of vertebrae uncertain.
Further Comparisons: Characters shared between both Wessex Fm. specimens but not other baryonychines							
Ceratosuchops + Riparovenator	28	Premaxilla, paradental plates: absent (0); present (1)	0*	0*	1	1	*Possibly taphonomic.
	29	Premaxilla, interalveolar space between 3rd and 4th alveoli, mesiodistal diameter: less (0); subequal or more (1) than ½ of 4th alveolus mesiodistal diameter (Ch. 512)	0	0	1	1	Interalveolar space can be variable in baryonychines, and heterodonty exhibited by spinosaurids generally. State 1 present in juvenile spinosaurid premaxillae (Lakin et al., 2019), suggesting character not influenced by ontogeny (but sample size low).
	30	Basioccipital, ventral occipital condyle margin in ventral view: V-shaped (0); gently curved (1)	1	1	0	0	Ventral condyle shape ontogenetically and individually variable in tyrannosaurids (Carr (2020): Ch 1020 – immature state observed in some adult *Tyrannosaurus*). Left ventrolateral margin in cf. *Suchomimus* possibly slighty damaged.
Further Comparisons: Characters shared between both Wessex Fm. specimens and *Suchomimus* but not *Baryonyx*							
Ceratosuchops + cf. Suchomimus	31	Enamel ornamentation*: lingually only (0); labially and lingually (1).	1	1	0	1	*Enamel ornamentation variable and potentially of limited significance (Fowler, 2007; Hendrickx et al., 2016; Hendrickx et al., 2019).
	32	Frontal, postorbital facet, anterior depth: less (0); more (1) than 2/5 facet length (Ch. 1053).	1	1	0	1	Cranial facets may be generally variable (Molnar, 1990), deeper facets affect larger specimens; Ontogeny/individual variation affects postorbital frontal process shape (and thus frontal postorbital facet shape, which accomodates the process) in *Tyrannosaurus* (Carr (2020): Ch 68, 69 – some young adults and adults display the immature "shorter" state re: facet height and length).
	33	Frontal, postorbital facet, deep longitudinal slot for postorbital: absent (0); present (1) (Ch. 1761).	1	1	0	1	Slot within frontal postorbital facet develops ontogenetically in *Tyrannosaurus* (Carr (2020): Ch 919 – groove acquired by young adult stage), smallest specimen (*Baryonyx*) does not produce slot.

Ceratosuchops + cf. Suchomimus (cont.)	34	Frontal, anterior margins of supratemporal fossa: poorly developped with little curvature (0) sharp and laterally curving (1).	1	1	0	1	Margins change shape (Carr, 1999) and become increasingly prominent in tyrannosaurids growth series but may be individually variable also (Carr (2020): Ch 935 – some young adults and adults stages display immature state); Trait affects larger baryonychine specimens.
	35	Basioccipital, ventral occipital condyle margin in posterior view: V-shaped, margins converge towards midline (0); gently curved (1).	1	1	0	1	State 0 reminiscent of immature tyrannosaurid state (Carr, 1999; Carr, 2020: Ch 1018 – mature "reniform" state acquired by young adult stage in *Tyrannosaurus*).
	36	Basioccipital, contribution to foramen magnum margin: large, exoccipitals widely separated (0); reduced, exoccipitals closely placed (1) (Ch. 974).	1	1	0	1	Closely appressed exoccipitals also in *Irritator* (S. Evers, pers. comms. 2021). Some variation in at least one tyrannosaurid (reduced contact in an immature *Gorgosaurus*, space normally wider in tyranosaurids –Bever et al. (2013): 25). More tangentially, basioccipital contribution to foramen magnum increases in *Psittacosaurus* ontogeny (hatchling and juveniles: 15%, adults 30%) (Bullar et al., 2019) but may decrease in some ceratopsids (Longrich et al. (2012): Ch 4).
	37	Basisphenoid, excavation of the collateral scars placed lateral to middle depression: absent (0); present and distinct on both sides (1) (Ch. 510).	1	1	0	1	Does affect a probably muscular insertion point (thus potential for individual variation in attachment morphology); "dished"/"concave" scars seen in adult tyrannosaurids (Carr, 1999).
	38	Basisphenoid, median recess, depth: shallow (0); deep (1) (Ch. 1566).	1	1	0	1	Pneumatic features generally variable (see above).
	39	Basisphenoid, ridges (cf. cristae ventrolateralis of some) binding the median recess laterally: absent (0); present (1).	1	1	0	1	Probably redundant with scar excavation (see row 41); Increase in ridge prominence throughout *Tyrannosaurus* ontogeny (Carr, 2020: Ch 1044), however immature state in latter already contains ridged margins.
	40	Basisphenoid, posteroventral edge of interbasipterygoidal web in sagittal section: sharp (0); rounded (1).	1	1	0	1	Web becomes thicker and convex during *Tyrannosaurus* ontogeny (blade-like in younger morphs; Carr, 2020: ch 1050).

Ceratosuchops + cf. Suchomimus (cont.)	41	Otoccipial, number of cranial nerve foramina lateral to occipital condyle: two (0); three (1).	1	1	0	1	Number can be variable in *Tyrannosaurus* (Bever et al., 2013: 22), unknown if number of foramina phylognetically informative at this stage (Brusatte et al., 2010).
	42	Prefrontal, presence of a boss-like process: absent (0); present (1)	1	1	?*	1	*Prefrontal recovered but potentially damaged.
Further Comparisons: Characters shared by at least one Wessex Fm. specimen and *Suchomimus*, but not *Baryonyx*							
Ceratosuchops + cf. Suchomimus	43	Premaxilla, narial fossa: absent (0); present (1) (Ch. 709).	1	?	0	1	Limited data on narial fossa variation in theropods. Tangentially, variation observed in *Gavialis* (Hone et al., 2020).
	44	Basioccipital, subcondylar recess bordered laterally by mediolaterally thick crests: absent (0); present (1).	0	1	1	0	Individual and ontogenetic varition observed in *Tyrannosaurus* "ascending scars" (Carr, 2020: Ch 1024 –some adult morphs display immature "prominent" state).
	45	Parietal, posterior rise of the nuchal crest in lateral view (angle measured in lateral view with the skull roof held horizontally; the vertex of the angle is located on the capitate process of the laterosphenoid (or preserved equvialent); the first ray projects to the dorsal nuchal crest; the second ray projects posteriorly): ≥ (0), or < (1) 45º.	1	?*	0	1	*Parietal damaged however general trend is likely comparable to that of cf. *Suchomimus* (42º) and *Ceratosuchops* (44º) rather than *Baryonyx* (70º).
Further Comparisons: Characters shared between both Wessex Fm. specimen and *Baryonyx* but not *Suchomimus*							
Ceratosuchops + Riparovenator + Baryonyx	46	Orbital margin, exposure of the orbital fossae in lateral view: orbital fossae visible (0); dorsal portion of orbital fossae partially obscured by overhang of the orbital rim (1).	0	0	0	1 *	*Taphonomic in c.f. *Suchomimus*?
	47	Basioccipital, proportions relative to basisphenoid (measured along midline ventral to occipital condyle to interbasipterygoidal web), in posterior view: basioccipital contribution shorter (0) or longer (1) than basisphenoid contribution.	0	0	0	1	
	48	Occiput, relationship between of basisphenoid oval scars and ventral portion of basioccipital apron: apron situated between oval scars (0); ventral plate overlaps oval scars (1)	1	1	1	0	

(cont.)	49	Basioccipital, foramina situated ventrolaterally occipital condyle: absent (0); present (1).	0	0	0	1 *	*Ambiguous as right side of *Suchomimus* not well exposed in available imagery. Observable foramina do not relate to foramina for X-XII.
Further Comparisons: Characters shared by at least one Wessex Fm. specimen and *Baryonyx* but not *Suchomimus*							
Ceratosuchops + Baryonyx	50	Premaxilla, subnarial process, slenderness: shorter than (0); longer than (1) 4 times its proximal depth (Ch. 697)	0	?	0	1	See also #10
	51	Premaxilla, dorsal midline: uncrested (0); crested (1)	0	?	0	1	
	52	Supraoccipital, dorsal process, width (measured between the foramina for the middle cerebral vein) relative to height (measured from a middle cerebral vein foramen to the tip of the dorsal process): width more than (0) or less than (1) 2/3 process height.	0	?	0	1	State 1 affects largest specimen, character could be allometrically variable.
	53	Supraoccipital, dorsal process, posterodorsal margins: in line with (0) or overhang (1) the rest of the dorsal process.	0	?	0	1 *	*Overhang potentially related to the development of cervical musuclature – process on dorsal end of supraoccipital identified as the tendinous insertion for the m. spinalis capitis in *Tyrannosaurus* (Tsuihiji, 2010).
Riparovenator + Baryonyx	54	Basioccipital, subcondylar recess bordered laterally by mediolaterally thick crests: absent (0); present (1).	0	1	1	0	Replicate (see #44)

A.7 Additional imagery of the diagnostic and differentiating cranial features of the Wessex Fm. spinosaurids.

A.7.1 Imagery of diagnostic the traits of *Ceratosuchops inferodios*

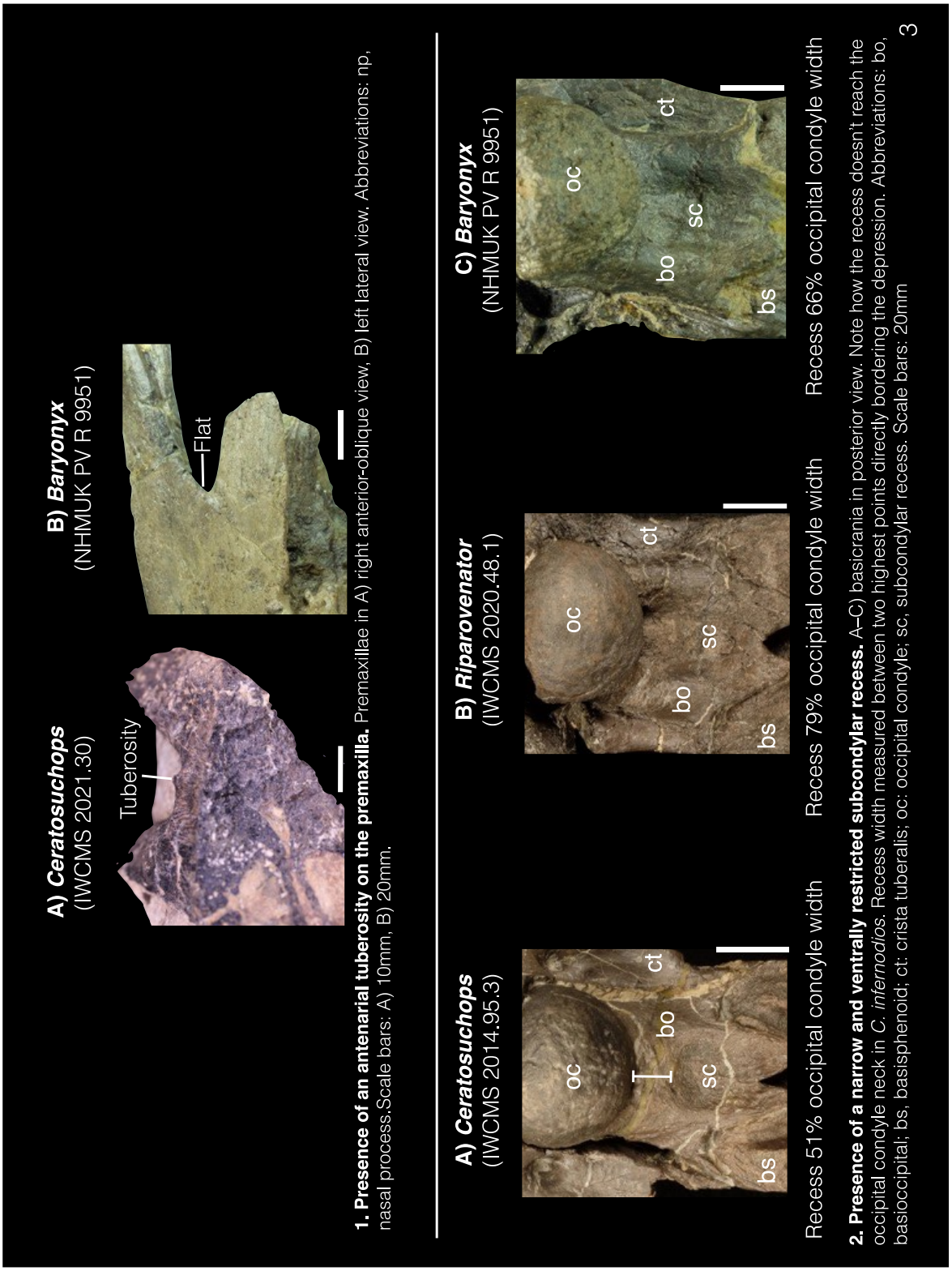

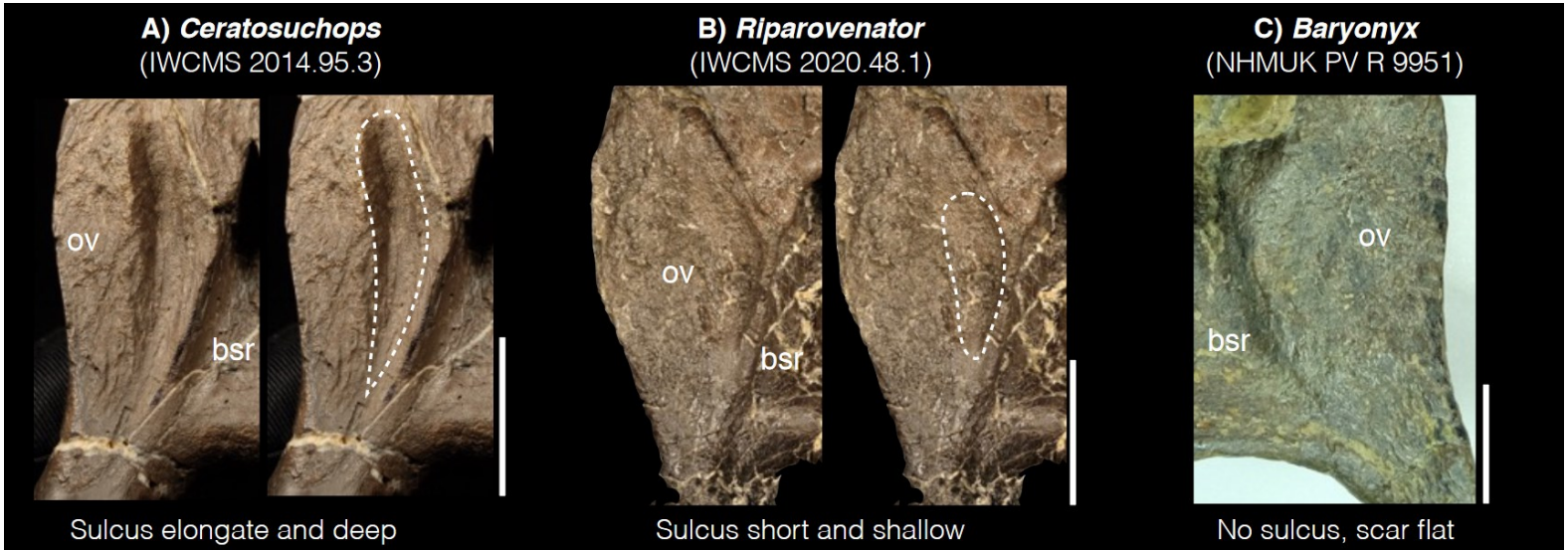

3. Presence of deep, elongate sulci excavating basisphenoid scars. Left (A, B) and right (C) basisphenoid oval scar in posterior view, A) and B) are stereopairs. Abbreviations: bsr, basisphenoid recess; ov, oval scar. Scale bars: 20mm.

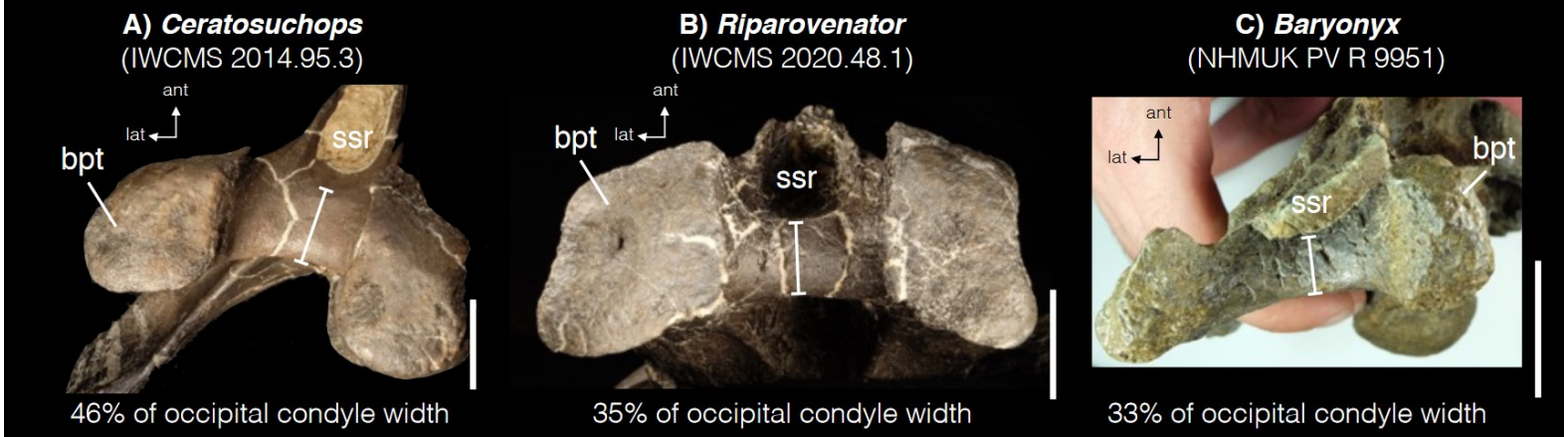

4. Presence of a relatively anteroposteriorly long interbasipterygoidal web. A–C) Basisphenoids in ventral view. Distance marked in A) 20.9mm, B) 16.3mm, C) 14.8 mm. Abbreviations: bpt, basipterygoid process; ssr, subsellar recess. Scale bars: 20mm.

4

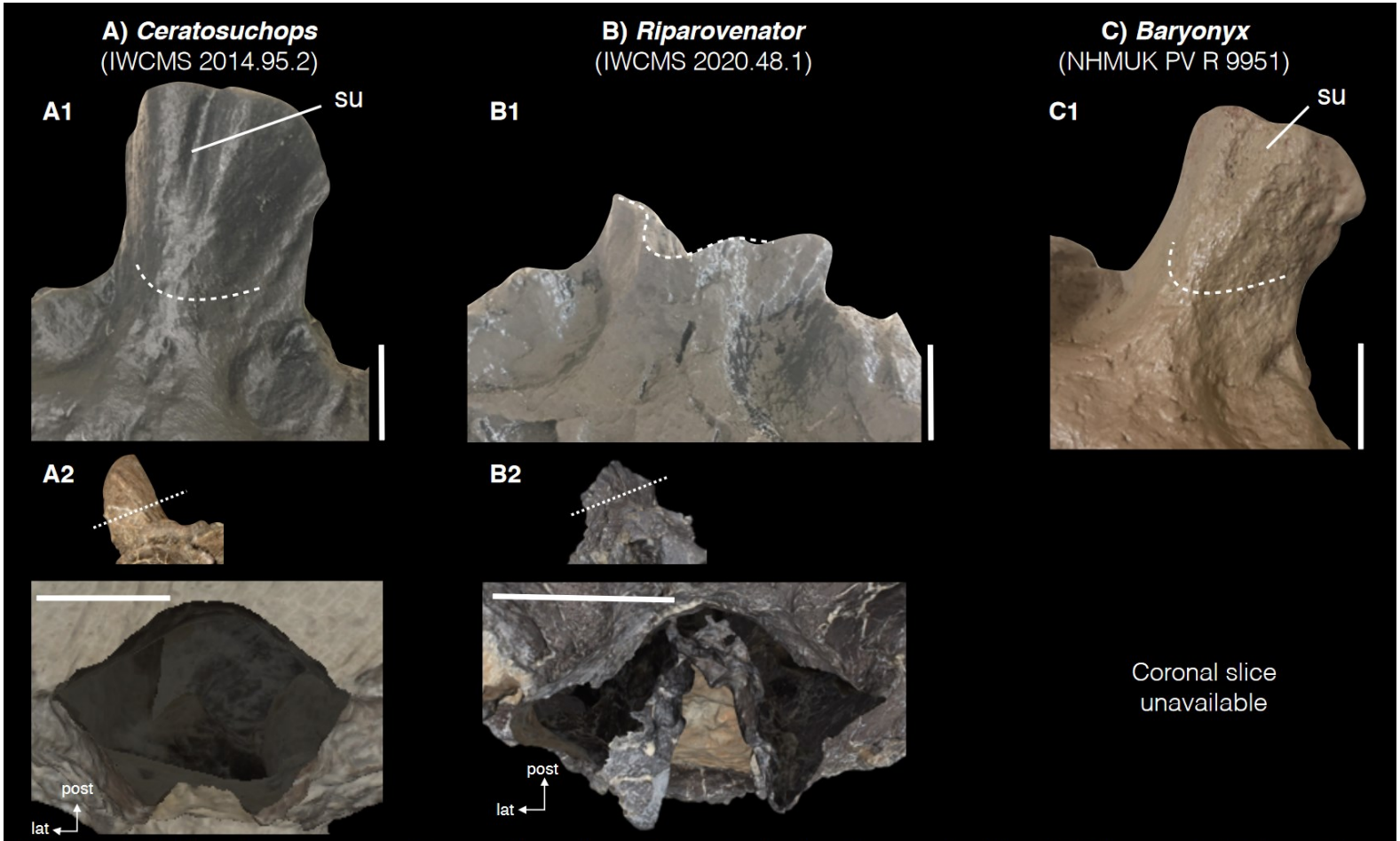

5. Supraoccipital dorsal process possessing a gently curving posteroventral surface in coronal section. A1–C1) supraoccipitals in posterior-oblique view. A2, B2) coronal slices of the dorsal process, generated in MeshLab. Note that the coronal slice of *Ceratosuchops* is based on an older surface scan of the un-prepared block, and the endocranial portion of the dorsal process is infilled with matrix. Abbreviations: su: sulcus. Scale bars: 20mm.

The posterior surface of the dorsal process in *Ceratosuchops* (below the dorsal sulcus) is gently curved (A2), and does not form the distinct and broad midline ridge of *Riparovenator*, which is clearly distinguished from the flatter lateral sides of the posterior dorsal process (B2). Whilst a coronal section was unavailable for *Baryonyx*, the ventral posterior surface of the dorsal process also differs from *Ceratosuchops*. possessing a more V-shaped cross-section.

A.7.2 Imagery of other distinguishing traits of *Ceratosuchops inferodios* relative to *Baryonyx walkeri* and/or *Riparovenator milnerae*

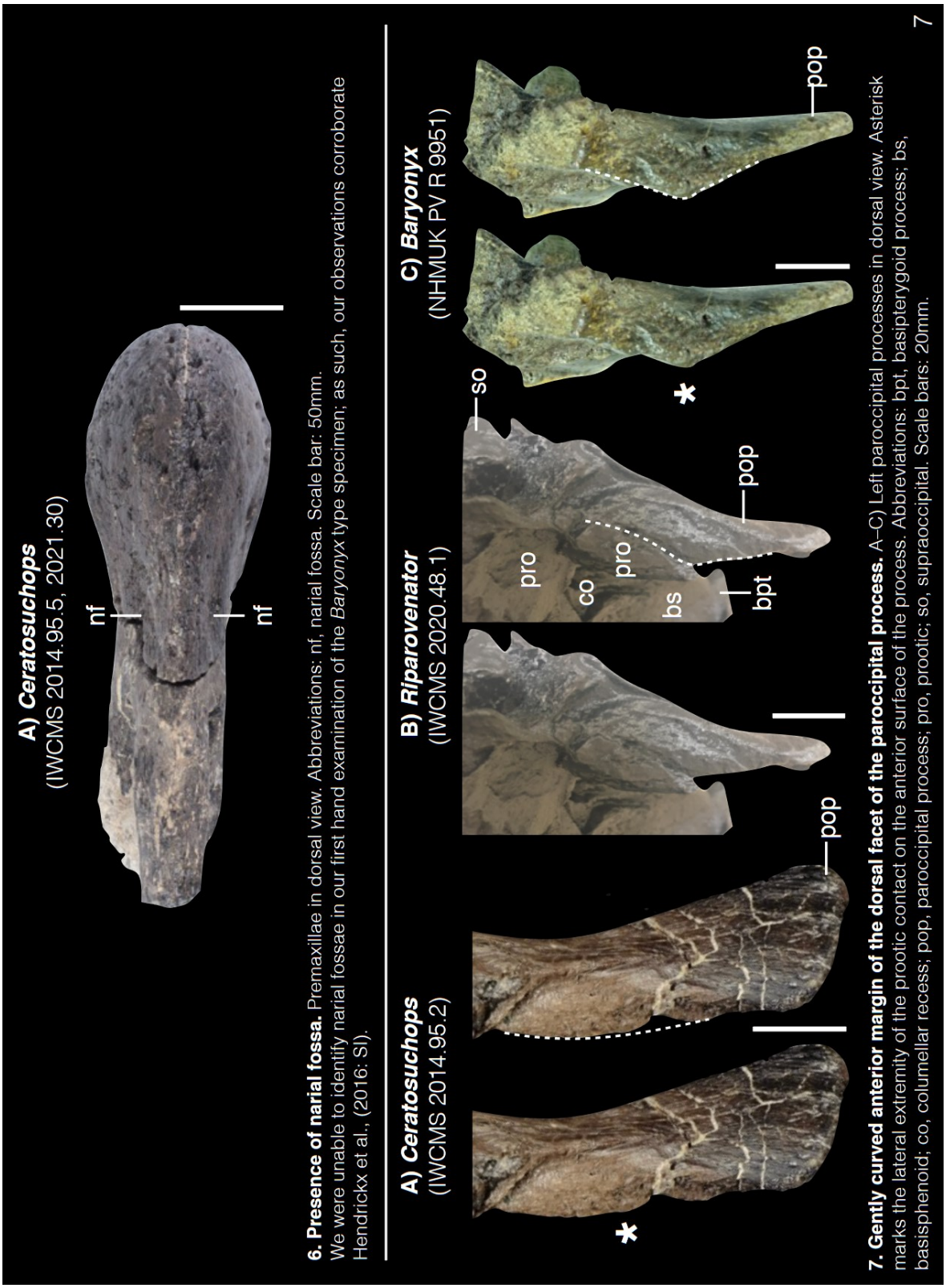

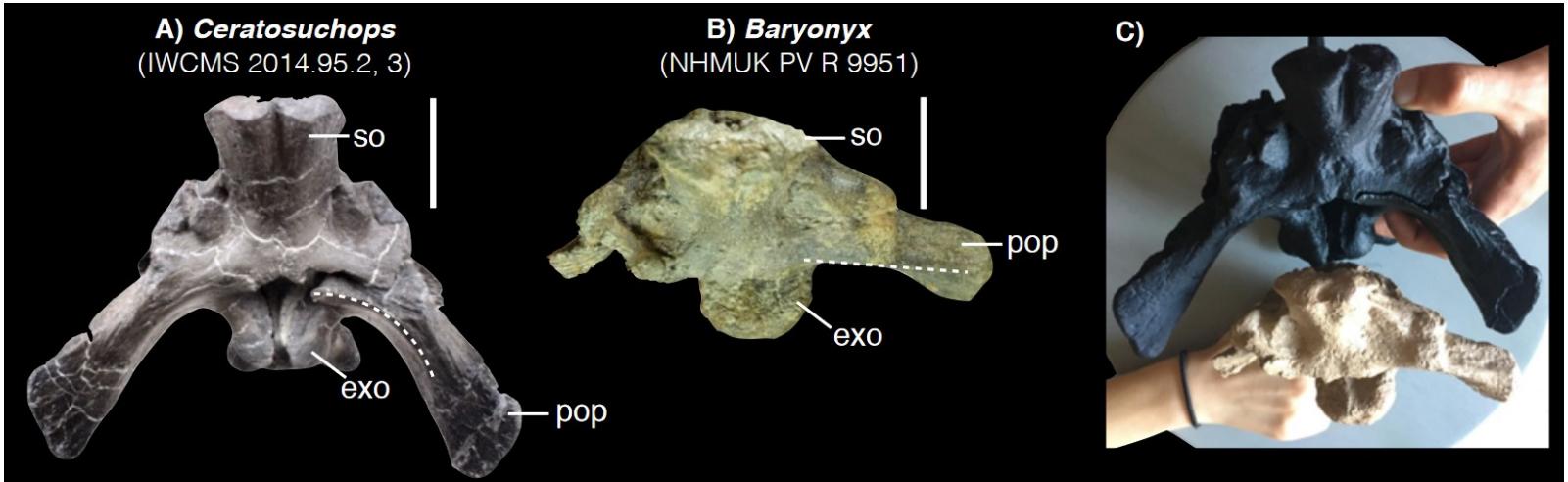

8. Posterolaterally projecting paroccipital processes. A, B) Basicranium in dorsal view. C) Comparison of life-size casts/3D prints of *Ceratosuchops* (top) and *Baryonyx* (bottom) in dorsal view. Abbreviations: exo, exoccipital; pop, paroccipital process; so, supraoccipital. Scale bar: 20mm.

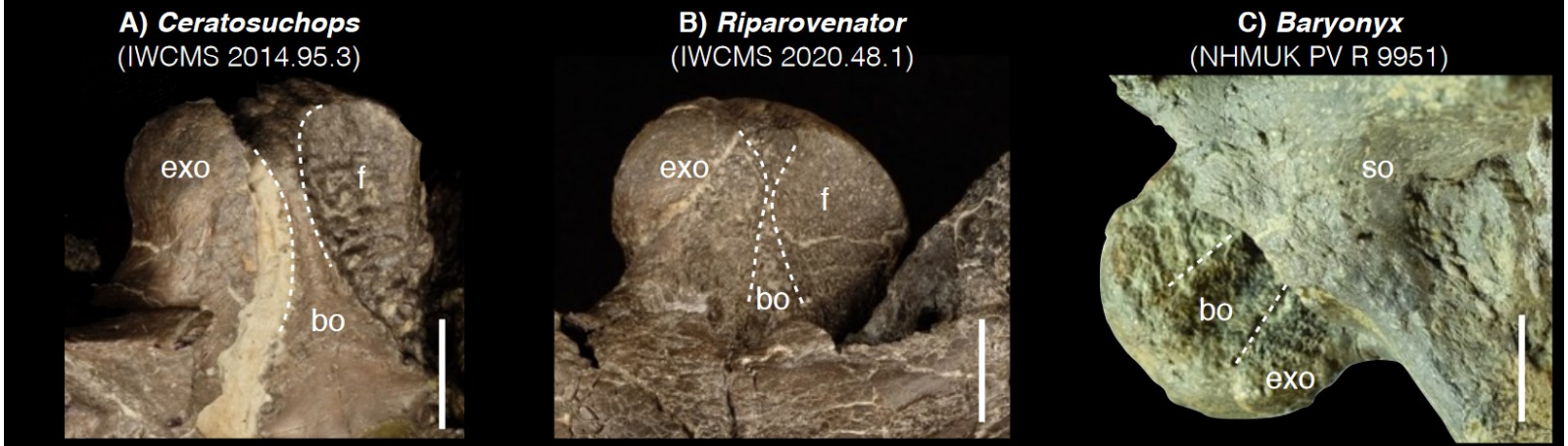

9. Closely placed exoccipitals on the dorsal occipital condyle. A–C) Occipital condyle in dorsal view. Abbreviations: bo, basioccipital; exo, exoccipital; f, exposed exoccipital facet on basioccipital; so, supraoccipital. Scale bars: 20mm.

8

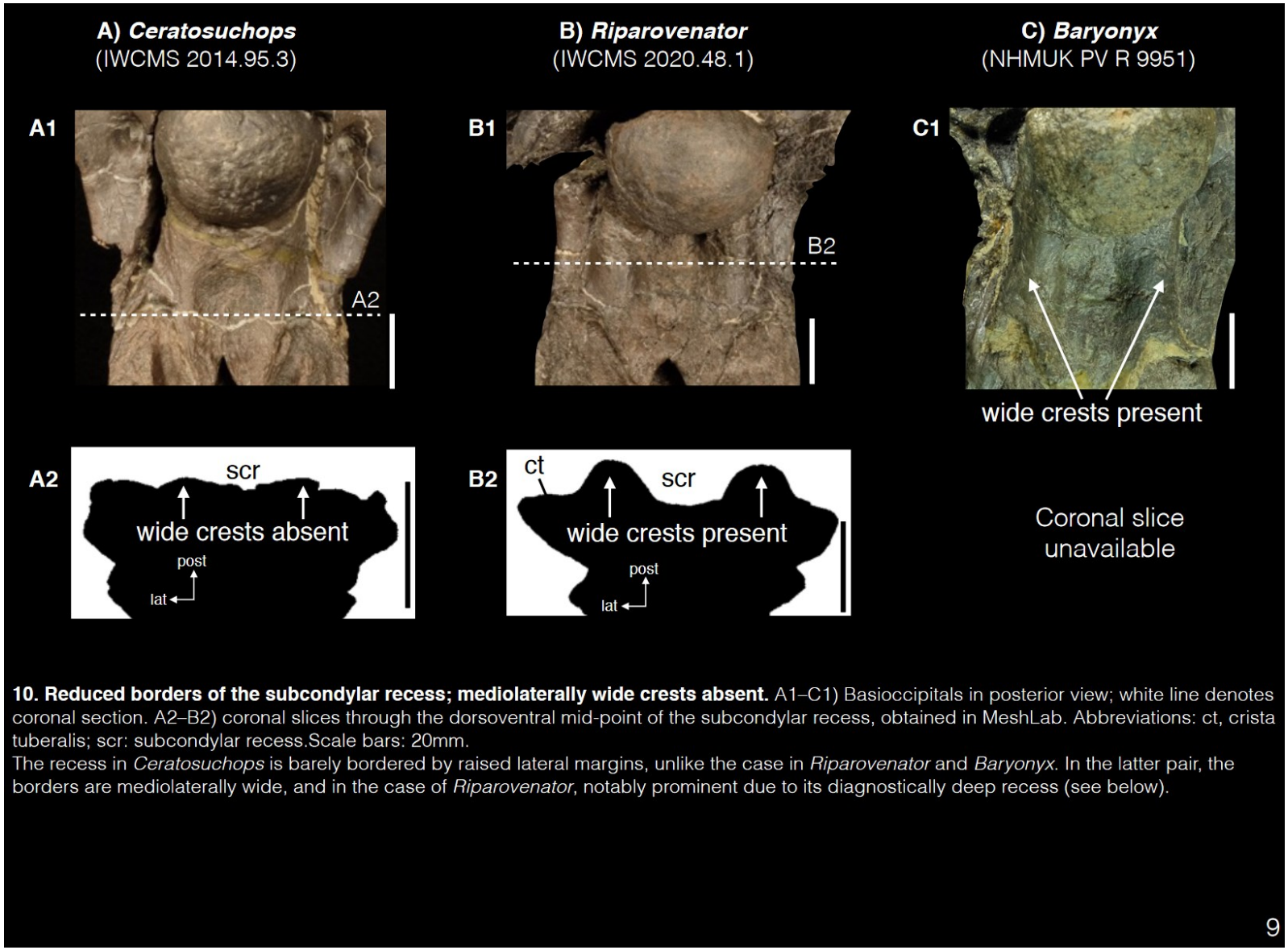

10. Reduced borders of the subcondylar recess; mediolaterally wide crests absent. A1–C1) Basioccipitals in posterior view; white line denotes coronal section. A2–B2) coronal slices through the dorsoventral mid-point of the subcondylar recess, obtained in MeshLab. Abbreviations: ct, crista tuberalis; scr: subcondylar recess.Scale bars: 20mm.

The recess in *Ceratosuchops* is barely bordered by raised lateral margins, unlike the case in *Riparovenator* and *Baryonyx*. In the latter pair, the borders are mediolaterally wide, and in the case of *Riparovenator*, notably prominent due to its diagnostically deep recess (see below).

A.7.3 Imagery of the diagnostic traits of *Riparovenator milnerae*

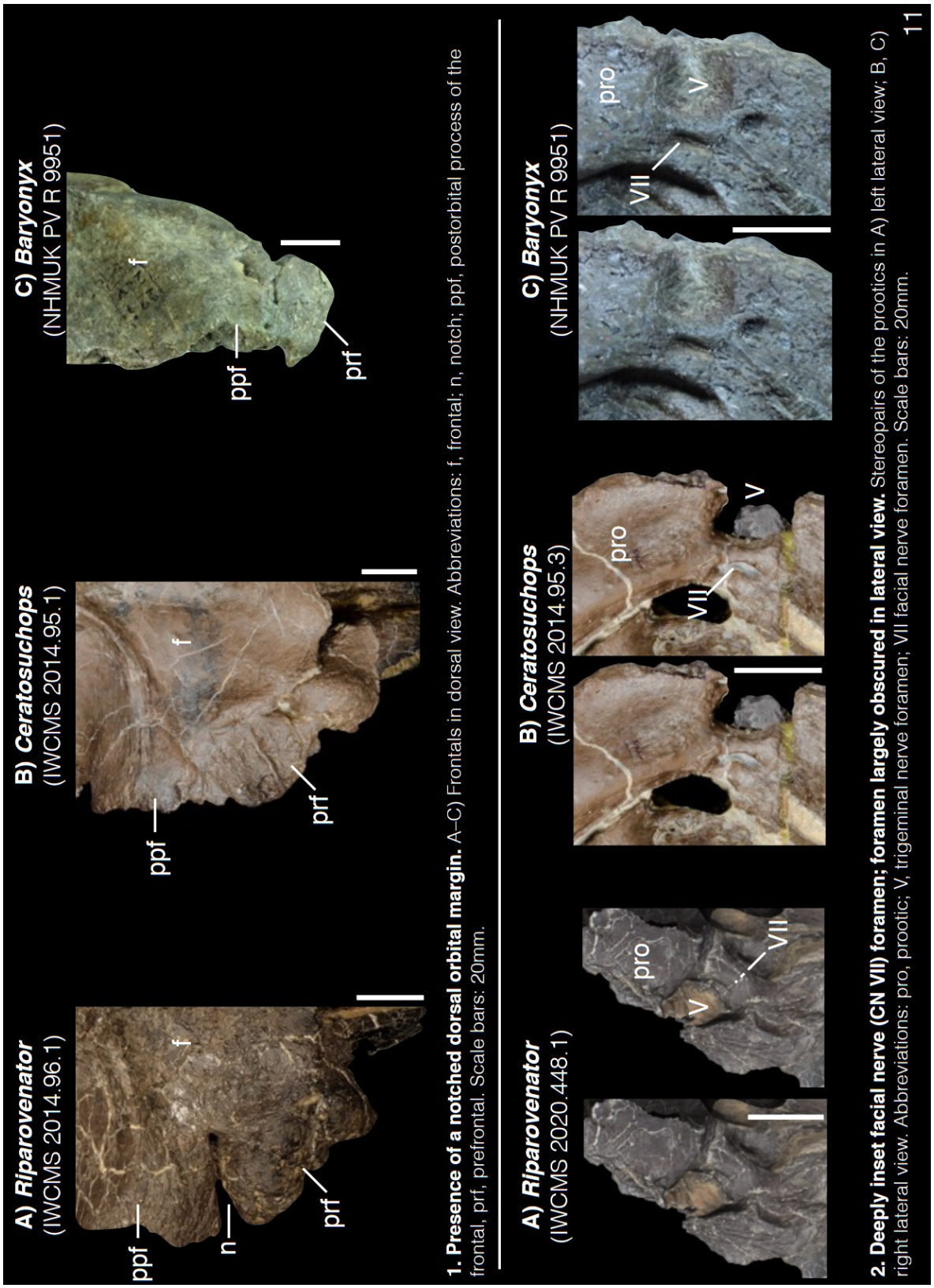

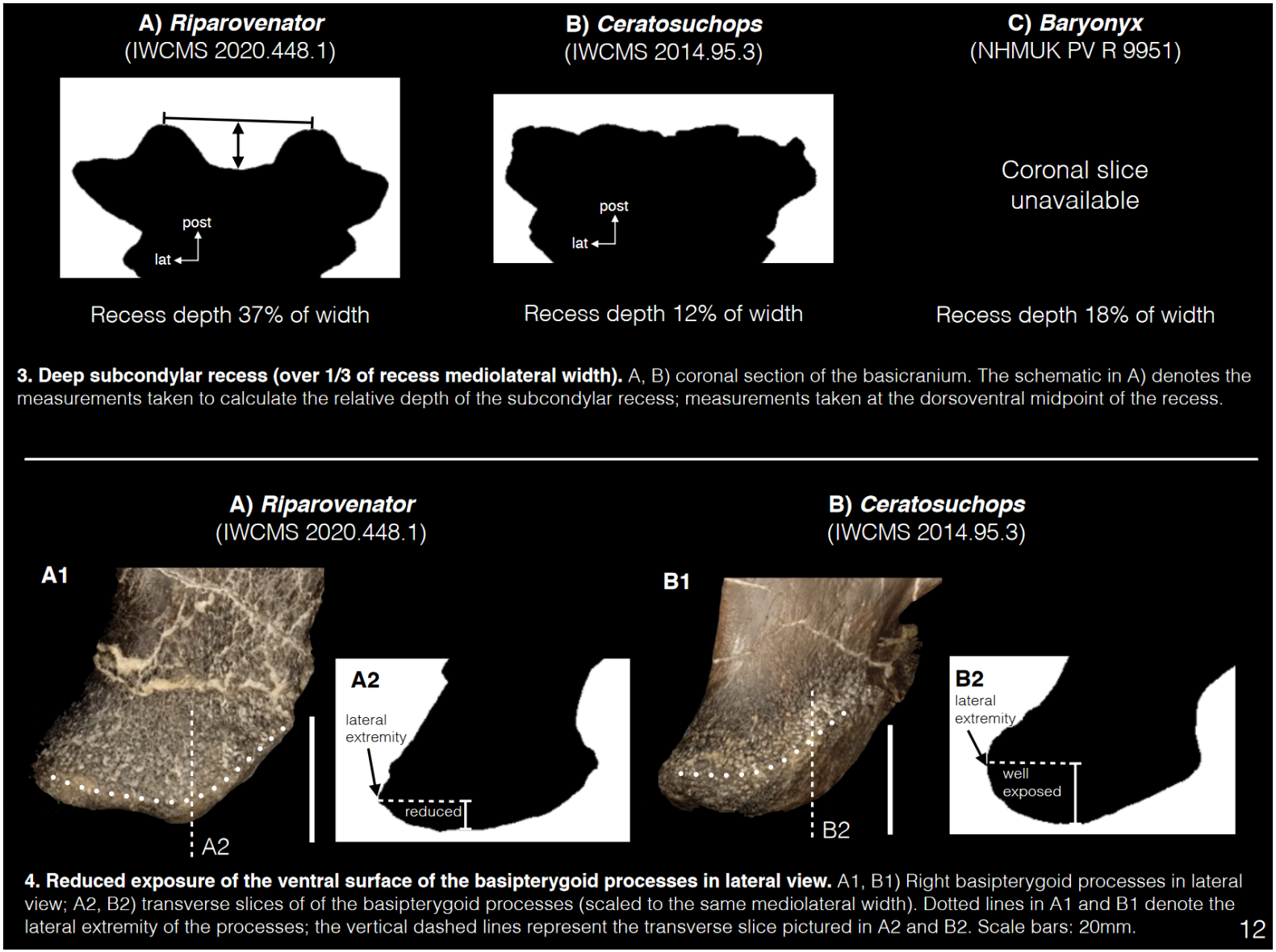
A) Riparovenator
(IWCMS 2020.448.1)
B) Ceratosuchops
(IWCMS 2014.95.3)
C) Baryonyx
(NHMUK PV R 9951)
post
lat
post
lat
Coronal slice unavailable
Recess depth 37% of width
Recess depth 12% of width
Recess depth 18% of width
3. Deep subcondylar recess (over 1/3 of recess mediolateral width). A, B) coronal section of the basicranium. The schematic in A) denotes the measurements taken to calculate the relative depth of the subcondylar recess; measurements taken at the dorsoventral midpoint of the recess.
A) Riparovenator
(IWCMS 2020.448.1)
B) Ceratosuchops
(IWCMS 2014.95.3)
A1
A2
lateral extremity
reduced
A2
B1
B2
B2
lateral extremity
well exposed
4. Reduced exposure of the ventral surface of the basipterygoid processes in lateral view. A1, B1) Right basipterygoid processes in lateral view; A2, B2) transverse slices of of the basipterygoid processes (scaled to the same mediolateral width). Dotted lines in A1 and B1 denote the lateral extremity of the processes; the vertical dashed lines represent the transverse slice pictured in A2 and B2. Scale bars: 20mm.

A.7.4 Imagery of other distinguishing traits of *Riparovenator milnerae* relative to *Baryonyx walkeri* and/or *Ceratosuchops inferodios*

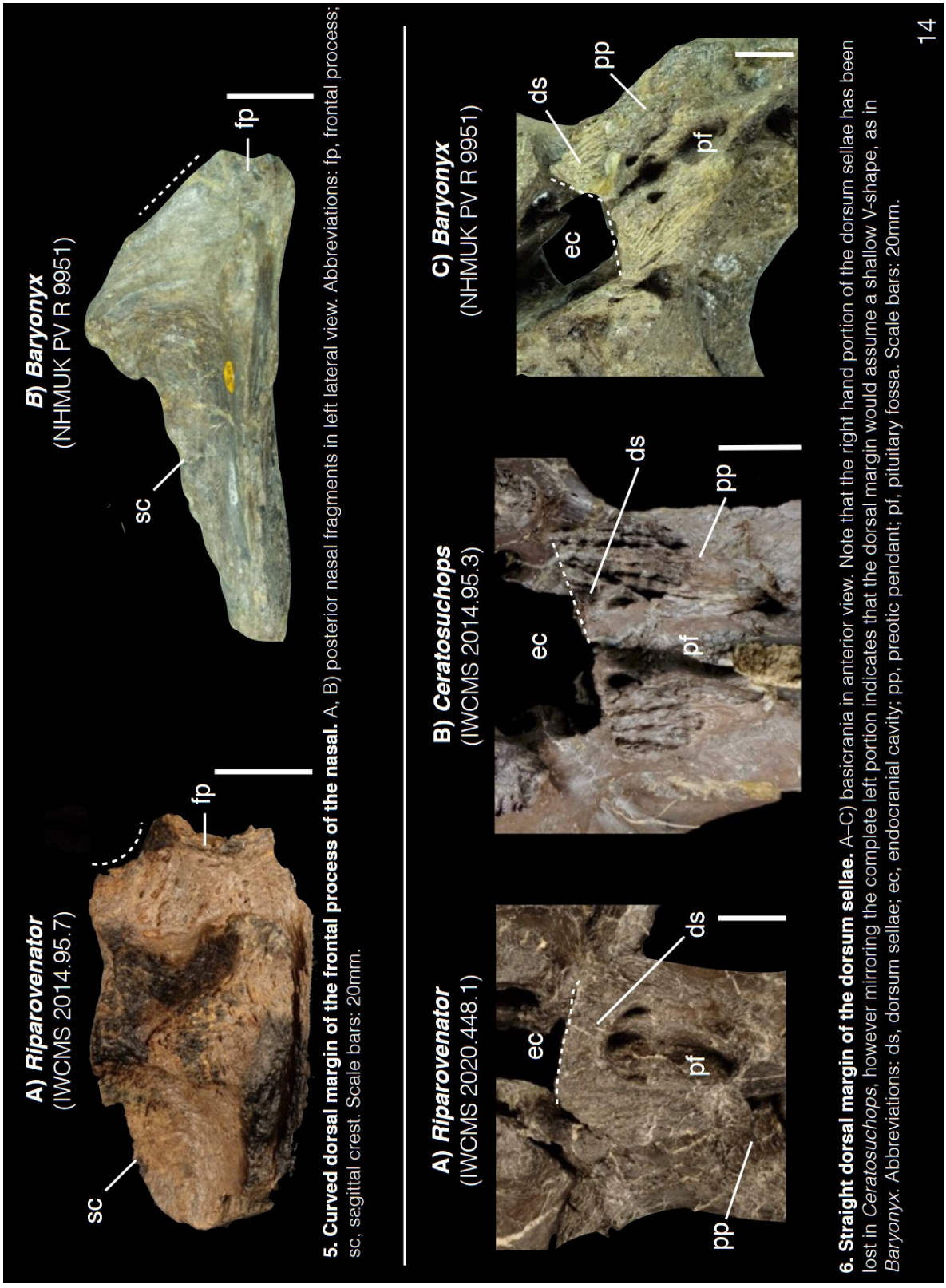

5. Curved dorsal margin of the frontal process of the nasal. A, B) posterior nasal fragments in left lateral view. Abbreviations: fp, frontal process; sc, sagittal crest. Scale bars: 20mm.

6. Straight dorsal margin of the dorsum sellae. A–C) basicrania in anterior view. Note that the right hand portion of the dorsum sellae has been lost in *Ceratosuchops*, however mirroring the complete left portion indicates that the dorsal margin would assume a shallow V-shape, as in *Baryonyx*. Abbreviations: ds, dorsum sellae; ec, endocranial cavity; pp, preotic pendant; pf, pituitary fossa. Scale bars: 20mm.

7. Closely placed exoccipitals on the dorsal occipital condyle. See *Ceratosuchops*, trait 9.

---

8. Prominent borders of the subcondylar recess. See *Ceratosuchops*, trait 10.

A) *Riparovenator*
(IWCMS 2020.448.1)

B) *Ceratosuchops*
(IWCMS 2014.95.3)

C) *Baryonyx*
(NHMUK PV R 9951)

9. Lateral margins of the basipterygoid processes concave in ventral view. A–C) basipterygoid process in ventral view. Note that the processes are too damaged in *Baryonyx* to provide comparison. Scale bars: 20mm.

15

Appendix B Supplementary information for Chapter 3

Isolated tooth reveals hidden spinosaurid dinosaur diversity in the British Wealden Supergroup (Lower Cretaceous)

Note that the full supplementary files, including scripts for the phylogenetic analyses, can be found with the published article online.

B.1 Full measurements of HASMG G369a

Table B 1 Measurements in millimetres (mm). Values based on reconstructed crown height (bold; see main text) marked with an asterisk (*).

Crown base length (CBL)	8.16
Crown base width (CBW)	7.03
Crown height (CH)	**17.2**
Apical length (AL)	?
Crown angle (CA)	74
Crown base ratio (CBR)	0.86
Crown height ratio (CHR)	2.1*
Midcrown length (MCL)	5.67*
Midcrown width (MCW)	4.54*
Midcrown ratio (MCR)	0.8*
Mesiobasal Denticle Extension (MDE)	?
Mesiobasal Carina Extension (MCE)	?
Mesial Serrated Carina Length (MSL)	?
Distal Serrated Carina Length (DSL)	?
Mesial Carina Length (MCAL)	?
Distal Carina Length (DCAL)	?
Distal Denticle Height (DDH)	0.195*

Distal Denticle Length (DDL)	0.171*
Distal Denticle Width (DDW)	0.253*
Mesial Denticle Height (MDH)	?
Mesial Denticle Length (MDL)	?
Mesial Denticle Width (MDW)	?
Distal Denticle Height Ratio (DHR)	1.14*
Distal Denticle Base Ratio (DBR)	1.48*
Mesial Denticle Height Ratio (MHR)	?
Mesial Denticle Base Ratio (MBR)	?
Distoapical Denticle Density (DA)	?
Distocentral Denticle Density (DC)	35*
Distobasal Denticle Density (DB)	?
Mesioapical Denticle Density (MA)	?
Mesiocentral Denticle Density (MC)	35*
Mesiobasal Denticle Density (MB)	?
Average Mesial Denticle Density (MAVG)	?
Average Distal Denticle Density (DAVG)	?
Denticle Size Density Index (DSDI)	1*
Transverse Undulation Density (TUD)	n/a
Marginal Undulation Density (TUD)	n/a
Labial Flutes (LAF)	7
Lingual Flutes (LAF)	5

B.2 Regression analyses

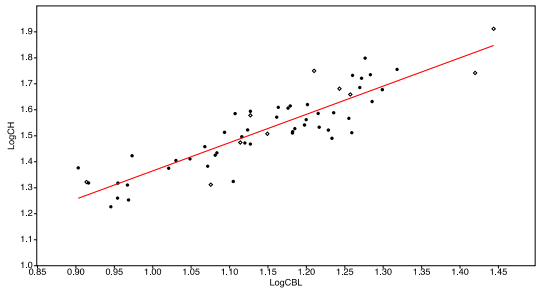

All spinosaurids (all positions), LogCH vs. LogCBL.
Slope: 1.0881, **intercept**: 0.27671, r2: 0.79069.

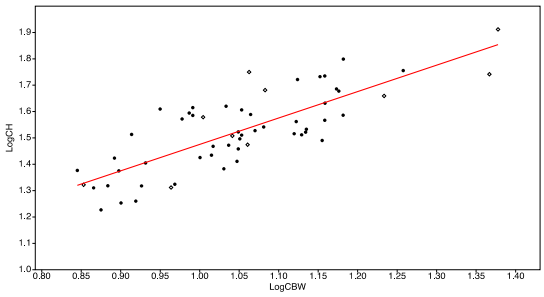

All spinosaurids (all positions), LogCH vs LogCBW.
Slope: 1.002, **intercept**: 0.47343, **r2**: 0.62588.

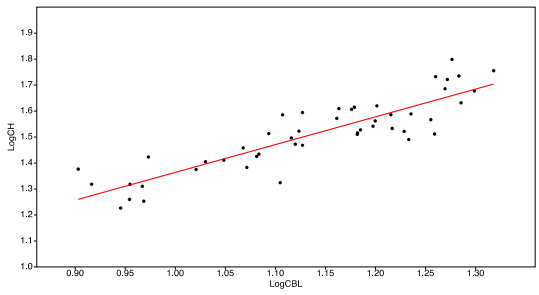

Baryonychine spinosaurids (all positions), LogCH vs. LogCBL.
Slope: 1.0686, **intercept**: 0.29548, **r2**: 0.77314.

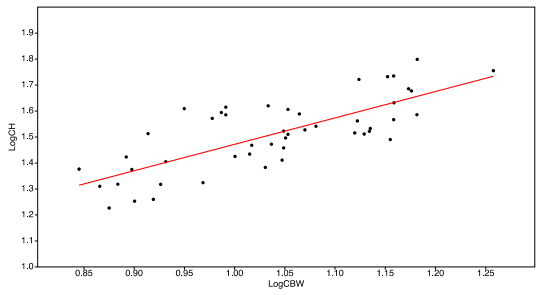

Baryonychine spinosaurids (all positions), LogCH vs. LogCBW.
Slope: 1.0161, **intercept**: 0.45603, **r2**: 0.582.

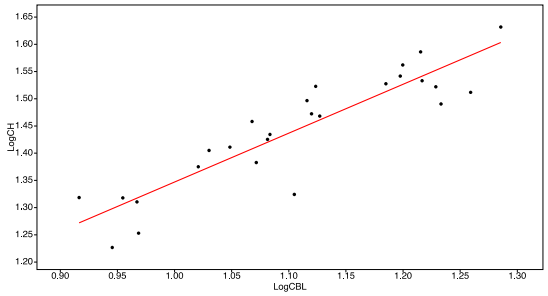

***Baryonyx* (all positions), LogCH vs. LogCBL.**
Slope: 0.89772, **intercept**: 0.44935, **r2**: 0.81304.

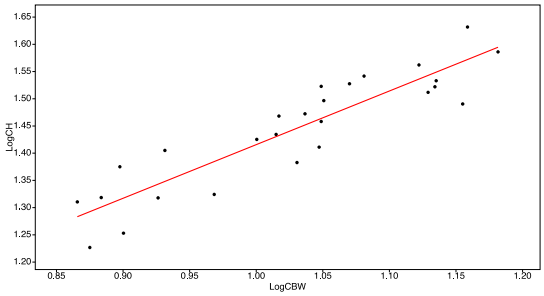

***Baryonyx* (all positions), LogCH vs. LogCBW.**
Slope: 0.9852, **intercept**: 0.43051, **r2**: 0.8198.

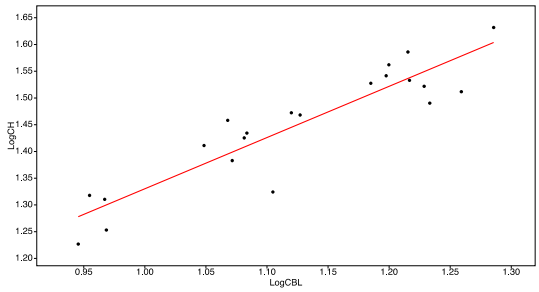

***Baryonyx* (lateral teeth only), LogCH vs. LogCBL.**
Slope: 0.95799, **intercept**: 0.37236, **r2**: 0.83866.

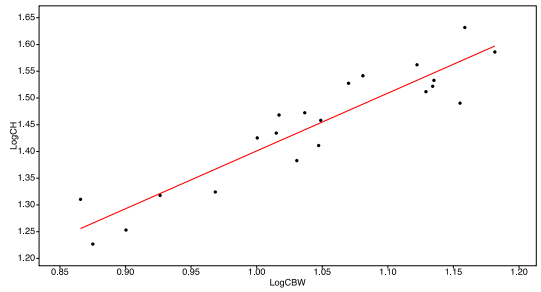

***Baryonyx* (lateral teeth only), LogCH vs. LogCBW.**
Slope: 1.0807, **intercept**: 0.32022, **r2**: 0.86066.

B.3 Phylogenetic analyses

B.3.1 Hendrickx et al. (2020) character scores for HASMG G369a

B.3.1.1 Whole dentition matrix

HASMGG369a(lateral)

??0?1211100000000100

100?000011?100?0??1?0?1?00200?0???00[03]0??????????????????0???0?

B.3.1.2 Crown-only matrix

HASMGG369a(lateral)

????????????????????????????0?12111000000001001 00?000011?100?0??1?0?1?00200?0???0

0[03]00???0

B.3.2 Full phylogenetic results

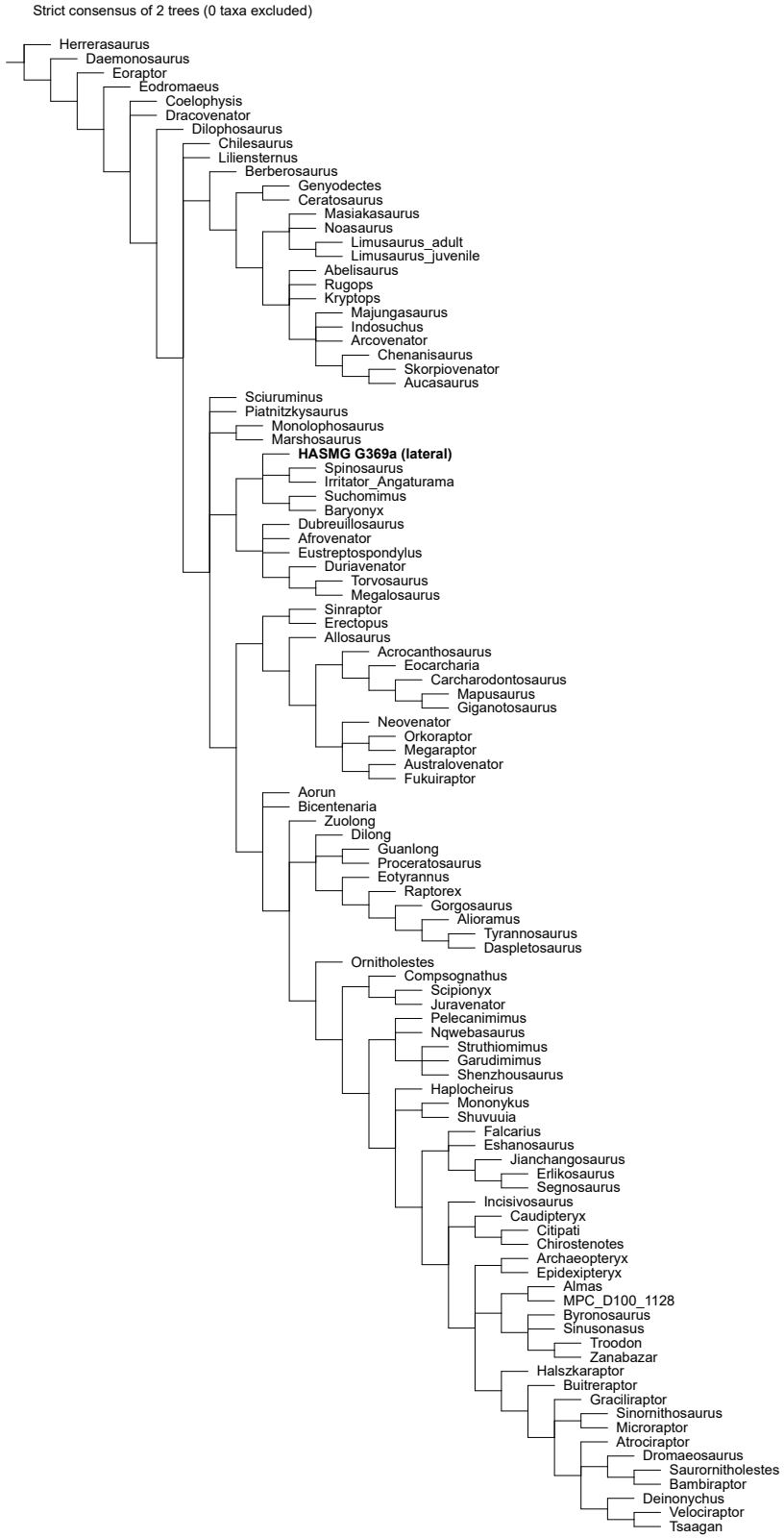

Fig B 1 Strict consensus of the constrained analysis using the whole dentition dataset.

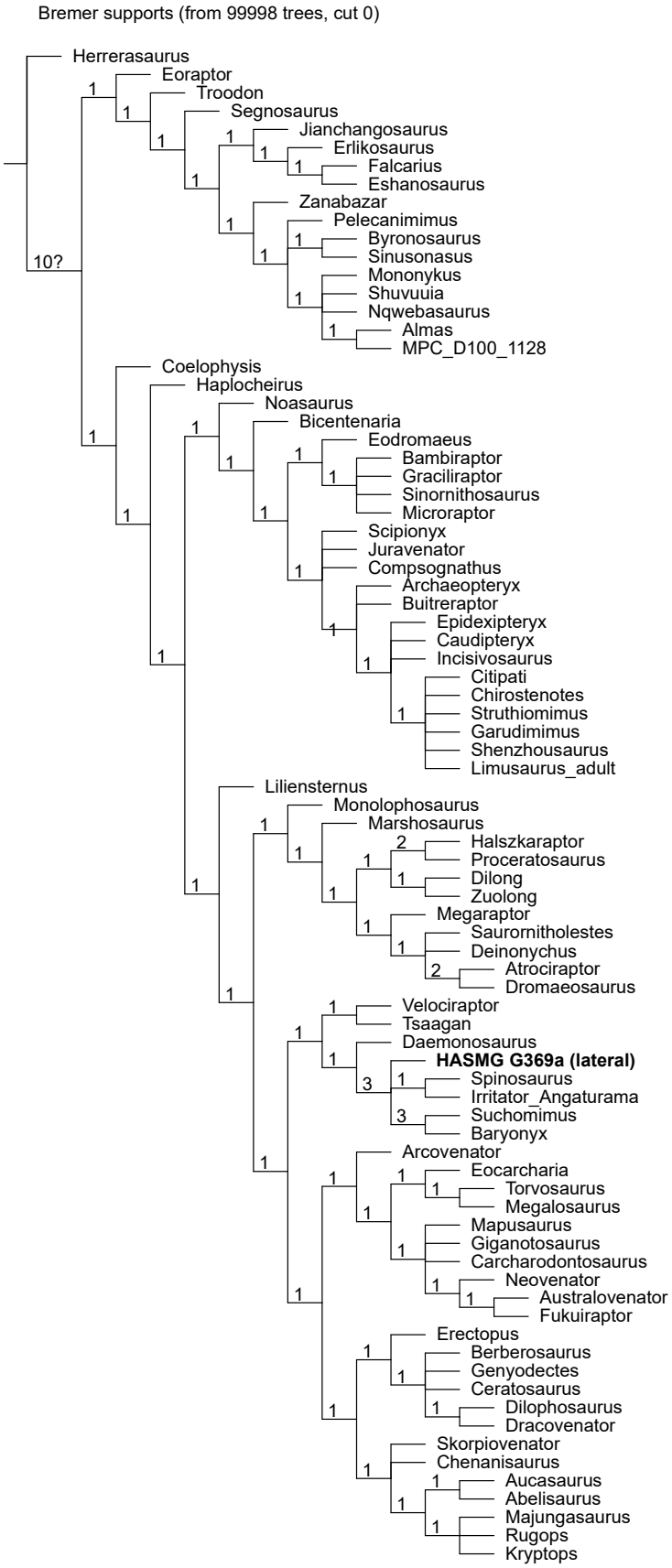

Fig B 2 Reduced consensus of the unconstrained analysis using the whole dataset.

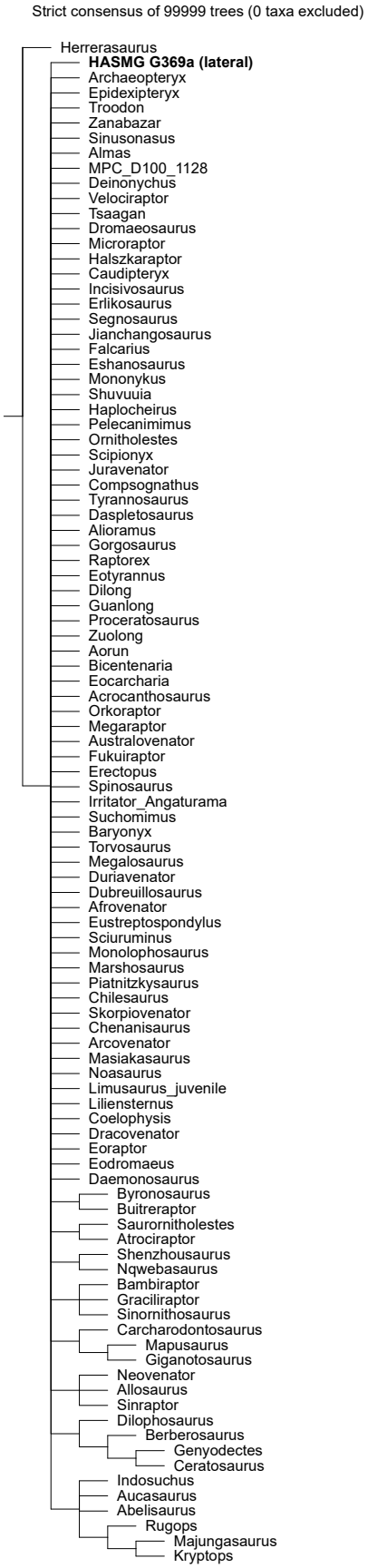

Fig B 3 Strict consensus of the unconstrained analysis using the crown-only dataset.

B.4 Cluster analyses:

Whole dataset – Hierarchical clustering

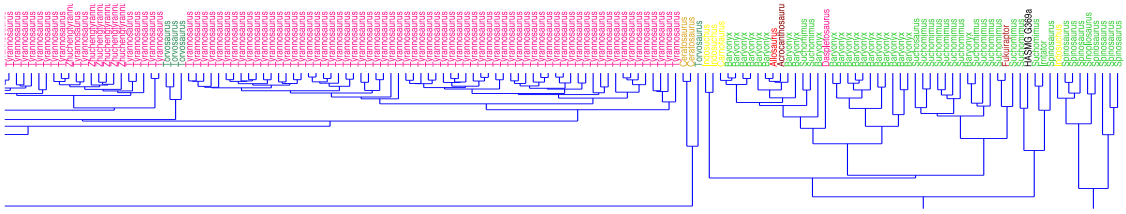

Whole dataset (no denticles = ?) – Hierarchical clustering

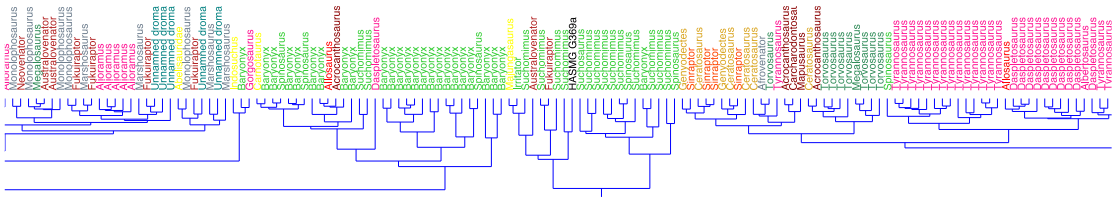

Reduced dataset – Hierarchical clustering

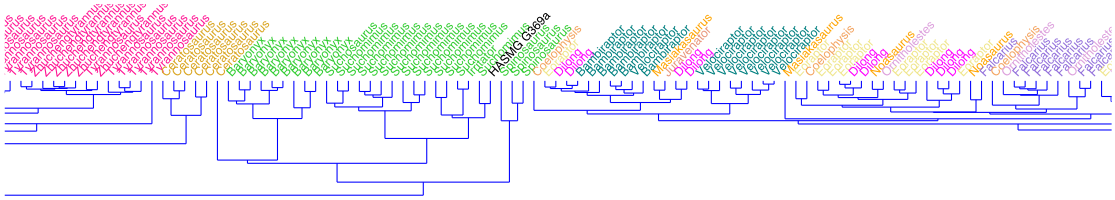

Reduced dataset (no denticles = ?) – Hierarchical clustering

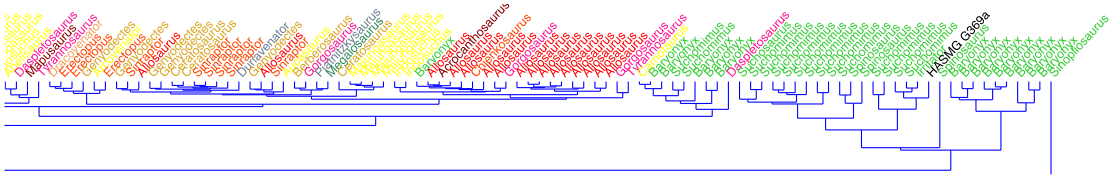

Whole dataset – Neighbour-joining

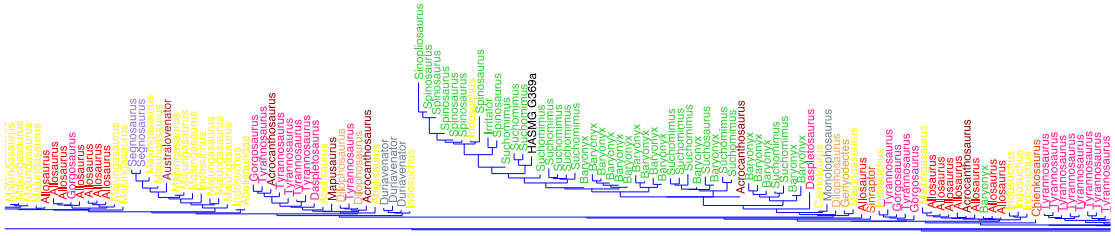

Whole dataset (no denticles = ?) – Neighbour-joining

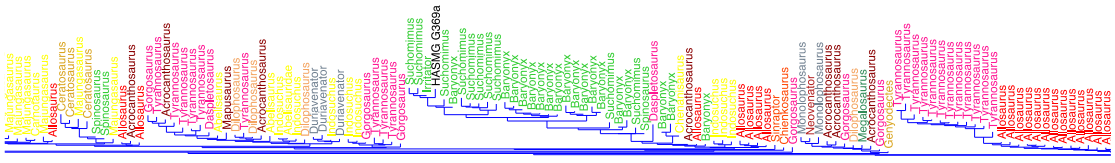

Reduced dataset – Neighbour-joining

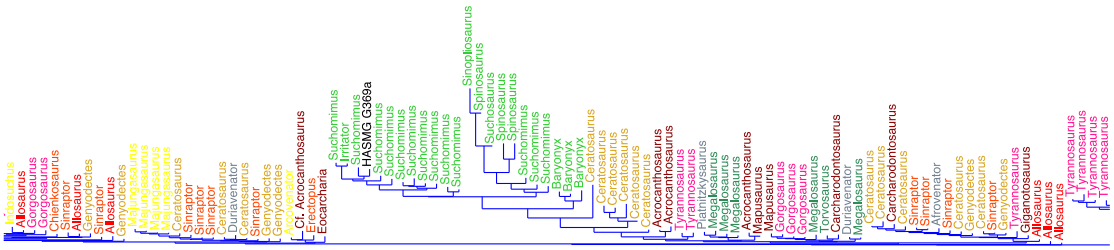

Reduced dataset (no denticles = ?) – Neighbour-joining

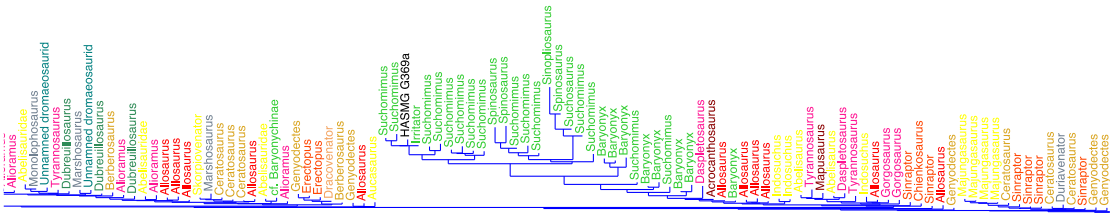

B.5 Quantitative analysis of XMDFEC V10010

B.5.1 Discriminant function analyses: results

Table B 2 Results of the discriminant function analyses on the various iterations of the pan-theropodan dataset, with XMDFEC V10010 treated as an unknown taxon

Dataset	**Discriminant Function Analysis**		**Reclassification Rate (RR)**	
	Clade level	**Taxon level**	**Clade level (%)**	**Taxon level (%)**
Whole dataset	Metriacanthosauridae	*Skorpiovenator*	60.84	61.14
Whole dataset (no denticles = ?)	Metriacanthosauridae	*Condorraptor*	62.12	59.34
My dataset	Metriacanthosauridae	*Skorpiovenator*	54.46	63.68
My dataset (no denticles = ?)	Metriacanthosauridae	*Erectopus*	59.29	60.3
Whole dataset with large teeth	Allosauridae	*Erectopus*	59.2	57.4
Whole dataset with large teeth (no denticles = ?)	Allosauridae	*Erectopus*	62.1	57.54
My dataset with large teeth	Metriacanthosauridae	*Erectopus*	58.54	61.56

My dataset with large teeth (no denticles = ?)	Metriacanthosauridae	*Erectopus*	60.8	62.06

Clade level		**Taxon level**		**Clade level (Eigenvalue)**		**Taxon level (Eigenvalue)**	
PC1 (%)	**PC2 (%)**	**PC1 (%)**	**PC2 (%)**	**Axis 1**	**Axis 2**	**Axis 1**	**Axis 2**
50.89	19.86	41.04	21.57	5.7081	2.2272	18.374	9.6563
50.08	19.11	42.86	17.09	5.7905	2.2091	18.01	7.1806
57.04	21.78	41.07	24.73	12.239	4.6732	24.992	15.051
54.09	22.79	41.4	25.68	11.008	4.6388	23.75	14.731
37.97	31.01	35.48	27.85	1.9237	1.5713	6.2636	4.9158
39.64	30.5	36.25	22.59	2.2061	1.6975	6.0601	3.7752
48.45	27.08	54.31	18.43	2.2474	1.2559	12.99	4.4081
57.88	22.98	45.27	21.19	3.4446	1.3678	9.3725	4.3866

B.5.2 Cluster analyses: results

Table B 3 Results of the cluster analyses on the various iterations of the pan-theropodan datasets, with XMDFEC V10010 treated as an unknown taxon.

Dataset	**Cluster Analysis**	
	Hierarchical clustering	**Neighbour joining**
Whole dataset	Abelisauridae indet.	Abelisauridae indet. *+ Fukuiraptor*
Whole dataset (no denticles = ?)	Abelisauridae indet.	Abelisauridae indet. *+ Fukuiraptor*
My dataset	Abelisauridae indet.	*Arcovenator*
My dataset (no denticles = ?)	Abelisauridae indet.	Abelisauridae indet.
Whole dataset with large teeth	Abelisauridae indet.	Abelisauridae indet.
Whole dataset with large teeth (no denticles = ?)	Abelisauridae indet.	Abelisauridae indet. *+ Fukuiraptor*
My dataset with large teeth	Abelisauridae indet.	Abelisauridae indet.

My dataset with large teeth (no denticles = ?)	Abelisauridae indet.	Abelisauridae indet.

Whole dataset – Hierarchical clustering

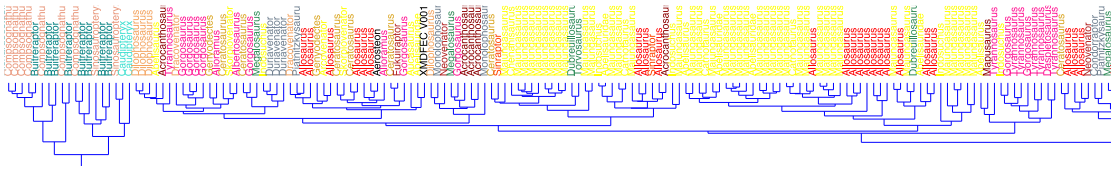

Whole dataset (no denticles = ?) – Hierarchical clustering

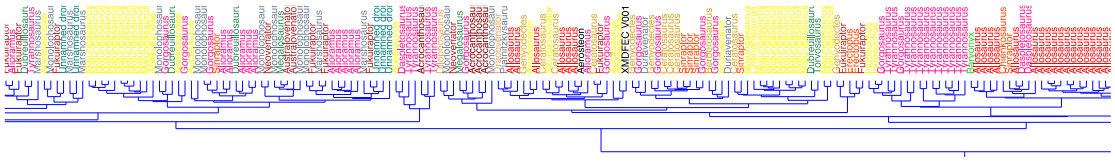

Reduced dataset – Hierarchical clustering

Reduced dataset (no denticles = ?) – Hierarchical clustering

Whole dataset large teeth only – Hierarchical clustering

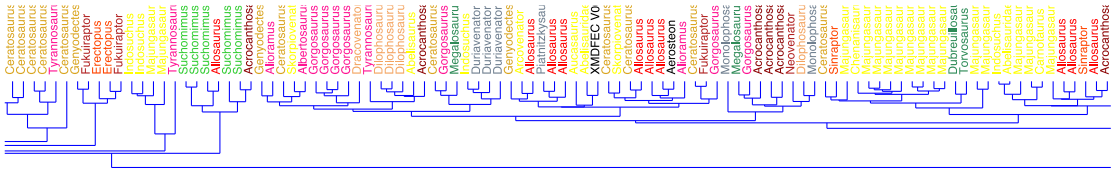

Whole dataset large teeth only (no denticles = ?) – Hierarchical clustering

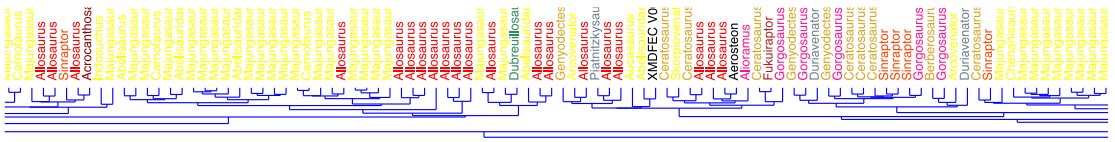

Reduced dataset with large teeth – Hierarchical clustering

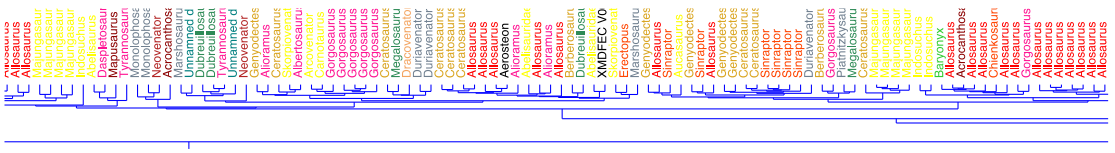

Reduced dataset with large teeth (no denticles = ?) – Hierarchical clustering

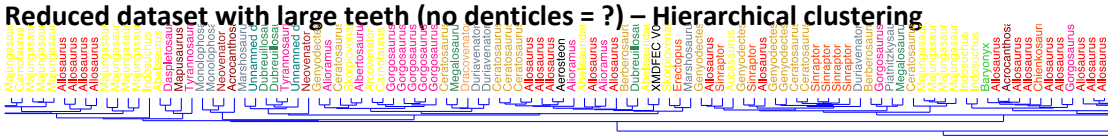

Whole dataset – Neighbour-joining

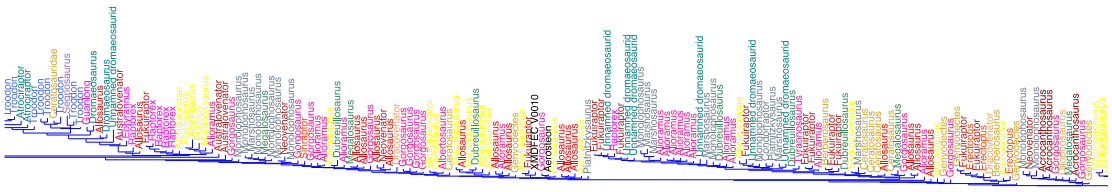

Whole dataset (no denticles = ?) – Neighbour-joining

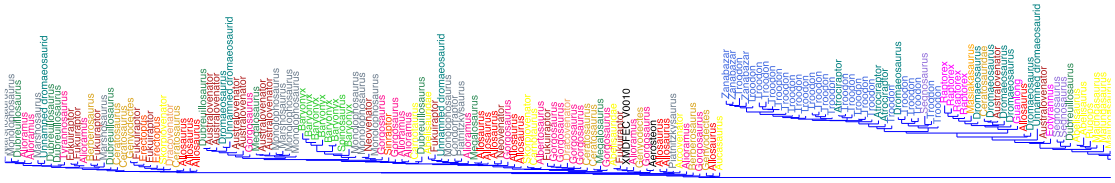

Reduced dataset – Neighbour-joining

Reduced dataset (no denticles = ?) – Neighbour-joining

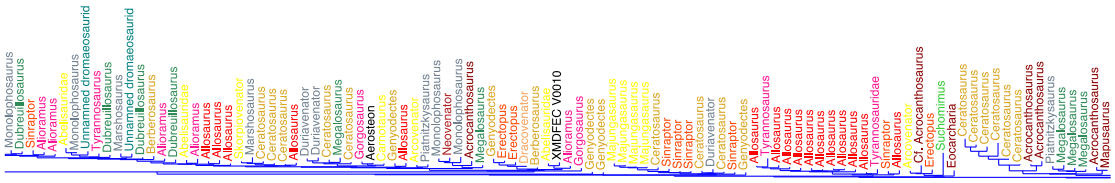

Whole dataset with large teeth– Neighbour-joining

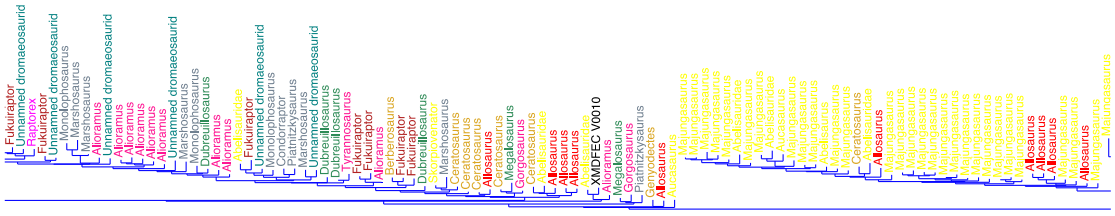

Whole dataset with large teeth (no denticles = ?) – Neighbour-joining

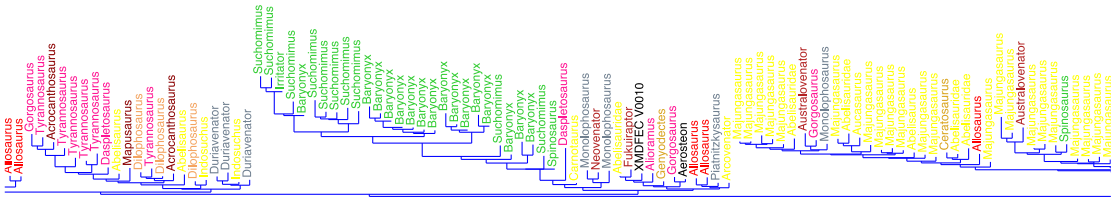

Reduced dataset with large teeth – Neighbour-joining

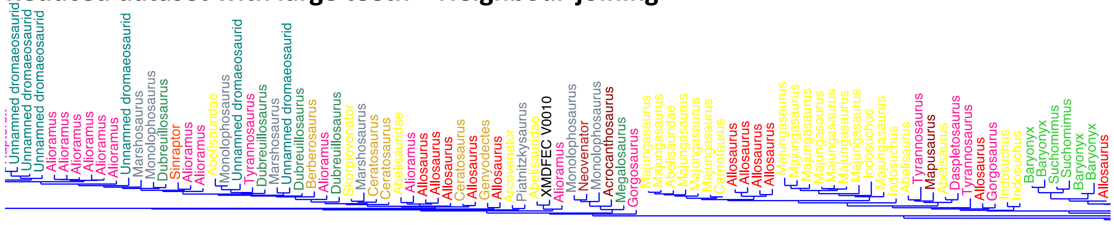

Reduced dataset with large teeth (no denticles = ?) – Neighbour-joining

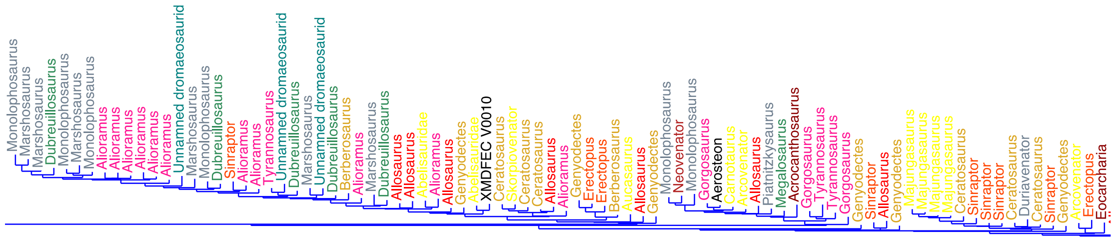

Appendix C Supplementary information for Chapter 4

A European giant: remains of a large spinosaurid (Dinosauria: Theropoda) from the Vectis Formation (Wealden Group, Early Cretaceous), UK.

Note that the full supplementary files, including scripts for the phylogenetic analyses, can be found with the published article online.

C.1 Indeterminate bone fragments:

Several other bone fragments were recovered along the stretch of foreshore near Compton Chine, covered in adhering matrix matching that of the White Rock Sandstone equivalent (Figure C 1). Unfortunately we were unable to identify these pieces, however we provide brief descriptions and imagery of the larger fragments below. The other pieces are largely bone shards and not dealt with here.

C.1.1 Fragment 1

Abrasion and exposure of the underling cancellous bone affects all surfaces and margins (to varying degrees), and what remains of the element has suffered three transverse cracks. As such, the true morphology of the fragment is unknown, and the element is only dealt with briefly here.

It has a maximum preserved length of 228 mm and mediolateral width of 79 mm. Exposure of the internal bone structure reveals cortical bone of various thicknesses and an absence of any internal cavitation. The cortical bone may be extremely thin in places (e.g. ~2mm where exposed in the large notch on the anterolateral surface). One side of the fragment possesses intact cortical bone and displays a flattened topology (Figure C 1.1A). Whilst the adjacent surface on the same side also appears similarly flattened, this portion has been abraded as evidenced by the exposure of the underlying cancellous bone. The topography of the opposite surface (Figure C 1.1B) is variable, producing a pair of convexities at either end; a coronal cross section through these structures would accordingly produce a hummocky margin (Figure C 1.1C).

C.1.2 Fragment 2

The large and slightly abraded piece vaguely resembles a peduncle of an ilium, with an exposed cross-section revealing thin cortical bone. One surface of the fragment is flat (Figure C 1.2A),

whilst the opposite produces a pair of concavities separated by a low ridge (Figure C 1.2B). The third preserved surface is convex and tapers towards one end (Figure C 1.2C). It has a maximum preserved length of 125.5 mm and height of 103.6 mm (when positioned as in Figure C 1.2A).

C.1.3 Fragments 3 and 4

These fragments likely pertain to pieces of ilium given their triradiate (Figure C 1.3) and triangular cross-sections (Figure C 1.4), although their precise position relative to the iliac pieces described in the main text are more difficult to ascertain.

The smaller fragment of the pair has thin cortical bone and produces two largely flat sides that converge towards one another (Figure C 1.A) and a notably concave third (Figure C 1.B). The latter has a maximum width of 92.8 mm and is pierced by three small (and presumably vascular) foramina inset within shallow channels.

The substantially abraded surface of the larger fragment (Figure C 1.A) suggesting it was closely associated with the fragments described in the main text; this abraded surface would thus correspond to the medial surface if genuine, with the opposite surface preserving part of the brevis fossa (Figure C 1.4B). The latter surface has a maximum width of 152.3 mm.

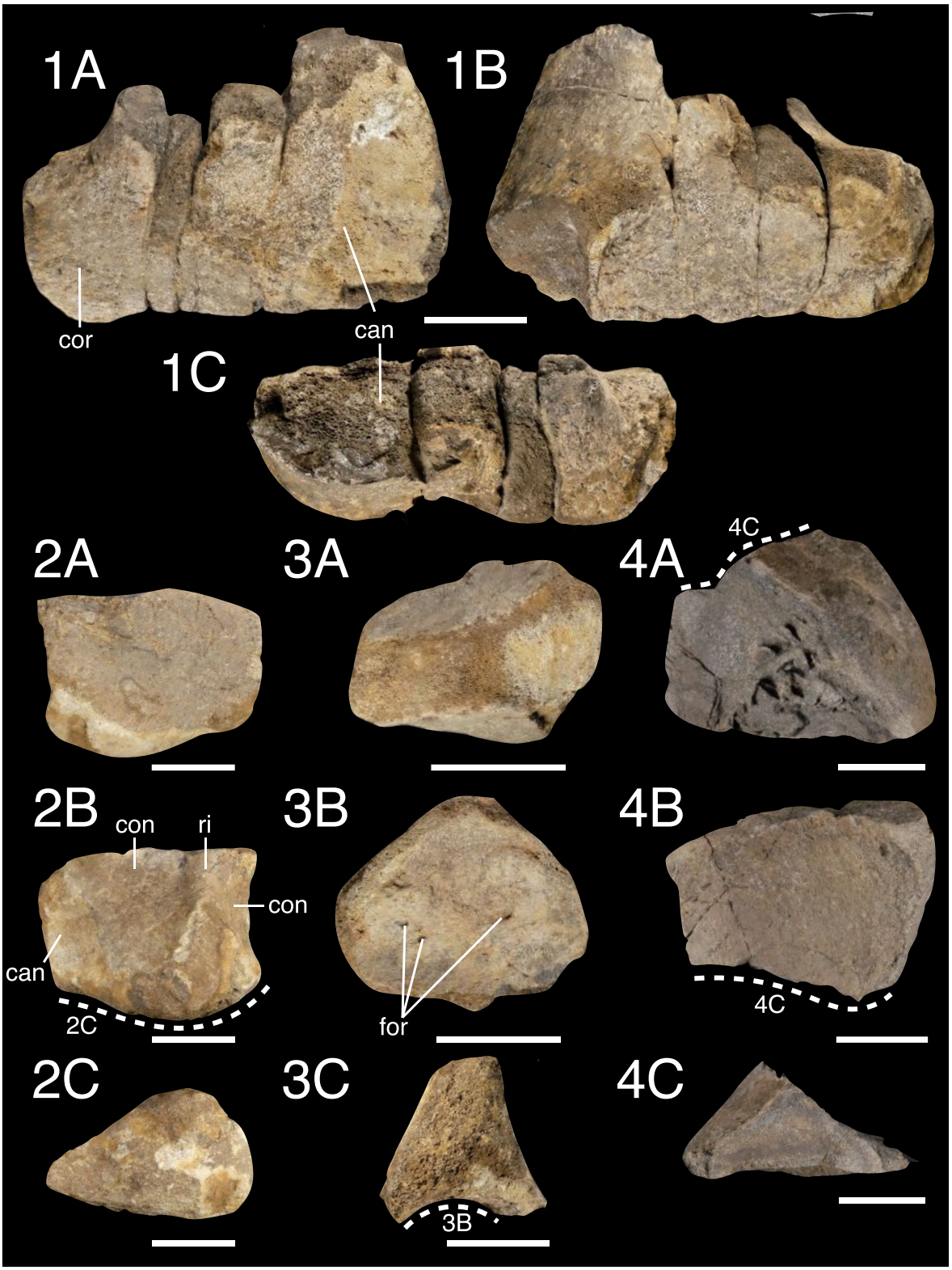

Figure C 1 Indeterminate bone fragments 1–4 (see Appendix C.1 for brief descriptions) referred to IWCMS 2018.30. Dashed lines indicate surfaces presented in other views (see respective enumeration). Abbreviations: can: cancellous bone; con: concavity; cor: cortical bone; for: foramina; ri, ridge. Scale bars: 50mm.

C.2 Phylogenetic results

C.2.1 Character scores for the phylogenetic analysis

The character string for the White Rock spinosaurid (see below) was added to the matrix presented in Appendix A.1.5. The full TNT script can be found online with the published article.

VectisSpino
??
??
??????????????????????1?????????????????????????????????101?1???????00????????????????????
??
?0?0??????????100????0???0?????????????????????????????????1?????????????????????????
??
??1????????
??????????????????????1??
??
??????????????????????????????????????0??
????????0?????????????????????1?????????????????????????????????00?0?????????????
??0??????????????????????
?????1??
??1??
????????????0????????????0??
??
??????????????????????????????????????0??
??????????????????0??
??????????????????????????????????1?????????????????????????1????????????????????????
0??
??????????????????????0???1?????????
????0?0

C.2.2 Full phylogenetic results

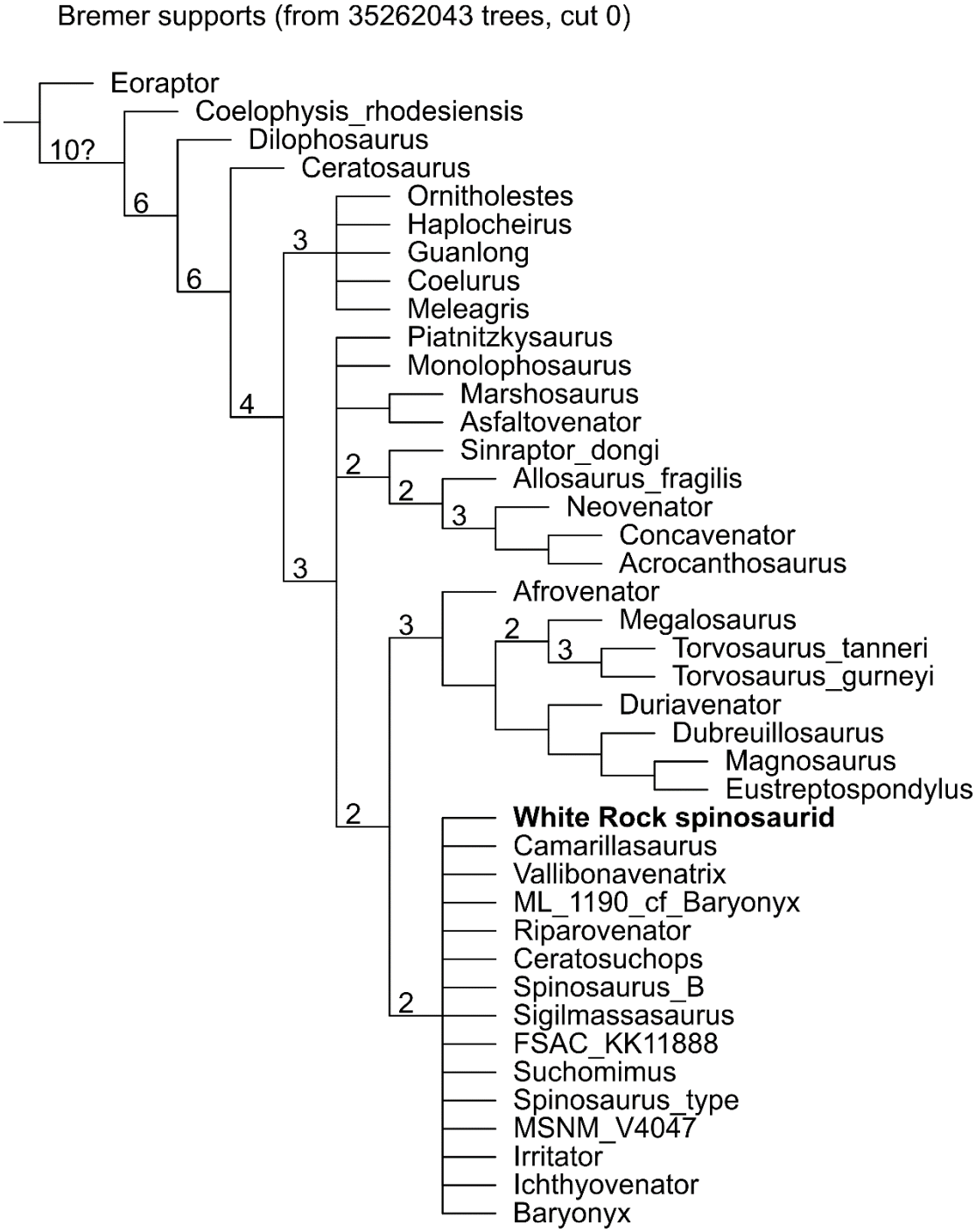

Figure C 2 Strict consensus tree. Numbers above the nodes indicate Bremer support values (>1).

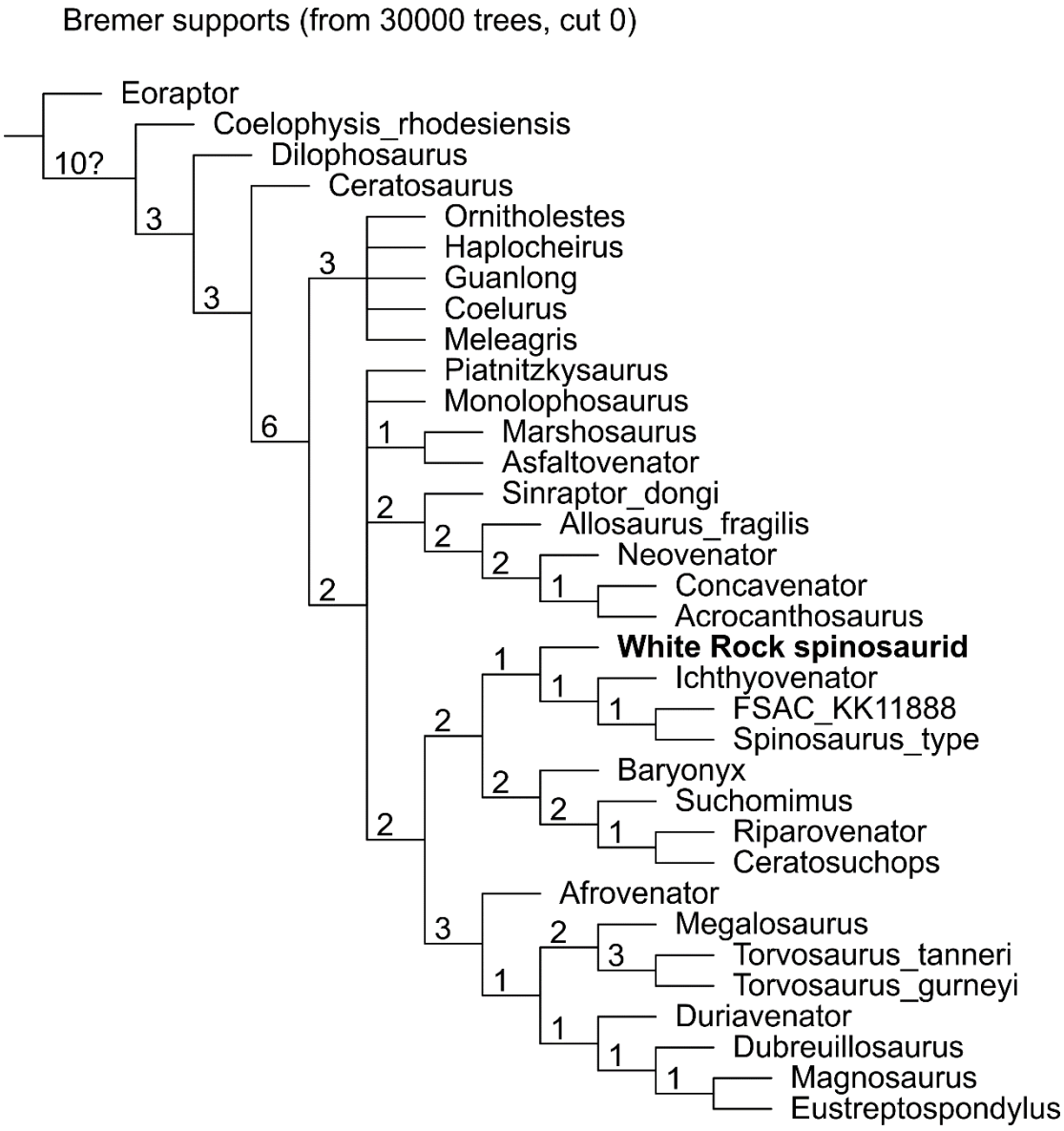

Figure C 3 Reduced consensus following pruning of wildcard OTUs. Numbers at nodes represent Bremer support values.

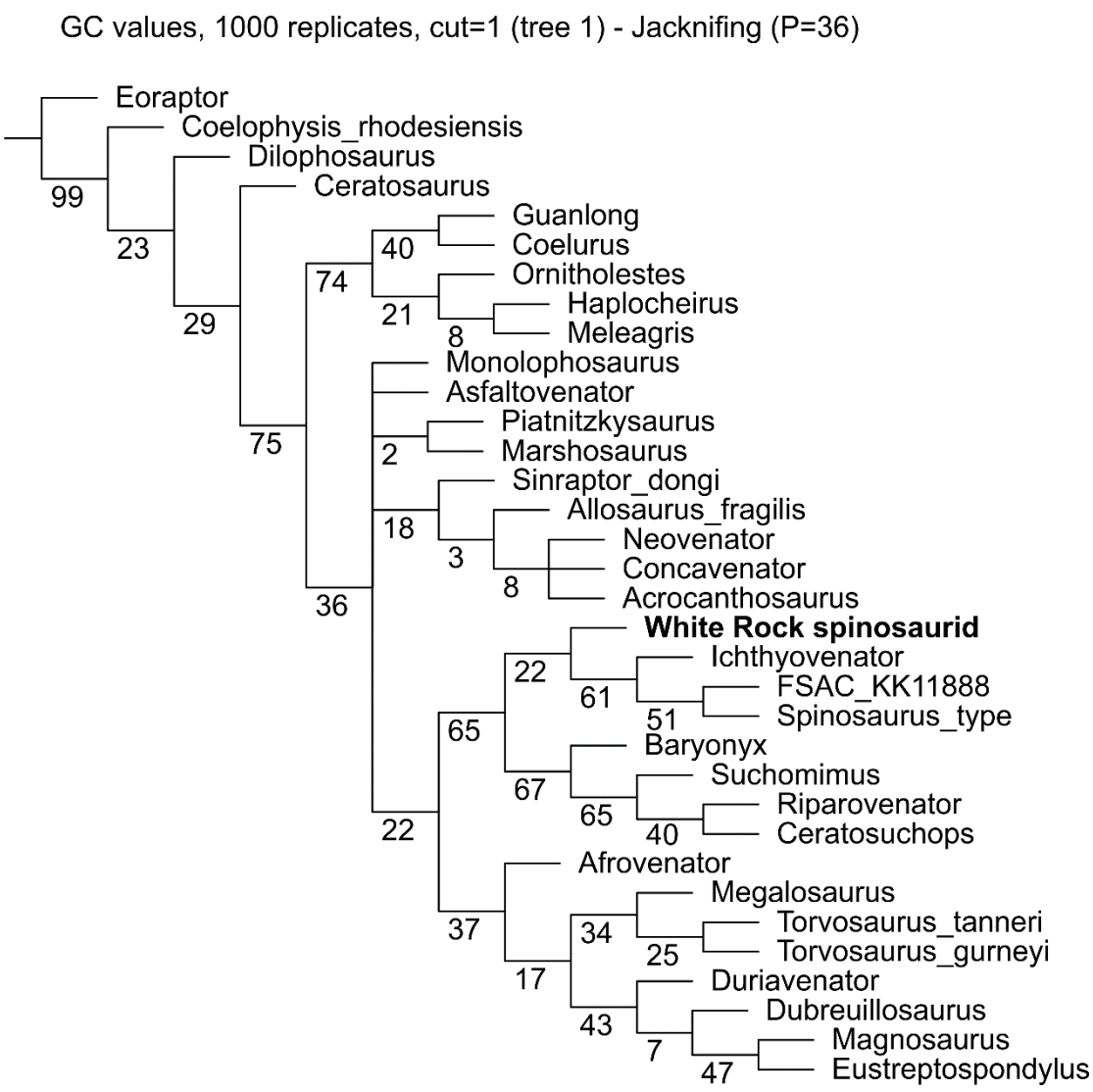

Figure C 4 Jackknife resampling for nodal support (absolute support) following exclusion of wildcard OTUs. Numbers below nodes indicate jackknife values.

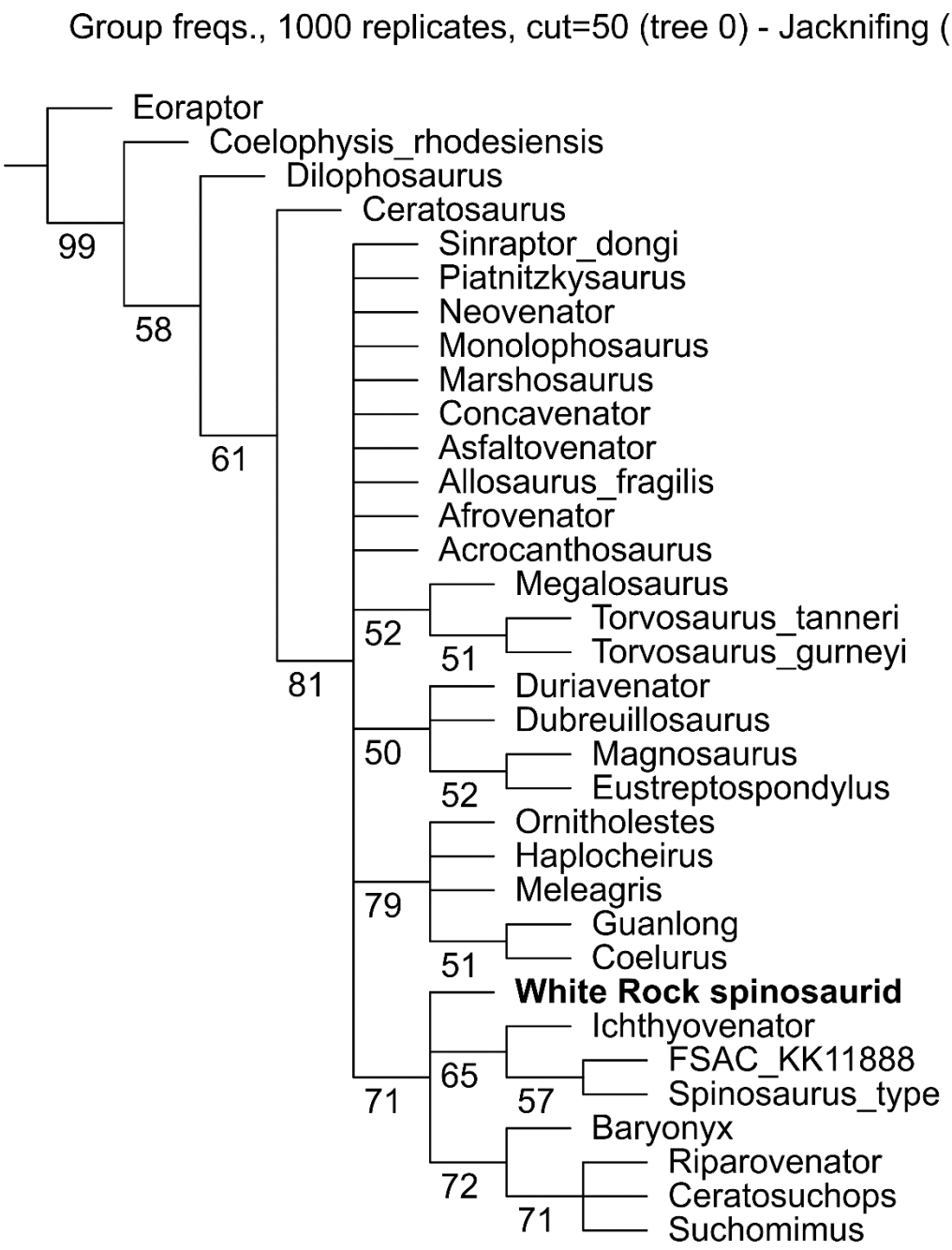

Figure C 5 Jackknife resampling for nodal support (GC frequency values) following exclusion of wildcard OTUs. Numbers below nodes indicate jackknife values.

Appendix D Supplementary information for Chapter 5

Modified skulls but conservative brains? The palaeoneurology and endocranial anatomy of baryonychine dinosaurs (Theropoda: Spinosauridae)

D.1 Methodology

Here we provide additional information regarding the rearticulation of the *Ceratosuchops* braincase and generation of the endocast figured and described in the main text. An overview of our workflow is provided in Fig. S1.

D.1.1 Braincase rearticulation and slice generation

We used 3D Slicer (v. 4.11.20210226) to rearticulate STLs of the braincase components via the registration of landmarks using the *Fiducial Registration Wizard* module, available through the *IGT extension* (Ungi et al., 2016). The registration of landmarks borrows from the method outlined by Carvalho et al. (2022). Alignment was achieved by the sequential addition of "floating" elements (the isolated right otoccipital of IWCMS 2014.95.3, followed by IWCMS 2014.95.2 and 2014.95.1) to a "static" element (the isolated basioccipital-basisphenoid complex IWCMS 2014.95.3).

Firstly, segmented braincase regions of interest (ROIs) were converted into contour meshes in ORS Dragonfly (*3D Modelling>Generate Contour Mesh*), exported as STLs (*Export>Mesh to File*), and then imported into 3D Slicer. Here, landmark point pairs were inserted, in the same order, on to the "static" element (*Fiducial Registration Wizard>From fiducials>Create new MarkupsFiducial*) and on the equivalent contacts on the "floating" elements (*Fiducial Registration Wizard>To fiducials>Create new MarkupsFiducial*).

A new linear transform node was generated (*Place fiducials using transforms>Registration result (From->To) transform>Create new LinearTransform*), with parameters set to *Rigid*, *Manual* and *Auto-update*. Application of this linear transformation was achieved in the *Data* module using the "static" model (*Subject hierarchy>Node>Applied transform* column). The rearticulated models were merged by first hardening the linear transformation (*Subject hierarchy>Node>Applied transform* column>*Harden transform*), followed by the *Merge Models* function in the *Surface Model* module. The newly rearticulated model now formed the basis of the next landmark registration, acting as the "static" model.

We consider the fully rearticulated braincase generated here to represent a "best fit" reconstruction. Whilst most contacts are relatively "clean", we do note that the left prootic likely possesses a minor degree of taphonomic distortion. This has resulted in the merging of this element with the ipsilateral otoccipital in its dorsal part, and we were unable to achieve the natural overlap of the former over the latter without sacrificing contacts elsewhere. This, however, has not impacted the morphology of the endocranial cavity.

Whilst 3D slicer can convert 3D models to 2D image stacks (e.g. *3D Slicer documentation>Developer Guide>Script repository>Rasterize a model and save it to a series of image files*) necessary for the segmentation of the endocranial cavity, this function repeatedly caused the computer to crash. Instead, we exported the rearticulated braincase STL from 3D Slicer and used *Voxelizer* (available at: https://drububu.com/miscellaneous/voxelizer/?out=obj) to convert the rearticulated braincase to a 2D image stack for segmentation of the endocranial cavity. To reduce the computational needs for this conversion, the rearticulated braincase STL was edited in Meshmixer (Autodesk Inc.) using the *Lasso* tool to remove portions of the braincase that did not immediately delineate the endocranium. This reduced braincase STL was subsequently converted into an image stack containing 1005 slices, the latter being reimported into ORS Dragonfly for segmentation. Unfortunately, this method does mean the rearticulated braincase data lacks appropriate voxel dimensions, and an inability to readjust to a common resolution using median voxel size (i.e. 103.3µm^3; R. Broadman, pers. comms., 2022) meant STLs of the endocranial cavity and CN II-V had to be scaled manually (see below).

D.1.2 Segmentation

Four disarticulated bone units contained neurovascular ROIs for segmentation:

1) The skull roof fragment (IWCMS 2014.95.1: CN II–V, both sides);
2) The supraoccipital-left otoccipital complex (IWCMS 2014.95.2: left CN IX–XII, posterior middle cerebral veins, left supraoccipital+otoccipital and right supraoccipital portions of the endosseous labyrinths).
3) A basicranial complex (IWCMS 2014.95.3: left CN VI and VII, right CN IV–VIII, carotid arteries, prootic portion of the endosseous labyrinth);
4) The isolated right otoccipital (IWCMS 2014.95.3: right CN IX–XII, partial endosseous labyrinth);

Segmentation of the individual neurovascular features posterior to cranial nerve (CN) V was conducted on the raw image files of IWCMS 2014.95.2–3, whilst the image stack of the rearticulated braincase generated above was used to segment the endocranial cavity and CN II-V.

ROIs were manually segmented in Dragonfly using the *Full* and *Adaptive Gaussian* brush tools between XY, YZ, and XZ planes. Segmentation of the rearticulated endocranial cavity also involved the *Polygon* tool in 3D view.

The right otoccipital is preserved detached from but in close association with the basioccipital-basisphenoid complex (IWCMS 2014.95.3); both are separated by a thin layer of matrix. These ROIs were segmented in 2D using the *Adaptive Gaussian* brush implemented with the *Multi-slice* function, using both upper and lower range functions across the filtered and original slices. All ROIs were submitted to a final round of processing via a Connected Components analysis (*Connected Components>New Multi-ROI (26 connected)>Analysis*) to remove stray voxels using a volume filter, implemented using the *Statistical Properties* of the *Object Analysis* dialog box. ROIs excluding stray voxels were selected and saved.

D.1.3 Endocast reassembly

In order to maintain the relative positioning between the neurovascular features in each bone unit (1-4, see above), individual neurovascular features within each unit were assimilated into a single ROI in ORS Dragonfly. Contour meshes of the new assimilated ROIs, whose properties are listed in Table D 1, were generated and saved as STLs.

Table D 1 Properties inputted in the *Dataset Tools* tab that were used to generate the neuroanatomical meshes in ORS Dragonfly prior to exportation as STL files.

Mesh No.	Neurovascular components	Threshold	Sampling	Smoothing (no. of iterations)
1	Endocranial cavity	50	2	10
2	Skull roof (CN II–IV)	50	2	5
3	Basicranial complex (left CN VI and VII, right CN VI–VIII, right endosseous labyrinth [prootic portion])	50	3	10
4	Right otoccipital (right CN IX–XII, right endosseous labyrinth [otoccipital portion])	50	3	10

5	Conjoined supraoccipital and left otoccipital complex (left CN IX–XII, left endosseous labyrinth (supraoccipital and otoccipital portions), right endosseous labyrinth [supraoccipital portion])	50	3	10

The STLs of the various neurovascular components were imported into Meshmixer for colouration and reassembly. Colouration of the STL surfaces occurred prior to reassembly and was achieved using the *Sculpt* function. The rearticulated braincase STL generated above was sagittally sliced using the *Plane Cut* function (*Edit>Plane Cut; Cut Type: Cut (Discard Half)*) along its mid-length to serve as a basis for the reassembly of the endocranial and neurovascular components. The better-preserved right side of the braincase was used for this purpose.

Reassembly utilised the *Transform* tool (*Edit>Transform*), using the *3D Transform Widget* to manually move the various STLs. Firstly, the endocast of the endocranial cavity and the CN II-V nerve trunks were combined and manually scaled using the *Uniform Scaling* tool and inserted into the corresponding cavity in the braincase. Landmarks such as the borders of the olfactory tract, CN II–IV foramina, and dorsal expansion of the endocast were used to ensure scaling was accurate. Scaling was not necessary for the more posterior neurovascular components given that these were generated from scan data on known voxel dimensions, and these were serially appended and combined. Various external foramina and endocranial cavity endocast topography were similarly used to ensure accurate reassembly of these latter components.

In order to reassemble the neurovascular components from the supraoccipital-left otoccipital unit (IWCMS 2019.45.2), a contour mesh of the conjoined bones was generated and exported as an STL. Both files were appended to the main endocast model. These were selected and manually superimposed in tandem onto the rearticulated half of the supraoccipital using the *Transform* function, with the bone model subsequently deleted once in place, thus leaving the neurovascular components appropriately reassembled.

Given the disarticulated nature of the *Ceratosuchops* braincase, we acknowledge that the reassembly outlined here represent an estimated, “best fit” reconstruction of the endocast.

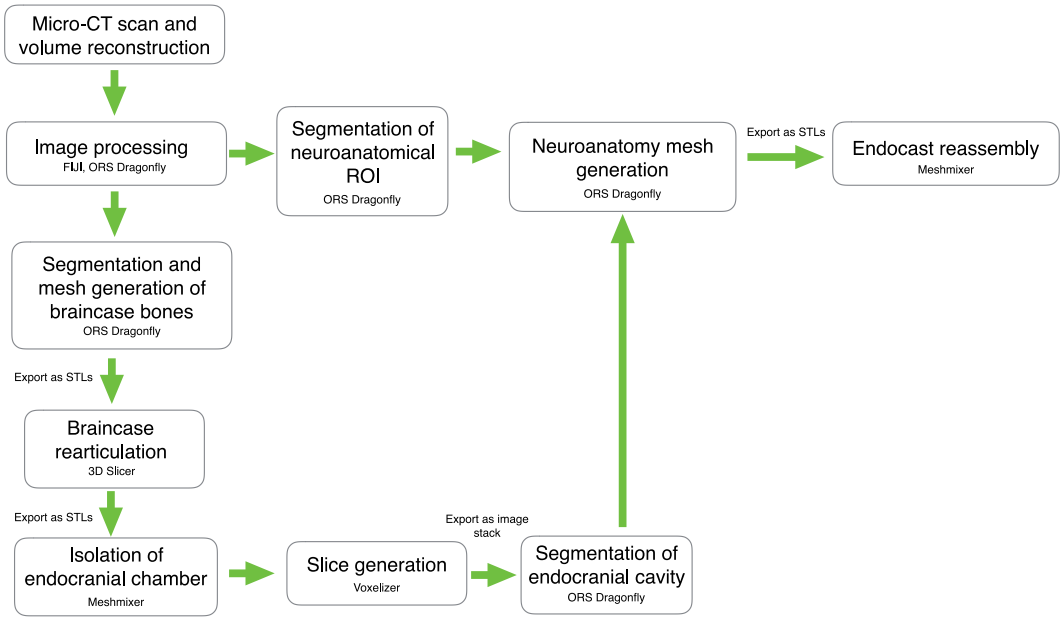

Figure D 1 Schematic workflow of the *Ceratosuchops* braincase rearticulation process, segmentation of the endocranial structures, and reassembly of the final endocast described in the main text.

Appendix E Supplementary information for Chapter 6

A highly pneumatic middle Cretaceous theropod from the British Lower Greensand

E.1 Phylogenetic analysis

Character scores for *Vectaerovenator inopinatus*, based on the character matrix of (Cau, 2018). The full TNT script is available online.

???
???
?????????????????????110?????????10110??0?0100?00??0-
001010??0???00???
???????????????????????????????????????0?0??????????????????0?0?????????????????????
???
?????????????????????????????????????0?????????????????????????????????0????????????
??0????????0??????
??????1???????1????????-
??????0???1???????0???????????1???
???????????????????0??0???????????0
1????????????1?????00?????????????????????????-
?????????????????????????0??????0?0??0??10?
0????????????????????????????0???????10??
??????????????????0??10??????????????????????????????????????0?0?????????????????????
????????????1??1??????0??????????????1??????
???
????????????????1????????????1??
?????????????????????????????????????0?????????????????????????????????01?????????????
???11???
?????????????1?????????????????????0???
??????????????????????????0???1?????????
????????????????????????????????

List of References

Abel, R. L., Laurini, C. R. and Richter, M. (2012) A palaeobiologist's guide to 'virtual'micro-CT preparation. *Palaeontologia Electronica*, 15(2), 1–-16.

Acuna, E. and Rodriguez, C. (2004) 'The treatment of missing values and its effect on classifier accuracy', in Banks, D. *et al.* (eds.) *Classification, clustering, and data mining applications*. Springer, 639–647.

Alfaro, M. E. and Holder, M. T. (2006) The posterior and the prior in Bayesian phylogenetics. *Annual Review of Ecology, Evolution, and Systematics*, 37, 19–42.

Allain, R. (2014) New material of the theropod *Ichthyovenator* from Ban Kalum type locality (Laos): implications for the synonymy of *Spinosaurus* and *Sigilmassasaurus* and the phylogeny of Spinosauridae, *74th Annual Meeting of Society of Vertebrate Paleontology*.

Allain, R., Vullo, R., Rozada, L., Anquetin, J., Bourgeais, R., Goedert, J., Lasseron, M., Martin, J. E., Pérez-García, A. and De Fabrègues, C. P. (2022) Vertebrate paleobiodiversity of the Early Cretaceous (Berriasian) Angeac-Charente Lagerstätte (southwestern France): implications for continental faunal turnover at the J/K boundary. *Geodiversitas*, 44(25), 683–752.

Allain, R., Xaisanavong, T., Richir, P. and Khentavong, B. (2012) The first definitive Asian spinosaurid (Dinosauria: Theropoda) from the early cretaceous of Laos. *Naturwissenschaften*, 99(5), 369–377.

Allemand, R., Abdul-Sater, J., Macrì, S., Di-Poï, N., Daghfous, G. and Silcox, M. T. (2022) Endocast, brain, and bones: Correspondences and spatial relationships in squamates. *The Anatomical Record*, 1–23.

Alonso, A. and Canudo, J. I. (2016) On the spinosaurid theropod teeth from the early Barremian (Early Cretaceous) Blesa Formation (Spain). *Historical Biology*, 28(6), 823–834.

Alonso, A., Gasca, J., Navarro-Lorbés, P., Rubio, C. and Canudo, J. (2018) A new contribution to our knowledge of the large-bodied theropods from the Barremian of the Iberian Peninsula: the "Barranco del Hocino" site (Spain). *Journal of Iberian Geology*, 44(1), 7–23.

Amiot, R., Buffetaut, E., Lécuyer, C., Fernandez, V., Fourel, F., Martineau, F. and Suteethorn, V. (2009) Oxygen isotope composition of continental vertebrate apatites from Mesozoic formations of Thailand; environmental and ecological significance. *Geological Society, London, Special Publications*, 315(1), 271–283.

Amiot, R., Buffetaut, E., Lécuyer, C., Wang, X., Boudad, L., Ding, Z., Fourel, F., Hutt, S., Martineau, F. and Medeiros, M. A. (2010a) Oxygen isotope evidence for semi-aquatic habits among spinosaurid theropods. *Geology*, 38(2), 139–142.

Amiot, R., Wang, X., Lécuyer, C., Buffetaut, E., Boudad, L., Cavin, L., Ding, Z., Fluteau, F., Kellner, A. W. and Tong, H. (2010b) Oxygen and carbon isotope compositions of middle Cretaceous vertebrates from North Africa and Brazil: ecological and environmental significance. *Palaeogeography, Palaeoclimatology, Palaeoecology*, 297(2), 439–451.

Andrews, W. and Jukes-Browne, A. (1894) The Purbeck beds of the Vale of Wardour. *Quarterly Journal of the Geological Society*, 50(1-4), 44–71.

Apesteguía, S., Smith, N. D., Valieri, R. J. and Makovicky, P. J. (2016) An unusual new theropod with a didactyl manus from the Upper Cretaceous of Patagonia, Argentina. *PloS one*, 11(7), e0157793.

Aragão, P. R. L. (2021) *Dentes fósseis de arcossauros da Formação Feliz Deserto (Cretáceo Inferior), Bacia de Sergipe-Alagoas*. Bachelors Thesis. Universidade Federal de Sergipe, Brazil.

Arai, M. and Assine, M. L. (2020) Chronostratigraphic constraints and paleoenvironmental interpretation of the Romualdo Formation (Santana Group, Araripe Basin, Northeastern Brazil) based on palynology. *Cretaceous Research*, 116, 104610.

Aranciaga Rolando, A. M., Novas, F. E. and Agnolín, F. L. (2019) A reanalysis of *Murusraptor barrosaensis* Coria & Currie (2016) affords new evidence about the phylogenetical relationships of Megaraptora. *Cretaceous Research*, 99, 104–127.

Arden, T. M. S., Klein, C. G., Zouhri, S. and Longrich, N. R. (2019) Aquatic adaptation in the skull of carnivorous dinosaurs (Theropoda: Spinosauridae) and the evolution of aquatic habits in spinosaurids. *Cretaceous Research*, 93, 275–284.

Assine, M. L., Perinotto, J. d. J., Custódio, M. A., Neumann, V., Varejão, F. and Mescolotti, P. (2014) Sequências deposicionais do andar Alagoas da Bacia do Araripe, nordeste do Brasil. *Boletim de Geociências da Petrobras*, 22(1), 3–28.

Aureliano, T., Ghilardi, A. M., Buck, P. V., Fabbri, M., Samathi, A., Delcourt, R., Fernandes, M. A. and Sander, M. (2018) Semi-aquatic adaptations in a spinosaur from the Lower Cretaceous of Brazil. *Cretaceous Research*, 90, 283–295.

Austen, P. A. and Batten, D. J. (2018) English Wealden fossils: an update. *Proceedings of the Geologists' Association*, 129(2), 171–201.

Bader, K. S., Hasiotis, S. T. and Martin, L. D. (2009) Application of forensic science techniques to trace fossils on dinosaur bones from a quarry in the Upper Jurassic Morrison Formation, northeastern Wyoming. *Palaios*, 24(3), 140–158.

Bailleul, A. M., O'Connor, J. and Schweitzer, M. H. (2019) Dinosaur paleohistology: Review, trends and new avenues of investigation. *PeerJ*, 7, e7764.

Bakker, R. T., Williams, M. and Currie, P. J. (1988) *Nanotyrannus*, a new genus of pygmy tyrannosaur, from the latest Cretaceous of Montana. *Hunteria*, 1(5), 1–30.

Balanoff, A. M., Bever, G., Colbert, M. W., Clarke, J. A., Field, D. J., Gignac, P. M., Ksepka, D. T., Ridgely, R. C., Smith, N. A. and Torres, C. R. (2016a) Best practices for digitally constructing endocranial casts: examples from birds and their dinosaurian relatives. *Journal of Anatomy*, 229(2), 173–190.

Balanoff, A. M., Bever, G. and Norell, M. A. (2014) Reconsidering the avian nature of the oviraptorosaur brain (Dinosauria: Theropoda). *PLoS One*, 9(12), e113559.

Balanoff, A. M. and Bever, G. S. (2020) 'The Role of Endocasts in the Study of Brain Evolution', in Kaas, J.H. (ed.) *Evolutionary Neuroscience (Second Edition)*. Academic Press: London, 29–49.

Balanoff, A. M., Smaers, J. B. and Turner, A. H. (2016b) Brain modularity across the theropod–bird transition: testing the influence of flight on neuroanatomical variation. *Journal of Anatomy*, 229(2), 204–214.

Balanoff, A. M., Xu, X., Kobayashi, Y., Matsufune, Y. and Norell, M. A. (2009) Cranial osteology of the theropod dinosaur *Incisivosaurus gauthieri* (Theropoda: Oviraptorosauria). *American Museum Novitates*, 2009(3651), 1–35.

Ballell, A., King, J. L., Neenan, J. M., Rayfield, E. J. and Benton, M. J. (2020) The braincase, brain and palaeobiology of the basal sauropodomorph dinosaur *Thecodontosaurus antiquus*. *Zoological Journal of the Linnean Society*, 193(2), 541–562.

Barker, C. T., Hone, D. W., Naish, D., Cau, A., Lockwood, J. A., Foster, B., Clarkin, C. E., Schneider, P. and Gostling, N. J. (2021) New spinosaurids from the Wessex Formation (Early Cretaceous, UK) and the European origins of Spinosauridae. *Scientific Reports*, 11, 19340

Barker, C. T., Lockwood, J. A., Naish, D., Brown, S., Hart, A., Tulloch, E. and Gostling, N. J. (2022) A European giant: a large spinosaurid (Dinosauria: Theropoda) from the Vectis Formation (Wealden Group, Early Cretaceous), UK. *PeerJ*, 10, e13543.

Barker, C. T., Naish, D., Clarkin, C. E., Farrell, P., Hullmann, G., Lockyer, J., Schneider, P., Ward, R. K. and Gostling, N. J. (2020) A highly pneumatic middle Cretaceous theropod from the British Lower Greensand. *Papers in Palaeontology*, 6(4), 661–679.

Barker, C. T., Naish, D., Newham, E., Katsamenis, O. L. and Dyke, G. (2017) Complex neuroanatomy in the rostrum of the Isle of Wight theropod *Neovenator salerii*. *Scientific Reports*, 7(1), 3749.

Barrett, P., Benson, R. and Upchurch, P. (2010) Dinosaurs of Dorset: Part II, the sauropod dinosaurs (Saurischia, Sauropoda) with additional comments on the theropods. *Proceedings of the Dorset Natural History and Archaeological Society*, 131, 113–126.

Barrett, P. M. (2021) Dinosaur material from the Lower Greensand Group of Upware, Cambridgeshire, and the age of 'Wealden vertebrates from the 'Bedfordshire Straits'. *Proceedings of the Geologists' Association*, 132(4), 497–505.

Barrett, P. M. and Bonsor, J. A. (2021) A revision of the non-avian dinosaurs '*Eucercosaurus tanyspondylus*' and '*Syngonosaurus macrocercus*' from the Cambridge Greensand, UK. *Cretaceous Research*, 118, 104638.

Barrett, P. M. and Rayfield, E. J. (2006) Ecological and evolutionary implications of dinosaur feeding behaviour. *Trends in Ecology & Evolution*, 21(4), 217–224.

Bartholomai, A. and Molnar, R. E. (1981) *Muttaburrasaurus*, a new iguanodontid (Ornithischia: Ornithopoda) dinosaur from the Lower Cretaceous of Queensland. *Memoirs of the Queensland Museum*, 20(2), 319–349.

Batten, D. J. (2011) 'Wealden Geology', in Batten, D.J. (ed.) *English Wealden Fossils*. The Palaeontological Association: London, 7–14.

Batten, D. J. and Austen, P. A. (2011) 'The Wealden of South-East England', in Batten, D.J. (ed.) *English Wealden Fossils*. The Paleontological Society: London, 15–51.

Beevor, T., Quigley, A., Smith, R. E., Smyth, R. S., Ibrahim, N., Zouhri, S. and Martill, D. M. (2021) Taphonomic evidence supports an aquatic lifestyle for *Spinosaurus*. *Cretaceous Research*, 117, 104627.

Behrensmeyer, A. K. (1978) Taphonomic and ecologic information from bone weathering. *Paleobiology*, 4(2), 150–162.

Benoit, J., Legendre, L., Farke, A., Neenan, J., Mennecart, B., Costeur, L., Merigeaud, S. and Manger, P. (2020) A test of the lateral semicircular canal correlation to head posture, diet and other biological traits in “ungulate” mammals. *Scientific reports*, 10, 19602.

Benson, R. B. (2010) A description of *Megalosaurus bucklandii* (Dinosauria: Theropoda) from the Bathonian of the UK and the relationships of Middle Jurassic theropods. *Zoological Journal of the Linnean Society*, 158(4), 882–935.

Benson, R. B., Brusatte, S. L., Hutt, S. and Naish, D. (2009a) A new large basal tetanuran (Dinosauria: Theropoda) from the Wessex Formation (Barremian) of the Isle of Wight, England. *Journal of vertebrate Paleontology*, 29(2), 612–615.

Benson, R. B., Butler, R. J., Carrano, M. T. and O'Connor, P. M. (2012) Air-filled postcranial bones in theropod dinosaurs: physiological implications and the ‘reptile’–bird transition. *Biological Reviews*, 87(1), 168–193.

Benson, R. B., Carrano, M. T. and Brusatte, S. L. (2010) A new clade of archaic large-bodied predatory dinosaurs (Theropoda: Allosauroidea) that survived to the latest Mesozoic. *Naturwissenschaften*, 97(1), 71–78.

Benson, R. B., Hunt, G., Carrano, M. T. and Campione, N. (2018) Cope's rule and the adaptive landscape of dinosaur body size evolution. *Palaeontology*, 61(1), 13–48.

Benson, R. B., Starmer-Jones, E., Close, R. A. and Walsh, S. A. (2017) Comparative analysis of vestibular ecomorphology in birds. *Journal of Anatomy*, 231(6), 990–1018.

Benson, R. B. J. and Barrett, P. (2009b) Dinosaurs of Dorset: part I, the carnivorous dinosaurs (Saurischia, Theropoda). *Proceedings of the Dorset Natural History and Archaeological Society*, 130, 133–147.

Benson, R. B. J., Mannion, P. D., Butler, R. J., Upchurch, P., Goswami, A. and Evans, S. E. (2013) Cretaceous tetrapod fossil record sampling and faunal turnover: Implications for biogeography and the rise of modern clades. *Palaeogeography, Palaeoclimatology, Palaeoecology*, 372, 88–107.

Benton, M., Martill, D. and Taylor, M. (1995a) The first Lower Jurassic dinosaur from Scotland: limb bone of a ceratosaur theropod from Skye. *Scottish Journal of Geology*, 31(2), 177–182.

Benton, M. J., Bouaziz, S., Buffetaut, E., Martill, D., Ouaja, M., Soussi, M. and Trueman, C. (2000) Dinosaurs and other fossil vertebrates from fluvial deposits in the Lower Cretaceous of southern Tunisia. *Palaeogeography, Palaeoclimatology, Palaeoecology*, 157(3-4), 227–246.

Benton, M. J. and Spencer, P. S. (1995b) *Fossil reptiles of Great Britain*. Dordrecht: Springer.

Benyoucef, M., Läng, E., Cavin, L., Mebarki, K., Adaci, M. and Bensalah, M. (2015) Overabundance of piscivorous dinosaurs (Theropoda: Spinosauridae) in the mid-Cretaceous of North Africa: The Algerian dilemma. *Cretaceous Research*, 55, 44–55.

Benyoucef, M., Pérez-García, A., Bendella, M., Ortega, F., Vullo, R., Bouchemla, I. and Ferré, B. (2022) The" mid"-Cretaceous (Lower Cenomanian) Continental Vertebrates of Gara Samani, Algeria. Sedimentological Framework and Palaeodiversity. *Frontiers in Earth Science*, 10, 927059.

Bertin, T. (2010) A catalogue of material and review of the Spinosauridae. *PalArch’s Journal of Vertebrate Palaeontology*, 7(4), 1–39.

Beurlen, K. (1971) As condições ecológicas e faciológicas da Formação Santana na Chapada do Araripe (Nordeste do Brasil). *Anais da Academia brasileira de Ciências*, 43(Supplement), 411–415.

Bever, G. S., Brusatte, S. L., Balanoff, A. M. and Norell, M. A. (2011) Variation, variability, and the origin of the avian endocranium: insights from the anatomy of *Alioramus altai* (Theropoda: Tyrannosauroidea). *PLoS One*, 6(8), e23393.

Bever, G. S., Brusatte, S. L., Carr, T. D., Xu, X., Balanoff, A. M. and Norell, M. A. (2013) The braincase anatomy of the Late Cretaceous dinosaur *Alioramus* (Theropoda: Tyrannosauroidea). *Bulletin of the American Museum of Natural History*, 2013(376), 1–72.

Bittencourt, J. and Kellner, A. W. A. (2004) On a sequence of sacrocaudal theropod dinosaur vertebrae from the Lower Cretaceous Santana Formation, northeastern Brazil. *Archivos do Museu Nacional do Rio de Janeiro*, 62(3), 309–320.

Blows, W. T. (1987) The armoured dinosaur *Polacanthus foxi* from the Lower Cretaceous of the Isle of Wight. *Palaeontology*, 30(3), 557–580.

Blows, W. T. (1995) The early Cretaceous brachiosaurid dinosaurs *Ornithopsis* and *Eucamerotus* from the Isle of Wight, England. *Palaeontology*, 38(1), 187–198.

Blows, W. T. (1998) A review of Lower and Middle Cretaceous dinosaurs of England. *New Mexico Museum of Natural History and Science Bulletin*, 14, 29–38.

Bouabdellah, F., Lessner, E. and Benoit, J. (2022) The rostral neurovascular system of *Tyrannosaurus rex*. *Palaeontologia Electronica*, 25(1), a3.

Bouaziz, S., Buffetaut, E., Ghanmi, M., Jaeger, J.-J., Martin, M., Mazin, J.-M. and Tong, H. (1988) Nouvelle decouvertes de vertebres fossiles dans l'Albien du Sud Tunisien. *Bulletin de la Société géologique de France*, 4(2), 335–339.

Bouckaert, R., Heled, J., Kühnert, D., Vaughan, T., Wu, C.-H., Xie, D., Suchard, M. A., Rambaut, A. and Drummond, A. J. (2014) BEAST 2: a software platform for Bayesian evolutionary analysis. *PLoS Comput Biol*, 10(4), e1003537.

Bremer, K. (1988) The limits of amino acid sequence data in angiosperm phylogenetic reconstruction. *Evolution*, 42(4), 795–803.

Bremer, K. (1994) Branch support and tree stability. *Cladistics*, 10(3), 295-304.

Britt, B. B. (1993) *Pneumatic cranial bones in dinosaurs and other archosaurs.* PhD thesis. University of Calgary.

Britt, B. B. (1997) 'Postcranial pneumaticity', in Currie, P.J. and Padian, K. (eds.) *The Encyclopedia of Dinosaurs*. Academic Press: San Diego, 590–593.

Britt, B. B., Eberth, D. A., Scheetz, R. D., Greenhalgh, B. W. and Stadtman, K. L. (2009) Taphonomy of debris-flow hosted dinosaur bonebeds at Dalton Wells, Utah (Lower Cretaceous, Cedar Mountain Formation, USA). *Palaeogeography, Palaeoclimatology, Palaeoecology*, 280(1–2), 1–22.

Britt, B. B., Scheetz, R. D. and Dangerfield, A. (2008) A suite of dermestid beetle traces on dinosaur bone from the Upper Jurassic Morrison Formation, Wyoming, USA. *Ichnos*, 15(2), 59–71.

Brochu, C. A. (1996) Closure of neurocentral sutures during crocodilian ontogeny: implications for maturity assessment in fossil archosaurs. *Journal of Vertebrate Paleontology*, 16(1), 49–62.

Brochu, C. A. (2000) A digitally-rendered endocast for *Tyrannosaurus rex*. *Journal of Vertebrate Paleontology*, 20(1), 1–6.

Brochu, C. A. (2003) Osteology of *Tyrannosaurus rex*: insights from a nearly complete skeleton and high-resolution computed tomographic analysis of the skull. *Journal of Vertebrate Paleontology*, 22(sup4), 1–138.

Bronzati, M., Benson, R. B., Evers, S. W., Ezcurra, M. D., Cabreira, S. F., Choiniere, J., Dollman, K. N., Paulina-Carabajal, A., Radermacher, V. J. and Roberto-da-Silva, L. (2021) Deep evolutionary diversification of semicircular canals in archosaurs. *Current Biology*, 31(12), 2520-2529.e6.

Brooks, K. (2008) Pierre Teilhard de Chardin 1881-1955. *Hastings & District Geological Society Journal*, 14, 30–33.

Brougham, T., Smith, E. T. and Bell, P. R. (2019) New theropod (Tetanurae: Avetheropoda) material from the 'mid'-Cretaceous Griman Greek Formation at Lightning Ridge, New South Wales, Australia. *Royal Society open science*, 6(1), 180826.

Brown, C. M., Arbour, J. H. and Jackson, D. A. (2012) Testing of the effect of missing data estimation and distribution in morphometric multivariate data analyses. *Systematic biology*, 61(6), 941–954.

Brown, C. M., Henderson, D. M., Vinther, J., Fletcher, I., Sistiaga, A., Herrera, J. and Summons, R. E. (2017) An exceptionally preserved three-dimensional armored dinosaur reveals insights into coloration and Cretaceous predator-prey dynamics. *Current Biology*, 27(16), 2514-2521.e3.

Brusatte, S. L., Benson, R. B. J. and Hutt, S. (2008) The osteology of *Neovenator salerii* (Dinosauria: Theropoda) from the Wealden Group (Barremian) of the Isle of Wight. *Monograph of the Palaeontographical Society*, 162(631), 1–75.

Brusatte, S. L., Carr, T. D. and Norell, M. A. (2012) The osteology of *Alioramus*, a gracile and long-snouted tyrannosaurid (Dinosauria: Theropoda) from the Late Cretaceous of Mongolia. *Bulletin of the American Museum of Natural History*, 2012(366), 1–197.

Brusatte, S. L., Chure, D. J., Benson, R. B. J. and Xu, X. (2010) The osteology of *Shaochilong maortuensis*, a carcharodontosaurid (Dinosauria: Theropoda) from the Late Cretaceous of Asia. *Zootaxa*, (2334), 1–46.

Brusatte, S. L. and Sereno, P. C. (2007) A new species of *Carcharodontosaurus* (Dinosauria: Theropoda) from the Cenomanian of Niger and a revision of the genus. *Journal of Vertebrate Paleontology*, 27(4), 902-916.

Bryant, D. (2003) A classification of consensus methods for phylogenetics. *DIMACS series in discrete mathematics and theoretical computer science*, 61, 163–184.

Buchholtz, E. A. and Seyfarth, E.-A. (1999) The gospel of the fossil brain: Tilly Edinger and the science of paleoneurology. *Brain research bulletin*, 48(4), 351–361.

Bucholtz, E. (2012) 'Dinosaur Paleoneurology', in Brett-Surman, K., Holtz Jr, T.R. and Farlow, J.O. (eds.) *The Complete Dinosaur (2nd Edition)*. Indiana University Press: Bloomington, 191-208.

Buckland, W. (1824) Notice on the *Megalosaurus* or great fossil lizard of Stonefield. *Transactions of the Geological Society of London*, 1(2), 390–396.

Buffetaut, E. (2007) The spinosaurid dinosaur *Baryonyx* (Saurischia, Theropoda) in the Early Cretaceous of Portugal. *Geological Magazine*, 144(6), 1021–1025.

Buffetaut, E. (2010) 'Spinosaurs before Stromer: early finds of spinosaurid dinosaurs and their interpretations', in Moody, R.T.J. *et al.* (eds.) *Dinosaurs and Other Extinct Saurians: A Historical Perspective*. The Geological Society of London: London, 175–188.

Buffetaut, E. (2012) An early spinosaurid dinosaur from the Late Jurassic of Tendaguru (Tanzania) and the evolution of the spinosaurid dentition. *Oryctos*, 10, 1–8.

Buffetaut, E. and Ingavat, R. (1986) Unusual theropod dinosaur teeth from the Upper Jurassic of Phu Wiang, northeastern Thailand. *Revue de Paléobiologie*, 5(2), 217–220.

Buffetaut, E., Martill, D. and Escuillié, F. (2004) Pterosaurs as part of a spinosaur diet. *Nature*, 430(6995), 33–33.

Buffetaut, E. and Nori, L. (2012) 'Dinosaur remains from the “Sables Verts” (Early Cretaceous, Albian) of the eastern Paris Basin', in Godefroit, P. (ed.) *Bernissart dinosaurs and Early Cretaceous terrestrial ecosystem*. Indiana University Press: Bloomington, 363–377.

Buffetaut, E. and Ouaja, M. (2002) A new specimen of *Spinosaurus* (Dinosauria, Theropoda) from the Lower Cretaceous of Tunisia, with remarks on the evolutionary history of the Spinosauridae. *Bulletin de la Société Géologique de France*, 173(5), 415–421.

Buffetaut, E., Suteethorn, S., Suteethorn, V., Tong, H. and Wongko, K. (2019) Spinosaurid teeth from the Lower Cretaceous of Ko Kut, eastern Thailand. *Annales de Paléontologie*, 105(3), 239–243.

Buffetaut, E., Suteethorn, V., Tong, H. and Amiot, R. (2008) An Early Cretaceous spinosaurid theropod from southern China. *Geological Magazine*, 145(5), 745–748.

Bullar, C. M., Zhao, Q., Benton, M. J. and Ryan, M. J. (2019) Ontogenetic braincase development in *Psittacosaurus lujiatunensis* (Dinosauria: Ceratopsia) using micro-computed tomography. *PeerJ*, 7, e7217.

Butler, R. J. and Barrett, P. M. (2008) Palaeoenvironmental controls on the distribution of Cretaceous herbivorous dinosaurs. *Naturwissenschaften*, 95(11), 1027–1032.

Caldas, I. V. and Schrago, C. G. (2019) Data partitioning and correction for ascertainment bias reduce the uncertainty of placental mammal divergence times inferred from the morphological clock. *Ecology and Evolution*, 9(4), 2255–2262.

Calvo, J. O., Porfiri, J. D., Veralli, C., Novas, F. and Poblete, F. (2004) Phylogenetic status of *Megaraptor namunhuaiquii* Novas based on a new specimen from Neuquén, Patagonia, Argentina. *Ameghiniana*, 41(4), 565–575.

Campione, N. E., Evans, D. C., Brown, C. M. and Carrano, M. T. (2014) Body mass estimation in non-avian bipeds using a theoretical conversion to quadruped stylopodial proportions. *Methods in Ecology and Evolution*, 5(9), 913–923.

Canale, J., Novas, F. and Haluza, H. (2008) Comments about the cervical vertebrae referred to the African theropods *Carcharodontosaurus* and *Sigilmassasaurus*, *III Congreso Latinoamericano de Paleontología de Vertebrados.* Neuquén.

Candeiro, C. R. A., Abranches, C., Abrantes, E., Avilla, L. d. S., Martins, V., Moreira, A., Torres, S. and Bergqvist, L. (2004) Dinosaurs remains from western São Paulo state, Brazil (Bauru Basin, Adamantina Formation, Upper Cretaceous). *Journal of South American Earth Sciences*, 18(1), 1–10.

Candeiro, C. R. A., Brusatte, S. L. and de Souza, A. L. (2017) Spinosaurid dinosaurs from the Early Cretaceous of North Africa and Europe: fossil record, biogeography and extinction. *Anuário do Instituto de Geociências*, 40(3), 294–302.

Canudo, J. I., Barco, J. L., Pereda-Suberbiola, X., Ruiz-Omeñaca, J. I., Salgado, L., Torcida Fernandez-Baldor, F. and Gasulla, J. M. (2009) What Iberian dinosaurs reveal about the bridge said to exist between Gondwana and Laurasia in the Early Cretaceous. *Bulletin de la Société Géologique de France*, 180(1), 5–11.

Canudo, J. I., Gasulla, J. M., Gómez-Fernández, D., Ortega, F., Sanz, J. L. and Yagüe, P. (2008) Primera evidencia de dientes aislados atribuidos a Spinosauridae (Theropoda) en el Aptiano inferior (Cretácico Inferior) de Europa: Formación Arcillas de Morella (España). *Ameghiniana*, 45(4), 649–662.

Carlson, W., Rowe, T., Ketcham, R. and Colbert, M. (2003) Applications of high-resolution X-ray computed tomography in petrology, meteoritics and palaeontology. *Geological Society, London, Special Publications*, 215(1), 7–22.

Carr, T. D. (1999) Craniofacial ontogeny in Tyrannosauridae (Dinosauria, Coelurosauria). *Journal of vertebrate Paleontology*, 19(3), 497–520.

Carr, T. D. (2020) A high-resolution growth series of *Tyrannosaurus rex* obtained from multiple lines of evidence. *PeerJ*, 8, e9192.

Carr, T. D., Varricchio, D. J., Sedlmayr, J. C., Roberts, E. M. and Moore, J. R. (2017) A new tyrannosaur with evidence for anagenesis and crocodile-like facial sensory system. *Scientific reports*, 7, 44942.

Carr, T. D. and Williamson, T. E. (2004) Diversity of late Maastrichtian Tyrannosauridae (Dinosauria: Theropoda) from western North America. *Zoological Journal of the Linnean Society*, 142(4), 479–523.

Carrano, M. T., Benson, R. B. and Sampson, S. D. (2012) The phylogeny of Tetanurae (Dinosauria: Theropoda). *Journal of Systematic Palaeontology*, 10(2), 211–300.

Carrano, M. T. and Sampson, S. D. (2008) The phylogeny of Ceratosauria (Dinosauria: Theropoda). *Journal of Systematic Palaeontology*, 6(2), 183–236.

Carvalho, F. S. R., Dos Santos, T. J. S., Neto, I. C. P., Soares, E. C. S. and Costa, F. W. G. (2022) Workflow in open-source software for computed tomography analysis. *British Journal of Oral and Maxillofacial Surgery*, 60(7), 987–990.

Casey, R. (1961) The stratigraphical palaeontology of the Lower Greensand. *Palaeontology*, 3(4), 487–621.

Casey, R. (1963) The dawn of the Cretaceous period in Britain. 117.

Cau, A. (2017) Specimen-level phylogenetics in paleontology using the Fossilized Birth-Death model with sampled ancestors. *PeerJ*, 5, e3055.

Cau, A. (2018) The assembly of the avian body plan: a 160-million-year long process. *Bollettino della Società Paleontologica Italiana*, 57(1), 1–25.

Cau, A., Dalla Vecchia, F. M. and Fabbri, M. (2013) A thick-skulled theropod (Dinosauria, Saurischia) from the Upper Cretaceous of Morocco with implications for carcharodontosaurid cranial evolution. *Cretaceous Research*, 40, 251–260.

Cerio, D. G. and Witmer, L. M. (2019) Intraspecific variation and symmetry of the inner-ear labyrinth in a population of wild turkeys: Implications for paleontological reconstructions. *PeerJ*, 7, e7355.

Cerroni, M. A. and Paulina-Carabajal, A. (2019) Novel information on the endocranial morphology of the abelisaurid theropod *Carnotaurus sastrei*. *Comptes Rendus Palevol*, 18(8), 985–995.

Charig, A. J. and Milner, A. C. (1986) *Baryonyx*, a remarkable new theropod dinosaur. *Nature*, 324(6095), 359–361.

Charig, A. J. and Milner, A. C. (1990) *The systematic position of Baryonyx walkeri, in the light of Gauthier's reclassification of the Theropoda*. Cambridge University Press. Dinosaur Systematics: Approaches and Perspectives.

Charig, A. J. and Milner, A. C. (1997) *Baryonyx walkeri*, a fish-eating dinosaur from the Wealden of Surrey. *Bulletin-Natural History Museum Geology Series*, 53, 11–70.

Chiarenza, A. A. and Cau, A. (2016) A large abelisaurid (Dinosauria, Theropoda) from Morocco and comments on the Cenomanian theropods from North Africa. *PeerJ*, 4, e1754.

Chiarenza, A. A., Mannion, P. D., Lunt, D. J., Farnsworth, A., Jones, L. A., Kelland, S.-J. and Allison, P. A. (2019) Ecological niche modelling does not support climatically-driven dinosaur diversity decline before the Cretaceous/Paleogene mass extinction. *Nature communications*, 10(1), 1–14.

Choiniere, J. N., Neenan, J. M., Schmitz, L., Ford, D. P., Chapelle, K. E., Balanoff, A. M., Sipla, J. S., Georgi, J. A., Walsh, S. A. and Norell, M. A. (2021) Evolution of vision and hearing modalities in theropod dinosaurs. *Science*, 372(6542), 610–613.

Chokchaloemwong, D., Hattori, S., Cuesta, E., Jintasakul, P., Shibata, M. and Azuma, Y. (2019) A new carcharodontosaurian theropod (Dinosauria: Saurischia) from the Lower Cretaceous of Thailand. *PLOS ONE*, 14(10), e0222489.

Chure, D. J. and Madsen Jr, J. H. (1996) Variation in aspects of the tympanic pneumatic system in a population of *Allosaurus fragilis* from the Morrison Formation (Upper Jurassic). *Journal of Vertebrate Paleontology*, 16(1), 63–66.

Cobbett, A., Wilkinson, M. and Wills, M. A. (2007) Fossils impact as hard as living taxa in parsimony analyses of morphology. *Systematic Biology*, 56(5), 753–766.

Congleton, J. D. (1990) *Vertebrate paleontology of the Koum Basin, northern Cameroon, and archosaurian paleobiogeography in the Early Cretaceous*. Masters thesis. Southern Methodist University.

Conroy, G. C. and Vannier, M. W. (1984) Noninvasive three-dimensional computer imaging of matrix-filled fossil skulls by high-resolution computed tomography. *Science*, 226(4673), 456–458.

Cope, J. C. W. (2006) 'Jurassic: the returning seas', in Brenchley, P.J. and Rawson, P.F. (eds.) *The Geology of England and Wales (2nd Edition)*. The Geological Society of London: London, 325–364.

Cope, J. C. W. (2007) Drawing the line: the history of the Jurassic—Cretaceous boundary. *Proceedings of the Geologists' Association*, 119(1), 105–117.

Coram, R. A. and Radley, J. D. (2021) Revisiting climate change and palaeoenvironments in the Purbeck Limestone Group (Tithonian–Berriasian) of Durlston Bay, southern UK. *Proceedings of the Geologists' Association*, 132(3), 392–404.

Coria, R. A. and Currie, P. J. (2006) A new carcharodontosaurid (Dinosauria, Theropoda) from the Upper Cretaceous of Argentina. *Geodiversitas*, 28(1), 71–118.

Coria, R. A. and Currie, P. J. (2016) A new megaraptoran dinosaur (Dinosauria, Theropoda, Megaraptoridae) from the Late Cretaceous of Patagonia. *PLoS One*, 11(7), e0157973.

Coria, R. A., Currie, P. J., Ortega, F. and Baiano, M. A. (2019) An Early Cretaceous, medium-sized carcharodontosaurid theropod (Dinosauria, Saurischia) from the Mulichinco Formation (upper Valanginian), Neuquén Province, Patagonia, Argentina. *Cretaceous Research*, 104319.

Cruzado-Caballero, P., Canudo, J. I., De Valais, S., Frigola, J., Barriuso, E. and Fortuny, J. (2021) Bioerosion and palaeoecological association of osteophagous insects in the Maastrichtian dinosaur *Arenysaurus ardevoli*. *Lethaia*, 54(5), 957–968.

Csiki, Z. (2006) 'Insect borings in dinosaur bone from the Maastrichtian of the Hateg Basin, Romania - paleoecological and paleoclimatic implications. 101-109', in Csiki, Z. (ed.) *Mesozoic and Cenozoic Vertebrates and Paleoenviroments. Tributes to the career of Prof. Dan Grigorescu.* Cambridge University Press: Cambridge, 95–104.

Cuesta, E., Ortega, F. and Sanz, J. L. (2019) Axial osteology of *Concavenator corcovatus* (Theropoda; Carcharodontosauria) from the Lower Cretaceous of Spain. *Cretaceous Research*, 95, 106–120.

Cuff, A. R. and Rayfield, E. J. (2013) Feeding mechanics in spinosaurid theropods and extant crocodilians. *PLoS One*, 8(5), e65295.

Cullen, T. M., Canale, J. I., Apesteguía, S., Smith, N. D., Hu, D. and Makovicky, P. J. (2020) Osteohistological analyses reveal diverse strategies of theropod dinosaur body-size evolution. *Proceedings of the Royal Society B*, 287(1939), 20202258.

Cunningham, J. A., Rahman, I. A., Lautenschlager, S., Rayfield, E. J. and Donoghue, P. C. (2014) A virtual world of paleontology. *Trends in Ecology & Evolution*, 29(6), 347–357.

Currie, P. J. (2003) Cranial anatomy of tyrannosaurid dinosaurs from the Late Cretaceous of Alberta, Canada. *Acta Palaeontologica Polonica*, 48(2), 191–226.

Currie, P. J. and Dong, Z. (2001) New information on *Shanshanosaurus huoyanshanensis*, a juvenile tyrannosaurid (Theropoda, Dinosauria) from the Late Cretaceous of China. *Canadian Journal of Earth Sciences*, 38(12), 1729–1737.

Currie, P. J. and Zhao, X.-J. (1993) A new carnosaur (Dinosauria, Theropoda) from the Jurassic of Xinjiang, People's Republic of China. *Canadian Journal of Earth Sciences*, 30(10), 2037–2081.

D'Emic, M. D., O'Connor, P. M., Sombathy, R. S., Cerda, I., Pascucci, T. R., Varricchio, D., Pol, D., Dave, A., Coria, R. A. and Curry Rogers, K. A. (2023) Developmental strategies underlying gigantism and miniaturization in non-avialan theropod dinosaurs. *Science*, 379(6634), 811–814.

Dai, H., Benson, R., Hu, X., Ma, Q., Tan, C., Li, N., Xiao, M., Hu, H., Zhou, Y. and Wei, Z. (2020) A new possible megalosauroid theropod from the Middle Jurassic Xintiangou Formation of Chongqing, People's Republic of China and its implication for early tetanuran evolution. *Scientific Reports*, 10(1), 1–16.

Dal Sasso, C., Maganuco, S., Buffetaut, E. and Mendez, M. A. (2005) New information on the skull of the enigmatic theropod *Spinosaurus*, with remarks on its size and affinities. *Journal of Vertebrate Paleontology*, 25(4), 888–896.

Dal Sasso, C., Maganuco, S. and Cau, A. (2018) The oldest ceratosaurian (Dinosauria: Theropoda), from the Lower Jurassic of Italy, sheds light on the evolution of the three-fingered hand of birds. *PeerJ*, 6, e5976.

Dal Sasso, C., Maganuco, S. and Iurino, D. A. (2014) Update on the internal structure of the snout of *Spinosaurus aegyptiacus*, *Second North African Vertebrate Palaeontology Congress - NAVEP2*. Ouarzazate, Morocco.

Dávalos, L. M., Velazco, P. M., Warsi, O. M., Smits, P. D. and Simmons, N. B. (2014) Integrating incomplete fossils by isolating conflicting signal in saturated and non-independent morphological characters. *Systematic Biology*, 63(4), 582–600.

David, R., Bronzati, M. and Benson, R. B. (2022) Comment on "The early origin of a birdlike inner ear and the evolution of dinosaurian movement and vocalization". *Science*, 376(6600), eabl6710.

de Andrade, M. B., Edmonds, R., Benton, M. J. and Schouten, R. (2011) A new Berriasian species of *Goniopholis* (Mesoeucrocodylia, Neosuchia) from England, and a review of the genus. *Zoological Journal of the Linnean Society*, 163(suppl_1), S66–S108.

Deepak, A., Dong, J. and Fernández-Baca, D. (2012) Identifying Rogue Taxa through Reduced Consensus: NP-Hardness and Exact Algorithms, Berlin, Heidelberg. Springer Berlin Heidelberg.

Delcourt, R. (2018) Ceratosaur palaeobiology: new insights on evolution and ecology of the southern rulers. *Scientific Reports*, 8, 9730

Deng, C., Ślipiński, A., Ren, D. and Pang, H. (2017) The oldest dermestid beetle from the Middle Jurassic of China (Coleoptera: Dermestidae). *Annales Zoologici*, 67(1), 109–112.

Dong, Z., Zhou, S. and Zhang, Y. (1983) Dinosaurs from the Jurassic of Sichuan. *Palaeontologica Sinica*, 162(C23), 1–151.

Dos Reis, M., Donoghue, P. C. and Yang, Z. (2016) Bayesian molecular clock dating of species divergences in the genomics era. *Nature Reviews Genetics*, 17(2), 71–80.

Drew, F. (1861) On the succession of the beds in the Hastings sands of the southern portion of the weald. *Quarterly Journal of the Geological Society of London*, 17, 217–286.

Drummond, A. J., Ho, S. Y. W., Phillips, M. J. and Rambaut, A. (2006) Relaxed phylogenetics and dating with confidence. *PLoS biology*, 4(5), e88.

Drummond, A. J. and Suchard, M. A. (2010) Bayesian random local clocks, or one rate to rule them all. *BMC biology*, 8(1), 1–12.

Drummond, A. J., Suchard, M. A., Xie, D. and Rambaut, A. (2012) Bayesian phylogenetics with BEAUti and the BEAST 1.7. *Molecular biology and evolution*, 29(8), 1969–1973.

Dudgeon, T. W., Maddin, H. C., Evans, D. C. and Mallon, J. C. (2020) The internal cranial anatomy of *Champsosaurus* (Choristodera: Champsosauridae): Implications for neurosensory function. *Scientific Reports*, 10, 7122

Dufeau, D. L. (2011) *The Evolution of Cranial Pneumaticity in Archosauria: Patterns of Paratympanic Sinus Development*. PhD Thesis. Ohio University.

Eaton, J. G., Kirkland, J. I., Howard Hutchison, J., Denton, R., O'Neill, R. C. and Michael Parrish, J. (1997) Nonmarine extinction across the Cenomanian-Turonian boundary, southwestern Utah, with a comparison to the Cretaceous-Tertiary extinction event. *Geological Society of America Bulletin*, 109(5), 560–567.

Eddy, D. R. and Clarke, J. A. (2011) New information on the cranial anatomy of *Acrocanthosaurus atokensis* and its implications for the phylogeny of Allosauroidea (Dinosauria: Theropoda). *PLOS ONE*, 6(3), e17932.

Egan, M. G. (2006) Support versus corroboration. *Journal of Biomedical Informatics*, 39(1), 72–85.

Evers, S. W., Joyce, W. G., Choiniere, J. N., Ferreira, G. S., Foth, C., Hermanson, G., Yi, H., Johnson, C. M., Werneburg, I. and Benson, R. B. (2022) Independent origin of large labyrinth size in turtles. *Nature Communications*, 13, 5807

Evers, S. W., Neenan, J. M., Ferreira, G. S., Werneburg, I., Barrett, P. M. and Benson, R. B. (2019) Neurovascular anatomy of the protostegid turtle *Rhinochelys pulchriceps* and comparisons of membranous and endosseous labyrinth shape in an extant turtle. *Zoological Journal of the Linnean Society*, 187(3), 800–828.

Evers, S. W. and Rauhut, O. W. (2012a) Evidence for spinosaurid affinities of *Sigilmassasaurus brevicollis* (Theropoda, Tetanurae) [Abstract S25]. Terra Nostra.

Evers, S. W., Rauhut, O. W. and Milner, A. C. (2012b) Was Stromer right? The affinities of *Sigilmassasaurus brevicollis* (theropoda, Tetanurae), *Journal of Vertebrate Paleontology, Programs and Abstracts*

Evers, S. W., Rauhut, O. W., Milner, A. C., McFeeters, B. and Allain, R. (2015) A reappraisal of the morphology and systematic position of the theropod dinosaur *Sigilmassasaurus* from the "middle" Cretaceous of Morocco. *PeerJ*, 3, e1323.

Fabbri, M., Navalon, G., Benson, R. B., Pol, D., O'Connor, J., Bhullar, B.-A. S., Erickson, G., Norell, M. A., Orkney, A. and Lamanna, M. C. (2022a) Sinking a giant: quantitative macroevolutionary comparative methods debunk qualitative assumptions. *bioRxiv*, 1–10.

Fabbri, M., Navalón, G., Benson, R. B., Pol, D., O'Connor, J., Bhullar, B.-A. S., Erickson, G. M., Norell, M. A., Orkney, A. and Lamanna, M. C. (2022b) Subaqueous foraging among carnivorous dinosaurs. *Nature*, 603(7903), 852–857.

Fanti, F., Cau, A., Martinelli, A. and Contessi, M. (2014) Integrating palaeoecology and morphology in theropod diversity estimation: a case from the Aptian-Albian of Tunisia. *Palaeogeography, Palaeoclimatology, Palaeoecology*, 410, 39–57.

Farke, A. A. and Phillips, G. E. (2017) The first reported ceratopsid dinosaur from eastern North America (Owl Creek Formation, Upper Cretaceous, Mississippi, USA). *PeerJ*, 5, e3342.

Farlow, J. O. and Holtz, T. R. (2002a) The fossil record of predation in dinosaurs. *Paleontological Society Papers*, 8, 251–266.

Farlow, J. O. and Planka, E. R. (2002b) Body size overlap, habitat partitioning and living space requirements of terrestrial vertebrate predators: implications for the paleoecology of large theropod dinosaurs. *Historical Biology*, 16(1), 21–40.

Farris, J. S. (1989) The retention index and the rescaled consistency index. *Cladistics*, 5(4), 417–419.

Fedorov, A., Beichel, R., Kalpathy-Cramer, J., Finet, J., Fillion-Robin, J.-C., Pujol, S., Bauer, C., Jennings, D., Fennessy, F. and Sonka, M. (2012) 3D Slicer as an image computing platform for the Quantitative Imaging Network. *Magnetic Resonance Imaging*, 30(9), 1323–1341.

Feldesman, M. R. (2002) Classification trees as an alternative to linear discriminant analysis. *American Journal of Physical Anthropology*, 119(3), 257–275.

Ferreira-Cardoso, S., Araújo, R., Martins, N., Martins, G., Walsh, S., Martins, R., Kardjilov, N., Manke, I., Hilger, A. and Castanhinha, R. (2017) Floccular fossa size is not a reliable proxy of ecology and behaviour in vertebrates. *Scientific Reports*, 7, 2005.

Fowler, D. (2007) Recently rediscovered baryonychine teeth (Dinosauria: Theropoda): New morphologic data, range extension & similarity to *Ceratosaurus*. *Journal of Vertebrate Paleontology*, 27(3), 76A.

Franzosa, J. and Rowe, T. (2005) Cranial endocast of the Cretaceous theropod dinosaur *Acrocanthosaurus atokensis*. *Journal of Vertebrate Paleontology*, 25(4), 859–864.

Franzosa, J. W. (2004) *Evolution of the brain in Theropoda (Dinosauria)*. PhD Thesis. The University of Texas at Austin.

Gale, A. (2019) *The Isle of Wight*. The Geologist's Association Geologist's Association Guide.

Galton, P. M. and Martin, L. D. (2002) Postcranial anatomy and systematics of *Enaliornis* Seeley, 1876, a foot-propelled diving bird (Aves: Ornithurae: Hesperornithiformes) from the Early Cretaceous of England. *Revue de Paléobiologie*, 21(2), 489–538.

Garwood, R., Sutton, M. and Rahman, I. (2014) *Techniques for virtual palaeontology*. John Wiley & Sons.

Gasca, J. M., Díaz-Martínez, I., Moreno-Azanza, M., Canudo, J. I. and Alonso, A. (2018) A hypertrophied ungual phalanx from the lower Barremian of Spain: Implications for the diversity and palaeoecology of Spinosauridae (Theropoda) in Iberia. *Cretaceous Research*, 84, 141–152.

Gauthier, J. (1986) Saurischian monophyly and the origin of birds. *Memoirs of the California Academy of sciences*, 8, 1–55.

Gauthier, J., Kluge, A. G. and Rowe, T. (1988) Amniote phylogeny and the importance of fossils. *Cladistics*, 4(2), 105–209.

Gavryushkina, A., Heath, T. A., Ksepka, D. T., Stadler, T., Welch, D. and Drummond, A. J. (2017) Bayesian total-evidence dating reveals the recent crown radiation of penguins. *Systematic biology*, 66(1), 57–73.

Gavryushkina, A., Welch, D., Stadler, T. and Drummond, A. J. (2014) Bayesian inference of sampled ancestor trees for epidemiology and fossil calibration. *PLoS Comput Biol*, 10(12), e1003919.

Gearty, W., McClain, C. R. and Payne, J. L. (2018) Energetic tradeoffs control the size distribution of aquatic mammals. *Proceedings of the National Academy of Sciences*, 115(16), 4194–4199.

George, I. D. and Holliday, C. M. (2013) Trigeminal nerve morphology in *Alligator mississippiensis* and its significance for crocodyliform facial sensation and evolution. *The Anatomical Record*, 296(4), 670–680.

Gheerbrant, E. and Rage, J.-C. (2006) Paleobiogeography of Africa: how distinct from Gondwana and Laurasia? *Palaeogeography, Palaeoclimatology, Palaeoecology*, 241(2), 224–246.

Gianechini, F. A., Méndez, A. H., Filippi, L. S., Paulina-Carabajal, A., Juárez-Valieri, R. D. and Garrido, A. C. (2021) A New Furileusaurian Abelisaurid from La Invernada (Upper Cretaceous, Santonian, Bajo De La Carpa Formation), Northern Patagonia, Argentina. *Journal of Vertebrate Paleontology*, e1877151.

Gilmore, C. W. (1920) Osteology of the carnivorous Dinosauria in the United States National museum: with special reference to the genera *Antrodemus* (*Allosaurus*) and *Ceratosaurus*. *Bulletin of the United States National Museum*, i-xi(110), 1–159.

Giribet, G. (2005) TNT: tree analysis using new technology. *Systematic Biology*, 54(1), 176–178.

Giribet, G. (2007) Efficient tree searches with available algorithms. *Evolutionary Bioinformatics*, 3, 341–356.

Gleich, O., Dooling, R. J. and Manley, G. A. (2005) Audiogram, body mass, and basilar papilla length: correlations in birds and predictions for extinct archosaurs. *Naturwissenschaften*, 92(12), 595–598.

Goloboff, P. A. (1999) Analyzing large data sets in reasonable times: solutions for composite optima. *Cladistics*, 15(4), 415–428.

Goloboff, P. A. (2002) 'Techniques for analyzing large data sets', in *Techniques in Molecular Systematics and Evolution*. Springer, 70–79.

Goloboff, P. A. and Catalano, S. A. (2016) TNT version 1.5, including a full implementation of phylogenetic morphometrics. *Cladistics*, 32(3), 221–238.

Goloboff, P. A., Farris, J. S. and Nixon, K. C. (2008) TNT, a free program for phylogenetic analysis. *Cladistics*, 24(5), 774–786.

Goloboff, P. A. and Pol, D. (2005) 'Parsimony and Bayesian phylogenetics', in Albert, V.A. (ed.) *Parsimony, phylogeny, and genomics*. Oxford University Press: New York, 148–159.

Goloboff, P. A. and Pol, D. (2007) On divide-and-conquer strategies for parsimony analysis of large data sets: Rec-I-DCM3 versus TNT. *Systematic biology*, 56(3), 485–495.

Goloboff, P. A. and Szumik, C. A. (2015) Identifying unstable taxa: efficient implementation of triplet-based measures of stability, and comparison with Phyutility and RogueNaRok. *Molecular phylogenetics and evolution*, 88, 93–104.

Gower, D. J. and Weber, E. (1998) The braincase of *Euparkeria*, and the evolutionary relationships of birds and crocodilians. *Biological Reviews*, 73(4), 367–411.

Grantham, T. (2004) The role of fossils in phylogeny reconstruction: Why is it so difficult to integrate paleobiological and neontological evolutionary biology? *Biology and Philosophy*, 19(5), 687–720.

Griffin, C. T. and Nesbitt, S. J. (2016) Anomalously high variation in postnatal development is ancestral for dinosaurs but lost in birds. *Proceedings of the National Academy of Sciences*, 113(51), 14757–14762.

Griffin, C. T., Stocker, M. R., Colleary, C., Stefanic, C. M., Lessner, E. J., Riegler, M., Formoso, K., Koeller, K. and Nesbitt, S. J. (2020) Assessing ontogenetic maturity in extinct saurian reptiles. *Biological Reviews*, 96(2), 470–525.

Gutarra, S. and Rahman, I. A. (2022) The locomotion of extinct secondarily aquatic tetrapods. *Biological Reviews*, 97(1), 67–98.

Hammer, Ø. and Harper, D. A. (2008) *Paleontological data analysis*. John Wiley & Sons.

Hammer, Ø., Harper, D. A. and Ryan, P. D. (2001) PAST: Paleontological statistics software package for education and data analysis. *Palaeontologia Electronica*, 4(1), 9.

Hanson, M., Hoffman, E. A., Norell, M. A. and Bhullar, B.-A. S. (2021) The early origin of a birdlike inner ear and the evolution of dinosaurian movement and vocalization. *Science*, 372(6542), 601–609.

Harris, J. D. (1998) *A reanalysis of Acrocanthosaurus atokensis, its phylogenetic status, and paleobiogeographic implications, based on a New Specimen from Texas*. New Mexico Museum of Natural History and Science.

Hasegawa, Y., Buffetaut E, Manabe M and Y, T. (2003) A possible spinosaurid tooth from the Sebayashi formation (Lower Cretaceous), Gunma, Japan. *Bulletin of Gunma Museum of Natural History*, 7, 1–6.

Hassler, A., Martin, J., Amiot, R., Tacail, T., Godet, F. A., Allain, R. and Balter, V. (2018) Calcium isotopes offer clues on resource partitioning among Cretaceous predatory dinosaurs. *Proceedings of the Royal Society B: Biological Sciences*, 285(1876), 20180197.

Hattori, S., Kawabe, S., Imai, T., Shibata, M., Miyata, K., Xu, X. and Azuma, Y. (2021) Osteology of *Fukuivenator paradoxus*: a bizarre maniraptoran theropod from the Early Cretaceous of Fukui, Japan. *Memoir of the Fukui Prefectural Dinosaur Museum*, 20, 1–82.

Haubitz, B., Prokop, M., Döhring, W., Ostrom, J. and Wellnhofer, P. (1988) Computed tomography of *Archaeopteryx*. *Paleobiology*, 14(2), 206–213.

Heath, T. A., Huelsenbeck, J. P. and Stadler, T. (2014) The fossilized birth–death process for coherent calibration of divergence-time estimates. *Proceedings of the National Academy of Sciences*, 111(29), E2957-E2966.

Heckeberg, N. S. and Rauhut, O. W. (2020) Histology of spinosaurid dinosaur teeth from the Albian-Cenomanian of Morocco: Implications for tooth replacement and ecology. *Palaeontologia Electronica*, 23(3), a48.

Heim, N. A., Knope, M. L., Schaal, E. K., Wang, S. C. and Payne, J. L. (2015) Cope's rule in the evolution of marine animals. *Science*, 347(6224), 867–870.

Heled, J. and Bouckaert, R. R. (2013) Looking for trees in the forest: summary tree from posterior samples. *BMC evolutionary biology*, 13(1), 1–11.

Henderson, D. M. (2000) Skull and tooth morphology as indicators of niche partitioning in sympatric Morrison Formation theropods. *Gaia*, 15, 219–226.

Henderson, D. M. (2018) A buoyancy, balance and stability challenge to the hypothesis of a semi-aquatic *Spinosaurus* Stromer, 1915 (Dinosauria: Theropoda). *PeerJ*, 6, e5409.

Hendrickx, C. and Mateus, O. (2014a) Abelisauridae (Dinosauria: Theropoda) from the Late Jurassic of Portugal and dentition-based phylogeny as a contribution for the identification of isolated theropod teeth. *Zootaxa*, 3759, 1–74.

Hendrickx, C. and Mateus, O. (2014b) *Torvosaurus gurneyi* n. sp., the largest terrestrial predator from Europe, and a proposed terminology of the maxilla anatomy in nonavian theropods. *PLoS One*, 9(3), e88905.

Hendrickx, C., Mateus, O. and Araújo, R. (2015a) The dentition of megalosaurid theropods. *Acta Palaeontologica Polonica*, 60(3), 627–642.

Hendrickx, C., Mateus, O. and Araújo, R. (2015b) A proposed terminology of theropod teeth (Dinosauria, Saurischia). *Journal of Vertebrate Paleontology*, 35(5), e982797.

Hendrickx, C., Mateus, O., Araújo, R. and Choiniere, J. (2019) The distribution of dental features in non-avian theropod dinosaurs: Taxonomic potential, degree of homoplasy, and major evolutionary trends. *Palaeontologia Electronica*, 22(3), 1–110.

Hendrickx, C., Mateus, O. and Buffetaut, E. (2016) Morphofunctional Analysis of the Quadrate of Spinosauridae (Dinosauria: Theropoda) and the Presence of Spinosaurus and a Second Spinosaurine Taxon in the Cenomanian of North Africa. *PLoS One*, 11(1), e0144695.

Hendrickx, C., Stiegler, J., Currie, P. J., Han, F., Xu, X., Choiniere, J. N. and Wu, X.-C. (2020a) Dental anatomy of the apex predator *Sinraptor dongi* (Theropoda: Allosauroidea) from the Late Jurassic of China. *Canadian Journal of Earth Sciences*, 57(9), 1127–1147.

Hendrickx, C., Tschopp, E. and d. Ezcurra, M. (2020b) Taxonomic identification of isolated theropod teeth: the case of the shed tooth crown associated with *Aerosteon* (Theropoda: Megaraptora) and the dentition of Abelisauridae. *Cretaceous Research*, 108, 104312.

Hirsch, K. F., Stadtman, K. L., Miller, W. E. and Madsen Jr, J. H. (1989) Upper Jurassic dinosaur egg from Utah. *Science*, 243(4899), 1711–1713.

Holtz Jr, T. R. (2000) A new phylogeny of the carnivorous dinosaurs. *Gaia*, 15, 5–61.

Holtz, T. R. (1998) Spinosaurs as crocodile mimics. *Science*, 282(5392), 1276–1277.

Holtz, T. R. (2002) 'Dinosaur predation', in Kelly, P.H., Koweleski, M. and Hansen, T.A. (eds.) *Predator—Prey Interactions in the Fossil Record*. Kluwer/Plenum: New York, 325–340.

Holtz, T. R., Molnar, R. E. and Currie, P. J. (2004) 'Basal Tetanurae', in Weishampel, D.B., Dodson, P. and Osmólska, H. (eds.) *The Dinosauria*. University of California Press: Berkley and Los Angeles, California, 71–110.

Hone, D. and Faulkes, C. (2014) A proposed framework for establishing and evaluating hypotheses about the behaviour of extinct organisms. *Journal of Zoology*, 292(4), 260–267.

Hone, D., Mallon, J. C., Hennessey, P. and Witmer, L. M. (2020) Ontogeny of a sexually selected structure in an extant archosaur *Gavialis gangeticus* (Pseudosuchia: Crocodylia) with implications for sexual dimorphism in dinosaurs. *PeerJ*, 8, e9134.

Hone, D., Xu, X. and Wang, D. (2010a) A probable baryonychine (Theropoda: Spinosauridae) tooth from the Upper Cretaceous of Henan Province, China. *Vertebrata PalAsiatica*, 48(1), 19–26.

Hone, D. W., Farke, A. A. and Wedel, M. J. (2016) Ontogeny and the fossil record: what, if anything, is an adult dinosaur? *Biology Letters*, 12(2), 20150947.

Hone, D. W. and Rauhut, O. W. (2010b) Feeding behaviour and bone utilization by theropod dinosaurs. *Lethaia*, 43(2), 232–244.

Hone, D. W., Wang, K., Sullivan, C., Zhao, X., Chen, S., Li, D., Ji, S., Ji, Q. and Xu, X. (2011) A new, large tyrannosaurine theropod from the Upper Cretaceous of China. *Cretaceous Research*, 32(4), 495–503.

Hone, D. W. E. and Holtz Jr, T. R. (2017) A century of spinosaurs - a review and revision of the Spinosauridae with comments on their ecology. *Acta Geologica Sinica - English Edition*, 91(3), 1120–1132.

Hone, D. W. E. and Holtz Jr, T. R. (2019) Comment on: Aquatic adaptation in the skull of carnivorous dinosaurs (Theropoda: Spinosauridae) and the evolution of aquatic habits in spinosaurids. 93: 275–284. *Cretaceous Research*, 134, 104152.

Hone, D. W. E. and Holtz Jr, T. R. (2021) Evaluating the ecology of *Spinosaurus*: Shoreline generalist or aquatic pursuit specialist? *Palaeontologia Electronica*, 23(3), a03.

Hooley, R. W. (1925) On the skeleton of *Iguanodon atherfieldensis* sp. nov., from the Wealden Shales of Atherfield (Isle of Wight). *Quarterly Journal of the Geological Society*, 81, 1–61.

Höpner, S. and Bertling, M. (2017) Holes in bones: ichnotaxonomy of bone borings. *Ichnos*, 24(4), 259–282.

Hopson, J. A. (1979) 'Paleoneurology', in Gans, C., Northcutt, R.C. and Ulinski, P. (eds.) *Biology of the Reptilia*. Academic Press: New York 39–146.

Hopson, J. A. and Farrant, A. R. (2015) *Geology of the Isle of Wight – a brief explanation of the geological sheet*. Nottingham: British Geological Survey. Sheet Explanation of the British Geological Survey.

Hopson, P. (2011) The geological history of the Isle of Wight: an overview of the 'diamond in Britain's geological crown'. *Proceedings of the Geologists' Association*, 122(5), 745–763.

Hopson, P., Wilkinson, I. and Woods, M. (2008) *A stratigraphical framework for the Lower Cretaceous of England* (RR/08/03) (0852726236).

Horner, J. R. (1979) Upper Cretaceous dinosaurs from the Bearpaw Shale (marine) of south-central Montana with a checklist of Upper Cretaceous dinosaur remains from marine sediments in North America. *Journal of Paleontology*, 566–577.

Hou, L., Yeh, H. and Zhao, X. (1975) Fossil reptiles from Fusui, Kwangshi. *Vertebrata PalAsiatica*, 13(1), 24–33.

Hovenkamp, P. (2004) Review of: TNT—Tree Analysis Using New Technology. Version 1.0, by P. Goloboff, JS Farris and K. Nixon. Available from the authors and from http://www.zmuc.dk/public/phylogeny. *Cladistics*, 20(4), 378–383.

Howitt, F. (1964) Stratigraphy and structure of the Purbeck inliers of Sussex (England). *Quarterly Journal of the Geological Society*, 120(1-4), 77–113.

Hu, K., King, J. L., Romick, C. A., Dufeau, D. L., Witmer, L. M., Stubbs, T. L., Rayfield, E. J. and Benton, M. J. (2021) Ontogenetic endocranial shape change in alligators and ostriches and implications for the development of the non-avian dinosaur endocranium. *The Anatomical Record*, 304(8), 1759–1775.

Huchet, J.-B. (2014) Insect remains and their traces: relevant fossil witnesses in the reconstruction of past funerary practices. *Anthropologie*, 52(3), 329–346.

Huelsenbeck, J. P., Ronquist, F., Nielsen, R. and Bollback, J. P. (2001) Bayesian inference of phylogeny and its impact on evolutionary biology. *Science*, 294(5550), 2310–2314.

Hulke, J. (1871) Note on a Large Reptillian Skull from Brooke, Isle of Wight, probably Dinosaurian, and referable to the Genus *Iguanodon*. *Quarterly Journal of the Geological Society*, 27(1–2), 199–206.

Hurlburt, G. R. (1996) *Relative brain size in recent and fossil amniotes: determination and interpretation*. PhD Thesis. University of Toronto Toronto.

Hurlburt, G. R., Ridgely, R. C. and Witmer, L. M. (2013) 'Relative size of brain and cerebrum in tyrannosaurid dinosaurs: an analysis using brain-endocast quantitative relationships in extant alligators', in Parrish, J.M. *et al.* (eds.) *Tyrannosaurid Paleobiology*. Indiana University Press: Bloomington, 135–156.

Hutchinson, J. R. (2001) The evolution of pelvic osteology and soft tissues on the line to extant birds (Neornithes). *Zoological Journal of the Linnean Society*, 131(2), 123–168.

Hutt, S., Martill, D. M. and Barker, M. J. (1996) The first European allosaurid dinosaur (Lower Cretaceous, Wealden Group, England). *Neues Jahrbuch für Geologie und Paläontologie-Monatshefte*, 10, 635–644.

Hutt, S., Naish, D., Martill, D. M., Barker, M. J. and Newbery, P. (2001) A preliminary account of a new tyrannosauroid theropod from the Wessex Formation (Early Cretaceous) of southern England. *Cretaceous Research*, 22(2), 227–242.

Hutt, S. and Newbery, P. (2004) An exceptional theropod vertebra from the Wessex Formation (Lower Cretaceous) Isle of Wight, England. *Proceedings of the Isle of Wight Natural History and Archaeological Society*, 20, 61–76.

Ibrahim, N., Maganuco, S., Dal Sasso, C., Fabbri, M., Auditore, M., Bindellini, G., Martill, D. M., Zouhri, S., Mattarelli, D. A. and Unwin, D. M. (2020a) Tail-propelled aquatic locomotion in a theropod dinosaur. *Nature*, 581(7806), 67–70.

Ibrahim, N., Sereno, P. C., Dal Sasso, C., Maganuco, S., Fabbri, M., Martill, D. M., Zouhri, S., Myhrvold, N. and Iurino, D. A. (2014) Semiaquatic adaptations in a giant predatory dinosaur. *Science*, 345(6204), 1613–1616.

Ibrahim, N., Sereno, P. C., Varricchio, D. J., Martill, D. M., Dutheil, D. B., Unwin, D. M., Baidder, L., Larsson, H. C., Zouhri, S. and Kaoukaya, A. (2020b) Geology and paleontology of the Upper Cretaceous Kem Kem Group of eastern Morocco. *ZooKeys*, 928, 1–216.

Insole, A., Daley, B. and Gale, A. (1998) *The Isle of WIght*. The Geologists' Association. Geologists' Association Guide, 60.

Insole, A. N. and Hutt, S. (1994) The palaeoecology of the dinosaurs of the Wessex Formation (Wealden Group, Early Cretaceous), Isle of Wight, Southern England. *Zoological Journal of the Linnean Society*, 112(1-2), 197–215.

Isasmendi, E., Navarro-Lorbés, P., Sáez-Benito, P., Viera, L. I., Torices, A. and Pereda-Suberbiola, X. (2022) New contributions to the skull anatomy of spinosaurid theropods: Baryonychinae maxilla from the Early Cretaceous of Igea (La Rioja, Spain). *Historical Biology*, 1–15.

Isasmendi, E., Sáez-Benito, P., Torices, A., Navarro-Lorbés, P. and Pereda-Suberbiola, X. (2020) New insights about theropod palaeobiodiversity in the Iberian Peninsula and Europe: Spinosaurid teeth (Theropoda, Megalosauroidea) from the Lower Cretaceous of La Rioja (Spain). *Cretaceous Research*, 116, 104600.

Ito, M. (1982) Cerebellar control of the vestibulo-ocular reflex—around the flocculus hypothesis. *Annual review of neuroscience*, 5(1), 275–297.

Jarzembowski, E. A. (2011) 'Insects excluding cockroaches', in Batten, D.J. (ed.) *English Wealden Fossils*. Palaeontological Association: London, 138–173.

Jones, L. A., Dean, C. D., Mannion, P. D., Farnsworth, A. and Allison, P. A. (2021) Spatial sampling heterogeneity limits the detectability of deep time latitudinal biodiversity gradients. *Proceedings of the Royal Society B*, 288(1945), 20202762.

Jukes, T. H. and Cantor, C. R. (1969) Evolution of protein molecules. *Mammalian protein metabolism*, 3, 21–132.

Kaikaew, S., Suteethorn, V., Deesri, U. and Suteethorn, S. (2023) The endocast of *Phuwiangosaurus sirindhornae* from the Lower Cretaceous of Thailand. *Cretaceous Research*, 144, 105434.

Katsuhiro, K. and Yoshikazu, T. Y. a. H. (2017) Second discovery of a spinosaurid tooth from the Sebayashi Formation (Lower Cretaceous), Kanna Town, Gunma Prefecture, Japan. *Bulletin of Gunma Museum of Natural History*, 21, 1–6.

Kawabe, S. and Hattori, S. (2022) Complex neurovascular system in the dentary of *Tyrannosaurus*. *Historical Biology*, 34(7), 1137–1145.

Kearney, M. (2002) Fragmentary taxa, missing data, and ambiguity: mistaken assumptions and conclusions. *Systematic biology*, 51(2), 369–381.

Kearney, M. and Clark, J. M. (2003) Problems due to missing data in phylogenetic analyses including fossils: a critical review. *Journal of Vertebrate Paleontology*, 23(2), 263–274.

Keating, J. N., Sansom, R. S., Sutton, M. D., Knight, C. G. and Garwood, R. J. (2020) Morphological phylogenetics evaluated using novel evolutionary simulations. *Systematic Biology*, 69(5), 897–912.

Kellner, A. (1996) Remarks on Brazilian dinosaurs. *Memoirs of the Queensland Museum*, 39(3), 611–626.

Kellner, A. W., Azevedo, S. A., Machado, E. B., Carvalho, L. B. d. and Henriques, D. D. (2011) A new dinosaur (Theropoda, Spinosauridae) from the Cretaceous (Cenomanian) Alcântara Formation, Cajual Island, Brazil. *Anais da Academia Brasileira de Ciências*, 83(1), 99–108.

Kellner, A. W. and Campos, D. d. A. (1996) First Early Cretaceous theropod dinosaur from Brazil with comments on Spinosauridae. *Neues Jahrbuch für Geologie und Paläontologie-Abhandlungen*, 151–166.

Kerr, A. C. (2014) 'Oceanic Plateaus', in Holland, H.D. and Turekian, K.K. (eds.) *Treatise on Geochemistry (Second Edition)*. Elsevier: Oxford, 631–667.

Kerth, M. and Hailwood, E. (1988) Magnetostratigraphy of the Lower Cretaceous Vectis Formation (Wealden Group) on the Isle of Wight, southern England. *Journal of the Geological Society*, 145(2), 351–360.

King, J. L., Sipla, J. S., Georgi, J. A., Balanoff, A. M. and Neenan, J. M. (2020) The endocranium and trophic ecology of *Velociraptor mongoliensis*. *Journal of Anatomy*, 237(5), 861–869.

King, L. (2021) *Macroevolutionary and ontogenetic trends in the anatomy and morphology of the non-avian dinosaur endocranium*. PhD Thesis. University of Bristol.

Kitching, I. J., Forey, P., Forey, P. L., Humphries, C. and Williams, D. (1998) 'Measures of character fit and character weighting', in *Cladistics: the theory and practice of parsimony analysis*. Oxford University Press, USA, 92–117.

Kluge, A. G. and Farris, J. S. (1969) Quantitative phyletics and the evolution of anurans. *Systematic Biology*, 18(1), 1–32.

Knoll, F., Buffetaut, E. and Buelow, M. (1999) A theropod braincase from the Jurassic of the Vaches Noires cliffs (Normandy, France); osteology and palaeoneurology. *Bulletin de la Société géologique de France*, 170(1), 103–109.

Knoll, F. and Kawabe, S. (2020) Avian palaeoneurology: Reflections on the eve of its 200th anniversary. *Journal of Anatomy*, 236(6), 965–979.

Knoll, F., Lautenschlager, S., Kawabe, S., Martínez, G., Espílez, E., Mampel, L. and Alcalá, L. (2021) Palaeoneurology of the early cretaceous iguanodont *Proa valdearinnoensis* and its bearing on the parallel developments of cognitive abilities in theropod and ornithopod dinosaurs. *Journal of Comparative Neurology*, 529(18), 3922–3945.

Knoll, F., Witmer, L. M., Ortega, F., Ridgely, R. C. and Schwarz-Wings, D. (2012) The braincase of the basal sauropod dinosaur *Spinophorosaurus* and 3D reconstructions of the cranial endocast and inner ear. *PloS one*, 7(1), e30060.

Kovarovic, K., Aiello, L. C., Cardini, A. and Lockwood, C. A. (2011) Discriminant function analyses in archaeology: are classification rates too good to be true? *Journal of archaeological science*, 38(11), 3006-3018.

Krumenacker, L., Simon, D. J., Scofield, G. and Varricchio, D. J. (2017) Theropod dinosaurs from the Albian–cenomanian Wayan Formation of eastern Idaho. *Historical Biology*, 29(2), 170–186.

Kundrát, M. (2007) Avian-like attributes of a virtual brain model of the oviraptorid theropod *Conchoraptor gracilis*. *Naturwissenschaften*, 94(6), 499–504.

Kundrát, M., Xu, X., Hančová, M., Gajdoš, A., Guo, Y. and Chen, D. (2018) Evolutionary disparity in the endoneurocranial configuration between small and gigantic tyrannosauroids. *Historical Biology*, 32(5), 620–634.

Lacerda, M. B., de Andrade, M. B., Sales, M. A., Aragão, P. R., Vieira, F. S., Bittencourt, J. S. and Liparini, A. (2023) The vertebrate fossil record from the Feliz Deserto Formation (Lower Cretaceous), Sergipe, NE Brazil: paleoecological, taphonomic, and paleobiogeographic implications. *Cretaceous Research*, 147, 105463.

Lacerda, M. B., Grillo, O. N. and Romano, P. S. (2021) Rostral morphology of Spinosauridae (Theropoda, Megalosauroidea): premaxilla shape variation and a new phylogenetic inference. *Historical Biology*, 34(11), 2089–2109.

Lake, R. D. and Shepard-Thorn, E. R. (1987) *Geology of the country around Hastings and Dungeness: Memoir for 1:50,000 Geological Sheets 320 and 321 (England and Wales)*. London: British Geological Survey Geological Memoirs & Sheet Explanations (England & Wales).

Lakin, R. J. and Longrich, N. R. (2019) Juvenile spinosaurs (Theropoda: Spinosauridae) from the middle Cretaceous of Morocco and implications for spinosaur ecology. *Cretaceous Research*, 93, 129–142.

Langer, M. C. (2004) 'Basal Saurischia', in Weishampel, D.B., Dodson, P. and OsmÓLska, H. (eds.) *The Dinosauria*. 2 edn. University of California Press, 25–46.

Langer, M. C. and Benton, M. J. (2006) Early dinosaurs: a phylogenetic study. *Journal of Systematic Palaeontology*, 4(4), 309–358.

Larsson, H. C., Sereno, P. C. and Wilson, J. A. (2000) Forebrain enlargement among nonavian theropod dinosaurs. *Journal of Vertebrate Paleontology*, 20(3), 615–618.

Lautenschlager, S. (2016) Reconstructing the past: methods and techniques for the digital restoration of fossils. *Royal Society Open Science*, 3(10), 160342.

Lautenschlager, S. and Hübner, T. (2013) Ontogenetic trajectories in the ornithischian endocranium. *Journal of Evolutionary Biology*, 26(9), 2044–2050.

Lautenschlager, S., Rayfield, E. J., Altangerel, P., Zanno, L. E. and Witmer, L. M. (2012) The endocranial anatomy of Therizinosauria and its implications for sensory and cognitive function. *PLoS One*, 7(12), e52289.

Le Loeuff, J., Metais, E., Dutheil, D. B., Rubino, J. L., Buffetaut, E., Lafont, F., Cavin, L., Moreau, F., Tong, H. and Blanpied, C. (2010) An Early Cretaceous vertebrate assemblage from the Cabao Formation of NW Libya. *Geological Magazine*, 147(5), 750–759.

Lee, M. S. (2016) Multiple morphological clocks and total-evidence tip-dating in mammals. *Biology Letters*, 12(7), 20160033.

Lee, M. S. Y. (2000) Tree robustness and clade significance. *Systematic Biology*, 829–836.

Lessner, E. J. (2021) Quantifying neurovascular canal branching patterns reveals a shared crocodylian arrangement. *Journal of Morphology*, 282(2), 185–204.

Lessner, E. J. and Holliday, C. M. (2022) A 3D ontogenetic atlas of *Alligator mississippiensis* cranial nerves and their significance for comparative neurology of reptiles. *The Anatomical Record*, 305(10), 2854–2882.

Lewis, P. O. (1998) A genetic algorithm for maximum-likelihood phylogeny inference using nucleotide sequence data. *Molecular biology and evolution*, 15(3), 277–283.

Lewis, P. O. (2001) A likelihood approach to estimating phylogeny from discrete morphological character data. *Systematic biology*, 50(6), 913–925.

Lipkin, C., Sereno, P. C. and Horner, J. R. (2007) The furcula in *Suchomimus tenerensis* and *Tyrannosaurus rex* (Dinosauria: Theropoda: Tetanurae). *Journal of Paleontology*, 81(6), 1523–1527.

Lockwood, J. (2016) Ichnological evidence for large predatory dinosaurs in the Wessex Formation (Wealden Group, Early Cretaceous) of the Isle of Wight. *Proceedings of the Isle of Wight Natural History and Archaeological Society*, 30, 103–110.

Lomax, D. R. and Tamura, N. (2014) *Dinosaurs of the British Isles*. Siri Scientific Press Manchester.

Longrich, N. R. and Field, D. J. (2012) *Torosaurus* is not *Triceratops*: ontogeny in chasmosaurine ceratopsids as a case study in dinosaur taxonomy. *PLOS ONE*, 7(7), e32623.

Longrich, N. R., Pereda-Suberbiola, X., Jalil, N.-E., Khaldoune, F. and Jourani, E. (2017) An abelisaurid from the latest Cretaceous (late Maastrichtian) of Morocco, North Africa. *Cretaceous Research*, 76, 40–52.

Lopez-Arbarello, A. (2012) Phylogenetic interrelationships of ginglymodian fishes (Actinopterygii: Neopterygii). *PLoS One*, 7(7), e39370.

Lydekker, R. (1888) *Catalogue of the Fossil Reptilia and Amphibia in the British Museum (Natural History). Part I.*

Madsen, J. H. (1976) *Allosaurus fragilis*: a revised osteology. *Utah Geological Survey Bulletin*, 109, 1–161.

Madzia, D. and Cau, A. (2017) Inferring 'weak spots' in phylogenetic trees: application to mosasauroid nomenclature. *PeerJ*, 5, e3782.

Mahler, L. (2005) Record of abelisauridae (Dinosauria: Theropoda) from the Cenomanian of Morocco. *Journal of Vertebrate Paleontology*, 25(1), 236–239.

Maisch, M. W. (2016) The nomenclatural status of the carnivorous dinosaur genus Altispinax v. Huene, 1923 (Saurischia, Theropoda) from the Lower Cretaceous of England. *Neues Jahrbuch für Geologie und Paläontologie-Abhandlungen*, 215–219.

Malafaia, E., Gasulla, J., Escaso, F., Narvaéz, I. and Ortega, F. (2020a) An update of the spinosaurid (Dinosauria: Theropoda) fossil record from the Lower Cretaceous of the Iberian Peninsula: distribution, diversity, and evolutionary history. *Journal of Iberian Geology*, 46, 431–444.

Malafaia, E., Gasulla, J. M., Escaso, F., Narváez, I., Sanz, J. L. and Ortega, F. (2020b) A new spinosaurid theropod (Dinosauria: Megalosauroidea) from the upper Barremian of Vallibona, Spain: Implications for spinosaurid diversity in the Early Cretaceous of the Iberian Peninsula. *Cretaceous Research*, 106, 104221.

Mallon, J. C. (2017) Recognizing sexual dimorphism in the fossil record: lessons from nonavian dinosaurs. *Paleobiology*, 43(3), 495–507.

Marsh, A. D. and Rowe, T. B. (2020) A comprehensive anatomical and phylogenetic evaluation of *Dilophosaurus wetherilli* (Dinosauria, Theropoda) with descriptions of new specimens from the Kayenta Formation of northern Arizona. *Journal of Paleontology*, 94(S78), 1–103.

Marsh, O. C. (1881) Principal characters of American Jurassic dinosaurs, part V. *American Journal of Science*, (125), 417–423.

Martill, D. M. (2001) 'Taphonomy', in Martill, D.M. and Naish, D. (eds.) *Dinosaurs of the Isle of Wight*. Palaeontological Association, London, 49–59.

Martill, D. M., Batten, D. J. and Loydell, D. K. (2000) A new specimen of the thyreophoran dinosaur cf. *Scelidosaurus* with soft tissue preservation. *Palaeontology*, 43(3), 549–559.

Martill, D. M., Cruickshank, A., Frey, E., Small, P. and Clarke, M. (1996a) A new crested maniraptoran dinosaur from the Santana Formation (Lower Cretaceous) of Brazil. *Journal of the Geological Society*, 153(1), 5–8.

Martill, D. M. and Hutt, S. (1996b) Possible baryonychid dinosaur teeth from the Wessex Formation (Lower Cretaceous, Barremian) of the Isle of Wight, England. *Proceedings of the Geologists' Association*, 107(2), 81–84.

Martill, D. M. and Naish, D. (eds.) (2001a) *Dinosaurs of the Isle of Wight*. Palaeontological Association, London.

Martill, D. M. and Naish, D. (2001b) 'The geology of the Isle of Wight', in Martill, D.M. and Naish, D. (eds.) *Dinosaurs of the Isle of Wight*. The Palaeontological Association: London, 25–43.

Martill, D. M., Naish, D. and Earland, S. (2006) Dinosaurs in marine strata: evidence from the British Jurassic, including a review of the allochthonous vertebrate assemblage from the marine Kimmeridge Clay Formation (Upper Jurassic) of Great Britain, *Actas de las III Jornadas sobre Dinosaurios y su Entorno. Salas de los Infantes, Burgos*.

Martill, D. M., Naish, D. and Hutt, S. (2001c) 'Introduction', in Martill, D.M. and Naish, D. (eds.) *Dinosaurs of the Isle of Wight*. Palaeontological Association, London, 11–24.

Martin, J. E., Raslan-Loubatié, J. and Mazin, J.-M. (2016) Cranial anatomy of *Pholidosaurus purbeckensis* from the Lower Cretaceous of France and its bearing on pholidosaurid affinities. *Cretaceous Research*, 66, 43–59.

Martin, J. E., Smith, T., Salaviale, C., Adrien, J. and Delfino, M. (2020) Virtual reconstruction of the skull of *Bernissartia fagesii* and current understanding of the neosuchian–eusuchian transition. *Journal of Systematic Palaeontology*, 18(13), 1079–1101.

Marugán-Lobón, J., Chiappe, L. M. and Farke, A. A. (2013) The variability of inner ear orientation in saurischian dinosaurs: testing the use of semicircular canals as a reference system for comparative anatomy. *PeerJ*, 1, e124.

Mateus, O., Araujo, R., Natário, C. and Castanhinha, R. (2011) A new specimen of the theropod dinosaur *Baryonyx* from the early Cretaceous of Portugal and taxonomic validity of *Suchosaurus*. *Zootaxa*, 2827(5), 54–68.

Mateus, O. and Estraviz-López, D. (2022) A new theropod dinosaur from the early cretaceous (Barremian) of Cabo Espichel, Portugal: Implications for spinosaurid evolution. *PloS one*, 17(2), e0262614.

McCurry, M. R., Evans, A. R., Fitzgerald, E. M., McHenry, C. R., Bevitt, J. and Pyenson, N. D. (2019) The repeated evolution of dental apicobasal ridges in aquatic-feeding mammals and reptiles. *Biological Journal of the Linnean Society*, 127(2), 245–259.

McFeeters, B. (2020) New mid-cervical vertebral morphotype of Spinosauridae from the Kem Kem Group of Morocco. *Vertebrate Anatomy Morphology Palaeontology*, 8(1), 182–193.

McFeeters, B., Ryan, M. J., Hinic-Frlog, S. and Schröder-Adams, C. (2013) A reevaluation of *Sigilmassasaurus brevicollis* (Dinosauria) from the Cretaceous of Morocco. *Canadian Journal of Earth Sciences*, 50(6), 636–649.

McHugh, J. B., Drumheller, S. K., Riedel, A. and Kane, M. (2020) Decomposition of dinosaurian remains inferred by invertebrate traces on vertebrate bone reveal new insights into Late Jurassic ecology, decay, and climate in western Colorado. *PeerJ*, 8, e9510.

McKeown, M., Brusatte, S. L., Williamson, T. E., Schwab, J. A., Carr, T. D., Butler, I. B., Muir, A., Schroeder, K., Espy, M. A. and Hunter, J. F. (2020) Neurosensory and sinus evolution as tyrannosauroid dinosaurs developed giant size: insight from the endocranial anatomy of *Bistahieversor sealeyi*. *The Anatomical Record*, 303(4), 1043–1059.

Medeiros, M. A. (2006) Large theropod teeth from the Eocenomanian of northeastern Brazil and the occurrence of Spinosauridae. *Revista brasileira de Paleontologia*, 9(3), 333–338.

Milner, A. C. (2002) Theropod dinosaurs of the Purbeck limestone group, Southern England. *Special Papers in Palaeontology*, 68, 191–202.

Milner, A. C. (2003) Fish-eating theropods: a short review of the systematics, biology and palaeobiogeography, *Actas de las II Jornadas Internacionales sobre Paleontología de Dinosaurios y su Entorno: Salas de los Infantes (Burgos, España), septiembre de 2001*. Caja de Burgos.

Milner, H. B. (1922) The geology of the country around Heathfield, Sussex: With report of excursion to heathfield, brightling, netherfield and robertsbridge. Saturday, June 4th, 1921. *Proceedings of the Geologists' Association*, 33(2), 142–151.

Molnar, R. E. (1990) 'Variation in theory and in theropods', in Carpenter, K. and Currie, P.J. (eds.) *Dinosaur Systematics: Approaches and Perspectives.* Cambridge University Press, 71–79.

Moro, D., Kerber, L., Müller, R. T. and Pretto, F. A. (2021) Sacral co-ossification in dinosaurs: The oldest record of fused sacral vertebrae in Dinosauria and the diversity of sacral co-ossification patterns in the group. *Journal of Anatomy*, 238(4), 828–844.

Myhrvold, N. P., Sereno, P. C., Baumgart, S. L., Formoso, K. K., Vidal, D., Fish, F. E. and Henderson, D. M. (2022) Spinosaurids as' subaqueous foragers' undermined by selective sampling and problematic statistical inference. *bioRxiv*, 1–5.

Naish, D. (2003) A definitive allosauroid (Dinosauria; Theropoda) from the Lower Cretaceous of east Sussex. *Proceedings of the Geologists' Association*, 114, 319–326.

Naish, D. (2011) 'Theropod dinosaurs', in Batten, D.J. (ed.) *English Wealden Fossils* The Palaeontological Association: London, 526–559.

Naish, D., Hutt, S. and Martill, D. M. (2001) 'Saurischian dinosaurs 2: Theropods. ', in Martill, D.M. and Naish, D. (eds.) *Dinosaurs of the Isle of Wight*. The Palaeontological Association London, 242–309.

Naish, D. and Martill, D. M. (2007) Dinosaurs of Great Britain and the role of the Geological Society of London in their discovery: basal Dinosauria and Saurischia. *Journal of the Geological Society*, 164(3), 493–510.

Naish, D. and Martill, D. M. (2008) Dinosaurs of Great Britain and the role of the Geological Society of London in their discovery: Ornithischia. *Journal of the Geological Society*, 165(3), 613–623.

Naish, D. and Sweetman, S. C. (2011) A tiny maniraptoran dinosaur in the Lower Cretaceous Hastings Group: evidence from a new vertebrate-bearing locality in south-east England. *Cretaceous Research*, 32(4), 464–471.

Nascimento, F. F., Dos Reis, M. and Yang, Z. (2017) A biologist's guide to Bayesian phylogenetic analysis. *Nature ecology & evolution*, 1(10), 1446–1454.

Neenan, J. M., Reich, T., Evers, S. W., Druckenmiller, P. S., Voeten, D. F., Choiniere, J. N., Barrett, P. M., Pierce, S. E. and Benson, R. B. (2017) Evolution of the sauropterygian labyrinth with increasingly pelagic lifestyles. *Current Biology*, 27(24), 3852-3858.e3.

Nesbitt, S. J. (2011) The early evolution of archosaurs: relationships and the origin of major clades. *Bulletin of the American Museum of Natural History*, 352, 1–292.

Neumann, V. and Assine, M. (2015) Stratigraphic proposal to the post-rift I tectonic-sedimentary sequence of Araripe Basin, Northeastern Brazil, *International Congress on Stratigraphy*.

Neumann, V. and Cabrera, L. (1999) Una nueva propuesta estratigrafica para la tectonosecuencia post-rifte de la cuenca de Araripe, noreste de Brasil, *Boletim do Simposio Sobre O Cretaceo Do Brasil*. 279–285.

Nicholl, C. S. C., Mannion, P. D. and Barrett, P. M. (2018) Sauropod dinosaur remains from a new Early Jurassic locality in the Central High Atlas of Morocco. *Acta Palaeontologica Polonica*, 63(1), 147–157.

Nityananda, V. and Read, J. C. (2017) Stereopsis in animals: evolution, function and mechanisms. *Journal of Experimental Biology*, 220(14), 2502–2512.

Nixon, K. C. (1999) The parsimony ratchet, a new method for rapid parsimony analysis. *Cladistics*, 15(4), 407–414.

Norell, M. A. and Clark, J. M. (1990) A reanalysis of *Bernissartia fagesii*, with comments on its phylogenetic position and its bearing on the origin and diagnosis of the Eusuchia. *Bulletin de l'Institut Royal des Sciences Naturelles de Belgique*, 60, 115–128.

Norman, D. B. (2004) 'Basal iguanodontia', in Weishampel, D.B., Dodson, P. and Osmólska, H. (eds.) *The Dinosauria*. University of California Press: Berkeley CA, 413–437.

Norman, D. B. (2011) 'Ornithopod dinosaurs', in Batten, D.J. (ed.) *English Wealden Fossils*. The Palaeontological Association: London, 407–475.

Novas, F. E. (2009) *The age of dinosaurs in South America*. Indiana University Press.

Novas, F. E., Agnolín, F. L., Ezcurra, M. D., Porfiri, J. and Canale, J. I. (2013) Evolution of the carnivorous dinosaurs during the Cretaceous: the evidence from Patagonia. *Cretaceous Research*, 45, 174–215.

Novas, F. E., Chatterjee, S., Rudra, D. K. and Datta, P. (2010) '*Rahiolisaurus gujaratensis*, n. gen. n. sp., a new abelisaurid theropod from the Late Cretaceous of India', in *New aspects of Mesozoic biodiversity*. Springer, 45–62.

O'Connor, P. M. (2006) Postcranial pneumaticity: an evaluation of soft-tissue influences on the postcranial skeleton and the reconstruction of pulmonary anatomy in archosaurs. *Journal of Morphology*, 267(10), 1199–1226.

O'Connor, P. M. (2007) The postcranial axial skeleton of *Majungasaurus crenatissimus* (Theropoda: Abelisauridae) from the Late Cretaceous of Madagascar. *Journal of Vertebrate Paleontology*, 27(S2), 127–163.

O'Reilly, J. E. and Donoghue, P. C. (2018) The efficacy of consensus tree methods for summarizing phylogenetic relationships from a posterior sample of trees estimated from morphological data. *Systematic biology*, 67(2), 354–362.

Ogg, J. G., Hasenyager II, R. W. and Wimbledon, W. A. (1994) Jurassic-Cretaceous boundary: Portland-Purbeck magnetostratigraphy and possible correlation to the Tethyan faunal realm. *Geobios*, 27, 519–527.

Orhan, K., Faria Vasconcelos, K. d. and Gaêta-Araujo, H. (2020) 'Artifacts in micro-CT', in *Micro-computed Tomography (micro-CT) in Medicine and Engineering*. Springer, 35–48.

Owen, R. (1840–1845) *Odontography; or, A treatise on the comparative anatomy of the teeth; their physiological relations, mode of development, and microscopic structure, in the vertebrate animals*. London: Hippolyte Baillière.

Owen, R. (1842) *Report on British Fossil Reptiles Part II*. London.

Owen, R. (1878) Monograph on the fossil Reptilia of the Wealden and Purbeck Formations, Supplement VIII: Crocodilia (*Goniopholis*, *Petrosuchus* and *Suchosaurus*). *Palaeontographical Society Monographs*, 1–15.

Owen, R. (1879) Monograph on the fossil Reptilia of the Wealden and Purbeck Formations, Supplement IX: Crocodilia (*Goniopholis*, *Brachydectes*, *Nannosuchus*, *Theriosuchus* and *Nuthetes*). *Palaeontographical Society Monographs*, 33, 1–19.

Padian, K., Hutchinson, J. R. and Holtz, T. R. (1999) Phylogenetic definitions and nomenclature of the major taxonomic categories of the carnivorous Dinosauria (Theropoda). *Journal of Vertebrate Paleontology*, 19(1), 69–80.

Paik, I. S. (2000) Bone chip-filled burrows associated with bored dinosaur bone in floodplain paleosols of the Cretaceous Hasandong Formation, Korea. *Palaeogeography, Palaeoclimatology, Palaeoecology*, 157(3-4), 213–225.

Palci, A., Caldwell, M. W. and Papazzoni, C. A. (2013) A new genus and subfamily of mosasaurs from the Upper Cretaceous of northern Italy. *Journal of Vertebrate Paleontology*, 33(3), 599–612.

Pasch, A. D. and May, K. C. (1997) First occurrence of a hadrosaur (Dinosauria) from the Matanuska Formation (Turonian) in the Talkeetna Mountains of south-central Alaska. *Short notes on Alaska geology*, 1997, 99–109.

Paul, G. S. (1988) *Predatory Dinosaurs of the World*. New York: Simon and Schuster.

Paulina-Carabajal, A. and Canale, J. I. (2010) Cranial endocast of the carcharodontosaurid theropod *Giganotosaurus carolinii* Coria & Salgado, 1995. *Neues Jahrbuch fur Geologie und Palaontologie–Abhandlungen*, 258, 249–256.

Paulina-Carabajal, A. and Currie, P. J. (2012) New information on the braincase of *Sinraptor dongi* Currie and Zhao (Theropoda, Allosauroidea): ethmoidal region, endocranial anatomy and pneumaticity. *Vertebrata PalAsiatica*, 50(2), 85–101.

Paulina-Carabajal, A. and Currie, P. J. (2017) The braincase of the theropod dinosaur *Murusraptor*: osteology, neuroanatomy and comments on the paleobiological implications of certain endocranial features. *Ameghiniana*, 54(5), 617–640.

Paulina-Carabajal, A., Currie, P. J., Dudgeon, T. W., Larsson, H. C. and Miyashita, T. (2021) Two braincases of *Daspletosaurus* (Theropoda: Tyrannosauridae): anatomy and comparison. *Canadian Journal of Earth Sciences*, 58(9), 885–910.

Paulina-Carabajal, A., Ezcurra, M. D. and Novas, F. E. (2019a) New information on the braincase and endocranial morphology of the Late Triassic neotheropod *Zupaysaurus rougieri* using computed tomography data. *Journal of Vertebrate Paleontology*, 39(3), e1630421.

Paulina-Carabajal, A. and Filippi, L. (2018) Neuroanatomy of the abelisaurid theropod *Viavenator*: The most complete reconstruction of a cranial endocast and inner ear for a South American representative of the clade. *Cretaceous Research*, 83, 84–94.

Paulina-Carabajal, A. and Nieto, M. N. (2019b) Brief comment on the brain and inner ear of *Giganotosaurus carolinii* (Dinosauria: Theropoda) based on CT scans. *Ameghiniana*, 57(1), 58–62.

Paulina-Carabajal, A. and Succar, C. (2014) The endocranial morphology and inner ear of the abelisaurid theropod *Aucasaurus garridoi*. *Acta Palaeontologica Polonica*, 60(1), 141–144.

Penn, S. J. and Sweetman, S. C. (2022) Microvertebrate-rich gutter casts from the basal Wessex Formation (Wealden Group, Lower Cretaceous) of Dungy Head, Dorset: insights into the palaeoecology and palaeoenvironment of a non-marine wetland. *Cretaceous Research*, 143, 105397.

Penn, S. J., Sweetman, S. C., Martill, D. M. and Coram, R. A. (2020) The Wessex Formation (Wealden Group, Lower Cretaceous) of Swanage Bay, southern England. *Proceedings of the Geologists' Association*, 131(6), 679–698.

Pereda-Suberbiola, X., Pérez-García, A., Corral, J. C., Murelaga, X., Martin, G., Larranaga, J., Bardet, N., Berreteaga, A. and Company, J. (2015) First dinosaur and turtle remains from the latest Cretaceous shallow marine deposits of Albaina (Lano quarry, Iberian Peninsula). *Comptes Rendus Palevol*, 14(6–7), 471–482.

Pereda-Suberbiola, X., Ruiz-Omeñaca, J. I., Canudo, J. I., Torcida, F. and Sanz, J. L. (2012) 'Dinosaur faunas from the Early Cretaceous (Valanginian-Albian) of Spain', in Godefroit, P. (ed.) *Bernissart dinosaurs and early Cretaceous terrestrial ecosystem*. Indiana University Press: Bloomington, 379–407.

Pérez-Ramos, A. and Figueirido, B. (2020) Toward an “Ancient” Virtual World: Improvement Methods on X-ray CT Data Processing and Virtual Reconstruction of Fossil Skulls. *Frontiers in Earth Science*, 8, 345.

Pfaff, C., Schultz, J. A. and Schellhorn, R. (2019) The vertebrate middle and inner ear: A short overview. *Journal of morphology*, 280(8), 1098–1105.

Pharisat, A. (1993) Vertèbres de dinosaure (Théropode) dans l'Oxfordien de Plaimbois-du-Miroir (Doubs). *Société d'Histoire Nat du Pays Montbéliard, Montbéliard, Bull*, 1993, 191-192.

Pirrone, C. A., Buatois, L. A. and Bromley, R. G. (2014) Ichnotaxobases for bioerosion trace fossils in bones. *Journal of Paleontology*, 88(1), 195–203.

Pol, D. and Escapa, I. H. (2009) Unstable taxa in cladistic analysis: identification and the assessment of relevant characters. *Cladistics*, 25(5), 515–527.

Pond, S., Lockley, M. G., Lockwood, J. A., Breithaupt, B. H. and Matthews, N. A. (2014) Tracking dinosaurs on the Isle of Wight: a review of tracks, sites, and current research. *Biological Journal of the Linnean Society*, 113(3), 737–757.

Porfiri, J. D., Novas, F. E., Calvo, J. O., Agnolín, F. L., Ezcurra, M. D. and Cerda, I. A. (2014) Juvenile specimen of *Megaraptor* (Dinosauria, Theropoda) sheds light about tyrannosauroid radiation. *Cretaceous Research*, 51, 35–55.

Porfiri, J. D., Valieri, R. D. J., Santos, D. D. and Lamanna, M. C. (2018) A new megaraptoran theropod dinosaur from the Upper Cretaceous Bajo de la Carpa Formation of northwestern Patagonia. *Cretaceous Research*, 89, 302–319.

Poropat, S. F., White, M. A., Vickers-Rich, P. and Rich, T. H. (2019) New megaraptorid (Dinosauria: Theropoda) remains from the Lower Cretaceous Eumeralla Formation of Cape Otway, Victoria, Australia. *Journal of Vertebrate Paleontology*, 39(4), e1666273.

Porter, W. R. and Witmer, L. M. (2015) Vascular patterns in iguanas and other squamates: blood vessels and sites of thermal exchange. *PLoS One*, 10(10), e0139215.

Porter, W. R. and Witmer, L. M. (2020) Vascular patterns in the heads of dinosaurs: Evidence for blood vessels, sites of thermal exchange, and their role in physiological thermoregulatory strategies. *The Anatomical Record*, 303(4), 1075–1103.

Puértolas-Pascual, E., Canudo, J. and Rabal-Garcés, R. (2015) Exceptional crocodylomorph biodiversity of "La Cantalera" site (lower Barremian; Lower Cretaceous) in Teruel, Spain. *Palaeontologia Electronica*, 18.2.28A, 1–16.

Racicot, R. (2017) Fossil secrets revealed: X-ray CT scanning and applications in paleontology. *The Paleontological Society Papers*, 22, 21–38.

Radley, J. D. and Allen, P. (2012a) The non-marine Lower Cretaceous Wealden strata of southern England. *Proceedings of the Geologists' Association*, 123(2), 235–244.

Radley, J. D. and Allen, P. (2012b) The southern English Wealden (non-marine Lower Cretaceous): overview of palaeoenvironments and palaeoecology. *Proceedings of the Geologists' Association*, 123(2), 382–385.

Radley, J. D. and Allen, P. (2012c) The Wealden (non-marine Lower Cretaceous) of the Weald sub-basin, southern England. *Proceedings of the Geologists' Association*, 123(2), 245–318.

Radley, J. D. and Allen, P. (2012d) The Wealden (non-marine Lower Cretaceous) of the Wessex Sub-basin, southern England. *Proceedings of the Geologists' Association*, 123(2), 319–373.

Radley, J. D. and Barker, M. J. (1998a) Stratigraphy, palaeontology and correlation of the Vectis Formation (Wealden Group, Lower Cretaceous) at Compton Bay, Isle of Wight, southern England. *Proceedings of the Geologists' Association*, 109(3), 187–195.

Radley, J. D., Barker, M. J. and Harding, I. C. (1998b) Palaeoenvironment and taphonomy of dinosaur tracks in the Vectis Formation (Lower Cretaceous) of the Wessex Sub-basin, southern England. *Cretaceous Research*, 19(3-4), 471–487.

Radley, J. D. and Coram, R. A. (2011) 'The Wealden of Dorset', in Batten, D.J. (ed.) *English Wealden Fossils*. The Palaeontological Association: London, 79–84.

Rambaut, A., Drummond, A. J., Xie, D., Baele, G. and Suchard, M. A. (2018) Posterior summarization in Bayesian phylogenetics using Tracer 1.7. *Systematic biology*, 67(5), 901–904.

Rauhut, O. W. (2003) *The Interrelationships and Evolution of Basal Theropod Dinosaurs*. Blackwell Publishing. Special Papers in Palaeontology, , 69.

Rauhut, O. W. (2005) Osteology and relationships of a new theropod dinosaur from the Middle Jurassic of Patagonia. *Palaeontology*, 48(1), 87–110.

Rauhut, O. W. (2011) Theropod dinosaurs from the Late Jurassic of Tendaguru (Tanzania). 86, 195–239.

Rauhut, O. W., Canudo, J. I. and Castanera, D. (2019a) A reappraisal of the Early Cretaceous theropod dinosaur *Camarillasaurus* from Spain, *European Association of Vertebrate Paleontologists (EAVP)*. Brussels. Program and Abstracts XVII Conference of the EAVP.

Rauhut, O. W., Foth, C., Tischlinger, H. and Norell, M. A. (2012) Exceptionally preserved juvenile megalosauroid theropod dinosaur with filamentous integument from the Late Jurassic of Germany. *Proceedings of the National Academy of Sciences*, 109(29), 11746–11751.

Rauhut, O. W., Huebner, T. R. and Lanser, K.-P. (2016) A new megalosaurid theropod dinosaur from the late Middle Jurassic (Callovian) of north-western Germany: Implications for theropod evolution and faunal turnover in the Jurassic. *Palaeontologia Electronica*, 19(2.26A), 1–65.

Rauhut, O. W., Piñuela, L., Castanera, D., García-Ramos, J.-C. and Cela, I. S. (2018) The largest European theropod dinosaurs: remains of a gigantic megalosaurid and giant theropod tracks from the Kimmeridgian of Asturias, Spain. *PeerJ*, 6, e4963.

Rauhut, O. W. and Pol, D. (2019b) Probable basal allosauroid from the early Middle Jurassic Cañadón Asfalto Formation of Argentina highlights phylogenetic uncertainty in tetanuran theropod dinosaurs. *Scientific Reports*, 9(1), 18826

Raven, T. J., Barrett, P. M., Pond, S. B. and Maidment, S. C. (2020) Osteology and Taxonomy of British Wealden Supergroup (Berriasian–Aptian) Ankylosaurs (Ornithischia, Ankylosauria). *Journal of Vertebrate Paleontology*, 40(4), e1826956.

Rawson, P. F. (1992) 'The Cretaceous', in Duff, P.M.D. and Smith, A.J. (eds.) *Geology of ENgland and Wales*. The Geological Society London, 355♥388.

Rawson, P. F. (2006) 'Cretaceous: sea levels peak as the North Atlantic opens', in Brenchley, P.J. and Rawson, P.F. (eds.) *The Geology of England and Wales (2nd edition)*. The Geological Society: London, 365–393.

Rayfield, E. J., Milner, A. C., Xuan, V. B. and Young, P. G. (2007) Functional morphology of spinosaur 'crocodile-mimic'dinosaurs. *Journal of Vertebrate Paleontology*, 27(4), 892–901.

Ree, R. H. and Smith, S. A. (2008) Maximum likelihood inference of geographic range evolution by dispersal, local extinction, and cladogenesis. *Systematic biology*, 57(1), 4–14.

Richter, U., Mudroch, A. and Buckley, L. G. (2013) Isolated theropod teeth from the Kem Kem beds (early Cenomanian) near Taouz, Morocco. *Paläontologische Zeitschrift*, 87(2), 291–309.

Robinson, S. A. and Hesselbo, S. P. (2004) Fossil-wood carbon-isotope stratigraphy of the non-marine Wealden Group (Lower Cretaceous, southern England). *Journal of the Geological Society*, 161(1), 133–145.

Rogers, R. R. (1992) Non-marine borings in dinosaur bones from the Upper Cretaceous Two Medicine Formation, northwestern Montana. *Journal of Vertebrate Paleontology*, 12(4), 528–531.

Rogers, S. W. (1998) Exploring dinosaur neuropaleobiology: computed tomography scanning and analysis of an *Allosaurus fragilis* endocast. *Neuron*, 21(4), 673–679.

Ross, A. J. and Cook, E. (1995) The stratigraphy and palaeontology of the Upper Weald Clay (Barremian) at Smokejacks Brickworks, Ockley, Surrey, England. *Cretaceous Research*, 16(6), 705–716.

Ruffell, A. (1988) Palaeoecology and event stratigraphy of the Wealden-Lower Greensand transition in the Isle of Wight. *Proceedings of the Geologists' Association*, 99(2), 133–140.

Ruffell, A. H., Hesselbo, S. P., Wach, G. D., Simpson, M. I. and Wray, D. S. (2002) Fuller's earth (bentonite) in the Lower Cretaceous (Upper Aptian) of Shanklin (Isle of Wight, southern England). *Proceedings of the Geologists Association*, 113, 281–290.

Ruiz-Omeñaca, J. I. (2003) Los restos directos de dinosaurios terópodos (excluyendo Aves) en España, *Dinosaurios y otros reptiles mesozoicos en España*. Universidad de La Rioja.

Ruiz-Omeñaca, J. I., Canudo, J. I., Cruzado-Caballero, P., Infante, P. and Moreno-Azanza, M. (2005) Baryonychine teeth (Theropoda: Spinosauridae) from the Lower Cretaceous of La Cantalera (Josa, NE Spain). *Kaupia*, 14, 59–63.

Russell, D. A. (1970) Tyrannosaurs from the Late Cretaceous of western Canada. *National Museum of Natural Sciences, Publications in Paleontology*, 1, 1–34.

Russell, D. A. (1972) Ostrich dinosaurs from the Late Cretaceous of western Canada. *Canadian Journal of Earth Sciences*, 9(4), 375–402.

Russell, D. A. (1996) Isolated dinosaur bones from the Middle Cretaceous of the Tafilalt, Morocco. *Bulletin du Muséum National d'Histoire Naturelle, 4ème série–section C–Sciences de la Terre, Paléontologie, Géologie, Minéralogie*, 18(2-3), 349–402.

Sadlier, R. W., Barrett, P. and Powell, H. P. (2008) The anatomy and systematics of *Eustreptospondylus oxoniensis*, a theropod dinosaur from the Middle Jurassic of Oxfordshire, England. *Monograph of the Palaeontological Society* 160, 1–82.

Sakamoto, M. (2010) Jaw biomechanics and the evolution of biting performance in theropod dinosaurs. *Proceedings of the Royal Society B: Biological Sciences*, 277(1698), 3327–3333.

Sakamoto, M. (2022) Estimating bite force in extinct dinosaurs using phylogenetically predicted physiological cross-sectional areas of jaw adductor muscles. *PeerJ*, 10, e13731.

Sales, M. A., Lacerda, M. B., Horn, B. L., de Oliveira, I. A. and Schultz, C. L. (2016) The "χ" of the matter: Testing the relationship between paleoenvironments and three theropod Clades. *PloS one*, 11(2), e0147031.

Sales, M. A., Liparini, A., de Andrade, M. B., Aragão, P. R. and Schultz, C. L. (2017a) The oldest South American occurrence of Spinosauridae (Dinosauria, Theropoda). *Journal of South American Earth Sciences*, 74, 83-88.

Sales, M. A. F. and Schultz, C. L. (2017b) Spinosaur taxonomy and evolution of craniodental features: Evidence from Brazil. *PLOS ONE*, 12(11), e0187070.

Salgado, L., Canudo, J. I., Garrido, A. C., Ruiz-Omenaca, J. I., García, R. A., Marcelo, S., Barco, J. L. and Bollati, R. (2009) Upper Cretaceous vertebrates from El Anfiteatro area, Río Negro, Patagonia, Argentina. *Cretaceous Research*, 30(3), 767–784.

Salisbury, S. W. (2002) Crocodilians from the Lower Cretaceous (Berriasian) Purbeck Limestone Group of Dorset, southern England. *Special Papers in Palaeontology: Life And Environments In Purbeck Times*, 68(68), 121–144.

Salisbury, S. W. and Naish, D. (2011) 'Crocodilians', in Batten, D.J. (ed.) *English Wealden Fossils*. The Palaeontological Association: London, 305–369.

Salisbury, S. W., Willis, P. M., Peitz, S. and Sander, P. M. (1999) The crocodilian *Goniopholis simus* from the Lower Cretaceous of north-western Germany. *Special Papers in Palaeontology*, 60(60), 121–148.

Samathi, A., Chanthasit, P. and Sander, P. M. (2019) A review of theropod dinosaurs from the Late Jurassic to mid-Cretaceous of Southeast Asia. *Annales de Paléontologie*, 105(3), 201–215.

Samathi, A., Sander, P. M. and Chanthasit, P. (2021) A spinosaurid from Thailand (Sao Khua Formation, Early Cretaceous) and a reassessment of *Camarillasaurus cirugedae* from the Early Cretaceous of Spain. *Historical Biology*, 1–15.

Sampson, S. D. and Witmer, L. M. (2007) Craniofacial anatomy of *Majungasaurus crenatissimus* (Theropoda : Abelisauridae) from the Late Cretaceous of Madagascar. *Journal of Vertebrate Paleontology*, 27(2), 32–102.

Sánchez-Hernández, B. and Benton, M. J. (2012) Filling the ceratosaur gap: A new ceratosaurian theropod from the Early Cretaceous of Spain. *Acta Palaeontologica Polonica*, 59(3), 581–600.

Sánchez-Hernández, B., Benton, M. J. and Naish, D. (2007) Dinosaurs and other fossil vertebrates from the Late Jurassic and Early Cretaceous of the Galve area, NE Spain. *Palaeogeography, Palaeoclimatology, Palaeoecology*, 249(1-2), 180–215.

Sanders, R. K. and Smith, D. K. (2005) The endocranium of the theropod dinosaur *Ceratosaurus* studied with computer tomography. *Acta Palaeontologica Polonica*, 50(3), 601–616.

Sanguino, F. (2020) Isolated archosaur teeth from Las Hoyas (Barremian, Cuenca, Spain) and the challenge of discriminating highly convergent teeth. *Journal of Iberian Geology*, 46(2), 223–251.

Sansom, R. S., Choate, P. G., Keating, J. N. and Randle, E. (2018) Parsimony, not Bayesian analysis, recovers more stratigraphically congruent phylogenetic trees. *Biology letters*, 14(6), 20180263.

Santos-Cubedo, A., de Santisteban, C., Poza, B. and Meseguer, S. (2023) A new spinosaurid dinosaur species from the Early Cretaceous of Cinctorres (Spain). *Scientific Reports*, 13(1), 6471.

Sauvage, H. E. (1897–1898) *Vertébrés fossiles du Portugal. Contribution à l'étude des poissons et des reptiles du Jurassique et du Crétacique.* . Lisbonne: Direction des Travaux géologiques du Portugal.

Schade, M., Rauhut, O. W. and Evers, S. W. (2020) Neuroanatomy of the spinosaurid *Irritator challengeri* (Dinosauria: Theropoda) indicates potential adaptations for piscivory. *Scientific Reports*, 10(1), 9259

Schade, M., Rauhut, O. W. M., Foth, C., Moleman, O. and Evers, S. W. (2023) A reappraisal of the cranial and mandibular osteology of the spinosaurid *Irritator challengeri* (Dinosauria: Theropoda). *Palaeontologia Electronica*, 26(2), a17.

Schindelin, J., Arganda-Carreras, I., Frise, E., Kaynig, V., Longair, M., Pietzsch, T., Preibisch, S., Rueden, C., Saalfeld, S. and Schmid, B. (2012) Fiji: an open-source platform for biological-image analysis. *Nature Methods*, 9(7), 676–682.

Schmidt-Lebuhn, A. N. (2016) TNT script for the Templeton Test.

Schneider, E. R., Gracheva, E. O. and Bagriantsev, S. N. (2016) Evolutionary specialization of tactile perception in vertebrates. *Physiology*, 31(3), 193–200.

Schwab, J. A., Young, M. T., Neenan, J. M., Walsh, S. A., Witmer, L. M., Herrera, Y., Allain, R., Brochu, C. A., Choiniere, J. N. and Clark, J. M. (2020) Inner ear sensory system changes as extinct crocodylomorphs transitioned from land to water. *Proceedings of the National Academy of Sciences*, 117(19), 10422–10428.

Schwarz, D. and Salisbury, S. W. (2005) A new species of *Theriosuchus* (Atoposauridae, Crocodylomorpha) from the late Jurassic (Kimmeridgian) of Guimarota, Portugal. *Geobios*, 38(6), 779–802.

Sedlmayr, J. C. (2002) *Anatomy, evolution, and functional significance of cephalic vasculature in Archosauria*. PhD. Ohio University.

Sepkoski, J. J. (1986) Phanerozoic Overview of Mass Extinction, *Patterns and Processes in the History of Life*. Berlin, Heidelberg. Springer Berlin Heidelberg, 277–295.

Sereno, P. C. (1991) Basal archosaurs: phylogenetic relationships and functional implications. *Journal of Vertebrate Paleontology*, 11(S4), 1–53.

Sereno, P. C. (1998) A rationale for phylogenetic definitions, with application to the higher-level taxonomy of Dinosauria. *Neues Jahrbuch für Geologie und Paläontologie-Abhandlungen*, 41–83.

Sereno, P. C., Beck, A. L., Dutheil, D. B., Gado, B., Larsson, H. C., Lyon, G. H., Marcot, J. D., Rauhut, O. W., Sadleir, R. W. and Sidor, C. A. (1998) A long-snouted predatory dinosaur from Africa and the evolution of spinosaurids. *Science*, 282(5392), 1298–1302.

Sereno, P. C. and Brusatte, S. L. (2008a) Basal abelisaurid and carcharodontosaurid theropods from the Lower Cretaceous Elrhaz Formation of Niger. *Acta Palaeontologica Polonica*, 53(1), 15–46.

Sereno, P. C., Martinez, R. N., Wilson, J. A., Varricchio, D. J., Alcober, O. A. and Larsson, H. C. E. (2008b) Evidence for Avian Intrathoracic Air Sacs in a New Predatory Dinosaur from Argentina. *PLOS ONE*, 3(9), e3303.

Sereno, P. C., Myhrvold, N., Henderson, D. M., Fish, F. E., Vidal, D., Baumgart, S. L., Keillor, T. M., Formoso, K. K. and Conroy, L. L. (2022) *Spinosaurus* is not an aquatic dinosaur. *eLife*, 11, e80092.

Serrano-Martínez, A., Ortega, F., Sciscio, L., Tent-Manclús, J. E., Bandera, I. F. and Knoll, F. (2015) New theropod remains from the Tiourarén Formation (? Middle Jurassic, Niger) and their bearing on the dental evolution in basal tetanurans. *Proceedings of the Geologists' Association*, 126(1), 107–118.

Serrano-Martínez, A., Vidal, D., Sciscio, L., Ortega, F. and Knoll, F. (2016) Isolated theropod teeth from the Middle Jurassic of Niger and the early dental evolution of Spinosauridae. *Acta Palaeontologica Polonica*, 61(2), 403–415.

Shu'an, J., Pei, Z. and Daolin, L. (2022) New materials of the Early Cretaceous spinosaurid (Theropoda) teeth of Napai Basin, Fusui County, Guangxi. *Geological Bulletin of China*, 41(9), 1509–1515.

Siebert, D. J. (1992) 'Tree statistics; trees and 'confidence'; consenss trees; alternatives to parsimony; character weighting; character conflict ad resolution', in Forey, P.L.D. *et al.* (eds.) *Cladistics: A practical course in systematics*. Clarendon Press: Oxford, 72–88.

Simões, T. R., Caldwell, M. W. and Pierce, S. E. (2020) Sphenodontian phylogeny and the impact of model choice in Bayesian morphological clock estimates of divergence times and evolutionary rates. *BMC biology*, 18(1), 1–30.

Smith, J. B., Lamanna, M. C., Mayr, H. and Lacovara, K. J. (2006) New information regarding the holotype of *Spinosaurus aegyptiacus*. *Journal of Paleontology*, 80(2), 400–406.

Smith, J. B., Vann, D. R. and Dodson, P. (2005) Dental morphology and variation in theropod dinosaurs: implications for the taxonomic identification of isolated teeth. *The Anatomical Record* 285(2), 699–736.

Smith, M. R. (2019) Bayesian and parsimony approaches reconstruct informative trees from simulated morphological datasets. *Biology letters*, 15(2), 20180632.

Smith, N. A., Koeller, K. L., Clarke, J. A., Ksepka, D. T., Mitchell, J. S., Nabavizadeh, A., Ridgley, R. C. and Witmer, L. M. (2022) Convergent evolution in dippers (Aves, Cinclidae): The only wing-propelled diving songbirds. *The Anatomical Record*, 305(7), 1563–1591.

Smith, N. D., Makovicky, P. J., Agnolin, F. L., Ezcurra, M. D., Pais, D. F. and Salisbury, S. W. (2008) A *Megaraptor*-like theropod (Dinosauria: Tetanurae) in Australia: support for faunal exchange across eastern and western Gondwana in the Mid-Cretaceous. *Proceedings of the Royal Society B: Biological Sciences*, 275(1647), 2085–2093.

Smyth, R. S., Ibrahim, N. and Martill, D. M. (2020) *Sigilmassasaurus* is *Spinosaurus*: a reappraisal of African spinosaurines. *Cretaceous Research*, 114, 104520.

Sone, M., Hirayama, R., He, T. Y., Yoshida, M. and Komatsu, T. (2015) First dinosaur fossils from Malaysia: spinosaurid and ornithischian teeth, *The 2nd International Symposium on Asian Dinosaurs (ISAD2015) Program and Abstract, Bangkok, 19–20 November 2015.* Nakhorn Ratchasima Rajabhat University and Department of Mineral Resources ….

Soto, M., Toriño, P. and Perea, D. (2020) *Ceratosaurus* (Theropoda, Ceratosauria) teeth from the Tacuarembó Formation (Late Jurassic, Uruguay). *Journal of South American Earth Sciences*, 103, 102781.

Spiekman, S. N., Ezcurra, M. D., Butler, R. J., Fraser, N. C. and Maidment, S. C. (2021) *Pendraig milnerae*, a new small-sized coelophysoid theropod from the Late Triassic of Wales. *Royal Society Open Science*, 8(10), 210915.

Spoor, F., Bajpai, S., Hussain, S. T., Kumar, K. and Thewissen, J. G. (2002) Vestibular evidence for the evolution of aquatic behaviour in early cetaceans. *Nature*, 417(6885), 163–166.

St. John, K. (2017) The shape of phylogenetic treespace. *Systematic biology*, 66(1), e83–e94.

Stadler, T. (2010) Sampling-through-time in birth–death trees. *Journal of Theoretical Biology*, 267(3), 396–404.

Steel, M. and Penny, D. (2000) Parsimony, likelihood, and the role of models in molecular phylogenetics. *Molecular biology and evolution*, 17(6), 839–850.

Stefanic, C. M. and Nesbitt, S. J. (2019) The evolution and role of the hyposphene-hypantrum articulation in Archosauria: phylogeny, size and/or mechanics? *Royal Society Open Science*, 6(10), 190258.

Stewart, D., Ruffell, A., Wach, G. and Goldring, R. (1991) Lagoonal sedimentation and fluctuating salinities in the Vectis Formation (Wealden Group, Lower Cretaceous) of the Isle of Wight, southern England. *Sedimentary Geology*, 72(1-2), 117–134.

Stromer, E. (1915) Ergebnisse der Forschungsreisen Prof. E. Stromers in den Wüsten Ägyptens. II. Wirbeltierreste der Baharîje Stufe (unterstes Cenoman). 3. Das Original des Theropoden *Spinosaurus aegyptiacus* nov. gen., nov. spec. . *Abhandlungen der Königlich Bayerischen Akademie der Wissenschaften, Mathematisch-physikalische Klasse Abhandlung* 28(3), 1–32.

Stromer, E. (1934) Ergebnisse der Forschungsreisen Prof. E. Stromers in den Wüsten Ägyptens. II. Wirbeltier-Reste der Baharije-Stufe (unterstes Cenoman). 13. Dinosauria. *Abhandlungen der Bayer- ischen Akademie der Wissenschaften Mathematisch-naturwissen- schaftliche Abteilung*, 22, 1–79.

Suchard, M. A., Lemey, P., Baele, G., Ayres, D. L., Drummond, A. J. and Rambaut, A. (2018) Bayesian phylogenetic and phylodynamic data integration using BEAST 1.10. *Virus evolution*, 4(1), vey016.

Sues, H. D., Frey, E., Martill, D. M. and Scott, D. M. (2002) *Irritator challengeri*, a spinosaurid (Dinosauria : Theropoda) from the Lower Cretaceous of Brazil. *Journal of Vertebrate Paleontology*, 22(3), 535–547.

Sutton, M., Rahman, I. and Garwood, R. (2016) Virtual paleontology—an overview. *The Paleontological Society Papers*, 22, 1–20.

Sutton, M. D. (2008) Tomographic techniques for the study of exceptionally preserved fossils. *Proceedings of the Royal Society B: Biological Sciences*, 275(1643), 1587–1593.

Sweetman, S. C. (2004) The first record of velociraptorine dinosaurs (Saurischia, Theropoda) from the Wealden (Early Cretaceous, Barremian) of southern England. *Cretaceous Research*, 25(3), 353–364.

Sweetman, S. C. (2011) 'The Wealden of the Isle of Wight', in Batten, D.J. (ed.) *English Wealden Fossils*. The Palaeontological Association: London, 52–78.

Sweetman, S. C. and Insole, A. N. (2010) The plant debris beds of the Early Cretaceous (Barremian) Wessex Formation of the Isle of Wight, southern England: their genesis and palaeontological significance. *Palaeogeography, Palaeoclimatology, Palaeoecology*, 292(3-4), 409–424.

Sweetman, S. C., Pedreira-Segade, U. and Vidovic, S. U. (2015) A new bernissartiid crocodyliform from the Lower Cretaceous Wessex Formation (Wealden Group, Barremian) of the Isle of Wight, southern England. *Acta Palaeontologica Polonica*, 60(2), 257–268.

Taquet, P. (1984) Une curieuse spécialisation du crâne de certains Dinosaures carnovores du Crétacé: le museau long et étroit des Spinosauridés. *Comptes-rendus des séances de l'Académie des sciences. Série 2, Mécanique-physique, chimie, sciences de l'univers, sciences de la terre*, 299(5), 217–222.

Taquet, P. and Russell, D. A. (1998) New data on spinosaurid dinosaurs from the Early Cretaceous of the Sahara. *Comptes Rendus de l'Académie des Sciences-Series IIA-Earth and Planetary Science*, 327(5), 347–353.

Tarasov, S. (2023) New phylogenetic Markov models for inapplicable morphological characters. *Systematic Biology*, (Early release version),

.

Tate, J. R. and Cann, C. E. (1982) High-resolution computed tomography for the comparative study of fossil and extant bone. *American Journal of Physical Anthropology*, 58(1), 67–73.

Templeton, A. R. (1983) Phylogenetic inference from restriction endonuclease cleavage site maps with particular reference to the evolution of humans and the apes. *Evolution*, 221–244.

Terras, R., Carbonera, M., Budke, G. and Leite, K. J. G. (2022) Família Spinosauridae (Dinosauria: Theropoda): taxonomia, paleobiogeografia e paleoecologia (uma revisão). *Paleontologia em Destaque - Boletim da Sociedade Brasileira de Paleontologia*, 37(77), 14-54.

Therrien, F. and Henderson, D. M. (2007) My theropod is bigger than yours… or not: estimating body size from skull length in theropods. *Journal of Vertebrate Paleontology*, 27(1), 108–115.

Therrien, F., Henderson, D. M. and Ruff, C. B. (2005) 'Bite me: biomechanical models of theropod mandibles and implications for feeding behavior', in Carpenter, K. (ed.) *The Carnivorous Dinosaurs*. Indiana University Press: Bloomington, 179–237.

Topley, W. (1875) *The Geology of the Weald (parts of the Counties of Kent, Surrey, Sussex, and Hants)*. London: HM Stationery Office.

Townson, W. G. (1975) Lithostratigraphy and deposition of the type Portlandian. *Journal of the Geological Society*, 131(6), 619–638.

Tschopp, E. and Upchurch, P. (2018) The challenges and potential utility of phenotypic specimen-level phylogeny based on maximum parsimony. *Earth and Environmental Science Transactions of the Royal Society of Edinburgh*, 109(1-2), 301–323.

Tsuihiji, T. (2010) Reconstructions of the axial muscle insertions in the occipital region of dinosaurs: evaluations of past hypotheses on Marginocephalia and Tyrannosauridae using the Extant Phylogenetic Bracket approach. *The Anatomical Record*, 293(8), 1360–1386.

Turmine-Juhel, P., Wilks, R., Brockhurst, D., Austen, P. A., Duffin, C. J. and Benton, M. J. (2019) Microvertebrates from the Wadhurst Clay Formation (Lower Cretaceous) of Ashdown Brickworks, East Sussex, UK. *Proceedings of the Geologists' Association*, 130(6), 752–769.

Ungi, T., Lasso, A. and Fichtinger, G. (2016) Open-source platforms for navigated image-guided interventions. *Medical Image Analysis*, 33, 181–186.

Upchurch, P. (1995) The evolutionary history of sauropod dinosaurs. *Philosophical Transactions of the Royal Society of London. Series B: Biological Sciences*, 349(1330), 365–390.

Upchurch, P., Barrett, P. M. and Dodson, P. (2004) 'Sauropoda', in Weishampel, D.B., Dodson, P. and Osmólska, H. (eds.) *The Dinosauria*. University of California Press, 259–322.

Upchurch, P., Mannion, P. D. and Barrett, P. M. (2011) 'Sauropod Dinosaurs', in Batten, D.J. (ed.) *English Wealden Fossils*. The Palaeontological Association: London, 476–525.

Van Valkenburgh, B. and Molnar, R. E. (2002) Dinosaurian and mammalian predators compared. *Paleobiology*, 28(4), 527–543.

Verdú, F. J., Cobos, A., Royo-Torres, R. and Alcalá, L. (2019) Diversity of large ornithopod dinosaurs in the upper Hauterivian-lower Barremian (Lower Cretaceous) of Teruel (Spain): a morphometric approach. *Spanish Journal of Palaeontology*, 34(2), 269–288.

Vermeiren, S., Bellefroid, E. J. and Desiderio, S. (2020) Vertebrate sensory ganglia: common and divergent features of the transcriptional programs generating their functional specialization. *Frontiers in Cell and Developmental Biology*, 8, 587699.

von Huene, F. (1923) Carnivorous saurischia in Europe since the Triassic. *Bulletin of the Geological Society of America*, 34(3), 449–458.

Voogd, J. and Wylie, D. R. (2004) Functional and anatomical organization of floccular zones: a preserved feature in vertebrates. *Journal of Comparative Neurology*, 470(2), 107–112.

Vullo, R., Abit, D., Ballevre, M., Billon-Bruyat, J.-P., Bourgeais, R., Buffetaut, E., Daviero-Gomez, V., Garcia, G., Gomez, B. and Mazin, J.-M. (2014) Palaeontology of the Purbeck-type (Tithonian, Late Jurassic) bonebeds of Chassiron (Oléron Island, western France). *Comptes Rendus Palevol*, 13(5), 421–441.

Vullo, R., Allain, R. and Cavin, L. (2016) Convergent evolution of jaws between spinosaurid dinosaurs and pike conger eels. *Acta Palaeontologica Polonica*, 61(4), 825–828.

Walsh, S. A., Barrett, P. M., Milner, A. C., Manley, G. and Witmer, L. M. (2009) Inner ear anatomy is a proxy for deducing auditory capability and behaviour in reptiles and birds. *Proceedings of the Royal Society B: Biological Sciences*, 276(1660), 1355–1360.

Walsh, S. A., Iwaniuk, A. N., Knoll, M. A., Bourdon, E., Barrett, P. M., Milner, A. C., Nudds, R. L., Abel, R. L. and Sterpaio, P. D. (2013) Avian cerebellar floccular fossa size is not a proxy for flying ability in birds. *PLoS One*, 8(6), e67176.

Walsh, S. A. and Knoll, M. A. (2011) Directions in palaeoneurology. *Special Papers in Palaeontology*, 86(1228), 263–279.

Warnock, R. C. and Wright, A. M. (2021) *Understanding the tripartite approach to Bayesian divergence time estimation*. Cambridge University Press.

Waskow, K. and Mateus, O. (2017) Dorsal rib histology of dinosaurs and a crocodylomorph from western Portugal: Skeletochronological implications on age determination and life history traits. *Comptes Rendus Palevol*, 16(4), 425–439.

Watanabe, A., Gignac, P. M., Balanoff, A. M., Green, T. L., Kley, N. J. and Norell, M. A. (2019) Are endocasts good proxies for brain size and shape in archosaurs throughout ontogeny? *Journal of Anatomy*, 234(3), 291–305.

Weishampel, D. B., Barrett, P., Coria, R. A., Le Loeuff, J., Xing, X. U., Xijin, Z., Sahni, A., Gomani, E. M. P. and Noto, C. R. (2004) 'Dinosaur distribution', in Weishampel, D.B., Dodson, P. and Osmólska, H. (eds.) *The Dinosauria*. University of California Press: London, England, 517–606.

Werneburg, I., Evers, S. W. and Ferreira, G. (2021) On the “cartilaginous rider” in the endocasts of turtle brain cavities. *Vertebrate Zoology*, 71, 403–418.

Westhead, R. and Mather, A. (1996) An updated lithostratigraphy for the Purbeck Limestone Group in the Dorset type-area. *Proceedings of the Geologists' Association*, 107(2), 117–128.

Wever, E. G. (1978) 'General anatomy of the reptilian ear', in *The Reptile Ear*. Princeton University Press, 59–88.

White, H. J. O. (1928) *The Geology of the Country Near Hastings and Dungeness*. London: Memoirs of the Geological Survey England.

White, M. A., Bell, P. R., Poropat, S. F., Pentland, A. H., Rigby, S. L., Cook, A. G., Sloan, T. and Elliott, D. A. (2020) New theropod remains and implications for megaraptorid diversity in the Winton Formation (lower Upper Cretaceous), Queensland, Australia. *Royal Society Open Science*, 7(1), 191462.

White, O. (1921) *A Short Account of the Geology of the Isle of Wight*. London: Memoirs of the Geological Survey.

Whitlock, J. A. (2011) A phylogenetic analysis of Diplodocoidea (Saurischia: Sauropoda). *Zoological Journal of the Linnean Society*, 161(4), 872–915.

Wiens, J. J. (2006) Missing data and the design of phylogenetic analyses. *Journal of biomedical informatics*, 39(1), 34–42.

Wiens, J. J. (2009) Paleontology, genomics, and combined-data phylogenetics: can molecular data improve phylogeny estimation for fossil taxa? *Systematic Biology*, 58(1), 87–99.

Wiens, J. J. and Moen, D. S. (2008) Missing data and the accuracy of Bayesian phylogenetics. *Journal of Systematics and Evolution*, 46(3), 307–314.

Wiens, J. J. and Morrill, M. C. (2011) Missing data in phylogenetic analysis: reconciling results from simulations and empirical data. *Systematic biology*, 60(5), 719–731.

Wilkinson, M. (1995) Coping with abundant missing entries in phylogenetic inference using parsimony. *Systematic biology*, 44(4), 501–514.

Wilkinson, M. (2003) Missing entries and multiple trees: instability, relationships, and support in parsimony analysis. *Journal of Vertebrate Paleontology*, 23(2), 311–323.

Wills, S., Underwood, C. J. and Barrett, P. M. (2021) Learning to see the wood for the trees: machine learning, decision trees, and the classification of isolated theropod teeth. *Palaeontology*, 64(1), 75–99.

Wilson, J. A., Michael, D., Ikejiri, T., Moacdieh, E. M. and Whitlock, J. A. (2011) A nomenclature for vertebral fossae in sauropods and other saurischian dinosaurs. *PLoS One*, 6(2), e17114.

Wilson, J. A. and Upchurch, P. (2003) A revision of *Titanosaurus* Lydekker (Dinosauria-Sauropoda), the first dinosaur genus with a ‘Gondwanan’distribution. *Journal of Systematic Palaeontology*, 1(3), 125–160.

Witmer, L. M. (1990) The craniofacial air sac system of Mesozoic birds (Aves). *Zoological Journal of the Linnean Society*, 100(4), 327–378.

Witmer, L. M. (1997a) 'Craniofacial air sinus systems', in Currie, P.J. and Padian, K. (eds.) *The Encyclopedia of Dinosaurs*. Academic Press: New York, 151–159.

Witmer, L. M. (1997b) The evolution of the antorbital cavity of archosaurs: a study in soft-tissue reconstruction in the fossil record with an analysis of the function of pneumaticity. *Journal of Vertebrate Paleontology*, 17(S1), 1–76.

Witmer, L. M., Chatterjee, S., Franzosa, J. and Rowe, T. (2003) Neuroanatomy of flying reptiles and implications for flight, posture and behaviour. *Nature*, 425(6961), 950–953.

Witmer, L. M. and Ridgely, R. C. (2009) New insights into the brain, braincase, and ear region of tyrannosaurs (Dinosauria, Theropoda), with implications for sensory organization and behavior. *The Anatomical Record: Advances in Integrative Anatomy and Evolutionary Biology*, 292(9), 1266–1296.

Witmer, L. M. and Ridgely, R. C. (2010) The Cleveland tyrannosaur skull (*Nanotyrannus* or *Tyrannosaurus*): new findings based on CT scanning, with special reference to the braincase. *Kirtlandia*, 57, 61–81.

Witmer, L. M., Ridgely, R. C., Dufeau, D. L. and Semones, M. C. (2008) 'Using CT to peer into the past: 3D visualization of the brain and ear regions of birds, crocodiles, and nonavian dinosaurs', in Endo, H. and Frey, R. (eds.) *Anatomical Imaging*. Springer, 67–87.

Wongko, K., Buffetaut, E., Khamha, S. and Lauprasert, K. (2019) Spinosaurid theropod teeth from the red beds of the Khok Kruat formation (Early Cretaceous) in Northeastern Thailand. *Tropical Natural History*, 19(1), 8–20.

Woolley, C. H., Thompson, J. R., Wu, Y.-H., Bottjer, D. J. and Smith, N. D. (2022) A biased fossil record can preserve reliable phylogenetic signal. *Paleobiology*, 1–16.

Wright, A. M. (2019) A systematist's guide to estimating Bayesian phylogenies from morphological data. *Insect systematics and diversity*, 3(3), 1–14.

Wright, A. M., Bapst, D. W., Barido-Sottani, J. and Warnock, R. C. (2022) Integrating fossil observations into phylogenetics using the fossilized birth–death model. *Annual Review of Ecology, Evolution, and Systematics*, 53, 251–273.

Wright, A. M. and Hillis, D. M. (2014) Bayesian analysis using a simple likelihood model outperforms parsimony for estimation of phylogeny from discrete morphological data. *PLoS One*, 9(10), e109210.

Xi-Jin, Z., Benson, R. B., Brusatte, S. L. and Currie, P. J. (2009) The postcranial skeleton of *Monolophosaurus jiangi* (Dinosauria: Theropoda) from the Middle Jurassic of Xinjiang, China, and a review of Middle Jurassic Chinese theropods. *Geological Magazine*, 147(1), 13–27.

Xing, L., Paulina-Carabajal, A., Currie, P. J., Xu, X., Zhang, J., Wang, T., Burns, M. E. and Dong, Z. (2014) Braincase anatomy of the basal theropod *Sinosaurus* from the Early Jurassic of China. *Acta Geologica Sinica-English Edition*, 88(6), 1653–1664.

Xing, L., Roberts, E. M., Harris, J. D., Gingras, M. K., Ran, H., Zhang, J., Xu, X., Burns, M. E. and Dong, Z. (2013) Novel insect traces on a dinosaur skeleton from the Lower Jurassic Lufeng Formation of China. *Palaeogeography, Palaeoclimatology, Palaeoecology*, 388, 58–68.

Yang, Z. (2014) 'Phylogeny reconstruction: overview', in *Molecular Evolution: A Statistical Approach*. Oxford University Press: New York, 70–101.

Young, C. C. (1944) On the Reptilian Remains from Weiyuan, Szechuan, China. *Bulletin of the Geological Society of China*, 24(3–4), 187–209.

Young, C. M., Hendrickx, C., Challands, T. J., Foffa, D., Ross, D. A., Butler, I. B. and Brusatte, S. L. (2019) New theropod dinosaur teeth from the Middle Jurassic of the Isle of Skye, Scotland. *Scottish Journal of Geology*, 55(1), 7–19.

Young, M. T., Steel, L., Foffa, D., Price, T., Naish, D. and Tennant, J. P. (2014) Marine tethysuchian crocodyliform from the ?Aptian-Albian (Lower Cretaceous) of the Isle of Wight, UK. *Biological Journal of the Linnean Society*, 113(3), 854–871.

Young, M. T., Tennant, J. P., Brusatte, S. L., Challands, T. J., Fraser, N. C., Clark, N. D. and Ross, D. A. (2016) The first definitive Middle Jurassic atoposaurid (Crocodylomorpha, Neosuchia), and a discussion on the genus *Theriosuchus*. *Zoological journal of the Linnean Society*, 176(2), 443–462.

Yu, C., Qin, F., Li, Y., Qin, Z. and Norell, M. (2022) CT segmentation of dinosaur fossils by deep learning. *Frontiers in Earth Science*, 9, 805271.

Yu, Y., Harris, A. J., Blair, C. and He, X. (2015) RASP (Reconstruct Ancestral State in Phylogenies): a tool for historical biogeography. *Molecular phylogenetics and evolution*, 87, 46–49.

Zelenitsky, D. K., Therrien, F. and Kobayashi, Y. (2009) Olfactory acuity in theropods: palaeobiological and evolutionary implications. *Proceedings of the Royal Society B: Biological Sciences*, 276(1657), 66–-673.

Zelenitsky, D. K., Therrien, F., Ridgely, R. C., McGee, A. R. and Witmer, L. M. (2011) Evolution of olfaction in non-avian theropod dinosaurs and birds. *Proceedings of the Royal Society B: Biological Sciences*, 278(1725), 3625–3634.